# NEURODEGENERATION, CELL SIGNALING AND NEUROREPARATIVE STRATEGIES

EDITED BY: Ana Rita Vaz, Valle Palomo and Ana Falcão
PUBLISHED IN: Frontiers in Pharmacology and Frontiers in Neuroscience

frontiers Research Topics

ISSN 1664-8714
ISBN 978-2-83250-674-5
DOI 10.3389/978-2-83250-674-5

## About Frontiers

Frontiers is more than just an open-access publisher of scholarly articles: it is a pioneering approach to the world of academia, radically improving the way scholarly research is managed. The grand vision of Frontiers is a world where all people have an equal opportunity to seek, share and generate knowledge. Frontiers provides immediate and permanent online open access to all its publications, but this alone is not enough to realize our grand goals.

## Frontiers Journal Series

The Frontiers Journal Series is a multi-tier and interdisciplinary set of open-access, online journals, promising a paradigm shift from the current review, selection and dissemination processes in academic publishing. All Frontiers journals are driven by researchers for researchers; therefore, they constitute a service to the scholarly community. At the same time, the Frontiers Journal Series operates on a revolutionary invention, the tiered publishing system, initially addressing specific communities of scholars, and gradually climbing up to broader public understanding, thus serving the interests of the lay society, too.

## Dedication to Quality

Each Frontiers article is a landmark of the highest quality, thanks to genuinely collaborative interactions between authors and review editors, who include some of the world's best academicians. Research must be certified by peers before entering a stream of knowledge that may eventually reach the public - and shape society; therefore, Frontiers only applies the most rigorous and unbiased reviews.
Frontiers revolutionizes research publishing by freely delivering the most outstanding research, evaluated with no bias from both the academic and social point of view. By applying the most advanced information technologies, Frontiers is catapulting scholarly publishing into a new generation.

## What are Frontiers Research Topics?

Frontiers Research Topics are very popular trademarks of the Frontiers Journals Series: they are collections of at least ten articles, all centered on a particular subject. With their unique mix of varied contributions from Original Research to Review Articles, Frontiers Research Topics unify the most influential researchers, the latest key findings and historical advances in a hot research area! Find out more on how to host your own Frontiers Research Topic or contribute to one as an author by contacting the Frontiers Editorial Office: frontiersin.org/about/contact

# NEURODEGENERATION, CELL SIGNALING AND NEUROREPARATIVE STRATEGIES

Topic Editors:
**Ana Rita Vaz,** University of Lisbon, Portugal
**Valle Palomo,** IMDEA Nanociencia, Spain
**Ana Falcão,** Universidade NOVA de Lisboa, Portugal

**Citation:** Vaz, A. R., Palomo, V., Falcão, A., eds. (2022). Neurodegeneration, Cell Signaling and Neuroreparative Strategies. Lausanne: Frontiers Media SA. doi: 10.3389/978-2-83250-674-5

# Table of Contents

frontiers | Frontiers in Pharmacology

TYPE Editorial
PUBLISHED 19 October 2022
DOI 10.3389/fphar.2022.1059923



OPEN ACCESS

EDITED AND REVIEWED BY
Nicholas M. Barnes,
University of Birmingham,
United Kingdom

*CORRESPONDENCE
Ana Rita Vaz,
armvaz@ff.ulisboa.pt

SPECIALTY SECTION
This article was submitted to Neuropharmacology, a section of the journal Frontiers in Pharmacology

RECEIVED 02 October 2022
ACCEPTED 06 October 2022
PUBLISHED 19 October 2022

CITATION
Vaz AR, Falcão AS and Palomo V (2022), Editorial: Neurodegeneration, cell signaling and neuroreparative strategies. *Front. Pharmacol.* 13:1059923. doi: 10.3389/fphar.2022.1059923



# Editorial: Neurodegeneration, cell signaling and neuroreparative strategies

Ana Rita Vaz[1,2]*, Ana Sofia Falcão[3] and Valle Palomo[4,5]

[1]Neuroinflammation, Signaling and Neuroregeneration Group, Research Institute for Medicines (iMed.ULisboa), Faculty of Pharmacy, Universidade de Lisboa, Lisbon, Portugal, [2]Department of Pharmaceutical Sciences and Medicines, Faculty of Pharmacy, Universidade de Lisboa, Lisbon, Portugal, [3]iNOVA4Health, NOVA Medical School, Faculdade de Ciências Médicas, NMS, FCM, Universidade Nova de Lisboa, Lisboa, Portugal, [4]Instituto Madrileño de Estudios Avanzados en Nanociencia (IMDEA-Nanociencia), Madrid, Spain, [5]Centro de Investigación Biomédica en Red de Enfermedades Neurodegenerativas (CIBERNED), Instituto de Salud Carlos III, Madrid, Spain

KEYWORDS

**neurodegenerative diseases, CNS-intracellular and extracellular communication, neuroinflammation and immunoregulation, therapeutic applications, paracrine signaling**

Editorial on the Research Topic
Neurodegeneration, cell signaling and neuroreparative strategies

Neurodegenerative diseases are usually characterized by the accumulation of misfolded proteins and malfunction of proteasomal, autophagosomal, lysosomal or mitochondrial systems, that lead to a progressive loss of vulnerable populations of neurons in specific regions of the central nervous system (CNS). Glial cells and neuroinflammation are key contributors for the neurodegenerative process but their precise role remains unclear. A better understanding of the cell-cell communication will contribute to unveil the pathophysiological mechanisms that trigger neurodegeneration and will help to find specific targets for modulation. Non-cellular players, including the overall secretome and the extracellular vesicles (EVs), including the small EVs (sEVs), also designated as exosomes, may be also important contributors for the maintenance and spread of pathological processes that depend on cell-to-cell communication, and may also constitute targets for modulation. Indeed, they are important in the intercellular communication due to their capacity to transfer multiple different messengers, such as proteins, lipids, nuclei acids or microRNAs.

This Research Topic gives an overview of the neuronal-glial pathophysiological mechanisms involved in several existing models of neurodegenerative diseases. In addition, new potential therapeutic strategies targeting either intercellular and intracellular communication are proposed for the several existing models of neurodegenerative diseases, through 10 articles by 51 authors, which contains 3 reviews and 1 mini-review, as well as 5 original research papers and 1 brief research report, (Total views: 21,535; as of 30 Sep 2022).

One of the reviews focuses on the recent progress in methods for manufacturing, isolation and engineering sEVs that may be used as a therapeutic strategy to overcome neurodegeneration in CNS pathologies, namely in models of Alzheimer's and Parkinson's Disease, Amyotrophic Lateral Sclerosis and Brain Tumours (Loch-Neckel et al.). Another review discusses the cell non-autonomous proteostasis function and decline along the aging process, by focusing on the systemic activation and mechanisms of the heat shock and unfolded protein responses of the endoplasmic reticulum and mitochondria, as well as transcellular chaperone signaling and transcellular transfer of proteotoxic material (Ferreira et al.). The third review focuses on the molecular mechanisms underlying ischemic stroke and presents the new systemic glutamate scavenging methods that may be used in combination or as an alternative to the current available drugs and therapeutic approaches for stroke patients (Kaplan-Arabaci et al.). There is also a mini-review that examines the pathophysiological mechanisms of spinal cord injury, emphasizing the important contribution of the inflammatory processes, and how its inhibition by Safflower Yellow, an HMGB1-TLR4-NF-κB signaling pathway inhibitor, have a reparative effect in injured spinal cord tissue (Wang et al.).

This Research Topic also contains original studies covering critical aspects of neurodegeneration and putative therapeutic strategies. Among them, two studies focused on the contribution of myelinating cells in models involving neurodegeneration. In the first one, the benefit of basic fibroblast growth factor (bFGF) to promote the facial nerve repair after injury was explored (Hu et al.). The Authors developed a thermosensitive *in situ* forming poloxamer hydrogel that was used as a vehicle to deliver bFGF for treating facial nerve injury (FNI) in rats. Data indicate that the bFGF-hydrogel promote facial nerve regeneration by promoting autophagy and inhibiting apoptosis. They also demonstrated that such repair is mediated by the PAK1 signaling pathway activation in Schwann cells, which may provide a promising strategy to be used for FNI recovery. The other study addressed the protective effect of GABA receptors agonists, namely baclofen and muscimol, against AMPA-induced excitotoxicity in cultured rat oligodendrocytes (Bayon-Cordero et al.). They found that GABA receptors activation initiates alternative molecular mechanisms that attenuate AMPA-mediated apoptotic excitotoxicity in oligodendrocytes, and propose GABA receptor agonists as potential oligodendroglial protectants in CNS disorders.

In another study, the neuroprotective effects of entinostat, a class I histone deacetylases (HDAC) inhibitor were studied in a model of spinal cord injury (SCI) (Dai et al.). For that, a mouse model of SCI and an *in vitro* model of oxygen-glucose deprivation (OGD) were used. The authors concluded that entinostat suppressed HDAC activation and also improved the motor function, histopathological damage, local inflammatory response and NLRP3 inflammasome activation in the spinal cord following SCI. Entionostat also had a neuroprotective role in the OGD-induced neuronal damage *via* the NLRP3 inflammasome, highlighting the interaction between the HDAC and NLRP3 inflammasome in the pathologic process of SCI.

Finally, three studies were focused in neurodegenerative disorders, namely using Alzheimer's Disease (AD) and Amyotrophic Lateral Sclerosis (ALS) models. Regarding AD, the first study aimed to determine whether the regulation of Rho protein kinase 2 (Rock2) by the activator of the E3 ubiquitin ligase anaphase-promoting complex/cyclosome (APC/C), Cdh1, is an important mechanistic event in AD (Lapresa et al.). For that, Authors used an oligomerized form of the amyloid-beta (Aβ) peptide (Aβ25-35) that was incubated in neuronal primary mice cultures and also injected intracerebroventricularly in the mice, to induce an *in vitro* and an *in vivo* AD model, respectively. Results identified a novel Cdh1-Rock2 pathway that is involved in Aβ-mediated neurotoxicity, which may open novel therapeutic opportunities for AD. The other study on AD used a co-culture system of two human cell lines, microRNA (miR)-124 modulated SWE SHSY-5Y-neurons and CHME3-microglia stimulated with interferon-gamma (IFNγ), to determine how miR-124 modulation in SWE cells influences microglia polarized subtypes in the context of inflammation (Garcia et al.). The authors found that SWE miR-124 inhibitor favored IFNγ-induced inflammatory signature in microglia, while the SWE miR-124 mimic reduced their activation. Microglia proteomics also identified 113 responsive proteins to SWE miR-124 levels, including a subgroup of proteins involved in immune function/inflammation. This study was innovative in suggesting that neuronal miR-124 reshapes microglia plasticity, highlighting the contribution of neuronal survival to the inflammatory mechanisms that occur in AD-associated pathophysiology. In the study regarding the ALS model, the authors compared the potential therapeutic effects of three Sigma-1 receptor (Sig-1R) ligands, namely the agonists PRE-084 and SA4503 and the antagonist BD1063, in the SOD1G93A mouse model of ALS (Gaja-Capdevila et al.). They found that PRE-084 and BD1063 treatment could preserve neuromuscular function of the hindlimbs and increased the number of surviving motor neurons in the ALS mice, while SA4503 only slightly improved motor function, concluding that Sig-1R ligands are promising tools to consider for ALS treatment.

Overall, this Research Topic discussed a few proofs of concept that non-neuronal cells and their communication actively contribute to the degenerative process in several models of neurodegeneration and how the modulation of such communication mechanisms could uncover novel therapeutic strategies. Some of these strategies are here highlighted, providing valuable information for the development of innovative strategies designed to overcome the neurodegenerative process.

## Author contributions

AV, VP, and ASF contributed to writing this Editorial.

## Funding

This work was partly supported by the grant UID/DTP/04138/2019-21 (iMed.ULisboa) as well as La Caixa Foundation and -Luzón Foundation through project HR21-00931. VP acknowledges financial support from the Spanish Ministry of Science through the Ramón y Cajal grant RYC2019-027489-I.

## Acknowledgments

The editors appreciate the contributions of all authors to this Research Topic, the constructive comments of all the reviewers, and the editorial support from Frontiers throughout the publication process.

## Conflict of interest

The authors declare that the research was conducted in the absence of any commercial or financial relationships that could be construed as a potential conflict of interest.

## Publisher's note

frontiers in Pharmacology

ORIGINAL RESEARCH
published: 26 November 2021
doi: 10.3389/fphar.2021.774539

# Entinostat Improves Motor Function and Neuronal Damage *Via* Downregulating NLRP3 Inflammasome Activation After Spinal Cord Injury

*Chen Dai*[1,2†], *Bin Liu*[3†], *Bibo Peng*[4], *Bo Qu*[5], *Jiezhi Lin*[6], *Baogan Peng*[2*] and *Duan-Ming Li*[2*]

[1]Orthopedics and Trauma Department, The 963rd (224th) Hospital of People's Liberation Army, 963rd Hospital of Joint Logistics Support Force of PLA, Jiamusi, China, [2]Department of Orthopedics, The Third Medical Center, General Hospital of the Chinese People's Liberation Army, Beijing, China, [3]Department of Orthopaedics, General Hospital of Northern Theater Command, Shenyang, China, [4]Outpatient Department, The Third Medical Center of Chinese People's Liberation Army General Hospital, Beijing, China, [5]Tianjin University, Tianjin Key Laboratory for Disaster and Emergency Medicine Technology, Tianjin, China, [6]Military Burn Center, The 963rd (224th) Hospital of People's Liberation Army, 963rd Hospital of Joint Logistics Support Force of PLA, Jiamusi, China

OPEN ACCESS

**Edited by:**
Ana Rita Vaz,
University of Lisbon, Portugal

**Reviewed by:**
Minfei Wu,
Second Affiliated Hospital of Jilin University, China
Yibo Ying,
The Second Affiliated Hospital and Yuying Children's Hospital of Wenzhou Medical University, China

***Correspondence:**
Baogan Peng
pengbaogan76611@163.com
Duan-Ming Li
liduanmin69@163.com

[†]These authors have contributed equally to this work and share first authorship

**Specialty section:**
This article was submitted to Neuropharmacology, a section of the journal Frontiers in Pharmacology

**Received:** 12 September 2021
**Accepted:** 25 October 2021
**Published:** 26 November 2021

**Citation:**
Dai C, Liu B, Peng B, Qu B, Lin J, Peng B and Li D-M (2021) Entinostat Improves Motor Function and Neuronal Damage Via Downregulating NLRP3 Inflammasome Activation After Spinal Cord Injury. Front. Pharmacol. 12:774539. doi: 10.3389/fphar.2021.774539

**Background:** Spinal cord injury (SCI), a major public health problem, has no effective treatment. A large number of studies have confirmed that histone deacetylases (HDACs) are involved in the physiologic processes that occur following SCI. We tried to uncover the potential neuroprotective role of entinostat (a class I HDAC inhibitor) in SCI.

**Methods:** We conducted a study on a preclinical mouse model of SCI and OGD-induced neuronal damage to present the role of entinostat by the analysis of motor function, histopathologic damage, local NLRP3 inflammasome activation, and neuronal damage.

**Results:** The results showed that entinostat suppressed HDAC activation (including HDAC1 and HDAC3 expression), improved the grip strength and BMS score, spinal edema, cell death, and local NLRP3 inflammasome activation in the spinal cord following SCI. Furthermore, entinostat significantly increased OGD-inhibited neuronal activity and decreased PI-positive cells, HDAC activation, caspase-1 activation, IL-1β and IL-18 levels, and NLRP3 expression.

**Conclusion:** In summary, we first documented that entinostat improved the motor function, histopathologic damage, and local inflammatory response and NLRP3 inflammasome activation in the spinal cord following SCI and also presented the neuroprotective role of OGD-induced neuronal damage *via* the NLRP3 inflammasome. Thus, our study has the potential to reveal the interaction between the HDAC and NLRP3 inflammasome in the pathologic process as well as SCI and further promote the clinical indications of HDACi entinostat and clinical treatment for the inflammatory response after SCI.

**Keywords: SCI, entinostat, HDAC, NLRP3 inflammasome, neuronal damage**

## BACKGROUND

With a high global incidence rate (10.4–83 per million people per year), spinal cord injury (SCI) results in severe long-term disability as it deprives many patients of motor function (Karsy and Hawryluk, 2019), induced by motor vehicle accidents, violence, falls, and recreational activities. In the United States, the incidence of traumatic SCI is 183, 000–230, 000 and is more common in males, with an average age of 31.7 years (McDonald and Sadowsky, 2002), and the average lifetime cost of treating an individual with traumatic SCI is between $1.1 m and $4.7 million per person that places an enormous financial burden on society and families (McDonald and Sadowsky, 2002; Karsy and Hawryluk, 2019). Although a large number of preclinical studies have been conducted to better understand the pathophysiology of acute SCI and to develop targeted therapies to improve SCI outcomes, there is still little clinical practice (Karsy and Hawryluk, 2019). Current clinical management of SCI includes aggressive intensive care measures, early surgical decompression, and stabilization followed by elevating blood pressure to decrease secondary injury (Fehlings et al., 2017; Shank et al., 2019).

Previous research studies have confirmed that damaged cells, axons, and blood vessels release toxic chemicals that attack intact neighboring cells after SCI, and the secondary events include excitotoxicity and inflammation (McDonald and Sadowsky, 2002; Fouad et al., 2021). In animal models of SCI and humans, inflammation is a result of the loss of control of sympathetic tone transmitted to the organs that directs metabolism or mediates immune responses (Fouad et al., 2021). Days or weeks after the initial trauma, a wave of cell death induced by secondary events might sweep through neurons and glial cells affecting the outcomes of the trauma site (McDonald and Sadowsky, 2002). The downstream consequences of inflammation could serve as modifiers of SCI functional outcomes in experimental or clinical indices of the severity of injury (Bloom et al., 2020; Kwiecien et al., 2020; Zrzavy et al., 2021). Several inflammatory treatment strategies have been documented to be effective in preclinical studies of SCI (Jorge et al., 2019; Kong et al., 2021). IL-10 significantly suppresses inflammatory cytokines, alters macrophage phenotype, preserves more axons within the rubrospinal and reticulospinal tracts through the injury site, and aids in functional recovery after SCI (Hellenbrand et al., 2019). Chen et al. have demonstrated that AZD8797, an inhibitor of CX3CR1, effectively blocks overwhelming inflammation, apoptosis, and necrosis after SCI and facilitates early recovery of locomotive function (Chen et al., 2020).

Histone deacetylases (HDACs) are epigenetic regulators that regulate histone modifications, which are also posttranscriptional modifiers that regulate protein acetylation in several pathophysiologic states (Kiany et al., 2020). HDAC inhibitors (HDACi) indicate an ability for targeting two main classes of HDAC enzymes, namely, class I HDAC: 1, 2, 3, and 8 and class II HDAC: 4, 5, 6, 7, 9, and 10 which are utilized in treating diseases ranging from neurodegenerative conditions to inflammatory diseases (Cantley and Haynes, 2013). Multiple HDACi, including trichostatin A (TSA), phenylbutyrate, vorinostat, givinostat, and valproic acid (VPA), have documented anti-inflammatory effects both *in vitro* and *in vivo* (Cantley and Haynes, 2013; Mohammadi et al., 2018). Acetylated histone proteins exert their neuroprotective effects by reducing inflammation and inhibiting neuronal death (Chen et al., 2018), which improve the neurologic functions in many neurologic diseases, including cerebral ischemia (Suda et al., 2015), traumatic brain injury (Sada et al., 2020), and SCI (Su et al., 2014; Chen et al., 2018). VPA inhibits the HDAC3 level and activity and increases STAT1 as well as NF-κB p65 acetylation, which attenuates the microglia-mediated central inflammatory response after SCI (Chen et al., 2018). Zhang et al. verified that the class I HDAC inhibitor CI-994 decreases neutrophil accumulation, inflammatory cytokine expressions, and neuronal loss as early as 3 days following SCI (Zhang H. et al., 2018). Tubastatin A promotes acetylation and stabilization of microtubules and thus restores transport function in nocodazole-treated cells and SCI mice by inhibiting HDAC 6, which may contribute to restored autophagic flux and increased axonal length (Zheng et al., 2020). Hendrix et al. have found specific HDAC 8 inhibition with PCI-34051 reduces the number of perilesional macrophages as measured by histologic analyses but does not improve functional recovery after SCI (Hendrix et al., 2020). Entinostat, a member of the benzamide group, is a narrow-spectrum HDAC inhibitor and affects class I HDAC with limited effect on HDAC 8, which is already used for conducting several phase I/II clinical trials on cancers (Kiany et al., 2020). Furthermore, entinostat has a potential protective effect in ischemic injury, including LPS-induced acute kidney injury by inhibiting ROS oxidative and endoplasmic reticulum stress (Zhang S. et al., 2018) and brain ischemia–induced neuronal death by mitochondrial preservation (Murphy et al., 2014) and NF-κB/RelA-mediated Bcl-xL and Bim levels (Lanzillotta et al., 2013). However, the powerful neuroprotective activity of entinostat in SCI has not been fully understood. Here, we investigated the potential neuroprotective effects of entinostat (15 mg/kg and 45 mg/kg) on improving cognitive impairment and reducing acute spinal damage in an SCI mice model and revealed its potential mechanism in an *in vitro* oxygen-glucose deprivation (OGD)–induced cell model, which may provide a preclinical experimental basis for further elaborating its potential role in the body and SCI clinical therapy.

## MATERIALS AND METHODS

### The Spinal Cord Injury Model and Entinostat Treatment *in vivo*

Male C57BL/6 mice (25 ± 2 g, 8 weeks) were subjected to SCI. All animal studies were conducted according to the Animal Welfare Guidelines of the United States National Institutes of Health with supervision and ratification from the Animal Care and Use Committee of the General Hospital of the Chinese People's Liberation Army under standard conditions, including adequate temperature and humidity (60%) and a 12 h light/12 h dark cycle. The mice had free access to water and food.

The SCI model was established as previously described (Jiao et al., 2020). The mice were anesthetized using 4% isoflurane with a rate of 1 L/min, exposed to the T6–T7 spinous process, and underwent laminectomy. Then, epidural compression of the spinal cord with a 24-g closure force was applied for 1 min at the T6–T7 level, resulting in SCI, while the mice that underwent laminectomy were regarded as the sham group. We assessed SCI levels at baseline and postoperative days 1, 2, 3, 7, 14, 21, and 28.

As previously reported (Bombardo et al., 2018; Mota et al., 2020), we dissolved entinostat (Selleck, Shanghai, China) in 0.1 M phosphate-buffered saline (PBS, as the vehicle) (pH 7.4), and it was administered to the animals (1, 5, or 10 mg/kg, gavage) at 4 h after SCI and again 24 and 48 h later. The sham group was treated with equal PBS volumes.

## The Forelimb Grip Strength Detection

The forelimb grip strength was assessed by using a Chatillon digital force meter (LTCM-100, Wintop Co., Shanghai, China). The mice tails were lifted and placed near the bars of a grip-measuring machine so they could grasp the bar. The mice were then gently pulled back horizontally away from the crossbar with a device that measured the grip strength in both front paws. While evaluating the grip of the other front paw, one front paw was taped. If the mouse cannot catch the crossbar, a score of 0 was obtained.

## Basso Mouse Scale

The BMS assessed the hind limb movements during locomotion in an open field, with a 0-to 9-point scale (a high score means better hind limb function). This measurement was conducted independently by two blinded experimenters over 5 min at pre-SCI conditions and 1, 2, 3, 7, 14, 21, and 28 days after SCI ($n = 8$ mice/group).

## Histological Evaluation

The tissues were immersed in 4% paraformaldehyde, dehydrated, and embedded in paraffin. The tissue sections were stained with hematoxylin and eosin (H&E). Microscopic observation of the histologic slides was performed using a light microscope.

## Terminal Deoxynucleotidyl Transferase dUTP Nick-End Labeling Staining

The tissues were obtained, fixed with 4% paraformaldehyde solution, dehydrated, and embedded in paraffin. 4-μm paraffin coronal sections (having proximity to and located in the injury site) were stained by using a DeadEnd™ Fluorometric terminal deoxynucleotidyl transferase–mediated dUTP nick-end labeling (TUNEL) System (Solarbio, Beijing, China, and then incubated with secondary antibodies. The cell nuclei were stained with DAPI (Solarbio). Images were obtained under the fluorescence microscope (Olympus, Osaka, Japan).

## Immunofluorescence Assays

The samples were obtained and fixed with 4% paraformaldehyde, blocked with 5% BSA, and then incubated with primary antibodies, namely, NLRP3 (Thermo Fisher Scientific, Waltham, MA, United States; 1:100) and caspase-1 (Proteintech, 1:100) and then incubated with secondary antibodies. The cell nuclei were stained with 4′,6-diamidino-2-phenylindole (DAPI, Sigma-Aldrich), 6 random high-power fields (200 ×) were chosen, and images were obtained using a fluorescence microscope (Leica, Oskar-Barnack, Germany).

## Primary Neuron Culture and Injury Model *in vitro*

Spinal neurons were obtained from E16 mouse embryos with a modified protocol from Jiao et al. (2020). Briefly, the neonatal pups of C57BL/6 mice were anesthetized by isoflurane, decapitated, and vertebral columns were removed. The spinal cord was isolated and cut into 1-$mm^3$ pieces after gently peeling off the meninges. The tissue pieces were digested by 0.25% trypsin for 10 min at 37°C, and then the cells were resuspended in a serum-free medium, including Neurobasal, B27, and penicillin/streptomycin (50 U/mL). 2.5 × $10^5$ cells were seeded in a 24-well plate at 37°C with 5% $CO_2$, and supplemented with 10 μM AraC (Sigma-Aldrich, St Louis, MO, United States) after 48 h. On the next day, the medium was replaced with Neurobasal containing supplements, excluding AraC, and changed every three days. The cells were cultured for 10 days and then OGD treatment was performed on them. Briefly, the spinal cord neurons were incubated in DMEM and cultured in an incubator containing 95% $N_2$/5% $CO_2$ for 4 h. Then, the DMEM was replaced with a standard neuronal culture medium for 24 h. The cells cultured in a standard neuronal culture medium in the presence of ambient 5% $CO_2$ served as the control. After OGD treatment, the neurons were either immediately treated with entinostat or not. The vehicle group received an equal volume of PBS.

## Cell Viability Detection

Cell damage was measured using the CellTiter 96® Aqueous One Solution Cell Proliferation Assay (Promega, Madison, WI, United States). The cells were plated in 96-well plates in triplicate at approximately 3 × $10^4$ cells per well and cultured in the growth medium. After treatment, MTS was added to the culture medium and incubated for 2 h at 37°C in 95% humidified air and 5% $CO_2$. The absorbance was measured at 490 nm using a microplate reader (Thermo Fisher Scientific).

## Propidium Iodide Staining

After being fixed in 4% paraformaldehyde for 5 min, the treated cells were washed thrice with PBS and then stained with 500 nM of propidium iodide (PI; Sigma-Aldrich) for 5 min. DAPI (Sigma-Aldrich) was used to stain nuclei, and images were obtained with a fluorescence microscope.

## ELISA Analysis

The spinal tissues and the cell culture medium supernatant were collected. A bicinchoninic acid (BCA) assay kit (Invitrogen, Carlsbad, CA, United States) was used to measure the protein concentration. ELISA analysis was performed using the TNF-α,

| | | |
|---|---|---|
| HDAC1 | Forward | 5′-TGATGCTGGGAGGAGGTG-3′ |
| | Reverse | 5′-GTTGGAAGGGCTGATGTG-3′ |
| HDAC2 | Forward | 5′-TGACAAACCAGAACACTCCAGAATA-3′ |
| | Reverse | 5′-GAATAGCTTGCATTTGAACACCAG-3′ |
| HDAC3 | Forward | 5′-AGCCTTAATGCCTTCAACGTGG-3′ |
| | Reverse | 5′-TCATTGACATAGCAGAAGCCAGAGG-3′ |
| HDAC4 | Forward | 5′-GCGAGCACAGAGGTGAAGATGAAG-3′ |
| | Reverse | 5′-AGACGGGGTGGTTGTAGGAGG-3′ |
| HDAC6 | Forward | 5′-TGGTGTTATGTCTGTCAGGCTTA-3′ |
| | Reverse | 5′-GCAGTGTGGTCTGGGATTTAGT-3′ |
| HDAC8 | Forward | 5′-TGTGACTCCCTGGCCAAGATCCC-3′ |
| | Reverse | 5′-TCATCGCCCTCTTGGCTGACCTT-3′ |
| HDAC11 | Forward | 5′-GTTTACAACCGCCACATCTACCC-3′ |
| | Reverse | 5′-TCCACCTTCTCCAGATATTCCTCAT-3′ |
| GAPDH | Forward | 5′- AACTTTGGCATTGTGGAAGG -3′ |
| | Reverse | 5′- GGATGCAGGGATGATGTTCT -3′ |

IL-1β, and IL-18 ELISA kit (Beyotime Biotechnology, Shanghai, China) following the manufacturer's instructions.

## Caspase-1 Activity Detection

Caspase-1 activity was detected using the Caspase-1 Activity Assay Kit (Solarbio). The specific steps were performed according to the manufacturer's instructions (Solarbio). The protein concentration was ensured from 1 μg/μl to 3 μg/μl. A standard curve was prepared using the pNA standard. Then, the optical density of the specimen was read on a microplate reader (Thermo Fisher Scientific) at 405 nm. The percentage of changes in caspase-1 activity was calculated by the ratio of $OD_{405}$ of the experimental well to that of the normal well.

## Histone Deacetylase Activity Analysis

HDAC enzyme activity was conducted by the EpiQuik HDAC Activity/Inhibition Assay Kit (Colorimetric) (Epigentek, Farmingdale, NY, United States). Briefly, nuclear cell lysates were extracted using the Nuclear Protein Extraction Kit (Solarbio), 50 μg of the lysates was incubated with the HDAC colorimetric substrate, and the color was immediately quantified through an ELISA reaction. HDAC activity was inversely proportional to the amount of the remaining acetylated histone substrates. HDAC activity or inhibition was calculated using the following formula: HDAC activity (OD/min/mg) = ((Sample OD−Blank OD)/ (Protein Amount (50 μg) ×60 min)) × 1,000.

## Western Blot Analysis

Spinal cord tissue and primary neurons were lysed by lysis buffer (Beyotime, Shanghai, China). After protein quantification, electrophoresis (12% SDS-PAGE gels), and Western transfer, the membranes were blocked with 5% BSA and incubated with the appropriate primary antibodies, such as HDAC1 (CST, 1:1,000), HDAC2 (Abcam, 1:800), HDAC3 (Abcam, 1:1,000), NLRP3 (Thermo Fisher Scientific, 1:1,000), caspase-1 (Proteintech, 1:800), and caspase-1 p20 (CST, 1:1,000) at 4°C overnight and then incubated

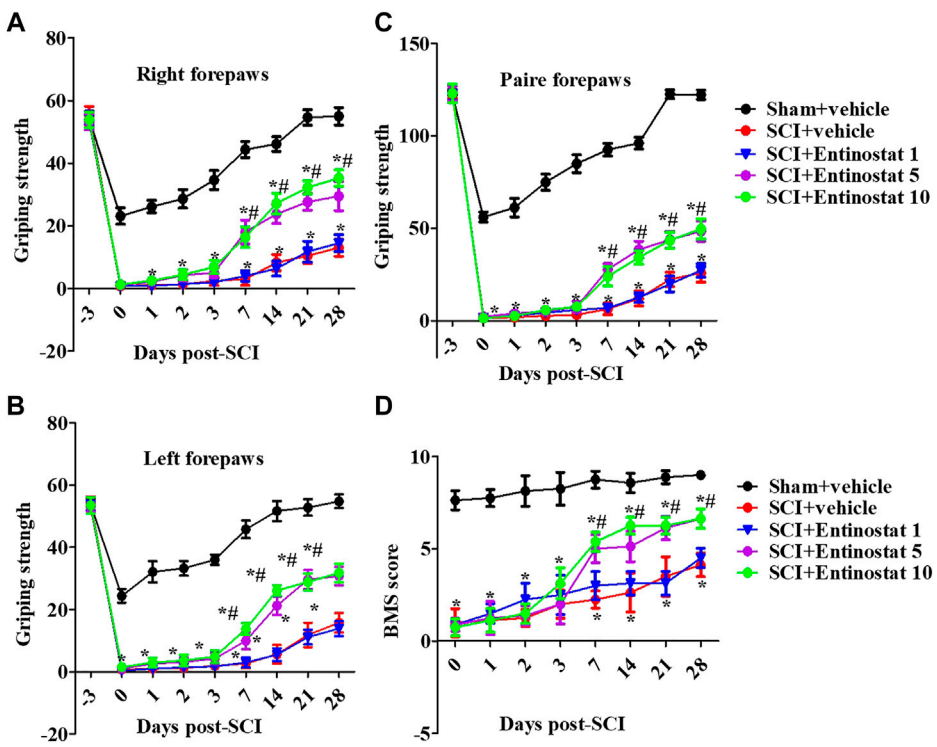


**FIGURE 1 |** Entinostat improves the motor function following SCI. Behavioral tests of SCI mice with entinostat (1, 5, or 10 mg/kg) or not and the grip strength of the right forepaw **(A)**, left forepaw **(B)**, and paired forepaws **(C)** was measured before the experiment and after surgery. **(D)** Measurement of the BMS score after SCI. Data are expressed as the mean ± SEM, $n = 8$. *$p < 0.05$, *vs.* the sham + vehicle group; #$p < 0.05$, *vs.* the SCI + vehicle group. BMS: basso mouse scale. SEM: standard error of the mean.

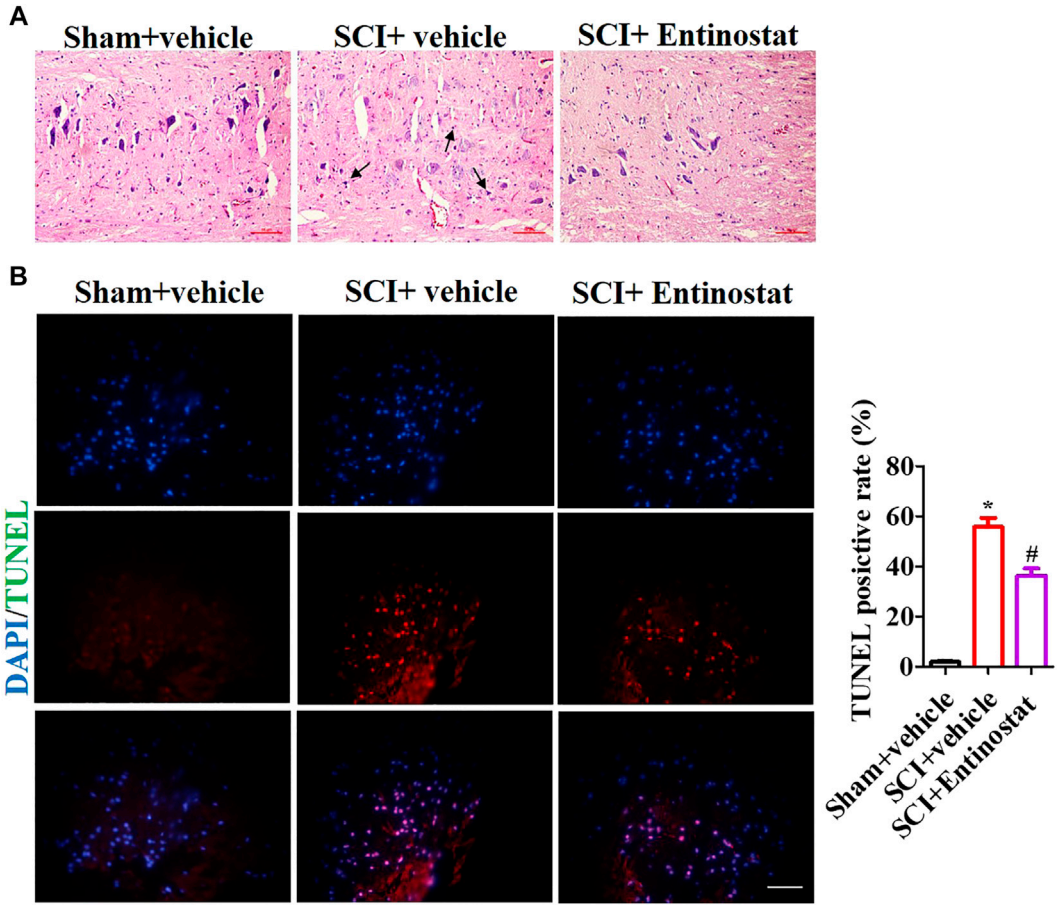


**FIGURE 2 |** Entinostat attenuates histopathologic damage following SCI. The histopathologic damage was assessed 7 days following SCI by H&E staining. **(A)** Black arrows indicating the neutrophil infiltration and TUNEL staining. **(B)** Nuclei were stained with DAPI. Histogram analysis of the TUNEL-positive cell. Data are expressed as the mean ± SEM, $n = 6$. Scale bar: 25 μm *$p < 0.05$, *vs.* the sham + vehicle group; #$p < 0.05$, *vs.* the SCI + vehicle group.

with secondary antibodies (Abgent, 1: 20,000) followed by the hypersensitivity chemiluminescent substrate (Bio-Rad, Hercules, CA, United States), and protein bands were photographed by using a ChemiDoc™ MP imaging system (Bio-Rad).

## QPCR Analysis

Total RNA was lysed by using the TRIzol reagent (Invitrogen) and reversely transcripted to cDNA using a HiFi-MMLV cDNA First-Strand Synthesis Kit (CW-Bio, Beijing, China). QRT-PCR analysis was executed using GoTaq qPCR Master Mix (Tiangen, Beijing, China) by the CFX96TM Real-Time System (Bio-Rad, Hercules, CA, United States). QPCR was performed on samples and standards in triplicate, and fold changes were calculated by applying the relative quantification ($2^{-\Delta\Delta Ct}$) method. GAPDH was used as an internal control, and primer sequences are listed as follows.

## Statistical Analysis

Data were expressed as the mean ± SEM. SPSS 22.0 was used for Student's *t*-test or one-way ANOVA followed by Tukey's multiple comparisons test (two-way ANOVA analysis for grip strength assessment). $P < 0.05$ was considered statistically significant.

# RESULTS

## Entinostat Improves the Motor Function Following Spinal Cord Injury

After the onset of SCI within 4 weeks, the motor function of mice was assessed by the forelimb grip strength test and BMS score. Before the experiment, all the mice showed consistent behavioral evaluations. SCI directly impaired motor function with decreased grip strength both of left, right, and paired forepaws (**Figures 1A–C**), and the grip strength had a slow recovery process during the 1 week following SCI. Entinostat improved the motor function in a concentration-dependent manner, at 7–28 days after SCI (but not during the 7 days following SCI) (**Figures 1A–C**), where 5 mg/kg and 10 mg/kg of entinostat showed significant protection of motor dysfunction (not the 1 mg/kg group) ($p < 0.05$, **Figures 1A–C**), but there was still a gap compared with the characteristics in the sham group (**Figures**

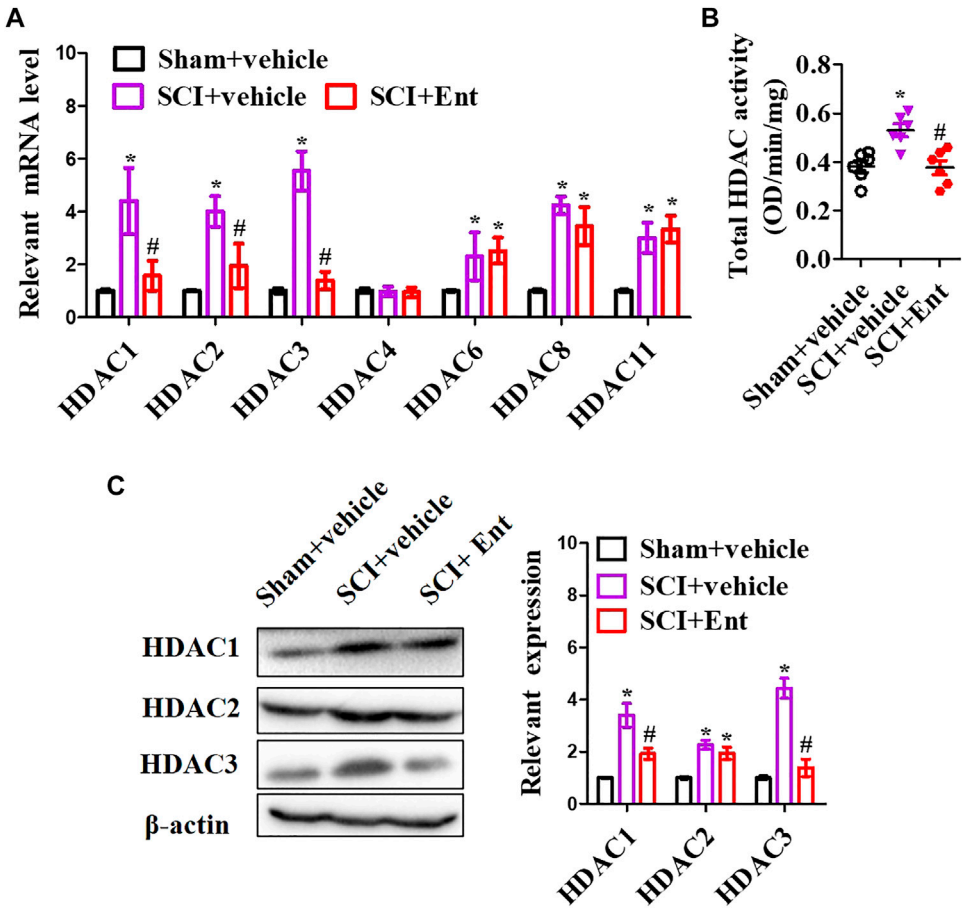


**FIGURE 3 |** Entinostat suppresses HDAC1 and HDAC3 expressions in the spinal cord after SCI. **(A)** 7 days following SCI, HDAC1, HDAC2, HDAC3, HDAC4, HDAC6, HDAC8, and HDAC11 mRNA concentrations were measured. **(B)** Enzymatic activity of total HDAC was evaluated using the EpiQuik HDAC Activity/Inhibition Assay Kit. **(C)** WB analysis of HDAC1, HDAC2, and HDAC3 expressions in the spinal cord following SCI at 7 days. Data are expressed as the mean ± SEM, $n = 5$. *$p <$ 0.05, *vs.* the sham + vehicle group; #$p < 0.05$, *vs.* the SCI + vehicle group.

**1A–C**). At 7–28 days after SCI, the BMS score was significantly improved in the entinostat 5 mg/kg and 10 mg/kg groups than the sham group ($p < 0.05$, **Figure 1D**). But, the entinostat 1 mg/kg group at 28 days post-SCI showed a statistically significant BMS score alteration compared with that of the sham group ($p < 0.05$, **Figure 1D**). The data showed that high concentrations of entinostat (5 mg/kg and 10 mg/kg) treatment presented the protection of motor function following SCI.

## Entinostat Attenuates Histopathologic Damage Following Spinal Cord Injury

To explore the protection of entinostat on histopathologic damage, H&E and TUNEL staining were performed to assess the pathologic alteration after treating with 5 mg/kg entinostat. The H&E staining results showed that the structure of the spinal cord was clear, the nucleus was complete and inerratic, and there was hypochromatic nucleus, neutrophil infiltration (as the black arrow indicating), neuronal disruption, and diffuse hemorrhage (**Figure 2A**). However, entinostat relieved histopathologic damage after SCI (**Figure 2A**). By TUNEL staining, the results found more TUNEL-positive cells (about 64.3%) in the SCI group compared with the sham group, and entinostat treatment significantly suppressed cell death (about 27.5% TUNEL positive cell) (**Figure 2B**). These results indicated that entinostat attenuates histopathologic damage and showed protection post-SCI.

## Entinostat Inhibits NLRP3 Inflammasome Activation After Spinal Cord Injury

After SCI at 7 days, HDACs were measured. As shown in **Figure 3A**, SCI increased class I HDAC levels, including HDAC1, HDAC2, HDAC3, HDAC6, HDAC8, and HDAC11 mRNA, while entinostat significantly suppressed SCI-induced class I HDAC levels ($p < 0.05$, **Figure 3A**). Total HDAC activation was also upregulated after SCI and decreased after entinostat treatment ($p < 0.05$, **Figure 3B**). WB results showed that the expressions of HDAC1, HDAC2, and HDAC3 were induced by SCI in the spinal cord and entinostat inhibited the

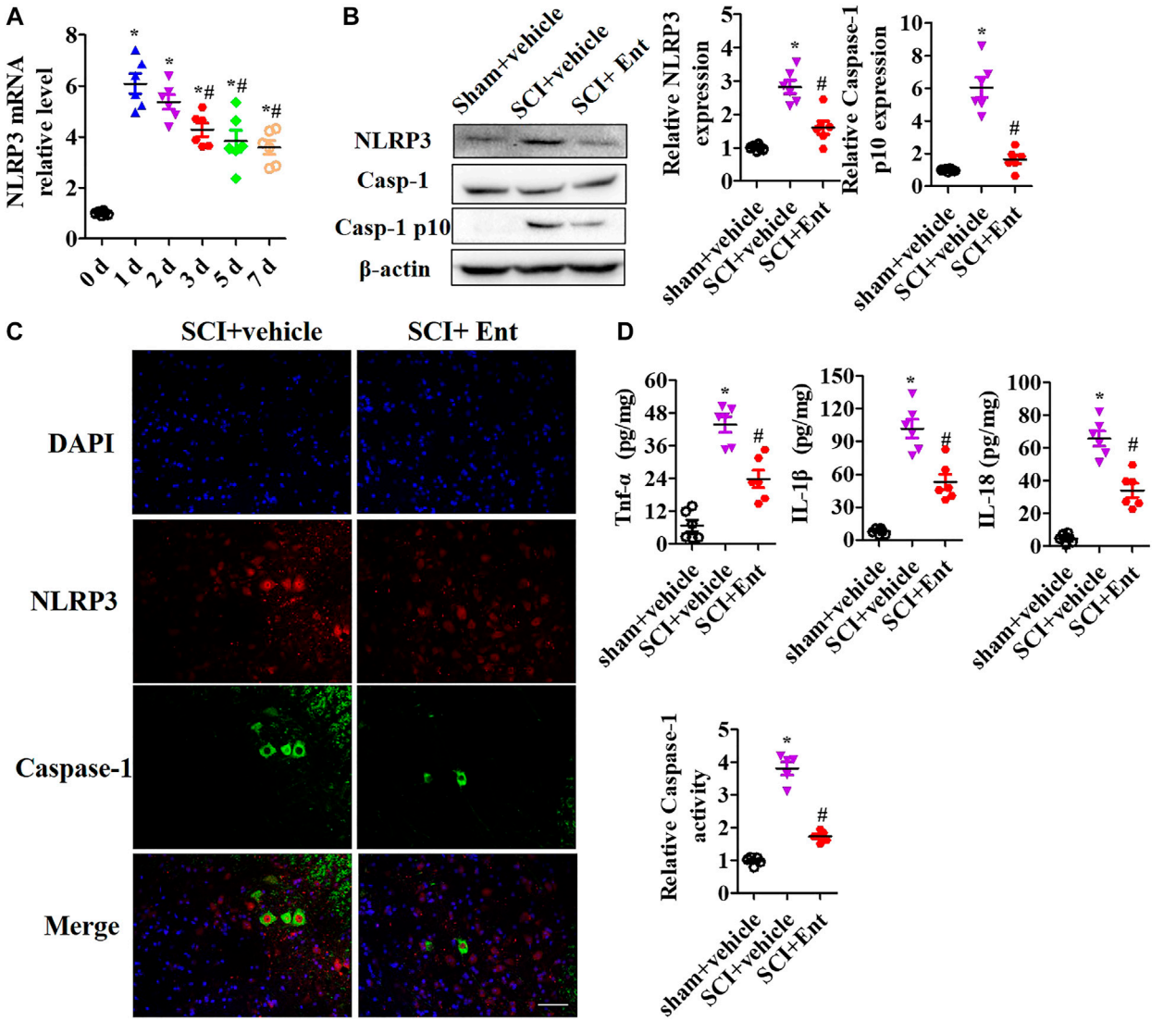


**FIGURE 4 |** Entinostat inhibits NLRP3 inflammasome activation in the spinal cord after SCI. NLRP3 inflammasome activation was measured in the spinal cord after SCI. **(A)** qPCR analysis of NLRP3 mRNA during 7 days post-SCI. **(B)** WB analysis of NLRP3, Caspase-1 expression in spinal cord after SCI at 7 days. Histogram analysis of the protein relative expression, *vs.* β-actin. **(C)** NLRP3/caspase-1 double staining was performed, and the nuclei were stained with DAPI. Scale bar: 50 μm. **(D)** ELISA analysis of the levels of TNF-α, IL-1β, and IL-18 in the spinal cord. **(E)** Caspase-1 activity was detected using Caspase-1 Activity Assay Kit after SCI. Data are expressed as the mean ± SEM, $n = 5$. *$p < 0.05$, *vs.* the sham + vehicle group; #$p < 0.05$, *vs.* the SCI + vehicle group.

expressions of HDAC1 and HDAC3, but the variation in HDAC2 expression was weak following treatment with entinostat (**Figure 3C**). The data showed that class I HDAC involved in the pathologic processes of SCI and entinostat suppressed HDAC1 and HDAC3 expression in the spinal cord. Furthermore, we analyzed NLRP3 inflammasome activation after SCI. As shown in **Figure 4A**, NLRP3 mRNA was increased with time dependence, which peaked at 24 h following SCI, then decreased gradually from 2 to 7 days, but was significantly upregulated at 7 days ($p < 0.05$, **Figure 4A**). Then, NLRP3 expression was measured at 7 days post-TBI in the spinal cord of entinostat-treated mice. Undoubtedly, SCI not only induced NLRP3 expression and caspase-1 p 10 fragment but also was significantly suppressed by entinostat compared with the SCI group ($p < 0.05$, **Figure 4B**). IF results demonstrated that entinostat inhibited NLRP3/caspase-1 staining (**Figure 4C**). Furthermore, NLPR3 inflammasome–mediated inflammation was also measured in the spinal cord. ELISA results showed that SCI increased the level of inflammatory factors, such as TNF-α, IL-1β, and IL-18 at 7 days post-SCI, whereas entinostat significantly decreased the levels of TNF-α ($p < 0.05$), IL-1β ($p < 0.01$), and IL-18 ($p < 0.01$) (**Figure 4D**). Caspase-1 activity assay also demonstrated that entinostat reversed the increase of caspase-1 activity after SCI ($p < 0.01$, **Figure 4E**). Thus, the results demonstrated that entinostat alleviated NLPR3 inflammasome activation in the spinal cord following SCI.

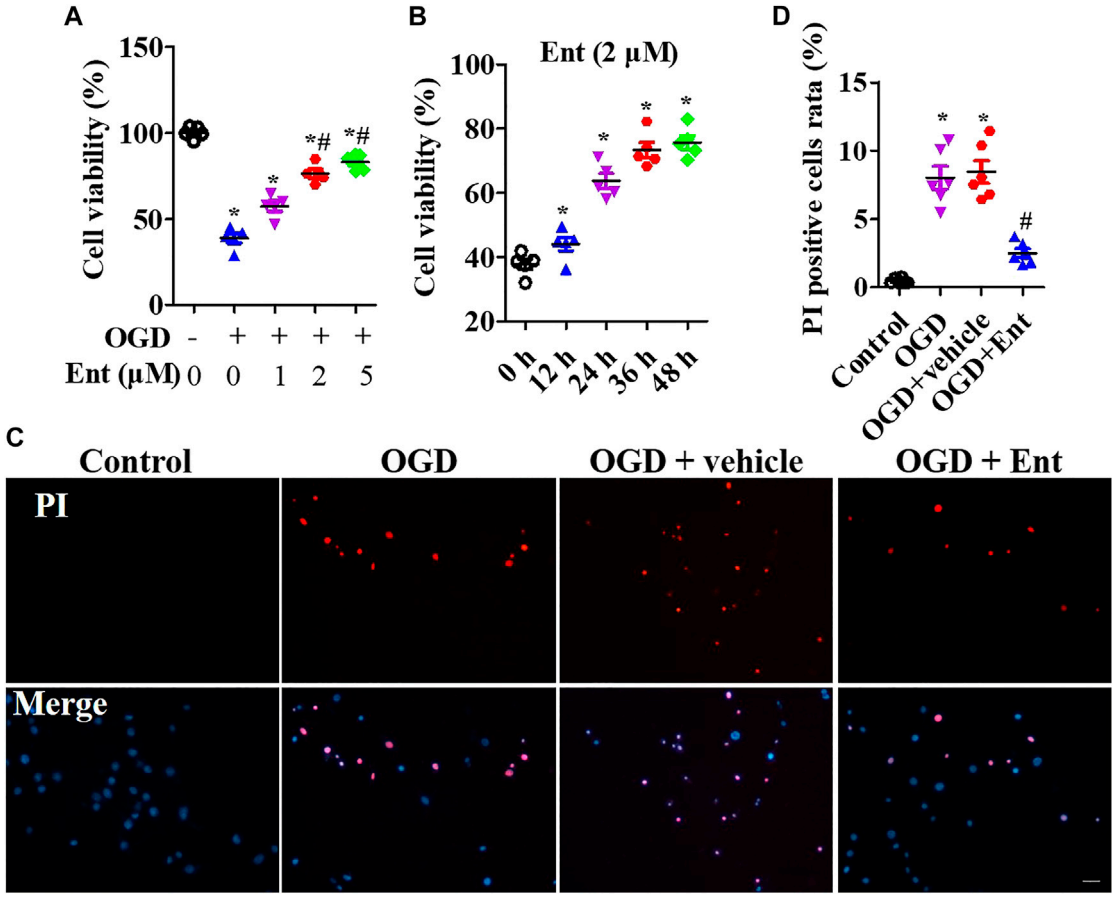


**FIGURE 5 |** Entinostat suppresses OGD-induced neuronal injury. In the OGD-induced neuronal damage model, cell viability was measured after being treated with 0, 1, 2, or 5 μM entinostat for 24 h **(A)** or treated with 2 μM entinostat for 12, 24, 36, or 48 h **(B)**. **(C)** PI staining of primal neurons at 24 h after being treated with 2 μM entinostat, and DAPI stained all cell nuclei. **(D)** Histogram analysis of PI-positive cells. Scale bars: 50 μm. Data are expressed as the mean ± SEM, $n = 4$. $^{*}p < 0.05$, *vs.* the control group; $\#p < 0.05$, *vs.* the OGD group.

## Entinostat Ameliorates NLPR3 Inflammasome Activation and Neuronal Damage

MTS was used to detect the cell viability of primal neurons. At the beginning of OGD, spinal cord neurons were immediately treated with entinostat (1, 2, and 5 μM) for 24 h or not. As shown in **Figure 5A**, OGD downregulated cell viability, and high concentration of entinostat (2 and 5 μM) could inhibit the decrease of cell activity, but the effect of 1 μM entinostat was weak (**Figure 5A**). Then, 2 μM entinostat was treated for 12, 24, 36, and 48 h. The longer the treatment time of entinostat, the better the cell activity of neurons (**Figure 5B**). So, the treated condition of entinostat was selected as 2 μM for 24 h. As shown in **Figures 5C,D**, PI staining showed that OGD induced the increase of PI-positive cells, and 2 μM entinostat significantly decreased the PI-positive cells. After entinostat treatment in OGD-induced primal neurons, total HDAC activation and caspase-1 activation were analyzed at 24 h. OGD significantly enhanced the total HDAC ($p < 0.05$, **Figure 6A**) and caspase-1 ($p < 0.05$, **Figure 6B**) activation, and entinostat reduced the total HDAC and caspase-1 activation ($p < 0.05$, **Figures 6A,B**). ELISA results showed that OGD increased the level of inflammatory factors, IL-1β and IL-18, whereas entinostat significantly decreased the levels of IL-1β and IL-18 ($p < 0.05$, **Figure 6C**). WB results further found that entinostat significantly decreased HDAC3 expression and NLRP3 inflammasome activation (including NLRP3 expression and caspase-1 p 10 level), related to the OGD group ($p < 0.05$, **Figure 6D**). Furthermore, IF results showed that OGD induced NLRP3 expression and entinostat suppressed NLRP3 expression in the OGD model (**Figure 6E**). The results demonstrated that entinostat alleviated NLPR3 inflammasome activation and neuronal damage in the OGD model.

## DISCUSSION

Entinostat is a narrow-spectrum HDAC inhibitor of class I HDAC that has been shown to possess neuroprotective functions in brain ischemia and intracerebral hemorrhage (Mota et al., 2020; Bonsack and Sukumari-Ramesh, 2021).

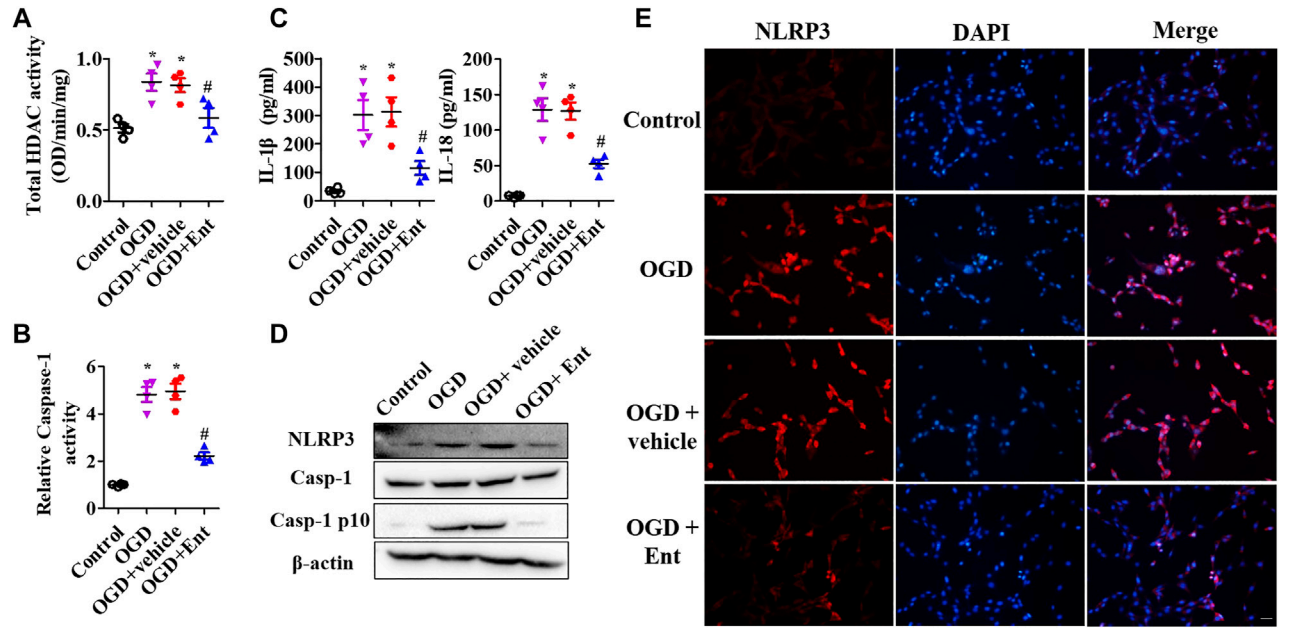


**FIGURE 6 |** Entinostat ameliorates OGD-induced NLPR3 inflammasome activation. In the OGD-induced neuronal damage model, enzymatic activity of total HDAC was evaluated using the EpiQuik HDAC Activity/Inhibition Assay Kit **(A),** and caspase-1 activity was detected using Caspase-1 Activity Assay Kit **(B)**. **(C)** ELISA analysis of the levels of IL-1β and IL-18 in primal neurons. **(D)** WB analysis of NLRP3, caspase-1, and caspase-1 p 10 levels. **(E)** IF analysis of NLRP3 expression in the OGD model, Scale bar: 50 μm. Data are expressed as the mean ± SEM, $n = 4$. *$p < 0.05$, *vs.* the control group; #$p < 0.05$, *vs.* the OGD group.

However, its role in SCI has not been reported. In this study, we showed that entinostat improved the motor function (including the grip strength and BMS score), histopathologic damage (spinal edema and cell death), and local NLRP3 inflammasome activation in the spinal cord following SCI. Furthermore, entinostat significantly increased OGD-inhibited neuronal activity and decreased PI-positive cell concentration, HDAC activation, caspase-1 activation, IL-1β and IL-18 levels, and NLRP3 expression.

A large number of studies have confirmed that HDACs are involved in the physiologic processes that occur following SCI (Zhang H. et al., 2018; Chen et al., 2018; Hendrix et al., 2020; Zhou et al., 2020). Recent studies have shown that HDACs tend to increase in PBMC nuclear extracts of SCI patients, including increased HDAC3 in PBMCs from SCI patients (Ma et al., 2015). In the animal SCI model, the HDAC expression is not consistent. Chen et al. documented that HDAC 1–3 is upregulated in the lesioned spinal cord of male Wistar rats 7 days after SCI, when compared to the sham group (Chen et al., 2018). The treatment with VPA inhibits HDAC3 protein expression and induced STAT1, as well as NF-κB p65 acetylation following SCI, without affecting the HDAC1 and the HDAC2 protein expressions, which attenuates the microglia-mediated central inflammatory response after SCI (Chen et al., 2018). Zhou et al. also verified that upregulated HDAC3 is presented in the spinal cord tissues of experimental SCI SD rats and HDAC3 knockdown restores the locomotor function via HDAC3/miR-27a/PAK6 axis (Zhou et al., 2020). Interestingly, Zhang et al. have shown that among class I HDACs, HDAC1 and HDAC3 expressions are significantly downregulated in the motor cortex of C57BL/6 J mice but not significantly altered in the lesion site of the spinal cord 14 days after SCI. No expression changes in HDAC1 and HDAC3 were measured in the spinal cord of CI-994-treated mice (Zhang S. et al., 2018). The administration of CI-994 inhibits class I HDAC activities in both the cortex and spinal cord, and CI-994 enhances functional recovery following SCI but does not enhance cervical sprouting of the corticospinal tract following SCI (Zhang H. et al., 2018). Although Zhang et al. showed that the variation trend of HDACs in the spinal cord of the SCI model is inconsistent with previous reports, they also revealed that the inhibition of both HDAC1 and HDAC 3 of CI-994 may exert a neuroprotective effect (Zhang S. et al., 2018). In our study, we found that HDAC1, HDAC2, and HDAC3 expressions were enhanced in the spinal cord after SCI and entinostat decreased HDAC1 and HDAC3 expressions but without affecting the HDAC2 expression. Entinostat, another class I HDAC inhibitor, has potential neuroprotective effects in brain damage (Zhang H. et al., 2018; Hendrix et al., 2020; Bonsack and Sukumari-Ramesh, 2021). Entinostat reduces NF-κB-p65 expression and nuclear accumulation as well as the neuroinflammatory response (TNF-α and IL-1β levels) in the hippocampus, which causes the improvement of postoperative cognitive dysfunction in rats (Wu et al., 2019). Local infusion of entinostat into the medial prefrontal cortex exerts robust antidepressant-like effects in the chronic social defeat stress paradigm in mice (Covington et al., 2015). Ma et al. documented that entinostat treatment contributes to the

recovery of actin-based NMDAR synaptic delivery and the rescue of autistic social preference deficits in Shank 3–deficient mice (Ma et al., 2018). Finelli et al. reported that entinostat treatment enhances the expression of genes associated with axon regeneration in sensory neurons and promotes axonal growth after SCI (Finelli et al., 2013). Furthermore, our experiment results first suggested the potential role of entinostat in the spinal cord that entinostat improved histopathologic damage and motor function of male C57BL/6 mice following SCI and showed the neuroprotective role of OGD-induced neuronal damage.

Current investigations have demonstrated that NLRP3 inflammasome–mediated cell death plays a critical role in the pathogenesis of multiple neurologic disorders (Heneka et al., 2018; Voet et al., 2019; Chen et al., 2021), as well as SCI (Jiang et al., 2017; Al Mamun et al., 2020). NLRP3 inhibitors play a neuroprotective role in SCI (Jiao et al., 2020), as well as the NLRP3 inflammasome upstream regulatory molecules, such as ROS, NF-Kb, NEK7, and ASC (Gao et al., 2019; Shiraishi et al., 2020; Ji et al., 2021). In SCI mouse models, NEK7 suppression attenuates local inflammatory response and inhibits NLRP3 inflammasome activation in microglia/macrophages of the injured spinal cord, and targeting the NEK7/NLRP3 signaling shows great promise in the treatment of inflammatory responses after SCI (Ji et al., 2021). In addition, several potential drugs also present a neuroprotective role by regulating NLRP3 activation (Gao et al., 2019; Kong et al., 2021). The administration of echinacoside enhances the BBB scores, decreases neuron loss, and improves tissue architecture via inhibiting the NLRP3 inflammasome signaling pathway after SCI (Gao et al., 2019). β-hydroxybutyrate inhibits an LPS + ATP-induced inflammatory response and NLRP3 levels, and a ketogenic diet attenuates neuroinflammation following SCI, probably by suppressing the NLRP3 inflammasome and shifting the activation state of microglia from M1 to the M2a phenotype (Kong et al., 2021). At the same time, we also demonstrated that entinsotat inhibited the local inflammatory response and NLRP3 inflammasome activation after SCI, which might explain its contribution to the improvement of motor function. Previously, correlations between HDAC and NLRP3 have been rarely reported. Ky-2, a hybrid compound HDACi, downregulates LPS-induced NLRP3, caspase-1 p 20, and IL-1β in THP-1 cells that may regulate M1 macrophage polarization via inhibiting NLRP3 inflammasome activation (Kaneko et al., 2018). In J774A.1 cells, hydroxamic acid derivatives of nigranoic acid and manwuweizic acid moderately enhance HDAC1/2/4/6 inhibition activity, which inhibits IL-1β maturation and caspase-1 cleavage, and Ni et al. suggest that the synthesis of HDACi may block NLRP3 inflammasome activation (Ni et al., 2021).

## CONCLUSION

In conclusion, we first documented that entinostat improved motor function, histopathologic damage, local inflammatory response, and NLRP3 inflammasome activation in the spinal cord following SCI and also presented the neuroprotection of OGD-induced neuronal damage via the NLRP3 inflammasome. Thus, our study has the potential to reveal the interaction between the HDAC and NLRP3 inflammasome in the pathologic process as well as SCI and further promote the clinical indications of HDACi entinostat and clinical treatment for inflammatory response after SCI.

## DATA AVAILABILITY STATEMENT

The original contributions presented in the study are included in the article/Supplementary Material; further inquiries can be directed to the corresponding authors.

## ETHICS STATEMENT

The animal study was reviewed and approved by General Hospital of the Chinese People's Liberation Army.

## AUTHOR CONTRIBUTIONS

CD and DL contributed to conceptualization. BL and BP contributed to experiment performance, data collection, and verification. CD, JZL, and BQ contributed to data analysis. CD contributed to writing the original draft. BP and DL contributed to writing, reviewing, and editing.

## FUNDING

This study was supported by a grant from the National Key R&D Program of China (NO.2019YFC1511201).

## REFERENCES

Al Mamun, A., Wu, Y., Monalisa, I., Jia, C., Zhou, K., Munir, F., et al. (2021). Role of Pyroptosis in Spinal Cord Injury and its Therapeutic Implications. *J. Adv. Res.* 28, 97–109. doi:10.1016/j.jare.2020.08.004

Bloom, O., Herman, P. E., and Spungen, A. M. (2020). Systemic Inflammation in Traumatic Spinal Cord Injury. *Exp. Neurol.* 325, 113143. doi:10.1016/j.expneurol.2019.113143

Bombardo, M., Chen, R., Malagola, E., Saponara, E., Hills, A. P., Graf, R., et al. (2018). Inhibition of Class I Histone Deacetylases Abrogates Tumor Growth Factor β Expression and Development of Fibrosis during Chronic Pancreatitis. *Mol. Pharmacol.* 94 (2), 793–801. doi:10.1124/mol.117.110924

Bonsack, F., and Sukumari-Ramesh, S. (2021). Entinostat Improves Acute Neurological Outcomes and Attenuates Hematoma Volume after Intracerebral Hemorrhage. *Brain Res.* 1752, 147222. doi:10.1016/j.brainres.2020.147222

Cantley, M. D., and Haynes, D. R. (2013). Epigenetic Regulation of Inflammation: Progressing from Broad Acting Histone Deacetylase (HDAC) Inhibitors to Targeting Specific HDACs. *Inflammopharmacology* 21 (4), 301–307. doi:10.1007/s10787-012-0166-0

Chen, G., Zhou, Z., Sha, W., Wang, L., Yan, F., Yang, X., et al. (20202020). A Novel CX3CR1 Inhibitor AZD8797 Facilitates Early Recovery of Rat Acute Spinal

Cord Injury by Inhibiting Inflammation and Apoptosis. *Int. J. Mol. Med.* 45 (5), 1373–1384. doi:10.3892/ijmm.2020.4509

Chen, S., Ye, J., Chen, X., Shi, J., Wu, W., Lin, W., et al. (2018). Valproic Acid Attenuates Traumatic Spinal Cord Injury-Induced Inflammation via STAT1 and NF-Kb Pathway Dependent of HDAC3. *J. Neuroinflammation* 15 (1), 150. doi:10.1186/s12974-018-1193-6

Chen, Y., Li, Y., Guo, L., Hong, J., Zhao, W., Hu, X., et al. (2020). Bibliometric Analysis of the Inflammasome and Pyroptosis in Brain. *Front. Pharmacol.* 11, 626502. doi:10.3389/fphar.2020.626502

Covington, H. E., Maze, I., Vialou, V., and Nestler, E. J. (2015). Antidepressant Action of HDAC Inhibition in the Prefrontal Cortex. *Neuroscience* 298, 329–335. doi:10.1016/j.neuroscience.2015.04.030

Fehlings, M. G., Tetreault, L. A., Wilson, J. R., Kwon, B. K., Burns, A. S., Martin, A. R., et al. (2017). A Clinical Practice Guideline for the Management of Acute Spinal Cord Injury: Introduction, Rationale, and Scope. *Glob. Spine J* 7 (3 Suppl. l), 84S–94S. doi:10.1177/2192568217703387

Finelli, M. J., Wong, J. K., and Zou, H. (2013). Epigenetic Regulation of Sensory Axon Regeneration after Spinal Cord Injury. *J. Neurosci.* 33 (50), 19664–19676. doi:10.1523/JNEUROSCI.0589-13.2013

Fouad, K., Popovich, P. G., Kopp, M. A., and Schwab, J. M. (2021). The Neuroanatomical-Functional Paradox in Spinal Cord Injury. *Nat. Rev. Neurol.* 17 (1), 53–62. doi:10.1038/s41582-020-00436-x

Gao, S., Xu, T., Guo, H., Deng, Q., Xun, C., Liang, W., et al. (20192019). Ameliorative Effects of Echinacoside against Spinal Cord Injury via Inhibiting NLRP3 Inflammasome Signaling Pathway. *Life Sci.* 237, 116978. doi:10.1016/j.lfs.2019.116978

Hellenbrand, D. J., Reichl, K. A., Travis, B. J., Filipp, M. E., Khalil, A. S., Pulito, D. J., et al. (2019). Sustained Interleukin-10 Delivery Reduces Inflammation and Improves Motor Function after Spinal Cord Injury. *J. Neuroinflammation* 16 (1), 93. doi:10.1186/s12974-019-1479-3

Hendrix, S., Sanchez, S., Ventriglia, E., and Lemmens, S. (2020). HDAC8 Inhibition Reduces Lesional Iba-1+ Cell Infiltration after Spinal Cord Injury without Effects on Functional Recovery. *Int. J. Mol. Sci.* 21 (12), 4539. doi:10.3390/ijms21124539

Heneka, M. T., McManus, R. M., and Latz, E. (2018). Inflammasome Signalling in Brain Function and Neurodegenerative Disease. *Nat. Rev. Neurosci.* 19 (10), 610–621. doi:10.1038/s41583-018-0055-7

Ji, X., Song, Z., He, J., Guo, S., Chen, Y., Wang, H., et al. (2021). NIMA-related Kinase 7 Amplifies NLRP3 Inflammasome Pro-inflammatory Signaling in Microglia/macrophages and Mice Models of Spinal Cord Injury. *Exp. Cel Res.* 398 (2), 112418. doi:10.1016/j.yexcr.2020.112418

Jiang, W., Li, M., He, F., Zhou, S., and Zhu, L. (2017). Targeting the NLRP3 Inflammasome to Attenuate Spinal Cord Injury in Mice. *J. Neuroinflammation* 14 (1), 207. doi:10.1186/s12974-017-0980-9

Jiao, J., Zhao, G., Wang, Y., Ren, P., and Wu, M. (2020). MCC950, a Selective Inhibitor of NLRP3 Inflammasome, Reduces the Inflammatory Response and Improves Neurological Outcomes in Mice Model of Spinal Cord Injury. *Front. Mol. Biosci.* 7, 37. doi:10.3389/fmolb.2020.00037

Jorge, A., Taylor, T., Agarwal, N., and Hamilton, D. K. (2019). Current Agents and Related Therapeutic Targets for Inflammation after Acute Traumatic Spinal Cord Injury. *World Neurosurg.* 132, 138–147. doi:10.1016/j.wneu.2019.08.108

Kaneko, J., Okinaga, T., Ariyoshi, W., Hikiji, H., Fujii, S., Iwanaga, K., et al. (2018). Ky-2, a Hybrid Compound Histone Deacetylase Inhibitor, Regulated Inflammatory Response in LPS-Driven Human Macrophages. *Cell Biol Int* 42 (12), 1622–1631. doi:10.1002/cbin.11058

Karsy, M., and Hawryluk, G. (2019). Modern Medical Management of Spinal Cord Injury. *Curr. Neurol. Neurosci. Rep.* 19 (9), 65. doi:10.1007/s11910-019-0984-1

Kiany, S., Harrison, D., and Gordon, N. (2020). The Histone Deacetylase Inhibitor Entinostat/Syndax 275 in Osteosarcoma. *Adv. Exp. Med. Biol.* 1257, 75–83. doi:10.1007/978-3-030-43032-0_7

Kong, G., Liu, J., Li, R., Lin, J., Huang, Z., Yang, Z., et al. (2021). Ketone Metabolite β-Hydroxybutyrate Ameliorates Inflammation after Spinal Cord Injury by Inhibiting the NLRP3 Inflammasome. *Neurochem. Res.* 46 (2), 213–229. doi:10.1007/s11064-020-03156-2

Kwiecien, J. M., Dabrowski, W., Dąbrowska-Bouta, B., Sulkowski, G., Oakden, W., Kwiecien-Delaney, C. J., et al. (2020). Prolonged Inflammation Leads to Ongoing Damage after Spinal Cord Injury. *PLoS One* 15 (3), e0226584. doi:10.1371/journal.pone.0226584

Lanzillotta, A., Pignataro, G., Branca, C., Cuomo, O., Sarnico, I., Benarese, M., et al. (2013). Targeted Acetylation of NF-kappaB/RelA and Histones by Epigenetic Drugs Reduces post-ischemic Brain Injury in Mice with an Extended Therapeutic Window. *Neurobiol. Dis.* 49, 177–189. doi:10.1016/j.nbd.2012.08.018

Ma, K., Qin, L., Matas, E., Duffney, L. J., Liu, A., and Yan, Z. (2018). Histone Deacetylase Inhibitor MS-275 Restores Social and Synaptic Function in a Shank3-Deficient Mouse Model of Autism. *Neuropsychopharmacology* 43 (8), 1779–1788. doi:10.1038/s41386-018-0073-1

Ma, Y. D., Fang, J., Liu, H., and Zhou, L. (2015). Increased HDAC3 and Decreased miRNA-130a Expression in PBMCs through Recruitment HDAC3 in Patients with Spinal Cord Injuries. *Int. J. Clin. Exp. Pathol.* 8 (2), 1682–1689.

McDonald, J. W., and Sadowsky, C. (2002). Spinal-cord Injury. *Lancet* 359 (9304), 417–425. doi:10.1016/S0140-6736(02)07603-1

Mohammadi, A., Sharifi, A., Pourpaknia, R., Mohammadian, S., and Sahebkar, A. (2018). Manipulating Macrophage Polarization and Function Using Classical HDAC Inhibitors: Implications for Autoimmunity and Inflammation. *Crit. Rev. Oncol. Hematol.* 128, 1–18. doi:10.1016/j.critrevonc.2018.05.009

Mota, M., Porrini, V., Parrella, E., Benarese, M., Bellucci, A., Rhein, S., et al. (2020). Neuroprotective Epi-Drugs Quench the Inflammatory Response and Microglial/macrophage Activation in a Mouse Model of Permanent Brain Ischemia. *J. Neuroinflammation* 17 (1), 361. doi:10.1186/s12974-020-02028-4

Murphy, S. P., Lee, R. J., McClean, M. E., Pemberton, H. E., Uo, T., Morrison, R. S., et al. (2014). MS-275, a Class I Histone Deacetylase Inhibitor, Protects the P53-Deficient Mouse against Ischemic Injury. *J. Neurochem.* 129 (3), 509–515. doi:10.1111/jnc.12498

Ni, D. X., Wang, Q., Li, Y. M., Cui, Y. M., Shen, T. Z., Li, X. L., et al. (2021). Synthesis of Nigranoic Acid and Manwuweizic Acid Derivatives as HDAC Inhibitors and Anti-inflammatory Agents. *Bioorg. Chem.* 109, 104728. doi:10.1016/j.bioorg.2021.104728

Sada, N., Fujita, Y., Mizuta, N., Ueno, M., Furukawa, T., and Yamashita, T. (2020). Inhibition of HDAC Increases BDNF Expression and Promotes Neuronal Rewiring and Functional Recovery after Brain Injury. *Cell Death Dis* 11 (8), 655. doi:10.1038/s41419-020-02897-w

Shank, C. D., Walters, B. C., and Hadley, M. N. (2019). Current Topics in the Management of Acute Traumatic Spinal Cord Injury. *Neurocrit. Care* 30 (2), 261–271. doi:10.1007/s12028-018-0537-5

Shiraishi, Y., Kimura, A., Kimura, H., Ohmori, T., Takahashi, M., and Takeshita, K. (2020). Deletion of Inflammasome Adaptor Protein ASC Enhances Functional Recovery after Spinal Cord Injury in Mice. *J. Orthop. Sci.* S0949-2658 (20), 30124–X. doi:10.1016/j.jos.2020.04.006

Su, Z., Niu, W., Liu, M. L., Zou, Y., and Zhang, C. L. (2014). *In Vivo* conversion of Astrocytes to Neurons in the Injured Adult Spinal Cord. *Nat. Commun.* 5, 3338. doi:10.1038/ncomms4338

Suda, S., Ueda, M., Nito, C., Nishiyama, Y., Okubo, S., Abe, A., et al. (2015). Valproic Acid Ameliorates Ischemic Brain Injury in Hyperglycemic Rats with Permanent Middle Cerebral Occlusion. *Brain Res.* 1606, 1–8. doi:10.1016/j.brainres.2015.02.013

Voet, S., Srinivasan, S., Lamkanfi, M., and van Loo, G. (2019). Inflammasomes in Neuroinflammatory and Neurodegenerative Diseases. *EMBO Mol. Med.* 11 (6), e10248. doi:10.15252/emmm.201810248

Wu, Y., Dou, J., Wan, X., Leng, Y., Liu, X., Chen, L., et al. (2019). Histone Deacetylase Inhibitor MS-275 Alleviates Postoperative Cognitive Dysfunction in Rats by Inhibiting Hippocampal Neuroinflammation. *Neuroscience* 417, 70–80. doi:10.1016/j.neuroscience.2019.08.020

Zhang, H., Zhang, W., Jiao, F., Li, X., Zhang, H., Wang, L., et al. (2018a). The Nephroprotective Effect of MS-275 on Lipopolysaccharide (LPS)-Induced Acute Kidney Injury by Inhibiting Reactive Oxygen Species (ROS)-Oxidative Stress and Endoplasmic Reticulum Stress. *Med. Sci. Monit.* 24, 2620–2630. doi:10.12659/MSM.906362

Zhang, S., Fujita, Y., Matsuzaki, R., and Yamashita, T. (2018b). Class I Histone Deacetylase (HDAC) Inhibitor CI-994 Promotes Functional Recovery Following Spinal Cord Injury. *Cel Death Dis* 9 (5), 460. doi:10.1038/s41419-018-0543-8

Zheng, Z., Zhou, Y., Ye, L., Lu, Q., Zhang, K., Zhang, J., et al. (2020). Histone Deacetylase 6 Inhibition Restores Autophagic Flux to Promote Functional

Recovery after Spinal Cord Injury. *Exp. Neurol.* 324, 113138. doi:10.1016/j.expneurol.2019.113138

Zhou, Q., Feng, X., Ye, F., Lei, F., Jia, X., and Feng, D. (2020). miR-27a Promotion Resulting from Silencing of HDAC3 Facilitates the Recovery of Spinal Cord Injury by Inhibiting PAK6 Expression in Rats. *Life Sci.* 260, 118098. doi:10.1016/j.lfs.2020.118098

Zrzavy, T., Schwaiger, C., Wimmer, I., Berger, T., Bauer, J., Butovsky, O., et al. (2021). Acute and Non-resolving Inflammation Associate with Oxidative Injury after Human Spinal Cord Injury. *Brain* 144 (1), 144–161. doi:10.1093/brain/awaa360

**Conflict of Interest:** The authors declare that the research was conducted in the absence of any commercial or financial relationships that could be construed as a potential conflict of interest.

**Publisher's Note:** All claims expressed in this article are solely those of the authors and do not necessarily represent those of their affiliated organizations, or those of the publisher, the editors, and the reviewers. Any product that may be evaluated in this article, or claim that may be made by its manufacturer, is not guaranteed or endorsed by the publisher.

frontiers in Pharmacology

ORIGINAL RESEARCH
published: 10 December 2021
doi: 10.3389/fphar.2021.780588

# Sigma-1 Receptor is a Pharmacological Target to Promote Neuroprotection in the SOD1$^{G93A}$ ALS Mice

*Núria Gaja-Capdevila*[1,2], *Neus Hernández*[1,2], *Xavier Navarro*[1,2] *and Mireia Herrando-Grabulosa*[1,2]*

[1]Institute of Neurosciences, Department Cell Biology, Physiology and Immunology, Universitat Autònoma de Barcelona, Bellaterra, Spain, [2]Centro de Investigación Biomédica en Red Sobre Enfermedades Neurodegenerativas (CIBERNED), Madrid, Spain

Amyotrophic Lateral Sclerosis (ALS) is a neurodegenerative disorder characterized by the death of motoneurons (MNs) with a poor prognosis. There is no available cure, thus, novel therapeutic targets are urgently needed. Sigma-1 receptor (Sig-1R) has been reported as a target to treat experimental models of degenerative diseases and, importantly, mutations in the Sig-1R gene cause several types of motoneuron disease (MND). In this study we compared the potential therapeutic effect of three Sig-1R ligands, the agonists PRE-084 and SA4503 and the antagonist BD1063, in the SOD1$^{G93A}$ mouse model of ALS. Pharmacological administration was from 8 to 16 weeks of age, and the neuromuscular function and disease progression were evaluated using nerve conduction and rotarod tests. At the end of follow up (16 weeks), samples were harvested for histological and molecular analyses. The results showed that PRE-084, as well as BD1063 treatment was able to preserve neuromuscular function of the hindlimbs and increased the number of surviving MNs in the treated female SOD1$^{G93A}$ mice. SA4503 tended to improve motor function and preserved neuromuscular junctions (NMJ), but did not improve MN survival. Western blot analyses revealed that the autophagic flux and the endoplasmic reticulum stress, two pathways implicated in the physiopathology of ALS, were not modified with Sig-1R treatments in SOD1$^{G93A}$ mice. In conclusion, Sig-1R ligands are promising tools for ALS treatment, although more research is needed to ascertain their mechanisms of action.

**Keywords: sigma-1 receptor, amyotrophic lateral sclerosis, motoneuron, SOD1 G93A transgenic, neurodegenerative disease**

OPEN ACCESS

***Edited by:***
*Valle Palomo, Consejo Superior de Investigaciones Científicas (CSIC), Spain*

***Reviewed by:***
*Jean-Charles LIEVENS, Université de Montpellier, France*
*Arnold Eino Ruoho, University of Wisconsin-Madison, United States*

***Correspondence:**
*Mireia Herrando-Grabulosa*
*Mireia.Herrando@uab.cat*

***Specialty section:***
*This article was submitted to Neuropharmacology, a section of the journal Frontiers in Pharmacology*

***Received:*** *21 September 2021*
***Accepted:*** *08 November 2021*
***Published:*** *10 December 2021*

***Citation:***
*Gaja-Capdevila N, Hernández N, Navarro X and Herrando-Grabulosa M (2021) Sigma-1 Receptor is a Pharmacological Target to Promote Neuroprotection in the SOD1$^{G93A}$ ALS Mice. Front. Pharmacol. 12:780588. doi: 10.3389/fphar.2021.780588*

## INTRODUCTION

Amyotrophic lateral sclerosis (ALS) is a fatal neurodegenerative disorder characterized by the progressive loss of upper and lower motoneurons (MNs), causing muscle paralysis and early death. Despite persistent efforts to develop treatments for this disease, no effective cure is available for ALS patients. Riluzole and edaravone are the only drugs approved by the FDA, but they have limited therapeutic benefits increasing the lifespan a few months (Edaravone (MCI-186) ALS 19 Study Group, 2017; Ludolph and Jesse, 2009). The exact pathophysiological mechanisms contributing to

MN degeneration in ALS remain unclear. Nevertheless, the generation of transgenic animal models carrying ALS-related mutations has accelerated the research on physiopathology and preclinical therapeutic assays for ALS. Since the first mutation identified in familiar ALS was in the SOD1 gene (Rosen et al., 1993), the SOD1$^{G93A}$ mouse is the most widely used ALS model, which develops the main clinical, electrophysiological and histopathological features of both familial and sporadic forms of the disease (Turner and Talbot, 2008; Mancuso et al., 2011b). Despite mutations in SOD1 gene are present in 20% of familiar ALS cases and only 2% of all ALS cases (Ragagnin et al., 2019), the interest of the SOD1 transgenic models is increased because alterations in SOD1 protein also occur in sporadic ALS cases (Bosco and Landers, 2010), and accumulation of wild-type SOD1 causes ALS (Graffmo et al., 2013).

Sigma-1 receptor (Sig-1R) is a protein ubiquitously expressed in the central nervous system (CNS) (Langa et al., 2003) and particularly enriched in the MNs. It is located in the endoplasmic reticulum (ER) cisternae at postsynaptic sites of C-terminals and at the mitochondria associated-endoplasmic reticulum membrane (MAM), an active and dynamic site in which there is crosstalk between mitochondria and ER (Hayashi and Su, 2007; Mavlyutov et al., 2012). Sig-1R is involved in numerous cellular processes, such as ion channel modulation, protein and lipid transport, ER stress response and mitochondria function (Penke et al., 2018; Herrando-Grabulosa et al., 2021). In recent years, genetic analyses revealed Sig-1R gene mutations involved in a juvenile form of ALS (Al-Saif et al., 2011; Watanabe et al., 2016) and in forms of motor neuropathies (Almendra et al., 2018; Ververis et al., 2019). Moreover, either accumulation of mutant SOD1 or absence of Sig-1R induced MAM disruption and mitochondrial dysfunction (Bernard-Marissal et al., 2015; Watanabe et al., 2016).

Nowadays, several Sig-1R ligands have interest as potential therapeutic agents against CNS disorders, including chronic neurological conditions such as pain, stroke, Huntington disease, among others (Bruna et al., 2018; Reilmann et al., 2019; Urfer et al., 2014). Regarding motoneuron diseases (MND), the Sig-1R agonist PRE-084 has shown positive effects reducing the MN death *in vitro* in organotypic culture of spinal cord subjected to excitotoxic damage (Guzmán-Lenis et al., 2009) and *in vivo* in the SOD1$^{G93A}$ murine model of ALS (Mancuso et al., 2012), in the wobbler mouse model of spontaneous MN degeneration (Peviani et al., 2014), and after spinal nerve injury in adult mice and rats (Gaja-Capdevila et al., 2021; Penas et al., 2011). Studies testing two other Sig-1R agonists, SA4503 and pridopidine, also showed that treatment ameliorates ALS pathology (Ionescu et al., 2019; Ono et al., 2014), and pridopidine is being tested in a clinical trial for ALS (ClinicalTrials.gov NCT04615923). However, Sig-1R ligands may act differently, and even contrarily, on neuroprotective mechanisms by modulating calcium homeostasis (Tadić et al., 2017). Thus, the Sig1-R appears as a promising target to promote MN protection, but more studies are needed to establish the role of Sig-1R ligands in MND models, and the type of ligand that may be most effective. Considering the recent data, the aim of the work reported here was to comparatively evaluate the therapeutic efficacy of three Sig-1R ligands in an *in vitro* model of MN degeneration and in the SOD1$^{G93A}$ mouse. Moreover, it was investigated whether the administration of Sig-1R ligands could promote the modulation of glial reactivity. Finally, regarding the importance of ER stress and autophagy in the ALS pathogenesis (Hetz and Saxena, 2017; Medinas et al., 2017; Nguyen et al., 2019), we investigated whether these Sig-1R ligands modulate these molecular pathways.

# MATERIAL AND METHODS

## Spinal Cord Organotypic Cultures

Spinal cord organotypic cultures (SCOCs) were prepared from lumbar sections of Sprague–Dawley pups (8–9 days-old) as previously described (Mòdol-Caballero et al., 2017). After harvesting, the spinal cord was cut in 350 μm thick transverse sections, that were transferred on Millicell-CM nets (0.4 μm, PICM03050, Millipore) and then into a six-well plate with the incubation medium [50% (v/v) minimal essential medium (MEM, M5775, Sigma), 2 mM glutamine, 25 mM HEPES, 25% (v/v) Hank's Balanced Salt Solution (HBSS−/−, 14,175, Gibco) supplemented with 25.6 mg/ml glucose and 25% (v/v) heat-inactivated horse serum (26,050–088, Gibco), pH = 7.2). After 7 days *in vitro* (DIV), chronic excitotoxicity was induced by adding DL-threo-β-hydroxyaspartic acid (THA; 100 μM), a selective inhibitor of glutamate transport (Rothstein et al., 1993). The Sig-1R ligands were simultaneously co-added in the culture medium and renewed at each medium change twice per week. Sig-1R ligands PRE-084, BD1063 and SA4503 (Tocris) were tested at three different concentrations (30, 3 and 0.3 μM). Riluzole (5 μM) was also assayed as positive control. Slices were maintained for 28 DIV and then fixed with 4% paraformaldehyde in phosphate-buffered saline (PBS). The *in vitro* experiments have been performed in three independent cultures and resulting in 12 slices for each experimental condition.

## Animals and Experimental Design

Transgenic SOD1$^{G93A}$ mice (B6SJL-Tg [SOD1-G93A] 1Gur) and non-transgenic wild type (WT) littermates were used. The transgenic offspring was identified by polymerase chain reaction (PCR) amplification of DNA extracted from the tail. Primer sequences were the following: hSOD1-forward CATCAG CCCTAATCCATCTGA, hSOD1 reverse CGCGACTAACAA TCAAAGTGA, mIL2 forward CTAGGCCACAGAATTGAA AGATCT and mIL2 reverse GTAGGTGGAAATTCTAGC ATCATCC. Mice were maintained under standard conditions with access to food and water ad libitum. The experimental procedures were approved by the Ethics Committee of the Universitat Autònoma de Barcelona and followed the European Communities Council Directive 2010/63/EU.

The study included B6SJL female WT and SOD1$^{G93A}$ mice divided in different experimental groups, either receiving vehicle or a Sig-1R ligand. We first performed a complete study in female mice, and after analyses, the study was also performed in male

mice with two compounds, considering the differences in disease progression between sexes in this transgenic mouse. For the functional studies the following experimental groups of $SOD1^{G93A}$ female mice were used: SOD1 + saline (n = 15), SOD1 + PRE-084 0.25 mg/kg (n = 14), SOD1 + BD1063 5 mg/kg (n = 12), SOD1 + SA4503 0.25 mg/kg (n = 7), SOD1 + SA4503 1 mg/kg (n = 7), in addition to untreated WT littermates (n = 15). Samples from these animals (n = 7–10) were collected for histological analysis at 16 weeks. Subgroups (n = 4–5) of WT, vehicle, PRE-084 and BD1063 groups were used for Western blot (WB) analyses at 8 and 16 weeks of age. For the functional studies in male the following groups of $SOD1^{G93A}$ mice were used: SOD1 + saline (n = 10), SOD1 + PRE-084 (n = 10), SOD1 + BD1063 (n = 5), and untreated WT littermates (n = 10).

## Pharmacological Treatment

The Sig-1R ligands were given once a day from 8 to 16 weeks of age by intraperitoneal (i.p) administration of agonists PRE-084 (0.25 mg/kg, TOCRIS) and SA4503 (0.25 mg/kg and 1 mg/kg, TOCRIS) and the antagonist BD1063 (5 mg/kg, TOCRIS). The compounds were dissolved in saline solution, that was administered in the same volume to the untreated control group. The Sig-1R ligands were administered in a volume of 10 ml/kg.

## Electrophysiological Tests

Motor nerve conduction tests were performed at 8 weeks of age to obtain baseline values (prior to drug administration) to distribute them between the experimental groups, and then at 11, 13 and 16 weeks of age. Briefly, the sciatic nerve was stimulated by single pulses of 20 μs duration delivered at the sciatic notch. The compound muscle action potential (CMAP) was recorded from tibialis anterior (TA), gastrocnemius (GM) and plantar interossei (PL) muscles with microneedle electrodes (Mancuso et al., 2011b). The recorded potentials were amplified and displayed on a digital oscilloscope to measure the latency to the onset and the amplitude of the CMAP. Pentobarbital (50 mg/kg i. p.) was used to anesthetise the mice during the tests and mice body temperature was maintained by means of a thermostated heating pad.

## Locomotion Tests

The rotarod test was performed to evaluate motor coordination and balance of the animals, weekly from 8 to 16 weeks of age in $SOD1^{G93A}$ and WT mice. Mice were placed onto the rod turning at 14 rpm, each mouse was given five trials and the longest latency without falling was recorded, with an arbitrary cut-off time of 180 s. The symptomatic disease onset for each mouse was determined as the first week when the mouse did not sustain 180 s on the rod.

## Histological and Immunohistochemical Analyses

SCOC were fixed, blocked with 5% normal horse serum in 0.3% Triton X-100 PBS solution (PBS-Tx), and incubated with primary antibody mouse anti-neurofilament H non-phosphorylated (SMI-32, 1:500; 801701, BioLegend) for 48 h at 4°C. Then, after several washes with 0.1% Tween-20 in PBS (PBS-Tw), slices were incubated with secondary antibody Alexa Fluor 488 donkey anti-mouse (1:500; A-2102, Invitrogen) for 2 h at RT. Cell nuclei were labeled with DAPI (1:5000; D9563, Sigma) and the sections were mounted with Fluoromount-G medium (SouthernBiotech). Images of the ventral horns were captured with a confocal microscope (LSM 700 Axio Observer, Carl Zeiss 20x/z0.5). The Cell Counter plugin of ImageJ software was used for quantifying SMI-32 positive neurons (MN survival) in each spinal cord.

At 16 weeks of age mice were sacrificed with an overdose of pentobarbital sodium and transcardially perfused with 4% paraformaldehyde in PBS. The lumbar segment of spinal cord was post-fixed for 2 h and cryopreserved in 30% sucrose solution in PB, whereas the hindlimb muscles were directly cryopreserved. For assessing MN survival, the spinal cord was serially cut in 20 μm thick transverse sections using a cryostat (Leica) and collected sequentially on series of 10 slides. Slices corresponding to L4-L5 spinal cord sections separated 100 μm were stained for 3 h with an acidified solution of 3.1 mM cresyl violet. Then, the slides were washed, dehydrated and mounted with DPX. MNs were identified by localization in the lateral ventral horn and strict morphological and size criteria: polygonal shape, prominent nucleoli and diameter larger than 20 μm.

For immunofluorescence analysis, lumbar spinal cord sections were blocked with blocking solution (10% normal donkey serum (NDS) and 0.2 mM glycine in PBS-Tx) for 1 h at RT, and then incubated overnight at 4°C with primary antibodies: anti-Iba1 (1: 500; 019–19,741, Wako), anti-GFAP (1:500; 13–0300, Invitrogen), SQSTM1/p62 (1:150; 155686, Abcam). After several washes, sections were incubated for 2 h at RT with the corresponding secondary antibody: Alexa Fluor 488-conjugated secondary antibody (1:500; A-21206, Invitrogen), Cy3-conjugated secondary antibody (1:500; AP182C, Millipore), Alexa Fluor 594-conjugated secondary antibody (1:300; A-21207,Invitrogen) or Alexa Fluor 647-conjugated secondary antibody (1:300; Ab150155,Abcam). NeuroTraceTM 500/525 Green Fluorescent Nissl (1:200; N21480, Invitrogen) and DAPI (1:2000; D9563, Sigma) were used to stain MNs and nuclei, respectively. Finally, samples were washed in PB and mounted with Fluoromount-G. To quantify the glial cell reactivity images of the ventral horn were captured at x40 under the same conditions (sensitivity and exposure time) for each analyzed marker, using fluorescence microscopy (Olympus BX51, Japan). Fluorescence signal intensity (Integrated density) was analyzed using ImageJ software after defining a threshold for background correction. To quantify p62/SQSTM1 immunolabeling, photographs of the ventral horn were taken with confocal microscopy (LSM 700 Axio Observer, Carl Zeiss, 40xOil/z0.5). Integrated density of p62/SQSTM1 was quantified in a total of more than 50 MNs for each animal using a ROI manage tool from ImageJ software. The p62/SQSTM1 integrated density was analyzed in the glia by quantifying the whole slide image and subtracting the intensity of the MNs.

For neuromuscular junctions (NMJ) labeling, GM muscle was serially cut in 50 μm thick longitudinal sections and collected in sequential series. After blocking, the sections were incubated for

**TABLE 1 |** Primary antibodies used for WB experiments.

| Antibody name | Dilution | Description | References number |
|---|---|---|---|
| LC3B | 1:500 | Rabbit polyclonal | #ab51520; Abcam |
| Beclin 1 | 1:1000 | Rabbit polyclonal | #3738; CST |
| XBP-1 | 1:300 | Rabbit polyclonal | #37152; Abcam |
| GADD153/CHOP | 1:500 | Mouse monoclonal | #sc-7351; SCBT |
| Sigma-1 Receptor | 1:250 | Rabbit polyclonal | # 223,702; Abcam |
| GRP78/BiP | 1:500 | Rabbit polyclonal | #G8918; Sigma-Aldrich |
| IRE1 (phospho S724) | 1:250 | Rabbit polyclonal | # ab48187; Abcam |
| IRE1α | 1:500 | Rabbit polyclonal | #3294; CST |
| β-Actin | 1:10,000 | Mouse monoclonal | #A5316; Sigma-Aldrich |
| α-tubulin | 1:10,000 | Mouse monoclonal | #T9026; Sigma-Aldrich |

48 h at 4°C with the primary antibodies anti-neurofilament 200 (NF200, 1:1000; AB5539, Millipore, United States) and anti-synaptophysin (1:500; AB32127, Abcam). After washes sections were incubated overnight with Alexa Fluor 594-conjugated secondary antibody (1:200; A11042-A21207, Invitrogen) and Alexa Fluor 488-conjugated alfa-bungarotoxin (1:500; B13422, Life Technologies). Slides were mounted in Fluoromount-G with DAPI. Images were captured by confocal microscopy (LSM 700 Axio Observer, Carl Zeiss, 40xOil/z0.5). The proportion of innervated NMJs was calculated by classifying each endplate as occupied or vacant. Four fields with a total of more than 60 endplates were analyzed per each mouse.

## Protein Extraction and Western Blot Analysis

At 8 or 16 weeks of age, mice were euthanized with an overdose of pentobarbital sodium. The lumbar spinal cord from WT and $SOD1^{G93A}$ of each experimental group was harvested and frozen in liquid nitrogen for storage. To lysate samples the RIPA lysis buffer with protease inhibitor cocktail (Sigma) and phosphatase inhibitors (PhosphoSTOP Roche) was used. Then, samples were sonicated and centrifuged at 12,000 rpm for 10 min at 4°C. Finally, total protein concentration was determined by the BCA Protein Assay Kit (Biorad). 20–30 μg of protein per sample were loaded into 7.5–15% SDS-polyacrylamide gels and transferred into a PVDF membrane. After blocking, primary antibodies were incubated at 4°C overnight (**Table 1**). After incubation with appropriate Horseradish peroxidase (HRP)-coupled secondary antibody (1:5000; Bio-rad) for 1 h at RT, proteins were visualized using the Clarity Western ECL Substrate (Cat#1705061, Bio-Rad Laboratories). Images were collected using a transilluminator (Chemidoc MP Imaging System, BioRad) and blots were analyzed using the Lane and band plugin of Image Lab software (Bio Rad). Data were normalized first by the loading control (actin or tubulin) and afterwards by the mean of the control (WT) samples (n = three to six samples were analyzed per each condition and time-point of the study).

## Statistical Analysis

GraphPad Prism 8 software was used to perform data analyses, all data is expressed as mean ± SEM. Electrophysiological and functional measurements were analyzed with repeated measurements Two-Way ANOVA and histological and molecular data were analyzed using One-way ANOVA. Bonferroni test was used as the post hoc test for multiple comparisons. Differences were considered significant at $p \leq 0.05$.

# RESULTS

## Sig-1R Ligands Exert Neuroprotection in SCOCs Under Chronic Excitotoxicity

Addition of THA to the SCOC induced a significant reduction of about 40% in the number of SMI-32 labeled MNs in the ventral horn after 21 DIV, compared to control slices (**Figure 1**). Slices treated with THA and PRE-084, BD1063 or SA4503 showed significant preservation of MNs at the two doses tested. The Sig-1R agonists PRE-084 and SA4503 significantly reduced MN death in a dose-dependent manner, with maximal protective effect at 30 μM (**Figures 1A,B**). The antagonist BD1063 also prevented MN death, with a highest effect at 3 μM (**Figure 1C**). Furthermore, the positive control against excitotoxicity Riluzole presented significant MN protection at similar levels than the Sig-1R ligands tested.

## Treatment With Sig-1R Ligands Preserves Neuromuscular Function in $SOD1^{G93A}$ Mice

$SOD1^{G93A}$ mice treated with Sig-1R ligands for 8 weeks maintained a gain of body weight throughout the study, and did not present any secondary effect, indicating lack of general toxicity of these ligands (**Figure 2A**).

In order to assess the effect of Sig-1R ligands on neuromuscular function of the $SOD1^{G93A}$ mice, we performed motor nerve conduction tests during the follow-up. Results showed that $SOD1^{G93A}$ mice treated with PRE-084 and with BD1063 had a significantly higher TA and GM CMAP amplitude compared to saline administered $SOD1^{G93A}$ mice at 13–16 weeks of age (**Figure 2B** and **Supplementary Figure S1A**). CMAP amplitude differences did not reach statistical significance in SA4503 treated group compared with untreated mice at the end of the follow up. Male $SOD1^{G93A}$ treated with PRE-084 had a significant preservation of TA and GM CMAP amplitude throughout the follow-up compared to the saline group, while

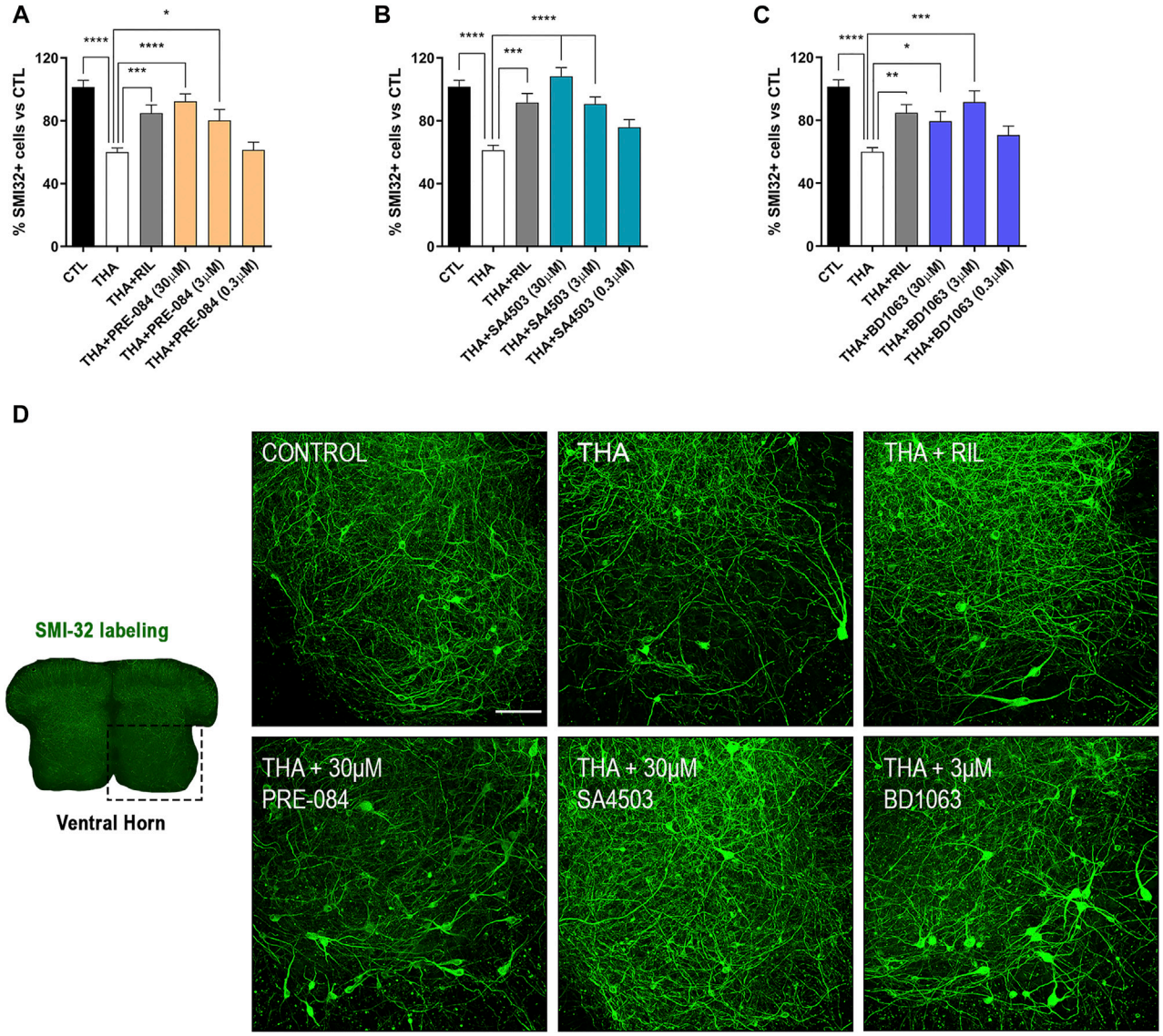


**FIGURE 1 |** PRE-084, BD1063 and SA4503 prevent MN death under chronic excitotoxicity *in vitro* **(A-C)** Plots showing the percentage of SMI-32 positive cells in the ventral horn of spinal cord hemislices under excitotoxicity by THA and the addition of Sig-1R ligands (mean ± SEM; n = 16–24 hemisections per treatment). One-way ANOVA followed with Bonferroni's post hoc test: ****$p < 0.0001$, ***$p < 0.001$; **$p < 0.01$, *$p < 0.05$ vs THA alone condition **(D)** Microphotograph of a SCOC slice labeled with SMI-32 antibody, and representative images of the ventral horn at 28 DIV of all tested conditions. Scale bar 100 μm.

BD1063 treatment has lower effect (**Supplementary Figure S1B, C**). The PL CMAP amplitude showed mild preservation for groups treated with PRE-084 and SA4503 at both doses, although it was only significant for PRE-084 (**Figure 2C**).

The rotarod test revealed that SOD1$^{G93A}$ mice treated with SA4503 at dose of 0.25 mg/kg and PRE-084 significantly improved the functional outcome compared with the untreated group, but animals treated with BD1063 and SA4503 1 mg/kg did not have any improvement (**Figure 2D**). Furthermore, the disease onset was delayed by 1 week (14 weeks of age) in mice treated with SA4503 (0.25 and 1 mg/kg) and PRE-084 versus the saline group (13 weeks) (**Figure 2E**).

The innervation of NMJ of the GM muscle was evaluated at 16 weeks of age. All the SOD1$^{G93A}$ mice treated with Sig-1R ligands had a significantly higher number of innervated endplates compared with the saline group, supporting the preservation of CMAP amplitude observed in the nerve conduction tests (**Figures 2E,F**).

## Sig-1R Ligands Promote MN Survival and Reduce Microglial Reactivity in SOD1$^{G93A}$ Mice

The quantification of α-MNs in the ventral horn of lumbar spinal cord sections stained with cresyl violet at 16 weeks of age, revealed

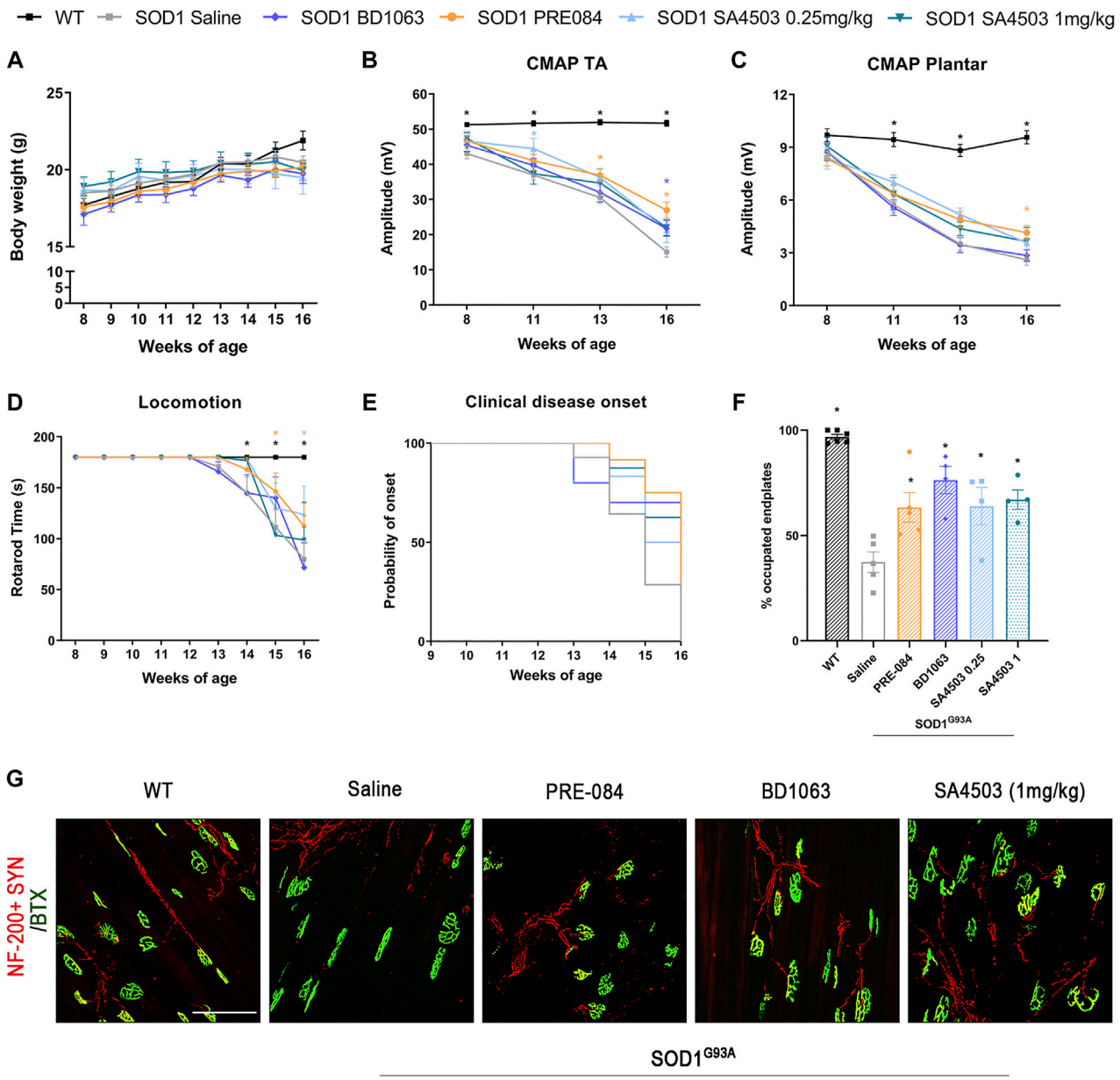


**FIGURE 2 |** Treatment with PRE-084, BD1063 and SA4503 enhances neuromuscular function in SOD1$^{G93A}$ female mice **(A)** Body weight of mice was monitored weekly during the 8 weeks of the follow-up **(B-C)** Values of the amplitude of compound muscle action potentials (CMAP) of tibialis anterior (TA) and plantar interosseus muscles **(D)** Graph showing the effect of the different Sig-1R treatment on functional outcome assessed with the rotarod test (n = 15 WT; n = 15 SOD1 saline; n = 12 SOD1 BD1063; n = 7 SOD1 SA4503 0.25 mg/kg; n = 7 SOD1 SA4503 1 mg/kg, and n = 14 SOD1 PRE-084 mice) **(E)** Probability of clinical onset of disease evaluated by the fall in the rotarod test. Some Sig-1R ligands delayed the onset of locomotion deficits but without significant differences **(F)** Plot of the percentage of innervated NMJ (overlap of signals) in the different experimental groups (n = four to six mice per group) **(G)** Representative confocal images of GA NMJs at 16 weeks of age. The maximum projection images shown were generated from 1.3 µm z projections. Scale bar 100 µm. Data are mean ± SEM, analyzed by One-way **(F)** and Two-way **(A-D)** ANOVA with Bonferroni's multiple comparisons test. *$p < 0.05$ vs SOD1$^{G93A}$ saline mice.

that treatment with PRE-084 and BD1063 mildly but significantly prevented the death of spinal MNs at the end-stage of the disease in comparison with untreated SOD1$^{G93A}$ mice, whereas SA4503 at both doses assessed did not have a noticeable effect (**Figures 3A,B**).

Microglial and astroglial response was found markedly increased in SOD1$^{G93A}$ compared to WT mice. Treatment with Sig-1R ligands reduced microglial reactivity, although only PRE-084 and SA4503 at 0.25 mg/kg caused a significant decrease, whereas the other treatments did not reach statistical significance (**Figures 3C,D**). Regarding

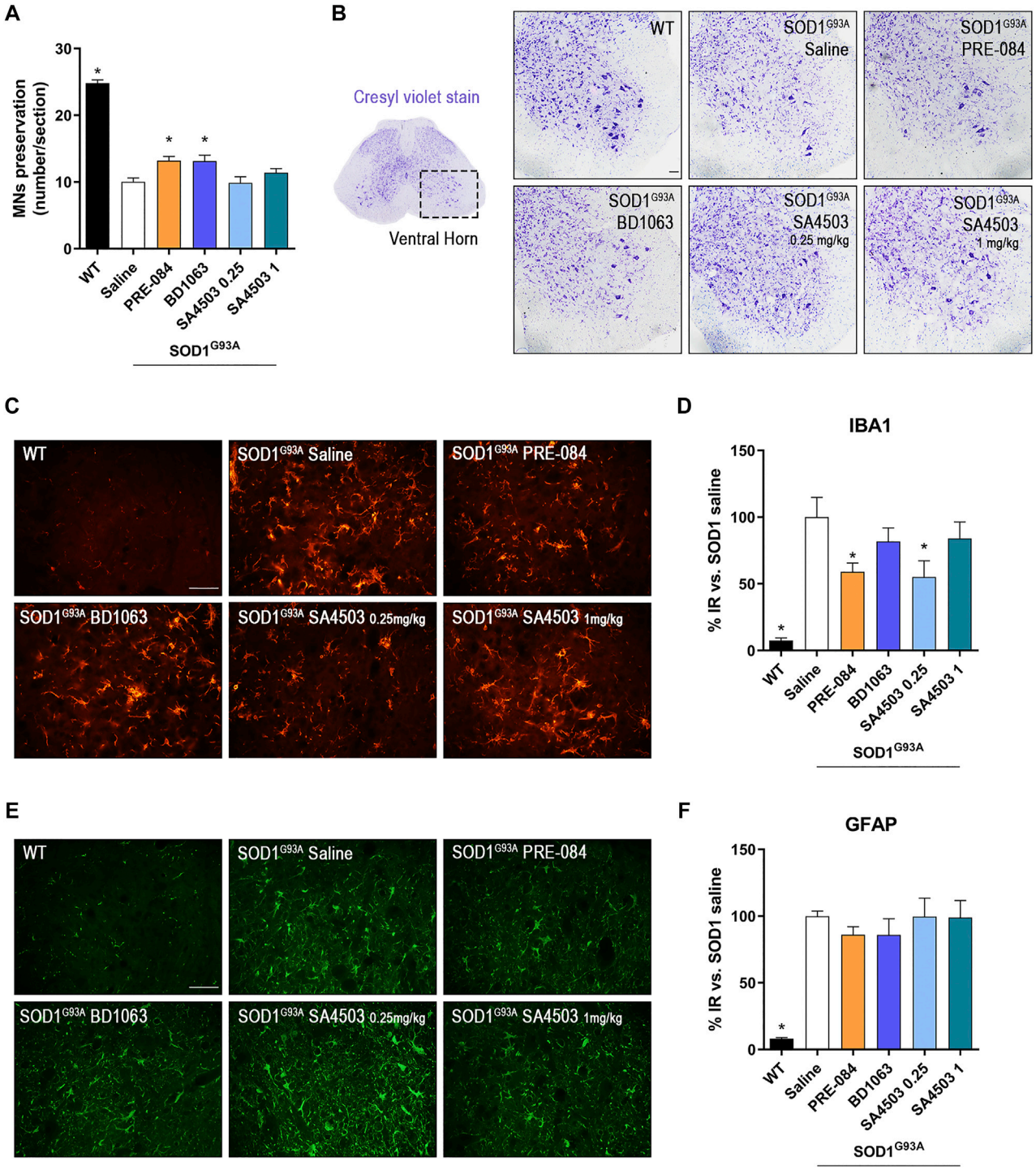


**FIGURE 3 |** PRE-084 and BD1063 reduce spinal MN degeneration and decrease microgliosis in SOD1$^{G93A}$ female mice at 16 weeks of age **(A)** Quantification of surviving MNs (mean number of MNs per section ±SEM) in the lumbar spinal cord, showing improved MN preservation with Sig-1R ligands PRE-084 and BD1063. **(B)** Representative spinal cord images of MNs stained with cresyl violet. Scale bar 100 µm. **(C, E)** Representative images of immunoreactivity for Iba1 **(C)**, a marker for microglia, and GFAP **(E)**, a marker of astrocytes, in the ventral horn of WT and SOD1$^{G93A}$ mice with or without Sig-1R treatments. Scale bar 50 µm. **D, F)** Graphs showing the quantification of percentage of Iba-1 **(D)** and GFAP **(F)** immunolabeling in ventral horn of spinal cord (n = 10 WT, n = 10 SOD1 saline, n = 8 SOD1 BD1063, n = 7 SOD1 SA4503 0.25 mg/kg, n = 7 SOD1 SA4503 1 mg/kg and n = 10 SOD1 PRE-084 mice). *$p < 0.05$ vs SOD1$^{G93A}$ saline mice.

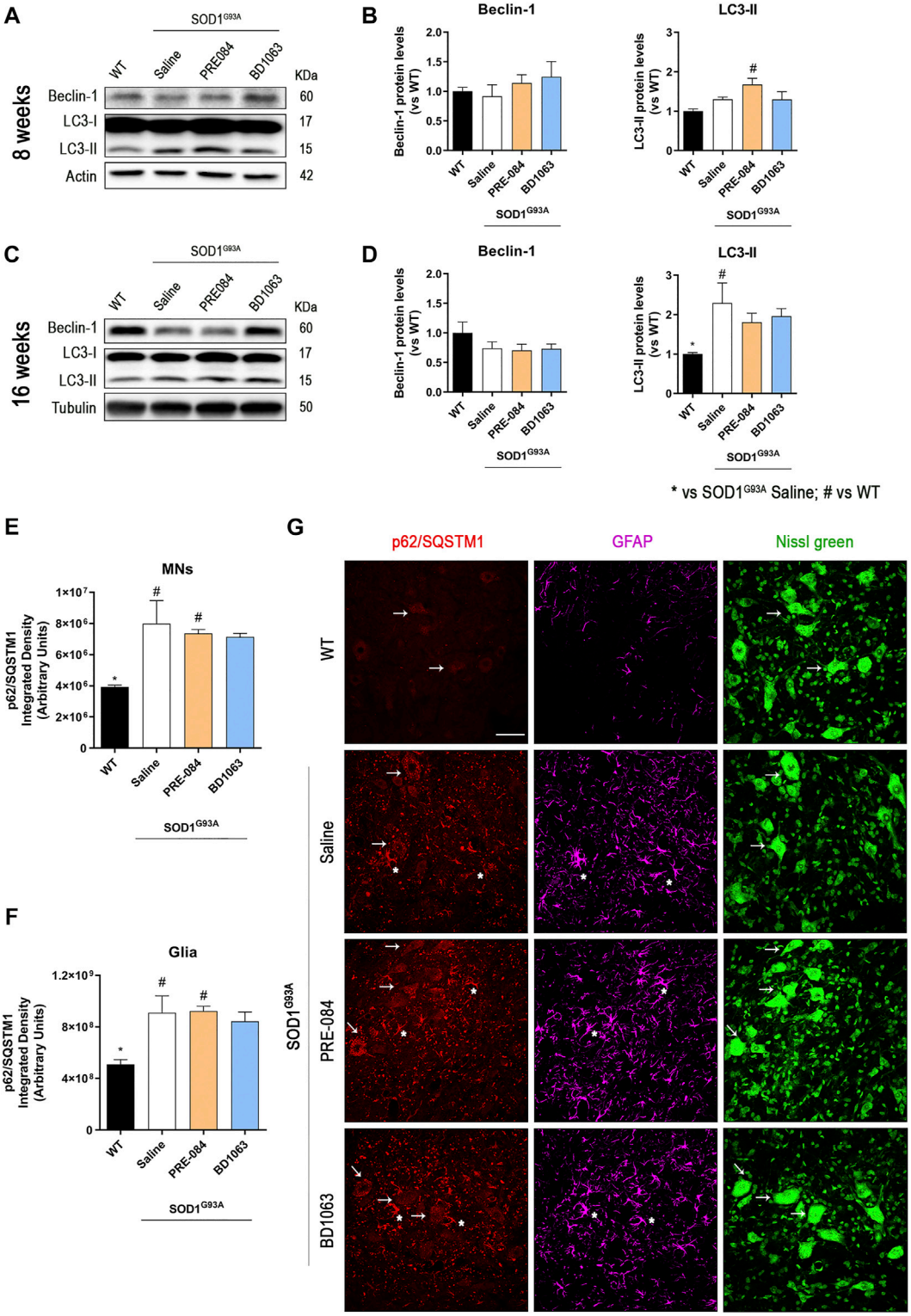


**FIGURE 4 |** Protein levels of autophagic flux markers in SOD1$^{G93A}$ female mice. Representative blots and protein level quantification of the autophagic markers Beclin-1 and LC3-II at 8 **(A, B)** and 16 **(C, D)** weeks of age. Quantification of the p62/SQSTM1 immunolabeling in the MNs **(E)** and in the glia (whole image without MNs) **(F)**. **(G)** Representative images of p62/SQSTM1 (red), GFAP (cyan) and FluoroNissl (green) immunofluorescence in the ventral horn of lumbar spinal cord of WT and SOD1$^{G93A}$ mice at 16 weeks. White arrows show examples of MNs with cytosolic p62 accumulation and asteriscs show p62 immunolabeling in the astroglia. Scale bar 50 µm. Data is mean ± SEM; n = three to five mice per group. One-way ANOVA followed with Bonferroni's post hoc test for multiple comparison. *$p < 0.05$ vs SOD1$^{G93A}$ saline, #$p < 0.05$ vs WT.

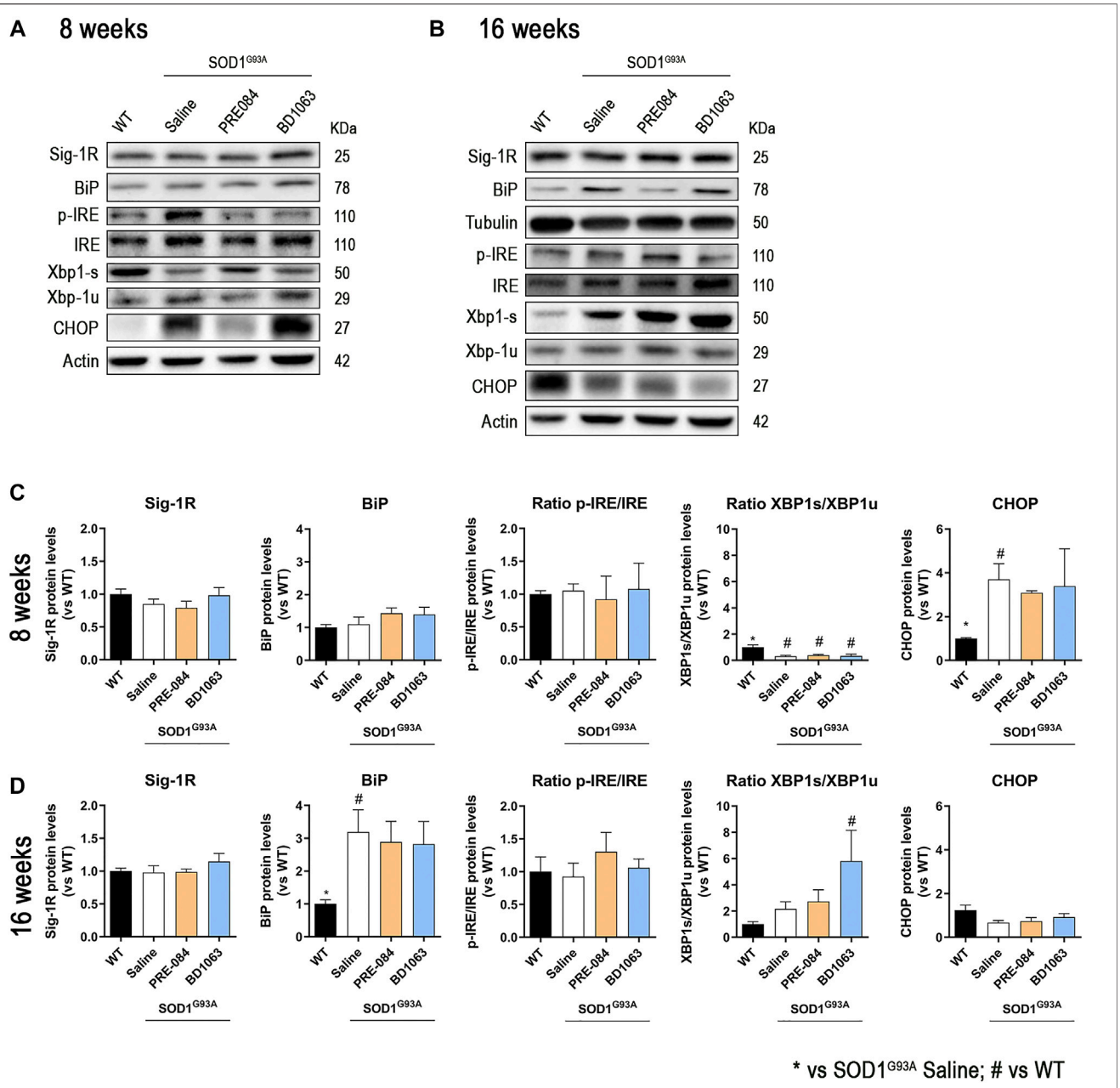


**FIGURE 5 |** Protein levels of ER stress markers in SOD1$^{G93A}$ female mice. Representative blots of ER stress markers at 8 **(A)** and 16 **(B)** weeks of age. Quantification of protein levels of Sig-1R, BiP, ratio p-IRE1/IRE1, ratio XBP1s/XBP1unspliced and CHOP at 8 **(C)** and 16 **(D)** weeks of age. Data is mean ± SEM; n = three to five mice per group. One-way ANOVA followed with Bonferroni's post hoc test for multiple comparison. *$p$ < 0.05 vs SOD1$^{G93A}$ saline, #$p$ < 0.05 vs WT.

astroglial immunoreactivity in the spinal cord ventral horn, we found that it was not modified by administration of the Sig-1R ligands in female SOD1$^{G93A}$ mice (**Figures 3E,F**).

## Analyses of Autophagic Flux and ER Stress During the Progression of ALS With Sig-1R Ligands

Considering that PRE-084 and BD1603 significantly preserved spinal MNs, we performed WB analyses of lumbar spinal cord lysates from WT and SOD1$^{G93A}$ saline, PRE-084 and BD1063 treated mice at 8 and 16 weeks of age to evaluate two main molecular pathways implicated in ALS pathogenesis. Three markers of autophagy flux (**Figure 4**) were analyzed and we found that there was no differences in Beclin-1 protein levels between WT and SOD1$^{G93A}$ mice groups at the two time points evaluated. A progressive increase of LC3-II levels was observed in SOD1$^{G93A}$ saline group, observing higher levels at 16 weeks of age compared with WT mice group. In contrast, at 8 weeks of age, higher LC3-II levels were detected in PRE-084 group that were

maintained at 16 weeks. No differences regarding LC3-II protein levels were detected in BD1063 group (**Figures 4A–D**). Immunofluorescence analyses of lumbar spinal cord sections revealed a significant accumulation of p62/SQSTM1 immunoreactive dots in the MNs and glial cells, mainly astroglia, of $SOD1^{G93A}$ animals at 16 weeks of age (**Figure 4E–G**). In summary, treatment with Sig-1R ligands PRE-084 and BD1063 did not markedly modify the protein levels of autophagic markers in comparison with saline $SOD1^{G93A}$ mice.

We also monitored the levels of ER stress markers in the spinal cord (**Figures 5A,B**). The protein levels of Sig-1R did not change at 8 and 16 weeks in $SOD1^{G93A}$ mice, as previously described (Mancuso et al., 2012), and administration of Sig-1R ligands PRE-084 and BD1063 did not modify the levels of this receptor (**Figures 5C,D**). During disease progression, WB analyses revealed a marked increase in the chaperone BiP at 16 weeks of age in $SOD^{G93A}$ mice (**Figure 5D**). There were no differences in the ratio p-IRE1/IRE between experimental groups at both time points evaluated, whereas there was a significant reduction of the ratio XBP1s/XBP1unspliced at 8 weeks, that was reverted to increased levels at 16 weeks in $SOD1^{G93A}$ mice, with a significant difference for the BD1063 treated compared to WT mice. We also observed a significant increase of CHOP levels in $SOD1^{G93A}$ mice at 8 weeks of age, though no differences were found at 16 weeks of age.

## DISCUSSION

The results of this study demonstrate the beneficial effects of the Sig-1R agonist PRE-084 as well as the Sig-1R antagonist BD1063, on preserving neuromuscular function and attenuating MNs loss in the $SOD1^{G93A}$ mouse model of ALS. The compound SA4503 showed lower effects in ameliorating the progression of the disease. Whereas previous studies have reported that PRE-084 (Mancuso et al., 2012) and SA4503 (Ono et al., 2014) treatment ameliorated the progression and survival of spinal MNs, we report for the first time that a Sig-1R antagonist, such as BD1063, has also neuroprotective effects in preclinical models of ALS. We have recently reported that all PRE-084, SA4503 and BD1063 also prevent MN death in a model of spinal root injury in mice (Gaja-Capdevila et al., 2021), emphasizing the interesting effects of Sig-1R ligands for improving motor neurodegenerative conditions.

Although similar outcomes were obtained in terms of MN preservation *in vitro* in the SCOC with the three Sig-1R ligands tested, there were noticeable differences in the *in vivo* model of ALS. Glutamate excitotoxicity is one of the main pathophysiological mechanisms implicated in ALS. Astrocytes are the main regulators of extracellular glutamate levels and excitatory amino acid transporter 2 (EAAT2) is the main astroglial synaptic glutamate reuptake transporter protein. The loss of EAAT2 has been reported in both ALS patients (Bristol and Rothstein, 1996) and rodent models (Howland et al., 2002). Our *in vitro* results showed that two considered Sig-1R agonists, PRE-084 and SA4503, and the antagonist BD1063 induced protection against chronic excitotoxicity, at the doses of 3–30 μM. Indeed, some reports reveal that binding to Sig-1R prevented neuronal death in *vitro* studies. Our group described that PRE-084 (at 10 μM) protected the SCOC against acute glutamate toxicity (Guzmán-Lenis et al., 2009). Ono and collaborators found that SA4503 (at 10 μM) protected the NSC34 cell line against $SOD1^{G93A}$ and serum free neurotoxicity (Ono et al., 2014). However, those protective effects were inhibited by the co-addition of a Sig-1R antagonist, BD1063 or BD1047, respectively. In our study we assessed each compound alone, without combining them, demonstrating that BD1063 had also similar neuroprotective effects.

Several reports have focused on Sig-1R ligands to modulate ALS progression. PRE-084 (0.25 mg/kg) daily administrated in $SOD1^{G93A}$ from 8 to 16 weeks of age showed neuroprotection, improving MN function and survival and extending the lifespan of $SOD1^{G93A}$ mice (Mancuso et al., 2012). SA4503 (1 mg/kg) treatment from 5 weeks of age extended survival time, but did not affect the onset time in the $SOD1^{G93A}$ mice (Ono et al., 2014). However, we found a delay of 1 week of disease onset compared to untreated mice. In addition, in our study we evaluate the number of MN survival to compare with the other two Sig-1R ligands. Even though SA4503 did not significantly preserve spinal MNs as PRE-084 and BD1063 treatment did, all the pharmacological treatments significantly preserved NMJ innervation in the hindlimb muscles at 16 weeks of age. This is a remarkable result, since NMJ disruption is an early event in ALS pathogenesis (Fischer et al., 2004; Mancuso et al., 2011a). Since SA4503 and PRE-084 had been shown to prolong the lifespan of $SOD1^{G93A}$ mice, a further study is needed to elucidate whether BD1063 has similar effect. Recently, pridopidine, a small molecule that modulates axonal transport deficit and causes a reduction in mutant SOD1 aggregates in the spinal cord of $SOD1^{G93A}$ mice though Sig-1R, was reported to attenuate also NMJ disruption (Ionescu et al., 2019). Taken together, it seems that Sig-1R ligands improve several cellular and histological hallmark pathologies related to ALS.

Despite the three Sig-1R compounds assessed, PRE-084, SA4503 and BD1063, have demonstrated potential to bind the Sig-1R, the neuroprotective effects observed in the $SOD1^{G93A}$ mouse model significantly differed between the three ligands. In the same line, Wang and others compared the Sig-1R ligands SA4503, PRE-084 and pentazocine (PTZ) in a model of severe retinopathy (Wang et al., 2020). *In vitro* results yielded similar outcomes, whereas neither PRE-084 or SA4503 afforded *in vivo* protection comparable to PTZ. A wide range of evidence is now available to support the role of Sig-1R in the treatment of several CNS disorders, such Parkinson disease or ischemia (Nguyen et al., 2017; Haga et al., 2019; Zhao et al., 2019). It is important to note that in this study Sig-1R ligands were classified as agonists or antagonist according to the BiP/Sig-1R association assay, in which the interaction between Sig-1R and the chaperone BiP is used to identify the functional nature (agonistic or antagonistic) of compounds. However, classification of Sig-

1R ligands causes a lot of controversy because some studies revealed different cellular function between compounds considered as agonists of Sig-1R. Indeed, Sig-1R ligands of the same type may act differently in each pathology/degenerative disease, even in opposite way (Tadić et al., 2017). For example, it has been shown that the agonist SA4503 normalized cytosolic $Ca^{2+}$ levels following activation by kainate and by bradykinin in embryonic MNs, whereas PRE-084 (also Sig-1R agonist) did not exert any significant effect (Tadić et al., 2017). Furthermore, we emphasize that the traditional concept of agonist or antagonist is controversial for Sig-1R ligands, that may act as modulators of this receptor promoting activity in different pathways with a delicate balance of effects (for review see Herrando-Grabulosa et al., 2021). Moreover, the total absence of Sig-1R in $SOD1^{G93A}$ ALS mice model accelerates the ALS pathology (Mavlyutov et al., 2013). Therefore, considering the positive results obtained, BD1063 might act pharmacologically as a partial agonist in our animal model. Further comparative studies with other ligands classified as antagonists such as BD1047 and studies related with ligand classification *in vivo* are needed.

A body of evidence has demonstrated the contribution of neuroinflammation, the role of non-neuronal cells including microglia and astrocytes in ALS pathogenesis. Genetic deletion of mutant SOD1 selectively in microglia increased the lifespan of ALS mice, despite the mutant protein was expressed in MNs and all other cell types (Boillée et al., 2006). We observed a reduction in microglia activation following treatment with PRE-084 and with SA4503 at a dose of 0.25 mg/kg (see **Figure 3D**), but not with BD1063. The effect of PRE-084 on reducing the microglial reactivity and improving the MN environment was already found in the $SOD1^{G93A}$ ALS model (Mancuso et al., 2012), as well as in a mouse model of spinal muscular atrophy ($SMA^{2B/-}$), in which PRE-084 treatment mitigated reactive gliosis restoring the altered M1/M2 balance (Cerveró et al., 2018). On the other hand, we did not observe any effect with any of the three Sig-1R ligands assessed on reactive astrogliosis. Contrarily, after spinal root injury, where MN death also occurs, PRE-084 reduced astroglia immunoreactivity (Penas et al., 2011; Gaja-Capdevila et al., 2021). All these studies highlight the role of Sig-1R ligands modulating the neuroinflammatory response.

The etiology underlying the development of ALS remains poorly understood, but abnormal protein aggregation and altered proteostasis are common features of sporadic and familial ALS forms (Medinas et al., 2017). To elucidate the mechanisms through which BD1063 and PRE-084 promote MN preservation we analyzed autophagic flux and ER stress. Autophagy is an intracellular lysosome degradation system responsible for the clearance of cytoplasmic components and organelles. Enhancement of autophagy has been reported in ALS with alterations in several steps. Thus, the level of LC3-II, which is correlated with the extent of autophagosome formation, was found increased in $SOD1^{G93A}$ transgenic mice at symptomatic stage (Morimoto et al., 2007; Tian et al., 2011), as we also found in this study. The marker of the late stage autophagosome, the autophagy adaptor p62, interacts with polyubiquitinated misfolded mutant SOD1 (mSOD1), sequestering mSOD1 into protein inclusions, so fusion of the autophagosome to the lysosome becomes insufficient at the end stage (Tian et al., 2011). Furthermore, autophagy is activated in the ventral spinal cord MNs in sporadic ALS patients, observed by immunostaining for LC3 and p62 (Mizuno et al., 2006; Sasaki, 2011). In our results, we also observed that there was an accumulation of SQSTM1/p62 in the MNs of spinal cord and in the glia cells in $SOD1^{G93A}$ mice. However, there was no difference between untreated group and animals treated with the Sig-1R ligands. It is worth to mention that in ALS the role of autophagy is confusing and it is still unknown whether activation or inhibition of autophagy may influence in the disease progression (Nguyen et al., 2019), and depending on the model used (Medinas et al., 2017).

On the other hand, increased expression of ER stress markers was observed in post-mortem tissues from ALS patients (Hetz et al., 2009), and correspondingly, in this work we observed up-regulation of BiP and XBP1s in the spinal cord of symptomatic $SOD1^{G93A}$ mice. The unfolded protein response (UPR) and the autophagy pathway have been linked (Hetz et al., 2009); thus, XBP1 conditional deletion in the nervous system ameliorated SOD1 mice pathogenesis, through up-regulation of the autophagy pathway boosting the degradation of mSOD1 aggregates. In the context of ALS, the functional significance of ER stress is still unclear, because activating UPR is a protective response to increase protein folding and quality control mechanisms, whereas chronic stress may represent a deleterious signaling due to irreversible disturbance of ER homeostasis. Although we found some differences in the markers analyzed by WB between WT and $SOD1^{G93A}$ mice, we did not observe changes induced by treatment with the Sig-1R ligands, indicating that autophagy and ER stress pathways are not significantly modified through Sig-1R modulation. However, specific immunolabeling analyses of the spinal cord may reveal changes in specific populations, either MNs or glial cells, that may be obscured in protein analyses of the whole spinal cord tissue. Thus, further experiments are needed to elucidate the mechanisms of action by which Sig-1R ligands yield neuroprotective effects.

## DATA AVAILABILITY STATEMENT

The data that support the findings of this study are available from the corresponding author under reasonable request.

## ETHICS STATEMENT

The animal study was reviewed and approved by Universitat Autonoma de Barcelona European Communities Council Directive 2010/63/EU.

## AUTHOR CONTRIBUTIONS

NG-C carried out the experiments and analyzed the data with the technical support of NH. NG-C, MH-G and XN wrote the manuscript. XN and MH-G made the experimental design, supervised the performed experiments, and involved in funding acquisition. All authors have read and agreed to the published version of the manuscript.

## FUNDING

This work was supported by project RTI 2018-096386-B-I00 from Ministerio de Ciencia, Innovación y Universidades of Spain, CIBERNED (CB06/05/1105) and TERCEL (RD16/0011/0014) funds from the Instituto de Salud Carlos III of Spain, cofunded by European Union (ERDF/ESF, "Investing in your future"). NG-C held a predoctoral fellowship of AGAUR, FI-DGR2017.

## ACKNOWLEDGMENTS

We thank Mònica Espejo and Jessica Jaramillo for the technical help.

## SUPPLEMENTARY MATERIAL

The Supplementary Material for this article can be found online at: https://www.frontiersin.org/articles/10.3389/fphar.2021.780588/full#supplementary-material

## REFERENCES

Al-Saif, A., Al-Mohanna, F., and Bohlega, S. (2011). A Mutation in Sigma-1 Receptor Causes Juvenile Amyotrophic Lateral Sclerosis. *Ann. Neurol.* 70 (6), 913–919. doi:10.1002/ana.22534

Almendra, L., Laranjeira, F., Fernández-Marmiesse, A., and Negrão, L. (2018). SIGMAR1 Gene Mutation Causing Distal Hereditary Motor Neuropathy in a Portuguese Family. *Acta Myol.* 37 (1), 2–4.

Bernard-Marissal, N., Médard, J. J., Azzedine, H., and Chrast, R. (2015). Dysfunction in Endoplasmic Reticulum-Mitochondria Crosstalk Underlies SIGMAR1 Loss of Function Mediated Motor Neuron Degeneration. *Brain* 138 (Pt 4), 875–890. doi:10.1093/brain/awv008

Boillée, S., Yamanaka, K., Lobsiger, C. S., Copeland, N. G., Jenkins, N. A., Kassiotis, G., et al. (2006). Onset and Progression in Inherited ALS Determined by Motor Neurons and Microglia. *Science* 312 (5778), 1389–1392. doi:10.1126/science.1123511

Bosco, D. A., and Landers, J. E. (2010). Genetic Determinants of Amyotrophic Lateral Sclerosis as Therapeutic Targets. *CNS Neurol. Disord. Drug Targets* 9 (6), 779–790. doi:10.2174/187152710793237494

Bristol, L. A., and Rothstein, J. D. (1996). Glutamate Transporter Gene Expression in Amyotrophic Lateral Sclerosis Motor Cortex. *Ann. Neurol.* 39 (5), 676–679. doi:10.1002/ana.410390519

Bruna, J., Videla, S., Argyriou, A. A., Velasco, R., Villoria, J., Santos, C., et al. (2018). Efficacy of a Novel Sigma-1 Receptor Antagonist for Oxaliplatin-Induced Neuropathy: A Randomized, Double-Blind, Placebo-Controlled Phase IIa Clinical Trial. *Neurotherapeutics* 15 (1), 178–189. doi:10.1007/s13311-017-0572-5

Cerveró, C., Blasco, A., Tarabal, O., Casanovas, A., Piedrafita, L., Navarro, X., et al. (2018). Glial Activation and Central Synapse Loss, but Not Motoneuron Degeneration, Are Prevented by the Sigma-1 Receptor Agonist PRE-084 in the Smn2B/- Mouse Model of Spinal Muscular Atrophy. *J. Neuropathol. Exp. Neurol.* 77 (7), 577–597. doi:10.1093/jnen/nly033

Edaravone MCI-186 ALS 19 Study Group (2017). Safety and Efficacy of Edaravone in Well Defined Patients with Amyotrophic Lateral Sclerosis: a Randomised, Double-Blind, Placebo-Controlled Trial. *Lancet Neurol.* 16 (7), 505–512. doi:10.1016/S1474-4422(17)30115-1

Fischer, L. R., Culver, D. G., Tennant, P., Davis, A. A., Wang, M., Castellano-Sanchez, A., et al. (2004). Amyotrophic Lateral Sclerosis Is a Distal Axonopathy: Evidence in Mice and Man. *Exp. Neurol.* 185 (2), 232–240. doi:10.1016/j.expneurol.2003.10.004

Gaja-Capdevila, N., Hernández, N., Zamanillo, D., Vela, J. M., Merlos, M., Navarro, X., et al. (2021). Neuroprotective Effects of Sigma 1 Receptor Ligands on Motoneuron Death after Spinal Root Injury in Mice. *Int. J. Mol. Sci.* 22 (13), 6956. doi:10.3390/ijms22136956

Graffmo, K. S., Forsberg, K., Bergh, J., Birve, A., Zetterström, P., Andersen, P. M., et al. (2013). Expression of Wild-type Human Superoxide Dismutase-1 in Mice Causes Amyotrophic Lateral Sclerosis. *Hum. Mol. Genet.* 22 (1), 51–60. doi:10.1093/hmg/dds399

Guzmán-Lenis, M. S., Navarro, X., and Casas, C. (2009). Selective Sigma Receptor Agonist 2-(4-Morpholinethyl)1-Phenylcyclohexanecarboxylate (PRE084) Promotes Neuroprotection and Neurite Elongation through Protein Kinase C (PKC) Signaling on Motoneurons. *Neuroscience* 162 (1), 31–38. doi:10.1016/j.neuroscience.2009.03.067

Haga, H., Matsuo, K., Yabuki, Y., Zhang, C., Han, F., and Fukunaga, K. (2019). Enhancement of ATP Production Ameliorates Motor and Cognitive Impairments in a Mouse Model of MPTP-Induced Parkinson's Disease. *Neurochem. Int.* 129, 104492. doi:10.1016/j.neuint.2019.104492

Hayashi, T., and Su, T. P. (2007). Sigma-1 Receptor Chaperones at the ER-Mitochondrion Interface Regulate Ca(2+) Signaling and Cell Survival. *Cell* 131 (3), 596–610. doi:10.1016/j.cell.2007.08.036

Herrando-Grabulosa, M., Gaja-Capdevila, N., Vela, J. M., and Navarro, X. (2021). Sigma 1 Receptor as a Therapeutic Target for Amyotrophic Lateral Sclerosis. *Br. J. Pharmacol.* 178 (6), 1336–1352. doi:10.1111/bph.15224

Hetz, C., and Saxena, S. (2017). ER Stress and the Unfolded Protein Response in Neurodegeneration. *Nat. Rev. Neurol.* 13 (8), 477–491. doi:10.1038/nrneurol.2017.99

Hetz, C., Thielen, P., Matus, S., Nassif, M., Court, F., Kiffin, R., et al. (2009). XBP-1 Deficiency in the Nervous System Protects against Amyotrophic Lateral Sclerosis by Increasing Autophagy. *Genes Dev.* 23 (19), 2294–2306. doi:10.1101/gad.1830709

Howland, D. S., Liu, J., She, Y., Goad, B., Maragakis, N. J., Kim, B., et al. (2002). Focal Loss of the Glutamate Transporter EAAT2 in a Transgenic Rat Model of SOD1 Mutant-Mediated Amyotrophic Lateral Sclerosis (ALS). *Proc. Natl. Acad. Sci. U S A.* 99 (3), 1604–1609. doi:10.1073/pnas.032539299

Ionescu, A., Gradus, T., Altman, T., Maimon, R., Saraf Avraham, N., Geva, M., et al. (2019). Targeting the Sigma-1 Receptor via Pridopidine Ameliorates Central Features of ALS Pathology in a SOD1G93A Model. *Cell Death Dis* 10 (3), 210. doi:10.1038/s41419-019-1451-2

Langa, F., Codony, X., Tovar, V., Lavado, A., Giménez, E., Cozar, P., et al. (2003). Generation and Phenotypic Analysis of Sigma Receptor Type I (Sigma 1) Knockout Mice. *Eur. J. Neurosci.* 18 (8), 2188–2196. doi:10.1046/j.1460-9568.2003.02950.x

Ludolph, A. C., and Jesse, S. (2009). Evidence-based Drug Treatment in Amyotrophic Lateral Sclerosis and Upcoming Clinical Trials. *Ther. Adv. Neurol. Disord.* 2 (5), 319–326. doi:10.1177/1756285609336399

Mancuso, R., Oliván, S., Osta, R., and Navarro, X. (2011a). Evolution of Gait Abnormalities in SOD1(G93A) Transgenic Mice. *Brain Res.* 1406, 65–73. doi:10.1016/j.brainres.2011.06.033

Mancuso, R., Oliván, S., Rando, A., Casas, C., Osta, R., and Navarro, X. (2012). Sigma-1R Agonist Improves Motor Function and Motoneuron Survival in ALS Mice. *Neurotherapeutics* 9 (4), 814–826. doi:10.1007/s13311-012-0140-y

Mancuso, R., Santos-Nogueira, E., Osta, R., and Navarro, X. (2011b). Electrophysiological Analysis of a Murine Model of Motoneuron Disease. *Clin. Neurophysiol.* 122 (8), 1660–1670. doi:10.1016/j.clinph.2011.01.045

Mavlyutov, T. A., Epstein, M. L., Liu, P., Verbny, Y. I., Ziskind-Conhaim, L., and Ruoho, A. E. (2012). Development of the Sigma-1 Receptor in C-Terminals of Motoneurons and Colocalization with the N,N'-dimethyltryptamine Forming Enzyme, Indole-N-Methyl Transferase. *Neuroscience* 206, 60–68. doi:10.1016/j.neuroscience.2011.12.040

Mavlyutov, T. A., Epstein, M. L., Verbny, Y. I., Huerta, M. S., Zaitoun, I., Ziskind-Conhaim, L., et al. (2013). Lack of Sigma-1 Receptor Exacerbates ALS Progression in Mice. *Neuroscience* 240, 129–134. doi:10.1016/j.neuroscience.2013.02.035

Medinas, D. B., Valenzuela, V., and Hetz, C. (2017). Proteostasis Disturbance in Amyotrophic Lateral Sclerosis. *Hum. Mol. Genet.* 26 (R2), R91–R104. doi:10.1093/hmg/ddx274

Mizuno, Y., Amari, M., Takatama, M., Aizawa, H., Mihara, B., and Okamoto, K. (2006). Immunoreactivities of P62, an Ubiqutin-Binding Protein, in the Spinal Anterior Horn Cells of Patients with Amyotrophic Lateral Sclerosis. *J. Neurol. Sci.* 249 (1), 13–18. doi:10.1016/J.JNS.2006.05.060

Mòdol-Caballero, G., Santos, D., Navarro, X., and Herrando-Grabulosa, M. (2017). Neuregulin 1 Reduces Motoneuron Cell Death and Promotes Neurite Growth in an *In Vitro* Model of Motoneuron Degeneration. *Front. Cell. Neurosci.* 11, 431. doi:10.3389/fncel.2017.00431

Morimoto, N., Nagai, M., Ohta, Y., Miyazaki, K., Kurata, T., Morimoto, M., et al. (2007). Increased Autophagy in Transgenic Mice with a G93A Mutant SOD1 Gene. *Brain Res.* 1167 (1), 112–117. doi:10.1016/J.BRAINRES.2007.06.045

Nguyen, D. K. H., Thombre, R., and Wang, J. (2019). Autophagy as a Common Pathway in Amyotrophic Lateral Sclerosis. *Neurosci. Lett.* 697, 34–48. doi:10.1016/J.NEULET.2018.04.006

Nguyen, L., Lucke-Wold, B. P., Mookerjee, S., Kaushal, N., and Matsumoto, R. R. (2017). Sigma-1 Receptors and Neurodegenerative Diseases: Towards a Hypothesis of Sigma-1 Receptors as Amplifiers of Neurodegeneration and Neuroprotection. *Adv. Exp. Med. Biol.* 964, 133–152. doi:10.1007/978-3-319-50174-1_10

Ono, Y., Tanaka, H., Takata, M., Nagahara, Y., Noda, Y., Tsuruma, K., et al. (2014). SA4503, a Sigma-1 Receptor Agonist, Suppresses Motor Neuron Damage in *In Vitro* and *In Vivo* Amyotrophic Lateral Sclerosis Models. *Neurosci. Lett.* 559, 174–178. doi:10.1016/j.neulet.2013.12.005

Penas, C., Pascual-Font, A., Mancuso, R., Forés, J., Casas, C., and Navarro, X. (2011). Sigma Receptor Agonist 2-(4-morpholinethyl)1 Phenylcyclohexanecarboxylate (Pre084) Increases GDNF and BiP Expression and Promotes Neuroprotection after Root Avulsion Injury. *J. Neurotrauma.* 28 (5), 831–840. doi:10.1089/neu.2010.1674

Penke, B., Fulop, L., Szucs, M., and Frecska, E. (2018). The Role of Sigma-1 Receptor, an Intracellular Chaperone in Neurodegenerative Diseases. *Curr. Neuropharmacol.* 16 (1), 97–116. doi:10.2174/1570159X15666170529104323

Peviani, M., Salvaneschi, E., Bontempi, L., Petese, A., Manzo, A., Rossi, D., et al. (2014). Neuroprotective Effects of the Sigma-1 Receptor (S1R) Agonist PRE-084, in a Mouse Model of Motor Neuron Disease Not Linked to SOD1 Mutation. *Neurobiol. Dis.* 62, 218–232. doi:10.1016/j.nbd.2013.10.010

Ragagnin, A. M. G., Shadfar, S., Vidal, M., Jamali, M. S., and Atkin, J. D. (2019). Motor Neuron Susceptibility in ALS/FTD. *Front. Neurosci.* 13, 532. doi:10.3389/fnins.2019.00532

Reilmann, R., McGarry, A., Grachev, I. D., Savola, J. M., Borowsky, B., Eyal, E., et al. (2019). Safety and Efficacy of Pridopidine in Patients with Huntington's Disease (PRIDE-HD): a Phase 2, Randomised, Placebo-Controlled, Multicentre, Dose-Ranging Study. *Lancet Neurol.* 18 (2), 165–176. doi:10.1016/S1474-4422(18)30391-0

Rosen, D. R., Siddique, T., Patterson, D., Figlewicz, D. A., Sapp, P., Hentati, A., et al. (1993). Mutations in Cu/Zn Superoxide Dismutase Gene Are Associated with Familial Amyotrophic Lateral Sclerosis. *Nature* 362 (6415), 59–62. doi:10.1038/362059a0

Rothstein, J. D., Jin, L., Dykes-Hoberg, M., and Kuncl, R. W. (1993). Chronic Inhibition of Glutamate Uptake Produces a Model of Slow Neurotoxicity. *Proc. Natl. Acad. Sci. U. S. A.* 90 (14), 6591–6595. doi:10.1073/pnas.90.14.6591

Sasaki, S. (2011). Autophagy in Spinal Cord Motor Neurons in Sporadic Amyotrophic Lateral Sclerosis. *J. Neuropathol. Exp. Neurol.* 70 (5), 349–359. doi:10.1097/NEN.0B013E3182160690

Tadić, V., Malci, A., Goldhammer, N., Stubendorff, B., Sengupta, S., Prell, T., et al. (2017). Sigma 1 Receptor Activation Modifies Intracellular Calcium Exchange in the G93AhSOD1 ALS Model. *Neuroscience* 359, 105–118. doi:10.1016/j.neuroscience.2017.07.012

Tian, F., Morimoto, N., Liu, W., Ohta, Y., Deguchi, K., Miyazaki, K., et al. (2011). *In Vivo* optical Imaging of Motor Neuron Autophagy in a Mouse Model of Amyotrophic Lateral Sclerosis. *Autophagy* 7 (9), 985–992. doi:10.4161/AUTO.7.9.16012

Turner, B. J., and Talbot, K. (2008). Transgenics, Toxicity and Therapeutics in Rodent Models of Mutant SOD1-Mediated Familial ALS. *Prog. Neurobiol.* 85 (1), 94–134. doi:10.1016/j.pneurobio.2008.01.001

Urfer, R., Moebius, H. J., Skoloudik, D., Santamarina, E., Sato, W., Mita, S., et al. (2014). Phase II Trial of the Sigma-1 Receptor Agonist Cutamesine (SA4503) for Recovery Enhancement after Acute Ischemic Stroke. *Stroke* 45 (11), 3304–3310. doi:10.1161/STROKEAHA.114.005835

Ververis, A., Dajani, R., Koutsou, P., Aloqaily, A., Nelson-Williams, C., Loring, E., et al. (2019). Distal Hereditary Motor Neuronopathy of the Jerash Type Is Caused by a Novel SIGMAR1 c.500A>T Missense Mutation. *J. Med. Genet.* 57 (3), 178–186. doi:10.1136/jmedgenet-2019-106108

Wang, J., Xiao, H., Barwick, S. R., and Smith, S. B. (2020). Comparison of Sigma 1 Receptor Ligands SA4503 and PRE084 to (+)-Pentazocine in the Rd10 Mouse Model of RP. *Invest. Ophthalmol. Vis. Sci.* 61 (13), 3. doi:10.1167/IOVS.61.13.3

Watanabe, S., Ilieva, H., Tamada, H., Nomura, H., Komine, O., Endo, F., et al. (2016). Mitochondria-associated Membrane Collapse Is a Common Pathomechanism in SIGMAR1- and SOD1-Linked ALS. *EMBO Mol. Med.* 8 (12), 1421–1437. doi:10.15252/emmm.201606403

Zhao, X., Zhu, L., Liu, D., Chi, T., Ji, X., Liu, P., et al. (2019). Sigma-1 Receptor Protects against Endoplasmic Reticulum Stress-Mediated Apoptosis in Mice with Cerebral Ischemia/reperfusion Injury. *Apoptosis* 24 (1–2), 157–167. doi:10.1007/s10495-018-1495-2

**Conflict of Interest:** The authors declare that the research was conducted in the absence of any commercial or financial relationships that could be construed as a potential conflict of interest.

**Publisher's Note:** All claims expressed in this article are solely those of the authors and do not necessarily represent those of their affiliated organizations, or those of the publisher, the editors and the reviewers. Any product that may be evaluated in this article, or claim that may be made by its manufacturer, is not guaranteed or endorsed by the publisher.

frontiers in Neuroscience

MINI REVIEW
published: 24 December 2021
doi: 10.3389/fnins.2021.803885

# The Repression of the HMGB1-TLR4-NF-κB Signaling Pathway by Safflower Yellow May Improve Spinal Cord Injury

*Lu Wang[1†], Benson O. A. Botchway[2†] and Xuehong Liu[1*]*

[1] Department of Histology and Embryology, Medical College, Shaoxing University, Shaoxing, China, [2] Institute of Neuroscience, Zhejiang University School of Medicine, Hangzhou, China

Spinal cord injury (SCI) often results in abnormal sensory and motor functions. Current interventions for SCI in the clinical setting are not effective partly due to the complexity concerning its pathophysiological mechanism. In the wake of SCI, considerable inflammatory cells assemble around the injured area that induces a series of inflammatory reactions and aggravates tissue lesions, thereby affecting the recovery of the damaged nerve tissue. Therefore, the inhibition of inflammatory responses can improve the repair of the injured spinal cord tissue. Safflower Yellow (SY) is the main active ingredient of Carthamus tinctorius. SY has anti-inflammatory effect, as it can inhibit IκBα phosphorylation to impede the NF-κB signaling pathway and p53 nuclear translocation. Besides, SY can limit the release of pro-inflammatory factors, which in turn may alleviate secondary SCI and prevent further complications. In this report, we analyze the pathophysiological mechanism of SCI, the role of inflammatory responses, and how SY interferes with the HMGB1-TLR-4-NF-κB signaling pathway to attenuate inflammatory responses in SCI.

**Keywords: safflower yellow, spinal cord injury, inflammatory reaction, glial scar, the HMGB1-TLR-4-NF-κB signaling pathway**

OPEN ACCESS

***Edited by:***
*Ana Rita Vaz,*
*University of Lisbon, Portugal*

***Reviewed by:***
*Falei Yuan,*
*Zhejiang Ocean University, China*
*María Cámara Quílez,*
*University of A Coruña, Spain*

***Correspondence:**
*Xuehong Liu*
*liuxueh6588@126.com*

*[†]These authors have contributed equally to this work*

***Specialty section:***
*This article was submitted to Neuropharmacology, a section of the journal Frontiers in Neuroscience*

***Received:*** *28 October 2021*
***Accepted:*** *07 December 2021*
***Published:*** *24 December 2021*

***Citation:***
*Wang L, Botchway BOA and Liu X (2021) The Repression of the HMGB1-TLR4-NF-κB Signaling Pathway by Safflower Yellow May Improve Spinal Cord Injury. Front. Neurosci. 15:803885. doi: 10.3389/fnins.2021.803885*

## INTRODUCTION

Spinal cord injury (SCI) is a serious central nervous system injury (Ahuja et al., 2017; Hodgetts and Harvey, 2017). In the past decade, significant number of people have suffered from SCI, with its incidence rate still on the rise. According to the National Spinal Cord Injury Statistical Center, there are about 12,500 new SCI cases each year in the North America (Alizadeh et al., 2019). SCI impairs sensorimotor circuits, culminating in motor and sensory dysfunctions (Hilton and Tetzlaff, 2018; Ganzer et al., 2020). SCI considerably affects an individual's quality of life, and causes an immense social and economic burden (Schattling et al., 2019). To date, the neuron-regenerative repair of SCI continues to be a challenge in the clinical setting (Lindsay et al., 2020). Although several factors could be attributed to this problem, the two main factors concerning the ineffective treatment of SCI are persistent neuro-inflammation and glial scar formation (Yoshizaki et al., 2021). After SCI, astrocytes around the lesion are activated under the action of inflammatory factors. These reactive astrocytes aggregate around the lesion and form glial scars to protect undamaged spinal cord tissue that impedes axonal regeneration (Okada et al., 2018).

Physical trauma can cause the rupture of blood vessels of the spinal cord, damage the blood spinal cord barrier, and result in local bleeding and ischemia, edema, and inflammation, and cell-death (Tran et al., 2018). SCI has two phases: primary SCI and secondary SCI (Hachem et al., 2017). Primary SCI is usually a mechanical damage that causes the destruction of the blood spinal cord barrier and induces local inflammatory responses (Stahel et al., 2012). Secondary injury occurs several hours, days or weeks after the primary SCI. This happens under the action of inflammatory factors, with secondary injury aggravating the damage to the spinal cord tissue (Fan et al., 2013; Tran et al., 2018). Cells within the lesion sites release ATP, DNA, glutamate and free radicals, leading to the formation of a post-damaged cytotoxic environment (Ahuja and Fehlings, 2016). In view of this, inflammatory responses are significant players in secondary SCI (Bethea and Dietrich, 2002).

## THE ROLE OF INFLAMMATORY REACTION IN SCI PROGRESSION

Inflammatory reaction is a protective mechanism of the body. However, excessive and persistent inflammatory microenvironment can hinder spinal cord repair (Li X. et al., 2020). In the wake of SCI, myelin debris are formed, which triggers complement-mediated inflammatory reaction (Kopper and Gensel, 2018). A distinctive consequence of SCI is the upregulation of multiple families of inflammatory molecules that involve cytokines and chemokines (Rice et al., 2007). Inflammatory reaction may aggravate SCI, and cause neuronal cell death, neurodegeneration, and neuroinflammation (Polcyn et al., 2020). Neuroinflammation is one of the key factors that drives secondary SCI (Gaojian et al., 2020). SCI can give rise to a comprehensive inflammatory cascade response induced by the activation of innate immune cells (microglia and astrocyte), leukocytes (neutrophil and macrophage), and neuronal cell death. These cells release pro-inflammatory cytokines, chemokines, free radicals, excitatory toxic amino acids, and nitric oxide (NO) (Hausmann, 2003; Anwar et al., 2016). The pro-inflammatory macrophage and the anti-inflammatory phenotype of the immune cells aggregate at the damage sites to initiate an immune inflammatory response following SCI (Rice et al., 2007; Fan et al., 2020). After SCI, astrocytes play a vital role in SCI pathology through a phenotypic change called reactive cells (Hara et al., 2017). Reactive astrocytes are commonly divided into A1 and A2 types, which are analogous to macrophages M1 and M2 (Liddelow and Barres, 2017; Liddelow et al., 2017; Vismara et al., 2020). Microglia refers to macrophage in the central nervous system (CNS) (Yu et al., 2021). Noteworthy is that invasive macrophages have different functions from microglia (Milich et al., 2019). Classical activated neuro-inflammatory microglia can induce the production of A1 reactive astrocytes (Liddelow et al., 2017). Activated macrophage/microglia are polarized into M1 and M2 sub-types, exhibiting pro-inflammatory and anti-inflammatory effects following SCI (Ransohoff, 2016; Lin et al., 2020). For instance, M1 phenotype generate pro-inflammatory cytokines (such as TNF-α and IL-1β), while M2 phenotype may curtail inflammation via IL-4 and IL-10 cytokines (Jiang et al., 2017). The ratio of M1 to M2 influences the microenvironment of the spinal cord tissue after injury, as the augmentation of M1 phenotype after SCI will negatively affect the injury repair (Fan et al., 2018). Besides, reactive oxygen species (ROS) can lead to cell and tissue dysfunction through the oxidation of DNA and cell membranes, which further causes inflammation (Hervera et al., 2018; Kertmen et al., 2018). SCI comprises of three stages; acute stage, acute secondary stage, and chronic stage (Nukolova et al., 2018).

### The Role of Inflammatory Reaction in Acute Spinal Cord Injury

Acute SCI is one of the stages of SCI. At this stage, cell fragments are formed and intracellular proteins are released as potent inflammatory stimuli. These injury-exposed fragment signals, also known as damage-associated molecular patterns (DAMPs), activate pattern recognition receptors (PRRs) on inflammatory cells after SCI (Orr and Gensel, 2018). The acute SCI includes primary and secondary injuries. Oxidative stress leads to the release of cytoplasmic components and mitochondrial dysfunction in primary SCI. Secondary injury begins as early as minutes after the primary SCI, and involves spinal cord ischemia and free radical-mediated peroxidation (Albayar et al., 2019; Pinchi et al., 2019). Oxidative stress is the main cause of neuronal tissue damage, as it can initiate cytotoxicity by enhancing lipid peroxidation in damaged neuronal tissue (Guan et al., 2020). In particular, lipid peroxidation is extremely important in acute SCI (Kwon et al., 2004). Secondary SCI has inflammatory reaction that leads to edema and hemorrhage, which in turn aggravates the injured area. Macrophages, neutrophils and T-cells invade damaged sites, leading to blood-brain barrier disruption (Lambrechts and Cook, 2021; **Figure 1**). The first infiltrated inflammatory cells are neutrophils, which peak around day 1 after acute SCI. Neutrophils decrease within 1 week of injury, while monocytes increase in the spinal cord. Similarly, T and B-lymphocytes being to gradually increase during the first week after injury (Wu et al., 2019; **Figure 1**). Subsequent to acute SCI, ischemia leads to the formation of an acidic environment. Moreover, macrophage infiltration and the activation of microglia further promote the release of pro-inflammatory factors, including TNF-α, IL-1β, and interleukin 6 (IL-6) (Xi et al., 2021; **Figure 1**). The microglia are the key immune cell type in CNS (DiSabato et al., 2016). Under normal circumstances, microglia perform immune defense mechanisms, regulate neuronal and synaptic activities, secrete nutritional factors and support neuronal survival and axon growth in CNS (DiSabato et al., 2016; Gaudet and Fonken, 2018). The microglia can be strongly activated and carry out double-edged tasks following SCI (Gaudet and Fonken, 2018). The microglial and macrophages can have beneficial roles in acute SCI. A large number of macrophages and microglia are recruited in the lesion epicenter within 7 days after SCI (Stirling and Yong, 2008). Activated microglial and macrophages secrete products that promote

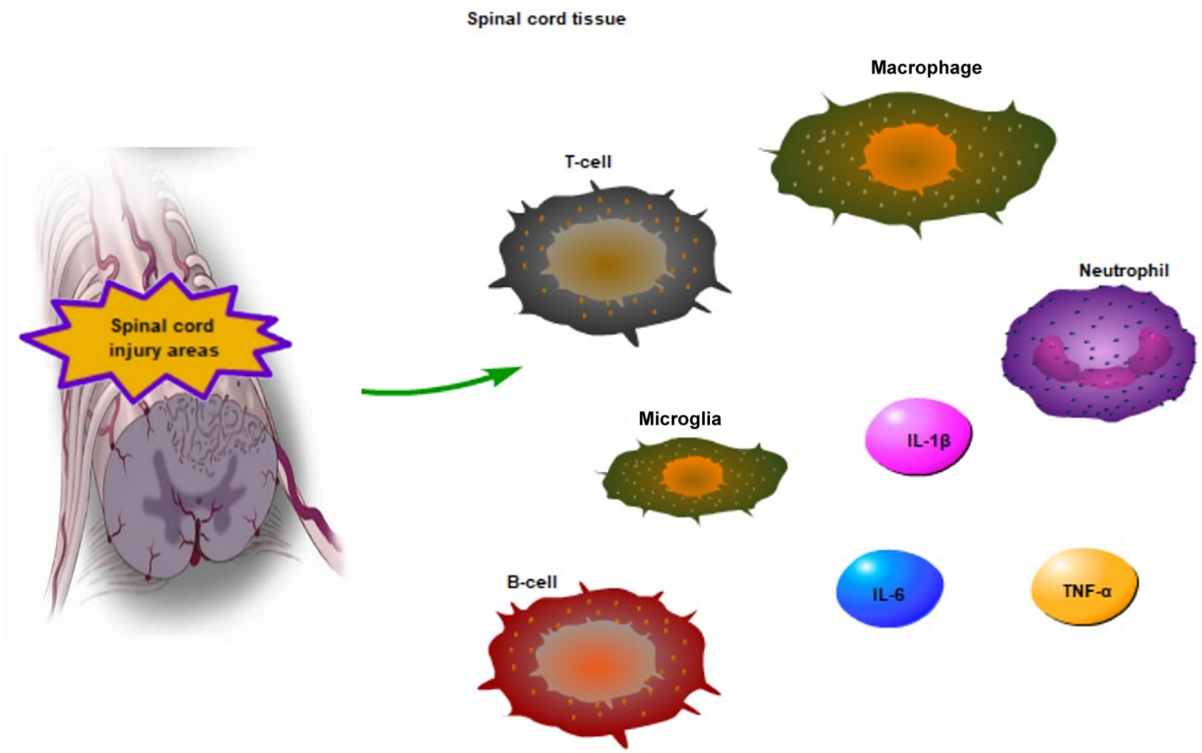


**FIGURE 1 |** The inflammatory reaction in acute SCI areas. The macrophage, T-cell, neutrophil invade damaged sites following SCI, T and B cells being to gradually increase within 1 week of injury. Moreover, macrophage infiltration and the activation of microglia regulate the release of pro-inflammatory factors, such as TNF-α, IL-6, and IL-1β in acute SCI.

axon growth. Zymosan-activated macrophages create a growth-microenvironment to increase the density of axons *in vivo* (Gensel et al., 2009). A study has showed that M1 phenotype cells can produce proteases and oxidative metabolities to kill neurons and glia, conversely, M2 phenotype cells can contribute to tissue repair via downregulating inflammatory responses in SCI (Kigerl et al., 2009). Acute SCI leads to chronic SCI, and chronic complications after acute SCI are detrimental (Chen et al., 2020).

## The Role of Inflammatory Reaction in Chronic Spinal Cord Injury

Systemic inflammation is key to chronic SCI (Diaz et al., 2021). Systemic inflammatory markers, such as c-reactive protein (CRP) and IL-6, are increased after chronic SCI (Hart et al., 2016; Lynch et al., 2017; Dugan et al., 2021). Chronic SCI can intensify IL-2 and TNF-α levels to upregulate the NF-κB transcriptional activity (Yarar-Fisher et al., 2016). Microglia appears to be strongly related to chronic neuroinflammation after SCI, and microglial cells expressing TNF-α may transform the polarization of astrocytes to neurotoxic phenotypes (Yoshizaki et al., 2021). Besides, natural killer cell numbers, cytotoxic activity levels, and T-lymphocytes in patients with chronic SCI exhibit abnormal function (**Figure 2**). There are indications that $CD4^+$ T cells are increased in the spinal tissue (Monahan et al., 2015; Herman et al., 2018). Therefore, several factors such as IL-2, IL-6, CRP, TNF-α and $CD4^+$T cells can be activated, however, NK cells can be inhibited in chronic SCI (**Figure 2**). Chronic SCI is a period of stabilization and low activity, where the nerve function around the injured areas gradually decreases (Rodríguez-Barrera et al., 2017).

# SAFFLOWER YELLOW CAN INHIBIT INFLAMMATORY REACTION

## The Biological Role of Safflower Yellow

Carthamus tinctorius is a plant of Compositae or Asteraceae family (Delshad et al., 2018). Safflower is the dry flower of Cathamus tinctorius, a commonly used traditional Chinese medicine that has been reported to improve trauma, gynecological disease, cardiovascular conditions, blood circulation, and remove blood stasis (Wang et al., 2011). SY is the effective component of safflower water-soluble extract, with its main component being hydroxysafflower yellow (Asgarpanah and Kazemivash, 2013; Li H. et al., 2020; Wang et al., 2020). The molecular formula of SY is C60H74O38, contains hydroxyl groups, carbonyl groups, aromatic rings and conjugated carbonyl groups. Hydroxysafflor yellow A-4′-O-b-D-glucopyranoside and 3′-hydroxyhydroxysafflor yellow A are separated from the SY (Zhang et al., 2020). SY has anti-infection and anti-inflammatory

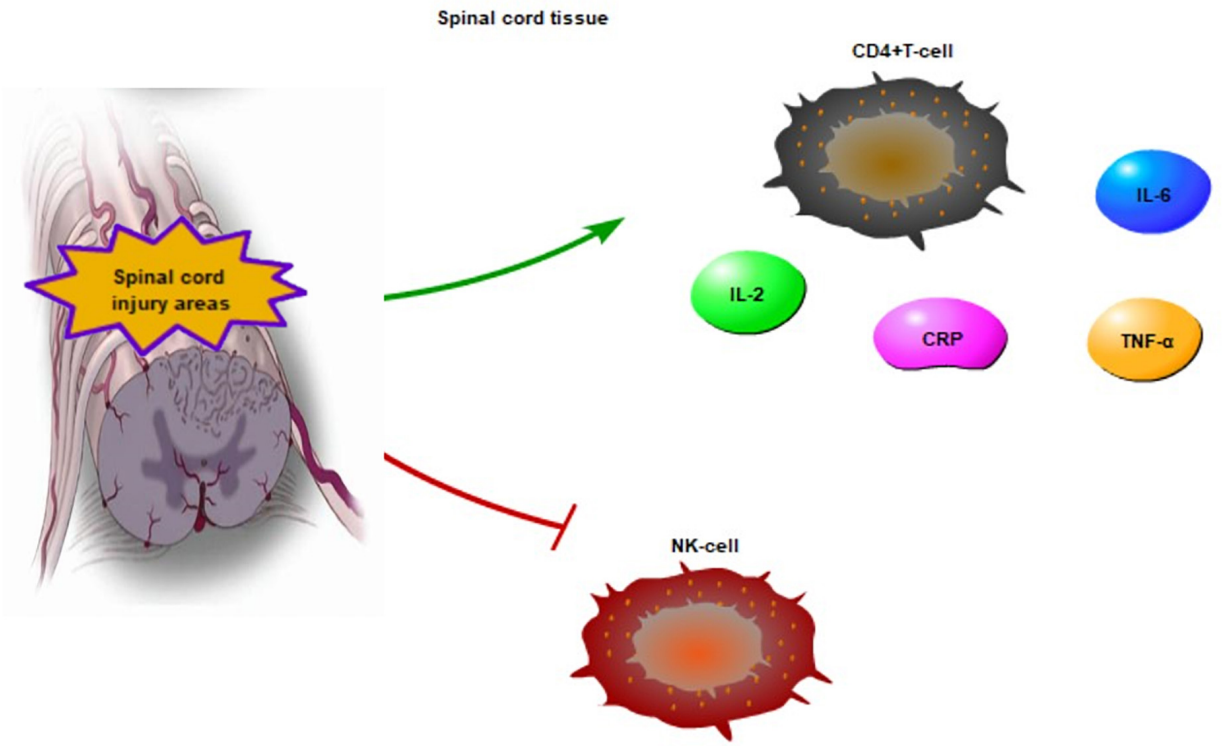


**FIGURE 2 |** The inflammatory reaction in chronic SCI areas. CD4 + T-cell, CRP, IL-6 are increased, IL-2 and TNF-α are activated to enhance the NF-κB transcriptional activity in chronic SCI. Meanwhile, the activity of NK cell is inhibited.

properties, and has been used for the clinical treatment of patients who suffer from severe sepsis and septic shock (Li et al., 2016). Furthermore, SY has anti-fibrotic (Wang et al., 2011), anti-oxidative (Wang et al., 2020), anti-coagulative (Sun et al., 2010), anti-obesity (Yan et al., 2020), anti-calcium-antagonist (Du et al., 2019), and neuroprotective effects (Pang et al., 2020). In recent times, the mediation of SY in inflammation has attracted significant attention.

## Safflower Yellow Inhibits the HMGB1-TLR4-NF-κB Signaling Pathway

High mobility group box 1 protein (HMGB1) is a nuclear non-histone DNA-binding protein expressed in all nuclear animal cells, and can be used as a potent inflammatory late mediator when passively secreted during inflammatory response (Scaffidi et al., 2010; Li et al., 2015). HMGB1, which can stimulate neuroinflammatory responses under deleterious conditions, is a damage-associated molecular pattern (DAMP) molecule (Yu et al., 2019). HMGB1 can induce intracellular signaling pathway by interacting with at least three pattern recognition receptors: Toll-like receptor-2 (TLR-2) and TLR-4, and the receptor for advanced glycation products (PAGE) (van Zoelen et al., 2009). Among them, TLR-2 and TLR-4 are key players, while PAGE has a minimal role (Park et al., 2004). The migration ability of breast cancer cells is closely related to HMGB1 (Lv et al., 2016). HMGB1 can be released from the nucleus to the cytoplasm under damage conditions to activate TLR4 signaling pathway and play a biological role (Lv et al., 2016; Antón et al., 2017; Xu et al., 2020). HMGB1 and TLR-4 interactions may lead to NF-κB upregulation, which results in producing and releasing inflammatory cytokines, such as IL-1β, TNF-α and IL-6 (Zhang et al., 2007; Kang et al., 2015; Wang et al., 2015; Xu et al., 2020; **Figure 3**). The HMGB1-TLR4-NF-κB signaling pathway is an inflammatory signaling pathway that mediates multiple inflammation-related pathways (Sun et al., 2019). NF-κB is a well-established inflammatory transcription factors produced by almost all animal cells. More importantly, the NF-κB signaling pathway has a significant number of target genes that can regulate a variety of biological functions, including inflammation, apoptosis, cell adhesion, cell stress response, and immunity (Jing and Lee, 2014). More importantly, the NF-κB signaling pathway is instrumental in inflammation (Ma and Hottiger, 2016). There is a positive feedback mechanism between inflammation and the NF-κB signaling pathway after SCI (Karova et al., 2019). Exposing neutrophils or macrophages to HMGB1 can lead to enhanced NF-κB signaling pathway and pro-inflammatory cytokine expression (Park et al., 2004). Interestingly, SY can improve inflammatory response and exert effect on inflammatory factors, like TNF-α, IL-1(IL-1β), and IL-6 (Zhou et al., 2018; Du et al., 2019; **Figure 3**). Furthermore, SY can inhibit the activation of the NF-κB signaling pathway by suppressing IκBα phosphorylation and cell nucleus translocation of p65 (Li et al., 2013; **Figure 3**). Moreover, SY may suppress the NF-κB signaling

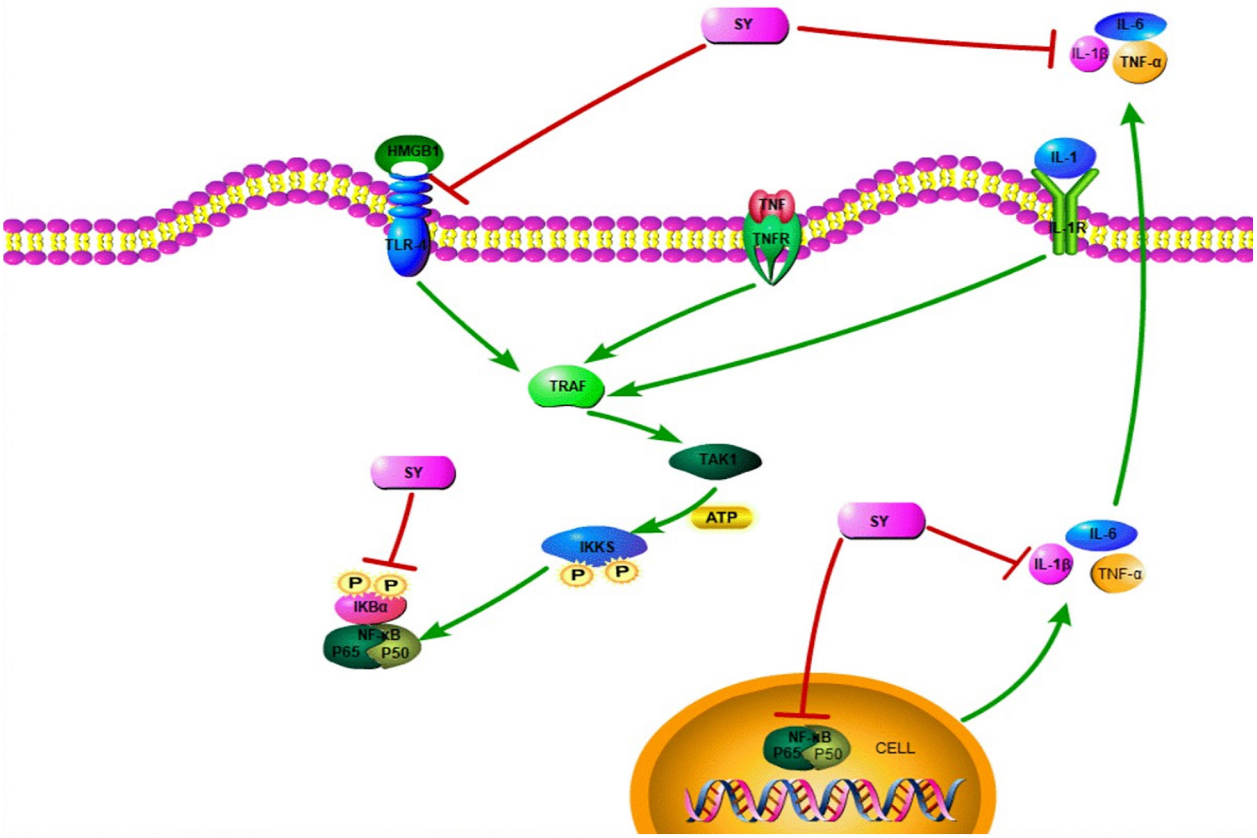


**FIGURE 3 |** The role of SY in SCI. SY moderates the release of pro-inflammatory factors (TNF-α, IL-6, and IL-1β). Additionally, SY inhibits IκBα phosphorylation and p53 nuclear translocation. Thus, SY can suppress the TLR-4-NF-κB signaling pathway.

**TABLE 1 |** Beneficial effects of SY in diseases.

| Diseases | Species | Doses | Outcome | References |
|---|---|---|---|---|
| Pulmonary fibrosis | Rats | 0.25 mg/ml | SY can inhibit α-SMA mRNA expression in lung fibroblast. | Wang et al., 2011 |
| Osteoarthritis | Rats | 50 μg/ml | SY can regulate NF-κB/SIRT1/AMPK signaling pathway, and prevent inflammation. | Wang et al., 2020 |
| Focal cerebral | Rats | 8 mg/kg | HSYA suppresses thrombin formation and inflammatory responses. | Sun et al., 2010 |
| Obesity | Mice | 120 mg/kg | SY may improve insulin sensitivity. | Yan et al., 2020 |
| Cerebral ischemia | Rats | 8 mg/kg | SYB can activate AMPK and reduce NF-κB mediated inflammation. | Du et al., 2019 |
| Alzheimer's disease (AD) | Mice | 30 mg/kg | SY can improve learning and memory functions. | Pang et al., 2020 |
| CNS | Cell | 80 μg/ml | SY can inhibit inflammatory response. | Yang et al., 2016 |
| AD | Mice | 100 mg/kg | SY can improve AD by decreasing the expression of proteins related to β-amyloid formation. | Shi et al., 2018 |
| ROS | Cell | / | SYB can effectively reduce ROS generation by decreasing NADPH oxidase activity. | Wang et al., 2013 |
| Bone fracture | Cell | 18 μg/ml | SY can promote angiogenesis to improve bone fracture. | Tang et al., 2018 |
| Obesity/diabetic | Mice | 80 μg/ml | SY can reduce body fat mass and improve insulin sensitivity. | Zhu et al., 2016 |
| Cardiovascular disease (CVD) | Mice | 25 μg/ml | SY has an effect on angiotensin II-induced adventitial fibroblast proliferation. | Liu et al., 2014 |
| CVD | Cell | 20 μg/ml | HSYA can decrease PDGF-BB-induced proliferation, migration, and Akt signaling pathway. | Song et al., 2014 |
| AD | Cell | 10 μg/ml | HSYA can inhibit neuroinflammation by reducing Aβ1-42-induced cytotoxicity in BV-2 cells. | Zhang et al., 2014 |
| SCI | Rabbits | 90 μg/ml | SY can improve SCI by enhancing Bcl-2 expression and inhibiting Bax and caspase-3 activation. | Zhou et al., 2013 |

pathway by restricting the TNF-α (Wang et al., 2020). SY has a significant role in the minimization of ROS level (Lu et al., 2019). Also, SY can downregulate the TLR-4 expression (Yang et al., 2015; **Figure 3**). Besides, SY can transform microglia from inflammatory M1 to anti-inflammatory M2, which then plays an anti-inflammatory role by hindering the TLR-4-NF-κB signaling pathway (Yang et al., 2016). SY has been widely studied in various diseases, most especially, SCI (**Table 1**).

## CONCLUDING REMARKS

Inflammation plays an important role in SCI, which have been expounded in this report. The NF-κB is a central transcription factor of inflammatory mediators, and the neuroinflammatory response caused by activated microglia through the NF-κB pathway is a consequential contributing factor to secondary injury (Chen et al., 2018). The HMGB1-TLR-4-NF-κB signaling is an inflammatory pathway upregulated during SCI. Particularly, HMGB1 and TLR-4 interactions can lead to NF-κB upregulation, which in turn results in the formation and release of inflammatory cytokines at increasing levels in secondary SCI (Zhang et al., 2007; Wang et al., 2015). SY has several pharmacological effects, such as anti-inflammation and anti-oxidation. SY may mitigate the release of pro-inflammatory factors, TNF-α, IL-1β, and IL-6. Far more, SY can inhibit the HMGB1-TLR-4-NF-κB signaling pathway to ameliorate inflammatory response and offer protection to the spinal cord in the event of an injury. Notwithstanding, the specific molecular mechanism of HMGB-TLR-4-NF-κB following SCI are presently unclear, and warrants further thorough investigations using appropriate experimental models.

## AUTHOR CONTRIBUTIONS

XL designed the study. LW, BOAB, and XL prepared the first draft of the manuscript and revised the manuscript. All authors approved the final manuscript.

## FUNDING

This work was supported by the Natural Science Foundation of Zhejiang Province (no. LY19H170001).

## REFERENCES

Ahuja, C. S., and Fehlings, M. (2016). concise review: bridging the gap: novel neuroregenerative and neuroprotective strategies in spinal cord injury. *Stem Cells Transl. Med.* 5, 914–924. doi: 10.5966/sctm.2015-0381

Ahuja, C. S., Nori, S., Tetreault, L., Wilson, J., Kwon, B., Harrop, J., et al. (2017). Traumatic spinal cord injury-repair and regeneration. *Neurosurgery* 80, S9–S22. doi: 10.1093/neuros/nyw080

Albayar, A. A., Roche, A., Swiatkowski, P., Antar, S., Ouda, N., Emara, E., et al. (2019). Biomarkers in spinal cord injury: prognostic insights and future potentials. *Front. Neurol.* 10:27. doi: 10.3389/fneur.2019.00027

Alizadeh, A., Dyck, S. M., and Karimi-Abdolrezaee, S. (2019). Traumatic spinal cord injury: an overview of pathophysiology, models and acute injury mechanisms. *Front. Neurol.* 10:282. doi: 10.3389/fneur.2019.00282

Antón, M., Alén, F., Gómez de Heras, R., Serrano, A., Pavón, F. J., Leza, J. C., et al. (2017). Oleoylethanolamide prevents neuroimmune HMGB1/TLR4/NF-kB danger signaling in rat frontal cortex and depressive-like behavior induced by ethanol binge administration. *Addict. Biol.* 22, 724–741. doi: 10.1111/adb.12365

Anwar, M. A., Al Shehabi, T. S., and Eid, A. H. (2016). Inflammogenesis of secondary spinal cord injury. *Front. Cell Neurosci.* 10:98. doi: 10.3389/fncel.2016.00098

Asgarpanah, J., and Kazemivash, N. (2013). Phytochemistry, pharmacology and medicinal properties of *Carthamus tinctorius* L. *Chin. J. Integr. Med.* 19, 153–159. doi: 10.1007/s11655-013-1354-5

Bethea, J. R., and Dietrich, W. D. (2002). Targeting the host inflammatory response in traumatic spinal cord injury. *Curr. Opin. Neurol.* 15, 355–360. doi: 10.1097/00019052-200206000-00021

Chen, G., Zhou, Z., Sha, W., Wang, L., Yan, F., Yang, X., et al. (2020). A novel CX3CR1 inhibitor AZD8797 facilitates early recovery of rat acute spinal cord injury by inhibiting inflammation and apoptosis. *Int. J. Mol. Med.* 45, 1373–1384. doi: 10.3892/ijmm.2020.4509

Chen, S., Ye, J., Chen, X., Shi, J., Wu, W., Lin, W., et al. (2018). Valproic acid attenuates traumatic spinal cord injury-induced inflammation via STAT1 and NF-κB pathway dependent of HDAC3. *J. Neuroinflammation* 15:150. doi: 10.1186/s12974-018-1193-6

Delshad, E., Yousefi, M., Sasannezhad, P., Rakhshandeh, H., and Ayati, Z. (2018). Medical uses of *Carthamus tinctorius* L. (Safflower): a comprehensive review from traditional medicine to modern medicine. *Electron. Phys.* 10, 6672–6681. doi: 10.19082/6672

Diaz, D., Lopez-Dolado, E., Haro, S., Monserrat, J., Martinez-Alonso, C., Balomeros, D., et al. (2021). Systemic inflammation and the breakdown of intestinal homeostasis are key events in chronic spinal cord injury patients. *Int. J. Mol. Sci.* 22:744. doi: 10.3390/ijms22020744

DiSabato, D. J., Quan, N., and Godbout, J. P. (2016). Neuroinflammation: the devil is in the details. *J. Neurochem.* 139 Suppl 2(Suppl. 2), 136–153. doi: 10.1111/jnc.13607

Du, S., Deng, Y., Yuan, H., and Sun, Y. (2019). Safflower yellow B protects brain against cerebral ischemia reperfusion injury through AMPK/NF-kB pathway. *Evid. Based Compl. Alternat. Med.* 2019:7219740. doi: 10.1155/2019/7219740

Dugan, E. A., Schachner, B., Jergova, S., and Sagen, J. (2021). Intensive locomotor training provides sustained alleviation of chronic spinal cord injury-associated neuropathic pain: a two-year pre-clinical study. *J. Neurotrauma* 38, 789–802. doi: 10.1089/neu.2020.7378

Fan, B., Wei, Z., Yao, X., Shi, G., Cheng, X., Zhou, X., et al. (2018). Microenvironment imbalance of spinal cord injury. *Cell Transplant.* 27, 853–866. doi: 10.1177/0963689718755778

Fan, H., Liu, X., Tang, H. B., Xiao, P., Wang, Y. Z., and Ju, G. (2013). Protective effects of batroxobin on spinal cord injury in rats. *Neurosci. Bull.* 29, 501–508. doi: 10.1007/s12264-013-1354-7

Fan, H., Tang, H. B., Chen, Z., Wang, H. Q., Zhang, L., Jiang, Y., et al. (2020). Inhibiting HMGB1-RAGE axis prevents pro-inflammatory macrophages/microglia polarization and affords neuroprotection after spinal cord injury. *J. Neuroinflammation* 17:295. doi: 10.1186/s12974-020-01973-4

Ganzer, P. D., Colachis, S. C. IV, Schwemmer, M. A., Friedenberg, D. A., Dunlap, C. F., Swiftney, C. E., et al. (2020). Restoring the sense of touch using a sensorimotor demultiplexing neural interface. *Cell* 181, 763–773.e12. doi: 10.1016/j.cell.2020.03.054

Gaojian, T., Dingfei, Q., Linwei, L., Xiaowei, W., Zheng, Z., Wei, L., et al. (2020). Parthenolide promotes the repair of spinal cord injury by modulating M1/M2 polarization via the NF-κB and STAT 1/3 signaling pathway. *Cell Death Discov.* 6:97. doi: 10.1038/s41420-020-00333-8

Gaudet, A. D., and Fonken, L. K. (2018). Glial cells shape pathology and repair after spinal cord injury. *Neurotherapeutics* 15, 554–577. doi: 10.1007/s13311-018-0630-7

Gensel, J. C., Nakamura, S., Guan, Z., van Rooijen, N., Ankeny, D. P., and Popovich, P. G. (2009). Macrophages promote axon regeneration with concurrent neurotoxicity. *J. Neurosci.* 29, 3956–3968. doi: 10.1523/JNEUROSCI.3992-08.2009

Guan, B., Chen, R., Zhong, M., Liu, N., and Chen, Q. (2020). Protective effect of oxymatrine against acute spinal cord injury in rats via modulating oxidative stress, inflammation and apoptosis. *Metab. Brain Dis.* 35, 149–157. doi: 10.1007/s11011-019-00528-8

Hachem, L. D., Ahuja, C. S., and Fehlings, M. G. (2017). Assessment and management of acute spinal cord injury: from point of injury to rehabilitation. *J. Spinal Cord Med.* 40, 665–675. doi: 10.1080/10790268.2017.1329076

Hara, M., Kobayakawa, K., Ohkawa, Y., Kumamaru, H., Yokota, K., Saito, T., et al. (2017). Interaction of reactive astrocytes with type I collagen induces astrocytic scar formation through the integrin-N-cadherin pathway after spinal cord injury. *Nat. Med.* 23, 818–828. doi: 10.1038/nm.4354

Hart, J. E., Morse, L., Tun, C. G., Brown, R., and Garshick, E. (2016). Cross-sectional associations of pulmonary function with systemic inflammation and oxidative stress in individuals with chronic spinal cord injury. *J. Spinal Cord Med.* 39, 344–352. doi: 10.1179/2045772315Y.0000000045

Hausmann, O. N. (2003). Post-traumatic inflammation following spinal cord injury. *Spinal Cord* 41, 369–378. doi: 10.1038/sj.sc.3101483

Herman, P., Stein, A., Gibbs, K., Korsunsky, I., Gregersen, P., and Bloom, O. (2018). Persons with chronic spinal cord injury have decreased natural killer cell and increased toll-like receptor/inflammatory gene expression. *J. Neurotrauma* 35, 1819–1829. doi: 10.1089/neu.2017.5519

Hervera, A., De Virgiliis, F., Palmisano, I., Zhou, L., Tantardini, E., Kong, G., et al. (2018). Reactive oxygen species regulate axonal regeneration through the release of exosomal NADPH oxidase 2 complexes into injured axons. *Nat. Cell Biol.* 20, 307–319. doi: 10.1038/s41556-018-0039-x

Hilton, B. J., and Tetzlaff, W. (2018). A brainstem bypass for spinal cord injury. *Nat. Neurosci.* 21, 457–458. doi: 10.1038/s41593-018-0099-z

Hodgetts, S. I., and Harvey, A. R. (2017). Neurotrophic Factors used to treat spinal cord injury. *Vitam. Horm.* 104, 405–457. doi: 10.1016/bs.vh.2016.11.007

Jiang, J., Luo, Y., Qin, W., Ma, H., Li, Q., Zhan, J., et al. (2017). Electroacupuncture suppresses the NF-κB signaling pathway by upregulating cylindromatosis to alleviate inflammatory injury in cerebral ischemia/reperfusion rats. *Front. Mol. Neurosci.* 10:363. doi: 10.3389/fnmol.2017.00363

Jing, H., and Lee, S. (2014). NF-κB in cellular senescence and cancer treatment. *Mol. Cells* 37, 189–195. doi: 10.14348/molcells.2014.2353

Kang, N., Hai, Y., Yang, J., Liang, F., and Gao, C. J. (2015). Hyperbaric oxygen intervention reduces secondary spinal cord injury in rats via regulation of HMGB1/TLR4/NF-κB signaling pathway. *Int. J. Clin. Exp. Pathol.* 8, 1141–1153.

Karova, K., Wainwright, J. V., Machova-Urdzikova, L., Pisal, R. V., Schmidt, M., Jendelova, P., et al. (2019). Transplantation of neural precursors generated from spinal progenitor cells reduces inflammation in spinal cord injury via NF-κB pathway inhibition. *J Neuroinflammation.* 16, 12. doi: 10.1186/s12974-019-1394-7

Kertmen, H., Celikoglu, E., Ozturk, O. C., Gürer, B., Bozkurt, H., Kanat, M. A., et al. (2018). Comparative effects of methylprednisolone and tetracosactide (ACTH1-24) on ischemia/reperfusion injury of the rabbit spinal cord. *Arch. Med. Sci.* 14, 1459–1470. doi: 10.5114/aoms.2017.65650

Kigerl, K. A., Gensel, J. C., Ankeny, D. P., Alexander, J. K., Donnelly, D. J., and Popovich, P. G. (2009). Identification of two distinct macrophage subsets with divergent effects causing either neurotoxicity or regeneration in the injured mouse spinal cord. *J. Neurosci.* 29, 13435–13444. doi: 10.1523/JNEUROSCI.3257-09.2009

Kopper, T. J., and Gensel, J. C. (2018). Myelin as an inflammatory mediator: myelin interactions with complement, macrophages, and microglia in spinal cord injury. *J. Neurosci. Res.* 96, 969–977. doi: 10.1002/jnr.24114

Kwon, B. K., Tetzlaff, W., Grauer, J. N., Beiner, J., and Vaccaro, A. R. (2004). Pathophysiology and pharmacologic treatment of acute spinal cord injury. *Spine J.* 4, 451–464. doi: 10.1016/j.spinee.2003.07.007

Lambrechts, M. J., and Cook, J. L. (2021). Nonsteroidal anti-inflammatory drugs and their neuroprotective role after an acute spinal cord injury: a systematic review of animal models. *Glob. Spine J.* 11, 365–377. doi: 10.1177/2192568220901689

Li, H., Kan, B., Song, L., Liu, Y., and Jian, X. (2020). Role of the Hippo signaling pathway in safflower yellow pigment treatment of paraquat-induced pulmonary fibrosis. *J. Int. Med. Res.* 48:300060520905425. doi: 10.1177/0300060520905425

Li, J., Zhang, S., Lu, M., Chen, Z., Chen, C., Han, L., et al. (2013). Hydroxysafflor yellow a suppresses inflammatory responses of BV2 microglia after oxygen-glucose deprivation. *Neurosci. Lett.* 535, 51–56. doi: 10.1016/j.neulet.2012.12.056

Li, L., Ling, Y., Huang, M., Yin, T., Gou, S. M., Zhan, N. Y., et al. (2015). Heparin inhibits the inflammatory response induced by LPS and HMGB1 by blocking the binding of HMGB1 to the surface of macrophages. *Cytokine* 72, 36–42. doi: 10.1016/j.cyto.2014.12.010

Li, X., Yu, Z., Zong, W., Chen, P., Li, J., Wang, M., et al. (2020). Deficiency of the microglial Hv1 proton channel attenuates neuronal pyroptosis and inhibits inflammatory reaction after spinal cord injury. *J. Neuroinflammation* 17:263. doi: 10.1186/s12974-020-01942-x

Li, X. J., Wang, R. R., Kang, Y., Liu, J., Zuo, Y. X., Zeng, X. F., et al. (2016). Effects of safflower yellow on the treatment of severe sepsis and septic shock: a randomized controlled clinical trial. *Evid Based Compl. Alternat. Med.* 2016:3948795. doi: 10.1155/2016/3948795

Liddelow, S. A., and Barres, B. A. (2017). Reactive astrocytes: production, function, and therapeutic potential. *Immunity* 46, 957–967. doi: 10.1016/j.immuni.2017.06.006

Liddelow, S. A., Guttenplan, K. A., Clarke, L. E., Bennett, F. C., Bohlen, C. J., Schirmer, L., et al. (2017). Neurotoxic reactive astrocytes are induced by activated microglia. *Nature* 541, 481–487. doi: 10.1038/nature21029

Lin, J., Huang, Z., Liu, J., Huang, Z., Liu, Y., Liu, Q., et al. (2020). Neuroprotective effect of ketone metabolism on inhibiting inflammatory response by regulating macrophage polarization after acute cervical spinal cord injury in rats. *Front. Neurosci.* 14:583611. doi: 10.3389/fnins.2020.583611

Lindsay, S. L., McCanney, G. A., Willison, A. G., and Barnett, S. C. (2020). Multi-target approaches to CNS repair: olfactory mucosa-derived cells and heparan sulfates. *Nat. Rev. Neurol.* 16, 229–240. doi: 10.1038/s41582-020-0311-0

Liu, Y., Tian, X., Cui, M., and Zhao, S. (2014). Safflower yellow inhibits angiotensin II-induced adventitial fibroblast proliferation and migration. *J. Pharmacol. Sci.* 126, 107–114. doi: 10.1254/jphs.14055fp

Lu, Q. Y., Ma, J. Q., Duan, Y. Y., Sun, Y., Yu, S., Li, B., et al. (2019). Carthamin yellow protects the heart against ischemia/reperfusion injury with reduced reactive oxygen species release and inflammatory response. *J. Cardiovasc. Pharmacol.* 74, 228–234. doi: 10.1097/FJC.0000000000000710

Lv, W., Chen, N., Lin, Y., Ma, H., Ruan, Y., Li, Z., et al. (2016). Macrophage migration inhibitory factor promotes breast cancer metastasis via activation of HMGB1/TLR4/NF kappa B axis. *Cancer Lett.* 375, 245–255. doi: 10.1016/j.canlet.2016.02.005

Lynch, M., Duffell, L., Sandhu, M., Srivatsan, S., Deatsch, K., Kessler, A., et al. (2017). Effect of acute intermittent hypoxia on motor function in individuals with chronic spinal cord injury following ibuprofen pretreatment: a pilot study. *J. Spinal Cord Med.* 40, 295–303. doi: 10.1080/10790268.2016.1142137

Ma, B., and Hottiger, M. O. (2016). Crosstalk between Wnt/β-Catenin and NF-κB signaling pathway during Inflammation. *Front. Immunol.* 7:378. doi: 10.3389/fimmu.2016.00378

Milich, L. M., Ryan, C. B., and Lee, J. K. (2019). The origin, fate, and contribution of macrophages to spinal cord injury pathology. *Acta Neuropathol.* 137, 785–797. doi: 10.1007/s00401-019-01992-3

Monahan, R., Stein, A., Gibbs, K., Bank, M., and Bloom, O. (2015). Circulating T cell subsets are altered in individuals with chronic spinal cord injury. *Immunol. Res.* 63, 3–10. doi: 10.1007/s12026-015-8698-1

Nukolova, N. V., Aleksashkin, A. D., Abakumova, T. O., Morozova, A. Y., Gubskiy, I. L., Kirzhanova, EA, et al. (2018). Multilayer polyion complex

nanoformulations of superoxide dismutase 1 for acute spinal cord injury. *J. Control Release* 270, 226–236. doi: 10.1016/j.jconrel.2017.11.044

Okada, S., Hara, M., Kobayakawa, K., Matsumoto, Y., and Nakashima, Y. (2018). Astrocyte reactivity and astrogliosis after spinal cord injury. *Neurosci. Res.* 126, 39–43. doi: 10.1016/j.neures.2017.10.004

Orr, M. B., and Gensel, J. C. (2018). Spinal cord injury scarring and inflammation: therapies targeting glial and inflammatory responses. *Neurotherapeutics* 15, 541–553. doi: 10.1007/s13311-018-0631-6

Pang, J., Hou, J., Zhou, Z., Ren, M., Mo, Y., Yang, G., et al. (2020). Safflower yellow improves synaptic plasticity in APP/PS1 mice by regulating microglia activation phenotypes and BDNF/TrkB/ERK signaling pathway. *Neuromol. Med.* 22, 341–358. doi: 10.1007/s12017-020-08591-6

Park, J. S., Svetkauskaite, D., He, Q., Kim, J. Y., Strassheim, D., Ishizaka, A., et al. (2004). Involvement of toll-like receptors 2 and 4 in cellular activation by high mobility group box 1 protein. *J. Biol. Chem.* 279, 7370–7377. doi: 10.1074/jbc.M306793200

Pinchi, E., Frati, A., Cantatore, S., D'Errico, S., Russa, R., Maiese, A., et al. (2019). Acute spinal cord injury: a systematic review investigating miRNA families involved. *Int. J. Mol. Sci.* 20:1841. doi: 10.3390/ijms20081841

Polcyn, R., Capone, M., Matzelle, D., Hossain, A., Chandran, R., Banik, N. L., et al. (2020). Enolase inhibition alters metabolic hormones and inflammatory factors to promote neuroprotection in spinal cord injury. *Neurochem. Int.* 139:104788. doi: 10.1016/j.neuint.2020.104788

Ransohoff, R. M. (2016). A polarizing question: do M1 and M2 microglia exist? *Nat. Neurosci.* 19, 987–991. doi: 10.1038/nn.4338

Rice, T., Larsen, J., Rivest, S., and Yong, V. W. (2007). Characterization of the early neuroinflammation after spinal cord injury in mice. *J. Neuropathol. Exp. Neurol.* 66, 184–195. doi: 10.1097/01.jnen.0000248552.07338.7f

Rodríguez-Barrera, R., Flores-Romero, A., Fernández-Presas, A. M., García-Vences, E., Silva-García, R., Konigsberg, M., et al. (2017). Immunization with neural derived peptides plus scar removal induces a permissive microenvironment, and improves locomotor recovery after chronic spinal cord injury. *BMC Neurosci.* 18:7. doi: 10.1186/s12868-016-0331-2

Scaffidi, P., Misteli, T., and Bianchi, M. E. (2010). Release of chromatin protein HMGB1 by necrotic cells triggers inflammation. Nature. 2002; 418(6894):191-5. *Erratum Nat.* 467:622. doi: 10.1038/nature00858

Schattling, B., Engler, J. B., Volkmann, C., Rothammer, N., Woo, M. S., Petersen, M., et al. (2019). Bassoon proteinopathy drives neurodegeneration in multiple sclerosis. *Nat. Neurosci.* 22, 887–896. doi: 10.1038/s41593-019-0385-4

Shi, X. M., Zhang, H., Zhou, Z. J., Ruan, Y. Y., Pang, J., Zhang, L., et al. (2018). Effects of safflower yellow on beta-amyloid deposition and activation of astrocytes in the brain of APP/PS1 transgenic mice. *Biomed. Pharmacother.* 98, 553–565. doi: 10.1016/j.biopha.2017.12.099

Song, Y., Long, L., Zhang, N., and Liu, Y. (2014). Inhibitory effects of hydroxysafflor yellow A on PDGF-BB-induced proliferation and migration of vascular smooth muscle cells via mediating Akt signaling. *Mol. Med. Rep.* 10, 1555–1560. doi: 10.3892/mmr.2014.2336

Stahel, P. F., VanderHeiden, T., and Finn, M. A. (2012). Management strategies for acute spinal cord injury: current options and future perspectives. *Curr. Opin. Crit. Care* 18, 651–660. doi: 10.1097/MCC.0b013e32835a0e54

Stirling, D. P., and Yong, V. W. (2008). Dynamics of the inflammatory response after murine spinal cord injury revealed by flow cytometry. *J. Neurosci. Res.* 86, 1944–1958. doi: 10.1002/jnr.21659

Sun, L., Zhao, L., Li, P., Liu, X., Liang, F., Jiang, Y., et al. (2019). Effect of hyperbaric oxygen therapy on HMGB1/NF-κB expression and prognosis of acute spinal cord injury: a randomized clinical trial. *Neurosci. Lett.* 692, 47–52. doi: 10.1016/j.neulet.2018.10.059

Sun, X., Wei, X., Qu, S., Zhao, Y., and Zhang, X. (2010). Hydroxysafflor yellow a suppresses thrombin generation and inflammatory responses following focal cerebral ischemia-reperfusion in rats. *Bioorg. Med. Chem. Lett.* 20, 4120–4124. doi: 10.1016/j.bmcl.2010.05.076

Tang, Z., Xie, H., Jiang, S., Cao, S., Pu, Y., Zhou, B., et al. (2018). Safflower yellow promotes angiogenesis through p-VHL/ HIF-1α/VEGF signaling pathway in the process of osteogenic differentiation. *Biomed. Pharmacother.* 107, 1736–1743. doi: 10.1016/j.biopha.2018.06.119

Tran, A. P., Warren, P. M., and Silver, J. (2018). The biology of regeneration failure and success after spinal cord injury. *Physiol. Rev.* 98, 881–917. doi: 10.1152/physrev.00017.2017

van Zoelen, M. A., Yang, H., Florquin, S., Meijers, J. C., Akira, S., Arnold, B., et al. (2009). Role of toll-like receptors 2 and 4, and the receptor for advanced glycation end products in high-mobility group box 1-induced inflammation in vivo. *Shock* 31, 280–284. doi: 10.1097/SHK.0b013e318186262d

Vismara, I., Papa, S., Veneruso, V., Mauri, E., Mariani, A., De Paola, M., et al. (2020). Selective modulation of A1 Astrocytes by drug-loaded nano-structured gel in spinal cord injury. *ACS Nano* 14, 360–371. doi: 10.1021/acsnano.9b05579

Wang, C., Gao, Y., Zhang, Z., Chi, Q., Liu, Y., Yang, L., et al. (2020). Safflower yellow alleviates osteoarthritis and prevents inflammation by inhibiting PGE2 release and regulating NF-κB/SIRT1/AMPK signaling pathways. *Phytomedicine* 78:153305. doi: 10.1016/j.phymed.2020.153305

Wang, C., He, Y., Yang, M., Sun, H., Zhang, S., and Wang, C. (2013). Safflor yellow B suppresses angiotensin II-mediated human umbilical vein cell injury via regulation of Bcl-2/p22(phox) expression. *Toxicol. Appl. Pharmacol.* 273, 59–67. doi: 10.1016/j.taap.2013.08.018

Wang, L., Jin, M., Zang, B. X., and Wu, Y. (2011). Inhibitory effect of safflor yellow on pulmonary fibrosis. *Biol. Pharm. Bull.* 34, 511–516. doi: 10.1248/bpb.34.511

Wang, Y. S., Li, Y. Y., Wang, L. H., Kang, Y., Zhang, J., Liu, Z. Q., et al. (2015). Tanshinone IIA attenuates chronic pancreatitis-induced pain in rats via downregulation of HMGB1 and TRL4 expression in the spinal cord. *Pain Phys.* 18, E615–E628.

Wu, F., Ding, X. Y., Li, X. H., Gong, M. J., An, J. Q., Lai, J. H., et al. (2019). Cellular inflammatory response of the spleen after acute spinal cord injury in rat. *Inflammation* 42, 1630–1640. doi: 10.1007/s10753-019-01024-y

Xi, K., Gu, Y., Tang, J., Chen, H., Xu, Y., Wu, L., et al. (2021). Microenvironment-responsive immunoregulatory electrospun fibers for promoting nerve function recovery. Nat Commun. 2020; 11(1):4504. *Erratum Nat. Commun.* 12:2882. doi: 10.1038/s41467-020-18265-3

Xu, B., Lang, L. M., Lian, S., Guo, J. R., Wang, J. F., Liu, J., et al. (2020). Neuroinflammation induced by secretion of acetylated HMGB1 from activated microglia in hippocampi of mice following chronic cold exposure. *Brain Res.* 1726:146495. doi: 10.1016/j.brainres.2019.146495

Yan, K., Wang, X., Zhu, H., Pan, H., Wang, L., Yang, H., et al. (2020). Safflower yellow improves insulin sensitivity in high-fat diet-induced obese mice by promoting peroxisome proliferator-activated receptor-γ2 expression in subcutaneous adipose tissue. *J. Diabetes Investig.* 11, 1457–1469. doi: 10.1111/jdi.13285

Yang, G., Zhou, X., Chen, T., Deng, Y., Yu, D., Pan, S., et al. (2015). Hydroxysafflor yellow A inhibits lipopolysaccharide-induced proliferation and migration of vascular smooth muscle cells via Toll-like receptor-4 pathway. *Int. J. Clin. Exp. Med.* 8, 5295–5302.

Yang, X. W., Li, Y. H., Zhang, H., Zhao, Y. F., Ding, Z. B., Yu, J. Z., et al. (2016). Safflower yellow regulates microglial polarization and inhibits inflammatory response in LPS-stimulated Bv2 cells. *Int. J. Immunopathol. Pharmacol.* 29, 54–64. doi: 10.1177/0394632015617065

Yarar-Fisher, C., Bickel, C. S., Kelly, N. A., Stec, M. J., Windham, S. T., McLain, A. B., et al. (2016). Heightened TWEAK-NF-κB signaling and inflammation-associated fibrosis in paralyzed muscles of men with chronic spinal cord injury. *Am. J. Physiol. Endocrinol. Metab.* 310, E754–E761. doi: 10.1152/ajpendo.00240.2015

Yoshizaki, S., Tamaru, T., Hara, M., Kijima, K., Tanaka, M., Konno, D. J., et al. (2021). Microglial inflammation after chronic spinal cord injury is enhanced by reactive astrocytes via the fibronectin/β1 integrin pathway. *J. Neuroinflammation* 18:12. doi: 10.1186/s12974-020-02059-x

Yu, L., Song, H., Fang, X., and Hu, Y. (2021). Role of MK2 signaling pathway mediating microglia/macrophages polarization in chronic compression injury of cervical spinal cord. *Ann. Palliat. Med.* 10, 1304–1312. doi: 10.21037/apm-20-396

Yu, S., Zhang, H., Hei, Y., Yi, X., Baskys, A., Liu, W., et al. (2019). High mobility group box-1 (HMGB1) antagonist BoxA suppresses status epilepticus-induced neuroinflammatory responses associated with Toll-like receptor 2/4 down-regulation in rats. *Brain Res.* 1717, 44–51. doi: 10.1016/j.brainres.2019.04.007

Zhang, H., Duan, C. P., Luo, X., Feng, Z. M., Yang, Y. N., Zhang, X., et al. (2020). Two new quinochalcone glycosides from the safflower yellow pigments. *J. Asian Nat. Prod. Res.* 22, 1130–1137. doi: 10.1080/10286020.2020.1846530

Zhang, H., Zhi, L., Moochhala, S., Moore, P. K., and Bhatia, M. (2007). Hydrogen sulfide acts as an inflammatory mediator in cecal ligation and puncture-induced

sepsis in mice by upregulating the production of cytokines and chemokines via NF-kappaB. *Am. J. Physiol. Lung Cell Mol. Physiol.* 292, L960–L971. doi: 10.1152/ajplung.00388.2006

Zhang, Z., Wu, Z., Zhu, X., Hui, X., Pan, J., and Xu, Y. (2014). Hydroxy-safflor yellow A inhibits neuroinflammation mediated by $A\beta_{1-42}$ in BV-2 cells. *Neurosci. Lett.* 562, 39–44. doi: 10.1016/j.neulet.2014.01.005

Zhou, D., Liu, B., Xiao, X., Dai, P., Ma, S., and Huang, W. (2013). The effect of safflower yellow on spinal cord ischemia reperfusion injury in rabbits. *Oxid. Med. Cell Longev.* 2013:692302. doi: 10.1155/2013/692302

Zhou, D., Qu, Z., Wang, H., Su, Y., Wang, Y., Zhang, W., et al. (2018). The effect of hydroxy safflower yellow A on coronary heart disease through Bcl-2/Bax and PPAR-γ. *Exp. Ther. Med.* 15, 520–526. doi: 10.3892/etm.2017.5414

Zhu, H., Wang, X., Pan, H., Dai, Y., Li, N., Wang, L., et al. (2016). The mechanism by which safflower yellow decreases body fat mass and improves insulin sensitivity in HFD-induced obese mice. *Front. Pharmacol.* 7:127. doi: 10.3389/fphar.2016.00127

**Conflict of Interest:** The authors declare that the research was conducted in the absence of any commercial or financial relationships that could be construed as a potential conflict of interest.

**Publisher's Note:** All claims expressed in this article are solely those of the authors and do not necessarily represent those of their affiliated organizations, or those of the publisher, the editors and the reviewers. Any product that may be evaluated in this article, or claim that may be made by its manufacturer, is not guaranteed or endorsed by the publisher.

frontiers in Pharmacology

REVIEW
published: 23 March 2022
doi: 10.3389/fphar.2022.866738

# Glutamate Scavenging as a Neuroreparative Strategy in Ischemic Stroke

*Oykum Kaplan-Arabaci[1,2], Alperen Acari[1], Pinar Ciftci[1] and Devrim Gozuacik[1,2,3]**

[1]Koç University Research Center for Translational Medicine (KUTTAM), Istanbul, Turkey, [2]Sabancı University Nanotechnology Research and Application Center (SUNUM), Istanbul, Turkey, [3]School of Medicine, Koç University, Istanbul, Turkey

Stroke is the second highest reason of death in the world and the leading cause of disability. The ischemic stroke makes up the majority of stroke cases that occur due to the blockage of blood vessels. Therapeutic applications for ischemic stroke include thrombolytic treatments that are in limited usage and only applicable to less than 10% of the total stroke patients, but there are promising new approaches. The main cause of ischemic neuronal death is glutamate excitotoxicity. There have been multiple studies focusing on neuroprotection via reduction of glutamate both in ischemic stroke and other neurodegenerative diseases that ultimately failed due to the obstacles in delivery. At that point, systemic glutamate grabbing, or scavenging is an ingenious way of decreasing glutamate levels upon ischemic stroke. The main advantage of this new therapeutic method is the scavengers working in the circulating blood so that there is no interference with the natural brain neurophysiology. In this review, we explain the molecular mechanisms of ischemic stroke, provide brief information about existing drugs and approaches, and present novel systemic glutamate scavenging methods. This review hopefully will elucidate the potential usage of the introduced therapeutic approaches in stroke patients.

**Keywords: stroke, glutamate, neuroreparation, excitotoxicity, neuroprotection, ischemia, TPA, brain**

OPEN ACCESS

***Edited by:***
*Valle Palomo,*
*Spanish National Research Council (CSIC), Spain*

***Reviewed by:***
*Kinga Szydlowska,*
*Nencki Institute of Experimental Biology (PAS), Poland*
*Pedro Ramos-Cabrer,*
*CIC biomaGUNE, Spain*
*Matthew Boyko,*
*Ben-Gurion University of the Negev, Israel*

****Correspondence:***
*Devrim Gozuacik*
*dgozuacik@ku.edu.tr*

***Specialty section:***
*This article was submitted to Neuropharmacology, a section of the journal Frontiers in Pharmacology*

***Received:*** *31 January 2022*
***Accepted:*** *08 March 2022*
***Published:*** *23 March 2022*

***Citation:***
*Kaplan-Arabaci O, Acari A, Ciftci P and Gozuacik D (2022) Glutamate Scavenging as a Neuroreparative Strategy in Ischemic Stroke. Front. Pharmacol. 13:866738. doi: 10.3389/fphar.2022.866738*

## INTRODUCTION

Stroke is the second leading cause of death after ischemic heart disease and the third cause of disability affecting more than six million lives per year, according to the latest report of the World Health Organization (WHO) (WHO, 2020). Stroke patients are broadly divided into ischemic and haemorrhagic stroke types while the majority has been driven by ischemia. The summation of damage done by both stroke types affect the life of 13,7 million people and cause 5,5 million deaths every year (Global GBD 2016 Stroke Collaborators, 2019). Considering the continuous increase in the human population as well as skyrocketing numbers in obesity and hypertension patients, it is likely to face severe circumstances in the upcoming years.

### Ischemic Stroke

The word ischemia is originated from two Greek words: ischō, meaning holding back and haima, meaning blood; expressing the phrase of stopping blood (Verdouw et al., 1998). As the name indicates, ischemic stroke simply occurs due to the interruption of blood supply to the brain. The human brain requires constant blood flow providing oxygen and nutrients as well as eliminating carbon dioxide and cell debris. When there is a disruption in the blood supply, the brain cells lose

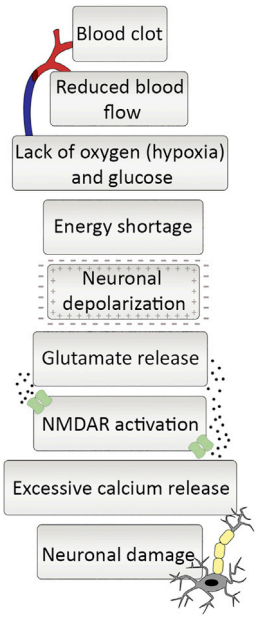


**FIGURE 1 |** Ischemic cascade at a glance. Occlusion of an artery starts a series of responses. Blood clot blocking artery causes reduced blood flow, which leads to lack of oxygen and glucose and ultimately a drastic decrease in energy supply. It leaves neurons in a depolarized state and reduction in glutamate reuptake gives rise to increase in extracellular glutamate levels. The increment in glutamate leads to NMDA receptor activation and neuronal calcium influx, and excessive amount of calcium release ending up with neuronal damage.

their only energy source glucose and eventually die because of the energy shortage combined with toxic waste that is accumulated in the cells. The ischemic brain could be classified into two regions based on the stroke's severity: the core zone which lost 90% of blood flow and shows the most severe effects, and the penumbra or peri-infarct region which surrounds the core zone (Appireddy et al., 2015). Even though the core zone experiences partial cell death as ischemia happens, the circulation in that region partially continues by the collateral arteries and the damage is reversible if the blood flow could be restored within a couple of hours (Heiss and Rosner, 1983). Consequently, the penumbra or peri-infarct region has been the primary target of pharmacological approaches with the hope to rescue invaluable neuronal cells from death (Castillo et al., 2016).

It is momentous to emphasize that more focused attempts for the prevention and treatment of ischemic stroke are desperately required. Modern treatment methods are simply dependent on re-sustaining blood flow as soon as possible and ensuring reperfusion in the affected area. Current clinical therapies offer only two efficient methods: intravenous administration of tissue plasminogen activator (tPA) and mechanical thrombectomy (Bhaskar et al., 2018). Globally, tPA application is the most widely accepted and implemented treatment method for ischemic stroke, although it is only effective when quickly applied in the time window of 4.5 h following the initiation of stroke (Yoo et al., 2011), and in some cases it can go up to 6 h (Snelling et al., 2019). In addition to the narrow time window, there is a certain risk of reperfusion damage that makes the treatment capacity of tPA limited on most patients (Kurth et al., 2007). If the size of the clot occluding the vein is large than the tPA treatment limits or the time window is outlasted, MT surgery is the alternative treatment in which a microcatheter is used to directly remove the clot, although it is a risk involved solution that is far from being perfect (Dong et al., 2020). Despite the fact that there are hundreds of treatment attempts for thrombectomy, they ultimately failed to translate to the clinics (Matei et al., 2021). Considering all modern applications, it is safe to say there is a desperate need for pharmacological therapeutics and drugs that could solve the urgent need of ischemic stroke patients.

## Cellular Mechanism of Ischemia

The mechanism of ischemic cell death in the brain is well-known at the cellular and molecular levels (Rossi et al., 2007). A clot blocking an artery disrupts the consistent flow of nutrient-rich blood. Inevitably, it causes inadequate glucose and oxygen supply that cannot meet the energy demands of neuronal cells. Since glucose-dependent oxidative phosphorylation sourced by the constant blood flow is the primary energy source of neural cells, inadequacy in the glucose supply causes ATP depletion even in minutes because of the absence of long-term energy reserves in the brain (Doyle et al., 2008). Neuronal cells cannot perform regular metabolic activities without glucose and oxygen, causing inevitable starvation-related cell death (**Figure 1**). A second emerging problem arises with energy scarcity. The function of ion pumps is essential for the information transfer between the adjacent neurons that maintain the concentration gradient of sodium ($Na^+$), potassium ($K^+$), and calcium ($Ca^{2+}$) between intracellular and extracellular environments but require ATP to function. The ion pumps are non-functional without energy, making the electrochemical gradient difference unsustainable. In the ATP depletion, the abnormal increase of $Na^+$ influx and $K^+$ efflux to neural cells causes depolarization. Following extracellular $K^+$ concentration increase, L-type voltage-gated channels open and allow the passage of $Ca^{2+}$ ions resulting in elevated intracellular $Ca^{2+}$ concentration (Luoma et al., 2011). The $Ca^{2+}$ cannot be pumped out of the cell by the ion pumps and exchangers without sufficient energy. The level of $Ca^{2+}$ causes the release of glutamate, which is one of the fundamental reasons for ischemia-induced excitotoxicity in neurons and glial cells. Glutamate is an excitatory amino acid and behaves as a neurotransmitter binding glutamate receptor to transmit signals. Glutamate is released by the activation of its postsynaptic receptors that are ionotropic or metabotropic receptors (mGluRs). Ionotropic receptors consist of three groups which are NMDA (N-methyl-D-aspartate), AMPA (a-amino-3-hydroxy-5-methyl-4-iso-xazolepropionic acid) or kainate receptors (Atoji and Sarkar, 2019). Metabotropic receptors act through the heterotrimeric guanine nucleotide-binding proteins that convey the signal to its effector channels or intracellular enzymes. The excitotoxic response is primarily regulated by NMDA type glutamate receptors (Gupta et al., 2013; Girling et al., 2018).

The accumulation of glutamate in the extracellular space led to the hyperactivation of glutamate receptors and then to massive

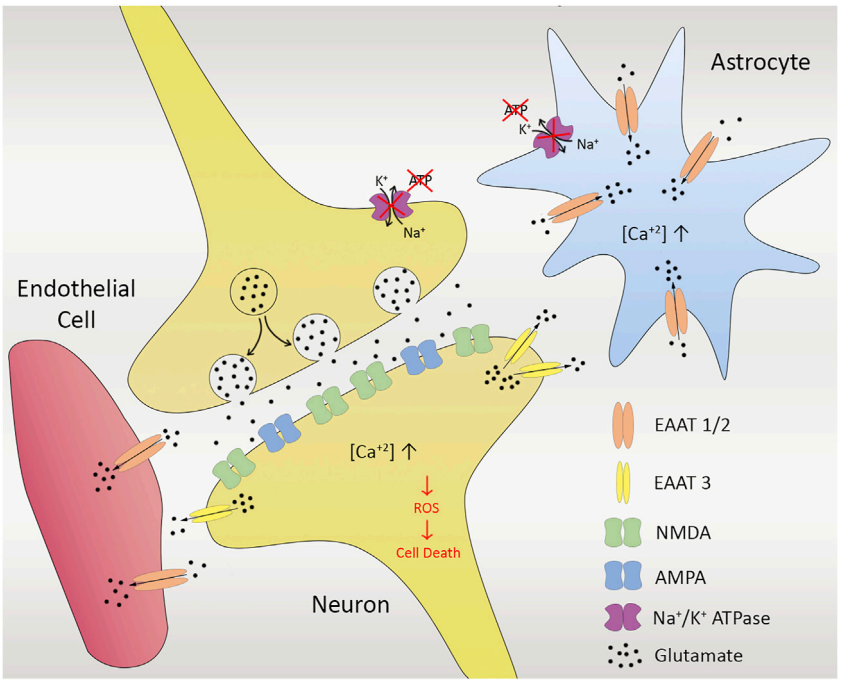


**FIGURE 2 |** Ischemia in cellular unit. Anoxic depolarization and decreased activity of glutamate uptake gives rise to enhanced glutamate levels, leading to calcium influx *via* NMDA receptors. Excessive glutamate released from presynapse of the neuron also leads to $Na^+$-dependent excitatory amino acid transporters (EAATs) in astrocytes (EAAT1/2) as well as neurons (EAAT3). Insufficient energy and lack of ion pump functioning cause massive increase in the intracellular $Ca^{2+}$, activating protein kinases and some other downstream $Ca^{2+}$-dependent enzymes, damaging the cell membrane, resulting in more $Ca^{2+}$entry into the cell, release of free radicals as well as reactive oxygen species (ROS) that gives rise to cell death in the end.

$Ca^{2+}$ influx. If there is sufficient energy supply, ion equilibrium of the cells are maintained by removing some positive ions *via* ion pumps and then uptake the cell. However, in the case of insufficient energy in the cell, the ion pumps do not function properly, causing an important increase in the intracellular $Ca^{2+}$. This intracellular $Ca^{2+}$ increase causes the activation of protein kinases and other downstream $Ca^{2+}$-dependent enzymes which damage significant molecules and disrupt the cell membrane, resulting in more $Ca^{2+}$ entry into the cell, release of free radicals from damaged mitochondria, and subsequent cell death (Papazian et al., 2018; Verma et al., 2018; Belov Kirdajova et al., 2020).

The uptake of excessive glutamate by astrocytes also causes constant activation of $Ca^{2+}$ channels that give rise to a pathological increase in intracellular $Ca^{2+}$ concentration. Toxic elements such as reactive oxygen species (ROS) and a group of $Ca^{2+}$-dependent degradative enzymes such as ATPases, endonucleases, proteases, and phospholipases are released from the neural cells (Sattler et al., 1999). Overall, the sequence of events results in the release of mitochondrial apoptotic signals and initiation of the caspase-dependent cell death (Belov Kirdajova et al., 2020) (**Figure 2**). The removal of excitatory neurotransmitters released to the synaptic cleft is also an energy-dependent action. Therefore, there is a huge increase in neurotransmitter concentrations, especially glutamate, in the ischemia, which acts as a mediator of neuronal degeneration.

## Glutamate and its Excitotoxicity

Glutamate is one of the most abundant amino acids in the human body participating in multiple metabolic pathways, and it is the most indispensable regulator in the central nervous system playing a vital role in regulating neural communication, plasticity, learning, memory, and more. Considering its broad range of metabolic activities and regulatory capacity, it is no wonder that glutamate-including pathways are highly regulated. The neurotransmitter function of glutamate requires its presence in the extracellular fluid part of the brain. Neuronal cells are sensitive to the changes in the extracellular glutamate level, where sustaining the balance is vital; therefore, the extracellular glutamate is regulated by release and restrain cycles. If the balance in the glutamate level is disturbed and the extracellular glutamate concentration increases in an uncontrollable manner, neuronal cells die inevitably because of the cumulative toxic effects (Zauner et al., 1996). This phenomenon is described as glutamate excitotoxicity and is known as a primary damaging mechanism that causes the cell death occured in stroke (Danbolt, 2001).

There are several mechanisms that supply glutamate to the extracellular fluid. The synaptic glutamate released from the presynapse is the main source of extracellular glutamate (Danbolt, 2001). The transfer of information at synapse requires receptor activation on postsynaptic side by sensing glutamate. As the postsynaptic receptors are outwardly located on the cell membrane, glutamate should be released from the

presynapse to the extracellular fluid via exocytosis of the synaptic vesicles. Besides, there are several non-vesicular mechanisms that supply glutamate to the extracellular fluid via anion channels and reversed operation of glutamate transporting proteins (Rossi et al., 2000). Once released, the extra glutamate should be eliminated rapidly to sustain the balance. There is no mechanism to remove extracellular glutamate besides cellular reuptake by astrocytes, neurons and endothelial cells. The cellular reuptake is strictly controlled by $Na^+$-dependent excitatory amino acid transporter family members, also known as excitatory amino acid transporters (EAATs) (Danbolt 2001; Grewer and Rauen, 2005; Tzingounis and Wadiche, 2007; Vandenberg and Ryan, 2013).

EAATs, which are a part of the solute carrier 1 (SLC1) family that uptake glutamate inside to the cell against the concentration gradient. There are five distinct types of these glutamate transporters. EAAT1 is predominantly expressed in the neocortex and cerebellum, specifically in astrocytes, whereas EAAT2 is the primary glutamate transporter found in the forebrain, widely expressed in astrocytes (Danbolt et al., 1990; Pines et al., 1992; Storck et al., 1992). Given that EAAT1 and EAAT2 have a broad expression in astrocytes, EAAT3 is mostly expressed in neurons (Rothstein et al., 1994; Mennerick et al., 1998). EAAT4 is also shown to be expressed in neurons, however the expression is limited to Purkinje cells. EAAT5 is on the other hand, only expressed at photoreceptor and bipolar cell terminals in the retina (Danbolt, 2001). In addition to that, EAATs also exist in endothelial cells (Campos et al., 2011b). All types of EAATs that are having similar mechanism act on clearing glutamate from the synaptic cleft (Magi et al., 2019).

Extracellular glutamate levels are strictly controlled *via* EAATs. EAATs that are found in astrocytes that bind and sequester the neurotransmitter for processing and recycling, promote the glutamate reuptake from synaptic junctions after neuronal excitation. As an alternative, glutamate can be transferred from the extracellular space *via* sodium-dependent transport on the antiluminal surface of brain capillary endothelial cells when the extracellular concentration is increased (Leibowitz et al., 2012). If the accumulation of glutamate concentration in the endothelial cells surpasses the plasma level, glutamate is transported from the luminal side into the bloodstream by facilitated diffusion. In this way, although there are adverse concentration gradients from central nervous system (CNS) to plasma, the endothelial regulation of CNS glutamate concentration can happen. After EAATs uptake glutamate from the synaptic cleft, it is converted in astrocytes to glutamine via glutamine synthetase or to α-ketoglutarate, which is involved in the tricarboxylic citric acid cycle (TCA) *via* glutamate dehydrogenase.

TCA cycle, also called as Krebs cycle or citric acid cycle (CAC) is a second stage of cellular respiration, in which cells decompose organic molecules in the presence of oxygen and produce energy to be able to survive. This event takes place in mitochondria in almost all living organisms including most of the bacteria. The TCA cycle starts with the catalyze of α-ketoglutarate to succinyl CoA via α-ketoglutarate dehydrogenase (KGDH). Multiple steps in the tricarboxylic acid (TCA) cycle convert the carbon skeleton to malate, which is ultimately turned to pyruvate by malic enzyme (ME). As an alternative, pyruvate kinase (PK) and phosphoenolpyruvate carboxykinase (PEPCK) work together to convert oxaloacetate (OAA) to pyruvate. For the complete oxidation of glutamate, ME or PEPCK with PK must operate in the direction of pyruvate. Pyruvate dehydrogenase (PDH) re-enters the TCA cycle, and the carbon skeleton derived from glutamate can be entirely oxidized to $CO_2$ in the TCA cycle through this pathway (Schousboe et al., 2014; Cooper and Jeitner, 2016) (**Figure 3**).

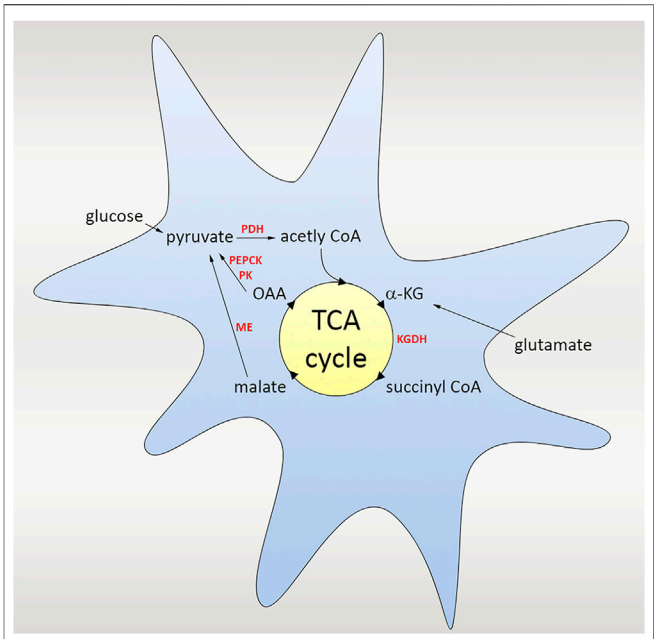


**FIGURE 3 |** Scheme of the glutamate uptake and the TCA cycle. TCA cycle is a second stage of cellular respiration taking place in mitochondria, in which cells decompose organic molecules in the presence of oxygen and produce energy. The cycle starts with the catalyze of α-ketoglutarate to succinyl CoA *via* α-ketoglutarate dehydrogenase (KGDH), followed by several steps in the TCA cycle converting the carbon skeleton to malate, which is ultimately turned to pyruvate by malic enzyme (ME). As an alternative, pyruvate kinase (PK) and phosphoenolpyruvate carboxykinase (PEPCK) work and convert oxaloacetate (OAA) to pyruvate. Pyruvate dehydrogenase (PDH) also re-enters the TCA cycle, and the carbon skeleton derived from glutamate could be oxidized to $CO_2$.

## Current Therapeutic Approaches in Ischemic Stroke

The treatment approach of stroke depends on the underlying cause of the disease because of the contradictory therapeutic requirements of hemorrhagic and ischemic types. While the hemorrhagic type requires immediate termination of bleeding, the ischemic type needs quick restoration of blood flow. The contrast between the motivations of treatment approaches makes the medical examination highly critical where misjudgment could worsen the existing damage on the brain. Once ischemia is identified, the medications aim the reperfusion of the affected area by either thrombolytic agents or mechanical thrombectomy

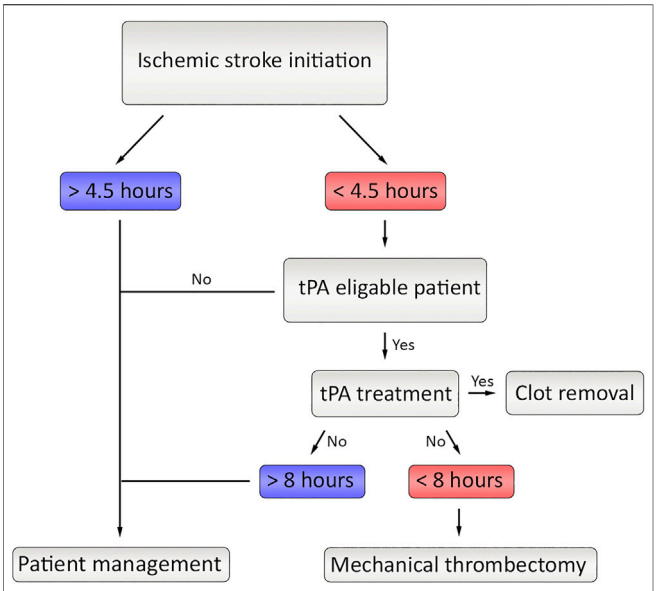


**FIGURE 4 |** The current flow of therapeutic approaches in ischemic stroke. After initiation of the stroke, if the time limit is under 4.5 h and if tPA is eligible, the tPA treatment is applied. If the clot is still not fully removed and if the time did not exceed 8 h, Mechanical thrombectomy could be applied.

(Dong et al., 2020) (**Figure 4**). Although there are several thrombolytic agents in the stage of clinical trials including alteplase, streptokinase and tenecteplase; only alteplase was approved by FDA. While streptokinase is eliminated because of the unacceptably high rates of hemorrhage, tenecteplase still requires further studies to verify benefits on ischemic stroke patients (Bhaskar et al., 2018).

## Alteplase (Tissue Plasminogen Activator, tPA)

By the day, tissue plasminogen activator (tPA or alteplase) is the only approved drug by the FDA and the golden standard of ischemic stroke treatment. tPA is a member of plasminogen activators that hydrolyze de arginine-valine peptide bond to activate plasminogen as plasmin (Lijnen and Collen, 1988). When given intravenously (IV), the tPA therapy can lyse the ischemia reasoning clot if it is performed within 3 h starting from the initiation of symptoms (National Institute of Neurological Disorders and Stroke rt-PA Stroke Study Group, 1995; Kwiatkowski et al., 1999; Bansal et al., 2013). If tPA treatment is applied directly to the affected area, therapy is generally accepted as successful up to the 4.5 h (Hacke et al., 2008). Although tPA therapy is the sharpest tool in the box, it is far from being perfect because thrombolytic therapy is still associated with bleeding that could be catastrophic (Goldstein et al., 2010). Therefore, there is a desperate and urgent need of new therapies in ischemic stroke.

## Mechanical Thrombectomy

Mechanical thrombectomy is a minimally invasive procedure that includes removal of the clot from the artery of the patient by using a microcatheter. The size of the clot can differ depending on the patient, and if it too big or tPA treatment time is surpassed, MT surgery is the only treatment that could be applied if the onset is before 8 h (Jovin et al., 2015). It has been observed that MT treatment supplied two times more survival rate and less disability in patients diagnosed with ischemic stroke (Smith et al., 2008). MT and pre-treatment with intravenous tPA treatment could be another therapeutic option. However, this therapy is also disadvantageous since handling the clot within the vessel could be risky in terms of mechanical injuries (Bhaskar et al., 2018).

## Peritoneal Dialysis

There is another strategy called as peritoneal dialysis have been developed in order to decrease blood glutamate levels by directing glutamate from brain to blood. The transient increase in glutamate is aimed to decrease via this dialysis method simply by exchanging fluids and dissolved substances between the blood and the dialysate across the peritoneum (Godino et al., 2013). It has been also demonstrated that this strategy significantly decrease glutamate levels in patients (Rogachev et al., 2013). This novel therapy can be an effective strategy for stroke patients, however it is not commonly used as a stroke therapy yet and clinical trials are needed to see the efficiancy in ischemic stroke patients.

## Stroke Prevention

Despite the fact that prevention of stroke is not a treatment itself, it is commonly used and quite effective therapeutic intervention method against stroke. Anticoagulants, antiplatelet therapy, statin treatment, drugs that are regulating blood pressure are currently used stroke prevention methods, and it has been foreseen that up to 80% of recurrent stroke cases can be averted by the usage of these methods. Therefore, mass stroke prevention strategy could be a very useful complementary strategy to decrease the increasing trend of global burden of stroke as well as subsequent disability (Sherzai and Elkind, 2015).

## Neuroprotective Therapies

Significant pharmacological strategies to this neurotoxic event have been improved by researchers thanks to the knowledge of the molecular mechanisms contained in glutamate excitotoxicity after cerebral ischemia. Initially, NMDA receptors (NMDAR) antagonism was investigated as a main focus; since NMDAR is a significant gateway for the numerous other downstream effects of glutamate excitotoxicity. Therefore, it ensured a reasonable target for drug design. Throughout this period, the knowledge of the structure and function of these receptors also increased owing to advances in protein biochemistry and small molecule design (Ogden and Traynelis, 2011). Various classes of NMDAR antagonists that have different sites of action, were improved that are the competitive NMDAR antagonist affecting for glutamate or glycine binding sites, noncompetitive allosteric inhibitors acting on other extracellular sites, and NMDAR channel blockers that influence sites in the receptor channel pore. Although there are promising results in animal research,

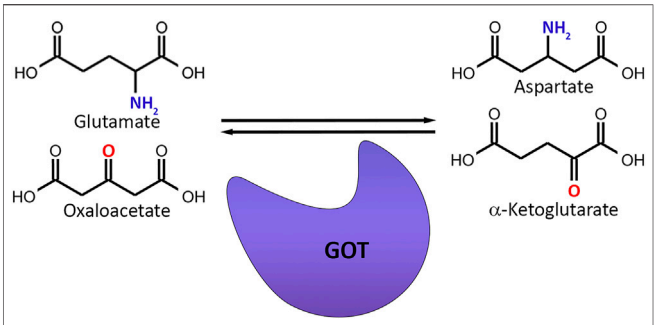


**FIGURE 5 |** Basic mechanism of glutamate scavenging. Glutamate-oxaloacetate Transaminase (GOT) transfers the amino group from glutamate to oxaloacetate while replacing the amino group of glutamate with a carbonyl group and converts glutamate and oxaloacetate to aspartate and α-ketoglutarate.

antagonist drugs like selfotel, gavestinel, and traxoprodil, have not dramatically succeeded in randomized and controlled clinical trials in humans. The failure of these NMDAR-targeting therapies has been explained with many different reasons. Some of them show important dose-limiting side effects and lack adequate brain penetration (Kalia et al., 2008; Grupke et al., 2015; Jia et al., 2015). There are also some unfavorable process profiles such as hallucinations, agitations, catatonia, peripheral sensory loss, nausea, and elevation in blood pressure (Muir, 2006). Furthermore, it is thought that glutamate excitotoxicity leads to harm in a narrow time frame during which the neurotransmitter performs its normal function in the condition of acute processes like stroke or traumatic brain injuries. Thus, unfavorable side effects due to the prolonged receptor blockade and less therapeutic efficacy may occur by using agents acting on NMDAR, which is a fundamental receptor of glutamate. Although there were initial failures, research about NMDAR antagonism has been conducted. Recent experiments focusing on the control of the upstream glutamate concentration and downstream protein signals have begun to expand beyond the NMDAR over the past 2 decades. Novel theraphy approaches related to NMDA receptors including death-signaling pathways have been developed. These downstream pathyways of the receptor are inhibited by using inhibitors without blocking NMDARs such as interfering peptides and pharmacological inhibitors. These agents particularly uncouple the neuronal death signaling from NMDARs and they don't change neither functional nor survival of the receptors. In contrast to the receptor antagonist therapies, this approach may have less side effects and also has a potential to supply a longer therapeutic effect for stroke (Wu and Tymianski, 2018). Currently, there is increasing interest in blood glutamate scavengers and other agents targeting downstream sites of the receptor to improve effective drug modalities (Ikonomidou and Turski, 2002; Korczyn et al., 2015; Castillo et al., 2016).

# GLUTAMATE SCAVENGING IN ISCHEMIC STROKE

## Definition and the Mechanism of Scavenging

The word scavenger means the elimination of unwanted substances in order to keep the biological environment stable. Since glutamate is the major element to control in the CNS, regulating glutamate levels by a scavenging mechanism would be a very smart way to preserve homeostasis. The basis of systemic glutamate scavenging is based on a simple reaction, in which a blood-resident enzyme glutamate-oxaloacetate transaminase (GOT), also referred as Aspartate Aminotransferase (AST) converts glutamate into α-ketoglutarate and aspartate in existence of oxaloacetate (Campos et al., 2012) (**Figure 5**). The GOT enzyme-based reaction is dependent to the pyridoxal-5-phosphate (P5P) cofactor, which is the active type of vitamin B6. It binds covalently to an active-site lysine in a reversible manner and help catalyze the reaction (Westerhuis and Hafkenscheid, 1983; Tutor-Crespo et al., 2004).

The main advantage of glutamate scavengers is that they are doing their job in the blood. Furthermore, this mechanism acts locally in the brain regions that have a high glutamate concentration, whereas other brain regions that have normal glutamate levels have been unaffected, which eliminates secondary effects by decreasing cumulative glutamate levels in the brain. The glutamate concentration in blood plasma is measured as 40–60 μM in healthy adults (Leibowitz et al., 2012; Bai et al., 2017), whereas glutamate levels in cerebrospinal fluid (CSF) or brain intercellular fluids is between 1 and 10 μM (Hawkins, 2009; Teichberg et al., 2009) revealing that the glutamate concentration is much higher in the blood than in the CSF. Due to that difference, there is intraparenchymal-blood glutamate concentration gradient occurring between blood and brain, and it is mainly dependent to the integrity of the BBB as well as endothelial glutamate transporters (EAATs) (Hawkins, 2009; Cohen-Kashi-Malina et al., 2012; Bai and Zhou, 2017). When stroke happens, glutamate concentration in the brain goes up to 10 times above normal that which leads to a higher glutamate concentration is higher in the brain side than the blood (Campos et al., 2012). Another advantage of glutamate scavengers is that the systemic glutamate scavenging process is self-controlled, and automatically stops if that imbalance between brain and blood glutamate levels is reverted to the normal. One of the most important features of this method is, these scavengers do not give any harm, meaning that if there is a stroke risk observed, these agents can be given for prevention of the disease safely. Compared to previously used NMDA receptor antagonists that are not successfully working as well as many side effects since their interference with regular receptor signaling, systemic glutamate scavenging may be the smartest way for future glutamate excitotoxicity treatment (Boyko et al., 2014).

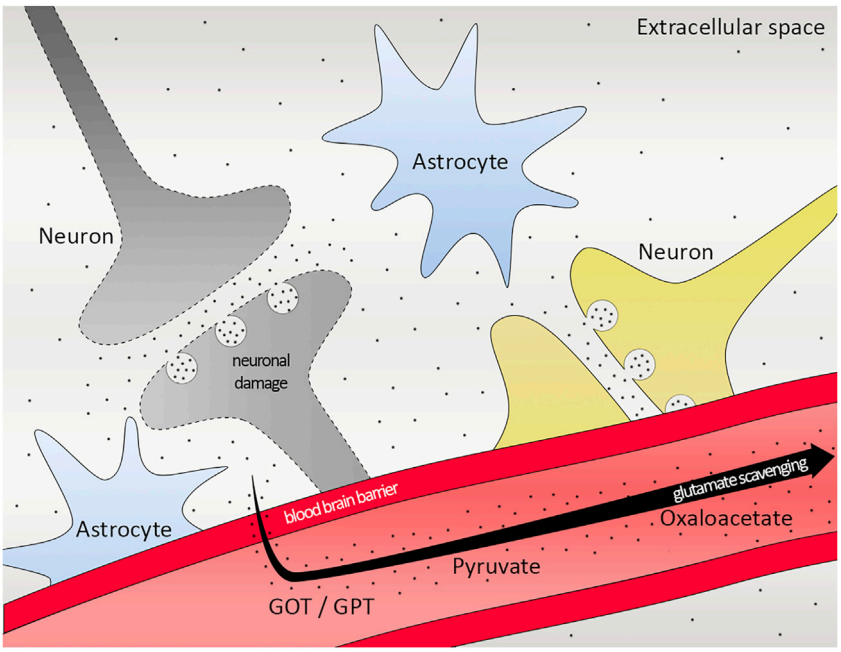


**FIGURE 6 |** Scheme of glutamate scavenging. Working mechanism of GOT/GPT, pyruvate and oxaloacetate in the brain. Black dots representing glutamate. GOT, Glutamate-oxaloacetate transaminase; GPT, Glutamate-pyruvate transaminase.

# CURRENT GLUTAMATE SCAVENGERS

## Glutamate-Oxaloacetate Transaminase and Glutamate-Pyruvate Transaminase

Based on the systemic glutamate scavenging method, it was first demonstrated that, upon glutamate increase in CSF, GOT and glutamate-pyruvate transaminase (GPT) lead to a significant reduction of glutamate in blood, further diminishing the extracellular glutamate amount in brain (Gottlieb et al., 2003). GOT and GPT, together with the addition of their co-substrates pyruvate and oxaloacetate, transform glutamate to α-ketoglutarate and aspartate. This was the starting point for the potential systemic glutamate scavenging method for the eradication of the redundant glutamate in the brain ventricles as well as CSF. Afterwards, there has been a focus on glutamate converting transaminases as a possible therapeutic approach. It has been shown that peripheral administration of GOT and GPT with and without oxaloacetate and pyruvate give rise to a decrease in blood glutamate levels (Zlotnik et al., 2007; Boyko et al., 2012a; Boyko et al., 2012b).

One of the interesting findings has come recently that by doing both transcriptome screening and qPCR, GOT levels are found to be increased in MCAO rat ischemic stroke model (Rink et al., 2010). This study is followed by a unique *in vitro* study and by using neuronal HT4 cells transfected with GOT siRNA and verifying diminished GOT mRNA level and GOT activity, neuroprotective effect of GOT under hypoglycemic and high extracellular glutamate conditions has been discovered (Rink et al., 2011). Another study elucidated that patients with big infarction have higher glutamate and lower GOT levels in blood due to the capacity of the to metabolize blood glutamate, which makes GOT a potential biomarker showing the severity of the stroke (Campos et al., 2011c). There has also been a comparison of GOT and GPT in ischemic stroke patients, highlighting that the effect of GOT levels are more significantly showing a better outcome than GPT levels (Campos et al., 2011b). Yet, *in vitro* mechanism of GOT still needs to be understood.

Very recently, neuroprotective outcome of a bioconjugate human recombinant glutamate oxaloacetate transaminase (hrGOT) has been studied and it has been observed that a single administration of hrGOT leads to a drastic decrease of glutamate in bloodstream up to a week. Neuroprotective effect of hrGOT has also been confirmed by decreased infarct volume and improved sensorimotor functions in ischemic rats. Interestingly, the innovative form, the blood brain barrier targeted hrGOT did not show a significant increase in terms of efficiency, stating that glutamate scavenging activity in blood is an effective and powerful technique for stroke neuroprotection (Zaghmi et al., 2020).

## Oxaloacetate

The neuroprotective role of oxaloacetate in ischemia is shown in rats by photothrombotic lesion and revealed that it reduces both blood and brain glutamate levels (Nagy et al., 2009). Interestingly, oxaloacetate injection in complete forebrain ischemia (2VO) model does also provide reestablishment of synaptic plasticity measured by LTP recordings in the CA1 region of hippocampus (Marosi et al., 2009). Further studies are done to be able to show the neuroprotective effect of oxaloacetate on diminishing blood as well as brain glutamate, by transient occlusion of the middle

cerebral artery (MCAO) ischemic model, it has been observed that intravenous oxaloacetate administration leads to a significant drop of glutamate levels both in blood and brain. Moreover, it is confirmed by magnetic resonance spectroscopy (MRS) of the brain clearly showing the neuroprotective outcome of oxaloacetate (Campos et al., 2011a). It has also been demonstrated that glutamate levels in brain extracellular fluid (ECF) can be cleared by oxaloacetate (Teichberg et al., 2009). In another study in which maleate, a glutamate-oxaloacetate transaminase-blocker used next to oxaloacetate elucidates that the neuroprotective activity is reversed, proving the systemic glutamate scavenging activity of oxaloacetate (Zlotnik et al., 2009). Neuroprotective effect of oxaloacetate is also confirmed by electrophysiological methods measuring somatosensory evoked responses upon MCAO, and histological methods (Campos et al., 2012; Knapp et al., 2015; Castillo et al., 2016).

### Pyruvate

The neuroprotective feature of pyruvate in ischemic stroke has been discovered 2 decades ago (Lee et al., 2001). It is followed by more studies showing the protective effect (Yi et al., 2007), as well as by another pyruvate derivative, ethyl pyruvate has also a role in neuroprotective outcome (Kim et al., 2005). However, the glutamate scavenging role of pyruvate is elucidated later by a rat model with closed head injury (Zlotnik et al., 2008). More studies have been done stating that glutamate–pyruvate transaminase together with pyruvate has a protective effect on ischemic rats after head trauma (Boyko et al., 2011), all in all emphasizing the therapeutic potential of glutamate grabber pyruvate in ischemic stroke (**Figure 6**).

## CONCLUSION AND FUTURE PROSPECTS

Ischemic stroke, one of the major reasons of death and disability worldwide, occurs because of the blockage of blood supply to the brain. Glucose and oxygen are limited by the decreased blood flow, causing insufficient energy supply in neurons. Neurons can no longer sustain their transmembrane gradient, leading to depolarization, which induces excitotoxicity *via* releasing neurotransmitters, especially glutamate. Glutamate excitotoxicity increases the production of harmful substances such as ROS that leads to endothelial apoptosis and blood-brain barrier damage and enhances the cerebral injury. Administration of tPA is still one and only therapy for ischemic stroke and the time frame is really short. Recent studies focusing on the glutamate excitotoxicity generates very promising data and scientists are improving novel therapeutic agents targeting different steps in the pathway. In this review, we sought to describe major strategies that are in development, namely systemic glutamate scavenging, which directly decreases extracellular glutamate in the CNS. In particular, systemic glutamate scavenging has received much attention as a new approach to prevent excitotoxicity. Moreover, they are extremely useful due to the fact that there are no side effects, which allow us to use them immediately if suspected and making therapy available for everybody. Since these different methods target to influence the glutamate-mediated damage at different levels, it may be interesting to explore the use of drug combinations to seek synergies in the future. Those trials will allow us to elucidate the application of this new therapeutic strategy. Last but not least, it is also crucial to understand the molecular mechanism behind the glutamate scavengers as well as permeability on blood brain barrier to be able to broaden the window of the current and future therapeutic options in ischemic stroke.

## AUTHOR CONTRIBUTIONS

OK-A, AA, PC, and DG designed the structure of the review. OK-A, AA, and PC wrote and edited the review article. AA prepared the figures. OK-A and PC contributed to the conceptualization of the figures. DG provided the funding.

## FUNDING

This work was supported by the Scientific and Technological Research Council of Turkey (TUBITAK, 219S086), the Natural Science Engineering Council of Canada (NSERC), Instituto de Salud Carlos III, and the Research Council of Norway (RCN) under the frame of EuroNanoMed III (GOTTARG project).

## REFERENCES

Appireddy, R. M., Demchuk, A. M., Goyal, M., Menon, B. K., Eesa, M., Choi, P., et al. (2015). Endovascular Therapy for Ischemic Stroke. *J. Clin. Neurol.* 11 (1), 1–8. doi:10.3988/jcn.2015.11.1.1

Atoji, Y., and Sarkar, S. (2019). Localization of AMPA, Kainate, and NMDA Receptor mRNAs in the pigeon Cerebellum. *J. Chem. Neuroanat.* 98, 71–79. doi:10.1016/j.jchemneu.2019.04.004

Bai, W., and Zhou, Y. G. (2017). Homeostasis of the Intraparenchymal-Blood Glutamate Concentration Gradient: Maintenance, Imbalance, and Regulation. *Front. Mol. Neurosci.* 10, 400. doi:10.3389/fnmol.2017.00400

Bai, W., Zhu, W. L., Ning, Y. L., Li, P., Zhao, Y., Yang, N., et al. (2017). Dramatic Increases in Blood Glutamate Concentrations Are Closely Related to Traumatic Brain Injury-Induced Acute Lung Injury. *Sci. Rep.* 7 (1), 5380. doi:10.1038/s41598-017-05574-9

Bansal, S., Sangha, K. S., and Khatri, P. (2013). Drug Treatment of Acute Ischemic Stroke. *Am. J. Cardiovasc. Drugs* 13 (1), 57–69. doi:10.1007/s40256-013-0007-6

Belov Kirdajova, D., Kriska, J., Tureckova, J., and Anderova, M. (2020). Ischemia-Triggered Glutamate Excitotoxicity from the Perspective of Glial Cells. *Front Cel Neurosci* 14, 51. doi:10.3389/fncel.2020.00051

Bhaskar, S., Stanwell, P., Cordato, D., Attia, J., and Levi, C. (2018). Reperfusion Therapy in Acute Ischemic Stroke: Dawn of a new era? *BMC Neurol.* 18 (1), 8. doi:10.1186/s12883-017-1007-y

Boyko, M., Gruenbaum, S. E., Gruenbaum, B. F., Shapira, Y., and Zlotnik, A. (2014). Brain to Blood Glutamate Scavenging as a Novel Therapeutic Modality: a Review. *J. Neural Transm. (Vienna).* 971–979. 121. doi:10.1007/s00702-014-1181-7

Boyko, M., Melamed, I., Gruenbaum, B. F., Gruenbaum, S. E., Ohayon, S., Leibowitz, A., et al. (2012a). The Effect of Blood Glutamate Scavengers Oxaloacetate and Pyruvate on Neurological Outcome in a Rat Model of Subarachnoid Hemorrhage. *Neurotherapeutics* 9 (3), 649–657. doi:10.1007/s13311-012-0129-6

Boyko, M., Stepensky, D., Gruenbaum, B. F., Gruenbaum, S. E., Melamed, I., Ohayon, S., et al. (2012b). Pharmacokinetics of Glutamate-Oxaloacetate Transaminase and Glutamate-Pyruvate Transaminase and Their Blood Glutamate-Lowering Activity in Naïve Rats. *Neurochem. Res.* 37 (10), 2198–2205. doi:10.1007/s11064-012-0843-9

Boyko, M., Zlotnik, A., Gruenbaum, B. F., Gruenbaum, S. E., Ohayon, S., Kuts, R., et al. (2011). Pyruvate's Blood Glutamate Scavenging Activity Contributes to the Spectrum of its Neuroprotective Mechanisms in a Rat Model of Stroke. *Eur. J. Neurosci.* 34 (9), 1432–1441. doi:10.1111/j.1460-9568.2011.07864.x

Campos, F., Rodríguez-Yáñez, M., Castellanos, M., Arias, S., Pérez-Mato, M., Sobrino, T., et al. (2011a). Blood Levels of Glutamate Oxaloacetate Transaminase Are More Strongly Associated with Good Outcome in Acute Ischaemic Stroke Than Glutamate Pyruvate Transaminase Levels. *Clin. Sci. (Lond)* 121 (1), 11–17. doi:10.1042/CS20100427

Campos, F., Sobrino, T., Ramos-Cabrer, P., Argibay, B., Agulla, J., Pérez-Mato, M., et al. (2011b). Neuroprotection by Glutamate Oxaloacetate Transaminase in Ischemic Stroke: an Experimental Study. *J. Cereb. Blood Flow Metab.* 31 (6), 1378–1386. doi:10.1038/jcbfm.2011.3

Campos, F., Sobrino, T., Ramos-Cabrer, P., Castellanos, M., Blanco, M., Rodríguez-Yáñez, M., et al. (2011c). High Blood Glutamate Oxaloacetate Transaminase Levels Are Associated with Good Functional Outcome in Acute Ischemic Stroke. *J. Cereb. Blood Flow Metab.* 31 (6), 1387–1393. doi:10.1038/jcbfm.2011.4

Campos, F., Sobrino, T., Ramos-Cabrer, P., and Castillo, J. (2012). Oxaloacetate: a Novel Neuroprotective for Acute Ischemic Stroke. *Int. J. Biochem. Cel Biol* 44 (2), 262–265. doi:10.1016/j.biocel.2011.11.003

Castillo, J., Loza, M. I., Mirelman, D., Brea, J., Blanco, M., Sobrino, T., et al. (2016). A Novel Mechanism of Neuroprotection: Blood Glutamate Grabber. *J. Cereb. Blood Flow Metab.* 36 (2), 292–301. doi:10.1177/0271678X15606721

Cohen-Kashi-Malina, K., Cooper, I., and Teichberg, V. I. (2012). Mechanisms of Glutamate Efflux at the Blood-Brain Barrier: Involvement of Glial Cells. *J. Cereb. Blood Flow Metab.* 32 (1), 177–189. doi:10.1038/jcbfm.2011.121

Cooper, A. J., and Jeitner, T. M. (2016). Central Role of Glutamate Metabolism in the Maintenance of Nitrogen Homeostasis in Normal and Hyperammonemic Brain. *Biomolecules* 6 (2), 16. doi:10.3390/biom6020016

Danbolt, N. C. (2001). Glutamate Uptake. *Prog. Neurobiol.* 65 (1), 1–105. doi:10.1016/s0301-0082(00)00067-8

Danbolt, N. C., Pines, G., and Kanner, B. I. (1990). Purification and Reconstitution of the Sodium- and Potassium-Coupled Glutamate Transport Glycoprotein from Rat Brain. *Biochemistry* 29 (28), 6734–6740. doi:10.1021/bi00480a025

Dong, X., Gao, J., Su, Y., and Wang, Z. (2020). Nanomedicine for Ischemic Stroke. *Int. J. Mol. Sci.* 21 (20), 7600. doi:10.3390/ijms21207600

Doyle, K. P., Simon, R. P., and Stenzel-Poore, M. P. (2008). Mechanisms of Ischemic Brain Damage. *Neuropharmacology* 55 (3), 310–318. doi:10.1016/j.neuropharm.2008.01.005

Girling, K. D., Demers, M. J., Laine, J., Zhang, S., Wang, Y. T., and Graham, R. K. (2018). Activation of Caspase-6 and Cleavage of Caspase-6 Substrates Is an Early Event in NMDA Receptor-Mediated Excitotoxicity. *J. Neurosci. Res.* 96 (3), 391–406. doi:10.1002/jnr.24153

Global GBD 2016 Stroke Collaborators (2019). Global, Regional, and National burden of Stroke, 1990-2016: a Systematic Analysis for the Global Burden of Disease Study 2016. *Lancet Neurol.* 18 (5), 439–458. doi:10.1016/S1474-4422(19)30034-1

Godino, Mdel. C., Romera, V. G., Sánchez-Tomero, J. A., Pacheco, J., Canals, S., Lerma, J., et al. (2013). Amelioration of Ischemic Brain Damage by Peritoneal Dialysis. *J. Clin. Invest.* 123 (10), 4359–4363. doi:10.1172/JCI67284

Goldstein, J. N., Marrero, M., Masrur, S., Pervez, M., Barrocas, A. M., Abdullah, A., et al. (2010). Management of Thrombolysis-Associated Symptomatic Intracerebral Hemorrhage. *Arch. Neurol.* 67 (8), 965–969. doi:10.1001/archneurol.2010.175

Gottlieb, M., Wang, Y., and Teichberg, V. I. (2003). Blood-mediated Scavenging of Cerebrospinal Fluid Glutamate. *J. Neurochem.* 87 (1), 119–126. doi:10.1046/j.1471-4159.2003.01972.x

Grewer, C., and Rauen, T. (2005). Electrogenic Glutamate Transporters in the CNS: Molecular Mechanism, Pre-steady-state Kinetics, and Their Impact on Synaptic Signaling. *J. Membr. Biol.* 203 (1), 1–20. doi:10.1007/s00232-004-0731-6

Grupke, S., Hall, J., Dobbs, M., Bix, G. J., and Fraser, J. F. (2015). Understanding History, and Not Repeating it. Neuroprotection for Acute Ischemic Stroke: from Review to Preview. *Clin. Neurol. Neurosurg.* 129, 1–9. doi:10.1016/j.clineuro.2014.11.013

Gupta, K., Hardingham, G. E., and Chandran, S. (2013). NMDA Receptor-dependent Glutamate Excitotoxicity in Human Embryonic Stem Cell-Derived Neurons. *Neurosci. Lett.* 543, 95–100. doi:10.1016/j.neulet.2013.03.010

Hacke, W., Kaste, M., Bluhmki, E., Brozman, M., Dávalos, A., Guidetti, D., et al. (2008). Thrombolysis with Alteplase 3 to 4.5 Hours after Acute Ischemic Stroke. *N. Engl. J. Med.* 359 (13), 1317–1329. doi:10.1056/NEJMoa0804656

Hawkins, R. A. (2009). The Blood-Brain Barrier and Glutamate. *Am. J. Clin. Nutr.* 90 (3), 867S–874S. doi:10.3945/ajcn.2009.27462BB

Heiss, W. D., and Rosner, G. (1983). Functional Recovery of Cortical Neurons as Related to Degree and Duration of Ischemia. *Ann. Neurol.* 14 (3), 294–301. doi:10.1002/ana.410140307

Ikonomidou, C., and Turski, L. (2002). Why Did NMDA Receptor Antagonists Fail Clinical Trials for Stroke and Traumatic Brain Injury? *Lancet Neurol.* 1 (6), 383–386. doi:10.1016/s1474-4422(02)00164-3

Jia, M., Njapo, S. A., Rastogi, V., and Hedna, V. S. (2015). Taming Glutamate Excitotoxicity: Strategic Pathway Modulation for Neuroprotection. *CNS drugs* 29 (2), 153–162. doi:10.1007/s40263-015-0225-3

Jovin, T. G., Chamorro, A., Cobo, E., de Miquel, M. A., Molina, C. A., Rovira, A., et al. (2015). Thrombectomy within 8 hours after Symptom Onset in Ischemic Stroke. *N. Engl. J. Med.* 372 (24), 2296–2306. doi:10.1056/NEJMoa1503780

Kalia, L. V., Kalia, S. K., and Salter, M. W. (2008). NMDA Receptors in Clinical Neurology: Excitatory Times Ahead. *Lancet Neurol.* 7 (8), 742–755. doi:10.1016/S1474-4422(08)70165-0

Kim, J. B., Yu, Y. M., Kim, S. W., and Lee, J. K. (2005). Anti-inflammatory Mechanism Is Involved in Ethyl Pyruvate-Mediated Efficacious Neuroprotection in the Postischemic Brain. *Brain Res.* 1060 (1-2), 188–192. doi:10.1016/j.brainres.2005.08.029

Knapp, L., Gellért, L., Kocsis, K., Kis, Z., Farkas, T., Vécsei, L., et al. (2015). Neuroprotective Effect of Oxaloacetate in a Focal Brain Ischemic Model in the Rat. *Cell Mol Neurobiol* 35 (1), 17–22. doi:10.1007/s10571-014-0064-7

Korczyn, A. D., Brainin, M., and Guekht., A. (2015). Neuroprotection in Ischemic Stroke: what Does the Future Hold? *Expert Rev. Neurother* 15 (3), 227–229. doi:10.1586/14737175.2015.1014806

Kurth, T., Heuschmann, P. U., Walker, A. M., and Berger, K. (2007). Mortality of Stroke Patients Treated with Thrombolysis: Analysis of Nationwide Inpatient Sample. *Neurology* 68 (9), 710–711. doi:10.1212/01.wnl.0000258816.02021.b9

Kwiatkowski, T. G., Libman, R. B., Frankel, M., Tilley, B. C., Morgenstern, L. B., Lu, M., et al. (1999). Effects of Tissue Plasminogen Activator for Acute Ischemic Stroke at One Year. National Institute of Neurological Disorders and Stroke Recombinant Tissue Plasminogen Activator Stroke Study Group. *N. Engl. J. Med.* 340 (23), 1781–1787. doi:10.1056/NEJM199906103402302

Lee, J. Y., Kim, Y. H., and Koh, J. Y. (2001). Protection by Pyruvate against Transient Forebrain Ischemia in Rats. *J. Neurosci.* 21 (20), RC171. doi:10.1523/jneurosci.21-20-j0002.2001

Leibowitz, A., Boyko, M., Shapira, Y., and Zlotnik, A. (2012). Blood Glutamate Scavenging: Insight into Neuroprotection. *Int. J. Mol. Sci.* 13 (8), 10041–10066. doi:10.3390/ijms130810041

Lijnen, H. R., and Collen, D. (1988). Mechanisms of Plasminogen Activation by Mammalian Plasminogen Activators. *Enzyme* 40 (2-3), 90–96. doi:10.1159/000469150

Luoma, J. I., Kelley, B. G., and Mermelstein, P. G. (2011). Progesterone Inhibition of Voltage-Gated Calcium Channels Is a Potential Neuroprotective Mechanism against Excitotoxicity. *Steroids* 76 (9), 845–855. doi:10.1016/j.steroids.2011.02.013

Magi, S., Piccirillo, S., Amoroso, S., and Lariccia, V. (2019). Excitatory Amino Acid Transporters (EAATs): Glutamate Transport and beyond. *Int. J. Mol. Sci.* 20 (22), 5674. doi:10.3390/ijms20225674

Marosi, M., Fuzik, J., Nagy, D., Rákos, G., Kis, Z., Vécsei, L., et al. (2009). Oxaloacetate Restores the Long-Term Potentiation Impaired in Rat hippocampus CA1 Region by 2-vessel Occlusion. *Eur. J. Pharmacol.* 604 (1-3), 51–57. doi:10.1016/j.ejphar.2008.12.022

Matei, N., Camara, J., and Zhang, J. H. (2020). The Next Step in the Treatment of Stroke. *Front. Neurol.* 11, 582605. doi:10.3389/fneur.2020.582605

Mennerick, S., Dhond, R. P., Benz, A., Xu, W., Rothstein, J. D., Danbolt, N. C., et al. (1998). Neuronal Expression of the Glutamate Transporter GLT-1 in Hippocampal Microcultures. *J. Neurosci.* 18 (12), 4490–4499. doi:10.1523/jneurosci.18-12-04490.1998

Muir, K. W. (2006). Glutamate-based Therapeutic Approaches: Clinical Trials with NMDA Antagonists. *Curr. Opin. Pharmacol.* 6 (1), 53–60. doi:10.1016/j.coph.2005.12.002

Nagy, D., Marosi, M., Kis, Z., Farkas, T., Rakos, G., Vecsei, L., et al. (2009). Oxaloacetate Decreases the Infarct Size and Attenuates the Reduction in Evoked Responses after Photothrombotic Focal Ischemia in the Rat Cortex. *Cel Mol Neurobiol* 29 (6-7), 827–835. doi:10.1007/s10571-009-9364-8

National Institute of Neurological Disorders and Stroke rt-PA Stroke Study Group (1995). Tissue Plasminogen Activator for Acute Ischemic Stroke. *N. Engl. J. Med.* 333 (24), 1581–1587. doi:10.1056/NEJM199512143332401

Ogden, K. K., and Traynelis, S. F. (2011). New Advances in NMDA Receptor Pharmacology. *Trends Pharmacol. Sci.* 32 (12), 726–733. doi:10.1016/j.tips.2011.08.003

Papazian, I., Kyrargyri, V., Evangelidou, M., Voulgari-Kokota, A., and Probert, L. (2018). Mesenchymal Stem Cell Protection of Neurons against Glutamate Excitotoxicity Involves Reduction of NMDA-Triggered Calcium Responses and Surface GluR1, and Is Partly Mediated by TNF. *Int. J. Mol. Sci.* 19 (3), 651. doi:10.3390/ijms19030651

Pines, G., Danbolt, N. C., Bjørås, M., Zhang, Y., Bendahan, A., Eide, L., et al. (1992). Cloning and Expression of a Rat Brain L-Glutamate Transporter. *Nature* 360 (6403), 464–467. doi:10.1038/360464a0

Rink, C., Gnyawali, S., Peterson, L., and Khanna, S. (2011). Oxygen-inducible Glutamate Oxaloacetate Transaminase as Protective Switch Transforming Neurotoxic Glutamate to Metabolic Fuel during Acute Ischemic Stroke. *Antioxid. Redox Signal.* 14 (10), 1777–1785. doi:10.1089/ars.2011.3930

Rink, C., Roy, S., Khan, M., Ananth, P., Kuppusamy, P., Sen, C. K., et al. (2010). Oxygen-sensitive Outcomes and Gene Expression in Acute Ischemic Stroke. *J. Cereb. Blood Flow Metab.* 30 (7), 1275–1287. doi:10.1038/jcbfm.2010.7

Rogachev, B., Tsesis, S., Gruenbaum, B. F., Gruenbaum, S. E., Boyko, M., Klein, M., et al. (2013). The Effects of Peritoneal Dialysis on Blood Glutamate Levels: Implementation for Neuroprotection. *J. Neurosurg. Anesthesiol* 25 (3), 262–266. doi:10.1097/ANA.0b013e318283f86a

Rossi, D. J., Brady, J. D., and Mohr, C. (2007). Astrocyte Metabolism and Signaling during Brain Ischemia. *Nat. Neurosci.* 10 (11), 1377–1386. doi:10.1038/nn2004

Rossi, D. J., Oshima, T., and Attwell, D. (2000). Glutamate Release in Severe Brain Ischaemia Is Mainly by Reversed Uptake. *Nature* 403 (6767), 316–321. doi:10.1038/35002090

Rothstein, J. D., Martin, L., Levey, A. I., Dykes-Hoberg, M., Jin, L., Wu, D., et al. (1994). Localization of Neuronal and Glial Glutamate Transporters. *Neuron* 13 (3), 713–725. doi:10.1016/0896-6273(94)90038-8

Sattler, R., Xiong, Z., Lu, W. Y., Hafner, M., MacDonald, J. F., and Tymianski, M. (1999). Specific Coupling of NMDA Receptor Activation to Nitric Oxide Neurotoxicity by PSD-95 Protein. *Science* 284 (5421), 1845–1848. doi:10.1126/science.284.5421.1845

Schousboe, A., Scafidi, S., Bak, L. K., Waagepetersen, H. S., and McKenna, M. C. (2014). Glutamate Metabolism in the Brain Focusing on Astrocytes. *Adv. Neurobiol.* 11, 13–30. doi:10.1007/978-3-319-08894-5_2

Sherzai, A. Z., and Elkind, M. S. (2015). Advances in Stroke Prevention. *Ann. N. Y Acad. Sci.* 1338, 1–15. doi:10.1111/nyas.12723

Smith, W. S., Sung, G., Saver, J., Budzik, R., Duckwiler, G., Liebeskind, D. S., et al. (2008). Mechanical Thrombectomy for Acute Ischemic Stroke: Final Results of the Multi MERCI Trial. *Stroke* 39 (4), 1205–1212. doi:10.1161/STROKEAHA.107.497115

Snelling, B., Mccarthy, D. J., Chen, S., Sur, S., Elwardany, O., Sheinberg, D. L., et al. (2019). Extended Window for Stroke Thrombectomy. *J. Neurosci. Rural Pract.* 10 (2), 294–300. doi:10.4103/jnrp.jnrp_365_18

Storck, T., Schulte, S., Hofmann, K., and Stoffel, W. (1992). Structure, Expression, and Functional Analysis of a Na(+)-dependent Glutamate/aspartate Transporter from Rat Brain. *Proc. Natl. Acad. Sci. U S A.* 89 (22), 10955–10959. doi:10.1073/pnas.89.22.10955

Teichberg, V. I., Cohen-Kashi-Malina, K., Cooper, I., and Zlotnik, A. (2009). Homeostasis of Glutamate in Brain Fluids: an Accelerated Brain-To-Blood Efflux of Excess Glutamate Is Produced by Blood Glutamate Scavenging and Offers protection from Neuropathologies. *Neuroscience* 158 (1), 301–308. doi:10.1016/j.neuroscience.2008.02.075

Tutor-Crespo, M. J., Hermida, J., and Tutor, J. C. (2004). Activation of Serum Aminotransferases by Pyridoxal-5' -phosphate in Epileptic Patients Treated with Anticonvulsant Drugs. *Clin. Biochem.* 37 (8), 714–717. doi:10.1016/j.clinbiochem.2004.03.007

Tzingounis, A. V., and Wadiche, J. I. (2007). Glutamate Transporters: Confining Runaway Excitation by Shaping Synaptic Transmission. *Nat. Rev. Neurosci.* 8, 935–947. doi:10.1038/nrn2274

Vandenberg, R. J., and Ryan, R. M. (2013). Mechanisms of Glutamate Transport. *Physiol. Rev.* 93 (4), 1621–1657. doi:10.1152/physrev.00007.2013

Verdouw, P. D., van den Doel, M. A., de Zeeuw, S., and Duncker, D. J. (1998). Animal Models in the Study of Myocardial Ischaemia and Ischaemic Syndromes. *Cardiovasc. Res.* 39 (1), 121–135. doi:10.1016/s0008-6363(98)00069-8

Verma, M., Wills, Z., and Chu, C. T. (2018). Excitatory Dendritic Mitochondrial Calcium Toxicity: Implications for Parkinson's and Other Neurodegenerative Diseases. *Front. Neurosci.* 12, 523. doi:10.3389/fnins.2018.00523

Westerhuis, L. W., and Hafkenscheid, J. C. (1983). Apoenzyme Content of Serum Aminotransferases in Relation to Plasma Pyridoxal-5'-Phosphate Concentration. *Clin. Chem.* 29 (5), 789–792. doi:10.1093/clinchem/29.5.789

WHO (2020). WHO Methods and Data Sources for Global burden of Disease Estimates 2000-2019. Available at: https://cdn.who.int/media/docs/default-source/gho-documents/global-health-estimates/ghe2019_daly-methods.pdf?sfvrsn=31b25009_7 (Accessed December 21, 2021).

Wu, Q. J., and Tymianski, M. (2018). Targeting NMDA Receptors in Stroke: new hope in Neuroprotection. *Mol. Brain* 11 (1), 15. doi:10.1186/s13041-018-0357-8

Yi, J. S., Kim, T. Y., Kyu Kim, D., and Koh, J. Y. (2007). Systemic Pyruvate Administration Markedly Reduces Infarcts and Motor Deficits in Rat Models of Transient and Permanent Focal Cerebral Ischemia. *Neurobiol. Dis.* 26, 94–104. doi:10.1016/j.nbd.2006.12.007

Yoo, A. J., Pulli, B., and Gonzalez, R. G. (2011). Imaging-based Treatment Selection for Intravenous and Intra-arterial Stroke Therapies: a Comprehensive Review. *Expert Rev. Cardiovasc. Ther.* 9 (7), 857–876. doi:10.1586/erc.11.56

Zaghmi, A., Dopico-López, A., Pérez-Mato, M., Iglesias-Rey, R., Hervella, P., Greschner, A. A., et al. (2020). Sustained Blood Glutamate Scavenging Enhances protection in Ischemic Stroke. *Commun. Biol.* 3 (1), 729. doi:10.1038/s42003-020-01406-1

Zauner, A., Bullock, R., Kuta, A. J., Woodward, J., and Young, H. F. (1996). Glutamate Release and Cerebral Blood Flow after Severe Human Head Injury. *Acta Neurochir Suppl.* 67, 40–44. doi:10.1007/978-3-7091-6894-3_9

Zlotnik, A., Gruenbaum, S. E., Artru, A. A., Rozet, I., Dubilet, M., Tkachov, S., et al. (2009). The Neuroprotective Effects of Oxaloacetate in Closed Head Injury in Rats Is Mediated by its Blood Glutamate Scavenging Activity: Evidence from the Use of Maleate. *J. Neurosurg. Anesthesiol* 21 (3), 235–241. doi:10.1097/ANA.0b013e3181a2bf0b

Zlotnik, A., Gurevich, B., Cherniavsky, E., Tkachov, S., Matuzani-Ruban, A., Leon, A., et al. (2008). The Contribution of the Blood Glutamate Scavenging Activity of Pyruvate to its Neuroprotective Properties in a Rat Model of Closed Head Injury. *Neurochem. Res.* 33 (6), 1044–1050. doi:10.1007/s11064-007-9548-x

Zlotnik, A., Gurevich, B., Tkachov, S., Maoz, I., Shapira, Y., and Teichberg, V. I. (2007). Brain Neuroprotection by Scavenging Blood Glutamate. *Exp. Neurol.* 203 (1), 213–220. doi:10.1016/j.expneurol.2006.08.021

**Conflict of Interest:** The authors declare that the research was conducted in the absence of any commercial or financial relationships that could be construed as a potential conflict of interest.

**Publisher's Note:** All claims expressed in this article are solely those of the authors and do not necessarily represent those of their affiliated organizations, or those of the publisher, the editors and the reviewers. Any product that may be evaluated in this article, or claim that may be made by its manufacturer, is not guaranteed or endorsed by the publisher.

frontiers in Pharmacology

REVIEW
published: 29 March 2022
doi: 10.3389/fphar.2022.839790

# Challenges in the Development of Drug Delivery Systems Based on Small Extracellular Vesicles for Therapy of Brain Diseases

*Gecioni Loch-Neckel*[1], *Ana Teresa Matos*[1], *Ana Rita Vaz*[1,2]* *and Dora Brites*[1,2]*

[1]Neuroinflammation, Signaling and Neuroregeneration Lab, Research Institute for Medicines (iMed.ULisboa), Faculty of Pharmacy, Universidade de Lisboa, Lisbon, Portugal, [2]Department of Pharmaceutical Sciences and Medicines, Faculty of Pharmacy, Universidade de Lisboa, Lisbon, Portugal

Small extracellular vesicles (sEVs) have ~30–200 nm diameter size and may act as carriers of different cargoes, depending on the cell of origin or on the physiological/pathological condition. As endogenous nanovesicles, sEVs are important in intercellular communication and have many of the desirable features of an ideal drug delivery system. sEVs are naturally biocompatible, with superior targeting capability, safety profile, nanometric size, and can be loaded with both lipophilic and hydrophilic agents. Because of their biochemical and physical properties, sEVs are considered a promising strategy over other delivery vehicles in the central nervous system (CNS) since they freely cross the blood-brain barrier and they can be directed to specific nerve cells, potentiating a more precise targeting of their cargo. In addition, sEVs remain stable in the peripheral circulation, making them attractive nanocarrier systems to promote neuroregeneration. This review focuses on the recent progress in methods for manufacturing, isolating, and engineering sEVs that can be used as a therapeutic strategy to overcome neurodegeneration associated with pathologies of the CNS, with particular emphasis on Alzheimer's, Parkinson's, and amyotrophic lateral sclerosis diseases, as well as on brain tumors.

**Keywords: drug delivery systems, microRNA nanocarriers, biomarkers, neurodegenerative diseases, brain tumors, cargo of sEVs/exosomes, isolation and loading of sEVs/exosomes**

OPEN ACCESS

***Edited by:***
*Christian Celia,*
*University of Studies G. d'Annunzio Chieti and Pescara, Italy*

***Reviewed by:***
*M. Carmen Martínez,*
*Université d'Angers, France*
*Maria Blanco Formoso,*
*University of Vigo, Spain*

***Correspondence:**
*Ana Rita Vaz*
*armvaz@ff.ulisboa.pt*
*Dora Brites*
*dbrites@ff.ulisboa.pt*

***Specialty section:***
*This article was submitted to Neuropharmacology, a section of the journal Frontiers in Pharmacology*

***Received:*** *20 December 2021*
***Accepted:*** *21 February 2022*
***Published:*** *29 March 2022*

***Citation:***
*Loch-Neckel G, Matos AT, Vaz AR and Brites D (2022) Challenges in the Development of Drug Delivery Systems Based on Small Extracellular Vesicles for Therapy of Brain Diseases. Front. Pharmacol. 13:839790. doi: 10.3389/fphar.2022.839790*

## 1 INTRODUCTION

The term "extracellular vesicles" refers to particles naturally released from the cell that do not contain a functional nucleus, i.e., they cannot replicate themselves (Johnstone, 2005). Extracellular vesicles (EVs) are released by most cell types and can be classified into different subtypes, including large and small extracellular vesicles (respectively, lEVs and sEVs), exomeres, supermeres, oncosomes, and apoptotic bodies (El Andaloussi et al., 2013; Brites, 2020; Zhang et al., 2021). These EVs are different in size, density, biochemical and biophysical properties, as well as in secretion pathways, which may depend on the donor cells that produce them (**Figure 1**). EVs can be taken up by the recipient cells through different mechanisms, including phagocytosis, micropinocytosis, receptor-ligand interaction, or membrane fusion.

Apoptotic bodies result from the fractionation/fragmentation of the cellular content of cells that die by apoptosis. These bodies are formed during membrane disintegration by a separation of the plasma membrane from the cytoskeleton (Jiang and Poon, 2019). Apoptotic bodies are

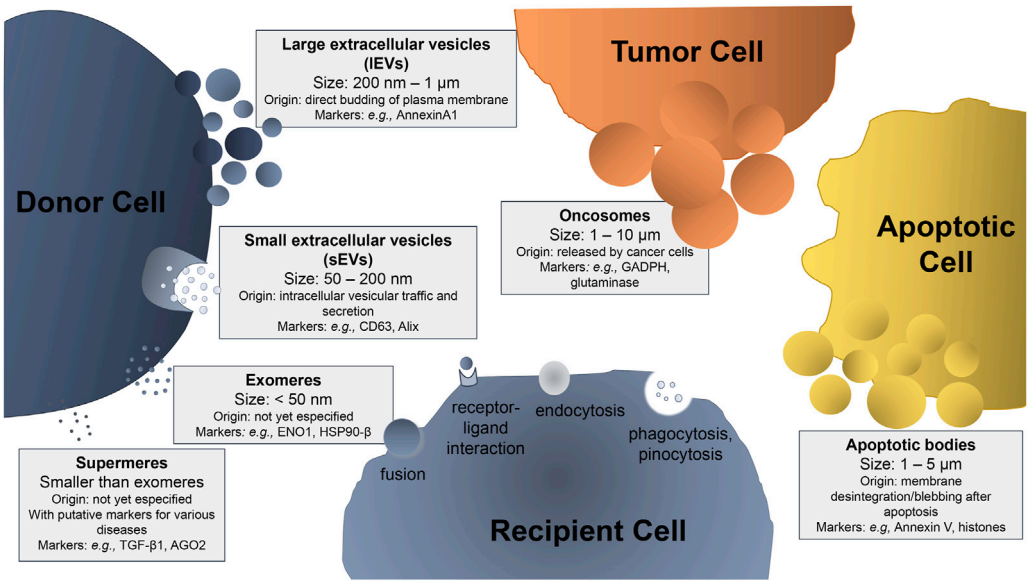


**FIGURE 1 |** Schematic representation of the extracellular vesicles (EVs) subtypes, sizes, and characteristic markers. Depending on their size and site of origin, EVs can be classified as: i) large extracellular vesicles (lEVs), also mentioned as ectosomes or microvesicles, when their size ranges from 200 nm to 1 µm, generated from the budding of the plasma membrane; ii) small extracellular vesicles (sEVs), also referred as exosomes, with a diameter from 50 to 200 nm, which are formed after inward budding of endosomal vesicle membrane and maturation in multivesicular bodies that later fuse with the plasma membrane to be secreted into the extracellular space; iii) oncosomes, which are EVs secreted by tumor cells, with a size ranging from 1 to 10 µm (relatively larger than lEVs) and responsible for the spreading of the tumor; iv) apoptotic bodies that are EVs secreted by apoptotic cells upon their membrane disintegration after apoptosis, with a size ranging from 1 to 5 µm; (v) amembraneous exomeres that present a size smaller than 50 nm, whose origin is not fully understood yet; and (vi) amembraneous supermeres that are smaller and morphologically distinct from exomeres. The cell that releases EVs into the medium is called the donor cell and the one that internalizes EVs is the recipient cell. EV internalization in the recipient cell can occur by dissecting mechanisms, such as: a) fusion, when the membrane of the vesicle becomes contiguous with the cell membrane, releasing its contents into the cell; b) receptor-ligand interaction, when the vesicle has a specific ligand in its membrane that will bind to a specific receptor on the cell membrane allowing its internalization; c) endocytosis, when the vesicle is internalized by the plasma membrane; d) phagocytosis, when the vesicle is larger than 0.5 µm, being engulfed by the target cell; and e) pinocytosis in the case of fluid absorption (macropinocytosis of solute molecules larger than 200 nm and micropinocytosis of smaller particles). Some examples of characteristic markers used in EV identification are included.

quite variable in size and cargo. They have a size ranging from 1 to 5 µm and their cellular contents includes intact organelles, with high levels of proteins associated with the nucleus, chromatin residues, DNA fragments, RNA (in a large amount), degraded proteins, organelles fragments, and glycosylated proteins (in a small amount) (Xu et al., 2019; Battistelli and Falcieri, 2020).

lEVs, also referred to in the literature as ectosomes or microvesicles (MVs), are originated from the cellular membrane through budding and fission. After their generation, lEVs are released within the extracellular space, enter in the circulation, and transfer their cargo to either neighboring or more distant cells (Akers et al., 2013). lEVs are quite heterogeneous in size, ranging from ~200 nm to more than 1–2 µm in diameter. Their cargo usually reflects both the intracellular origin and the cell type from which they are derived, and may contain cytoskeletal proteins, heat shock proteins, integrins, nucleic acids, bioactive lipids, and other active components expressed by the cells of origin (Lv et al., 2019). Some markers used in their characterization are included in **Figure 1**, though their specific characterization is not trivial (Phan et al., 2021) and some of the markers despite being more abundant in lEVs can be also found in sEVs and vice-versa (Théry et al., 2018; Saludas et al., 2022).

sEVS, also referred to as exosomes, derive from the endosome pathway. They have tightly controlled biogenesis and regulated secretion into the extracellular media. sEVs are typically 30–200 nm in diameter and are the most homogeneous (in both shape and size) population of extracellular vesicles (Yuyama and Igarashi, 2016). They are lipid bilayer bound vesicles that are easily uptaken by the mononuclear phagocyte system, allowing them to reach other cellular targets beyond the ones from which they derive (Antimisiaris et al., 2018). sEVs are constitutively or stimulus-dependently secreted from many different cell types, including those of the nervous system, such as neurons, astrocytes, oligodendrocytes, and microglia (Caruso Bavisotto et al., 2019; Song Z. et al., 2020). sEVs are important mediators in cell-to-cell and inter-tissue communication, by carrying small noncoding ribonucleic acids (ncRNAs), messenger RNAs (mRNAs), lipid molecules, and proteins. sEVs play critical roles in regulating both physiological and pathological processes. Indeed, in pathological conditions, the cargo transferred by sEVs may have detrimental effects, while contributing for the spread of the disease, which has been described in inflammation-associated and neurodegenerative diseases, as well as in tumor growth (Johnstone, 2005; Ciregia et al., 2017; Isola and Chen, 2017; Busatto et al., 2021). Recent evidence indicates that sEVs released

by the different tissues can be collected from body fluids, in order to evaluate their unique protein or RNA content to be used as disease biomarkers, or as therapeutic tools in different pathologies (Barile and Vassalli, 2017). Some examples were already described in the cancer field, where the tumor-derived sEVs were demonstrated to be enriched in certain miRNAs that could act as tumor markers (Kumar et al., 2015), or in circulating sEVs derived from glioblastoma patients, which have showed increased levels of Epidermal Growth Factor Receptor (EGFR)-vIII mRNA (Skog et al., 2008). Other examples related with the central nervous system (CNS) disorders include the AT270 phospho-tau, a biomarker for Alzheimer's disease (AD), detected in sEVs collected from the cerebrospinal fluid (CSF) of patients with mild disease (Saman et al., 2012), and syntenin one that was found elevated in the circulating sEVs isolated from the serum of Parkinson's disease (PD) patients (Tomlinson et al., 2015). Several studies using different body fluids and their isolated sEVs propose them as potential candidates for early diagnosis in neurodegenerative diseases based on the disease-associated mutant proteins and miRNAs (Hornung et al., 2020; Rastogi et al., 2021). However, the majority of the studies are retrospective with incomplete clinical and pathological informations (Wong and Chen, 2019). Moreover, though the quick and accurate isolation of sEVs is key for their application, current methods still have limitations, such as time-consuming processes, presence of contaminants, and high costs (Xiao et al., 2020). Standard isolation protocols are not yet established and sEVs usually represent a heterogenous population derived from different cell sources. Lately, separation of sEVs originated from neurons, microglia and astrocytes were achieved by using specific cell surface markers and magnetic beads (Kumar et al., 2021).

Another type of EVs referred to as oncosomes are atypical EVs derived from cancer cells, with larger sizes (1–10 μm), which may carry abnormal macromolecules including oncoproteins. They are produced from non-apoptotic plasma membrane blebbing from cancer cells and can mediate the communication between cancer and non-cancer cells within the tumor microenvironment (Jaiswal and Sedger, 2019).

In recent years, a novel population of EVs smaller than sEVs (<30 nm of diameter) that can be isolated from the sEVs by an ultracentrifugation-based method was described (Zhang Q. et al., 2019). Although their function is still a matter of debate, it is known that exomeres are enriched in proteins involved in cellular bioenergetics, namely in glycolysis and Mechanistic Target of Rapamycin Complex 1 (mTORC1) metabolic pathways, suggesting their potential association with mitochondrial function. In the same study, the authors demonstrated that exomeres are enriched in proteins associated with the endoplasmic reticulum, mitochondria, and microtubules, suggesting that these proteins may be implicated in their biogenesis or even secretion. Nucleic acids and lipids are also reported as part of exomeres' cargo. Lately, supermeres, nanoparticles smaller than sEVs and exomeres, and morphologically distinct from exomeres, were described to be easily ingested and enriched with cargo involved in several cancers, as well as Alzheimer's and cardiovascular diseases (Zhang et al., 2021). They are enriched in proteins and miRNAs, as well as miRNA-processing proteins such as Argonaute RISC Catalytic Component 2 (AGO2), and are functional agents of intercellular communication, also constituting candidate biomarkers and therapeutic targets (Clancy et al., 2021).

Such heterogeneity of EVs needs further attention to understand the nature of each subpopulation in a more specific manner. In this review we recapitulate recent progress in methods for manufacturing, isolating, and engineering sEVs, and how they can be used to treat brain diseases. As endogenous nanovesicles, sEVs also have many of the desirable features of a good drug delivery system. They are naturally biocompatible, with superior targeting capability, safety profile, nanometric size, and can be loaded with both lipophilic and hydrophilic agents. Because of these highly desirable properties and their ability to penetrate biological barriers, sEVs represent ideal natural nanocarriers for the treatment of brain diseases (Busatto et al., 2021; Elliott and He, 2021). In terms of their transport and properties, sEVs are promising carrier vehicles for the transfer of drugs across the blood–brain barrier (BBB).

## 2 BIOGENESIS, PRODUCTION, AND STORAGE OF sEVs

Due to the growing number of studies using EVs in the last years, there was a need to create guidelines for the standardization of protocols of separation and characterization, nomenclature, and usage of the different types of EVs. Guidelines were part of the first Minimal Information for Studies of Extracellular Vesicles (MISEV) document, which was released in 2014 by the International Society for Extracellular Vesicles (ISEV). More recently, MISEV2018 guidelines were published in the *Journal of Extracellular Vesicles* (Théry et al., 2018). The purpose of this document was to provide an overview of the recommended procedures among the standardized methods in EV research. The information related with EV biogenesis, uptake, and signaling is more consensual, although storage and stability issues remain a matter of discussion among the scientific community, as well as the processes of EV fusion with the target cells (Russell et al., 2019). In this chapter, we will summarize the current knowledge on biogenesis, production, and storage of sEVs.

### 2.1 Origin

sEVs are secreted by all cells and are originated as intraluminal vesicles during the process of multivesicular body formation. The biogenesis of sEVs has been addressed by many publications (Baumann, 2021; Brites, 2020; Russell et al., 2019; van Niel et al., 2018). Briefly, the biogenesis of sEVs (**Figure 2A**) consists of three different stages: (1) the formation of endocytic vesicles from the plasma membrane, (2) the inward budding of the endosomal vesicle membrane that maturates in multivesicular bodies (MVBs), which consist of intraluminal vesicles (ILVs), and (3) the fusion of MVBs with the plasma membrane (instead of being sent to degradation into the lysosomes), allowing the release of

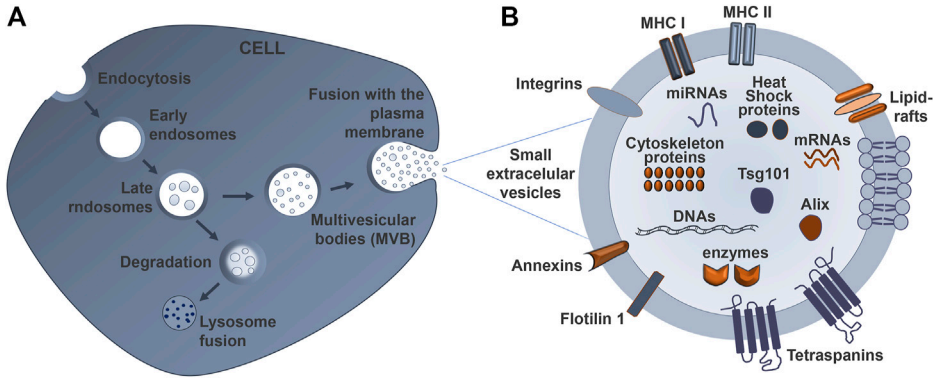


**FIGURE 2 |** Schematic representation of sEV biogenesis and its typical structure. **(A)** Early endosomes mature into late endosomes named multivesicular bodies (MVBs), which are formed after inward budding of the plasma membrane. The MVBs can either fuse with lysosomes to degrade their cargo, or fuse with the cell membrane to release small extracellular vesicles (sEVs) into the extracellular space, thus mediating cell-to-cell communication. **(B)** The sEV is limited by a lipid bilayer that includes ceramide sphingolipids and phospholipids. The sEV membrane also contains various proteins involved in the antigen presentation (major histocompatibility complexes–MHC I and II), as well as targeting and adhesion (integrin and tetraspanins) proteins, together with annexins. The cytosol content of the sEVs varies according to the cell and tissue from which they derive, and may contain lipids, nucleic acids, and proteins, among other components.

these ILVs, including sEVs, into the extracellular space (Zhang Y. et al., 2019). The pattern of nanospherical membrane-type is derived from the parent cells from which the sEVs are formed. Their respective cargo will likewise vary depending on the cell type of origin and status (Kang et al., 2021). The sEV membrane is formed by two layers of proteins and lipids, including cholesterol, phospholipids, glycerophospholipids, and sphingolipids that maintain its stability and structure (**Figure 2B**). Their lipid composition accounts for their unique rigidity (Skotland et al., 2019; Lin Y. et al., 2020).

After sEV release by exocytosis, their cargo is protected from enzymes like proteases and ribonucleases by their lipid bilayer membrane (Lorenc et al., 2020) (**Figure 3**). Once at the extracellular space, sEVs are transferred into the recipient cells through interaction with proteins that facilitate subsequent endocytosis by specific processes, such as receptor interaction, membrane fusion, and internalization. The internalization step of sEVs by the recipient cells can occur via receptor-ligand interactions, direct fusion of membranes, or internalization via endocytosis, and is normally dependent on the cell type, as recently reviewed by Malloci and others (Malloci et al., 2019). For example, the selective transfer of sEVs from oligodendrocytes and their subsequent uptake by microglia through a macropinocytosis mechanism does not require binding to the specific receptor (Fitzner et al., 2011). Another example is the injection of oligodendroglia sEVs in mouse brain, which results in a functional retrieval of sEV cargo in neurons through a clathrin-dependent endocytosis (Fruhbeis et al., 2013). Another study refers to the release of EVs from primary cortical astrocytes and microglial cells being triggered by ATP-mediated activation of P2X7 receptors after contact with phosphatidylserine at the cell surface (Bianco et al., 2009). sEVs carrying a multitude of proteins, such as myelin proteins, as well as RNA, are released from oligodendrocytes and endocytosed by neurons (Frohlich et al., 2014). In addition, the release of serotonin from neurons has been implicated in the release of microglial sEVs, upon binding of serotonin to specific receptors found in the microglia, suggesting a neurotransmitter dependent release (Glebov et al., 2015). To sum up, sEV uptake is determined by multiple mechanisms, together with cell-dependent different combinations of strategies. These specificities should be considered when designing sEV-based therapies.

## 2.2 Source

sEVs exert unique biological activities by stimulating regeneration and modulating pathological conditions, properties that can be explored for medicinal purposes. Namely, they are able to transfer RNA and proteins from donor cells to other cells in the surrounding milieu (Simons and Raposo, 2009). Furthermore, EVs derived from mesenchymal stem cells (MSCs) appear particularly useful in enhancing recovery from various injuries. MSCs are commonly used as a source of sEVs because they can recapitulate the biological activity of MSCs and have been used as a cell-free therapeutic (Harrell et al., 2021). For example, stem cells may modulate their biological effects through the delivery of genetic information that will alter the gene expression of the target cells (Zhao et al., 2019). In addition, EVs from both immune and non-immune cells are shown to suppress or stimulate both adaptive and innate immunity, which effects likely depend on the environmental context, as well as on the type of EV from a particular immune cell (Kim et al., 2005; Bu et al., 2015). sEVs are potential fingerprints of their originating cells and their composition largely depends on the donar cell, although it can also be determined by the cell metabolism and its needs, as well as be influenced by cellular and environmental factors (Bell and Taylor, 2017). As an example, release of miRNAs from cells into sEVs can occur either passively or actively. Therefore, it is very important to choose the cell lines that will act as the source of sEVs, once the donor cell will determine their ability to selectively target cells (Sancho-Albero et al., 2019). It has been shown that the interaction between the drug delivery systems is affected by

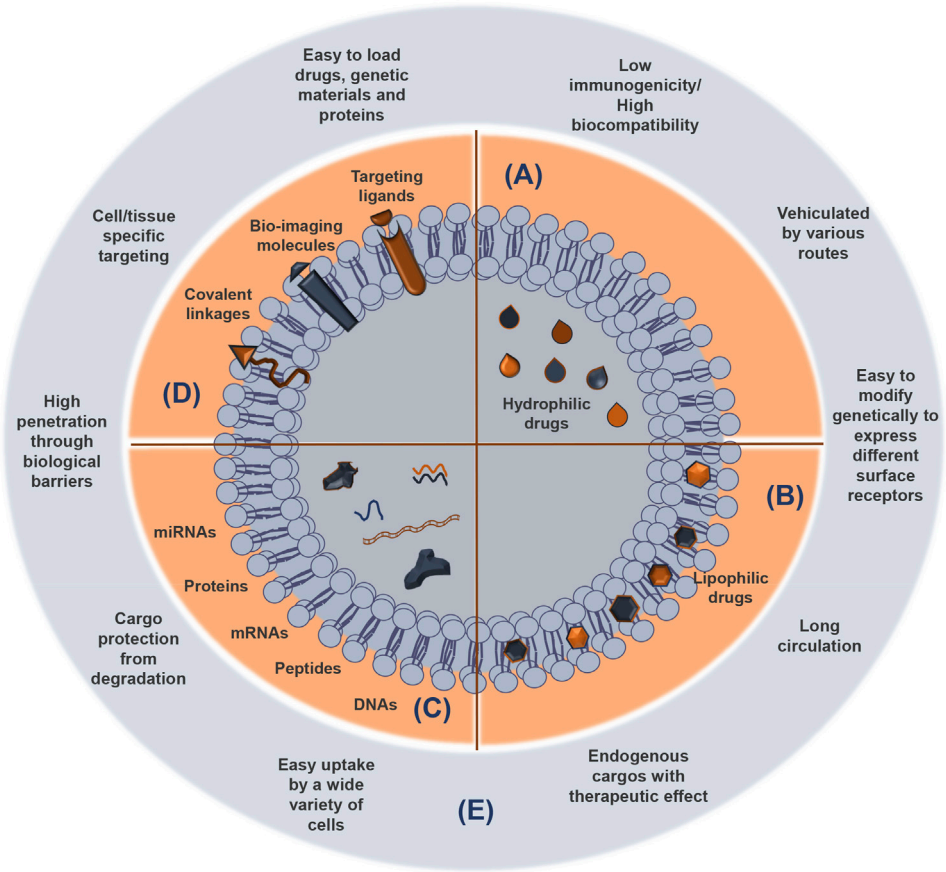


**FIGURE 3 |** sEV cargoes and advantages as delivery systems of functional and therapeutic molecules. Small extracellular vesicles (sEVs) consist of an aqueous compartment surrounded by a lipid bilayer. sEVs can compartmentalize and solubilize hydrophilic compounds in the aqueous compartments **(A)** and lipophilic molecules almost totally entrapped in the lipid layer **(B)**, which protects them from degradation. Agents with intermediary partition coefficient are equally distributed between the aqueous and the lipid compartments. Protein, peptides, and genetic material can be also released from sEVs **(C)**. Attachment of targeting compounds, bio-imaging molecules, and covalent linkage to sEV surface contribute to enhance their utility as vehicles to deliver biomolecules and drugs **(D)**. The most important advantages of the sEVs as therapeutic nanocarriers are indicated **(E)**.

the EV surface proteins (Yin et al., 2013). The ability of different types of EVs to modulate immune responses allows their therapeutic potential as a tool with theragnostic applications in nanomedicine (Thomas et al., 2021). Therefore, we may enrich sEVs with promising curative molecules or engineering cell lines to produce sEVs with a specific and desired target specificity (Gao et al., 2018).

## 2.3 Strategies to Enhance Production

The use of sEV technology as drug delivery vehicles must meet two basic requirements: first, a reproducible and scalable isolation with established production protocols to achieve high purity and elevated yield of a defined population of sEVs for clinical use; and second, the high drug-loading content in sEVs must be enough to obtain a therapeutic response (Armstrong and Stevens, 2018; Lin Y. et al., 2020; Wu Z. et al., 2021). Cells may produce higher or lower number of sEVs depending on several factors, but what will be important is that the production of enormous quantities of vesicles does not modify cell characteristics and behavior. Alterations in the composition and function of the sEVs may be performed using environmental parameters, such as pH gradients, mass transfer, or hydrodynamic force during scale-up processes. The number of sEVs released depends on the cell type, physiological state, and microenvironmental conditions. The production increases in cancer cells under hypoxic conditions, in melanoma cells under acidic microenvironment, and under cell stress induction with calcium ionophores (Zaborowski et al., 2015). It was indicated that immature dendritic cells produce a limited number of sEVs in the μg range (Alvarez-Erviti et al., 2011). However, MSCs secrete more elevated amounts, usually in the milligram range (Chen et al., 2011), making them a more relevant source for the production of therapeutic EVs targeting neurodegenerative diseases. Nevertheless, it should be taken into account that MSCs may undergo senescence after a few passages, a condition that will lead to the production of sEVs with impaired regenerative capacity as compared to those from younger cells (Severino et al., 2013). The confluence of cell

cultures also plays a critical role in the biogenesis and secretion of sEVs. Cell culture in a pre-confluent state showed a decreased sEV secretion compared to the confluent one, potentially due to changes in cholesterol metabolism (Llorente et al., 2013). In addition, sEV secretion rate from the 3D cultured cells is better when cells are close to confluence (Thippabhotla et al., 2019).

Contact inhibition between cells can also reduce sEV release, since these cells become quiescent and do not actively divide (Whitford and Guterstam, 2019). Apart from the individual characteristics of the cell culture and of the cell type that originates the sEVs, some methods are designed to increase their total yield, such as intracellular calcium production (Savina et al., 2003), external stress (de Jong et al., 2012), cytoskeletal blocking (Parolini et al., 2009), drug stimulation (Datta et al., 2018; Wang et al., 2020), and induction of gene expression factors (Boker et al., 2018). In spite of increasing the sEV yield, such methods should be considered with caution, since they may also alter sEV composition, therapeutic efficacy, and safety (Emam et al., 2018; Whitford and Guterstam, 2019). Another aspect to take into consideration is the increased risk of contamination with apoptotic bodies (Emam et al., 2018; Whitford and Guterstam, 2019), although their presence was referred to also have important regulatory roles, and can be a mechanism to immunomodulate dying cells (Caruso and Poon, 2018).

Some recent studies report the relevance of neural cell-derived sEVs to be used in neurodegenerative conditions (Huo et al., 2021). The direct conversion of somatic cells into induced neural precursor cells (iNPCs) provides abundant production of sEVs (Ma et al., 2019; Yuan P. et al., 2021), mainly if using bioreactors (Baghbaderani et al., 2011; Miranda et al., 2016). These sEVs after transplantation revealed to have therapeutic properties in ischemic stroke (Zhang et al., 2020). Lately, studies considered that milk is a viable and safe source of sEVs for therapeutic delivery. For instance, breast milk was shown to contain EVs in large quantities and with an enriched cargo in miRNAs (Jiang et al., 2021). Moreover, it has been demonstrated that milk sEVs improve oral drug bioavailability by protecting their cargo against degradation by low pH, RNases, or conditions that mimic digestion in the gastrointestinal tract (Izumi et al., 2012). Other biofluids, such as saliva, blood, and urine, were also demonstrated to be an alternative source of sEVs. Nevertheless, each body fluid has a clearly distinct vesicle profile and it is not clear what is the delivery potential and safety of these systems for continuous or long-term continuous exposure (Yuana et al., 2013).

## 2.4 Large-Scale Production

Applying the sEV-based therapies to clinics has been slowed down due to sEV low availability and difficulties for large-scale production. Beyond the use of small molecule modulators capable of enhancing sEV secretion, e.g., norepinephrine, N-methyldopamine, and forskolin recently described for MSCs (Wang et al., 2020), other upscaling approaches and technologies for their production have been reported, assuring not only high quality but also high quantity (Andriolo et al., 2018; Mendt et al., 2018). These strategies involve standardized production methods that increase the volume of cell culture from flasks to containers, bioreactors, or hollow fibers, aiming production toward a good manufacturing practice–grade (GMP-grade) of sEVs. Different methods have allowed researchers to isolate and characterize sEV populations in a more accurate way. First works describing methods for the production, purification, and characterization of clinical grade sEVs (cGMP) emerged in the beginning of 2000 (Lamparski et al., 2002; Navabi et al., 2005).

Bioreactors and hollow-fiber perfusion bioreactors have been used in cell culture systems for a long time and they improve sEV yield. These reactors support large numbers of cells at high densities in a continuous mode without the need of splitting or subculturing these cells (Yamashita et al., 2018; Yoo et al., 2018). Using a hollow fiber bioreactor, Watson and others showed that the yield of sEVs obtained from the conditioned media of human embryonic kidney 239 cells (HEK293 cells) was $100 \times 10^7$ particles per μg EV protein, instead of $20 \times 10^7$ by the conventional flask culture (Watson et al., 2016). In another study with MSCs, the authors showed that once compared to the conventional methods, the bioreactor led to a 5.7-fold increase of EV concentration in the conditioned medium, with a threefold increase in the number generated per cell (MSC from bone marrow originated an average of $3 \times 10^{11}$ EV particles per 60 ml final volume) (de Almeida Fuzeta et al., 2020). Additional advantages include less risk of contamination and less labor, besides the higher yield in a short incubation period. However, ideal criteria for production of large-scale GMP-grade EVs, such as scalability, reproducibility, size distribution, safety, surface charge, and purity of the resulting product still remain to be determined (Yamashita et al., 2018). Nevertheless, biomanufacturing of cells engineered to produce therapeutic proteins is well established, and practices or lessons from this area of industry could be transferred into the production of sEVs to be used in biomedicine.

## 2.5 Storage Conditions

Stability of products is mandatory and required for biomedical applications, such as the case of drug delivery systems. There are few research groups trying to understand the relationship between storage conditions and the integrity of sEVs (Jeyaram and Jay, 2017). The ISEV recommends that sEVs must be suspended in phosphate buffered saline (PBS) and stored at −80°C (Witwer et al., 2013). This recommendation was based on previous works showing that the structural and biological stability of the sEVs stored at −80°C for periods of up to 5 months have not been affected. Mendt and collaborators showed that the number and size distribution of sEVs after freezing (for 45 d or 6 months) and thawing are not affected as evaluated by Nanoparticle Tracking Analysis (NanoSight) and electron microscopy compared with freshly prepared sEVs and for up to 48 h when stored at room temperature or 4°C (Mendt et al., 2018). Recently, it has been shown that sEVs should be stored at 4°C or -20°C for short-term preservation; for longer periods of storage for therapeutic application, the most suitable temperature of preservation of sEVs is −80°C (Wu JY. et al., 2021). The effects

**TABLE 1 |** Advantages and disadvantages of most used methods to isolate small extracellular vesicles (sEVs).

| Methods | Advantages | Disadvantages | References |
|---|---|---|---|
| Differential ultracentrifugation | Relatively simple and low cost, high purity, high-enrichment isolation, potentially sterile, reduced contamination risks with separation reagents, large sample capacity, scalable | Requires ultracentrifuge machine, laborious and large sample volume, low recovery, protein contamination risks, potential exosomal aggregation, subject to operator-based variability, high speed centrifugation may damage sEVs | (Whitford and Guterstam, 2019; Konoshenko et al. (2018) |
| Density gradient centrifugation | More specific for certain sEV types, higher separation efficiency, separated components are not mixing again, maintains the structure and functions of sEVs | Complex, time-consuming, considerable sEV loss, expensive | (Lamparski et al., 2002; Zhang et al., 2019a; Lane et al., 2017; Théry et al. (2006) |
| Ultrafiltration | Sterile, fast, no special equipment required, direct RNA extraction possible, highest exosomal RNA yield, scalable | Low purity, loss of sEVs due to their attaching to the membranes, shear stress that can induce deterioration | (Zhang et al., 2019b; Lane et al., 2017; Oeyen et al., 2018; Heinemann et al. (2014) |
| SEV precipitation | Simple procedure, low number of steps, preservation of bioactivity, potential high yield, does not require specialized equipment, large and scalable sample capacity | Long running time, co-precipitation of other non-exosomal contaminants (e.g., proteins and polymeric materials) | (Momen-Heravi et al., 2013; Patel et al., 2019; Niu et al. (2017) |
| Immunological separation | Excellent for isolation of specific sEVs, rapid, easy to use, requires less sample volume, high RNA yield, high sensitivity and specificity, low number of steps | High reagent costs, low yield, difficulty in completely removing antibody from sample | (Théry et al., 2006; Momen-Heravi et al., 2013; Tauro et al., 2012; Cai et al. (2018) |
| Microfluidics-based technologies | Biocompatibility, requires low sample volumes, high purity, high resolution, contact-free manipulation, low cost, high-throughput, and precision | Low sample capacity, no distinction between the vesicles with the same surface markers | (Guo et al., 2018; Contreras-Naranjo et al., 2017; Sancho-Albero et al. (2020) |
| Tuneable resistive pulse sensing | High resolution, more accuracy, allows high-throughput analysis and simultaneous evaluation of size and zeta potential | Risk of pores getting clogged, lacks sensitivity, no detection of small sEVs, no distinction between types of particles | (Kurian et al., 2021; Lane et al., 2015; Akers et al., 2016; Coumans et al. (2014) |

of storage do not seem to depend on the sEV cellular or tissue source (Maroto et al., 2017).

A correct cryopreservation of biological material intended for therapeutic use is also crucial. When frozen and kept properly, specimens maintain their viability and prevent osmotic damage through the use of cryoprotectants, such as sucrose or trehalose (Kusuma et al., 2018). These cryoprotectants do not penetrate in the cell membrane. Instead, they stabilize and preserve the cell membranes, allowing regulated extracellular ice growth during controlled cooling, thus protecting sEVs from cryodamage (Bosch et al., 2016). There is still a critical need to develop protocols for collection and storage of sEV samples due to the still undefined standard operation procedures for their preservation conditions after isolation. Emerging techniques for EV storage include the lyophilization and freeze-dried sEVs can be stored at −20°C, a technique considered as a cost-saving strategy and holding great promise for translation into therapeutic protocols (Yuan F. et al., 2021). However, such studies are preliminary and require further investigation and standard protocols. More work is needed in this area and the impact on long-term storage and cold chain processes shall be considered.

# 3 ISOLATION AND CHARACTERIZATION OF sEVs

MISEV guidelines provide recommendations for the nomenclature, collection and pre-processing, separation and concentration, characterization and functional studies of EVs (Théry et al., 2018). Standardized methods for sEV isolation and analysis are needed to meet the regulatory requirements of their use as drug delivery systems (Rai et al., 2021). Several conventional methods have been employed to isolate sEVs, each one with its own pros and cons, influencing even the yield of sEVs. **Table 1** summarizes the advantages and disadvantages of the most common methods for sEV isolation. After sEV isolation, a detailed characterization is required to determine their physicochemical properties, as well as biochemical and molecular composition. There are several techniques to perform such characterization and, usually, more than one method is used to better define the sEV characteristics, as described in this article.

## 3.1 Traditional and Novel Methods for the Extraction

### 3.1.1 Differential Ultracentrifugation

Differential ultracentrifugation is the gold standard and the most used isolation method for sEV isolation from body fluids and conditioned media. Although various protocols are available, generally it consists of multiple steps: 1) relative low-speed centrifugation (1,000 g for 10 min), to remove cells and apoptotic debris; 2) higher speed spin (varies among laboratories, from 1,000 g to 20,000 g for 1 h) to eliminate larger vesicles; and 3) a high-speed centrifugation (100,000 g for 2 h) to precipitate sEVs (Zhang P. et al., 2019). Note that biological samples with high viscosity require a longer

ultracentrifugation step and higher speed of centrifugation. An additional filtration step is recommended prior to the ultracentrifugation process to remove microparticles, which are selected according to their size (pore diameters of 0.10, 0.22, or 0.45 μm). Importantly, the additional steps in sEV purification (washing and microfiltration) increase the purity of sEVs but also decrease the yield of sEVs that are obtained (Konoshenko et al., 2018; Whitford and Guterstam, 2019). This approach has several advantages, such as easy to use and little technical expertise, but it is also time-consuming. For more purified sEVs and to eliminate contaminations, the pellet can be washed again in a large volume of PBS and centrifuged one last time at 100,000 g for 2 h (Konoshenko et al., 2018). Lately, the isolation of exomeres with a ultra centrifugation at 167,000 g and of supermeres by an additional 367,000 g ultracentrifugation of the exomere supernatant (Clancy et al., 2021) was described. Pellets should be resuspended in PBS and stored at -80°C for further characterization and analysis.

### 3.1.2 Density Gradient Centrifugation

Density gradient centrifugation is another ultracentrifugation procedure frequently employed. It uses an inert gradient medium for centrifugal sedimentation or sedimentation equilibration (Lane et al., 2017). The sample is placed on a preconstructed density gradient, such as sucrose, iohexol, or iodoxinol, and when a certain centrifugal force is applied, the particles will begin their sedimentation through the gradient in separate zones according to their size, shape density, and the sedimentation coefficient(s) (Théry et al., 2006; Zhang P. et al., 2019). Samples are centrifuged for 16–24 h at 120,000 g at 4°C, and the resulting pellet contains the isolated sEVs collected at their characteristic density zone (1.1–1.2 g/ml) to separate from other components in the sample (Lamparski et al., 2002; Choi et al., 2021). Factors such as centrifugation time, relative centrifuge force, and temperature are particularly important and can lead to inconsistencies in isolated material. Therefore, an adequate centrifugation time avoids the presence of contaminating particles in the sEV fractions due to similar densities (Théry et al., 2006; Lane et al., 2017).

### 3.1.3 Ultrafiltration

Ultrafiltration is one of the most popular size-based techniques for the isolation of sEVs. The currently available commercial membrane filters have pores of different diameters to allow size distribution, simplifying the process of particle isolation. In some differential centrifugation methods, filtration is used in combination with ultracentrifugation or as an additional step in gel filtration chromatography (Lane et al., 2017; Oeyen et al., 2018). Based on their size, sEVs can be isolated using membrane filters with defined molecular weight or size exclusion limits (Heinemann et al., 2014). During the initial step, the larger vesicles are removed by filters with a pore diameter of 0.80 and 0.45 μm, and the particles with a smaller size than sEVs are separated from the filtrated at the next stage, and a concentrated sEV population is collected. The isolation step requires a relatively short period of time, although the method needs a pre-incubation of the silicon structure with the PBS buffer (Lane et al., 2017). In the following step, the sEV population is concentrated on the filtration membrane. Currently, there are commercial sEV isolation kits available that allow their extraction in shorter periods of time (Hu et al., 2021). Although filtration technologies are faster than ultracentrifugation and do not require special equipment, it is difficult to remove the remaining proteins that adhere to the nanomembrane and hamper the elution of sEVs. Additionally, the use of mechanical pressure may result in the deformation and breaking up of large EVs (Heinemann et al., 2014; Zhang P. et al., 2019).

### 3.1.4 sEV Precipitation

sEVs can be isolated from biological fluids, by altering their solubility or dispersibility. This method is based on the precipitation of sEVs in solutions of superhydrophilic polymers. One of them is polyethylene glycol (PEG), which has been used to change the sEV membrane surface structure. The use of PEG can help to solve the problem of rapid sEV clearance by phagocytic systems. Indeed, PEG confers more stable properties to sEVs, increasing their time in circulation (Kooijmans et al., 2016), which may be important to improve their efficacy as drug delivery systems. The procedure usually includes mixing the biological fluid with a polymer containing the precipitation solution, incubation at 4°C overnight, and sedimentation of sEVs by low-speed centrifugation (1,500 g). The resulting pellet is then resuspended in PBS for further analysis and sedimentation of sEVs by low-speed centrifugation (1,500 g) to remove cellular debris (Momen-Heravi et al., 2013; Patel et al., 2019). The water-excluding polymers (usually PEG of 8,000 Da) tie up water molecules and exclude less soluble components. sEV precipitation is easy to use, does not require any specialized equipment, has minimal costs, and can be scalable for larger quantities. Moreover, the precipitation with PEG allows us to work in physiological pH ranges and without dependence on the ion concentrations. However, polymer-based sEV precipitation is accompanied by co-precipitation of other non-sEVs contaminants, such as proteins and polymers (Niu et al., 2017; Patel et al., 2019). Currently, several commercial kits using PEG for sEVs isolation are available and easy to use, without the need of additional steps.

### 3.1.5 Immunological Separation

Immunoaffinity approaches exploit the highly specific affinity interactions between an antigen and an antibody. All the molecules in the surface of sEVs, such as proteins, receptors, lipids, and polysaccharides, are potential ligands. Ideally, sEV biomarkers for immune isolation are highly concentrated or only present on the surface of sEVs and lack free counterparts. Some of the sEV biomarkers (**Figure 2B**) include tetraspanins, heat shock proteins and MHC antigens, CD9, CD10, CD24, CD63, CD81, EpCAM, Alix, AQP2, FLT1, TSG101, and HSP70 (Tauro et al., 2012; Konoshenko et al., 2018). Several techniques of immunological separation of sEVs have been developed and include antibody-coated magnetic beads, immune-modified superparamagnetic nanoparticles, and microplate-based enzyme-linked immunosorbent assay (ELISA). Antibody-

coated magnetic beads and paramagnetic beads coated with antibodies are usually incubated with conditioned culture medium for 24 h at room temperature and sEV complexes are isolated from the magnetic particles with the help of a magnet. Afterward, the obtained sEVs are washed and then assayed, using sEV intracellular proteins as specific markers for their isolation. The diversity of antibodies and fixed phases has given rise to a large number of protocols for the isolation of sEVs, but isolation from larger volumes encounters certain difficulties (Momen-Heravi et al., 2013; Cai et al., 2018). Microplate-based ELISA methods have been developed for capturing and quantifying sEVs from biological samples (plasma, serum, and urine) and the results are expressed as absorbance values relative to the expression of known surface biomarkers. The absorbance values can also be extrapolated to quantify the captured sEVs through calibration using standards with known sEV counts (Théry et al., 2006). It is then possible to characterize and quantify sEV proteins with antibodies against sEV-associated antigens, either common to all sEVs, or specific to sEVs from certain cell types or cell conditions. Following isolation of sEVs, the sub-populations of interest can be separated by differentiating protein markers, avoiding contaminants. The method is applied for detection, analysis, and quantification of both common and cell type-specific sEV proteins (Tauro et al., 2012). The main advantage of the immunological separation is the high purity of the resulting isolated sEVs. Moreover, this approach has a comparable or even greater yield when compared to ultracentrifugation and precipitation-based methods. Nonetheless, this technique has high costs and difficulties related to the detachment of molecules, the analysis of intact vesicles, and the availability of antibodies (Tauro et al., 2012; Momen-Heravi et al., 2013).

### 3.1.6 Microfluidic-Based Technologies

In the last decade, research efforts have been made to develop microfluidic platforms that offer advantages in combining the separation and detection of sEVs into a single chip (Guo et al., 2018). Microfluidic technologies use small volumes of fluids (nano to microliters) and can be classified as size-based sEV and immunoaffinity-based sEV isolation procedures (Contreras-Naranjo et al., 2017). The system of size-based sEV isolation uses principles of chromatography and has the advantage of obtaining uniformly sized samples (Sancho-Albero et al., 2020). Samples are filtrated through two membranes with a pore size of 20 and 200 nm in diameter and the particles greater than 200 nm remain in the sample chamber (Lin S. et al., 2020).

Dialysis membrane can be used to increase the separation efficiency and purity of samples, or electrophoresis can be employed to force passage of particles across the filter (Contreras-Naranjo et al., 2017). Immunoaffinity-based microfluidic devices are comprised of modified microchannels with antibodies or magnetic beads constructed to capture sEVs based on specific biomarkers, such as CD63, CD81, and the major histocompatibility complex I (MHCI) (Lin S. et al., 2020). In one of the proposed systems, the multiple circular wells are connected through straight channels to increase the interaction with the functionalized surface, with additional narrow channels between the chambers to allow the changes in fluid velocities (Kanwar et al., 2014). Microfluidic-based technologies offer advantages such as high purity even for small quantities of fluids, fast isolation speed, high yield, and low cost in comparison with classical purification methods. Nevertheless, they require expensive and advanced equipment, as well as premixing and incubation of capture beads with samples (Guo et al., 2018; Kurian et al., 2021).

### 3.1.7 Tunable Resistive Pulse Sensing

Tunable Resistive Pulse Sensing (TRPS) allows high-throughput measurement of individual particles that move through a size-tunable nanopore. TRPS technology, usually applied for a particle size distribution and concentration measurement, has shown promising results as a method for the analysis of sEV samples (Lane et al., 2015). Particles like lEVs and sEVs are detected as a transient change in the ionic current when they move across the size-tunable nanopore, resulting in a resistive pulse signal (Akers et al., 2016). The signal obtained can then be used to calculate the size, charge, and concentration of particles by correlating the fluctuations in the current flow after calibration with a known standard (Kurian et al., 2021). The size of this pore can be adjusted allowing its usage for a variety of samples of different sizes. The technique provides higher resolution, high-throughput analysis, and more accuracy than by light scattering based-techniques (Coumans et al., 2014; Lane et al., 2015). The disadvantages of the TRPS include the lack of sensitivity to sEVs and the risk of pore obstruction with repeated usage (Coumans et al., 2014).

## 3.2 Size and Morphology

Standard flow cytometry is one of the most common and prevalent tools used to analyze the origin, size, and morphology of lEVs, while high resolution flow cytometry and imaging flow cytometers have been used for sEVs, as reviewed in MISEV 2018 guidelines (Théry et al., 2018) and recently published (Botha et al., 2021) Such a high-throughput, multi-parametric technique quantitates thousands of single cells or particles and quickly analyzes both their relative size and granulation (Ko et al., 2016; Tertel et al., 2020; Botha et al., 2021).

The working principle of a flow cytometer is that a laser beam with a specific wavelength is directed through a stream of fluid containing suspended particles and the scattered light is converted to an intensity-associated voltage pulse that can be quantified later. The degree of light scattering depends on the presence of particles in the samples, and sEVs can be quantified and/or classified accordingly to antigen expression levels using specific fluorescently labeled antibodies (Konoshenko et al., 2018). This same approach is also used by some commercially available kits and enables parallel multiple surface biomarker detection with different fluorescent antibodies. However, sEVs are too small to allow that the standard flow cytometry captures the florescence signal, which can be increased through the usage of immunoconjugated beads (Ko et al., 2016). Flow cytometry is a methodology that can be combined with molecular methods increasing statistical robustness and allowing simultaneous analysis of various antigens. Nevertheless, there is still a lack

of robust protocols reported, and many studies regarding flow cytometry of sEVs have incomplete methodological descriptions and insufficient calibration and standardization processes to generate the data, as indicated in MISEV guidelines for flow cytometry experiment with EVs (MIFlowCyt-EV) (Welsh et al., 2020). Some studies have used engineered CD63eGFP-labeled sEVs and imaging flow cytometry as a robust multi-parametric detection and quantification of single sEVs and sEV subsets in heterogeneous samples (Görgens et al., 2019). In recent years, ExoView® platform was proposed. It allows the addition of fluorescent antibodies on single sEVs and other EVs. No purification is required, allowing us to quantify the expression of relative proteins with a single fluorescent antibody sensitivity, while simultaneously measuring their size and number (Harkonen et al., 2019). Some of the biophysical approaches routinely used for the characterization of sEVs are focused on measuring the size distribution and morphology. Dynamic light scattering (DLS) allows the assessment of sEV size distribution based on the intensity of the scattered light (Frisken, 2001). Similar to DLS, the nanoparticle tracking analyzer (NTA) uses a laser beam to illuminate sEVs in the sample (Filipe et al., 2010). The suspended sEVs are illuminated by a laser, and the intensity of the light fluctuates over time since sEVs go through Brownian motion, that is, they are then identified and related by movement and particle size based on the Stokes-Einstein equation, where the diffusion velocities are inversely proportional to the size of particles. Both methods provide accurate and sensitive size distributions, but while DLS gives the diameter range of the analyzed vesicles, NTA is capable of tracking a single sEV overcoming polydispersity problems (Frisken, 2001; Filipe et al., 2010). Lately, sEV protein detection has been possible thanks to the quantum dot method coupled with immunomagnetic capture and enrichment. sEVs are captured by magnetic beads based on CD81 protein expression and subsequently detected by fluorescent spectroscopy (Vinduska et al., 2021).

Transmission electron microscopy (TEM) has a higher resolution compared with the other electronic microscopy techniques and has similar procedures for fixation and contrast enhancement. It is widely used to characterize the structure, morphology, and size of various biological components (**Figure 1**) (Théry et al., 2006). In the scanning electron microscopy (SEM) technique, a focused electron beam causes electron emission from the sEV surface. Samples are chemically or cryogenically fixed followed by dehydration and sputter-coated with a thin layer of gold or carbon for imaging (Chuo et al., 2018). These electrons are collected and magnified using a special lens. Usage of immune-gold labeling in TEM and SEM, as well as cryo-TEM allows the observation of EVs in their hydrated-like native state (Linares et al., 2017).

## 3.3 Biochemical Analysis of sEVs Markers

ExoCarta was previously described in 2009 and is routinely used by researchers to validate and/or characterize their findings in sEVs (Mathivanan and Simpson, 2009). ExoCarta is an online database that allows various groups to establish sEV markers with detailed information about lipids, proteins, and RNA sequences that were identified in specific sEV preparations (Mathivanan et al., 2012). Up to now, approximately 10,000 different proteins and more than 3,000 mRNAs have been characterized (http://www.exocarta.org/). ExoCarta contains annotations on the study that identified the molecule, the sEVs isolated from a particular sample, the employed methods of isolation and identification, and the date of publication. Free web-based resources like Exocarta, and others such as EVpedia and Vesiclepedia, help the scientific community in elucidating the molecular mechanisms and pathophysiological effects of EVs, specifically of sEVs, on target cells, as well as on their therapeutic potential (Mathivanan et al., 2012; Simpson et al., 2012). Recently, the topics on EVs have been updated, providing suggestions on molecular markers for their characterization based on protein composition, as well as on isolation and standardization techniques (Théry et al., 2018).

Western blot is used to separate and identify proteins and can be applied to detect and confirm the presence and expression levels of the sEV-specific proteins in purified sEV samples of tissue homogenate or extracts (He et al., 2014). After sEV isolation, they can be lysed and used for proteomics or be transferred onto a membrane for Western blotting. The specific markers frequently used as sEV markers are the characteristic proteins that belong to their biogenesis process and include, besides those pointed out in **Section 3.1.5**, Rab GTPase, annexins, flotillin, and the endosomal sorting complexes required for transport (ESCRT) pathway-dependent protein Alix (Simpson et al., 2009). It is a useful technique to identify proteins that are associated with sEVs once it can process multiple proteins at the same time. It is also important to state that although Western blot is often used to detect and confirm the presence of proteins in sEVs, it cannot completely exclude contaminants from different vesicles (He et al., 2014; Zhang P. et al., 2019). An alternative to Western blot, ELISA may be performed, which is a less time-consuming technique that also requires a smaller amount of sample. This technique uses sEV target specific antibodies immobilized to a solid surface to capture sEVs, and is followed by labeling with a detection antibody (Logozzi et al., 2020). Nevertheless, both Western blot and ELISA have some disadvantages, such as low specificity and quality, as well as higher costs.

One of the important characteristics of sEVs is that they may contain nucleic acids (DNAs, RNAs, miRNAs) that will play a crucial role in cell-to-cell communication and gene regulation in the target cell. These nucleic acids can be easily quantified by real-time quantitative reverse transcription polymerase chain reaction (RT-qPCR). This technique has several advantages since it does not need high sample volumes, it has higher sensitivity and resolution capacity, while allows a high-throughput analysis and absolute quantification (Chevillet et al., 2014). RT-qPCR is also important for the characterization of sEVs after transcriptomics. miRNAs have been described either as biomarkers and targets for modulation in several pathologies, including the neurodegenerative diseases (Brites, 2020), which turn these EVs as important tools for disease diagnosis and better understand the disease spread. Recent studies reported other forms of DNA (e.g., genomic and mitochondrial DNA) inside

**TABLE 2 |** Main differences between conventional nanocarriers and small extracellular vesicles (sEVs) as drug delivery systems.

| | Conventional nanocarriers | sEVs |
|---|---|---|
| Size | 10–300 nm | 50–200 nm |
| Composition | Polymers (natural or artificial; hydrophilic or lipophilic), lipids, silver, polysaccharides | Lipids, proteins, mRNAs, miRNAs, depending on cell of origin |
| Advantages | Loaded cargo hydrophilic and/or lipophilic drugs, long circulating (PEGylated), manufacturing methods available (liposomes) | Long body circulation, loaded cargo hydrophilic and/or lipophilic drugs, targeted delivery, biocompatibility, safe, biodegradable, cargo protection, immuno-compatibility (homologous), possibility of specific organotropism, high stability |
| Disadvantages | Immuno-compatibility of some materials, rapid clearance after *in vivo* administration, irregular biodistribution | Low drug loading, diversity of composition depending on cell source, difficult to obtain, long-term effect unclear, possibility of contamination with other EVs |

sEVs (Thakur et al., 2014; Sansone et al., 2017), although the exact role of them and the underlying mechanisms are still to be elucidated. Preliminary studies relate mitochondrial DNA as a biomarker of cancer aggressiveness (Arance et al., 2021) and its depletion in sEVs from astrocytes was associated with cell malfunction and spread of pathology (Ha et al., 2021).

# 4 sEVs-LOADING WITH THERAPEUTIC AGENTS

sEVs show the advantage to have membranes structurally comparable to other membranous structures found in cells in terms of lipid composition. Several proteins including receptors, transcription factors, enzymes, extracellular matrix proteins, lipids, and nucleic acids (DNAs, mRNAs, and miRNAs) are inside and on the surface of sEVs (Mashouri et al., 2019). In terms of lipids, the existence of lipid rafts deserves to be noted (**Figure 2B**), with ceramides, sphingolipids, and cholesterol, as well as phosphatidylserine and phosphatidylcholine, though to a lesser extent (Skotland et al., 2019). In addition, enzymes, such as phosphatases, proteases, and glycosidases, may also be present in sEVs where they often recapitulate the cell of origin and their metabolic activity (Skotland et al., 2017). sEVs have been referred as being enriched in sphingolipids, cholesterol, and phosphatidylserine in comparison with the donor cells, which may promote a higher stability of these vesicles against detergents than other EVs (Skotland et al., 2019). This means that they have important properties, namely high biocompatibility, enhanced stability, potential targeting, docking modalities, and limited immunogenicity (schematically represented in **Figure 3**). Cell adhesion molecules (CAMs), such as integrins, tetraspanins, and MHC class I and II, are some examples of specific types of sEV proteins. Also present are the less specific Rab2, Rab7, flotillin, annexin, Alix, heat shock proteins, and cytoskeleton proteins (e.g., actin, myosin, and tubulin) (Mashouri et al., 2019). Together with the MHC class II are integrins involved in antigen presentation and pattern recognition receptors important for innate immunity (Brites and Fernandes, 2015).

All these properties provide potential advantages of sEVs over conventional drug delivery nanocarrier systems and are summarized in **Table 2**. A variety of therapeutic material, such as drugs, short interfering-RNA (siRNA), antagomirs, pre-miRNAs, and recombinant proteins can be loaded into sEVs during their formation or after their isolation. These approaches may result in different loading efficiencies and stabilities of the drugs in the sEVs**.**

## 4.1 Cell-Based Loading Approach

The therapeutic agents (drugs, proteins, and nucleic acids) can be incorporated into cells that encapsulate the material during the production of sEVs. This strategy is more limited, since it depends on the cellular processes that are responsible for the production of sEVs as well as the cargo loading of the molecules. It also requires that the cellular source (cell line, primary culture) used is compatible and retains viability during the production of sEVs. In this case, after incubation with the therapeutic agents, the donor cells secrete sEVs that will be loaded with both biologically produced components and/or the drug. Such an approach requires that the donor cell can tolerate high concentrations of the drugs in order to be effective (Pessina et al., 2011). As so, it is also difficult to control the loading efficiency of the therapeutic molecule, which may suffer degradation in the host cells. Nevertheless, a major advantage is to specifically target sEVs against disease mechanisms (Garcia-Manrique et al., 2018). Another approach is to transfect the donor cells by genetic engineering with the drug-encoding DNA, which can then be expressed and sorted into sEVs. sEVs full of proteins encoded by the inserted genes can be obtained by isolating and purifying the sEVs through the natural packaging processes. Some disadvantages in this case are that the drug entrance is limited for its encoding DNA yield, depends on the transfection efficiency, and the transfection agents may lead to a reduction of cell viability (Johnsen et al., 2014; Batrakova and Kim, 2015).

## 4.2 Cargo Loading of sEVs Isolated From Donor Cells

The simplest strategy for loading therapeutic agents into sEVs is mixing them with the free drugs, as first demonstrated by Pascucci and others in 2014. Paclitaxel was selectively taken up by MSCs and then incorporated into the released sEVs, at a concentration sufficient to inhibit the growth of tumor cells *in vitro* (Pascucci et al., 2014). The process can also be used to load sEVs with small molecules. For cargo loading after isolation, sEVs are isolated and purified from biological fluids, such as cell

culture media, plasma, serum, or milk for the downstream processing. Several methods have been proposed to encapsulate therapeutic agents in sEVs with the common goal of permeating its membrane. These techniques include freeze-thaw cycles, saponin permeabilization, sonication, extrusion, and electroporation procedure. The process of loading should allow the maintenance of the structure and activity of the drugs.

In the method of freeze-thaw cycles, drugs are incubated with sEVs at room temperature for a fixed amount of time, and the mixture is subsequently frozen at −80°C or in liquid nitrogen, and re-thawed at room temperature. This process is repeated for at least three cycles to ensure drug encapsulation. However, the method can induce aggregation of the sEVs, while the drug loading efficiency is generally lower than that of sonication or extrusion methods. sEVs are shown to resist multiple freeze-thaw cycles and are stable when stored from −20°C to −80°C and when subjected to multiple freeze-thaw cycles (Haney et al., 2015; Sato et al., 2016).

Another way to encapsulate drugs in sEVs is to perform a permeabilization with saponin. Saponin, as a natural surfactant, interacts with membrane-bound cholesterol, creating pores that increase the permeability of sEV membrane, thus favoring the encapsulation (Chen et al., 2021). The method appears to not be affected by sEV morphology. However, such an approach is described to have poor stability *in vivo*, as well as low encapsulation yield when saponin is added (Fuhrmann et al., 2015; Haney et al., 2015).

Sonication consists of a method where sEVs derived from donor cells are mixed with drugs or proteins using a sonicator probe. The mechanical shear force from the sonicator probe induces deformation, compromises the membrane integrity of the sEVs, and allows the drug to flow into the sEVs. Nevertheless, in some cases, drugs can also be found in the outer layer of the sEV membrane. There are no significant changes in the structure and content of their membranes after sonication, and the drug sEV formulation has shown to be kept stable under various conditions for over a month (Kim et al., 2016; Liu et al., 2019).

Another method is extrusion. In this method, sEVs from donor cells are mixed with a drug, and the mixture is loaded into a syringe-based lipid extruder and extruded through membranes with 100–400 nm porous size, under a controlled temperature. During the extrusion, the sEV membrane is disrupted and vigorously mixed with the drug, resulting in drug loading into the sEVs. However, the use of this method can lead to changes in EV size, composition, and delivery capacity (Fuhrmann et al., 2015; Haney et al., 2015).

Finally, in electroporation, an electrical field (short, high-voltage pulses) is applied to a suspension of sEVs and the drug cargo of choice, creating small pores in their membrane, thereby facilitating the passage of cargo into the lumen of the sEVs. The integrity of the vesicle membrane is then recovered, resulting in the formation of drug-loaded vesicles. Electroporating a mixture of drug and sEVs at 1000 kV for 5 min was demonstrated to successfully load the drug into the sEVs (Kim et al., 2016; O'Loughlin et al., 2017).

Lately, efficient delivery of siRNAs and miRNAs into sEVs was shown to be achieved with commercial transfection kits, as the Exo-Fect$^{TM}$ from System Biosciences (SBI; System Biosciences, Palo Alto, CA) (Chivero et al., 2020). It was demonstrated to be more efficient than electroporation, heat shock, saponin, or cholesterol-mediated, at least for miRNAs, where more than 1000-fold upregulation was achieved, as compared to native sEVs (de Abreu et al., 2021).

## 4.3 sEV-Mimetic Nanovesicles as Delivery Systems

sEVs are stable and long-circulating endogenous nanocarriers that provide protection of the drug cargo from degradation, while increasing drug delivery to the targeted tissues. One of their major advantages is that they can cross the BBB, thus penetrating into the CNS. On the other hand, some disadvantages may arise from the fact that some components carried by natural sEVs are incompatible with therapeutic purposes, with difficulties in the purification methods and also that cells release relatively low quantities of sEVs (Zhang Y. et al., 2019). In this context, liposomes may be an alternative, as they are small artificial vesicles of spherical shape that can be created from cholesterol and natural non-toxic phospholipids. Due to their size and unique structure, liposomes can compartmentalize and solubilize both hydrophilic and hydrophobic materials. However, liposomes also have some limitations due to their poor stability under shelf and *in vivo* conditions (Akbarzadeh et al., 2013). Modified sEVs with other nanostructures, such as liposomes, may be considered a new outlook of biological drug delivery systems. They are inspired in EVs but represent novel biological nanocarriers. sEV-mimetic nanovesicles contain only the crucial components of natural EVs and are highly biocompatible with efficient targeting ability (Garcia-Manrique et al., 2018). These EVs are obtained by: i) subjecting cells to physical processes producing EVs of nano-dimensions; ii) fusing the membranes of sEVs and liposomes; and iii) coating nanoparticles with a lipid bilayer of cell plasma membranes (Luan et al., 2017; Colao et al., 2018), as detailed in this section.

### 4.3.1 Cell Membrane-Derived EVs as Bioactive Nanocarriers

Cell membrane-derived EVs are the natural analogs of liposomes. They can be fashioned from larger membrane structures, commonly prepared by size extrusion of monocytes or macrophages (Whitford and Guterstam, 2019). The forceful and sequential passage of cells through polycarbonate membrane filters (10, 5, and 1 μm pore sizes) leads to the generation of a large amount of nanovesicles, with a final size between 50 and 200 nm. Nanovesicles can also be obtained through the passage of cells over hydrophilic microchannels, generating a delivery system for endogenous material with technical features similar to those of sEVs (Jang et al., 2013; Lunavat et al., 2016). The production of nanovesicles can reach a high yield of cell-derived vesicles from living cells over a relatively brief period of time, achieving until 100 times more yield in comparison with the production of sEVs by using the same number of cells. Encapsulation efficiency is dependent on the initial amount of the added drug (Jang et al., 2013).

#### 4.3.2 Engineering sEVs by Fusion With Liposomes as Hybrid Nanocarriers

Hybrid systems produced after fusion between liposomes and sEVs are an attractive opportunity that, in principle, may decrease the immunogenicity of liposomes and increase their colloidal stability, while improving the half-life of the system in the blood. There are two approaches: i) drug-loaded liposomes are incubated with donor cells to produce sEVs or ii) sEVs are treated with drug-loaded liposomes composed of fusogenic lipids (Sato et al., 2016; Garcia-Manrique et al., 2018). In both strategies, features of sEVs depend on the properties of the liposome preparations used for the incubation processes, as well as cell uptake capabilities that vary with the cell type. When compared to neutral or anionic liposomes, cationic liposomes showed different uptake propensities and higher encapsulation than both cationic liposomes and/or non-fusogenic sEVs. Engineered hybrid sEVs seem to improve cellular delivery efficiency of therapeutic agents, as compared to the free drug or to the drug-loaded liposome precursor. Moreover, liposomes coated with peptides or antibodies as targeting moieties or PEG can be used to modify properties of the sEV surface. Furthermore, this approach may promote an efficient loading of larger molecules, mixing the cargo of the synthetic vesicles with that of their natural equivalent, while preserving their intrinsic content and biological properties. Generally, the fusion of cells/sEVs with liposomes increases sEV yield by conventional separation methods (Sato et al., 2016; Luan et al., 2017; Yamashita et al., 2018).

#### 4.3.3 Cell Membrane-Coated Nanoparticles as Nanomedical Tools

Nanoparticles coated by cell membranes mimic the properties of the source cells from which their membrane is derived, providing the ability to synthetic core structures to carry therapeutic cargo. They consist of a synthetic nanoparticle core covered by a natural cell membrane layer, with the advantages of immune-compatibility, long circulation, and disease-relevant targeting (Jang et al., 2013; Whitford and Guterstam, 2019). Recently, many types of membranes, such as those from erythrocytes, immune cells, platelets, stem cells, endothelial cells, activated fibroblast cells, cancer cells, and even *E. coli*, have been developed as carriers to facilitate the undetected targeted delivery of core nanoparticles independently of their properties. Natural cell membranes contain a series of functional moieties (proteins, antigens, and carbohydrates) that participate in protection, specific recognition, and intracellular communication, facilitating appropriate nanoparticle delivery (Fan et al., 2018; Fang et al., 2018; Luchini and Vitiello, 2019). The conventional approaches for production of cell membrane-coated nanoparticles involves three steps: i) membrane extraction from source cells; ii) inner core nanocarrier production; and iii) fusion process of the membranes with nanoparticulate cores (Fang et al., 2018). The cell membrane extraction requires large volumes of cells and includes membrane lysis and membrane purification, which should be as gentle as possible. This process is determined by the cell type of interest and includes freeze-thaw cycling, electroporation, and osmosis-based lysis coupled with physical homogenization. A variety of materials (organic or inorganic) may be utilized to produce cell membrane-coated nanoparticles, but the main criterion is that the nanoparticles have a negative zeta potential, which will facilitate orientation of the membrane around the nanoparticle. After extraction of the cell membrane and the introduction of the inner core nanocarrier, these two materials need to be fused together, without drug loss or protein denaturation (Zhai et al., 2017; Fang et al., 2018). Membrane extrusion, ultrasonic fusion, or electroporation are frequently used. However, for the success of these strategies, optimizations are needed in the voltage, duration, and flow velocity, as well as in the cell membrane-to-nanoparticles ratio, which should be carefully controlled to ensure complete surface coverage with the cell membrane (Fan et al., 2018).

## 5 sEVs AS DRUG DELIVERY SYSTEMS FOR NEUROREGENERATION

### 5.1 Migration Across the Blood-Brain Barrier

Significant efforts have been made to deliver small therapeutic molecules/drugs and diagnostic agents into the brain. The discovery of different types of EV cargo and their ability to interact and be taken up by specific cells has led investigators to concentrate on the potential of sEVs as delivery vehicles for therapeutic applications (Luan et al., 2017; Yamashita et al., 2018). sEVs have an efficient capability to cross the BBB, to deliver their intact content into a specific target cell, while also remain stable in the peripheral circulation, thus contributing to be considered potential attractive nanocarriers in the treatment of several CNS diseases (Alvarez-Erviti et al., 2011; Kojima et al., 2018; Busatto et al., 2021). A study carried out in 2016 reported the transfer of a tight junction protein from the endothelial cells to the leukocytes through EVs, thus supporting their cell-to-cell migration (Paul et al., 2016). In another work using rats with a fluorescently tagged protein expressed selectively in the brain tissue, the authors recovered the labeled sEVs in the blood of those animals and demonstrated that sEVs crossed the BBB in a bi-directional manner (Gomez-Molina et al., 2019). Chen et al. (2016) also showed that sEVs are internalized by brain microvascular endothelial cells through endocytosis, by using confocal microscopy and co-localizing sEVs with endosomes (Chen et al., 2016). In addition, sEVs are internalized by target cells through a variety of endocytic pathways. In particular, they use endogenous receptors that are highly expressed at the surface of the BBB, such as transferrin and insulin receptors, confirming sEVs as having a key role in intercellular communications and passage through the BBB in both directions (Yamashita et al., 2018). However, little is still known about the mechanistic details of sEV migration across the BBB and further investigation is required.

## 5.2 sEVs as miRNA Carriers

The content of sEVs can reflect the cell of origin and depends on the physiological or pathological conditions during their formation, suggesting horizontal transfer of genetic information (Zhang Y. et al., 2019). However, sEVs may also be enriched with a particular set of proteins and microRNAs (miRNAs), through selective mechanisms of protein cargo sorting controlled by specific post-translational modifications (PTMs) (van Niel et al., 2006). miRNAs are short nucleotide sequences of non-coding RNAs and can regulate gene expression in various cell types, constituting a critical factor in intracellular communication between origin and target cells (Simpson et al., 2009; Hessvik and Llorente, 2018; Zhang Y. et al., 2019). In the nervous system, a range of cell types have been shown to release miRNA-containing sEVs, including Schwann cells, microglia, oligodendrocytes, astrocytes, and neurons. For instance, miR-21, usually implicated in the microglial anti-inflammatory response, is transferred from neurons to microglia in a process that is mediated by sEVs (Fernandes et al., 2018). On the other hand, the most abundant miRNA of the CNS, the miR-124, is released from neurons as an sEV cargo and is taken up by astrocytes (Morel et al., 2013). Another study proposed that the delivery of miR-155 from microglia to adjacent cells may be mediated by sEVs (Cunha et al., 2016). In this study, the authors found that the expression profile of inflammation-associated miRNAs in sEVs recapitulated those in the cells on exposure to lipopolysaccharide (LPS), a pro-inflammatory stimulus. Increased expression of miR-21 released by Schwann cells in sEVs constitutes an important feature of the repair program of these cells, contributing to axonal regeneration and functional recovery after nerve injury (Lopez-Leal et al., 2020). miRNA profiles identified in sEVs of the CSF/blood in neurodegenerative disorders reinforce the important role of specific sEVs-miRNAs in the regulation of the neuroinflammatory processes (Ciregia et al., 2017; Yoo et al., 2018). In particular, we recently showed that increased levels of miR-124 in neurons derived from induced pluripotent cells generated from AD patients reduces amyloid precursor protein (APP) gene expression, tau hyperphosphorylation, and prevents dendritic spine deterioration (Garcia et al., 2021). In contrast, upregulation of miR-124 in SOD1G93A mutant motor neurons as a model of amyotrophic lateral sclerosis (ALS) evidenced to associate with neurodegeneration and homeostatic cell imbalance (Vaz et al., 2021). Therefore, miRNA sorting in sEVs may either work as a protective mechanism or be a sign of injury to neighboring cells and is dictated by the cell's own metabolism. Therefore, these sEVs-containing miRNAs are cell specific and may be involved in many biological and pathological processes, as further detailed in the next section. All these factors should be considered when choosing the cell source of sEVs to be used as therapeutic carriers.

## 5.3 sEVs as Delivery Systems of Therapeutic Agents in Brain Pathology

To date, cell-derived EVs provide multiple advantages over traditional synthetic delivery vehicles and potential new drug delivery methods, such as limited immunogenicity, natural composition, small size (nanoscale), enhanced stability in circulation, slightly negative zeta potential for long circulation, and deformable cytoskeleton. As drug delivery carriers, sEVs have the ability to cross many biological barriers, such as the BBB (Elliott and He, 2021; Yamashita et al., 2018). The main advantages of sEVs to be used as drug delivery systems in neurological diseases were addressed in previous sections and are indicated in **Figure 3**. To note, however, that the low residence time of sEVs in the circulation because of their rapid clearance by phagocytosis may compromise their efficiency and the generation of invisible sEVs has been attempted (Parada et al., 2021). We next will summarize the application that sEVs may have to prevent, halt, or even regenerate neural cell malfunction in age-associated neurodegenerative diseases and brain tumors.

### 5.3.1 Alzheimer's Disease

AD is the most common form of dementia, affecting brain regions that exhibit high synaptic activity implicated in important brain functions, such as memory and learning. sEV content seems to be specific for a particular activation or disease state. It was shown, for example, that sEV levels of both phosphorylated tau and amyloid beta (Aβ) proteins detected in the blood of AD patients were significantly higher than in controls, from 1 to 10 years before disease diagnosis (Fiandaca et al., 2015). Due to the complex pathophysiological process of this disease, its treatment is restricted to a few conventional oral medications that act only superficially (Jaul and Barron, 2017). In the incessant search for new therapeutic strategies, sEVs showed up as innovative approaches to be adopted in AD treatment. Alvarez-Erviti and others (2011) were the first to demonstrate that systemically injected sEVs could cross the BBB. They expressed a fusion protein of Lamp2b and rabies virus glycoprotein (RVG) in dendritic cells, which was incorporated into sEVs. Purified sEVs were loaded with exogenous GAPDH siRNA against BACE1 by electroporation and injected intravenously into mice. Systemic injection of RVG-targeted sEV loaded with GADPH siRNA induced specific gene knockdown in neurons, microglia, and oligodendrocytes and a 60% decrease of BACE1 mRNA in the brain cortex 3 d after administration. Besides the application of the sEVs in gene silencing strategies targeting the brain, also provided insights for their utilization in other tissues, as well.

Another study reported that sEVs, isolated from the serum of thr5xFAD mouse model and patients, when injected in the wild type mice brain are taken up by neurons, shuttle Aβ into the cells, and cause cell death by apoptosis, suggesting that disruption of Aβ at the sEV surface may protect from its induced neurotoxicity (Elsherbini et al., 2020). In contrast, sEVs, isolated from the adipose tissue-derived MSCs, decreased the levels of Aβ in an *in vitro* AD model by increasing the levels of neprilysin, important for Aβ degradation (Katsuda et al., 2013). Another compound that has been studied for many years for its beneficial role in AD is curcumin. Curcumin has anti-inflammatory, anti-lipidemic, and anti-oxidative properties. Due to these effects, it is suggested that curcumin can reduce tau protein clumping in the

brain, slowing cognitive deterioration in patients with AD. Curcumin has been shown to improve AD-like symptoms in mice (Strimpakos and Sharma, 2008). Despite these advantages, curcumin exhibits low bioavailability because of its poor solubility, low permeability, and absorption, as well as a faster metabolism rate. Nanoformulations of curcumin in sEVs may overcome such limitations, thus potentiating its usage in the treatment of neurodegenerative diseases. Sun and collaborators (Sun et al., 2010) were the first to demonstrate that sEVs loaded with curcumin increase the bioavailability and stability of the compound *in vivo*. Inspired by all these properties, Wang et al. ((2019) produced sEVs as a specifically designed carrier able to carry curcumin by injection in the right ventral hippocampus of an induced AD mouse model. They used okadaic acid to induce tau hyperphosphorylation and sEVs-enriched in curcumin to prevent neuronal death. In this study, they fabricated sEVs secreted by curcumin-treated mouse macrophage cells (curcumin-primed sEVs) to improve their solubility, stability, and tissue bioavailability. Compared with non-encapsulated curcumin, curcumin-primed sEVs enhanced the stability, and bioavailability of curcumin, inhibiting tau phosphorylation mediated by the AKT/GSK-3β pathway, thus contributing to the effective amelioration of learning and memory deficiencies in the induced-AD mice. Administration of curcumin loaded sEVs isolated from mESCs and administered by alternate nostrils in ischemia injured mice reduced post-ischemic events and restored the neurovascular unit, while the fluorescent sEVs were identified in the brain cortical region (Kalani et al., 2016). Nevertheless, additional *in vivo* studies are needed to better understand the specificity of the curcumin-primed-sEVs for other specific brain areas.

Quercetin is a natural bioactive flavonoid with significant pharmacological effects that has been lately widely studied for its antioxidant biological properties connected to its antioxidant activity (Albarracin et al., 2012; Song X. et al., 2020), and with benefits to counteract the neurodegenerative processes. Recently, it was shown that quercetin is able to inhibit tau hyperphosphorylation by reducing the formation of insoluble neurofibrillary tangles associated with AD (Calfio et al., 2020). In another study, plasma sEVs were chosen as therapeutic cargo carriers, improving the solubility and the brain targeting of quercetin in an animal model of AD (Qi et al., 2020). Quercetin-loaded sEVs were enriched with heat shock protein 70 (HSP70) to improve the BBB crossing by specific active targeting between sEV carrying HSP70 and endothelial Toll-like receptor 4 (TLR4) in the brain. Compared to free quercetin, plasma sEVs loaded with quercetin improved the drug bioavailability in AD and further relieved the symptoms of AD in this model by inhibiting the cyclin-dependent kinase 5-mediated phosphorylation of tau and reducing formation of insoluble neurofibrillary tangles, suggesting its potential therapeutic benefit in AD.

### 5.3.2 Parkinson's Disease

PD is a brain disorder characterized by the degeneration of nigrostriatal dopaminergic neurons, as well as by the presence of Lewy bodies resulting from misfolded α-synuclein in the surviving neurons in the striatum. Levodopa, a prodrug of dopamine, remains as one of the main drugs in the treatment of PD because dopamine cannot cross the BBB (Banks, 2016). An alternative strategy adopted by Qu et al. (2018) was to combine sEVs and dopamine, enabling the permeation of dopamine through the BBB with maximum biocompatibility and minimum toxicity. The authors isolated sEVs from human blood and loaded sEVs with a saturated solution of dopamine (24 h at room temperature) and tested the uptake of the loaded sEVs by mouse brain endothelial cells *in vitro* and the targeting ability of labeled sEVs *in vivo*. In both experiments, the authors observed that blood sEVs crossed the BBB and delivered dopamine into the brain through an interaction between transferrin and its receptor. Loaded blood sEVs demonstrated a 15-fold improvement in dopamine brain distribution and showed less toxicity than free dopamine by intravenously systemic administration. The sEVs loaded with dopamine had a continuous dopaminergic stimulation and a more stable treatment effect, with better therapeutic effect in the PD mouse model, demonstrating that this strategy seems to be efficient for obtaining a regular distribution of molecules in the brain (Qu et al., 2018). In another study, it was found that sEVs facilitated the entrance of catalase into the brain parenchyma of PD mice by intranasal administration, which produced a potent neuroprotective effect (Haney et al., 2015). In this study, researchers compared several active cargo-loading techniques for the loading of catalase into RAW264.7 macrophage-derived sEVs. The approach used by Haney and others (2015) focused on direct manipulations of sEVs and their membranes to obtain a more effective drug loading. Another strategy may be the usage of cellular modifications to originate sEVs with increased targeting ability. Indeed, a previous study from the same research group demonstrated that systemic administration of macrophages that were genetically modified to overexpress catalase in the released sEVs with incorporated DNA, mRNA, transcription factors, and the encoded proteins. This resulted in the sustained catalase expression by these macrophages and subsequent potent anti-inflammatory and neuroprotective outcomes in a mouse model of PD (Haney et al., 2013). In both approaches, the catalase was the therapeutic agent delivered by sEVs. Catalase is one of the most important antioxidant enzymes that mitigate oxidative stress to a considerable extent by destroying cellular hydrogen peroxide to produce water and oxygen. Deficiency or malfunction of catalase is postulated to be related with the pathogenesis of many age-associated degenerative diseases among which is PD, though the therapeutic delivery of this protein to the brain is restricted by the BBB (Jaul and Barron, 2017). Making use of a set of sEV transfer into cells, devices enabled efficient and customizable production of designer sEVs in engineered mammalian cells (endogenous modification-based approach). Kojima et al. (2018) also confirmed the functionality of these engineered sEVs to deliver therapeutic catalase mRNA for PD treatment. These genetically encoded devices in sEV donor cells optimized the therapeutic sEV release and controlled the delivery of intended biomolecules, without the need to concentrate sEVs. More importantly, engineered donar cells implanted in living mice allowed for a consistent delivery of mRNA cargo into the brain. The catalase mRNA via sEVs from implanted donor cells

attenuated neurotoxicity and neuroinflammation in *in vitro* and *in vivo* models of PD, opening new therapeutic opportunities by enabling the delivery of therapeutic mRNAs *in vivo*. Moreover, recent evidence supports the benefits of blood-derived sEVs from healthy volunteers when intraperitoneally injected in the MPTP-treated C57BL/6 mice, as a model of PD, for neuroprotection, as well as counteract inflammatory pathogenic features and recover motor ability (Sun et al., 2020).

### 5.3.3 Amyotrophic Lateral Sclerosis Disease

ALS is a progressive and fatal disease that affects motor neurons and glial cells in the brain and the spinal cord. Although most cases are sporadic, aggregation of mutated superoxide dismutase 1 (mSOD1) is a pathological hallmark of a subset of familial ALS. Propagation of mSOD1 may occur though the solubilized protein or by cell-derived sEVs (Grad et al., 2014). However, it was also proposed that sEVs from adipose-derived stem cells (ADSC) of healthy humans promote tissue repair in neuronal stem cells isolated from the subventricular zone of mSOD1 mice carrying the G93A mutation due to their strong immunosuppressive and regenerative effects through the release of paracrine factors (Lee et al., 2016). In this study, the authors proposed that ADSC-derived sEVs are effective in treating cellular phenotypes of ALS, including SOD1 aggregation and mitochondrial dysfunction. Based on these facts, the use of stem cells-derived sEVs may provide considerable advantages over their source cells, with better safety and making them attractive therapeutic strategies in neurodegenerative diseases. Indeed, a study performed in mSOD1 mice showed that systemic injection of adipose-derived MSCs delayed motor deterioration for 4–6 weeks and pointed the up-regulation of glial-derived neurotrophic factor (GDNF) and basic fibroblast growth factor (bFGF) produced by these MSCs via paracrine signaling as candidates for such benefits (Marconi et al., 2013). It was also shown that the incubation of sEVs derived from adipose-stromal cells in ALS motor neurons (NSC-34 cell line) has a neuroprotective effect following an oxidative insult, supporting the idea that sEVs mimic or are even better than neuroprotection by stem cells (Bonafede et al., 2016). A recent *in vivo* study from the same group tested the effects of sEVs isolated from ADSC on the mSOD1 mice and compared the intravenous and intranasal routes of administration (Bonafede et al., 2020). They found that treated mSOD1 mice with either intravenous or intranasal repeated administrations presented an improved motor performance, less cell death of lumbar motor neurons, and lower glial activation, as well as an improved neuromuscular junction functionality and muscle fiber morphology. Interestingly, through magnetic resonance imaging, the authors found that labeled ASC-sEVs reached the CNS administered by the intranasal route and accumulated in the typical lesioned sites of the mSOD1 mice brain, making this a promising tool for effective drug delivery into the CNS.

In another study using ALS NSC-34-motor neurons in a co-culture system with microglia, it was noticed that microglial cells were the main recipients of sEVs derived from ALS motor neurons, and that these sEVs induced phenotypic microglial alterations (Pinto et al., 2017). Since these sEVs are enriched in miR-124, it is conceivable that the modulation of this miRNA may have potential benefits to halt microglia activation and associated effects in motor neuron degeneration in this pathology. Indeed, we recently reported that miR-124 normalization in mSOD1 motor neurons prevented their dysregulation in terms of neurite network, and mitochondria and synaptic dynamics (Vaz et al., 2021). Importantly, this study demonstrated that the secretome (including sEVs), derived from mSOD1 motor neurons modulated with anti-miR-124 was able to counteract the pathology observed in the spinal organotypic cultures from mSOD1 mice in the early symptomatic stage. Such work highlighted miR-124 (either in cells, secretome, and/or sEVs) as a new therapeutic target to be considered in ALS. On the other hand, transfection with pre-miR-146a in astrocytes from mSOD1 cortical brain of mice pups abrogated the aberrant markers described for this cellular population (Gomes et al., 2019; Barbosa et al., 2021). Interestingly, this cellular transfection also counteracted miR-146a depletion in sEVs and led to secretome-mediated miR-146a enhancement in motor neurons and microglia, while recovered their function, reinforcing the miRNA modulation and consequent production of a more neuroprotective secretome/sEVs as emerging therapeutic targets in ALS.

### 5.3.4 Brain Tumors

sEVs derived from brain endothelial cells were used to deliver chemotherapeutics such as paclitaxel and doxorubicin across the BBB (Yang et al., 2015). In this study, four types of sEVs derived from different cells were isolated from the culture media (glioblastoma astrocytoma U-87 MG, endothelial bEND.3, neuroectodermal tumor PFSK-1, and glioblastoma A-172) and drugs such as rhodamine 123, paclitaxel, or doxorubicin were added to sEVs in PBS and incubated at 37°C for 2 h. The ability of sEVs to deliver drugs that crossed the BBB was examined *in vivo* by injecting bEND.3-derived sEVs loaded with the three molecules in the zebrafish model. Studies of drug biodistribution showed that when delivered by bEND.3 sEVs, there was a significant penetration of the fluorescent marker and of the two anticancer drugs into the brain region of the zebrafish embryos, reinforcing the ability of sEVs to cross the BBB. In the brain cancer model, sEVs with anticancer drugs significantly decreased fluorescent intensity of xenotransplant cancer cells and of the tumor growth marker vascular endothelial growth factor (VEGF) (Yang et al., 2015). The data showed significant therapeutic efficacy in the zebrafish brain model treated with sEVs with doxorubicin compared to doxorubicin alone, showing the potential of sEVs to deliver both small and big molecule drugs across the BBB for the treatment of brain cancers. In addition, an *in vivo* study using genetically engineered EVs carrying the suicide gene for cytosine deaminase (CD) fused to uracil phosphoribosyltransferase (UPRT) demonstrated a

reduction in the tumor growth in the glioblastoma mice model after treatment with the CD-UPRT-enriched EVs (Erkan et al., 2017). Zhuang et al. (2011) tested sEVs loaded with the signal transducer and activator of transcription 3 (STAT3) inhibitor and evaluated its effect on brain tumor-bearing mice model. In this model, mice treated intranasally with these loaded sEVs presented enhanced tumor apoptosis and significantly delayed GL26 tumor model, leading to increased survival. Another study observed that sEVs derived from marrow stromal cells were able to deliver anti-tumor miR-146b in an *in vivo* rodent model of malignant glioma, with consequent significant reduction of the tumor volume (Katakowski et al., 2013). Lately, Zhu and others (2019) used sEVs derived from embryonic stem cells (ESCs), which are known to have anti-tumor properties, and showed that they inhibited glioblastoma growth both *in vitro* and *in vivo*. The ESCs-sEVs modified with a targeting ligand for cancer chemotherapy at their surface facilitated their ability to cross the BBB (Zhu et al., 2019). In the same study, the authors also used paclitaxel (a mitotic inhibitor to tumor cells), loaded in the sEVs, and demonstrated that this strategy significantly improved the therapeutic effects of paclitaxel in glioblastoma enhancing mice survival. These results suggest that sEVs derived from ESCs are powerful therapeutic vehicles for glioblastoma treatment.

### 5.3.5 Other Brain-Associated Diseases

As indicated in **Section 5.3.1**, curcumin displays a variety of pharmacologic properties, attributed to its antioxidant and anti-inflammatory effects. Curcumin administration by nanocarriers improves several clinically relevant parameters, and considerably increases the chemical stability of curcumin by preventing its enzymatic and pH degradation (Loch-Neckel et al., 2015). Strategies to exploit sEVs and curcumin for the treatment of brain diseases have also been reported. Zhuang et al. (2011) prepared curcumin-loaded sEVs (5 min at 22°C) and evaluated *in vivo* effects in different disease models, namely in the LPS-induced brain inflammation model, and in the experimental autoimmune encephalitis (EAE) after intranasal administration. The effects of the administration of curcumin-loaded sEVs showed significant anti-inflammatory effects and blockade of LPS-induced brain inflammation, as well as of the reduction of myelin oligodendrocyte glycoprotein (MOG) in the EAE model. In these models a concomitant reduction in disease progression was observed, suggesting that intranasal delivery of anti-inflammatory agents provides a promising non-invasive approach for the treatment of brain inflammatory-related diseases. The combination of curcumin and the potentials of sEVs were also adopted by Kalani et al. (2016), aiming at neurovascular restoration following ischemia-reperfusion injury. Curcumin was loaded into sEVs in a proportion of 1: 4 and the method of nanopreparation was the rapid freeze-thawing. To determine the therapeutic efficacy of curcumin-loaded sEVs, the authors evaluated the neurological score, lesion volume, and cerebral edema in ischemia reperfusion-injured mice. These results showed that treatment with sEVs isolated from mouse embryogenic stem cells were effective in reducing infarct volume, edema, inflammation, and astrogliosis, while also restored NeuN positive neurons. The intranasal administration for 7 d was able to protect the tight junctions from dysfunction and BBB from disruption following injury by ischemia reperfusion injury in mice. Lately, sEVs from bone MSCs administered by the retro-orbital route into the C57BL/6 mice after traumatic brain injury were shown to modulate microglia/macrophage polarization and ameliorate early inflammatory responses (Ni et al., 2019). To highlight that sEVs isolated from the serum of 3-month-old mice (young) and intravenously injected in the 18-month-old recipient mice (old) reversed the expression of aging biomarkers in the lungs and the livers, but one can expect the same effect in the brain (Lee et al., 2018). All these results demonstrate that sEVs can effectively reach the CNS through different administration routes and are a novel and promising therapeutic approach for brain disorders (Kalani et al., 2016).

## 6 CONCLUSION AND FINAL CONSIDERATIONS

In recent years, sEVs were proposed as a powerful therapeutic tool that may be used to target brain pathology since they present numerous advantages as therapeutic nanocarriers, as schematically represented in **Figure 3**. Considering their biocompatibility and ability as efficient cell-to-cell messengers, sEVs may be delivered by various administration routes, to overcome biological barriers and reach the CNS. sEVs have low immunogenicity and are more stable in the circulation than other nanoparticle systems due to their endogenous origin and special surface composition. Moreover, they have the capability of loading multiple molecules, such as drugs, mRNAs, miRNAs, and proteins, allowing a more efficient delivery into specific cells or tissues, by properly modifying their surface based on the parental cell status and/or the source of donor cells. By doing that, their usage avoids most of the drugs being delivered to accumulate in other sites than the intended target. Lately, sEVs can be manipulated to be loaded with specific therapeutic molecules and miRNAs, through the generation of sEV-mimetics or by manipulation of their donor cells. Notwithstanding all the positive evidence to use sEVs as nanocarriers, some aspects still need to be further elucidated, such as the biodistribution analysis of sEVs, the mechanism of the brain entrance through the BBB, and their stability and pharmacokinetic properties. A critical issue that must be considered is the choice of sEV donor cells. Additional information on the complex molecular constitution of sEVs, i.e., their cargo dependence on their cell source, among others, will be imperative for the choice of the therapeutic goal and their usage. In addition, further studies are still required to explore the effects of sEVs *in vivo*, in terms of safety, effective delivery, and avoidance of off-target effects. A better knowledge into the sEV cargo and their cell/tissue specific targets will certainly provide new therapeutic strategies to overcome CNS disorders.

## AUTHOR CONTRIBUTIONS

GL-N, AV, and DB contributed to the conceptualization, analysis, and interpretation of the relevant literature, drafting of the manuscript, and visualization. DB contributed to funding acquisition. GN and AM helped in the preparation of figures and tables and contributed to review and editing. AV and DB edited the whole manuscript, and critically revised the final version, making a substantial, direct, and intellectual contribution to the work. All authors read and approved the final manuscript.

## FUNDING

This work was funded by Fundação para a Ciência e a Tecnologia (FCT), through projects PTDC/MED-NEU/31395/2017 and PTDC/MED-NEU/2382/2021 (to DB), by La Caixa Foundation-Luzón Foundation through project HR21-00931 (to DB) and in part and by La Caixa Foundation-Luzón Foundation through project HR21-00931 (to DB) by the grant UID/DTP/04138/2019-20 (to iMed.ULisboa), as well as by the Programa Operacional Regional de Lisboa and the Programa Operacional Competitividade e Internacionalização (LISBOA-01–0145-FEDER-031395 to DB).

## REFERENCES

Akbarzadeh, A., Rezaei-Sadabady, R., Davaran, S., Joo, S. W., Zarghami, N., Hanifehpour, Y., et al. (2013). Liposome: Classification, Preparation, and Applications. *Nanoscale Res. Lett.* 8, 102. doi:10.1186/1556-276X-8-102

Akers, J. C., Gonda, D., Kim, R., Carter, B. S., and Chen, C. C. (2013). Biogenesis of Extracellular Vesicles (EV): Exosomes, Microvesicles, Retrovirus-like Vesicles, and Apoptotic Bodies. *J. Neurooncol.* 113, 1–11. doi:10.1007/s11060-013-1084-8

Akers, J. C., Ramakrishnan, V., Nolan, J. P., Duggan, E., Fu, C. C., Hochberg, F. H., et al. (2016). Comparative Analysis of Technologies for Quantifying Extracellular Vesicles (EVs) in Clinical Cerebrospinal Fluids (CSF). *PLoS One* 11, e0149866. doi:10.1371/journal.pone.0149866

Albarracin, S. L., Stab, B., Casas, Z., Sutachan, J. J., Samudio, I., Gonzalez, J., et al. (2012). Effects of Natural Antioxidants in Neurodegenerative Disease. *Nutr. Neurosci.* 15, 1–9. doi:10.1179/1476830511Y.0000000028

Alvarez-Erviti, L., Seow, Y., Yin, H., Betts, C., Lakhal, S., and Wood, M. J. (2011). Delivery of siRNA to the Mouse Brain by Systemic Injection of Targeted Exosomes. *Nat. Biotechnol.* 29, 341–345. doi:10.1038/nbt.1807

Andriolo, G., Provasi, E., Lo Cicero, V., Brambilla, A., Soncin, S., Torre, T., et al. (2018). Exosomes from Human Cardiac Progenitor Cells for Therapeutic Applications: Development of a GMP-Grade Manufacturing Method. *Front. Physiol.* 9, 1169. doi:10.3389/fphys.2018.01169

Antimisiaris, S. G., Mourtas, S., and Marazioti, A. (2018). Exosomes and Exosome-Inspired Vesicles for Targeted Drug Delivery. *Pharmaceutics* 10, 218. doi:10.3390/pharmaceutics10040218

Arance, E., Ramírez, V., Rubio-Roldan, A., Ocaña-Peinado, F. M., Romero-Cachinero, C., Jódar-Reyes, A. B., et al. (2021). Determination of Exosome Mitochondrial DNA as a Biomarker of Renal Cancer Aggressiveness. *Cancers (Basel)* 14, 1. doi:10.3390/cancers14010199

Armstrong, J. P. K., and Stevens, M. M. (2018). Strategic Design of Extracellular Vesicle Drug Delivery Systems. *Adv. Drug Deliv. Rev.* 130, 12–16. doi:10.1016/j.addr.2018.06.017

Baghbaderani, B. A., Mukhida, K., Hong, M., Mendez, I., and Behie, L. A. (2011). A Review of Bioreactor Protocols for Human Neural Precursor Cell Expansion in Preparation for Clinical Trials. *Curr. Stem Cel Res Ther* 6, 229–254. doi:10.2174/157488811796575378

Banks, W. A. (2016). From Blood-Brain Barrier to Blood-Brain Interface: New Opportunities for CNS Drug Delivery. *Nat. Rev. Drug Discov.* 15, 275–292. doi:10.1038/nrd.2015.21

Barbosa, M., Gomes, C., Sequeira, C., Gonçalves-Ribeiro, J., Pina, C. C., Carvalho, L. A., et al. (2021). Recovery of Depleted miR-146a in ALS Cortical Astrocytes Reverts Cell Aberrancies and Prevents Paracrine Pathogenicity on Microglia and Motor Neurons. *Front Cel Dev Biol* 9, 634355. doi:10.3389/fcell.2021.634355

Barile, L., and Vassalli, G. (2017). Exosomes: Therapy Delivery Tools and Biomarkers of Diseases. *Pharmacol. Ther.* 174, 63–78. doi:10.1016/j.pharmthera.2017.02.020

Batrakova, E. V., and Kim, M. S. (2015). Using Exosomes, Naturally-Equipped Nanocarriers, for Drug Delivery. *J. Control. Release* 219, 396–405. doi:10.1016/j.jconrel.2015.07.030

Battistelli, M., and Falcieri, E. (2020). Apoptotic Bodies: Particular Extracellular Vesicles Involved in Intercellular Communication. *Biology (Basel)* 9, 21. doi:10.3390/biology9010021

Baumann, K. (2021). Making More Exosomes. *Nat. Rev. Mol. Cel Biol* 22, 242. doi:10.1038/s41580-021-00358-6

Bell, E., and Taylor, M. A. (2017). Functional Roles for Exosomal MicroRNAs in the Tumour Microenvironment. *Comput. Struct. Biotechnol. J.* 15, 8–13. doi:10.1016/j.csbj.2016.10.005

Bianco, F., Perrotta, C., Novellino, L., Francolini, M., Riganti, L., Menna, E., et al. (2009). Acid Sphingomyelinase Activity Triggers Microparticle Release from Glial Cells. *EMBO J.* 28, 1043–1054. doi:10.1038/emboj.2009.45

Böker, K. O., Lemus-Diaz, N., Rinaldi Ferreira, R., Schiller, L., Schneider, S., and Gruber, J. (2018). The Impact of the CD9 Tetraspanin on Lentivirus Infectivity and Exosome Secretion. *Mol. Ther.* 26, 634–647. doi:10.1016/j.ymthe.2017.11.008

Bonafede, R., Scambi, I., Peroni, D., Potrich, V., Boschi, F., Benati, D., et al. (2016). Exosome Derived from Murine Adipose-Derived Stromal Cells: Neuroprotective Effect on *In Vitro* Model of Amyotrophic Lateral Sclerosis. *Exp. Cel Res.* 340, 150–158. doi:10.1016/j.yexcr.2015.12.009

Bonafede, R., Turano, E., Scambi, I., Busato, A., Bontempi, P., Virla, F., et al. (2020). ASC-exosomes Ameliorate the Disease Progression in SOD1(G93A) Murine Model Underlining Their Potential Therapeutic Use in Human ALS. *Int. J. Mol. Sci.* 21, 3651. doi:10.3390/ijms21103651

Bosch, S., de Beaurepaire, L., Allard, M., Mosser, M., Heichette, C., Chrétien, D., et al. (2016). Trehalose Prevents Aggregation of Exosomes and Cryodamage. *Sci. Rep.* 6, 36162. doi:10.1038/srep36162

Botha, J., Pugsley, H. R., and Handberg, A. (2021). Conventional, High-Resolution and Imaging Flow Cytometry: Benchmarking Performance in Characterisation of Extracellular Vesicles. *Biomedicines* 9, 124. doi:10.3390/biomedicines9020124

Brites, D., and Fernandes, A. (2015). Neuroinflammation and Depression: Microglia Activation, Extracellular Microvesicles and microRNA Dysregulation. *Front Cel Neurosci* 9, 476. doi:10.3389/fncel.2015.00476

Brites, D. (2020). Regulatory Function of microRNAs in Microglia. *Glia* 68, 1631–1642. doi:10.1002/glia.23846

Bu, N., Wu, H. Q., Zhang, G. L., Zhan, S. Q., Zhang, R., Fan, Q. Y., et al. (2015). Immature Dendritic Cell Exosomes Suppress Experimental Autoimmune Myasthenia Gravis. *J. Neuroimmunol* 285, 71–75. doi:10.1016/j.jneuroim.2015.04.009

Busatto, S., Morad, G., Guo, P., and Moses, M. A. (2021). The Role of Extracellular Vesicles in the Physiological and Pathological Regulation of the Blood-Brain Barrier. *FASEB Bioadv* 3, 665–675. doi:10.1096/fba.2021-00045

Cai, S., Luo, B., Jiang, P., Zhou, X., Lan, F., Yi, Q., et al. (2018). Immuno-modified Superparamagnetic Nanoparticles via Host-Guest Interactions for High-Purity Capture and Mild Release of Exosomes. *Nanoscale* 10, 14280–14289. doi:10.1039/c8nr02871k

Calfio, C., Gonzalez, A., Singh, S. K., Rojo, L. E., and Maccioni, R. B. (2020). The Emerging Role of Nutraceuticals and Phytochemicals in the Prevention and Treatment of Alzheimer's Disease. *J. Alzheimers Dis.* 77, 33–51. doi:10.3233/JAD-200443

Caruso Bavisotto, C., Scalia, F., Marino Gammazza, A., Carlisi, D., Bucchieri, F., Conway de Macario, E., et al. (2019). Extracellular Vesicle-Mediated Cell¯Cell

Communication in the Nervous System: Focus on Neurological Diseases. *Int. J. Mol. Sci.* 20, 434. doi:10.3390/ijms20020434

Caruso, S., and Poon, I. K. H. (2018). Apoptotic Cell-Derived Extracellular Vesicles: More Than Just Debris. *Front. Immunol.* 9, 1486. doi:10.3389/fimmu.2018.01486

Chen, C. C., Liu, L., Ma, F., Wong, C. W., Guo, X. E., Chacko, J. V., et al. (2016). Elucidation of Exosome Migration across the Blood-Brain Barrier Model *In Vitro*. *Cell Mol Bioeng* 9, 509–529. doi:10.1007/s12195-016-0458-3

Chen, H., Wang, L., Zeng, X., Schwarz, H., Nanda, H. S., Peng, X., et al. (2021). Exosomes, a New Star for Targeted Delivery. *Front. Cel Dev Biol* 9, 751079. doi:10.3389/fcell.2021.751079

Chen, T. S., Arslan, F., Yin, Y., Tan, S. S., Lai, R. C., Choo, A. B., et al. (2011). Enabling a Robust Scalable Manufacturing Process for Therapeutic Exosomes through Oncogenic Immortalization of Human ESC-Derived MSCs. *J. Transl Med.* 9, 47. doi:10.1186/1479-5876-9-47

Chevillet, J. R., Kang, Q., Ruf, I. K., Briggs, H. A., Vojtech, L. N., Hughes, S. M., et al. (2014). Quantitative and Stoichiometric Analysis of the microRNA Content of Exosomes. *Proc. Natl. Acad. Sci. U S A.* 111, 14888–14893. doi:10.1073/pnas.1408301111

Chivero, E. T., Liao, K., Niu, F., Tripathi, A., Tian, C., Buch, S., et al. (2020). Engineered Extracellular Vesicles Loaded with miR-124 Attenuate Cocaine-Mediated Activation of Microglia. *Front. Cel Dev Biol* 8, 573. doi:10.3389/fcell.2020.00573

Choi, D., Rak, J., and Gho, Y. S. (2021). Isolation of Extracellular Vesicles for Proteomic Profiling. *Methods Mol. Biol.* 2261, 193–206. doi:10.1007/978-1-0716-1186-9_11

Chuo, S. T., Chien, J. C., and Lai, C. P. (2018). Imaging Extracellular Vesicles: Current and Emerging Methods. *J. Biomed. Sci.* 25, 91. doi:10.1186/s12929-018-0494-5

Ciregia, F., Urbani, A., and Palmisano, G. (2017). Extracellular Vesicles in Brain Tumors and Neurodegenerative Diseases. *Front. Mol. Neurosci.* 10, 276. doi:10.3389/fnmol.2017.00276

Clancy, J. W., Boomgarden, A. C., and D'Souza-Schorey, C. (2021). Profiling and Promise of Supermeres. *Nat. Cel Biol* 23, 1217–1219. doi:10.1038/s41556-021-00808-5

Colao, I. L., Corteling, R., Bracewell, D., and Wall, I. (2018). Manufacturing Exosomes: A Promising Therapeutic Platform. *Trends Mol. Med.* 24, 242–256. doi:10.1016/j.molmed.2018.01.006

Contreras-Naranjo, J. C., Wu, H. J., and Ugaz, V. M. (2017). Microfluidics for Exosome Isolation and Analysis: Enabling Liquid Biopsy for Personalized Medicine. *Lab. Chip* 17, 3558–3577. doi:10.1039/c7lc00592j

Coumans, F. A., van der Pol, E., Böing, A. N., Hajji, N., Sturk, G., van Leeuwen, T. G., et al. (2014). Reproducible Extracellular Vesicle Size and Concentration Determination with Tunable Resistive Pulse Sensing. *J. Extracell Vesicles* 3, 25922. doi:10.3402/jev.v3.25922

Cunha, C., Gomes, C., Vaz, A. R., and Brites, D. (2016). Exploring New Inflammatory Biomarkers and Pathways during LPS-Induced M1 Polarization. *Mediators Inflamm.* 2016, 6986175. doi:10.1155/2016/6986175

Datta, A., Kim, H., McGee, L., Johnson, A. E., Talwar, S., Marugan, J., et al. (2018). High-throughput Screening Identified Selective Inhibitors of Exosome Biogenesis and Secretion: A Drug Repurposing Strategy for Advanced Cancer. *Sci. Rep.* 8, 8161. doi:10.1038/s41598-018-26411-7

de Abreu, R. C., Ramos, C. V., Becher, C., Lino, M., Jesus, C., da Costa Martins, P. A., et al. (2021). Exogenous Loading of miRNAs into Small Extracellular Vesicles. *J. Extracell Vesicles* 10, e12111. doi:10.1002/jev2.12111

de Almeida Fuzeta, M., Bernardes, N., Oliveira, F. D., Costa, A. C., Fernandes-Platzgummer, A., Farinha, J. P., et al. (2020). Scalable Production of Human Mesenchymal Stromal Cell-Derived Extracellular Vesicles under Serum-/Xeno-free Conditions in a Microcarrier-Based Bioreactor Culture System. *Front. Cel Dev Biol* 8, 553444. doi:10.3389/fcell.2020.553444

de Jong, O. G., Verhaar, M. C., Chen, Y., Vader, P., Gremmels, H., Posthuma, G., et al. (2012). Cellular Stress Conditions Are Reflected in the Protein and RNA Content of Endothelial Cell-Derived Exosomes. *J. Extracell Vesicles* 1, 1. doi:10.3402/jev.v1i0.18396

El Andaloussi, S., Mäger, I., Breakefield, X. O., and Wood, M. J. (2013). Extracellular Vesicles: Biology and Emerging Therapeutic Opportunities. *Nat. Rev. Drug Discov.* 12, 347–357. doi:10.1038/nrd3978

Elliott, R. O., and He, M. (2021). Unlocking the Power of Exosomes for Crossing Biological Barriers in Drug Delivery. *Pharmaceutics* 13, 122. doi:10.3390/pharmaceutics13010122

Elsherbini, A., Qin, H., Zhu, Z., Tripathi, P., Crivelli, S. M., and Bieberich, E. (2020). *In Vivo* evidence of Exosome-Mediated Aβ Neurotoxicity. *Acta Neuropathol. Commun.* 8, 100. doi:10.1186/s40478-020-00981-y

Emam, S. E., Ando, H., Abu Lila, A. S., Shimizu, T., Ukawa, M., Okuhira, K., et al. (2018). A Novel Strategy to Increase the Yield of Exosomes (Extracellular Vesicles) for an Expansion of Basic Research. *Biol. Pharm. Bull.* 41, 733–742. doi:10.1248/bpb.b17-00919

Erkan, E. P., Senfter, D., Madlener, S., Jungwirth, G., Ströbel, T., Saydam, N., et al. (2017). Extracellular Vesicle-Mediated Suicide mRNA/protein Delivery Inhibits Glioblastoma Tumor Growth *In Vivo*. *Cancer Gene Ther.* 24, 38–44. doi:10.1038/cgt.2016.78

Fan, Z., Li, P. Y., Deng, J., Bady, S. C., and Cheng, H. (2018). Cell Membrane Coating for Reducing Nanoparticle-Induced Inflammatory Responses to Scaffold Constructs. *Nano Res.* 11, 5573–5583. doi:10.1007/s12274-018-2084-y

Fang, R. H., Kroll, A. V., Gao, W., and Zhang, L. (2018). Cell Membrane Coating Nanotechnology. *Adv. Mater.* 30, e1706759. doi:10.1002/adma.201706759

Fernandes, A., Ribeiro, A. R., Monteiro, M., Garcia, G., Vaz, A. R., and Brites, D. (2018). Secretome from SH-Sy5y APPSwe Cells Trigger Time-dependent CHME3 Microglia Activation Phenotypes, Ultimately Leading to miR-21 Exosome Shuttling. *Biochimie* 155, 67–82. doi:10.1016/j.biochi.2018.05.015

Fiandaca, M. S., Kapogiannis, D., Mapstone, M., Boxer, A., Eitan, E., Schwartz, J. B., et al. (2015). Identification of Preclinical Alzheimer's Disease by a Profile of Pathogenic Proteins in Neurally Derived Blood Exosomes: A Case-Control Study. *Alzheimers Dement* 11, 600–e1. doi:10.1016/j.jalz.2014.06.008

Filipe, V., Hawe, A., and Jiskoot, W. (2010). Critical Evaluation of Nanoparticle Tracking Analysis (NTA) by NanoSight for the Measurement of Nanoparticles and Protein Aggregates. *Pharm. Res.* 27, 796–810. doi:10.1007/s11095-010-0073-2

Fitzner, D., Schnaars, M., van Rossum, D., Krishnamoorthy, G., Dibaj, P., Bakhti, M., et al. (2011). Selective Transfer of Exosomes from Oligodendrocytes to Microglia by Macropinocytosis. *J. Cel Sci* 124, 447–458. doi:10.1242/jcs.074088

Frisken, B. J. (2001). Revisiting the Method of Cumulants for the Analysis of Dynamic Light-Scattering Data. *Appl. Opt.* 40, 4087–4091. doi:10.1364/ao.40.004087

Fröhlich, D., Kuo, W. P., Frühbeis, C., Sun, J. J., Zehendner, C. M., Luhmann, H. J., et al. (2014). Multifaceted Effects of Oligodendroglial Exosomes on Neurons: Impact on Neuronal Firing Rate, Signal Transduction and Gene Regulation. *Philos. Trans. R. Soc. Lond. B Biol. Sci.* 369, 20130510. doi:10.1098/rstb.2013.0510

Frühbeis, C., Fröhlich, D., Kuo, W. P., Amphornrat, J., Thilemann, S., Saab, A. S., et al. (2013). Neurotransmitter-triggered Transfer of Exosomes Mediates Oligodendrocyte-Neuron Communication. *Plos Biol.* 11, e1001604. doi:10.1371/journal.pbio.1001604

Fuhrmann, G., Serio, A., Mazo, M., Nair, R., and Stevens, M. M. (2015). Active Loading into Extracellular Vesicles Significantly Improves the Cellular Uptake and Photodynamic Effect of Porphyrins. *J. Control. Release* 205, 35–44. doi:10.1016/j.jconrel.2014.11.029

Garcia, G., Pinto, S., Cunha, M., Fernandes, A., Koistinaho, J., and Brites, D. (2021). Neuronal Dynamics and miRNA Signaling Differ between SH-Sy5y APPSwe and PSEN1 Mutant iPSC-Derived AD Models upon Modulation with miR-124 Mimic and Inhibitor. *Cells* 10, 2424. doi:10.3390/cells10092424

García-Manrique, P., Matos, M., Gutiérrez, G., Pazos, C., and Blanco-López, M. C. (2018). Therapeutic Biomaterials Based on Extracellular Vesicles: Classification of Bio-Engineering and Mimetic Preparation Routes. *J. Extracell Vesicles* 7, 1422676. doi:10.1080/20013078.2017.1422676

Glebov, K., Löchner, M., Jabs, R., Lau, T., Merkel, O., Schloss, P., et al. (2015). Serotonin Stimulates Secretion of Exosomes from Microglia Cells. *Glia* 63, 626–634. doi:10.1002/glia.22772

Gomes, C., Cunha, C., Nascimento, F., Ribeiro, J. A., Vaz, A. R., and Brites, D. (2019). Cortical Neurotoxic Astrocytes with Early ALS Pathology and miR-146a Deficit Replicate Gliosis Markers of Symptomatic SOD1G93A Mouse Model. *Mol. Neurobiol.* 56, 2137–2158. doi:10.1007/s12035-018-1220-8

Gómez-Molina, C., Sandoval, M., Henzi, R., Ramírez, J. P., Varas-Godoy, M., Luarte, A., et al. (2019). Small Extracellular Vesicles in Rat Serum Contain

Astrocyte-Derived Protein Biomarkers of Repetitive Stress. *Int. J. Neuropsychopharmacol.* 22, 232–246. doi:10.1093/ijnp/pyy098

Görgens, A., Bremer, M., Ferrer-Tur, R., Murke, F., Tertel, T., Horn, P. A., et al. (2019). Optimisation of Imaging Flow Cytometry for the Analysis of Single Extracellular Vesicles by Using Fluorescence-Tagged Vesicles as Biological Reference Material. *J. Extracell Vesicles* 8, 1587567. doi:10.1080/20013078.2019.1587567

Grad, L. I., Yerbury, J. J., Turner, B. J., Guest, W. C., Pokrishevsky, E., O'Neill, M. A., et al. (2014). Intercellular Propagated Misfolding of Wild-type Cu/Zn Superoxide Dismutase Occurs via Exosome-dependent and -independent Mechanisms. *Proc. Natl. Acad. Sci. U S A.* 111, 3620–3625. doi:10.1073/pnas.1312245111

Guo, S. C., Tao, S. C., and Dawn, H. (2018). Microfluidics-based On-A-Chip Systems for Isolating and Analysing Extracellular Vesicles. *J. Extracell Vesicles* 7, 1508271. doi:10.1080/20013078.2018.1508271

Ha, B. G., Heo, J. Y., Jang, Y. J., Park, T. S., Choi, J. Y., Jang, W. Y., et al. (2021). Depletion of Mitochondrial Components from Extracellular Vesicles Secreted from Astrocytes in a Mouse Model of Fragile X Syndrome. *Int. J. Mol. Sci.* 22, 410. doi:10.3390/ijms22010410

Haney, M. J., Klyachko, N. L., Zhao, Y., Gupta, R., Plotnikova, E. G., He, Z., et al. (2015). Exosomes as Drug Delivery Vehicles for Parkinson's Disease Therapy. *J. Control. Release* 207, 18–30. doi:10.1016/j.jconrel.2015.03.033

Haney, M. J., Zhao, Y., Harrison, E. B., Mahajan, V., Ahmed, S., He, Z., et al. (2013). Specific Transfection of Inflamed Brain by Macrophages: a New Therapeutic Strategy for Neurodegenerative Diseases. *PLoS One* 8, e61852. doi:10.1371/journal.pone.0061852

Härkönen, K., Oikari, S., Kyykallio, H., Capra, J., Hakkola, S., Ketola, K., et al. (2019). CD44s Assembles Hyaluronan Coat on Filopodia and Extracellular Vesicles and Induces Tumorigenicity of MKN74 Gastric Carcinoma Cells. *Cells* 8, 276. doi:10.3390/cells8030276

Harrell, C. R., Volarevic, A., Djonov, V., and Volarevic, V. (2021). Mesenchymal Stem Cell-Derived Exosomes as New Remedy for the Treatment of Neurocognitive Disorders. *Ijms* 22, 1433. doi:10.3390/ijms22031433

He, M., Crow, J., Roth, M., Zeng, Y., and Godwin, A. K. (2014). Integrated Immunoisolation and Protein Analysis of Circulating Exosomes Using Microfluidic Technology. *Lab. Chip* 14, 3773–3780. doi:10.1039/c4lc00662c

Heinemann, M. L., Ilmer, M., Silva, L. P., Hawke, D. H., Recio, A., Vorontsova, M. A., et al. (2014). Benchtop Isolation and Characterization of Functional Exosomes by Sequential Filtration. *J. Chromatogr. A.* 1371, 125–135. doi:10.1016/j.chroma.2014.10.026

Hessvik, N. P., and Llorente, A. (2018). Current Knowledge on Exosome Biogenesis and Release. *Cell Mol Life Sci* 75, 193–208. doi:10.1007/s00018-017-2595-9

Hornung, S., Dutta, S., and Bitan, G. (2020). CNS-derived Blood Exosomes as a Promising Source of Biomarkers: Opportunities and Challenges. *Front. Mol. Neurosci.* 13, 38. doi:10.3389/fnmol.2020.00038

Hu, S., Qiao, L., and Cheng, K. (2021). Generation and Manipulation of Exosomes. *Methods Mol. Biol.* 2158, 295–305. doi:10.1007/978-1-0716-0668-1_22

Huo, L., Du, X., Li, X., Liu, S., and Xu, Y. (2021). The Emerging Role of Neural Cell-Derived Exosomes in Intercellular Communication in Health and Neurodegenerative Diseases. *Front. Neurosci.* 15, 738442. doi:10.3389/fnins.2021.738442

Isola, A. L., and Chen, S. (2017). Exosomes: The Messengers of Health and Disease. *Curr. Neuropharmacol* 15, 157–165. doi:10.2174/1570159x14666160825160421

Izumi, H., Kosaka, N., Shimizu, T., Sekine, K., Ochiya, T., and Takase, M. (2012). Bovine Milk Contains microRNA and Messenger RNA that Are Stable under Degradative Conditions. *J. Dairy Sci.* 95, 4831–4841. doi:10.3168/jds.2012-5489

Jaiswal, R., and Sedger, L. M. (2019). Intercellular Vesicular Transfer by Exosomes, Microparticles and Oncosomes - Implications for Cancer Biology and Treatments. *Front. Oncol.* 9, 125. doi:10.3389/fonc.2019.00125

Jang, S. C., Kim, O. Y., Yoon, C. M., Choi, D. S., Roh, T. Y., Park, J., et al. (2013). Bioinspired Exosome-Mimetic Nanovesicles for Targeted Delivery of Chemotherapeutics to Malignant Tumors. *ACS Nano* 7, 7698–7710. doi:10.1021/nn402232g

Jaul, E., and Barron, J. (2017). Age-Related Diseases and Clinical and Public Health Implications for the 85 Years Old and over Population. *Front. Public Health* 5, 335. doi:10.3389/fpubh.2017.00335

Jeyaram, A., and Jay, S. M. (2017). Preservation and Storage Stability of Extracellular Vesicles for Therapeutic Applications. *AAPS J.* 20, 1. doi:10.1208/s12248-017-0160-y

Jiang, L., and Poon, I. K. H. (2019). Methods for Monitoring the Progression of Cell Death, Cell Disassembly and Cell Clearance. *Apoptosis* 24, 208–220. doi:10.1007/s10495-018-01511-x

Jiang, X., You, L., Zhang, Z., Cui, X., Zhong, H., Sun, X., et al. (2021). Biological Properties of Milk-Derived Extracellular Vesicles and Their Physiological Functions in Infant. *Front. Cel Dev Biol* 9, 693534. doi:10.3389/fcell.2021.693534

Johnsen, K. B., Gudbergsson, J. M., Skov, M. N., Pilgaard, L., Moos, T., and Duroux, M. (2014). A Comprehensive Overview of Exosomes as Drug Delivery Vehicles - Endogenous Nanocarriers for Targeted Cancer Therapy. *Biochim. Biophys. Acta* 1846, 75–87. doi:10.1016/j.bbcan.2014.04.005

Johnstone, R. M. (2005). Revisiting the Road to the Discovery of Exosomes. *Blood Cell Mol Dis* 34, 214–219. doi:10.1016/j.bcmd.2005.03.002

Kalani, A., Chaturvedi, P., Kamat, P. K., Maldonado, C., Bauer, P., Joshua, I. G., et al. (2016). Curcumin-loaded Embryonic Stem Cell Exosomes Restored Neurovascular Unit Following Ischemia-Reperfusion Injury. *Int. J. Biochem. Cel Biol* 79, 360–369. doi:10.1016/j.biocel.2016.09.002

Kang, T., Atukorala, I., and Mathivanan, S. (2021). Biogenesis of Extracellular Vesicles. *Subcell Biochem.* 97, 19–43. doi:10.1007/978-3-030-67171-6_2

Kanwar, S. S., Dunlay, C. J., Simeone, D. M., and Nagrath, S. (2014). Microfluidic Device (ExoChip) for On-Chip Isolation, Quantification and Characterization of Circulating Exosomes. *Lab. Chip* 14, 1891–1900. doi:10.1039/c4lc00136b

Katakowski, M., Buller, B., Zheng, X., Lu, Y., Rogers, T., Osobamiro, O., et al. (2013). Exosomes from Marrow Stromal Cells Expressing miR-146b Inhibit Glioma Growth. *Cancer Lett.* 335, 201–204. doi:10.1016/j.canlet.2013.02.019

Katsuda, T., Tsuchiya, R., Kosaka, N., Yoshioka, Y., Takagaki, K., Oki, K., et al. (2013). Human Adipose Tissue-Derived Mesenchymal Stem Cells Secrete Functional Neprilysin-Bound Exosomes. *Sci. Rep.* 3, 1197. doi:10.1038/srep01197

Kim, M. S., Haney, M. J., Zhao, Y., Mahajan, V., Deygen, I., Klyachko, N. L., et al. (2016). Development of Exosome-Encapsulated Paclitaxel to Overcome MDR in Cancer Cells. *Nanomedicine* 12, 655–664. doi:10.1016/j.nano.2015.10.012

Kim, S. H., Lechman, E. R., Bianco, N., Menon, R., Keravala, A., Nash, J., et al. (2005). Exosomes Derived from IL-10-treated Dendritic Cells Can Suppress Inflammation and Collagen-Induced Arthritis. *J. Immunol.* 174, 6440–6448. doi:10.4049/jimmunol.174.10.6440

Ko, J., Carpenter, E., and Issadore, D. (2016). Detection and Isolation of Circulating Exosomes and Microvesicles for Cancer Monitoring and Diagnostics Using Micro-/nano-based Devices. *Analyst* 141, 450–460. doi:10.1039/c5an01610j

Kojima, R., Bojar, D., Rizzi, G., Hamri, G. C., El-Baba, M. D., Saxena, P., et al. (2018). Designer Exosomes Produced by Implanted Cells Intracerebrally Deliver Therapeutic Cargo for Parkinson's Disease Treatment. *Nat. Commun.* 9, 1305. doi:10.1038/s41467-018-03733-8

Konoshenko, M. Y., Lekchnov, E. A., Vlassov, A. V., and Laktionov, P. P. (2018). Isolation of Extracellular Vesicles: General Methodologies and Latest Trends. *Biomed. Res. Int.* 2018, 8545347. doi:10.1155/2018/8545347

Kooijmans, S. A. A., Fliervoet, L. A. L., van der Meel, R., Fens, M. H. A. M., Heijnen, H. F. G., van Bergen En Henegouwen, P. M. P., et al. (2016). PEGylated and Targeted Extracellular Vesicles Display Enhanced Cell Specificity and Circulation Time. *J. Control. Release* 224, 77–85. doi:10.1016/j.jconrel.2016.01.009

Kumar, A., Kim, S., Su, Y., Sharma, M., Kumar, P., Singh, S., et al. (2021). Brain Cell-Derived Exosomes in Plasma Serve as Neurodegeneration Biomarkers in Male Cynomolgus Monkeys Self-Administrating Oxycodone. *EBioMedicine* 63, 103192. doi:10.1016/j.ebiom.2020.103192

Kumar, D., Gupta, D., Shankar, S., and Srivastava, R. K. (2015). Biomolecular Characterization of Exosomes Released from Cancer Stem Cells: Possible Implications for Biomarker and Treatment of Cancer. *Oncotarget* 6, 3280–3291. doi:10.18632/oncotarget.2462

Kurian, T. K., Banik, S., Gopal, D., Chakrabarti, S., and Mazumder, N. (2021). Elucidating Methods for Isolation and Quantification of Exosomes: A Review. *Mol. Biotechnol.* 63, 249–266. doi:10.1007/s12033-021-00300-3

Kusuma, G. D., Barabadi, M., Tan, J. L., Morton, D. A. V., Frith, J. E., and Lim, R. (2018). To Protect and to Preserve: Novel Preservation Strategies for Extracellular Vesicles. *Front. Pharmacol.* 9, 1199. doi:10.3389/fphar.2018.01199

Lamparski, H. G., Metha-Damani, A., Yao, J. Y., Patel, S., Hsu, D. H., Ruegg, C., et al. (2002). Production and Characterization of Clinical Grade Exosomes Derived from Dendritic Cells. *J. Immunol. Methods* 270, 211–226. doi:10.1016/s0022-1759(02)00330-7

Lane, R. E., Korbie, D., Anderson, W., Vaidyanathan, R., and Trau, M. (2015). Analysis of Exosome Purification Methods Using a Model Liposome System and Tunable-Resistive Pulse Sensing. *Sci. Rep.* 5, 7639. doi:10.1038/srep07639

Lane, R. E., Korbie, D., Trau, M., and Hill, M. M. (2017). Purification Protocols for Extracellular Vesicles. *Methods Mol. Biol.* 1660, 111–130. doi:10.1007/978-1-4939-7253-1_10

Lee, B. R., Kim, J. H., Choi, E. S., Cho, J. H., and Kim, E. (2018). Effect of Young Exosomes Injected in Aged Mice. *Int. J. Nanomedicine* 13, 5335–5345. doi:10.2147/ijn.S170680

Lee, M., Ban, J. J., Kim, K. Y., Jeon, G. S., Im, W., Sung, J. J., et al. (2016). Adipose-derived Stem Cell Exosomes Alleviate Pathology of Amyotrophic Lateral Sclerosis *In Vitro*. *Biochem. Biophys. Res. Commun.* 479, 434–439. doi:10.1016/j.bbrc.2016.09.069

Lin, S., Yu, Z., Chen, D., Wang, Z., Miao, J., Li, Q., et al. (2020a). Progress in Microfluidics-Based Exosome Separation and Detection Technologies for Diagnostic Applications. *Small* 16, e1903916. doi:10.1002/smll.201903916

Lin, Y., Lu, Y., and Li, X. (2020b). Biological Characteristics of Exosomes and Genetically Engineered Exosomes for the Targeted Delivery of Therapeutic Agents. *J. Drug Target.* 28, 129–141. doi:10.1080/1061186X.2019.1641508

Linares, R., Tan, S., Gounou, C., and Brisson, A. R. (2017). Imaging and Quantification of Extracellular Vesicles by Transmission Electron Microscopy. *Methods Mol. Biol.* 1545, 43–54. doi:10.1007/978-1-4939-6728-5_4

Liu, H., Shen, M., ZhaoRu, D., Ru, D., Duan, Y., Ding, C., et al. (2019). The Effect of Triptolide-Loaded Exosomes on the Proliferation and Apoptosis of Human Ovarian Cancer SKOV3 Cells. *Biomed. Res. Int.* 2019, 2595801. doi:10.1155/2019/2595801

Llorente, A., Skotland, T., Sylvänne, T., Kauhanen, D., Róg, T., Orłowski, A., et al. (2013). Molecular Lipidomics of Exosomes Released by PC-3 Prostate Cancer Cells. *Biochim. Biophys. Acta* 1831, 1302–1309. doi:10.1016/j.bbalip.2013.04.011

Loch-Neckel, G., Santos-Bubniak, L., Mazzarino, L., Jacques, A. V., Moccelin, B., Santos-Silva, M. C., et al. (2015). Orally Administered Chitosan-Coated Polycaprolactone Nanoparticles Containing Curcumin Attenuate Metastatic Melanoma in the Lungs. *J. Pharm. Sci.* 104, 3524–3534. doi:10.1002/jps.24548

Logozzi, M., Di Raimo, R., Mizzoni, D., and Fais, S. (2020). Immunocapture-based ELISA to Characterize and Quantify Exosomes in Both Cell Culture Supernatants and Body Fluids. *Methods Enzymol.* 645, 155–180. doi:10.1016/bs.mie.2020.06.011

López-Leal, R., Díaz-Viraqué, F., Catalán, R. J., Saquel, C., Enright, A., Iraola, G., et al. (2020). Schwann Cell Reprogramming into Repair Cells Increases miRNA-21 Expression in Exosomes Promoting Axonal Growth. *J. Cel Sci* 133, jcs239004. doi:10.1242/jcs.239004

Lorenc, T., Klimczyk, K., Michalczewska, I., Słomka, M., Kubiak-Tomaszewska, G., and Olejarz, W. (2020). Exosomes in Prostate Cancer Diagnosis, Prognosis and Therapy. *Int. J. Mol. Sci.* 21, 2118. doi:10.3390/ijms21062118

Luan, X., Sansanaphongpricha, K., Myers, I., Chen, H., Yuan, H., and Sun, D. (2017). Engineering Exosomes as Refined Biological Nanoplatforms for Drug Delivery. *Acta Pharmacol. Sin* 38, 754–763. doi:10.1038/aps.2017.12

Luchini, A., and Vitiello, G. (2019). Understanding the Nano-Bio Interfaces: Lipid-Coatings for Inorganic Nanoparticles as Promising Strategy for Biomedical Applications. *Front. Chem.* 7, 343. doi:10.3389/fchem.2019.00343

Lunavat, T. R., Jang, S. C., Nilsson, L., Park, H. T., Repiska, G., Lässer, C., et al. (2016). RNAi Delivery by Exosome-Mimetic Nanovesicles - Implications for Targeting C-Myc in Cancer. *Biomaterials* 102, 231–238. doi:10.1016/j.biomaterials.2016.06.024

Lv, Y., Tan, J., Miao, Y., and Zhang, Q. (2019). The Role of Microvesicles and its Active Molecules in Regulating Cellular Biology. *J. Cel Mol Med* 23, 7894–7904. doi:10.1111/jcmm.14667

Ma, Y., Li, C., Huang, Y., Wang, Y., Xia, X., and Zheng, J. C. (2019). Exosomes Released from Neural Progenitor Cells and Induced Neural Progenitor Cells Regulate Neurogenesis through miR-21a. *Cell Commun Signal* 17, 96. doi:10.1186/s12964-019-0418-3

Malloci, M., Perdomo, L., Veerasamy, M., Andriantsitohaina, R., Simard, G., and Martínez, M. C. (2019). Extracellular Vesicles: Mechanisms in Human Health and Disease. *Antioxid. Redox Signal.* 30, 813–856. doi:10.1089/ars.2017.7265

Marconi, S., Bonaconsa, M., Scambi, I., Squintani, G. M., Rui, W., Turano, E., et al. (2013). Systemic Treatment with Adipose-Derived Mesenchymal Stem Cells Ameliorates Clinical and Pathological Features in the Amyotrophic Lateral Sclerosis Murine Model. *Neuroscience* 248, 333–343. doi:10.1016/j.neuroscience.2013.05.034

Maroto, R., Zhao, Y., Jamaluddin, M., Popov, V. L., Wang, H., Kalubowilage, M., et al. (2017). Effects of Storage Temperature on Airway Exosome Integrity for Diagnostic and Functional Analyses. *J. Extracell Vesicles* 6, 1359478. doi:10.1080/20013078.2017.1359478

Mashouri, L., Yousefi, H., Aref, A. R., Ahadi, A. M., Molaei, F., and Alahari, S. K. (2019). Exosomes: Composition, Biogenesis, and Mechanisms in Cancer Metastasis and Drug Resistance. *Mol. Cancer* 18, 75. doi:10.1186/s12943-019-0991-5

Mathivanan, S., Fahner, C. J., Reid, G. E., and Simpson, R. J. (2012). ExoCarta 2012: Database of Exosomal Proteins, RNA and Lipids. *Nucleic Acids Res.* 40, D1241–D1244. doi:10.1093/nar/gkr828

Mathivanan, S., and Simpson, R. J. (2009). ExoCarta: A Compendium of Exosomal Proteins and RNA. *Proteomics* 9, 4997–5000. doi:10.1002/pmic.200900351

Mendt, M., Kamerkar, S., Sugimoto, H., McAndrews, K. M., Wu, C. C., Gagea, M., et al. (2018). Generation and Testing of Clinical-Grade Exosomes for Pancreatic Cancer. *JCI Insight* 3, e99263. doi:10.1172/jci.insight.99263

Miranda, C. C., Fernandes, T. G., Diogo, M. M., and Cabral, J. M. (2016). Scaling up a Chemically-Defined Aggregate-Based Suspension Culture System for Neural Commitment of Human Pluripotent Stem Cells. *Biotechnol. J.* 11, 1628–1638. doi:10.1002/biot.201600446

Momen-Heravi, F., Balaj, L., Alian, S., Mantel, P. Y., Halleck, A. E., Trachtenberg, A. J., et al. (2013). Current Methods for the Isolation of Extracellular Vesicles. *Biol. Chem.* 394, 1253–1262. doi:10.1515/hsz-2013-0141

Morel, L., Regan, M., Higashimori, H., Ng, S. K., Esau, C., Vidensky, S., et al. (2013). Neuronal Exosomal miRNA-dependent Translational Regulation of Astroglial Glutamate Transporter GLT1. *J. Biol. Chem.* 288, 7105–7116. doi:10.1074/jbc.M112.410944

Navabi, H., Croston, D., Hobot, J., Clayton, A., Zitvogel, L., Jasani, B., et al. (2005). Preparation of Human Ovarian Cancer Ascites-Derived Exosomes for a Clinical Trial. *Blood Cell Mol Dis* 35, 149–152. doi:10.1016/j.bcmd.2005.06.008

Ni, H., Yang, S., Siaw-Debrah, F., Hu, J., Wu, K., He, Z., et al. (2019). Exosomes Derived from Bone Mesenchymal Stem Cells Ameliorate Early Inflammatory Responses Following Traumatic Brain Injury. *Front. Neurosci.* 13, 14. doi:10.3389/fnins.2019.00014

Niu, Z., Pang, R. T. K., Liu, W., Li, Q., Cheng, R., and Yeung, W. S. B. (2017). Polymer-based Precipitation Preserves Biological Activities of Extracellular Vesicles from an Endometrial Cell Line. *PLoS One* 12, e0186534. doi:10.1371/journal.pone.0186534

O'Loughlin, A. J., Mäger, I., de Jong, O. G., Varela, M. A., Schiffelers, R. M., El Andaloussi, S., et al. (2017). Functional Delivery of Lipid-Conjugated siRNA by Extracellular Vesicles. *Mol. Ther.* 25, 1580–1587. doi:10.1016/j.ymthe.2017.03.021

Oeyen, E., Van Mol, K., Baggerman, G., Willems, H., Boonen, K., Rolfo, C., et al. (2018). Ultrafiltration and Size Exclusion Chromatography Combined with Asymmetrical-Flow Field-Flow Fractionation for the Isolation and Characterisation of Extracellular Vesicles from Urine. *J. Extracell Vesicles* 7, 1490143. doi:10.1080/20013078.2018.1490143

Parada, N., Romero-Trujillo, A., Georges, N., and Alcayaga-Miranda, F. (2021). Camouflage Strategies for Therapeutic Exosomes Evasion from Phagocytosis. *J. Adv. Res.* 31, 61–74. doi:10.1016/j.jare.2021.01.001

Parolini, I., Federici, C., Raggi, C., Lugini, L., Palleschi, S., De Milito, A., et al. (2009). Microenvironmental pH Is a Key Factor for Exosome Traffic in Tumor Cells. *J. Biol. Chem.* 284, 34211–34222. doi:10.1074/jbc.M109.041152

Pascucci, L., Coccè, V., Bonomi, A., Ami, D., Ceccarelli, P., Ciusani, E., et al. (2014). Paclitaxel Is Incorporated by Mesenchymal Stromal Cells and Released in Exosomes that Inhibit *In Vitro* Tumor Growth: a New Approach for Drug Delivery. *J. Control. Release* 192, 262–270. doi:10.1016/j.jconrel.2014.07.042

Patel, G. K., Khan, M. A., Zubair, H., Srivastava, S. K., Khushman, M., Singh, S., et al. (2019). Comparative Analysis of Exosome Isolation Methods Using

Culture Supernatant for Optimum Yield, Purity and Downstream Applications. *Sci. Rep.* 9, 5335. doi:10.1038/s41598-019-41800-2

Paul, D., Baena, V., Ge, S., Jiang, X., Jellison, E. R., Kiprono, T., et al. (2016). Appearance of Claudin-5+ Leukocytes in the central Nervous System during Neuroinflammation: a Novel Role for Endothelial-Derived Extracellular Vesicles. *J. Neuroinflammation* 13, 292. doi:10.1186/s12974-016-0755-8

Pessina, A., Bonomi, A., Coccè, V., Invernici, G., Navone, S., Cavicchini, L., et al. (2011). Mesenchymal Stromal Cells Primed with Paclitaxel Provide a New Approach for Cancer Therapy. *PLoS One* 6, e28321. doi:10.1371/journal.pone.0028321

Phan, T. H., Divakarla, S. K., Yeo, J. H., Lei, Q., Tharkar, P., Pansani, T. N., et al. (2021). New Multiscale Characterization Methodology for Effective Determination of Isolation-Structure-Function Relationship of Extracellular Vesicles. *Front. Bioeng. Biotechnol.* 9, 669537. doi:10.3389/fbioe.2021.669537

Pinto, S., Cunha, C., Barbosa, M., Vaz, A. R., and Brites, D. (2017). Exosomes from NSC-34 Cells Transfected with hSOD1-G93a Are Enriched in miR-124 and Drive Alterations in Microglia Phenotype. *Front. Neurosci.* 11, 273. doi:10.3389/fnins.2017.00273

Qi, Y., Guo, L., Jiang, Y., Shi, Y., Sui, H., and Zhao, L. (2020). Brain Delivery of Quercetin-Loaded Exosomes Improved Cognitive Function in AD Mice by Inhibiting Phosphorylated Tau-Mediated Neurofibrillary Tangles. *Drug Deliv.* 27, 745–755. doi:10.1080/10717544.2020.1762262

Qu, M., Lin, Q., Huang, L., Fu, Y., Wang, L., He, S., et al. (2018). Dopamine-loaded Blood Exosomes Targeted to Brain for Better Treatment of Parkinson's Disease. *J. Control. Release* 287, 156–166. doi:10.1016/j.jconrel.2018.08.035

Rai, A., Fang, H., Fatmous, M., Claridge, B., Poh, Q. H., Simpson, R. J., et al. (2021). A Protocol for Isolation, Purification, Characterization, and Functional Dissection of Exosomes. *Methods Mol. Biol.* 2261, 105–149. doi:10.1007/978-1-0716-1186-9_9

Rastogi, S., Sharma, V., Bharti, P. S., Rani, K., Modi, G. P., Nikolajeff, F., et al. (2021). The Evolving Landscape of Exosomes in Neurodegenerative Diseases: Exosomes Characteristics and a Promising Role in Early Diagnosis. *Ijms* 22, 440. doi:10.3390/ijms22010440

Russell, A. E., Sneider, A., Witwer, K. W., Bergese, P., Bhattacharyya, S. N., Cocks, A., et al. (2019). Biological Membranes in EV Biogenesis, Stability, Uptake, and Cargo Transfer: an ISEV Position Paper Arising from the ISEV Membranes and EVs Workshop. *J. Extracell Vesicles* 8, 1684862. doi:10.1080/20013078.2019.1684862

Saludas, L., Garbayo, E., Ruiz-Villalba, A., Hernández, S., Vader, P., Prósper, F., et al. (2022). Isolation Methods of Large and Small Extracellular Vesicles Derived from Cardiovascular Progenitors: A Comparative Study. *Eur. J. Pharm. Biopharm.* 170, 187–196. doi:10.1016/j.ejpb.2021.12.012

Saman, S., Kim, W., Raya, M., Visnick, Y., Miro, S., Saman, S., et al. (2012). Exosome-associated Tau Is Secreted in Tauopathy Models and Is Selectively Phosphorylated in Cerebrospinal Fluid in Early Alzheimer Disease. *J. Biol. Chem.* 287, 3842–3849. doi:10.1074/jbc.M111.277061

Sancho-Albero, M., Navascués, N., Mendoza, G., Sebastián, V., Arruebo, M., Martín-Duque, P., et al. (2019). Exosome Origin Determines Cell Targeting and the Transfer of Therapeutic Nanoparticles towards Target Cells. *J. Nanobiotechnology* 17, 16. doi:10.1186/s12951-018-0437-z

Sancho-Albero, M., Sebastián, V., Sesé, J., Pazo-Cid, R., Mendoza, G., Arruebo, M., et al. (2020). Isolation of Exosomes from Whole Blood by a New Microfluidic Device: Proof of Concept Application in the Diagnosis and Monitoring of Pancreatic Cancer. *J. Nanobiotechnology* 18, 150. doi:10.1186/s12951-020-00701-7

Sansone, P., Savini, C., Kurelac, I., Chang, Q., Amato, L. B., Strillacci, A., et al. (2017). Packaging and Transfer of Mitochondrial DNA via Exosomes Regulate Escape from Dormancy in Hormonal Therapy-Resistant Breast Cancer. *Proc. Natl. Acad. Sci. U S A.* 114, E9066–E9075. doi:10.1073/pnas.1704862114

Sato, Y. T., Umezaki, K., Sawada, S., Mukai, S. A., Sasaki, Y., Harada, N., et al. (2016). Engineering Hybrid Exosomes by Membrane Fusion with Liposomes. *Sci. Rep.* 6, 21933. doi:10.1038/srep21933

Savina, A., Furlán, M., Vidal, M., and Colombo, M. I. (2003). Exosome Release Is Regulated by a Calcium-dependent Mechanism in K562 Cells. *J. Biol. Chem.* 278, 20083–20090. doi:10.1074/jbc.M301642200

Severino, V., Alessio, N., Farina, A., Sandomenico, A., Cipollaro, M., Peluso, G., et al. (2013). Insulin-like Growth Factor Binding Proteins 4 and 7 Released by Senescent Cells Promote Premature Senescence in Mesenchymal Stem Cells. *Cell Death Dis* 4, e911. doi:10.1038/cddis.2013.445

Simons, M., and Raposo, G. (2009). Exosomes--vesicular Carriers for Intercellular Communication. *Curr. Opin. Cel Biol* 21, 575–581. doi:10.1016/j.ceb.2009.03.007

Simpson, R. J., Kalra, H., and Mathivanan, S. (2012). ExoCarta as a Resource for Exosomal Research. *J. Extracell Vesicles* 1, 1. doi:10.3402/jev.v1i0.18374

Simpson, R. J., Lim, J. W., Moritz, R. L., and Mathivanan, S. (2009). Exosomes: Proteomic Insights and Diagnostic Potential. *Expert Rev. Proteomics* 6, 267–283. doi:10.1586/epr.09.17

Skog, J., Würdinger, T., van Rijn, S., Meijer, D. H., Gainche, L., Sena-Esteves, M., et al. (2008). Glioblastoma Microvesicles Transport RNA and Proteins that Promote Tumour Growth and Provide Diagnostic Biomarkers. *Nat. Cel Biol* 10, 1470–1476. doi:10.1038/ncb1800

Skotland, T., Hessvik, N. P., Sandvig, K., and Llorente, A. (2019). Exosomal Lipid Composition and the Role of Ether Lipids and Phosphoinositides in Exosome Biology. *J. Lipid Res.* 60, 9–18. doi:10.1194/jlr.R084343

Skotland, T., Sandvig, K., and Llorente, A. (2017). Lipids in Exosomes: Current Knowledge and the Way Forward. *Prog. Lipid Res.* 66, 30–41. doi:10.1016/j.plipres.2017.03.001

Song, X., Wang, Y., and Gao, L. (2020a). Mechanism of Antioxidant Properties of Quercetin and Quercetin-DNA Complex. *J. Mol. Model.* 26, 133. doi:10.1007/s00894-020-04356-x

Song, Z., Xu, Y., Deng, W., Zhang, L., Zhu, H., Yu, P., et al. (2020b). Brain Derived Exosomes Are a Double-Edged Sword in Alzheimer's Disease. *Front. Mol. Neurosci.* 13, 79. doi:10.3389/fnmol.2020.00079

Strimpakos, A. S., and Sharma, R. A. (2008). Curcumin: Preventive and Therapeutic Properties in Laboratory Studies and Clinical Trials. *Antioxid. Redox Signal.* 10, 511–545. doi:10.1089/ars.2007.1769

Sun, D., Zhuang, X., Xiang, X., Liu, Y., Zhang, S., Liu, C., et al. (2010). A Novel Nanoparticle Drug Delivery System: the Anti-inflammatory Activity of Curcumin Is Enhanced when Encapsulated in Exosomes. *Mol. Ther.* 18, 1606–1614. doi:10.1038/mt.2010.105

Sun, T., Ding, Z. X., Luo, X., Liu, Q. S., and Cheng, Y. (2020). Blood Exosomes Have Neuroprotective Effects in a Mouse Model of Parkinson's Disease. *Oxid Med. Cel Longev* 2020, 3807476. doi:10.1155/2020/3807476

Tauro, B. J., Greening, D. W., Mathias, R. A., Ji, H., Mathivanan, S., Scott, A. M., et al. (2012). Comparison of Ultracentrifugation, Density Gradient Separation, and Immunoaffinity Capture Methods for Isolating Human colon Cancer Cell Line LIM1863-Derived Exosomes. *Methods* 56, 293–304. doi:10.1016/j.ymeth.2012.01.002

Tertel, T., Bremer, M., Maire, C., Lamszus, K., Peine, S., Jawad, R., et al. (2020). High-Resolution Imaging Flow Cytometry Reveals Impact of Incubation Temperature on Labeling of Extracellular Vesicles with Antibodies. *Cytometry A* 97, 602–609. doi:10.1002/cyto.a.24034

Thakur, B. K., Zhang, H., Becker, A., Matei, I., Huang, Y., Costa-Silva, B., et al. (2014). Double-stranded DNA in Exosomes: a Novel Biomarker in Cancer Detection. *Cell Res* 24, 766–769. doi:10.1038/cr.2014.44

Théry, C., Witwer, K. W., Aikawa, E., Alcaraz, M. J., Anderson, J. D., Andriantsitohaina, R., et al. (2018). Minimal Information for Studies of Extracellular Vesicles 2018 (MISEV2018): a Position Statement of the International Society for Extracellular Vesicles and Update of the MISEV2014 Guidelines. *J. Extracell Vesicles* 7, 1535750. doi:10.1080/20013078.2018.1535750

Théry, C., Amigorena, S., Raposo, G., and Clayton, A. (2006). Isolation and Characterization of Exosomes from Cell Culture Supernatants and Biological Fluids. *Curr. Protoc. Cel Biol.* 30, 1. doi:10.1002/0471143030.cb0322s30

Thippabhotla, S., Zhong, C., and He, M. (2019). 3D Cell Culture Stimulates the Secretion of *In Vivo* like Extracellular Vesicles. *Sci. Rep.* 9, 13012. doi:10.1038/s41598-019-49671-3

Thomas, S. C., Kim, J. W., Pauletti, G. M., Hassett, D. J., and Kotagiri, N. (2021). Exosomes: Biological Pharmaceutical Nanovectors for Theranostics. *Front. Bioeng. Biotechnol.* 9, 808614. doi:10.3389/fbioe.2021.808614

Tomlinson, P. R., Zheng, Y., Fischer, R., Heidasch, R., Gardiner, C., Evetts, S., et al. (2015). Identification of Distinct Circulating Exosomes in Parkinson's Disease. *Ann. Clin. Transl Neurol.* 2, 353–361. doi:10.1002/acn3.175

van Niel, G., D'Angelo, G., and Raposo, G. (2018). Shedding Light on the Cell Biology of Extracellular Vesicles. *Nat. Rev. Mol. Cel Biol* 19, 213–228. doi:10.1038/nrm.2017.125

van Niel, G., Porto-Carreiro, I., Simoes, S., and Raposo, G. (2006). Exosomes: a Common Pathway for a Specialized Function. *J. Biochem.* 140, 13–21. doi:10.1093/jb/mvj128

Vaz, A. R., Vizinha, D., Morais, H., Colaço, A. R., Loch-Neckel, G., Barbosa, M., et al. (2021). Overexpression of miR-124 in Motor Neurons Plays a Key Role in ALS Pathological Processes. *Int. J. Mol. Sci.* 22, 6128. doi:10.3390/ijms22116128

Vinduska, V., Gallops, C. E., O'Connor, R., Wang, Y., and Huang, X. (2021). Exosomal Surface Protein Detection with Quantum Dots and Immunomagnetic Capture for Cancer Detection. *Nanomaterials (Basel)* 11, 1853. doi:10.3390/nano11071853

Wang, H., Sui, H., Zheng, Y., Jiang, Y., Shi, Y., Liang, J., et al. (2019). Curcumin-primed Exosomes Potently Ameliorate Cognitive Function in AD Mice by Inhibiting Hyperphosphorylation of the Tau Protein through the AKT/GSK-3β Pathway. *Nanoscale* 11, 7481–7496. doi:10.1039/c9nr01255a

Wang, J., Bonacquisti, E. E., Brown, A. D., and Nguyen, J. (2020). Boosting the Biogenesis and Secretion of Mesenchymal Stem Cell-Derived Exosomes. *Cells* 9, 660. doi:10.3390/cells9030660

Watson, D. C., Bayik, D., Srivatsan, A., Bergamaschi, C., Valentin, A., Niu, G., et al. (2016). Efficient Production and Enhanced Tumor Delivery of Engineered Extracellular Vesicles. *Biomaterials* 105, 195–205. doi:10.1016/j.biomaterials.2016.07.003

Welsh, J. A., Van Der Pol, E., Arkesteijn, G. J. A., Bremer, M., Brisson, A., Coumans, F., et al. (2020). MIFlowCyt-EV: a Framework for Standardized Reporting of Extracellular Vesicle Flow Cytometry Experiments. *J. Extracell Vesicles* 9, 1713526. doi:10.1080/20013078.2020.1713526

Whitford, W., and Guterstam, P. (2019). Exosome Manufacturing Status. *Future Med. Chem.* 11, 1225–1236. doi:10.4155/fmc-2018-0417

Witwer, K. W., Buzás, E. I., Bemis, L. T., Bora, A., Lässer, C., Lötvall, J., et al. (2013). Standardization of Sample Collection, Isolation and Analysis Methods in Extracellular Vesicle Research. *J. Extracell Vesicles* 2, 1. doi:10.3402/jev.v2i0.20360

Wong, C. H., and Chen, Y. C. (2019). Clinical Significance of Exosomes as Potential Biomarkers in Cancer. *World J. Clin. Cases* 7, 171–190. doi:10.12998/wjcc.v7.i2.171

Wu, J. Y., Li, Y. J., Hu, X. B., Huang, S., and Xiang, D. X. (2021a). Preservation of Small Extracellular Vesicles for Functional Analysis and Therapeutic Applications: a Comparative Evaluation of Storage Conditions. *Drug Deliv.* 28, 162–170. doi:10.1080/10717544.2020.1869866

Wu, Z., He, D., and Li, H. (2021b). Bioglass Enhances the Production of Exosomes and Improves Their Capability of Promoting Vascularization. *Bioact Mater.* 6, 823–835. doi:10.1016/j.bioactmat.2020.09.011

Xiao, Y., Zhong, J., Zhong, B., Huang, J., Jiang, L., Jiang, Y., et al. (2020). Exosomes as Potential Sources of Biomarkers in Colorectal Cancer. *Cancer Lett.* 476, 13–22. doi:10.1016/j.canlet.2020.01.033

Xu, X., Lai, Y., and Hua, Z. C. (2019). Apoptosis and Apoptotic Body: Disease Message and Therapeutic Target Potentials. *Biosci. Rep.* 39, BSR20180992. doi:10.1042/BSR20180992

Yamashita, T., Takahashi, Y., and Takakura, Y. (2018). Possibility of Exosome-Based Therapeutics and Challenges in Production of Exosomes Eligible for Therapeutic Application. *Biol. Pharm. Bull.* 41, 835–842. doi:10.1248/bpb.b18-00133

Yang, T., Martin, P., Fogarty, B., Brown, A., Schurman, K., Phipps, R., et al. (2015). Exosome Delivered Anticancer Drugs across the Blood-Brain Barrier for Brain Cancer Therapy in *Danio rerio*. *Pharm. Res.* 32, 2003–2014. doi:10.1007/s11095-014-1593-y

Yin, W., Ouyang, S., Li, Y., Xiao, B., and Yang, H. (2013). Immature Dendritic Cell-Derived Exosomes: a Promise Subcellular Vaccine for Autoimmunity. *Inflammation* 36, 232–240. doi:10.1007/s10753-012-9539-1

Yoo, K. W., Li, N., Makani, V., Singh, R. N., Atala, A., and Lu, B. (2018). Large-Scale Preparation of Extracellular Vesicles Enriched with Specific microRNA. *Tissue Eng. Part. C Methods* 24, 637–644. doi:10.1089/ten.TEC.2018.0249

Yuan, F., Li, Y. M., and Wang, Z. (2021a). Preserving Extracellular Vesicles for Biomedical Applications: Consideration of Storage Stability before and after Isolation. *Drug Deliv.* 28, 1501–1509. doi:10.1080/10717544.2021.1951896

Yuan, P., Ding, L., Chen, H., Wang, Y., Li, C., Zhao, S., et al. (2021b). Neural Stem Cell-Derived Exosomes Regulate Neural Stem Cell Differentiation through miR-9-Hes1 Axis. *Front. Cel Dev Biol* 9, 601600. doi:10.3389/fcell.2021.601600

Yuana, Y., Sturk, A., and Nieuwland, R. (2013). Extracellular Vesicles in Physiological and Pathological Conditions. *Blood Rev.* 27, 31–39. doi:10.1016/j.blre.2012.12.002

Yuyama, K., and Igarashi, Y. (2016). Physiological and Pathological Roles of Exosomes in the Nervous System. *Biomol. Concepts* 7, 53–68. doi:10.1515/bmc-2015-0033

Zaborowski, M. P., Balaj, L., Breakefield, X. O., and Lai, C. P. (2015). Extracellular Vesicles: Composition, Biological Relevance, and Methods of Study. *Bioscience* 65, 783–797. doi:10.1093/biosci/biv084

Zhai, Y., Su, J., Ran, W., Zhang, P., Yin, Q., Zhang, Z., et al. (2017). Preparation and Application of Cell Membrane-Camouflaged Nanoparticles for Cancer Therapy. *Theranostics* 7, 2575–2592. doi:10.7150/thno.20118

Zhang, G., Zhu, Z., Wang, H., Yu, Y., Chen, W., Waqas, A., et al. (2020). Exosomes Derived from Human Neural Stem Cells Stimulated by Interferon Gamma Improve Therapeutic Ability in Ischemic Stroke Model. *J. Adv. Res.* 24, 435–445. doi:10.1016/j.jare.2020.05.017

Zhang, P., Yeo, J. C., and Lim, C. T. (2019a). Advances in Technologies for Purification and Enrichment of Extracellular Vesicles. *SLAS Technol.* 24, 477–488. doi:10.1177/2472630319846877

Zhang, Q., Higginbotham, J. N., Jeppesen, D. K., Yang, Y. P., Li, W., McKinley, E. T., et al. (2019b). Transfer of Functional Cargo in Exomeres. *Cell Rep* 27, 940–e6. doi:10.1016/j.celrep.2019.01.009

Zhang, Q., Jeppesen, D. K., Higginbotham, J. N., Graves-Deal, R., Trinh, V. Q., Ramirez, M. A., et al. (2021). Supermeres Are Functional Extracellular Nanoparticles Replete with Disease Biomarkers and Therapeutic Targets. *Nat. Cel Biol* 23, 1240–1254. doi:10.1038/s41556-021-00805-8

Zhang, Y., Liu, Y., Liu, H., and Tang, W. H. (2019c). Exosomes: Biogenesis, Biologic Function and Clinical Potential. *Cell Biosci* 9, 19. doi:10.1186/s13578-019-0282-2

Zhao, L., Hu, C., Zhang, P., Jiang, H., and Chen, J. (2019). Genetic Communication by Extracellular Vesicles Is an Important Mechanism Underlying Stem Cell-Based Therapy-Mediated protection against Acute Kidney Injury. *Stem Cel Res Ther* 10, 119. doi:10.1186/s13287-019-1227-8

Zhu, Q., Ling, X., Yang, Y., Zhang, J., Li, Q., Niu, X., et al. (2019). Embryonic Stem Cells-Derived Exosomes Endowed with Targeting Properties as Chemotherapeutics Delivery Vehicles for Glioblastoma Therapy. *Adv. Sci. (Weinh)* 6, 1801899. doi:10.1002/advs.201801899

Zhuang, X., Xiang, X., Grizzle, W., Sun, D., Zhang, S., Axtell, R. C., et al. (2011). Treatment of Brain Inflammatory Diseases by Delivering Exosome Encapsulated Anti-inflammatory Drugs from the Nasal Region to the Brain. *Mol. Ther.* 19, 1769–1779. doi:10.1038/mt.2011.164

Gao, X., Ran, N., Dong, X., Zuo, B., Yang, R., Zhou, Q., et al. (2018). Erratum for the Research Article: "Anchor peptide captures, targets, and loads exosomes of diverse origins for diagnostics and therapy. *Sci Transl Med.* 10, eaaw0534, doi:10.1126/scitranslmed.aaw0534

**Conflict of Interest:** The authors declare that the research was conducted in the absence of any commercial or financial relationships that could be construed as a potential conflict of interest.

**Publisher's Note:** All claims expressed in this article are solely those of the authors and do not necessarily represent those of their affiliated organizations, or those of the publisher, the editors, and the reviewers. Any product that may be evaluated in this article, or claim that may be made by its manufacturer, is not guaranteed or endorsed by the publisher.

frontiers | Frontiers in Pharmacology

ORIGINAL RESEARCH
published: 01 April 2022
doi: 10.3389/fphar.2022.778680

# Delivery of Basic Fibroblast Growth Factor Through an *In Situ* Forming Smart Hydrogel Activates Autophagy in Schwann Cells and Improves Facial Nerves Generation *via* the PAK-1 Signaling Pathway

*Binbin Hu[1,2†], Hanbo Zhang[2†], Menglu Xu[1,2], Lei Li[2], Man Wu[2], Susu Zhang[2], Xuejun Liu[1], Weidong Xia[3], Ke Xu[2], Jian Xiao[2*], Hongyu Zhang[2*] and Liyan Ni[1*]*

[1]Department of Otorhinolaryngology, The Second Affiliated Hospital and Yuying Children's Hospital of Wenzhou Medical University, Wenzhou, China, [2]Key Laboratory of Biotechnology and Pharmaceutical Engineering, School of Pharmaceutical Sciences, Cixi Biomedical Research Institute, Wenzhou Medical University, Wenzhou, China, [3]Department of Burn, First Affiliated Hospital of Wenzhou Medical University, Wenzhou, China

Although studies have shown that basic fibroblast growth factor (bFGF) can activate autophagy and promote peripheral nerve repair, the role and the molecular mechanism of action of bFGF in the facial nerve are not clear. In this study, a thermosensitive *in situ* forming poloxamer hydrogel was used as a vehicle to deliver bFGF for treating facial nerve injury (FNI) in the rat model. Using H&E and Masson's staining, we found that bFGF hydrogel can promote the functional recovery and regeneration of the facial nerve. Furthermore, studies on the mechanism showed that bFGF can promote FNI recovery by promoting autophagy and inhibiting apoptosis. Additionally, this study demonstrated that the role of hydrogel binding bFGF in nerve repair was mediated through the activation of the PAK1 signaling pathway in Schwann cells (SCs). These results indicated that poloxamer thermosensitive hydrogel loaded with bFGF can significantly restore the morphology and function of the injured facial nerve by promoting autophagy and inhibiting apoptosis by activating the PAK1 pathway, which can provide a promising strategy for FNI recovery.

**Keywords: facial nerve injury, autophagy, Pak1, *in situ* forming hydrogel, basic fibroblast growth factor**

OPEN ACCESS

***Edited by:***
*Ana Falcão,*
*Universidade NOVA de Lisboa, Portugal*

***Reviewed by:***
*Patricia Schoenlein,*
*Augusta University, United States*
*Guicai Li,*
*Nantong University, China*

***Correspondence:**
*Jian Xiao*
*Xfxj2000@126.com*
*Hongyu Zhang*
*st_hyz@126.com*
*Liyan Ni*
*niliyan0128@foxmail.com*

*†These authors have contributed equally to this work*

***Specialty section:***
*This article was submitted to Neuropharmacology, a section of the journal Frontiers in Pharmacology*

***Received:*** *17 September 2021*
***Accepted:*** *14 March 2022*
***Published:*** *01 April 2022*

***Citation:***
*Hu B, Zhang H, Xu M, Li L, Wu M, Zhang S, Liu X, Xia W, Xu K, Xiao J, Zhang H and Ni L (2022) Delivery of Basic Fibroblast Growth Factor Through an In Situ Forming Smart Hydrogel Activates Autophagy in Schwann Cells and Improves Facial Nerves Generation via the PAK-1 Signaling Pathway. Front. Pharmacol. 13:778680. doi: 10.3389/fphar.2022.778680*

## INTRODUCTION

About 20 out of 100,000 people are diagnosed with facial nerve injury (FNI) annually, and it is mostly caused by trauma and iatrogenic injury (Brown et al., 2019). Currently, even if an injured nerve can be repaired by experienced surgeons through delicate surgery, it is still difficult to completely restore the damaged nerve function (Ali et al., 2020). After facial nerve damage, the lesion area and its distal stump can undergo Wallerian degeneration (WD), including axon degeneration, demyelination and phagocytosis. The destruction of myelin sheaths during WD produces a large amount of myelin debris and seriously hinders the regeneration and functional recovery of the nerves (Colavincenzo and Levine, 2000; Zhou et al., 2019). Around 40–50% of residual myelin debris was removed by the

Schwann cells (SCs) in the first five to 7 days after injury (Niemi et al., 2013; Jessen and Mirsky, 2016). Moreover, some studies reported that the cellular mechanism of impaired myelin degradation during WD was closely related to the activation of autophagy in SCs (Gomez-Sanchez et al., 2015; Wakatsuki et al., 2017; Wang et al., 2019). Autophagy is a common cellular protection process in eukaryotes. It plays a key role in maintaining the homeostasis of cells and tissues by removing damaged organelles, pathological proteins, and dysfunctional macromolecules in cells. Autophagy regulates various physiological and pathological processes through lysosomal degradation pathways, such as nerve regeneration, myelin development, myelin degradation and neuropathic pain (Marinelli et al., 2014; Gomez-Sanchez et al., 2015; Jang et al., 2015; Jang et al., 2016).

Hence, a new therapeutic strategy to repair FNI is to activate the autophagy pathway in the early stage after FNI. The basic fibroblast growth factor (bFGF) is a powerful neurotrophic factor secreted by SCs and different neuronal populations (Jungnickel et al., 2006). After peripheral nerve injury (PNI), the upregulation of the mRNA and protein of bFGF cannot maintain the survival of neurons, and the axon prolongs (Grosheva et al., 2016). The overexpression of bFGF through a lentivirus transfection in SCs promotes muscular reinnervation and stimulates the regeneration of motor and sensory neurons in the peripheral nervous system (PNS) (Allodi et al., 2014). Additionally, bFGF has several biological properties associated with nerve protection, neuronal occurrence and angiogenesis in the PNS (Beenken and Mohammadi, 2009; Anderson et al., 2018). However, bFGF has a very short half-life and is easily inactivated in body fluids by various proteases (Rapraeger et al., 1991). Thus, it is important to use a suitable drug carrier to maintain the biological activity and availability of bFGF in the lesion and to control the release of bFGF. Thermosensitive hydrogel poloxamer 407 (P 407) is a suitable carrier and a controlled-release system for protein drugs (Al Khateb et al., 2016; Gausterer et al., 2020; Yang et al., 2020). It can maintain the stability of the protein and improve its bioavailability. We found that a thermosensitive heparin-poloxamer hydrogel combined with bFGF can effectively facilitate SC proliferation, axonal regeneration and recovery of motor function in diabetic rats with PNI (Li et al., 2018). Heparin can cause coagulation dysfunction, and the synthesis of heparin-poloxamer is time-consuming and laborious. In our study, poloxamer loaded with bFGF (P-bFGF) was used, and once the thermosensitive P-bFGF was injected into the FNI lesion, it turned from liquid to hydrogel *in situ*. The hydrogel remained at the site of the lesion for a long time and maintains the biological activity and availability of bFGF. Additionally, the protein was released slowly, resulting in a lasting bFGF therapy for FNI. Additionally, previous studies have also shown that the role of bFGF in the regulation of early peripheral nerve regeneration was closely related to the SC-mediated autophagy activation to remove myelin debris (Jiang et al., 2021).

Nevertheless, the molecular mechanism underlying the relationship between bFGF-induced nerve regeneration and SC-mediated myelin phagocytosis remains to be elucidated. P21-activated kinases 1 (PAK1) is a conserved serine/threonine-protein kinase. It needs phosphorylation of threonine 423 to be fully activated and is involved in various signal cascades on the surface of and within cells. It affects the cell cycle, proliferation, apoptosis, transformation, and migration of cells, and redox, inflammation, metabolism, gene expression and other processes. It is also associated with many diseases, such as cancer, nervous system diseases and heart diseases (Diebold et al., 2004; Han et al., 2017). A study reported that P21 activated autophagy by regulating the phosphorylation of Akt and AMPK to protect against cardiac hypertrophy, which was validated in a P21-knockout mouse model (Xu et al., 2019). The expression of PAK1 in DU145 (a kind of human prostate cancer cell) was knocked out by the short hairpin RNA (shRNA) method, the expressions of p-PAK1, mTOR and Beclin1 decreased, and the ratio of LC3B2/LC3B1 (microtubule-associated protein 1 light chain 3 beta) showed a downward trend, implying autophagy degradation and suggesting that PAK-1 was involved in cell autophagy (Wang et al., 2017a). However, there are no more studies on the relationship between PAK-1 and autophagy. Although bFGF has been shown to activate PAK-1, additional relevant reports and studies are lacking (Wary, 2003).

In this study, bFGF was loaded with thermosensitive poloxamer hydrogel to treat injured facial nerves, and it was uniformly distributed and slowly released at the site of the injury. We speculated that bFGF facilitated the recovery of nerve injury by activating the PAK1 pathway to promote autophagy and inhibit apoptosis. Our study provided a new target and therapeutic strategy for the treatment of peripheral nerve injury by bFGF.

# METHODS AND MATERIALS

## Reagents

We obtained bFGF lyophilized powder from the School of Pharmacy, Wenzhou Medical University (Wenzhou, China). Poloxamer 407 (P2443) was obtained from Sigma-Aldrich (Shanghai, China). Inhibitor targeting PAK1 activation-3 (IPA-3) and Bafilomycin A1 (Baf A1) were obtained from Selleck Chemicals (42521-82-4, 88899-55-2, Shanghai, China). Cy5.5-NHS was obtained from Aladdin (1469277-96-0, Shanghai, China). The primary and secondary antibodies used in this study are listed here. Rabbit monoclonal anti-PAK1 (ab223849), rabbit polyclonal anti-Bcl2 (ab196495), mouse monoclonal anti-P62 (ab56416), rabbit polyclonal anti-Beclin1 (ab62557), donkey anti-mouse IgG H&L Alexa Fluor 488-conjugated secondary antibody (ab150105), donkey anti-rabbit IgG H&L Alexa Fluor 647-conjugated secondary antibody (ab150075) were obtained from Abcam. Rabbit polyclonal anti-Myelin basic protein (MBP, 10458-1-AP), mouse monoclonal anti-S100 (66616-1-Ig), mouse monoclonal anti-GAPDH (60004-1-Ig), horseradish peroxidase (HRP)-conjugated Affinipure Goat Anti-Mouse IgG (H + L) (SA00001-1), and HRP-conjugated Affinipure Goat Anti-Rabbit IgG (H + L) (SA00001-2) were obtained from Proteintech. Rabbit polyclonal phospho-PAK1 (Thr423) (AF4463) was obtained from Affinity. Rabbit anti-BAX

(#2772), and rabbit anti-Cleaved Caspase-3 (#9661) were obtained from Cell Signaling Technology. Rabbit polyclonal anti-LC3B (L7543) was purchased from Sigma-Aldrich. Rabbit polyclonal anti-ATG5 (autophagy-related protein 5, AP6026) was purchased from Bioworld.

## The Fabrication and Characterization of P-bFGF Hydrogel

Poloxamer 407 and bFGF powder were mixed in saline and stirred gently at 4°C. The final concentration of the P-bFGF solution was 200 mg/ml for poloxamer and 0.1 mg/ml (or 0.3 mg/ml) for bFGF. The P-bFGF solution was lyophilized, fixed to a copper sheet, and sprayed with gold to take shape. Its microstructure was observed using a scanning electron microscope (SEM, Regulus8230; HITACHI, Tokyo, Japan) and its elemental composition was determined by SEM-EDS (energy-dispersive X-ray spectroscopy).

## Cell Culture and Treatment

The Schwann cell line RSC96 (ScienCell, Shanghai, China) was cultured in Dulbecco's Modified Eagle Medium (DMEM)containing 10% fetal bovine serum and 1% penicillin-streptomycin solution in an incubator at 37°C and 5% $CO_2$. The cells were seeded in a six-well plate at an initial density of $2 \times 10^5$ cells/mL. To determine the effect of P-bFGF, we divided the RSC96 cells into six groups: control group, $H_2O_2$ group, poloxamer group, bFGF group, P-bFGF group and IPA-3 group. The control group was cultured in normal DMEM, while the other groups were stimulated with 500 μmol $H_2O_2$ for 2 h. Four hours before $H_2O_2$ stimulation, the poloxamer group, bFGF group, and P-bFGF group were pretreated with poloxamer (200 mg/ml), bFGF (0.1 mg/ml), and P-bFGF (0.1 mg/ml) respectively. While the IPA-3 group was treated with P-bFGF (0.1 mg/ml) and IPA-3 (25 μM). To determine how bFGF and IPA-3 affect autolysosomal flux, we divided the RSC96 cells into seven groups: control group, $H_2O_2$ group, $H_2O_2$+bFGF group, $H_2O_2$+Baf group, $H_2O_2$+bFGF + Baf group, $H_2O_2$+bFGF + Baf + IPA-3 group, and $H_2O_2$+bFGF + IPA-3 group. We treated the cells with Baf A1 (1 nM) 4 h before $H_2O_2$ stimulation.

## Peripheral Nerve Injury Animal Model and Tissue Preparation

Male Sprague Dawley (SD) rats (200–220 g) were purchased from Charles River Laboratories (Beijing, China). The animal experiment in this study was approved by the Animal Experiment Ethics Committee of Wenzhou Medical University. The FNI model was estabilished following a previous study (Xia et al., 2020). Briefly, the rats were anesthetized by an intraperitoneal injection of 1% pentobarbital sodium (40 mg/kg). We exposed the main trunk of the left facial nerve 0.5 cm away from the stylomastoid foramen, and clamped a nerve (~2 mm long) for 60 s with a hemostatic forceps. The rats were randomly divided into five groups ($n$ = 10 per group): sham group, FNI group, poloxamer group (FNI treated with poloxamer), bFGF group (FNI treated with bFGF) and P-bFGF group (FNI treated with P-bFGF). The poloxamer group and P-bFGF group were injected with 15 μL poloxamer (200 mg/ml) and P-bFGF (200 mg/ml poloxamer and 0.3 mg/ml bFGF) on D0, respectively. The sham group, FNI group and bFGF group were injected with 15 μL of normal saline, normal saline, and bFGF (0.1 mg/ml) on D0, D3, and D7, respectively. On D7, five rats in each group were sacrificed. Facial nerves (1.5 cm long), including those from injured sites, were dissected and immediately stored in liquid nitrogen for western blotting. On D14, four to five rats in each group were sacrificed. The facial nerve was fixed in 4% paraformaldehyde (PFA) overnight, dehydrated with gradient absolute ethanol, and embedded in paraffin. The sample was cut into sections (5 μm thick) using a microtome (HistoCore AUTOCUT; Leica, Wetzlar, Germany).

## Fluorescence Labeling of bFGF With Cy5.5-NHS and Fluorescence Imaging *In Vivo*

To track the distribution and residence time of bFGF in the *in vivo* experiment, bFGF used in both P-bFGF and bFGF solutions was labeled with Cy5.5-NHS (Zhao et al., 2014). Briefly, after Cy5.5-NHS was mixed with bFGF (mass ratio 1:100), they were stirred overnight at 4°C in the dark. The unconjugated Cy5.5-NHS was eliminated through dialysis and gel chromatography, and the Cy5.5-bFGF solution was freeze-dried to obtain the Cy5.5-bFGF powder.

The Cy5.5-conjugated P-bFGF and bFGF were used to treat FNI rats. At 0, 6 h, 1, 3, and 7 day, the bioluminescence intensities of the two groups were recorded using an *in vivo* imaging instrument (IVIS Lumina XRMS, Shanghai, China). The luminous intensity was analyzed and quantified by the Living Image® Software.

## Facial Nerve Functional Scoring

According to the method described by Wang et al. (2006), Blink reflex (BR), Vibrissae movement (VM) and tip position (TP) are the three main aspects to assess facial nerve function. For BR, the air was discharged 2 cm away from the injured eye quickly with a 5 ml syringe, and the eyelid movement of the rats was scored with 0 points for no difference between the two sides, 1 point for delayed action on the injured side, and 2 points for unclosed eyelid on the injured side. For VM, bilateral beard movement was counted for 30 s with 0 points for no difference between the two sides, 1 point for weakened movement on the injured side, and 2 points for the loss of beard movement. For TP, 0 points represented nose tip centered, and 1 point for nose tip not centered. The FNI model was considered to be successfully established when the score was 5. After modeling, the facial nerve function of rats was evaluated on D0, D3, D7 and D14, respectively. H&E and Masson's staining were also performed to confirm that the modeling was successful.

## Hematoxylin and Eosin and Masson's Trichrome Staining

According to the manufacturer's protocol, the prepared sections were stained by H&E or Masson's trichrome staining. Initially, the sections were dried at 56°C for 30 min, then immersed in

xylene to dewax, and hydrated with gradient absolute ethanol and pure water. Then, different staining reagents were added to the sections. For H&E staining, the sample was immersed in hematoxylin for 7 min and eosin for 2 min. For Masson's trichrome staining, the nucleus of the section was stained with hematoxylin for 5 min, and Ponceau/Acid Fuchsin solution was added to cover the entire tissue for 5 min. Then, the section was stained in 1% phosphomolybdic acid solution for 30 s and stained in aniline blue reagent for 1 min. Finally, the glass slide was mounted with neutral resin. The stained section was observed and imaged using an inverted microscope (DMILLED; Leica).

## Immunofluorescence Staining

The tissue sections were subjected to antigen repair with high temperature and pressure. The cells were fixed in 4% PFA at room temperature for 30 min and then incubated with 0.5% Triton X-100 for 15 min. Then, the tissue sections or cells were blocked with 5% BSA for 30 min, and the tissues or cells were incubated with primary antibodies against MBP (1:100), S100 (1:100), LC3B (1:300), and Cleaved Caspase-3 (1:400) at 4°C overnight. After washing, these samples were incubated with Alexa Fluor conjugated secondary antibody (1:200) at room temperature for 1 h, and finally mounted with DAPI. Fluorescence images were captured using a laser confocal scanning fluorescence microscope (TCS SP8; Leica), and the fluorescence intensity was quantified by the ImageJ software.

## Western Blot

The facial nerve was placed in the RIPA lysis buffer containing 1% PMSF and lysed in a multi-sample tissue homogenizer (Bionoon-24LD; BIONOON, Shanghai, China) for 10 min. The RSC96 cells were placed in the RIPA lysis buffer containing 1% PMSF. Subsequently, the homogenized facial nerve or cell suspension was centrifuged at 12,000 rpm at 4°C for 15 min, and the protein concentration in the supernatant was quantified by the BCA reagent. The same amount of total protein was separated by SDS (Sodium dodecyl sulfate)-polyacrylamide gel electrophoresis and transferred to a PVDF (polyvinylidene fluoride) membrane. The membrane was blocked using skim milk and incubated overnight with primary antibodies (including GAPDH, Bcl2, BAX, beclin1, LC3B, ATG5, p62, p-PAK1 and PAK1) at 4°C. On the following day, the membrane was incubated with a secondary antibody conjugated with HRP for 2 h at room temperature. An enhanced chemiluminescence kit was used to detect the protein band, and the band density was quantified using the ImageJ software.

## Statistical Analysis

The data were analyzed using Graphpad Prism9 statistical software. One-way ANOVA was performed for analyzing data with **Figures 2D,E**, **3B,D–G**, **4B,D,E**, **5B–G,I,J**, **6B,D,E**. For two variables, two-way ANOVA was performed (**Figure 2A**). The difference was considered to be statistically significant at $p < 0.05$.

# RESULTS

## Poloxamer Hydrogel Loaded With Basic Fibroblast Growth Factor Maintained Thermal Sensitivity and the Porous Structure and P-bFGF Constantly Released bFGF *In Situ*

To gelate at body temperature, we prepared a poloxamer solution with a concentration of 17% (w/w), which was found to be the most suitable in previous studies (Wang et al., 2017b). The poloxamer was in a liquid form at 4°C and turned into a hydrogel at 37°C (**Figure 1A**). Moreover, the ultrastructure of the poloxamer hydrogel was observed by SEM (**Figure 1B**). The results showed that the internal crosslinking of hydrogel formed a loose porous network, and the internal porous network was unchanged after bFGF was loaded. SEM-EDS was performed to analyze the elements of P-bFGF. The C and O elements represented poloxamer hydrogel, and the N and S elements represented bFGF. We found that bFGF was evenly distributed in the poloxamer hydrogel (**Figure 1C**).

To observe whether P-bFGF can continuously release bFGF *in situ*, Cy5.5-bFGF was used to treat FNI rats. Through *in vivo* imaging, we discovered that in the bFGF group, the bFGF solution diffused in the tissue, while in the P-bFGF group, bFGF was attached to the facial nerve, which allowed us to see the contour of the facial nerve clearly. With the passage of time, we found that the bioluminescence intensity of bFGF decreasd, while the bioluminescence intensity of the P-bFGF group rats became stronger than that of the bFGF group rats (**Figure 1D**). The quantification of bioluminescence intensity showed the same trend (**Figure 1E**), which proved that P-bFGF constantly released bFGF in the injured nerve *in situ*, and maximized the therapeutic effect of bFGF *in vivo*. The results showed that P-bFGF was suitable for local uniform delivery and slow-release after nerve injury *in vivo*.

## P-bFGF Improved Functional Recovery of Early Facial Nerve Injury

To determine whether P-bFGF treatment promoted the recovery of facial nerve function, facial nerve function scoring was performed 0, 3, 7 and 14 days after surgery. On D0 after surgery, the score in each group was 5 points, suggesting that the model was successfully established. With time, the facial nerve function improved in all the groups, but the facial nerve function scoring revealed that the scores of the P-bFGF group and bFGF group were lower than those of the FNI group and poloxamer group. P-bFGF group was significantly lower than FNI group ($^{****}p < 0.0001$) and poloxamer group ($^{****}p < 0.0001$) and bFGF group was not significantly lower than FNI group and poloxamer group, which might be attributed to the long-lasting protection of the poloxamer hydrogel for bFGF bioactivity and slow drug release at the site of the facial lesion (**Figure 2A**). In summary, poloxamer alone had no therapeutic effect. This was also reflected in all the experiments that followed. We found that bFGF alone may not promote the recovery of the facial nerve function. P-bFGF, a mixture of bFGF and poloxamer, can

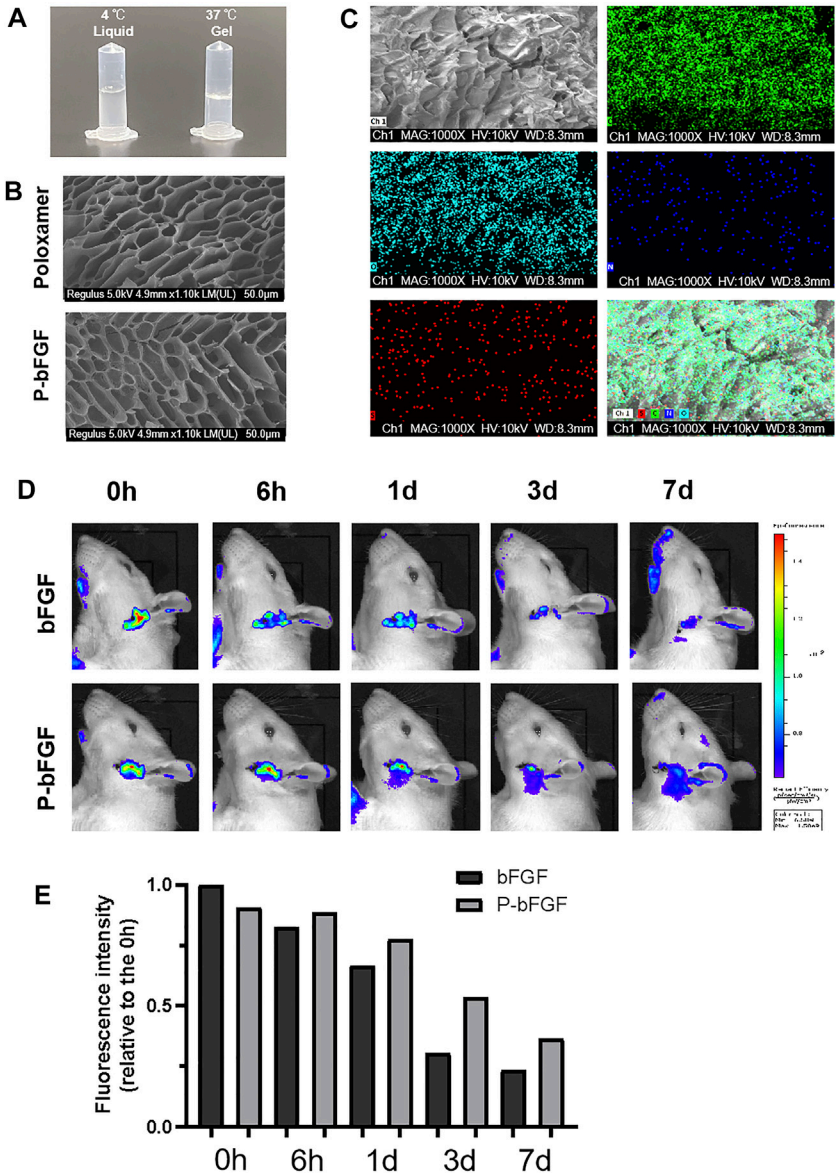


**FIGURE 1 |** Thermosensitivity, microstructure, relevant element analysis and *in vivo* local residence time of P-bFGF hydrogel. **(A)** The state of P-bFGF at 4 and 37°C. **(B)** The SEM image of poloxamer and P-bFGF hydrogel morphology; scale bar = 50 μm. **(C)** The SEM-EDS image analysis of P-bFGF hydrogel morphology. Channel 1 (Ch1), Channel C, Channel O, Channel N and Channel S were merged as one Channel. Scale bar = 50 μm. **(D)** Representative bioluminescence imaging of rats in different treatment groups at different times. **(E)** Quantitative calculation of the luminous intensity.

significantly promoted the early functional recovery of facial nerve injury.

## P-bFGF Accelerated Facial Nerve Regeneration and Functional Protein Expression

Hematoxylin & Eosin and Masson's staining were used to evaluate the histological recovery of injured nerves in each group. Both H&E and Masson's staining demonstrated that the nerve fibers in the FNI group and the poloxamer group were sparse and atrophic. The abnormal morphologies in the bFGF group and P-bFGF group improved. The nerve fibers in the P-bFGF group regenerated significantly and more regularly compared to those of the bFGF group (**Figure 2B**). This suggested that P-bFGF can promote the recovery of histological morphology of injured nerve fibers.

The S100 maker of Schwann cells can regulate the metabolism, movement and proliferation of cells. The presence of MBP (myelin basic protein) indicates myelin formation. Double IF staining of S100 and MBP showed that the functional protein expression and myelin density of the P-bFGF group and bFGF group were significantly higher than those of the FNI group and poloxamer group, and P-bFGF was higher than bFGF

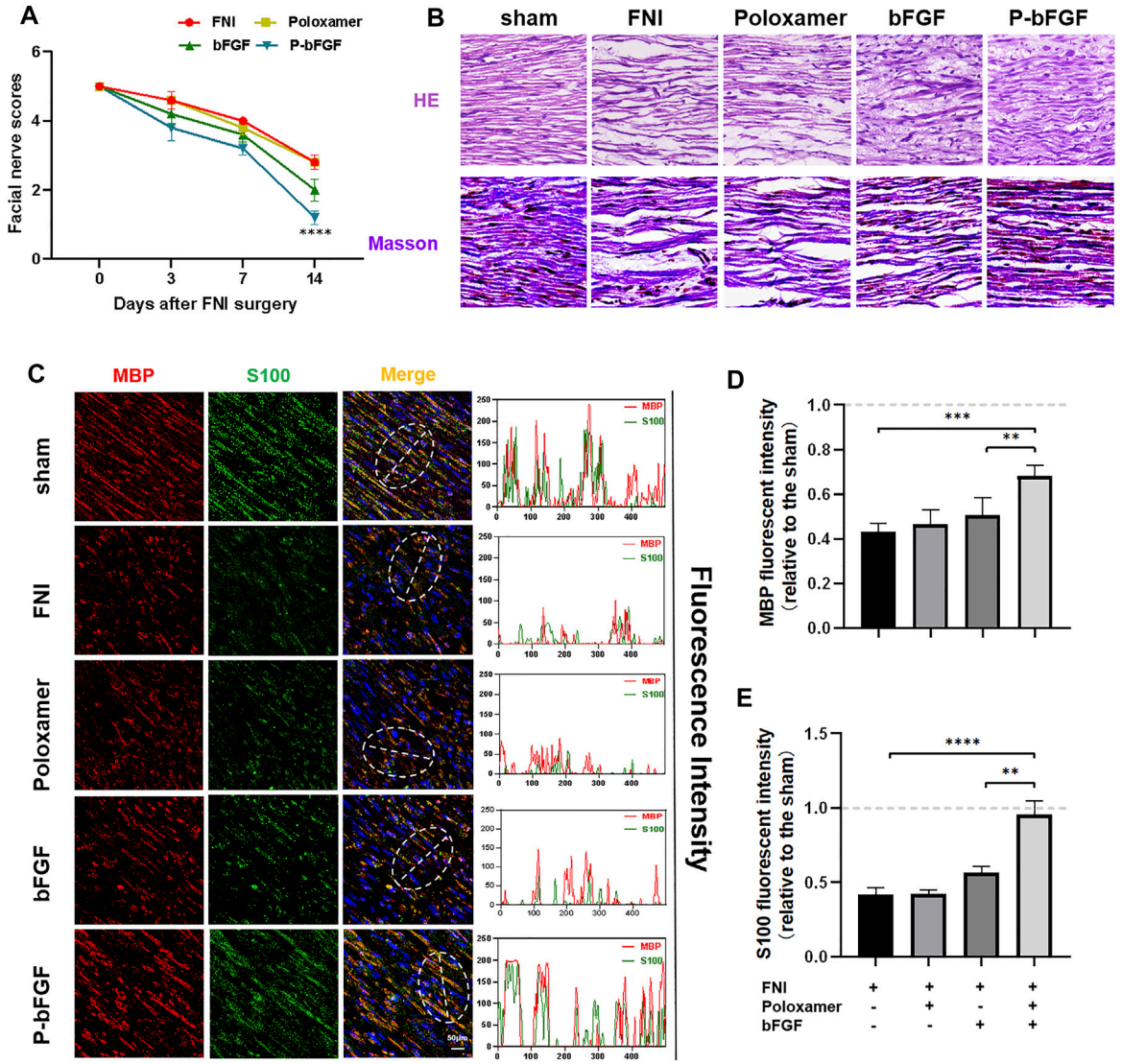


**FIGURE 2 |** The functional and histological recovery of the injured nerve 2 weeks after treatment. **(A)** Facial nerve function scoring was performed 0, 3, 7, and 14 days after surgery. The data were expressed as mean ± SEM ($n$ = 5); P-bFGF group vs. FNI group: ****$p$ < 0.0001, P-bFGF group vs. poloxamer group: ****$p$ < 0.0001. **(B)** Injured nerves were stained with H&E and Masson's stain, respectively; scale bar = 100 μm. **(C)** Confocal laser scanning micrograph of immunofluorescence staining with anti-MBP (red) and anti-S100 (green) antibodies; scale bar = 50 μm. The co-localization of MBP and S100 was shown by a plot profile analysis in Image J. **(D,E)** Quantitative calculation of the mean of the MBP and S100 fluorescence. The data were expressed as mean ± SEM ($n$ = 4); ****$p$ < 0.0001, ***$p$ < 0.001 and **$p$ < 0.01. A dashed line at 1.0 represented sham group.

(**Figure 2C**). The qualitative fluorescence co-localization expression analysis and respective quantitative analysis of S100 and MBP showed the similar trend (**Figures 2D,E**). The results indicated that P-bFGF upregulated the functional protein S100 of Schwann cells and boosted the remyelination of the SCs.

## P-bFGF Promoted Nerve Repair by Activating Autophagy and Inhibiting Apoptosis

To determine whether P-bFGF activated autophagy for facial nerve repair, we performed tissue IF staining and WB to detect the expression of autophagy-related proteins (including LC3B, Beclin1, P62, and ATG5). The IF staining showed that FNI slightly increased the fluorescence intensity of LC3B, and the bFGF and P-bFGF treatment further enhanced the fluorescence intensity of LC3B, the fluorescence intensity of the P-bFGF group was significantly higher than that of the bFGF group (**Figure 3A**). The quantitative analysis of fluorescence intensity showed a similar trend (**Figure 3B**). The WB results showed that the expression trends of LC3B-II, Beclin1, and ATG5 were consistent with the fluorescence intensity of LC3B, while the expression trend of P62 was the opposite (**Figures 3C–G**). These results indicated that P-bFGF activated autophagy in FNI.

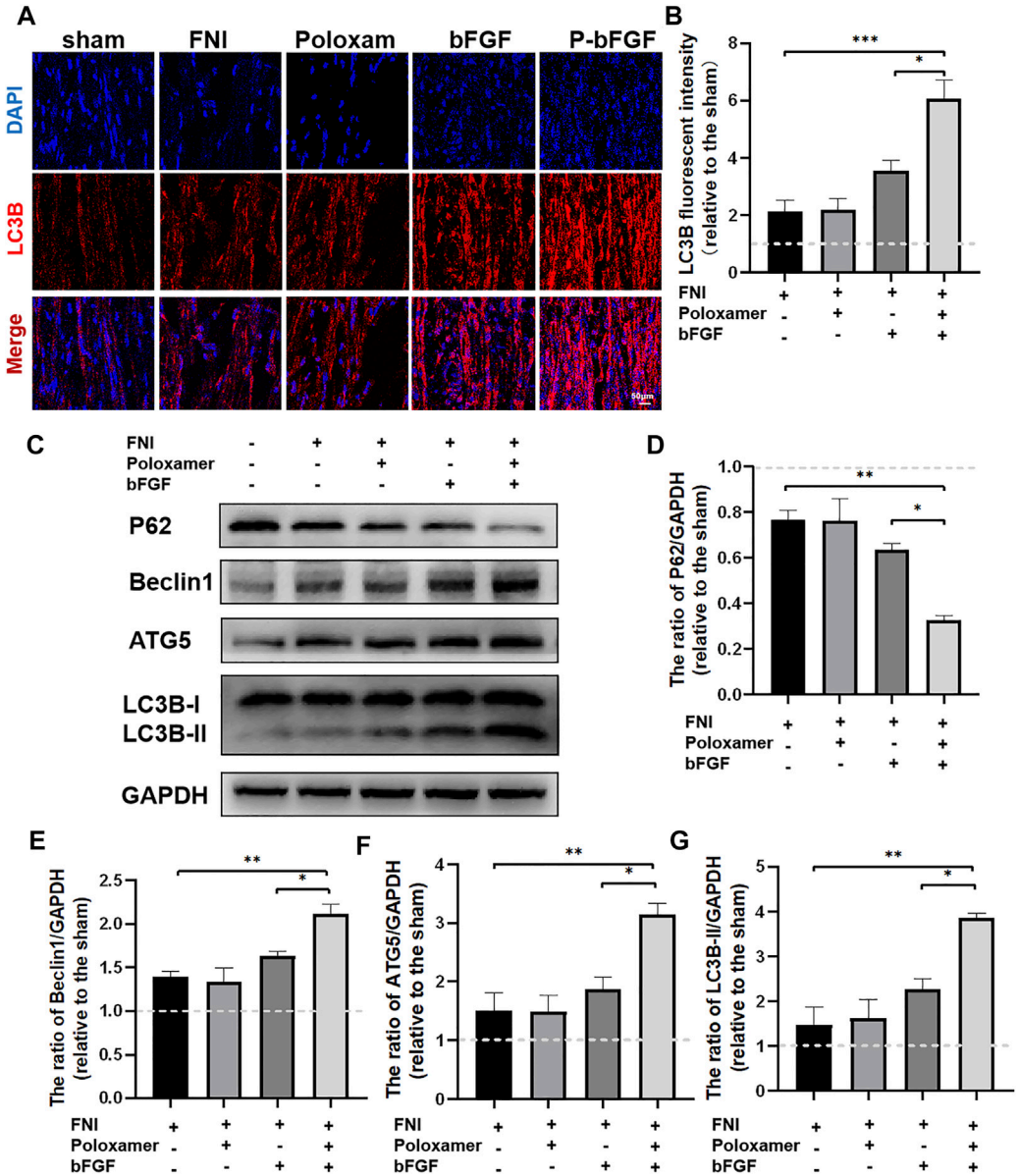


**FIGURE 3 |** P-bFGF activated autophagy in order to promote facial nerve repair. **(A)** Representative immunofluorescence staining of LC3B of injured nerves 2 weeks after treatment; scale bar = 50 μm. **(B)** Quantitative calculation of the mean of LC3B fluorescence. The data were expressed as mean ± SEM ($n$ = 4); FNI group vs. P-bFGF group: ***$p$ < 0.001, bFGF group vs. P-bFGF group: *$p$ < 0.05. **(C–G)** Representative western blot images of P62, Beclin1, ATG5, and LC3B-II expression in FNI 7 days after treatment and quantification of protein levels. The data were expressed as mean ± SEM ($n$ = 3); FNI group vs. P-bFGF group: **$p$ < 0.01, bFGF group vs. P-bFGF group: *$p$ < 0.05. A dashed line at 1.0 represented sham group.

To further determine whether P-bFGF treatment contributed to cell survival, we also measured the expression of apoptosis-related proteins by IF staining (Cleaved Caspase-3) and western blotting (BAX and Bcl2), and assessed the ability of P-bFGF to activate autophagy, which can help to reduce apoptosis after FNI. The pro-apoptosis protein Cleaved Caspase-3 and BAX were downregulated, while the anti-apoptosis protein Bcl2 was upregulated in the bFGF group and P-bFGF group, compared to their levels in the FNI group (**Figures 4A,C**). The quantitative analysis of fluorescence intensity and WB gray value showed a similar trend (**Figures 4B,D,E**). The above results confirmed that P-bFGF can promotes FNI repair by reducing apoptosis for the survival of nerve cells.

## P-bFGF Activated Autophagy and Maintained the Fluent Autophagic Flux *In Vitro* Through the PAK-1 Signaling Pathway

To study the molecular mechanism underlying the autophagy activation of P-bFGF, we performed the above treatment on

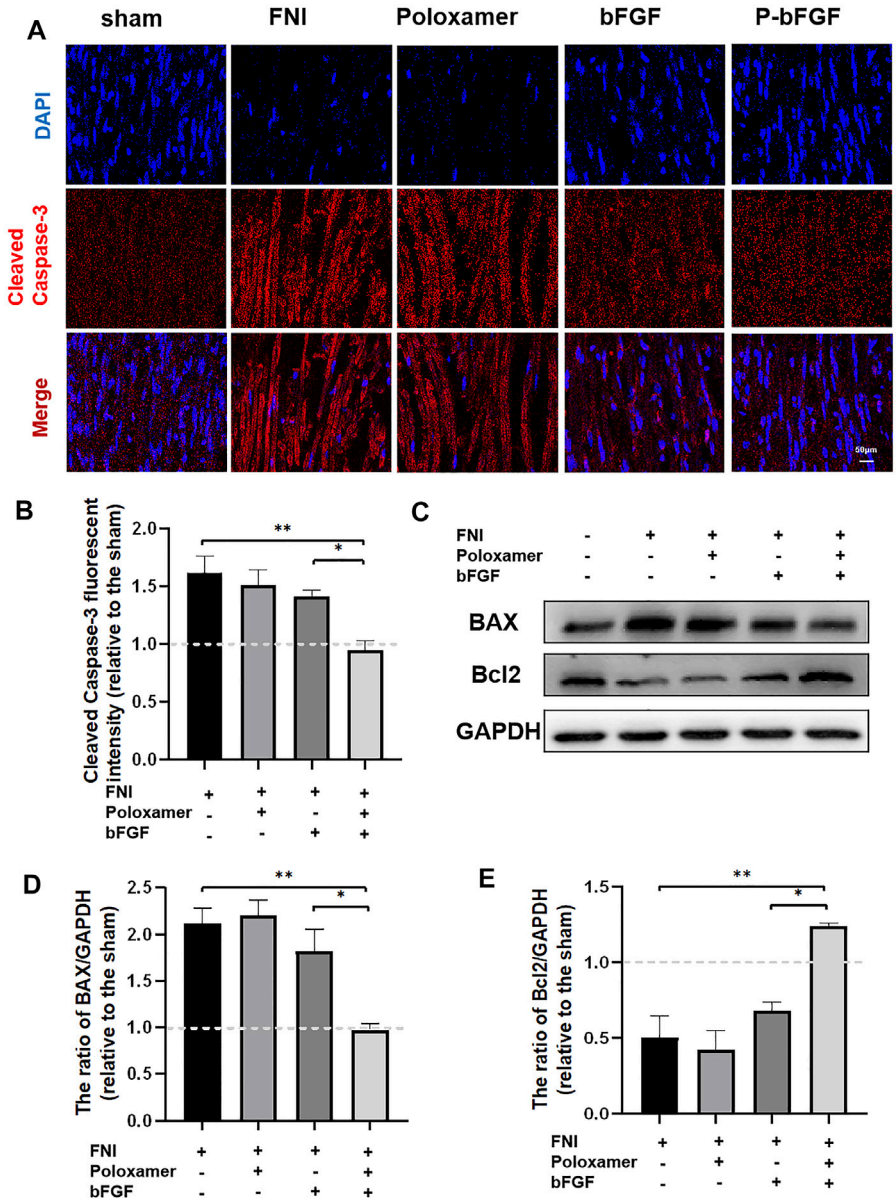


**FIGURE 4 |** P-bFGF inhibited apoptosis in order to promote facial nerve repair. **(A)** Representative immunofluorescence staining of Cleaved Caspase-3 of the injured nerves 2 weeks after treatment; Scale bar = 50 μm. **(B)** Quantitative calculation of the mean of Cleaved Caspase-3 fluorescence. The data were expressed as mean ± SEM ($n$ = 4); FNI group vs. P-bFGF group: $^{**}p < 0.01$, bFGF group vs. P-bFGF group: $^{*}p < 0.05$. **(C–E)** Representative western blot images of BAX and Bcl2 expression in FNI 7 days after treatment and quantification of protein levels. The data were expressed as mean ± SEM ($n$ = 3); FNI group vs. P-bFGF group: $^{**}p < 0.01$, bFGF group vs. P-bFGF group: $^{*}p < 0.05$. A dashed line at 1.0 represented sham group.

different groups of RSC96 cells. The expressions of pathway-related proteins (including PAK1 and p-PAK1) and autophagy-related proteins (including LC3B, Beclin1, P62, and ATG5) were detected. Through the WB assay, we found that the phosphorylation level of PAK1 increased in the $H_2O_2$ group and the poloxamer group. The phosphorylation level of PAK1 further increased in the bFGF group and P-bFGF group. IPA-3 partially reversed the effect in the P-bFGF group. The expression of PAK1 was opposite to that of p-PAK1 (**Figures 5A–C**). This showed that bFGF activated the PAK1 pathway, but IPA-3 inhibited the activation of bFGF in the PAK1 pathway. The expressions of ATG5, Beclin1 and LC3B-II in the P-bFGF group significantly increased compared with the $H_2O_2$ group ($^{**}p < 0.01$, $^{***}p < 0.001$ and $^{***}p < 0.001$, respectively), while the use of IPA-3 significantly reversed the treatment of P-bFGF ($^{*}p < 0.05$, $^{**}p < 0.01$ and $^{*}p < 0.05$, respectively). The expression of P62 showed an opposite trend to the expression of ATG5, Beclin1 and LC3B-II (**Figures 5A,D–G**). To confirm the continuous autolysosomal function in the cells treated by bFGF and determine how IPA-3 affected autolysosomal flux. We used

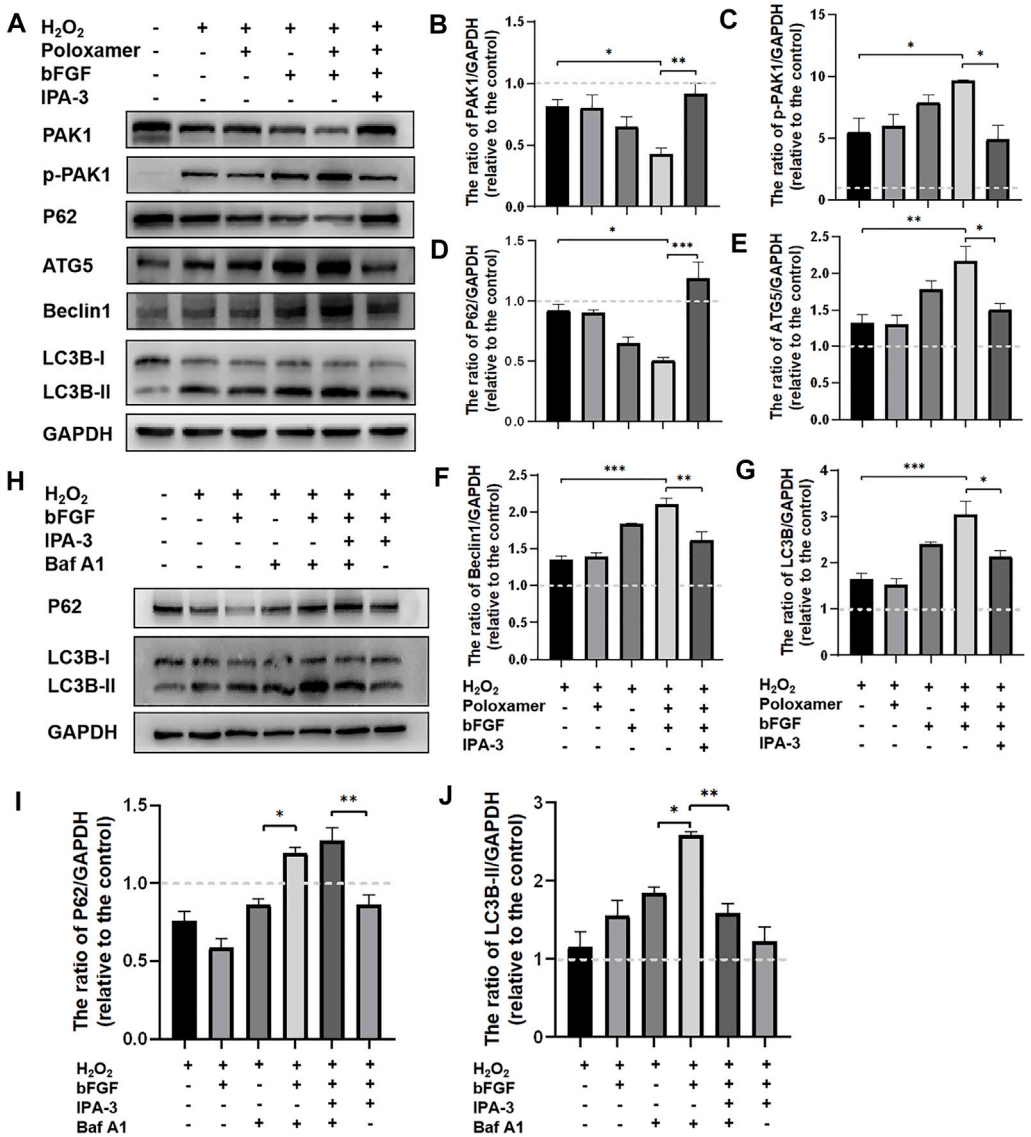


**FIGURE 5 |** P-bFGF activated the PAK1 pathway to promote autophagy of SCs. **(A)** Representative western blot images of PAK1, p-PAK1, P62, ATG5, Beclin1 and LC3B expression. **(B)** Quantification of the levels of PAK1 protein; $H_2O_2$ group vs. P-bFGF group: $^{*}p < 0.05$, P-bFGF group vs. IPA-3 group: $^{**}p < 0.01$. **(C)** Quantification of the levels of p-PAK1 protein; $H_2O_2$ group vs. P-bFGF group: $^{*}p < 0.05$, P-bFGF group vs. IPA-3 group: $^{*}p < 0.05$. **(D)** Quantification of the levels of P62 protein; $H_2O_2$ group vs. P-bFGF group: $^{*}p < 0.05$, P-bFGF group vs. IPA-3 group: $^{***}p < 0.001$. **(E)** Quantification of the levels of ATG5 protein; $H_2O_2$ group vs. P-bFGF group: $^{**}p < 0.01$, P-bFGF group vs. IPA-3 group: $^{*}p < 0.05$. **(F)** Quantification of the levels of the Beclin1 protein; $H_2O_2$ group vs. P-bFGF group: $^{***}p < 0.001$, P-bFGF group vs. IPA-3 group: $^{**}p < 0.01$. **(G)** Quantification of the levels of the LC3B-II protein; $H_2O_2$ group vs. P-bFGF group: $^{***}p < 0.001$, P-bFGF group vs. IPA-3 group: $^{*}p < 0.05$. **(H)** Representative western blot images of P62 and LC3B expression. **(I)** Quantification of the levels of the P62 protein; $H_2O_2$+Baf group vs. $H_2O_2$+bFGF + Baf group: $^{*}p < 0.05$, $H_2O_2$+bFGF + Baf + IPA-3 group vs. $H_2O_2$+bFGF + IPA-3 group: $^{**}p < 0.01$. **(J)** Quantification of the levels of the LC3B-II protein; $H_2O_2$+Baf group vs. $H_2O_2$+bFGF + Baf group: $^{*}p < 0.05$, $H_2O_2$+bFGF + Baf group vs. $H_2O_2$+bFGF + Baf + IPA-3 group: $^{**}p < 0.01$. The data above were expressed as mean ± SEM ($n = 3$). A dashed line at 1.0 represented control group.

Baf A1, an inhibitor of late autophagy, to treat RSC96 cells after the administration of bFGF. Baf A1 further raised the expression of LC3B-II and P62, while IPA-3 reversed the expression of LC3B-II and further increased P62 (**Figures 5H–J**). This indicated that the autophagic flux was activated by bFGF and blocked by IPA-3, which suggested that P-bFGF activated autophagy through the PAK1 pathway.

## P-bFGF Inhibited Apoptosis *In Vitro* Through the PAK-1 Signaling Pathway

To further confirm the molecular mechanism underlying the reduction of P-bFGF in $H_2O_2$-induced apoptosis of SCs, cell IF staining was performed to detect the expression of Cleaved Caspase-3, and WB was performed to detect the expressions of BAX and Bcl2. The fluorescence intensity of the pro-apoptosis

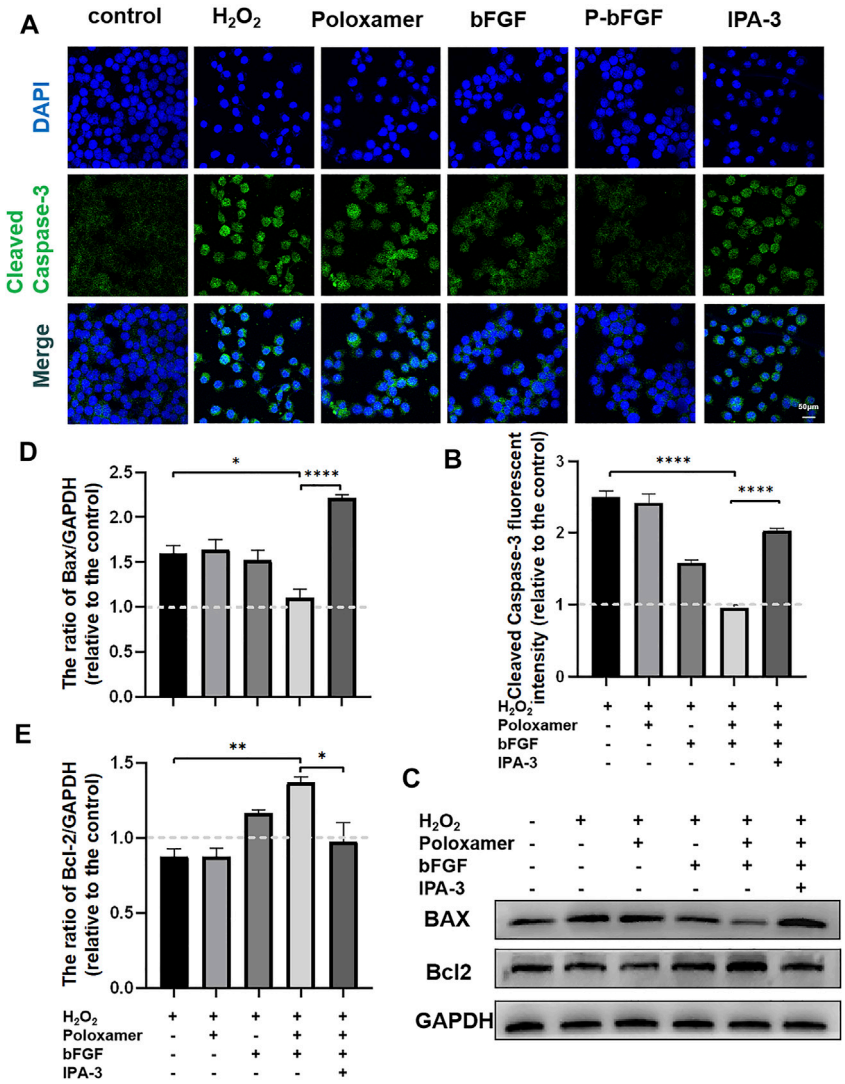


**FIGURE 6 |** P-bFGF activated PAK1 and inhibited the apoptosis of SCs. **(A)** Representative immunofluorescence staining of Cleaved Caspase-3 of SCs after treatment; scale bar = 50 μm. **(B)** Quantitative calculation of the mean of Cleaved Caspase-3 fluorescence. The data were expressed as mean ± SEM ($n = 4$); $H_2O_2$ group vs. P-bFGF group: $^{****}p < 0.0001$, P-bFGF group vs. IPA-3 group: $^{****}p < 0.0001$. **(C)** Representative western blot images of the BAX and Bcl2 expression in SCs after treatment. **(D)** Quantification of the levels of the BAX protein; $H_2O_2$ group vs. P-bFGF group: $^{*}p < 0.05$, P-bFGF group vs. IPA-3 group: $^{****}p < 0.0001$. **(E)** Quantification of the levels of the Bcl2 protein; $H_2O_2$ group vs. P-bFGF group: $^{**}p < 0.01$, P-bFGF group vs. IPA-3 group: $^{*}p < 0.05$. The data above were expressed as mean ± SEM ($n = 3$). A dashed line at 1.0 represented control group.

protein Cleaved Caspase-3 in the P-bFGF group was significantly lower than that in the $H_2O_2$ group ($^{****}p < 0.0001$), and IPA-3 treatment reversed the effect of the P-bFGF treatment ($^{****}p < 0.0001$, **Figures 6A,B**). The grayscale value of the pro-apoptosis protein BAX was significantly lower than that in the $H_2O_2$ group ($^{*}p < 0.05$), and IPA-3 treatment reversed the effect of the P-bFGF treatment ($^{****}p < 0.0001$, **Figures 6C,D**). Moreover, the grayscale value trend of the anti-apoptosis protein Bcl2 was opposite to that of BAX. The value of the P-bFGF group was significantly higher than that of the $H_2O_2$ group ($^{**}p < 0.01$), and IPA-3 treatment reversed the effect of the P-bFGF treatment ($^{*}p < 0.05$, **Figures 6C,E**). These results indicated that P-bFGF protected SCs from being apoptotic via the PAK1 pathway.

## DISCUSSION

The restoration of the function of the damaged facial nerves to a near-normal is challenging. Patients often suffer from partial or permanent disability in sensory and motor nerve function. Exogenous bFGF can promote FNI repair (Li et al., 2018; Jiang et al., 2021), but maintaining the release of bFGF at the appropriate location and time is a major obstacle to effective therapy. We used poloxamer thermosensitive hydrogel with excellent biocompatibility as the carrier. Using the rat FNI model, we found that P-bFGF promoted facial nerve repair by 1) maintaining the survival of nerve cells and inhibiting their apoptosis, 2) activating the autophagy of

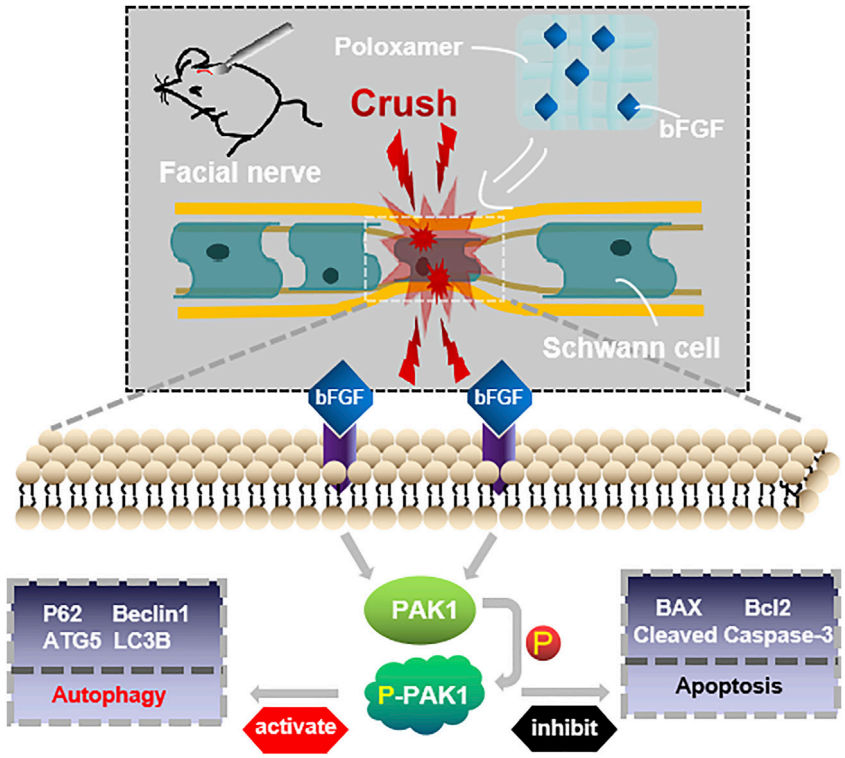


**FIGURE 7 |** Conceptualization. The treatment of injured facial nerve with thermosensitive poloxamer loaded with bFGF. The bFGF was released steadily and continuously at the original site of injury, and bFGF treated the injured facial nerve by activating the PAK1 signaling pathway to promote autophagy and inhibit apoptosis.

SCs and promoting the removal of myelin debris, and 3) facilitating axon growth and remyelination. These were consistent with previous studies on other peripheral nerve injuries (Wang et al., 2003; Pollak et al., 2014; Jiang et al., 2021). Through *in vitro* experiments, we found that the molecular mechanism underlying the positive effect of P-bFGF involved the activation of the PAK1 signaling pathway. Our research offers new insight into the role of bFGF in promoting the repair of damaged facial nerves by activating autophagy and inhibiting apoptosis (**Figure 7**).

Poloxamer hydrogel is an ideal drug delivery tool that is compatible with most tissues, thus, it has a wide range of applications in neuroprotection and regeneration. Poloxamer is in a liquid form at 4°C, making it easy to load bFGF. At body temperature, it transforms into a gel and provides an appropriate mechanical strength (**Figure 1A**). We found that bFGF could be loaded in large quantities in a three-dimensional network (**Figure 1B**) and was evenly diffused in these structures (**Figure 1C**). Therefore, bFGF can be uniformly and steadily released into the injured area over time (**Figures 1D,E**). We investigated the effects of bFGF with three injections on D0, D3, and D7, but for P-bFGF, only one injection was administered on D0, which showed that P-bFGF had considerable advantages in neuroprotection, regeneration, and functional recovery, and was superior to bFGF (**Figures 2A,B**). After FNI, the denervated SCs dedifferentiated, migrated, proliferated and transformed into repaired SCs. The repaired SCs removed degenerated myelin debris and secreted neurotrophic factors in order to create a favorable microenvironment for the regeneration of nerve cells (Jessen et al., 2015). Therefore, the regeneration and functional recovery of peripheral nerves are crucial to promote the proliferation and remyelination of SCs in the distal end of the lesion and inhibit their apoptosis (Jessen and Mirsky, 2016). S100 is a functional protein of SCs, whose level in the cell indicates the strength of proliferation. MBP indicates myelination and can represent the degree of remyelination. The results of immunofluorescence double-staining experiments also showed that after the application of bFGF, especially when it was loaded into poloxamer hydrogel, the proliferation and remyelination ability of SCs were enhanced (**Figure 2C**). Autophagy activation plays an active role in the repair of PNI, and the bFGF-mediated removal of myelin debris is driven by the activation of autophagy (Jiang et al., 2021). In our study, after FNI, the autophagy markers (P62, Beclin1, ATG5, and LC3B) changed in the direction of autophagy activation, which was caused by the obstacle of the fusion of the autophagosome with lysosome (Jiang et al., 2021). We discovered that bFGF could enhance autophagy, and the effect of P-bFGF treatment was better than that of bFGF treatment (**Figures 3A–F**). BAX, Bcl2 and Cleaved Caspase-3 were involved in the regulation of apoptosis. bFGF can also upregulate the anti-apoptotic protein Bcl2 and downregulate the pro-apoptotic proteins BAX and Cleaved Caspase-3. Similarly, the effect of P-bFGF treatment was better than that of bFGF treatment (**Figures 4A–E**).

Previously, PAK1 was shown to play a unique role in brain ontogeny and reconstruction of the neural cytoskeleton. It was also involved in various neurodevelopmental processes, such as neuron migration, neurite growth, neuron polarity, neuron differentiation and axon development (Zhang et al., 2020). PAK1 controls the correct direction, morphology and radial migration of neurons in the developing cerebral cortex (Zhong et al., 2003). In the growth cone of neurons, PAK1 can interact with NCAM (neural cell adhesion molecule), a member of the Ig superfamily, to induce the activation of the PAK1-LIMK1-cofilin pathway and facilitate cytoskeleton remodeling and Filopodia movement, to aid the growth and the direction of development of axons (Li et al., 2013). From *in vitro* cell experiments, we found that the expression of PAK1 decreased, while the expression of p-PAK1 increased after SCs injury. After bFGF and P-bFGF treatment, the expression of PAK1 further decreased, while the expression of p-PAK1 increased. The therapeutic effect of P-bFGF was better than that of bFGF, and the use of the PAK1 inhibitor IPA-3 partially reversed the effect of P-bFGF. We also found that autophagy-related proteins (P62, Beclin1, ATG5, and LC3B) were expressed in the direction of autophagy activation. The protein expression trend coincided with that of *in vivo* experiments, and IPA-3 could partially reverse the role of P-bFGF in autophagy activation (**Figures 5A–G**). We found that Baf A1 further raised the expression of LC3B-II and P62, while IPA-3 reversed the expression of LC3B-II and further increased P62. This indicated that bFGF could maintain fluent autophagic flux to enhance the level of autophagy through the PAK1 pathway (**Figures 5H–J**). The level of apoptosis also significantly decreased after P-bFGF treatment. Similar to the *in vivo* experiments, IPA-3 could partially reverse the anti-apoptotic effect of P-bFGF (**Figures 6A–E**). The above results suggested that the P-bFGF treatment of injured SCs was probably mediated by the activation of the PAK1 pathway, which increased autophagy and the anti-apoptotic effect. PAK1 can regulate the cytoskeleton and internode length to facilitate oligodendrocyte differentiation and myelination (Brown et al., 2021). bFGF induces autophagy activation, maintains the fluent autophagic flux in SCs to degrade myelin sheath fragments, and repairs peripheral nerves in the early stage of injury (Jiang et al., 2021). Moreover, autophagy activation can remove excess cytoplasm in SCs and promote myelin compaction, which plays a key role in the maturation and structural plasticity of SCs (Jang et al., 2015). A study on Alzheimer's disease found that the activation of the PAK1 signaling pathway can promote the autophagy of microglia, while its inhibitor IPA-3 can lower autophagy (Qi et al., 2021). The activation of PAK1 is closely related to the remodeling of the actin cytoskeleton (Davidson et al., 2021). In 1992, it was established that starved cells treated with actin depolymerization agents did not produce autophagosomes (Aplin et al., 1992). Subsequent studies also showed that actin can co-localize with important autophagy markers (Reggiori et al., 2005; Aguilera et al., 2012). The knockout of the ATG7 gene in mice not only inhibited the formation of autophagosomes but also induced serious defects in actin assembly (Zhuo et al., 2013). Hence, we speculated that bFGF activated the PAK1 signaling pathway to regulate autophagy by remodeling the actin cytoskeleton in FNI treatment. In future experiments, we aim to study how the actin cytoskeleton remodeling is involved in activating autophagy.

Our results indicated that P-bFGF could effectively promote cell proliferation, myelination and functional recovery and also reduce the apoptosis of nerve cells after FNI. The protective effect of P-bFGF on nerves is probably facilitated by the activation of the PAK1 pathway in SCs. The activation of the PAK1 pathway increases autophagy to degrade myelin fragments, promotes myelin formation, and inhibits the apoptosis of SCs. Therefore, our study was intended to find a new therapeutic method and a targeted treatment site for FNI and provide a new strategy for the treatment and mechanism of PNI in the future.

## DATA AVAILABILITY STATEMENT

The original contributions presented in the study are included in the article/**Supplementary Material**, further inquiries can be directed to the corresponding authors.

## ETHICS STATEMENT

The animal study was reviewed and approved by the Animal Experiment Ethics Committee of Wenzhou Medical University.

## AUTHOR CONTRIBUTIONS

Designed the studies: BH, HbZ, HyZ and LN. Undertook the experimental work: BH, MX, LL, MW and SZ. Analyzed the data: BH and LN. Contributed to figures and manuscript preparation: BH, HbZ, XL, WX, KX, JX, HyZ and LN. The manuscript was written through contributions of all authors. All authors have approved the final version of the manuscript.

## FUNDING

This study was jointly supported by the National Natural Science Foundation of China (81972150, 81802251, and 81772450), Zhejiang Provincial Natural Science Foundation of China (LR18H50001), Wenzhou Science and Technology Innovation Project (ZY2020023 and ZY2020026), and CAMS Innovation Fund for Medical Sciences (2019-I2M-5-028).

## SUPPLEMENTARY MATERIAL

The Supplementary Material for this article can be found online at: https://www.frontiersin.org/articles/10.3389/fphar.2022.778680/full#supplementary-material

## REFERENCES


Aguilera, M. O., Berón, W., and Colombo, M. I. (2012). The Actin Cytoskeleton Participates in the Early Events of Autophagosome Formation upon Starvation Induced Autophagy. *Autophagy* 8 (11), 1590–1603. doi:10.4161/auto.21459

Al Khateb, K., Ozhmukhametova, E. K., Mussin, M. N., Seilkhanov, S. K., Rakhypbekov, T. K., Lau, W. M., et al. (2016). *In Situ* gelling Systems Based on Pluronic F127/Pluronic F68 Formulations for Ocular Drug Delivery. *Int. J. Pharm.* 502 (1-2), 70–79. doi:10.1016/j.ijpharm.2016.02.027

Ali, S. A., Stebbins, A. W., Hanks, J. E., Kupfer, R. A., Hogikyan, N. D., Feldman, E. L., et al. (2020). Facial Nerve Surgery in the Rat Model to Study Axonal Inhibition and Regeneration[J]. *J. Vis. Exp.* 5(159), 2020.

Allodi, I., Mecollari, V., González-Pérez, F., Eggers, R., Hoyng, S., Verhaagen, J., et al. (2014). Schwann Cells Transduced with a Lentiviral Vector Encoding Fgf-2 Promote Motor Neuron Regeneration Following Sciatic Nerve Injury. *Glia* 62 (10), 1736–1746. doi:10.1002/glia.22712

Anderson, M. A., O'Shea, T. M., Burda, J. E., Ao, Y., Barlatey, S. L., Bernstein, A. M., et al. (2018). Required Growth Facilitators Propel Axon Regeneration across Complete Spinal Cord Injury. *Nature* 561 (7723), 396–400. doi:10.1038/s41586-018-0467-6

Aplin, A., Jasionowski, T., Tuttle, D. L., Lenk, S. E., and Dunn, W. A. (1992). Cytoskeletal Elements Are Required for the Formation and Maturation of Autophagic Vacuoles. *J. Cel Physiol* 152 (3), 458–466. doi:10.1002/jcp.1041520304

Beenken, A., and Mohammadi, M. (2009). The FGF Family: Biology, Pathophysiology and Therapy. *Nat. Rev. Drug Discov.* 8 (3), 235–253. doi:10.1038/nrd2792

Brown, S., Isaacson, B., Kutz, W., Barnett, S., and Rozen, S. M. (2019). Facial Nerve Trauma: Clinical Evaluation and Management Strategies. *Plast. Reconstr. Surg.* 143 (5), 1498–1512. doi:10.1097/PRS.0000000000005572

Brown, T. L., Hashimoto, H., Finseth, L. T., Wood, T. L., and Macklin, W. B. (2021). PAK1 Positively Regulates Oligodendrocyte Morphology and Myelination. *J. Neurosci.* 41 (9), 1864–1877. doi:10.1523/JNEUROSCI.0229-20.2021

Colavincenzo, J., and Levine, R. L. (2000). Myelin Debris Clearance during Wallerian Degeneration in the Goldfish Visual System. *J. Neurosci. Res.* 59 (1), 47–62. doi:10.1002/(sici)1097-4547(20000101)59:1<47::aid-jnr7>3.0.co;2-p

Davidson, A., Tyler, J., Hume, P., Singh, V., and Koronakis, V. (2021). A Kinase-independent Function of PAK Is Crucial for Pathogen-Mediated Actin Remodelling. *Plos Pathog.* 17 (8), e1009902. doi:10.1371/journal.ppat.1009902

Diebold, B. A., Fowler, B., Lu, J., Dinauer, M. C., and Bokoch, G. M. (2004). Antagonistic Cross-Talk between Rac and Cdc42 GTPases Regulates Generation of Reactive Oxygen Species. *J. Biol. Chem.* 279 (27), 28136–28142. doi:10.1074/jbc.M313891200

Gausterer, J. C., Saidov, N., Ahmadi, N., Zhu, C., Wirth, M., Reznicek, G., et al. (2020). Intratympanic Application of Poloxamer 407 Hydrogels Results in Sustained N-Acetylcysteine Delivery to the Inner Ear. *Eur. J. Pharm. Biopharm.* 150, 143–155. doi:10.1016/j.ejpb.2020.03.005

Gomez-Sanchez, J. A., Carty, L., Iruarrizaga-Lejarreta, M., Palomo-Irigoyen, M., Varela-Rey, M., Griffith, M., et al. (2015). Schwann Cell Autophagy, Myelinophagy, Initiates Myelin Clearance from Injured Nerves. *J. Cel Biol* 210 (1), 153–168. doi:10.1083/jcb.201503019

Grosheva, M., Nohroudi, K., Schwarz, A., Rink, S., Bendella, H., Sarikcioglu, L., et al. (2016). Comparison of Trophic Factors' Expression between Paralyzed and Recovering Muscles after Facial Nerve Injury. A Quantitative Analysis in Time Course. *Exp. Neurol.* 279, 137–148. doi:10.1016/j.expneurol.2016.02.020

Han, B., Zhao, J. Y., Wang, W. T., Li, Z. W., He, A. P., and Song, X. Y. (2017). Cdc42 Promotes Schwann Cell Proliferation and Migration through Wnt/β-Catenin and P38 MAPK Signaling Pathway after Sciatic Nerve Injury. *Neurochem. Res.* 42 (5), 1317–1324. doi:10.1007/s11064-017-2175-2

Jang, S. Y., Shin, Y. K., Park, S. Y., Park, J. Y., Lee, H. J., Yoo, Y. H., et al. (2016). Autophagic Myelin Destruction by Schwann Cells during Wallerian Degeneration and Segmental Demyelination. *Glia* 64 (5), 730–742. doi:10.1002/glia.22957

Jang, S. Y., Shin, Y. K., Park, S. Y., Park, J. Y., Rha, S. H., Kim, J. K., et al. (2015). Autophagy Is Involved in the Reduction of Myelinating Schwann Cell Cytoplasm during Myelin Maturation of the Peripheral Nerve. *PLoS One* 10 (1), e0116624. doi:10.1371/journal.pone.0116624

Jessen, K. R., Mirsky, R., and Lloyd, A. C. (2015). Schwann Cells: Development and Role in Nerve Repair. *Cold Spring Harb Perspect. Biol.* 7 (7), a020487. doi:10.1101/cshperspect.a020487

Jessen, K. R., and Mirsky, R. (2016). The Repair Schwann Cell and its Function in Regenerating Nerves. *J. Physiol.* 594 (13), 3521–3531. doi:10.1113/JP270874

Jiang, Y., Liang, J., Li, R., Peng, Y., Huang, J., and Huang, L. (2021). Basic Fibroblast Growth Factor Accelerates Myelin Debris Clearance through Activating Autophagy to Facilitate Early Peripheral Nerve Regeneration. *J. Cel Mol Med* 25 (5), 2596–2608. doi:10.1111/jcmm.16274

Jungnickel, J., Haase, K., Konitzer, J., Timmer, M., and Grothe, C. (2006). Faster Nerve Regeneration after Sciatic Nerve Injury in Mice Over-expressing Basic Fibroblast Growth Factor. *J. Neurobiol.* 66 (9), 940–948. doi:10.1002/neu.20265

Li, R., Li, Y., Wu, Y., Zhao, Y., Chen, H., Yuan, Y., et al. (2018). Heparin-Poloxamer Thermosensitive Hydrogel Loaded with bFGF and NGF Enhances Peripheral Nerve Regeneration in Diabetic Rats. *Biomaterials* 168, 24–37. doi:10.1016/j.biomaterials.2018.03.044

Li, S., Leshchyns'Ka, I., Chernyshova, Y., Schachner, M., and Sytnyk, V. (2013). The Neural Cell Adhesion Molecule (NCAM) Associates with and Signals through P21-Activated Kinase 1 (Pak1). *J. Neurosci.* 33 (2), 790–803. doi:10.1523/JNEUROSCI.1238-12.2013

Marinelli, S., Nazio, F., Tinari, A., Ciarlo, L., D'Amelio, M., Pieroni, L., et al. (2014). Schwann Cell Autophagy Counteracts the Onset and Chronification of Neuropathic Pain. *Pain* 155 (1), 93–107. doi:10.1016/j.pain.2013.09.013

Niemi, J. P., DeFrancesco-Lisowitz, A., Roldán-Hernández, L., Lindborg, J. A., Mandell, D., and Zigmond, R. E. (2013). A Critical Role for Macrophages Near Axotomized Neuronal Cell Bodies in Stimulating Nerve Regeneration. *J. Neurosci.* 33 (41), 16236–16248. doi:10.1523/JNEUROSCI.3319-12.2013

Pollak, D. D., Minh, B. Q., Cicvaric, A., and Monje, F. J. (2014). A Novel Fibroblast Growth Factor Receptor Family Member Promotes Neuronal Outgrowth and Synaptic Plasticity in aplysia. *Amino Acids* 46 (11), 2477–2488. doi:10.1007/s00726-014-1803-2

Qi, L. F., Liu, S., Liu, Y. C., Li, P., and Xu, X. (2021). Ganoderic Acid A Promotes Amyloid-β Clearance (*In Vitro*) and Ameliorates Cognitive Deficiency in Alzheimer's Disease (Mouse Model) through Autophagy Induced by Activating Axl. *Int. J. Mol. Sci.* 22 (11), 5559. doi:10.3390/ijms22115559

Rapraeger, A. C., Krufka, A., and Olwin, B. B. (1991). Requirement of Heparan Sulfate for bFGF-Mediated Fibroblast Growth and Myoblast Differentiation. *Science* 252 (5013), 1705–1708. doi:10.1126/science.1646484

Reggiori, F., Monastyrska, I., Shintani, T., and Klionsky, D. J. (2005). The Actin Cytoskeleton Is Required for Selective Types of Autophagy, but Not Nonspecific Autophagy, in the Yeast Saccharomyces cerevisiae. *Mol. Biol. Cel* 16 (12), 5843–5856. doi:10.1091/mbc.e05-07-0629

Wakatsuki, S., Tokunaga, S., Shibata, M., and Araki, T. (2017). GSK3B-mediated Phosphorylation of MCL1 Regulates Axonal Autophagy to Promote Wallerian Degeneration. *J. Cel Biol* 216 (2), 477–493. doi:10.1083/jcb.201606020

Wang, H., Wang, X., Zhang, K., Wang, Q., Cao, X., Wang, Z., et al. (2019). Rapid Depletion of ESCRT Protein Vps4 Underlies Injury-Induced Autophagic Impediment and Wallerian Degeneration. *Sci. Adv.* 5 (2), eaav4971. doi:10.1126/sciadv.aav4971

Wang, H. B., Feng, H. Y., Fan, Z. M., Xu, L., and Wang, L. J. (2006). Experimental Study of the Facial Nerve Paralysis Induced by Herpes Simplex Virus Type 1 Infection in Mice. *Zhonghua Er Bi Yan Hou Tou Jing Wai Ke Za Zhi* 41 (1), 13–16.

Wang, Q., He, Y., Zhao, Y., Xie, H., Lin, Q., He, Z., et al. (2017). A Thermosensitive Heparin-Poloxamer Hydrogel Bridges aFGF to Treat Spinal Cord Injury. *ACS Appl. Mater. Inter.* 9 (8), 6725–6745. doi:10.1021/acsami.6b13155

Wang, S., Cai, Q., Hou, J., Bei, J., Zhang, T., Yang, J., et al. (2003). Acceleration Effect of Basic Fibroblast Growth Factor on the Regeneration of Peripheral Nerve through a 15-mm gap. *J. Biomed. Mater. Res. A.* 66 (3), 522–531. doi:10.1002/jbm.a.10008

Wang, Z., Jia, G., Li, Y., Liu, J., Luo, J., Zhang, J., et al. (2017). Clinicopathological Signature of P21-Activated Kinase 1 in Prostate Cancer and its Regulation of Proliferation and Autophagy via the mTOR Signaling Pathway. *Oncotarget* 8 (14), 22563–22580. doi:10.18632/oncotarget.15124

Wary, K. K. (2003). Signaling through Raf-1 in the Neovasculature and Target Validation by Nanoparticles. *Mol. Cancer* 2, 27. doi:10.1186/1476-4598-2-27

Xia, W., Zhu, J., Wang, X., Tang, Y., Zhou, P., Wei, X., et al. (2020). Overexpression of Foxc1 Regenerates Crushed Rat Facial Nerves by Promoting Schwann Cells Migration via the Wnt/β-Catenin Signaling Pathway. *J. Cel Physiol* 235 (12), 9609–9622. doi:10.1002/jcp.29772

Xu, M., Wan, C. X., Huang, S. H., Wang, H. B., Fan, D., Wu, H. M., et al. (2019). Oridonin Protects against Cardiac Hypertrophy by Promoting P21-Related Autophagy. *Cell Death Dis* 10 (6), 403. doi:10.1038/s41419-019-1617-y

Yang, X., Yang, R., Chen, M., Zhou, Q., Zheng, Y., Lu, C., et al. (2020). KGF-2 and FGF-21 Poloxamer 407 Hydrogel Coordinates Inflammation and Proliferation Homeostasis to Enhance Wound Repair of Scalded Skin in Diabetic Rats. *BMJ Open Diabetes Res. Care* 8 (1), e001009. doi:10.1136/bmjdrc-2019-001009

Zhang, K., Wang, Y., Fan, T., Zeng, C., and Sun, Z. S. (2020). The P21-Activated Kinases in Neural Cytoskeletal Remodeling and Related Neurological disorders [J]. *Protein Cell* 13, 6-25. doi:10.1007/s13238-020-00812-9

Zhao, Y. Z., Tian, X. Q., Zhang, M., Cai, L., Ru, A., Shen, X. T., et al. (2014). Functional and Pathological Improvements of the Hearts in Diabetes Model by the Combined Therapy of bFGF-Loaded Nanoparticles with Ultrasound-Targeted Microbubble Destruction. *J. Control. Release* 186, 22–31. doi:10.1016/j.jconrel.2014.04.054

Zhong, J. L., Banerjee, M. D., and Nikolic, M. (2003). Pak1 and its T212 Phosphorylated Form Accumulate in Neurones and Epithelial Cells of the Developing Rodent. *Dev. Dyn.* 228 (1), 121–127. doi:10.1002/dvdy.10351

Zhou, T., Zheng, Y., Sun, L., Badea, S. R., Jin, Y., Liu, Y., et al. (2019). Microvascular Endothelial Cells Engulf Myelin Debris and Promote Macrophage Recruitment and Fibrosis after Neural Injury. *Nat. Neurosci.* 22 (3), 421–435. doi:10.1038/s41593-018-0324-9

Zhuo, C., Ji, Y., Chen, Z., Kitazato, K., Xiang, Y., Zhong, M., et al. (2013). Proteomics Analysis of Autophagy-Deficient Atg7-/- MEFs Reveals a Close Relationship between F-Actin and Autophagy. *Biochem. Biophys. Res. Commun.* 437 (3), 482–488. doi:10.1016/j.bbrc.2013.06.111

**Conflict of Interest:** The authors declare that the research was conducted in the absence of any commercial or financial relationships that could be construed as a potential conflict of interest.

**Publisher's Note:** All claims expressed in this article are solely those of the authors and do not necessarily represent those of their affiliated organizations, or those of the publisher, the editors and the reviewers. Any product that may be evaluated in this article, or claim that may be made by its manufacturer, is not guaranteed or endorsed by the publisher.

frontiers | Frontiers in Pharmacology

ORIGINAL RESEARCH
published: 14 April 2022
doi: 10.3389/fphar.2022.884470

# Amyloid-β Induces Cdh1-Mediated Rock2 Stabilization Causing Neurodegeneration

*Rebeca Lapresa*[1,2†], *Jesus Agulla*[1,2†], *Sonia Gonzalez-Guerrero*[1,2], *Juan P. Bolaños*[1,2] *and Angeles Almeida*[1,2*]

[1]Institute of Functional Biology and Genomics, CSIC, University of Salamanca, Salamanca, Spain, [2]Institute of Biomedical Research of Salamanca, University Hospital of Salamanca, CSIC, University of Salamanca, Salamanca, Spain

Alzheimer's disease (AD) is a neurodegenerative disorder characterized by progressive cognitive decline, which is causally related to the accumulation of abnormally folded amyloid-β (Aβ) peptide and hyperphosphorylated tau protein aggregates. The dendritic spine regulator Rho protein kinase 2 (Rock2) accumulates in the brain at the earliest stages of AD and remains increased during disease progression. However, the molecular mechanism that upregulates Rock2 in AD, and its role in the disease progression, are unknown. Here, we found that oligomers of the amyloidogenic fragment 25–35 of the Aβ peptide (Aβ25-35) trigger Rock2 accumulation and activation in mouse cortical neurons in primary culture and in mouse hippocampus *in vivo*. Neuronal apoptotic death and memory impairment caused by Aβ25-35 administration were rescued by genetic and pharmacological inhibition of Rock2 activity. Mechanistically, Aβ25-35 elicited cyclin dependent kinase-5 (Cdk5)-mediated phosphorylation of Cdh1, a cofactor that is essential for the activity of the E3 ubiquitin ligase anaphase-promoting complex/cyclosome (APC/C) in neurons. Notably, phosphorylated Cdh1 was disassembled from the APC/C complex, causing its inactivation and subsequent Rock2 protein stabilization and activation. Moreover, Aβ25-35-induced neuronal apoptosis was prevented by expressing a phosphodefective form of Cdh1, but not by a phosphomimetic Cdh1. Finally, Cdh1 inactivation, using both genetic and pharmacological approaches, enhanced Aβ25-35-mediated neuronal death through a mechanism that was prevented by inhibition of Rock2 activity. These results indicate that the Cdk5-Cdh1 signaling pathway accounts for the increased Rock2 activity by amyloidogenic Aβ peptides and that this mechanism may contribute to neurodegeneration and memory loss in AD.

**Keywords: amyloid-β, CDK5, CDH1, ROCK2, neurodegenaration, Alzheimer's disease**

OPEN ACCESS

***Edited by:***
*Ana Rita Vaz,*
*University of Lisbon, Portugal*

***Reviewed by:***
*Ana Lloret,*
*University of Valencia, Spain*
*Karen Litwa,*
*East Carolina University, United States*

***Correspondence:**
*Angeles Almeida*
*aaparra@usal.es*

*[†]These authors have contributed equally to this work and share first authorship*

***Specialty section:***
*This article was submitted to Neuropharmacology, a section of the journal Frontiers in Pharmacology*

***Received:*** *26 February 2022*
***Accepted:*** *01 April 2022*
***Published:*** *14 April 2022*

***Citation:***
*Lapresa R, Agulla J, Gonzalez-Guerrero S, Bolaños JP and Almeida A (2022) Amyloid-β Induces Cdh1-Mediated Rock2 Stabilization Causing Neurodegeneration. Front. Pharmacol. 13:884470. doi: 10.3389/fphar.2022.884470*

## INTRODUCTION

Alzheimer's disease (AD) is the leading cause of dementia (Alzheimer's Association, 2021), affecting around 35 million individuals worldwide hence representing an important strain on health resources (Cummings et al., 2021). However, effective disease-modifying pharmacologic therapies for AD are not currently available (Tatulian 2022). AD is causally related to the accumulation of abnormally folded amyloid-β (Aβ) peptide and hyperphosphorylated tau (pTau) protein aggregates, leading to synapse loss, neurodegeneration, and progressive cognitive decline. The widely accepted amyloid

cascade hypothesis posits that the accumulation of Aβ peptides in the brain parenchyma is a key event of AD pathogenesis. Furthermore, a large body of evidence now indicates that soluble Aβ oligomers, rather than their insoluble fibrillar aggregates, are responsible for the synapto- and neurotoxicity of the Aβ peptide (Walsh et al., 2002; Karran et al., 2011). The soluble Aβ oligomers initiate a cascade of pathological pathways that trigger dendritic and synaptic alterations, which ultimately lead to synaptic plasticity impairment, neurodegeneration, and AD dementia (Selkoe and Hardy 2016; Ricciarelli and Fedele 2017). However, the underlying molecular mechanisms are not fully understood hence preventing the development of effective treatments.

The Rho protein kinase (Rock) is a serine/threonine protein kinase whose activity is regulated by the small GTPase RhoA (Strassheim et al., 2019). Once active, Rock phosphorylates various cellular substrates involved in actin cytoskeleton dynamics, hence regulating cell adhesion, contraction, migration, and division, as well as survival (Strassheim et al., 2019). The predominant brain Rock isoform is Rock2, which phosphorylates cofilin to regulate actin cytoskeleton (Zhang et al., 2006; Newell-Litwa et al., 2015), dendritic spine morphology and synaptic plasticity (Hensel et al., 2015). We recently described that Rock2 accumulation and activation in neurons triggers dendrite disruption and synapse loss, leading to memory impairment (Bobo-Jimenez et al., 2017). Moreover, Rock2 expression resulted in lower dendritic spine density (Henderson et al., 2019), whereas Rock inhibition increases the number of thin spines and filopodia, which would enhance synapse formation and neuronal plasticity (Swanger et al., 2015; Cai et al., 2021). Interestingly, dendritic dystrophy (Cochran et al., 2014; Shi et al., 2020) and synapse loss (Terry et al., 1991; Scheff et al., 2007) have both been detected in early-stage AD brains and are correlated with cognitive decline. Moreover, Rock2 protein accumulates in the neurons of early-stage human AD brain and remain elevated throughout the disease progression (Herskowitz et al., 2013). In experimental models, enhanced Rock2 activity is associated with typical AD hallmarks, such as Aβ aggregation, tau hyperphosphorylation, neuroinflammation, synaptic damage and neuronal death (Gao et al., 2019; Cai et al., 2021). However, the molecular mechanism that leads to Rock accumulation and activation in AD is unknown.

Previous results from our group have shown that the activator of the E3 ubiquitin ligase anaphase-promoting complex/cyclosome (APC/C), Cdh1, is essential for dendritic network integrity, synaptic plasticity, and neuronal survival (Almeida et al., 2005; Maestre et al., 2008; Almeida 2012; Bobo-Jimenez et al., 2017). Recently, we found that APC/C-Cdh1 targets Rock2 for proteasomal degradation in neurons, and that the loss of Cdh1 causes Rock2 stabilization and activation, triggering dendrite disruption, and dendritic spine and synapse loss in the adult brain following neurodegeneration and cognitive impairment (Bobo-Jimenez et al., 2017). Here, we hypothesized whether the regulation of Rock2 by APC/C-Cdh1 is an important mechanistic event in AD. In summary, using *in vitro* and *in vivo* experimental mouse models, we found that Aβ25-35 oligomers induce cyclin dependent kinase-5 (Cdk5)-mediated Cdh1 phosphorylation leading to APC/C inactivation and neuronal apoptosis. Interestingly, through this mechanism, Aβ25-35 triggers Rock2 accumulation and activation in neurons, inducing memory loss that could be rescued by selectively inhibiting Rock2 activity. Thus, here we identify a novel Cdh1-Rock2 pathway that is involved in Aβ neurotoxicity, which may open a new avenue for the development of therapeutic strategies to combat cognitive impairment in AD.

# MATERIAL AND METHODS

## Culture of Primary Cortical Neurons

Neuronal cultures were prepared from C57BL/6J mouse embryo (E14.5) cortices. Animals were maintained in specific-pathogen free facilities at the University of Salamanca, in accordance with Spanish legislation (RD53/2013) under license from the Spanish government and the European Union (2010/63/EU). Protocols were reviewed and approved by the Bioethics Committee of the University of Salamanca. All efforts were made to minimize the numbers of animals used. Neurons were seeded at $1.8 \times 10^5$ cells/cm$^2$ in Neurobasal medium (Invitrogen) supplemented with 2% B27 (Invitrogen) and 2 mM glutamine (Invitrogen) and incubated at 37°C in a humidified 5% $CO_2$-containing atmosphere. Culture medium was replaced with fresh medium every 3 days. Neurons were used for the experiments on day 9–10 *in vitro* (Delgado-Esteban et al., 2013).

## Cell Transfections and Treatments

To achieve the silencing of proteins, we used the following commercial pre-designed small interference RNA (siRNA) (Ambion): s201147 for Cdk5; s80428 for Cdh1; s73020 for Rock2. The Silencer Select Negative Control No. 1 siRNA was used as control. Neurons were transfected with siRNA (9 nM) using Lipofectamine RNAiMAX (Invitrogen), following the manufacturer's instructions, and used after 48 h. The efficacy of siRNAs in targeting Cdk5, Cdh1 and Rock2 is shown in **Supplementary Figures S1A–C**.

The active truncated amyloid-β peptide Aβ25-35 (BioNova Cientifica S.L., Madrid, Spain), was dissolved in distilled water at a concentration of 1 mg/ml and then incubated at 37°C for 3 days to induce its oligomerization (Lapresa et al., 2019). Neurons were incubated in culture medium in the absence (control) or presence of oligomerized Aβ25-35 (10 μM; BioNova Cientifica S.L.), during the time periods indicated in the Figures. When indicated, neurons were incubated in the presence of the Cdk5 inhibitor, roscovitine (10 μM Rosc; Sigma), the APC/C inhibitor, ProTAME (10 μM; Sigma), the Rock inhibitor fasudil (10 μM; Selleck Chemicals) or the Rock2 inhibitor SR3677 (10 μM; Tocris Bioscience), for the time periods indicated in the Figures.

## Western Blot Analysis and Immunoprecipitation Assay

Cells were lysed in RIPA buffer (2% sodium dodecylsulphate, 2 mM EDTA, 2 mM EGTA and 50 mM Tris pH 7.5)

supplemented with phosphatase inhibitors (1 mM $Na_3VO_4$ and 50 mM NaF) and protease inhibitors (100 μM phenylmethylsulfonyl fluoride, 50 μg/ml anti-papain, 50 μg/ml pepstatin, 50 μg/ml amastatin, 50 μg/ml leupeptin, 50 μg/ml bestatin and 50 μg/ml soybean trypsin inhibitor), stored on ice for 30 min and boiled for 5 min. For *in vivo* studies, animals were sacrificed by anesthesia overdose, 5 days after intracerebroventricular (icv) injections. The brain was quickly removed from the skull, and the hippocampus was extracted and frozen in liquid $N_2$. Brain tissue was homogenized in RIPA buffer, supplemented with the protease and phosphatase inhibitors, and boiled for 5 min. Extracts were centrifuged at 17,500 × *g* at 4°C for 30 min. The supernatants were collected and stored at −80°C until further use. Protein concentrations were determined with the BCA method (BCA Protein Assay kit, Thermo Fisher Scientific). Neuronal extracts were subjected to SDS-polyacrylamide gel (MiniProtean; Bio-Rad). The antibodies used were anti-Cdh1 (1:1,000; Ab-1 DH01 clone, Thermo Fisher Scientific), anti-phosphoserine (pSer; ab9332, Abcam); anti-APC3 (35/CDC27; 610455, BD Pharmingen); anti-Rock2 (1:500; D-11, Santa Cruz Biotechnology); anti-MBS (1:500, BioLegend), anti-phospho(Thr853)-MBS (1:500, MyBioSource), and anti-GAPDH (1:40000; Ambion) overnight at 4°C. GAPDH was used as loading control. After incubation with horseradish peroxidase-conjugated goat anti-rabbit IgG (Pierce, Thermo Scientific) or goat anti-mouse IgG (Bio-Rad), membranes were incubated with the enhanced chemiluminescence SuperSignal West Dura (Pierce) for 5 min or Immobilon Western Chemiluminiscent HRP Substrate (Merck Millipore; Darmstadt, Germany) for 1 min, before exposure to Kodak XAR-5 film for 1–5 min, and the autoradiograms were scanned (Veas-Perez de Tudela et al., 2015b).

For immunoprecipitation of endogenous Cdh1, neurons were lysed in RIPA buffer supplemented with the phosphatase and protease inhibitor cocktail indicated above. Cell extracts were clarified by centrifugation, and the supernatants (100 μg protein) were incubated with anti-Cdh1 (1 μg) for 4 h at 4°C, followed by the addition of 20 μL of protein A-agarose (GE Healthcare Life Sciences) for 2 h at 4°C. Inmunoprecipitates were washed with lysis buffer and proteins detected by western blot analysis (Maestre et al., 2008).

## Cdk5 Activity Assay

Neurons were lysed in ice-cold buffer containing 50 mM Tris (pH 7.5), 150 mM NaCl, 2 mM EDTA, 1% NP-40, supplemented with the phosphatase and protease inhibitors cited above. After clearing debris by centrifugation, extracts (200 μg protein) were incubated with anti-Cdk5 (1 μg) for 4 h, at 4°C, followed by the addition of 30 μL of protein A-sepharose (GE Healthcare Life Sciences) for 2 h, at 4°C. Immunoprecipitates were washed in lysis buffer and resuspended in kinase buffer (50 mM Hepes pH 7.5, 10 mM $MgCl_2$, 1 mM EDTA and 0.1 mM dithiothreitol) containing 20 μM ATP, 2 μCi of [γ-$^{32}$P]ATP and histone H1 (1 mg/ml; Sigma). Samples were subjected to SDS-polyacrylamide gel (12%) electrophoresis and transferred proteins were visualized by autoradiography or blotted with anti-Cdk5 (Lapresa et al., 2019).

## APC/C Ubiquitin Ligase Activity Assay

Active APC/C was immunoprecipitated from neurons using monoclonal anti-APC3 antibody (BD Pharmingen) and immobilized on Dynabeads Protein A (Invitrogen). Immunoprecipitates were incubated at 37°C in 10 μL of buffer (0.1 M KCl, 2.5 mM $MgCl_2$, 2 mM ATP, 7.5 μg ubiquitin, 0.3 mM dithiothreitol, 135 mM MG132, 1 mM ubiquitin aldehyde, 2.5 mM His-UbcH10 and 2.5 μM UbcH5a in 20 mM Tris-HCl, pH 7.5) containing 2.5 μL of APC/C beads and 1 μL of [$^{35}$S]cyclin B1. Reactions were stopped at the indicated time points with SDS sample buffer, mixtures resolved by SDS-polyacrylamide gel electrophoresis and visualized by phosphorimaging. APC/C activity was expressed as densitometry of the bands using ImageJ 1.48u4 software (National Institutes of Health, United States) (Delgado-Esteban et al., 2013).

## Neuronal Apoptosis Determination by Flow Cytometry and Active Caspase-3 Fluorimetric Detection

Neurons were carefully detached from the plates using 1 mM EDTA tetrasodium salt in PBS (pH 7.4) at room temperature and neuronal apoptosis was assessed by flow cytometry. Neurons were stained with annexin V-allophycocyanin (APC; Becton Dickinson Biosciences, New Jersey, United States) and 7-aminoactinomycin D (7-AAD; Becton Dickinson Biosciences) in binding buffer (100 mM HEPES, 140 mM NaCl, 2.5 mM CaCl2) to quantitatively determine the percentage of apoptotic neurons by flow cytometry. The annexin V-APC-stained neurons that were 7-AAD-negative were apoptotic. Triplicates obtained from four different neuronal cultures were analysed on a FACScalibur flow cytometer (15 mW argon ion laser tuned at 488 nm. CellQuest software, Becton Dickinson Biosciences) (Gomez-Sanchez et al., 2011).

A fluorimetric caspase-3 assay kit (Sigma) was used following the manufacture's protocol. Cells were lysed with 50 mM HEPES, 5 mM CHAPS, 5 mM DTT, pH 7.4 for 20 min on ice, and the assay buffer containing the Ac-DEVD-AMC (acetyl-Asp-Glu-Val-Asp-7-amino-4-methylcoumarin) substrate (20 mM HEPES, 2 mM EDTA, 0.1% CHAPS, 5 mM DTT, 16 μM Ac-DEVD-AMC, pH 7.4) was added. Aliquots of 200 μL were transferred to a 96-wells plate and the fluorescence was recorded at 5 min intervals for 30 min at 37°C using a Fluoroskan Ascent FL (Thermo Scientific) fluorimeter (excitation: 360 nm, emission: 460 nm). Caspase-3 activity was determined as (7-amino-4-methylcoumarin) AMC release rate extrapolating the slopes to those obtained from the AMC standard curve. Results were expressed as pmol/h/μg protein (Sanchez-Moran et al., 2020).

## Immunocytochemistry

Neurons grown on glass coverslips were fixed with 4% (w/v, in PBS) paraformaldehyde for 30 min and immunostained with mouse anti-Cdh1 (1:250; Ab-1 DH01 clone, Thermo Fisher Scientific), mouse anti-Map2 (1:500; Sigma), rabbit anti-cleaved caspase-3 (1:300; Cell Signaling Technology), mouse anti-Rock2 (1:300; D-11, Santa Cruz Biotechnology), and rabbit anti-Map2 (1:500; Abcam). Immunolabeling was

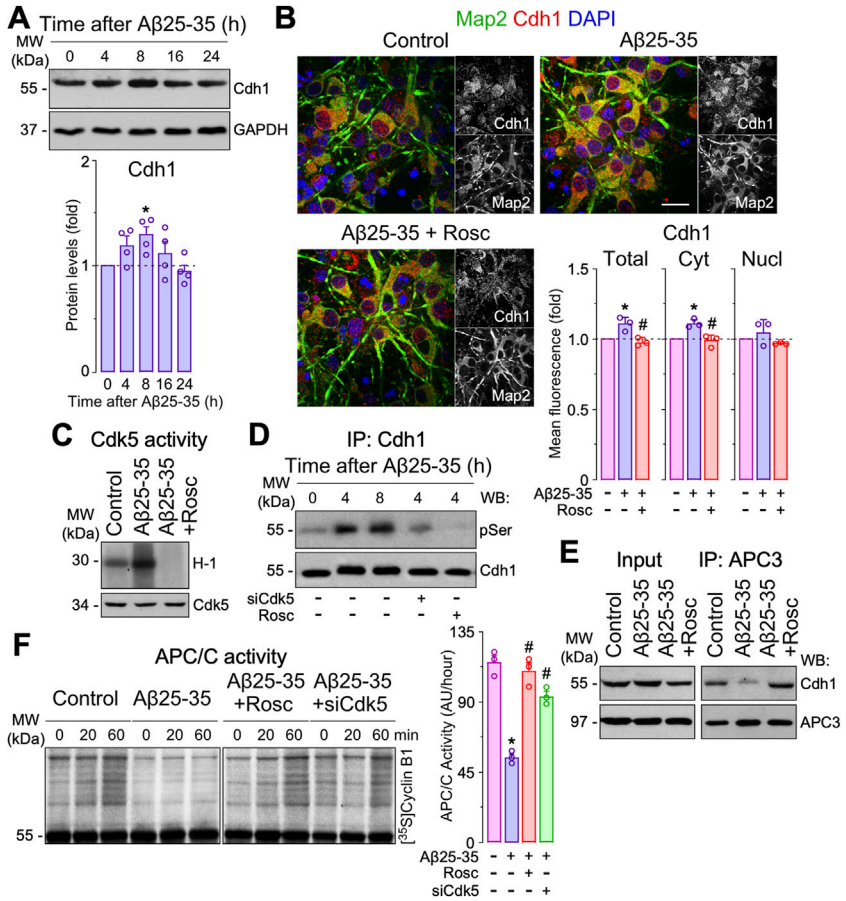


**FIGURE 1 |** Amyloid-β (Aβ)-induced Cdh1 phosphorylation disassembles Cdh1 from APC3 leading to APC/C inactivation. Primary cortical neurons were incubated in culture medium in the absence (control) or the presence of oligomerized Aβ25-35 (10 μM). When indicated, medium was supplemented with roscovitine (10 μM; Rosc). **(A)** Cdh1 western blot analysis in neurons at different time points of Aβ25-35 incubation (GAPDH, loading control). Cdh1 western blot bands were quantified by densitometry and data were expressed as the fold change relative to 0 time ($n$ = 4 neuronal cultures). **(B)** Cdh1 and Map2 (neuronal marker) immunocytochemical analysis in neurons treated with Aβ25-35 and roscovitine for 8 h. Scale bar = 20 μm. Total, nuclear and cytosolic Cdh1 mean fluorescence were quantified and data were expressed as the fold change relative to control ($n$ = 4 neuronal cultures). **(C)** Western blot analysis showing Cdk5 activity in neurons at 2 h of Aβ25-35 incubation. **(D)** Neurons on day 6 *in vitro* were transfected with siRNA control (9 nM) or with siRNA against Cdk5 (siCdk5; 9 nM) for 2 days and then treated with Aβ25-35. Immunoprecipitated Cdh1 followed by pSerine (pSer) western blot analysis in neurons at different time points of Aβ25-35 incubation. Representative blots are shown. Protein abundance quantification from three different neuronal cultures is shown in **Supplementary Figure S1D**. **(E)** Coimmunoprecipitation assay showing that Aβ25-35 (4 h of incubation) disrupted Cdh1 and APC3 interaction in neurons, which was prevented by roscovitine. **(F)** APC/C activity in neurons at 4 h of Aβ25-35 incubation, as assessed by the ability of neuronal extracts to ubiquitylate, *in vitro*, 35S-cyclin B1. Time (min) indicates the reaction time of incubation with 35S-cyclin B1. APC/C activity was expressed as densitometry of the bands (60 min) from three different neuronal cultures ($n$ = 3). Data are mean ± SEM for the indicated number of neuronal cultures. *$p$ < 0.05 *versus* control; #$p$ < 0.05 *versus* Aβ25-35.

detected using IgG-Cy2 (1:500) or IgG-Cy3 (1:500) secondary antibodies (Jackson ImmunoResearch Inc.). Nuclei were stained with 6-diamidino-2-phenylindole (DAPI, Sigma D9542). Coverslips were washed, mounted with SlowFace light antifade reagent (Invitrogen) and examined under an Olympus IX81 Spinning disk confocal microscope (Olympus) (Lapresa et al., 2019).

## Mice and Mouse Model of Single Intracerebroventricular Injection of Aβ25-35

Mice were maintained in specific-pathogen free facilities at the University of Salamanca, in accordance with Spanish legislation (RD53/2013) under license from the Spanish government and the European Union (2010/63/EU). Mouse model protocols were approved by the Bioethics Committee of the University of Salamanca. All efforts were made to minimize the numbers of animals used. The study included C57BL/6J male mice divided in three experimental groups, either receiving saline (control), oligomerized Aβ25-35 (Aβ25-35) or oligomerized Aβ25-35 plus Rock2 inhibitor (Aβ25-35 + SR3677).

Stereotaxic injections were performed as previously done (Lapresa et al., 2019). Twelve-week-old male mice were anesthetized by inhalatory induction (4%) and maintained (2.5%) with sevoflurane (Sevorane; Abbot) in a gas mixture of 70% $N_2O$, 30% $O_2$, using a gas distribution column (Hersill

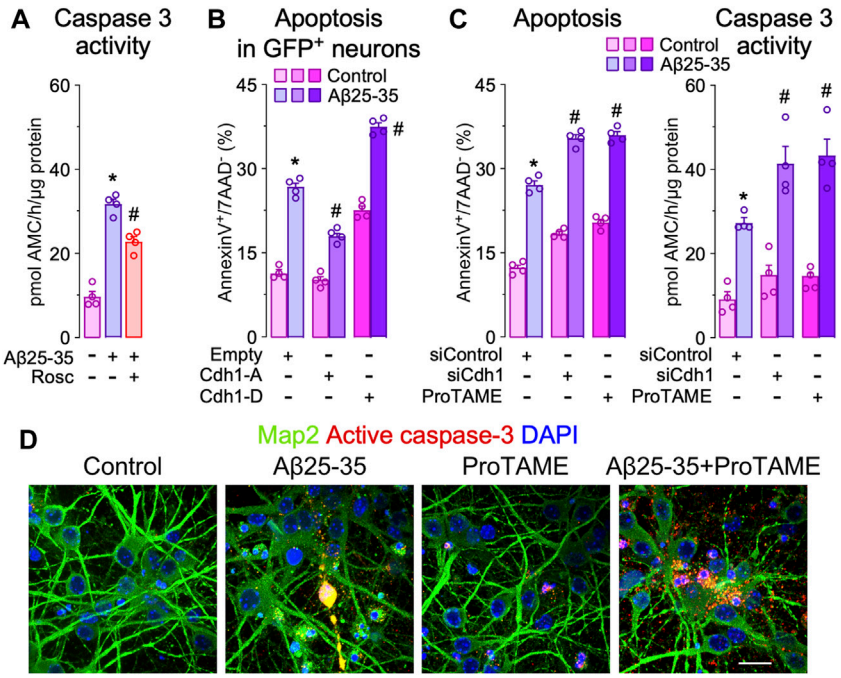


**FIGURE 2 |** Cdh1 phosphorylation mediates Aβ25-35 neurotoxicity. Primary cortical neurons were incubated in culture medium in the absence (control) or the presence of oligomerized Aβ25-35 (10 μM). When indicated, medium was supplemented with roscovitine (10 μM; Rosc) or ProTAME (10 μM). **(A)** Caspase-3 activity determination in neurons at 24 h of incubation with Aβ25-35 and roscovitine ($n = 4$ neuronal cultures). **(B)** Neurons on day 6 *in vitro* were transfected with empty vector or vectors co-expressing GFP and either the phosphodefective (Cdh1-A) or the phosphomimetic (Cdh1-D) forms of Cdh1 and were subjected to Aβ25-35 exposure for 24 h. Apoptosis was measured by flow cytometry in $GFP^+$ (transfected) neurons ($n = 4$ neuronal cultures). **(C)** Neurons on day 6 *in vitro* were transfected with siRNA control (9 nM) or with siRNA against Cdh1 (siCdh1; 9 nM) for 2 days and then treated with Aβ25-35 oligomerized and ProTAME. Neuronal apoptosis and caspase-3 activity were analyzed in neurons at 24 h of incubation with Aβ25-35 ($n = 4$ neuronal cultures). **(D)** Active caspase-3 and Map2 (neuronal marker) immunocytochemical analysis in neurons treated with Aβ25-35 and ProTAME for 24 h. Scale bar = 20 μm. Data are mean ± SEM for the indicated number of neuronal cultures. *$p < 0.05$ *versus* control; #$p < 0.05$ *versus* Aβ25-35.

H-3) and a vaporizer (InterMed Penlons Sigma Delta). Mice were placed in a stereotaxic alignment system (Model 1900; David Kopf Instruments) with digital read out (Wizard 550, Anilam). Injection was performed into the right ventricle at coordinates: 0.22 mm posterior to bregma, 1 mm lateral to midline, and 2.5 mm ventral to dura, using a 5-μL Hamilton syringe (Microliter 65RN, Hamilton) with a 26 S needle (type 2 tip). Either 4 μL of saline (control) or oligomerized Aβ25-35 (9 nmol) were injected using a mini-pump (UltraMicroPump III, World Precision Instruments) and a digital controller (Micro4 UMC4; World Precision Instruments), at a rate of 0.8 μL/min during 5 min. The syringe was left in place for 10 min before slowly retracting it to allow for Aβ infusion and to prevent reflux. Wounds were sutured, and animals were allowed to recover from anesthesia in cages placed on a 37°C thermostatic plate (Plactronic Digital, 25 × 60, JP Selecta). When indicated, animals were intracerebroventricularly injected with both oligomerized Aβ25-35 and Rock2 inhibitor, SR3677 (2 mg/kg, Tocris Bioscience) (Herskowitz et al., 2013). Hippocampal samples from these animals ($n = 3$ male mice per experimental group) were collected for western blot analysis at 1, 3 and 5 days after injections. In addition, functional studies were performed, as described below ($n = 7$ male mice per experimental condition).

## Behavioral Tests

Male mice (3 months old) were left to acclimate in the room for no less than 45 min at the same time of day. Tracking was carried out one at a time using a video-tracking system (ANY-maze, Stoelting Europe), and the apparatus was wiped thoroughly between each mouse session to avoid olfactory cues.

*Open-field Test (OF).* Mice were placed in an ANY-box core (40 × 40 cm). The arena of the box was divided in two zones, namely border (8 cm wide) and centre (a 20 × 20 cm square at the centre of the arena). The animals were allowed to freely explore the field for 10 min, and the distance, time and number of entries to the centre area were recorded. Mice were tested 5 days after icv injection. (Jimenez-Blasco et al., 2020).

*Novel object recognition task (NORT).* The test consisted of two phases. A familiarization phase, where mice were placed in the same ANY-box core with two identical objects located in the upper left and lower right corner of the arena 8 cm away frow the walls. The animals were allowed to freely explore the objects for 5 min and returned to their cages immediately afterwards for 30 min. Short-term memory was evaluated in the recognition phase, in which the animals were returned to the arena, where one of the objects was replaced for a novel one. We registered the number of explorations and the time exploring each object were

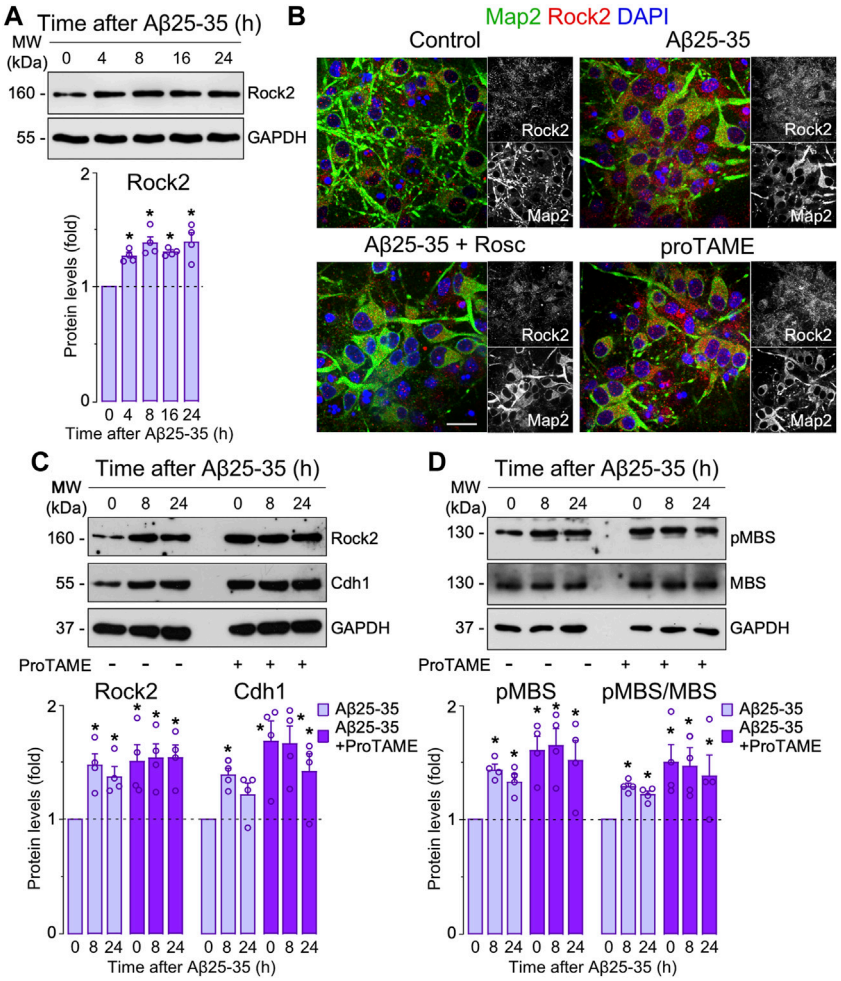


**FIGURE 3 |** Amyloid-β (Aβ)-induced APC/C-Cdh1 inactivation triggers Rock2 stabilization and activation. Primary cortical neurons were incubated in culture medium in the absence (control) or the presence of Aβ25-35 oligomerized (10 μM). When indicated, medium was supplemented with roscovitine (10 μM; Rosc) or ProTAME (10 μM). **(A)** Rock2 western blot analysis in neurons at different time points of Aβ25-35 incubation (GAPDH, loading control). Rock2 western blot bands were quantified by densitometry and data were expressed as the fold change relative to 0 time ($n$ = 4 neuronal cultures). **(B)** Rock2 and Map2 (neuronal marker) immunocytochemical analysis in neurons from one culture treated with Aβ25-35 or ProTAME for 24 h. Scale bar = 20 μm. **(C)** Rock2 and Cdh1 western blot analysis in neurons at different time points of Aβ25-35 and ProTAME incubation (GAPDH, loading control). Rock2 and Cdh1 western blot bands were quantified by densitometry and data were expressed as the fold change relative to 0 time in the absence of ProTAME ($n$ = 4 neuronal cultures). **(D)** MBS and pMBS western blot analysis in neurons at different time points of Aβ25-35 and ProTAME incubation (GAPDH, loading control). MBS and pMBS western blot bands were quantified by densitometry and data were expressed as the fold change relative to 0 time in the absence of ProTAME. Data are mean ± SEM for the indicated number of neuronal cultures. *$p < 0.05$ *versus* 0 time of Aβ25-35 incubation (control).

recorded, and analyzed the discrimination index using the formula $DI=(t_N-t_F)/(t_N + t_F)$, where $t_N$ is the time spent exploring the new object, and $t_F$ is the time spent exploring the familiar one. Mice were tested 5 days after icv injection (Vicente-Gutierrez et al., 2019).

*Barnes Maze*. The apparatus consisted of a grey circular platform, 120 cm in diameter elevated 90 cm above the floor. Along its perimeter were 20 evenly spaced holes. The maze has one removable escape box that could be fitted under any of these holes and was filled with the animal bedding before each experiment. Black and white patterned pictures were used as spatial visual cues. All sessions were performed under a room lightning of 400 lux to increase the mouse aversion for the platform. The test consisted of three phases. First, the habituation phase, where the animals were left to explore the platform freely for 5 min 1-day before the training sessions. Afterwards, the animals underwent the training phase where they were allowed to locate the scape hole for a maximum of 5 min, for 3 days with 4 sessions per day. Finally, for the probe phase, mice were tested for spatial memory. In this session the escape box was removed, and the platform was virtually divided into four quadrants, each containing five holes. Mice were allowed to explore the maze for 5 min and the time spent in the quadrant that previously contained the escape box was quantified. The animals were tested before and 5 days after icv injection (Islam et al., 2021).

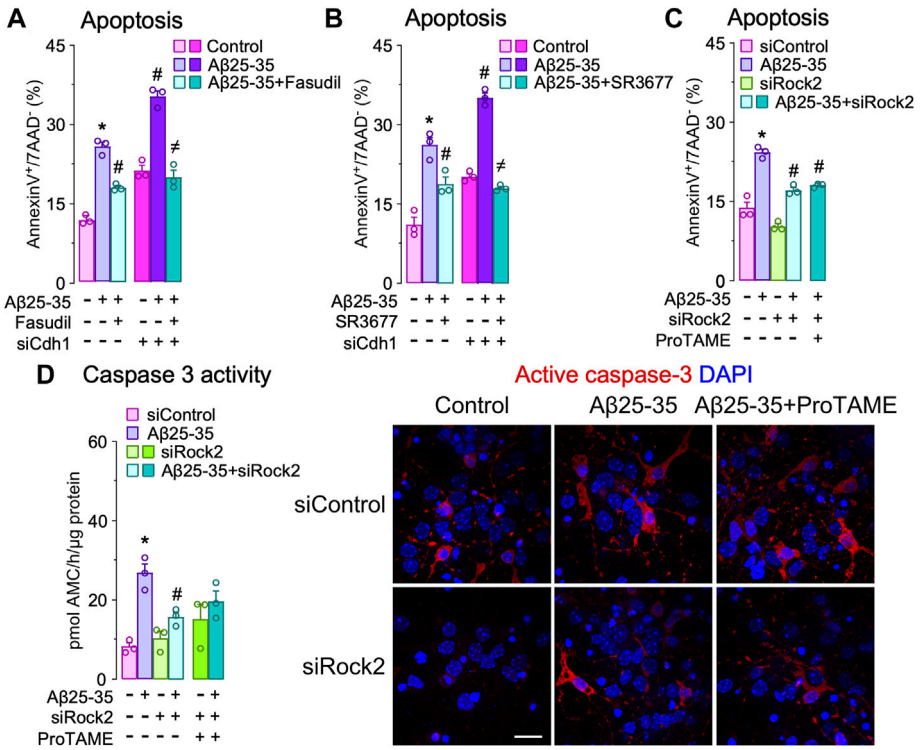


**FIGURE 4 |** Cdh1-induced Rock2 activation is involved in amyloid-β (Aβ) neurotoxicity. Primary cortical neurons were incubated in culture medium in the absence (control) or the presence of oligomerized Aβ25-35 (10 μM). When indicated, medium was supplemented with fasudil (10 μM), Rock2 inhibitor SR3677 (10 μM) or ProTAME (10 μM). **(A,B)** Neurons on day 6 *in vitro* were transfected with siRNA control (9 nM) or with siRNA against Cdh1 (siCdh1; 9 nM) for 2 days and then treated with oligomerized Aβ25-35 and **(A)** fasudil or **(B)** SR3677. Neuronal apoptosis was analyzed in neurons at 24 h of incubation with Aβ25-35 ($n$ = 3 neuronal cultures). **(C,D)** Neurons on day 6 *in vitro* were transfected with siRNA control (9 nM) or with siRNA against Rock2 (siRock2; 9 nM) for 2 days and then treated with Aβ25-35 oligomerized and ProTAME. **(C)** Neuronal apoptosis and **(D)** caspase-3 activity were analyzed in neurons at 24 h of incubation with Aβ25-35 ($n$ = 3 neuronal cultures). Active caspase-3 immunocytochemical analysis in neurons treated with Aβ25-35 and ProTAME for 24 h. Data are mean ± SEM for the indicated number of neuronal cultures. *$p$ < 0.05 *versus* control; #$p$ < 0.05 *versus* Aβ25-35; ≠$p$ < 0.05 *versus* Aβ25-35 + ProTAME.

## Statistical Analysis

Results are expressed as mean ± SEM. A one-way or two-way ANOVA with Tukey's post hoc test was used to compare values between multiple groups, and a two-tailed, unpaired Student's t-test was used for two-group comparisons. In all cases, $p < 0.05$ were considered significant. Statistical analyses were performed using SPSS Statistics 24.0 for Macintosh (IBM).

## RESULTS

**Aβ-induced Cdh1 phosphorylation causes APC/C inactivation and neuronal apoptosis.** To understand the potential role of the Cdh1-Rock2 pathway in Aβ neurotoxicity, we first analyzed the effect of Aβ on APC/C-Cdh1 activity. Cdh1 is the main activator of APC/C in neurons, where it is regulated by autoubiquitination, Cdk5-mediated phosphorylation and subcellular localization (Maestre et al., 2008; Almeida 2012). Treatment of neurons with oligomers of the amyloidogenic fragment Aβ25-35 time-dependently enhanced Cdh1 protein levels (**Figure 1A**) until 8 h of incubation, especially in the cytosol (**Figure 1B**); this effect was prevented by roscovitine, a cyclin dependent kinase-5 (Cdk5) inhibitor (**Figure 1B**), suggesting that Aβ25-35 might cause Cdh1 phosphorylation (Maestre et al., 2008; Veas-Perez de Tudela et al., 2015b; Fuchsberger et al., 2016). In accordance with our previous results (Lapresa et al., 2019), Aβ25-35 rapidly (2 h) activated Cdk5 (**Figure 1C**), resulting in a time-dependent phosphorylation of Cdh1 (**Figure 1D** and **Supplementary Figure S1D**). Since Cdh1 phosphorylation at Cdk5-cognate residues disrupts Cdh1 assembly from its APC/C complex core protein APC3, leading to APC/C-Cdh1 inactivation in neurons (Veas-Perez de Tudela et al., 2015b), we next assessed whether these effects could be mimicked by Aβ25-35 treatment. As shown in **Figure 1E**, APC3-Cdh1 interaction was disrupted by Aβ25-35, an effect that was rescued with roscovitine. Moreover, Aβ25-35 treatment caused APC/C inactivation, as revealed by the decreased ubiquitination of its well-known substrate, cyclin B1 (Zachariae et al., 1998), in a manner that could be prevented by roscovitine and Cdk5 knock down (siCdk5) (**Figure 1F**). Thus, Aβ25-35-induced Cdk5 activation promotes the accumulation of phosphorylated (inactive) Cdh1 and its disassembly from APC3, leading to APC/C-Cdh1 inactivation.

Given that the inactivation of APC/C-Cdh1 caused by Cdh1 phosphorylation promotes neuronal apoptosis (Maestre et al.,

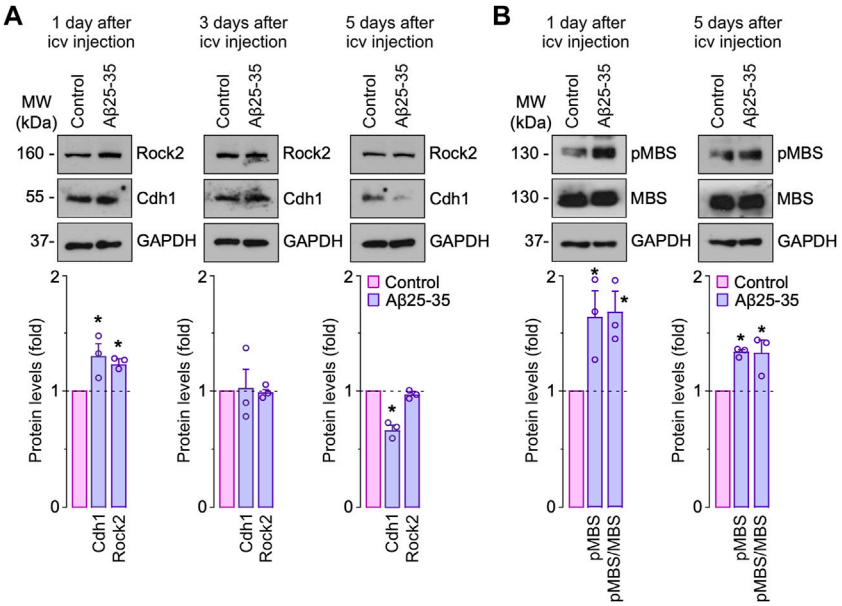


**FIGURE 5 |** Amyloid-β (Aβ) promotes Rock2 stabilization and activation in the hippocampus *in vivo*. Intracerebroventricular stereotactic injections of saline (control) or oligomerized Aβ25-35 (9 nmol) were performed into 12-week-old male mice. Hippocampus extracts were obtained at different days after injections. **(A)** Rock2 and Cdh1 western blot analysis in hippocampus extracts (GAPDH, loading control). Rock2 and Cdh1 western blot bands were quantified by densitometry and results were expressed as the fold change relative to control. **(B)** MBS and pMBS western blot analysis in hippocampus extracts (GAPDH, loading control). MBS and pMBS western blot bands were quantified by densitometry and results were expressed as the fold change relative to control. Data are mean ± SEM from 3 mice. *$p < 0.05$ *versus* control.

2008; Veas-Perez de Tudela et al., 2015b; Veas-Perez de Tudela et al., 2015a), we next evaluated the impact of Cdh1 in Aβ25-35 toxicity. As shown in **Figure 2A**, Aβ25-35-induced caspase 3 activation that was partially prevented by roscovitine. Then we investigated whether Cdh1 phosphorylation by Cdk5 impacted in Aβ25-35 neurotoxicity. To this end, a phosphomimetic (Cdh1-D) or a phosphodefective (Cdh1-A) form of Cdh1 were expressed in neurons followed by Aβ25-35 treatment. As previously described, Cdh1-D resulted in neuronal apoptosis (Maestre et al., 2008; Veas-Perez de Tudela et al., 2015b). In contrast, Cdh1-A prevented Aβ25-35-induced neuronal apoptosis (**Figure 2B** and **Supplementary Figure S2A**). Moreover, inhibition of APC/C using ProTAME and Cdh1 knock down (siCdh1) enhanced Aβ25-35-induced neurotoxicity, as revealed by the increased neuronal apoptosis and caspase 3 activation (**Figures 2C,D** and **Supplementary Figure S2A–C**). Thus, Cdk5-mediated Cdh1 phosphorylation triggers APC/C inhibition, which is important in Aβ25-35 neurodegeneration.

**Aβ-induced APC/C- Cdh1 inactivation triggers Rock2 stabilization and activation leading to neuronal apoptosis.** Next, we sought to identify the APC/C-Cdh1 target that is involved in Aβ25-35 neurotoxicity. We specifically focused on Rock2, given that it is a well-known APC/CCdh1 substrate (Bobo-Jimenez et al., 2017) that accumulates in the brain of AD patients (Herskowitz et al., 2013). To do so, we first treated neurons with Aβ25-35 and found that Rock2 protein levels time-dependently increased (**Figure 3A**) through a mechanism that could be prevented with roscovitine (**Figure 3B**). Moreover, inactivation of APC/C-Cdh1 with ProTAME promoted the accumulation of its cognate targets, Cdh1 and Rock2, an effect that was maintained during all the time of Aβ25-35 presence (**Figure 3C**). To ascertain whether Aβ25-35-induced Rock2 accumulation was translated into Rock2 activity, we measured the Thr853 phosphorylation of the Rock2-subtrate myosin phosphatase myosin-binding subunit (MBS) (Tanaka et al., 2006; Bobo-Jimenez et al., 2017). As shown in **Figure 3D**, Aβ25-35 increased MBS phosphorylation, indicating increased Rock2 activity, and effect that was potentiated by ProTAME. These results confirm that Aβ25-35 inactivates APC/C-Cdh1 to regulate Rock2 activity (Bobo-Jimenez et al., 2017). We then aimed to investigate whether the Cdh1-Rock2 axis impacts on Aβ25-35 neurotoxicity. To do this, neurons were treated with the clinically approved Rock inhibitor, fasudil, and with the Rock2 inhibitor, SR3677. As shown in **Figures 4A,B**, these treatments partially rescued Aβ25-35-induced neuronal apoptosis. Furthermore, either fasudil or SR3677 reduced Aβ25-35 neurotoxicity in Cdh1-knocked down neurons (**Figures 4A,B**). Neuronal viability was not affected by fasudil or SR3677 treatments (**Supplementary Figure S2D**). Although SR3677 demonstrated an approximately eightfold selectivity of Rock2 over Rock1, at a concentration of 10 μM it is likely that SR3677 also inhibits Rock1 (Feng et al., 2008). Next, we specifically knocked down Rock2 in neurons (siRock2), which did not affect Rock1 levels (**Supplementary Figure S1C**). Interestingly, Rock2 knock down also protected neurons against Aβ25-35-induced

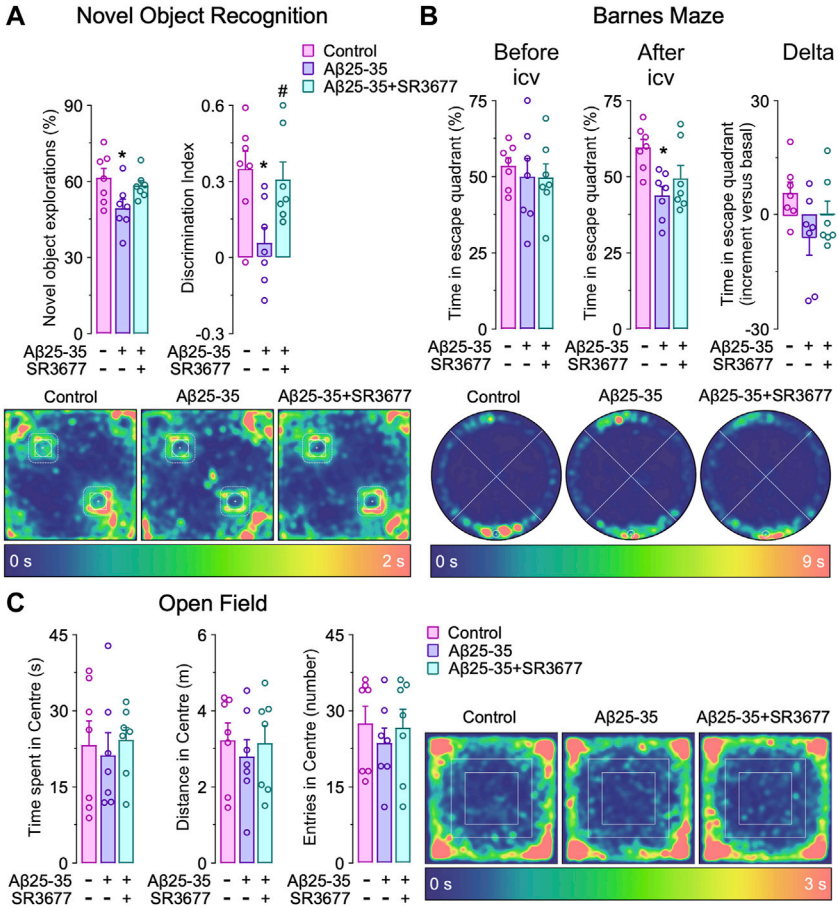


**FIGURE 6 |** Rock2 inhibition rescues amyloid-β (Aβ)-induced cognitive impairment *in vivo*. Intracerebroventricular stereotactic injections of saline (control) or oligomerized Aβ25-35 (9 nmol) were performed into 12-week-old male mice. When indicated, Rock2 inhibitor SR3677 (2 mg/kg) was intracerebroventricularly injected together with Aβ25-35 oligomers. Behavioral tests were performed at 5 days after injections. **(A)** Novel object recognition test showing novel object explorations and the discrimination index (familiar object in the upper left corner, novel object in the lower right corner). Spatiotemporal quantitative heatmaps are shown. **(B)** Barnes maze test showing time in scape (target) quadrant (lower) before and after Aβ25-35 and SR3677 injections ($n = 7$ male mice per condition). Spatiotemporal quantitative heatmaps are shown. **(C)** Open field test showing the time spent, distance and entries in the center area. Spatiotemporal quantitative heatmaps are shown. Data are mean ± SEM from 7 male mice. *$p < 0.05$ *versus* control; #$p < 0.05$ *versus* Aβ25-35.

apoptotic death (**Figures 4C,D**), an effect that was mimicked by the APC/C-Cdh1 inhibitor ProTAME (**Figure 4D**). Altogether, these results indicate that Aβ25-35-induced Cdh1 phosphorylation inactivates APC/C-Cdh1, which results in Rock2 stabilization and activation, eventually leading to neuronal apoptosis.

**Rock2 inhibition rescues cognitive impairment induced by Aβ *in vivo*.** Finally, we asked whether the Aβ 25–35-Cdh1-Rock2 pathway herein described takes place *in vivo*. To this end, saline (control) or oligomerized Aβ25-35 were intracerebroventricularly injected in the mouse brain as previously done (Lapresa et al., 2019). One day after injection, we found that both Cdh1 and Rock2 were accumulated in the hippocampus (**Figure 5A**, left panel); however, at day 3, Cdh1 and Rock2 levels decreased to normal values (**Figure 5**, middle panel) and, at day 5, Cdh1 levels decreased below controls whereas Rock2 levels were maintained (**Figure 5A**, right panel). The increase in Rock2 abundance was paralleled by enhanced activity, as revealed by the increase in MBS phosphorylation in the hippocampus that was maintained after 5 days of injection (**Figure 5B**). To investigate whether Rock2 activation is implicated in the cognitive impairment caused by Aβ25-35, the Rock2 inhibitor SR3677 was intracerebroventricularly administered in the mice together with the Aβ25-35 oligomers. We found that Rock2 inhibition prevented the decrease in the novel object explorations and discrimination index caused by Aβ25-35 (**Figure 6A**), indicating an improvement in memory performance. In the Barnes maze test, Aβ25-35-injected mice displayed fewer time in scape (target) quadrant than control mice, indicating spatial memory deficits, an effect that was rescued by Rock2 inhibition (**Figure 6B**). No alterations in the time spent, distance run and number of entries in the center distance were found in the open field test, discarding any motor impairment in this model (**Figure 6C**). Together, these results indicate that Aβ25-35

enhances Rock2 activity in the mouse hippocampus causing memory loss.

## DISCUSSION

Here, we characterize a novel signaling pathway involved in Aβ neurotoxicity that may open new therapeutic strategies to combat cognitive impairment in AD. We describe that Aβ25-35 oligomers induce cyclin dependent kinase-5 (Cdk5)-mediated phosphorylation of the APC/C-cofactor, Cdh1, leading to inhibition of APC/C and, eventually, neuronal apoptosis. Moreover, we show that Aβ25-35-induced APC/C-Cdh1 inhibition causes Rock2 accumulation and activation in neurons. Finally, we demonstrate that the memory loss caused by Aβ25-35 can be prevented by a pharmacological approach based on the selective inhibition of Rock2 activity. Given that Rock2 accumulates in the neurons of early-stage human AD brain (Herskowitz et al., 2013) and is associated with AD hallmarks (Gao et al., 2019; Cai et al., 2021), our data showing efficacy of the Rock2 inhibitor, compound SR3677, against Aβ25-35 memory impairment in mice should be considered as a potential therapeutic approach in AD.

We herein also characterize the signaling pathway that connects Aβ25-35 with Rock2. It was known that dysregulation of $Ca^{2+}$ homeostasis is a key event in AD pathogenesis (LaFerla 2002) and that Aβ causes p35 cleavage to p25 -a potent Cdk5 activator- in a $Ca^{2+}$-dependent manner (Fuchsberger et al., 2016; Lapresa et al., 2019). Notably, p25 accumulates, and Cdk5 is active, in the brain of AD patients before the onset of clinical symptoms (Patrick et al., 1999). In good agreement with these previous findings, here we demonstrate that the activation of Cdk5 by Aβ is a rapid process, as is the phosphorylation of Cdk5 substrate, Cdh1. Once phosphorylated, Cdh1 becomes disassembled from the APC/C complex, inhibiting its ubiquitin ligase activity for a long period of time. Given that Rock2 is a substrate of APC/C-Cdh1 complex, its inhibition by Cdh1 phosphorylation causes stabilization of Rock2 protein, which is maintained elevated and active also for long periods. Interestingly, this sequence of events mirrors that of Rock2 in AD patients, in which Rock2 is found elevated from the early stages of the disease and remains high throughout the AD progression (Herskowitz et al., 2013). This analogy between our data and those found in humans suggest that the early biochemical changes that we describe, namely Cdk5 activation and Cdh1 phosphorylation, might be considered as potential biomarkers of early AD detection and progression.

Our work also describes an intriguing biphasic effect of the temporal changes in Cdh1 protein abundance by Aβ25-35. Thus, Cdh1 is known to be a substrate of APC/C-Cdh1 and, therefore, when APC/C-Cdh1 is active, Cdh1 undergoes autoubiquitination and proteasomal degradation (Veas-Perez de Tudela et al., 2015b), which is considered a major regulatory system of Cdh1 homeostasis in neurons. Accordingly, in our hands, Aβ25-35 initially triggered APC/C-Cdh1 inactivation, which explains Cdh1 accumulation at the early time points after Aβ exposure, both *in vitro* and *in vivo*. However, at longer time periods, Cdh1 proteins levels underwent a progressive decrease, a result that is compatible with a previous study (Fuchsberger et al.) in which it was found that long-term incubation of neurons with Aβ oligomers causes a proteasome-dependent degradation of Cdh1. These observations suggest that Cdh1 may be subjected to regulation by alternative ubiquitin ligase(s) that could explain the maintained low protein levels of Cdh1. Notably, the F-box and WD-40 domain protein 11, FBXW11, has been observed in the hippocampus of AD mouse models (Sun et al., 2021). Whether FBXW11, which ubiquitinates phosphorylated substrates, including Cdh1 -in proliferative cells (Fukushima et al., 2013)- is responsible for the long-term neuronal degradation of Cdh1, is an interesting possibility that remains to be investigated in the context of AD pathogenesis.

Finally, our data may also provide clues for future development of pharmacological strategies aimed to specifically interfere in the Cdk5-Cdh1-Rock2 axis. Thus, Cdh1 needs to be phosphorylated by Cdk5 to be inactive and, therefore, to maintain Rock2 elevated upon Aβ treatment. These specific Cdk5-dependent phosphorylation sites on Cdh1 are Ser-40, Thr-121 and Ser-163 (Maestre et al., 2008). In fact, Aβ-induced neuronal apoptosis was prevented by expressing a triple phosphodefective ($Ser^{40}$Ala, $Thr^{121}$Ala and $Ser^{163}$Ala) Cdh1 mutant, but not by expressing a triple phosphomimetic ($Ser^{40}$Asp, $Thr^{121}$Asp and $Ser^{163}$Asp) Cdh1 mutant. We propose that these findings may be useful for the design of small molecules aimed to competitively and selectively antagonize these Cdh1 phosphorylation sites. If so, the subsequent disruption of the Cdk5-Cdh1 pathway might eventually serve to prevent aberrant Rock2 accumulation and neurodegeneration in AD.

In summary, our results provide evidence for a key role of the Cdh1-Rock2 signaling pathway in mediating neuronal apoptosis and memory impairment caused by Aβ25-35 oligomers. Thus, Aβ25-35 phosphorylates and inactivates Cdh1, which results in Rock2 stabilization and activation, leading to neurodegeneration. As Rock2 accumulates in the earliest stages of AD and remains elevated throughout the disease progression (Herskowitz et al., 2013), our data set the basis for a future development of therapeutic strategies to overcome neuronal loss and memory impairment in AD.

## DATA AVAILABILITY STATEMENT

The original contributions presented in the study are included in the article/**Supplementary Material**, further inquiries can be directed to the corresponding author.

## ETHICS STATEMENT

The animal study was reviewed and approved by The Bioethics Committee of the University of Salamanca.

## AUTHOR CONTRIBUTIONS

RL and JA performed the *in vitro* experiments and analyzed biochemical data. RL, JA, and SG-G performed the *in vivo* experiments. RL and JA organized the database and performed the statistical analysis. JB, RL, JA and AA analyzed data and design the experiments. AA conceived the idea, supervised the project, and wrote the manuscript. All authors contributed to the discussion of the results and read, revised, and approved the final version of the manuscript.

## FUNDING

The work was funded by The Instituto de Salud Carlos III (to AA, PI21/00727 and RD21/0006/0005); European Regional Development Fund; European Union's Horizon 2020 Research and Innovation Programme (to AA, grant agreement 686009); and Junta de Castilla y León (to AA and JB, CSI151P20 and CLU201703 P.O.FEDER CyL1420), and the Agencia Estatal de Investigación (to JB, PID 2019-105699RB-I00, MCIN/AEI/10.13039/501100011033 and European Union NextGenerationEU/PRTR). RL, JA and SG-G are funded by Junta de Castilla y León (to RL and JA, CSI151P20; to SG-G, EDU/601/2020).

## ACKNOWLEDGMENTS

The technical assistances of Lucía Martín, Mónica Carabias, Mónica Resch and Carmen Castro are acknowledged. The authors are grateful to Bodegas R. López de Heredia Viña Tondonia for funding part of the study.

## SUPPLEMENTARY MATERIAL

The Supplementary Material for this article can be found online at: https://www.frontiersin.org/articles/10.3389/fphar.2022.884470/full#supplementary-material

## REFERENCES

Almeida, A., Bolaños, J. P., and Moreno, S. (2005). Cdh1/Hct1-APC Is Essential for the Survival of Postmitotic Neurons. *J. Neurosci.* 25, 8115–8121. doi:10.1523/JNEUROSCI.1143-05.2005

Almeida, A. (2012). Regulation of APC/C-Cdh1 and its Function in Neuronal Survival. *Mol. Neurobiol.* 46 (3), 547–554. doi:10.1007/s12035-012-8309-2

Alzheimer´s Association (2021). 2021 Alzheimer's Disease Facts and Figures. *Alzheimers Dement* 17 (3), 327–406. doi:10.1002/alz.12328

Bobo-Jiménez, V., Delgado-Esteban, M., Angibaud, J., Sánchez-Morán, I., de la Fuente, A., Yajeya, J., et al. (2017). APC/CCdh1-Rock2 Pathway Controls Dendritic Integrity and Memory. *Proc. Natl. Acad. Sci. U S A.* 114 (17), 4513–4518. doi:10.1073/pnas.1616024114

Cai, R., Wang, Y., Huang, Z., Zou, Q., Pu, Y., Yu, C., et al. (2021). Role of RhoA/ROCK Signaling in Alzheimer's Disease. *Behav. Brain Res.* 414, 113481. doi:10.1016/j.bbr.2021.113481

Cochran, J. N., Hall, A. M., and Roberson, E. D. (2014). The Dendritic Hypothesis for Alzheimer's Disease Pathophysiology. *Brain Res. Bull.* 103, 18–28. doi:10.1016/j.brainresbull.2013.12.004

Cummings, J., Lee, G., Zhong, K., Fonseca, J., and Taghva, K. (2021). Alzheimer's Disease Drug Development Pipeline: 2021. *A&d Transl Res. Clin. Interv.* 7 (1), e12179. doi:10.1002/trc2.12179

Delgado-Esteban, M., García-Higuera, I., Maestre, C., Moreno, S., and Almeida, A. (2013). APC/C-Cdh1 Coordinates Neurogenesis and Cortical Size during Development. *Nat. Commun.* 4, 2879. doi:10.1038/ncomms3879

Feng, Y., Yin, Y., Weiser, A., Griffin, E., Cameron, M. D., Lin, L., et al. (2008). Discovery of Substituted 4-(pyrazol-4-Yl)-Phenylbenzodioxane-2-Carboxamides as Potent and Highly Selective Rho Kinase (ROCK-II) Inhibitors. *J. Med. Chem.* 51 (21), 6642–6645. doi:10.1021/jm800986w

Fuchsberger, T., Martínez-Bellver, S., Giraldo, E., Teruel-Martí, V., Lloret, A., and Viña, J. (2016). Aβ Induces Excitotoxicity Mediated by APC/C-Cdh1 Depletion that Can Be Prevented by Glutaminase Inhibition Promoting Neuronal Survival. *Sci. Rep.* 6, 31158. doi:10.1038/srep31158

Fukushima, H., Ogura, K., Wan, L., Lu, Y., Li, V., Gao, D., et al. (2013). SCF-mediated Cdh1 Degradation Defines a Negative Feedback System that Coordinates Cell-Cycle Progression. *Cell Rep* 4 (4), 803–816. doi:10.1016/j.celrep.2013.07.031

Gao, Y., Yan, Y., Fang, Q., Zhang, N., Kumar, G., Zhang, J., et al. (2019). The Rho Kinase Inhibitor Fasudil Attenuates Aβ1-42-Induced Apoptosis via the ASK1/JNK Signal Pathway in Primary Cultures of Hippocampal Neurons. *Metab. Brain Dis.* 34 (6), 1787–1801. doi:10.1007/s11011-019-00487-0

Gomez-Sanchez, J. C., Delgado-Esteban, M., Rodriguez-Hernandez, I., Sobrino, T., Perez de la Ossa, N., Reverte, S., et al. (2011). The Human Tp53 Arg72Pro Polymorphism Explains Different Functional Prognosis in Stroke. *J. Exp. Med.* 208 (3), 429–437. doi:10.1084/jem.20101523

Henderson, B. W., Greathouse, K. M., Ramdas, R., Walker, C. K., Rao, T. C., Bach, S. V., et al. (2019). Pharmacologic Inhibition of LIMK1 Provides Dendritic Spine Resilience against β-amyloid. *Sci. Signal.* 12 (587), eaaw9318. doi:10.1126/scisignal.aaw9318

Hensel, N., Rademacher, S., and Claus, P. (2015). Chatting with the Neighbors: Crosstalk between Rho-Kinase (ROCK) and Other Signaling Pathways for Treatment of Neurological Disorders. *Front. Neurosci.* 9, 198. doi:10.3389/fnins.2015.00198

Herskowitz, J. H., Feng, Y., Mattheyses, A. L., Hales, C. M., Higginbotham, L. A., Duong, D. M., et al. (2013). Pharmacologic Inhibition of ROCK2 Suppresses Amyloid-β Production in an Alzheimer's Disease Mouse Model. *J. Neurosci.* 33 (49), 19086–19098. doi:10.1523/JNEUROSCI.2508-13.2013

Islam, M. R., Valaris, S., Young, M. F., Haley, E. B., Luo, R., Bond, S. F., et al. (2021). Exercise Hormone Irisin Is a Critical Regulator of Cognitive Function. *Nat. Metab.* 3 (8), 1058–1070. doi:10.1038/s42255-021-00438-z

Jimenez-Blasco, D., Busquets-Garcia, A., Hebert-Chatelain, E., Serrat, R., Vicente-Gutierrez, C., Ioannidou, C., et al. (2020). Glucose Metabolism Links Astroglial Mitochondria to Cannabinoid Effects. *Nature* 583 (7817), 603–608. doi:10.1038/s41586-020-2470-y

Karran, E., Mercken, M., and De Strooper, B. (2011). The Amyloid cascade Hypothesis for Alzheimer's Disease: an Appraisal for the Development of Therapeutics. *Nat. Rev. Drug Discov.* 10 (9), 698–712. doi:10.1038/nrd3505

LaFerla, F. M. (2002). Calcium Dyshomeostasis and Intracellular Signalling in Alzheimer's Disease. *Nat. Rev. Neurosci.* 3 (11), 862–872. doi:10.1038/nrn960

Lapresa, R., Agulla, J., Sánchez-Morán, I., Zamarreño, R., Prieto, E., Bolaños, J. P., et al. (2019). Amyloid-ß Promotes Neurotoxicity by Cdk5-Induced P53 Stabilization. *Neuropharmacology* 146, 19–27. doi:10.1016/j.neuropharm.2018.11.019

Maestre, C., Delgado-Esteban, M., Gomez-Sanchez, J. C., Bolaños, J. P., and Almeida, A. (2008). Cdk5 Phosphorylates Cdh1 and Modulates Cyclin B1 Stability in Excitotoxicity. *Embo J.* 27 (20), 2736–2745. doi:10.1038/emboj.2008.195

Newell-Litwa, K. A., Badoual, M., Asmussen, H., Patel, H., Whitmore, L., and Horwitz, A. R. (2015). ROCK1 and 2 Differentially Regulate Actomyosin Organization to Drive Cell and Synaptic Polarity. *J. Cell Biol* 210 (2), 225–242. doi:10.1083/jcb.201504046

Patrick, G. N., Zukerberg, L., Nikolic, M., de la Monte, S., Dikkes, P., and Tsai, L. H. (1999). Conversion of P35 to P25 Deregulates Cdk5 Activity and Promotes Neurodegeneration. *Nature* 402 (6762), 615–622. doi:10.1038/45159

Ricciarelli, R., and Fedele, E. (2017). The Amyloid Cascade Hypothesis in Alzheimer's Disease: It's Time to Change Our Mind. *Curr. Neuropharmacol* 15 (6), 926–935. doi:10.2174/1570159X15666170116143743

Sánchez-Morán, I., Rodríguez, C., Lapresa, R., Agulla, J., Sobrino, T., Castillo, J., et al. (2020). Nuclear WRAP53 Promotes Neuronal Survival and Functional Recovery after Stroke. *Sci. Adv.* 6 (41). doi:10.1126/sciadv.abc5702

Scheff, S. W., Price, D. A., Schmitt, F. A., DeKosky, S. T., and Mufson, E. J. (2007). Synaptic Alterations in CA1 in Mild Alzheimer Disease and Mild Cognitive Impairment. *Neurology* 68 (18), 1501–1508. doi:10.1212/01.wnl.0000260698.46517.8f

Selkoe, D. J., and Hardy, J. (2016). The Amyloid Hypothesis of Alzheimer's Disease at 25 Years. *EMBO Mol. Med.* 8 (6), 595–608. doi:10.15252/emmm.201606210

Shi, Y. B., Tu, T., Jiang, J., Zhang, Q. L., Ai, J. Q., Pan, A., et al. (2020). Early Dendritic Dystrophy in Human Brains with Primary Age-Related Tauopathy. *Front. Aging Neurosci.* 12, 596894. doi:10.3389/fnagi.2020.596894

Strassheim, D., Gerasimovskaya, E., Irwin, D., Dempsey, E. C., Stenmark, K., and Karoor, V. (2019). RhoGTPase in Vascular Disease. *Cells* 8 (6). doi:10.3390/cells8060551

Sun, J., Qin, X., Zhang, X., Wang, Q., Zhang, W., and Wang, M. (2021). FBXW11 Deletion Alleviates Alzheimer's Disease by Reducing Neuroinflammation and Amyloid-β Plaque Formation via Repression of ASK1 Signaling. *Biochem. Biophys. Res. Commun.* 548, 104–111. doi:10.1016/j.bbrc.2020.12.081

Swanger, S. A., Mattheyses, A. L., Gentry, E. G., and Herskowitz, J. H. (2015). ROCK1 and ROCK2 Inhibition Alters Dendritic Spine Morphology in Hippocampal Neurons. *Cell Logist* 5 (4), e1133266. doi:10.1080/21592799.2015.1133266

Tanaka, T., Nishimura, D., Wu, R. C., Amano, M., Iso, T., Kedes, L., et al. (2006). Nuclear Rho Kinase, ROCK2, Targets P300 Acetyltransferase. *J. Biol. Chem.* 281 (22), 15320–15329. doi:10.1074/jbc.M510954200

Tatulian, S. A. (2022). Challenges and Hopes for Alzheimer's Disease. *Drug Discov. Today* 27, 1027–1043. doi:10.1016/j.drudis.2022.01.016

Terry, R. D., Masliah, E., Salmon, D. P., Butters, N., DeTeresa, R., Hill, R., et al. (1991). Physical Basis of Cognitive Alterations in Alzheimer's Disease: Synapse Loss Is the Major Correlate of Cognitive Impairment. *Ann. Neurol.* 30 (4), 572–580. doi:10.1002/ana.410300410

Veas-Pérez de Tudela, M., Delgado-Esteban, M., Maestre, C., Bobo-Jiménez, V., Jiménez-Blasco, D., Vecino, R., et al. (2015a). Regulation of Bcl-xL-ATP Synthase Interaction by Mitochondrial Cyclin B1-cyclin-dependent Kinase-1 Determines Neuronal Survival. *J. Neurosci.* 35 (25), 9287–9301. doi:10.1523/JNEUROSCI.4712-14.2015

Veas-Pérez de Tudela, M., Maestre, C., Delgado-Esteban, M., Bolaños, J. P., and Almeida, A. (2015b). Cdk5-mediated Inhibition of APC/C-Cdh1 Switches on the Cyclin D1-Cdk4-pRb Pathway Causing Aberrant S-phase Entry of Postmitotic Neurons. *Sci. Rep.* 5, 18180. doi:10.1038/srep18180

Vicente-Gutierrez, C., Bonora, N., Bobo-Jimenez, V., Jimenez-Blasco, D., Lopez-Fabuel, I., Fernandez, E., et al. (2019). Astrocytic Mitochondrial ROS Modulate Brain Metabolism and Mouse Behaviour. *Nat. Metab.* 1, 201–211. doi:10.1038/s42255-018-0031-6

Walsh, D. M., Klyubin, I., Fadeeva, J. V., Cullen, W. K., Anwyl, R., Wolfe, M. S., et al. (2002). Naturally Secreted Oligomers of Amyloid Beta Protein Potently Inhibit Hippocampal Long-Term Potentiation *In Vivo*. *Nature* 416 (6880), 535–539. doi:10.1038/416535a

Zachariae, W., Schwab, M., Nasmyth, K., and Seufert, W. (1998). Control of Cyclin Ubiquitination by CDK-Regulated Binding of Hct1 to the Anaphase Promoting Complex. *Science* 282, 1721–1724. doi:10.1126/science.282.5394.1721

Zhang, Z., Ottens, A. K., Larner, S. F., Kobeissy, F. H., Williams, M. L., Hayes, R. L., et al. (2006). Direct Rho-Associated Kinase Inhibition [correction of Inhibiton] Induces Cofilin Dephosphorylation and Neurite Outgrowth in PC-12 Cells. *Cell Mol Biol Lett* 11 (1), 12–29. doi:10.2478/s11658-006-0002-x

**Conflict of Interest:** The authors declare that the research was conducted in the absence of any commercial or financial relationships that could be construed as a potential conflict of interest.

**Publisher's Note:** All claims expressed in this article are solely those of the authors and do not necessarily represent those of their affiliated organizations, or those of the publisher, the editors and the reviewers. Any product that may be evaluated in this article, or claim that may be made by its manufacturer, is not guaranteed or endorsed by the publisher.

frontiers | Frontiers in Pharmacology

ORIGINAL RESEARCH
published: 10 May 2022
doi: 10.3389/fphar.2022.833066

# Protective Signature of IFNγ-Stimulated Microglia Relies on miR-124-3p Regulation From the Secretome Released by Mutant APP Swedish Neuronal Cells

*Gonçalo Garcia*[1,2], *Adelaide Fernandes*[2,3], *Frank Stein*[4] *and Dora Brites*[1]*

[1]Neuroinflammation, Signaling and Neuroregeneration Laboratory, Research Institute for Medicines (iMed.ULisboa), Faculty of Pharmacy, Universidade de Lisboa, Lisbon, Portugal, [2]Department of Pharmaceutical Sciences and Medicines, Faculty of Pharmacy, Universidade de Lisboa, Lisbon, Portugal, [3]Central Nervous System, Blood and Peripheral Inflammation, Research Institute for Medicines (iMed.ULisboa), Faculty of Pharmacy, Universidade de Lisboa, Lisbon, Portugal, [4]Proteomics Core Facility, European Molecular Biology Laboratory (EMBL), Heidelberg, Germany

Microglia-associated inflammation and miRNA dysregulation are key players in Alzheimer's disease (AD) pathophysiology. Previously, we showed miR-124 upregulation in APP Swedish SH-SY5Y (SWE) and PSEN1 iPSC-derived neurons and its propagation by the secretome (soluble and exosomal fractions). After modulation with miR-124 mimic/inhibitor, we identified common responsive mechanisms between such models. We also reported miR-124 colocalization with microglia in AD patient hippocampi. Herein, we determined how miR-124 modulation in SWE cells influences microglia polarized subtypes in the context of inflammation. We used a coculture system without cell-to-cell contact formed by miR-124 modulated SWE cells and human CHME3 microglia stimulated with interferon-gamma (IFNγ-MG), in which we assessed their adopted gene/miRNA profile and proteomic signature. The increase of miR-124 in SWE cells/secretome (soluble and exosomal) was mimicked in IFNγ-MG. Treatment of SWE cells with the miR-124 inhibitor led to RAGE overexpression and loss of neuronal viability, while the mimic caused RAGE/HMGB1 downregulation and prevented mitochondria membrane potential loss. When accessing the paracrine effects on microglia, SWE miR-124 inhibitor favored their IFNγ-induced inflammatory signature (upregulated RAGE/HMGB1/iNOS/IL-1β; downregulated IL-10/ARG-1), while the mimic reduced microglia activation (downregulated TNF-α/iNOS) and deactivated extracellular MMP-2/MMP-9 levels. Microglia proteomics identified 113 responsive proteins to SWE miR-124 levels, including a subgroup of 17 proteins involved in immune function/inflammation and/or miR-124 targets. A total of 72 proteins were downregulated (e.g., MAP2K6) and 21 upregulated (e.g., PAWR) by the mimic, while the inhibitor also upregulated 21 proteins and downregulated 17 (e.g., TGFB1, PAWR, and EFEMP1). Other targets were associated with neurodevelopmental mechanisms, synaptic function, and vesicular trafficking. To examine the source of miR-124 variations in microglia, we silenced the RNase III endonuclease Dicer1 to block miRNA canonical biogenesis. Despite this suppression, the coculture with SWE cells/exosomes still raised microglial miR-124 levels, evidencing miR-124 transfer from neurons to

OPEN ACCESS

**Edited by:**
*Morena Zusso, University of Padua, Italy*

**Reviewed by:**
*Stanley M. Stevens Jr, University of South Florida, United States*
*Imran Khan Mohammed, Indiana University, United States*

***Correspondence:**
*Dora Brites*
*dbrites@ff.ul.pt*

**Specialty section:**
*This article was submitted to Neuropharmacology, a section of the journal Frontiers in Pharmacology*

**Received:** *10 December 2021*
**Accepted:** *25 March 2022*
**Published:** *10 May 2022*

**Citation:**
*Garcia G, Fernandes A, Stein F and Brites D (2022) Protective Signature of IFNγ-Stimulated Microglia Relies on miR-124-3p Regulation From the Secretome Released by Mutant APP Swedish Neuronal Cells. Front. Pharmacol. 13:833066. doi: 10.3389/fphar.2022.833066*

microglia. This study is pioneer in elucidating that neuronal miR-124 reshapes microglia plasticity and in revealing the relevance of neuronal survival in mechanisms underlying inflammation in AD-associated neurodegeneration. These novel insights pave the way for the application of miRNA-based neuropharmacological strategies in AD whenever miRNA dysregulated levels are identified during patient stratification.

**Keywords: neuronal miR-124-3p mimic/inhibitor, IFNγ-primed CHME3 microglia, SH-SY5Y APPSwedish cell, inflammatory gene expression, mir-124-dependent microglia proteomic changes, MMP-2/MMP-9 deactivation, secretome/exosome (sEVs) paracrine signaling, miRNA-depleted microglia with siDicer1**

## 1 INTRODUCTION

Alzheimer's disease (AD) is the most prevalent neurodegenerative disorder in developed countries. The most common molecular hallmarks are extracellular β-amyloid (Aβ) plaques and neurofibrillary tangles of hyperphosphorylated tau protein. Besides, alterations in the neuroinflammatory status caused by dysregulated microglia are also reported in AD (Leng and Edison, 2021). Initially assumed to be excessively activated in response to amyloid deposition and neuronal dysfunction, evidence indicates that microglia actively participate in AD pathogenesis since disease early stages (Fan et al., 2017). The identification of new potential therapeutic microglial targets (Sierksma et al., 2020), as well as the classification of several microglial subtypes in health and disease (Uriarte Huarte et al., 2021), created new opportunities for immunomodulation-based strategies in opposition to previous approaches based on counteracting or inducing a unique phenotype (Deczkowska et al., 2018). However, the lack of translation from the bench to the clinic is still one of the most limiting factors for the success of drug development in AD (Vitek et al., 2020). Many studies rely on specific animal models, such as rodents, which do not entirely share the human disease pathophysiology. Despite not fully recapitulating the human disease and/or brain inflammation in a dish, human cell models are considered important steps toward AD mechanistic studies (Drummond and Wisniewski, 2017). In addition, though still controversial, another key point is to define which approach should be used in AD pathogenicity to reprogram microglia into protective and pro-regenerative phenotypes and in which context, disease stage, and patient subtypes should be applied.

miRNAs have gained increasing interest in the field of AD, emerging as potential biomarkers in several diseases, as their expression is altered in different patients, stages, and models (Fernandes et al., 2018; Kumar and Reddy, 2018; Brites, 2020; Garcia et al., 2021). By regulating hundreds of several targets in different cells and tissues, miRNA modulation may be a key strategy to counteract multifactorial and complex disorders, including neurodegenerative and cancer diseases (Saito and Saito, 2012). Specific miRNAs are known to regulate essential functions that are compromised in AD, such as neurite outgrowth and synaptic plasticity (Hu and Li, 2017; McGowan et al., 2018; Garcia et al., 2021), revealing their potential also as therapeutic targets. In particular, miR-124, as one of the most predominant cerebral miRNAs, was shown to be critically involved in multiple neuronal mechanisms, such as differentiation, axonal growth, synaptic function, and homeostasis maintenance (Sun et al., 2015; Xue et al., 2016; Yardeni et al., 2018), and to be dysregulated upon stress conditions (Sun et al., 2015). Though miR-124 is almost exclusively expressed by neurons (Åkerblom et al., 2012), we found miR-124 colocalization with microglia in hippocampal slices from Braak stage IV AD patients, together with a general miR-124 overexpression in whole hippocampal lysates that revealed significantly upregulated levels in Braak stage III patient postmortem samples (Brites, 2020). In contrast, accumulating studies demonstrate consistent benefits of miR-124 in microglia by triggering their pro-regenerative function (Ponomarev et al., 2011; Yu et al., 2017; Fumagalli et al., 2018). Together, these reports confirmed that miR-124 is closely involved in AD pathological processes and may play an important regulator role in microglial function. However, it is still unclarified if microglia are stimulated to overexpress miR-124 in a specific context or suffer the influence of miR-124 in the cell microenvironment.

The role of miR-124 in AD is still a matter of debate, with contradicting reports demonstrating increased (Wang et al., 2018) and decreased (An et al., 2017) levels in the disease and different perspectives about its *modus operandi*. It seems clear that miR-124 is a key player in AD (Sonntag et al., 2012), though its function may critically depend on the specific requirements of cell metabolism and the model used to recapitulate the condition (Garcia et al., 2021). Despite being able to control different AD hallmarks in SH-SY5Y cells constitutively expressing the APP Swedish form (SWE) and in neurons differentiated from induced pluripotent stem cells (iPSCs) generated from a patient with the PSEN1ΔE9 mutation, in such study, we showed that miR-124 was upregulated in both cell models and their derived exosomes (EXOs). Such findings support the potential of the SWE cell model to further explore the miR-124 dynamics in neuron-microglia cultures and investigate how it may contribute to microglia polarization/depolarization under an inflammatory condition. For instance, miR-124-loaded EXOs were revealed to attenuate microglia activation by cocaine (Chivero et al., 2020), supporting miRNA-based strategies as new delivery systems for therapeutic intervention in AD. Such small extracellular vesicles, herein identified as EXOs, are recognized as Aβ seeders and propagators of AD pathological mediators between brain regions (Eitan et al.,

2016; Yuyama and Igarashi, 2017). Moreover, EXOs are believed to act as paracrine vectors in miRNA specialized delivery to recover target cell function (Shirazi et al., 2021; Zheng et al., 2021). In that regard, we have previously shown that neuronal-derived EXOs carrying miR-124 modify microglia function and their immune properties (Pinto et al., 2017; Fernandes et al., 2018). This finding is not without precedent, since multiple therapeutic approaches using EXO-based delivery of miR-124 have been recently developed (Lee et al., 2017; Yang et al., 2017; Jiang et al., 2020).

In this study, we first validated increased miR-124 levels in the SWE cells when compared to SH-SY5Y (SH) counterparts. Then, we investigated how the miR-124 release by AD neuronal cells influenced microglia activation when both cells were in coculture. For that, we stimulated the human CHME-3 microglia with interferon-gamma (IFNγ), a well-known pro-inflammatory cytokine, reported to induce microglia activation in the AD context (Abbas et al., 2002; Mastrangelo et al., 2009; Belkhelfa et al., 2014). After establishing and characterizing the SWE-CHME3 cell coculture, we transfected SWE cells with the miR-124 inhibitor or the mimic to reduce or increase its expression levels, respectively. We monitored the consequences of downregulating and upregulating miR-124 in each of the cocultured cells and their secretome, with emphasis on inflammatory gene expression signature and the microglial proteomic profile. Finally, we assessed the neuron-microglia trafficking of miR-124, either in the coculture experiments or when incubating IFNγ-stimulated CHME-3 microglia with SWE-derived exosomes. Our results provide novel insights on neuronal miR-124 as a powerful neuro-immune regulator of microglia gene expression signature and highlight its modulation as representing a promising double-edge sword strategy in the AD field targeting both neurons and microglia.

# 2 MATERIALS AND METHODS

## 2.1 Culture and Differentiation of Human SH-SY5Y Neuronal Cell Lines

SH and SWE cells were a gift from Professor Anthony Turner (Belyaev et al., 2010). Cells were maintained in Dulbecco's Modified Eagle's Medium (DMEM) (Gibco, Thermo Fisher Scientific, Waltham, MA, United States), supplemented with 10% fetal bovine serum (FBS) and 2% AB/AM in T75 flasks under a humidified atmosphere with 5% $CO_2$, at 37°C, as we previously described (Fernandes et al., 2018; Garcia et al., 2021). For experiments, cells were seeded onto 12-well plates coated with poly-D-lysine (100 μg/ml, Sigma-Aldrich, St. Louis, MO, United States) and laminin (4 μg/ml, Gibco) at a final concentration of $5 \times 10^4$ cells per well, and differentiated with retinoic acid (RA) at the concentration of 10 μM, administered every day in fresh medium, until day 7 (Korecka et al., 2013; Garcia et al., 2021). Only for immunocytochemistry, cells were plated onto 12-well plates containing HCl-washed coverslips with the same poly-D-lysine/laminin coating described above.

## 2.2 Culture and Stimulation of Human CHME3 Microglia Cell Line

Human CHME3 microglial cells, also known as HMC3, were kindly provided by Professor Marc Tardieu (Janabi et al., 1995). Cells were cultured in T75 culture flasks in DMEM supplemented with 10% FBS, 2% AB/AM (Sigma-Aldrich) and 1% L-glutamine (L-glu) (Sigma-Aldrich) in a humidified atmosphere containing 5% $CO_2$, at 37°C, as usual in our lab (Fernandes et al., 2018). Medium was changed every other day. For experiments, cells were seeded onto 12-well non-coated plates, at a final concentration of $5 \times 10^4$ cells per well. To mimic microglia phenotypes in an inflammatory milieu we stimulated the cells with human IFNγ (BACHEM, Bubendorf, Switzerland) at 50 ng/ml during 2, 12, and 24 h.

## 2.3 Evaluation of Cell Viability by the Nexin Assay

In order to determine the viability of either neuroblastoma or microglial cells, both floating and adherent cells detached with trypsin were collected, mixed, and spun down at 500 g for 5 min. Then, pellets were resuspended in 1% bovine serum albumin (BSA) in PBS and stained with phycoerythrin-conjugated annexin V (V-PE) and 7-amino-actinomycin D (7-AAD), using the Guava Nexin Reagent® (Merck Millipore, Burlington, MA, United States). Stained cells were analyzed using a flow cytometer (Guava easyCyte 5 HT, Merck-Millipore), operated by Guava Nexin Software. Four cellular populations were distinguished: viable cells (annexin V-PE and 7-AAD double-negative), early apoptotic cells (annexin V-PE positive and 7-AAD negative), late apoptotic cells (annexin V-PE and 7-AAD double-positive), and necrotic cells/cellular debris (annexin V-PE negative and 7-AAD positive).

## 2.4 Isolation and Characterization of EXOs

Cells were cultured for 24 h in FBS-free medium to ensure sufficient EXO release and prevent the influence of FBS-associated EXOs. Cell culture media were collected from at least three independent experiments, and EXOs were isolated using the differential ultracentrifugation, as we previously described (Fernandes et al., 2018; Garcia et al., 2021). Briefly, equal volumes of cell media were promptly centrifuged at 1,000 g for 10 min to pellet cell debris. The supernatants were transferred into new tubes and centrifuged at 16,000 g for 1 h to pellet and discard large extracellular vesicles. The remaining supernatant containing EXOs was filtered through a 0.22 μm pore size membrane and centrifuged at 100,000 g for 2 h in an Ultra L-XP100 centrifuge (Beckman Coulter, Brea, CA, United States). The pellet was resuspended/washed in PBS and centrifuged once again at 100,000 g for 2 h. The pellet of EXOs was suspended in a 200 μl lysis buffer for RNA extraction with the miRCURY Isolation Kit-Cell to determine miRNA content

(Exiqon, Gill StreetWoburn, MA, United States). For the characterization of EXO markers by western blot, EXOs isolated from three independent experiments of 40 ml supernatants were pooled, suspended in 50 µl cell lysis buffer (Cell Signaling, Danvers, MA, United States), transferred into microtubes, snap-frozen, and stored at −80°C until analysis. Three characteristic markers of EXOs (ALIX, CD63, and flotillin) were assessed by western blot. For transmission electron microscopy (TEM), freshly isolated EXOs were suspended and kept in ice-cold PBS during 1–2 days until analysis. Then, equal volumes of freshly isolated EXO suspensions were dried onto freshly "glow discharged" 300 mesh formvar/carbon-coated TEM grids (Ted Pella, Redding, CA, United States), negatively stained with 2% aqueous uranyl acetate and observed under a JEOL JEM 1400 transmission electron microscope (JEOL Ltd., Tokyo, Japan) at an accelerating voltage of 120 kV. Images were digitally recorded using a Gatan SC 1100 ORIUS CCD camera (Gatan Inc., Warrendale, PA, United States). Round cup-shaped structures, ranging from 50 to 200 nm size, were considered as EXOs.

## 2.5 Determination of Soluble miRNAs and Cytokines/Chemokines

EXO-free cell media (depleted in EXOs after differential ultracentrifugation) were used to evaluate soluble miRNAs and cytokine/chemokine content. For miRNA determination, total RNA was extracted from the media using the miRNeasy Serum/Plasma kit (Qiagen, Venlo, Netherlands) according to the manufacturer's instructions and processed for RT-qPCR as detailed below. Concerning cytokine release, multiple cytokines and chemokines, including IL-1β, IL-8, IL-10, IL-18, TNF-α, and IL-6, were evaluated using the LEGENDplex multiplex immunoassay (BioLegend, San Diego, CA, United States), according to the manufacturer's instructions. Data were recorded on a Guava easyCyte 5 HT flow cytometer (Merck Millipore), operated by Guava Nexin Software, and further processed by LEGENDplex™ Data Analysis Software V8.0 (BioLegend, San Diego, California).

## 2.6 RNA Extraction and RT-qPCR

Total RNA was extracted from neuroblastoma and CHME3 cells using TRIzol® reagent (Life Technologies, Carlsbad, CA, United States), according to the manufacturer's instructions. Total RNA obtained from the cells, EXOs, and EXO-free cell media was quantified in Nanodrop® ND-100 Spectrophotometer (NanoDrop Technologies, Wilmington, DE, United States). In order to determine miRNA expression, equal amounts of RNA were reverse-transcribed into cDNA using the Universal cDNA Synthesis Kit (Qiagen). Then, miRNA expression was determined by RT-qPCR using the miRCURY LNA™ Universal RT miRNA PCR kit (Qiagen) with predesigned primers (**Supplementary Table S1**). Running conditions consisted of polymerase activation/denaturation and well-factor determination at 95°C for 10 min, followed by 50 amplification cycles at 95°C for 10 s and 60°C for 1 min (ramp-rate 1.6°C/s). In order to determine mRNA levels (gene expression), equal amounts of total RNA were reverse-transcribed into cDNA using the GRS cDNA Synthesis Master Mix kit (GRiSP, Porto, Portugal), and RT-qPCR was performed using Xpert Fast Sybr Blue (GRiSP) as a master mix with specific predesigned primers (**Supplementary Table S1**). Running conditions were as follows: 50°C for 2 min followed by 95°C for 2 min and finally 40 cycles at 95°C for 5 s and 62°C for 30 s. Both miRNA and mRNA RT-qPCRs were performed on a QuantStudio 7 Flex Real-Time PCR System (Applied Biosystems, Waltham, MA, United States). A melt-curve analysis was performed to verify amplification specificity immediately after the amplification protocol. Non-specific PCR products were not found. miRNA/gene expression data of at least four independewas inconsistentnt experiments were processed using the ΔΔCT method. Glyceraldehyde 3-phosphate dehydrogenase (GAPDH) was used as a reference gene for mRNAs because the β-actin expression was inconsistent upon miRNA modulation. For miRNA expression, U6 and spike-in were used as a reference miRNA and an internal standard, respectively. Results were normalized and expressed as $2^{-\Delta\Delta CT}$ (fold-change) and/or $\log_2$-transformed, as appropriate. All samples were quantified in duplicate and compared to respective controls, depending on the performed analysis.

## 2.7 Quantification of Nitrite Levels

Nitric oxide (NO) levels in CHME3 microglia culture supernatants were estimated by determining the concentration of nitrites ($NO_2$), the stable end-product generated from NO metabolism, using the Griess method, as previously published (Silva et al., 2011). Briefly, cell media was centrifuged at 15,000 *g* for 10 min to pellet cellular debris and mixed with the Griess reagent (1:1) in the 96-well tissue culture plates for 10 min, in the dark and at RT. A calibration curve was used for each assay. The absorbance at 540 nm was measured in duplicate samples, using a microplate reader, and the mean value used in the quantification.

## 2.8 Immunofluorescence, Image Acquisition, and Analysis

Cells were plated onto coverslips and cultured for the established periods of time. Then, cells were fixed with paraformaldehyde (4% w/v in PBS) for 20 min, washed with PBS, and permeabilized with Triton-X100 0.2% in PBS for 10 min. Blocking was performed with BSA at 3% in PBS for 30 min. F-actin was stained using AlexaFluor® 594 Phalloidin (1:100 in BSA 1% diluted in PBS, Thermo Fisher). As primary antibodies, mouse anti-iNOS (1:150) and/or mouse anti-MAP-2 (1:100) were used in separate experiments. As a secondary antibody, we used goat anti-mouse Alexa Fluor 488 (1:1,000). All antibodies were diluted in PBS containing 1% BSA. Then, coverslips were dipped in PBS for washing and incubated for 2 min with Hoechst 33258 dye diluted at 1:1,000 (BSA 1% in PBS) to stain nuclei. Excessive dye was removed by another PBS wash before coverslips were immersed in methanol and mounted on a glass slide with DPX mounting media. Fluorescence was recorded using an AxioScope A1 fluorescent microscope with an adapted camera AxioCam HRm (Zeiss, Oberkochen, Germany). Fluorescence

images of at least ten representative random microscopic fields were acquired (original magnification: ×400). A iNOS fluorescence intensity per cell, from a total of 600 cells, (iNOS) was assessed with Fiji software tools (Schindelin et al., 2012). Dendrite length of individual neurons was measured from the immunofluorescence images using MAP-2 dendritic marker and the NeuronJ plugin included in Fiji software, as indicated before (Garcia et al., 2021).

## 2.9 MitoTracker Active Mitochondria Labeling

In order to stain active mitochondria, cells were incubated for 30 min at 37°C with 500 nM of MitoTracker Red CMXRos, according to the manufacturer's instructions (Thermo Fisher Scientific). Then, they were fixed with 4% (w/v) paraformaldehyde, as described before (Garcia et al., 2021). Nuclei were stained with Hoechst 33,258 dye. Images were acquired, and total fluorescence intensity (FI) of the MitoTracker Red was assessed using Fiji software tools. Briefly, FI and cell area were automatically measured using (Analyze > Analyze Particles) with the options "area" and "integrated intensity" selected from the menu "set measurements." Then, the FI of MitoTracker Red intensity of more than 300 cells of each condition was normalized to the respective cell area.

## 2.10 Modulation of miR-124 Levels in Neuroblastoma SWE Cells

After 7 days of RA differentiation, SWE cells were changed to Optimem media (Gibco, Thermo Fisher) and transfected pre-miR-124-3p (mimic) and anti-miR-124-3p (inhibitor) (Ambion, Austin, TX, United States), each at 15 nM/well, in the presence of the transfection agent X-tremeGENE (100 μM) (Sigma-Aldrich), and cultured overnight. Mock transfected and negative controls (Scramble sequences provided by Ambion) for both mimic and inhibitor were equally performed in parallel under the same conditions. Transfection efficiency was ensured in each experiment after and before coculture. Because we observed that mock and negative controls produced identical results, only mock control was used as a reference to compare the effects of the mimic and the inhibitor in the next assays. For the isolation of EXOs, SWE cells were cultured in EXO-free FBS media for 24 h after transfection, before collection and secretome processing.

## 2.11 Neuroblastoma-Microglia Coculture

Both cells were initially cultured in separated 12-well plates at a final concentration of $5 \times 10^4$ cells per well to establish a coculture of SWE neurons with CHME3 microglia, followed by differentiation and miR-124 modulation with mimic and inhibitor (only in SWE cells), or IFNγ stimulation (only in CHME3 microglia). In the case of CHME3 microglia, cells were plated in wells containing HCl-washed coverslips with four small paraffin spacers on the outlined border and transferred into the 12-well plates containing the SWE cells to establish cocultures, as previously described by us (Fernandes et al., 2018). Because the CHME3 and SWE cells were separated by the paraffin spacers, this type of coculture setup avoids cell physical contact, but it still allows intercellular communication through the cell media. Similar approaches have been used in other studies for isolating different cell types from the same coculture showing no signs of cross-contamination (Phatnani et al., 2013; Wasilewski et al., 2022). Then, both cell types were cocultured during 2, 12, and 24 h in DMEM (Gibco, Thermo Fisher) with 1% FBS, 1% L-glutamine, and 2% AB/AM. Both CHME3-containing coverslips and SWE cells were separately processed for RNA/protein extraction immediately after each coculture period and selected time. The secretome (common to both cell types in the coculture) was immediately used for NO and matrix metalloproteinases (MMPs) determination, and the remaining media were frozen for further analysis.

## 2.12 Proteomics

### 2.12.1 Mass Spectrometric (MS) Analysis

Cellular lysates of three experimental conditions were collected in triplicate and analyzed for proteomic analysis: 1) CHME-3 microglia cocultured with the non-modulated (mock control) SWE cells; 2) CHME-3 microglia cocultured with the SWE cells treated with the miR-124 inhibitor; and 3) CHME-3 microglia cocultured with the SWE cells treated with the miR-124 mimic. The cellular lysates were collected in TRIzol® reagent (Life Technologies), and the protein fraction (denser) was isolated separately and immediately stored at −80°C. Total protein precipitation was performed by adding 10% trichloroacetic acid (TCA) to acetone, followed by three washing cycles with acetone containing 20 mM dithiothreitol (DTT) and centrifuged at 15,000 g for 10 min. The protein pellet was dissolved in a buffer containing 8 M urea, 1% SDS (1:1), and protease inhibitor (1:25) and resuspended by sonication, followed by centrifugation at 3,200 g for 10 min to remove insoluble particles. Thereafter, protein samples were sent for analysis at EMBL Proteomics Core Facility in Heidelberg, Germany. There, samples were subjected to an in-solution tryptic digest using a modified version of the Single-Pot Solid-Phase-enhanced Sample Preparation (SP3) protocol (Moggridge et al., 2018). Samples were added to Sera-Mag Beads (Thermo Fisher) suspended in 40 μl of a solution of 15% formic acid and ethanol solution (1:3, respectively). Protein binding was achieved by 15 min of shaking at RT, followed by SDS removal by washing four times with 200 μl of 70% ethanol. For digestion, proteins were left overnight at RT with 0.4 μg of sequencing grade modified trypsin (Promega, Madison, WI, United States) in 40 μl Hepes/NaOH, pH 8.4 in the presence of 1.25 mM TCEP and 5 mM chloroacetamide (Sigma-Aldrich). Beads were separated and washed with 10 μl of a 2% DMSO aqueous solution until the combined eluates were dried. Digested peptides were reconstituted in 10 μl of $H_2O$ and reacted for 1 h at RT with a TMT10plex (Thermo Fisher) label reagent (80 μg dissolved in 4 μl of acetonitrile) as previously described (Moggridge et al., 2018). TMT-labeled peptides were dried and reconstituted in 100 μl of 0.1% formic acid in H2O. After that, 5 μl (corresponding to 5% of the volume) was mixed with 5 μl of the other samples. Each sample was subjected to a reverse-phase clean-up step (OASIS) and then measured on our

Lumos system using a 1 h gradient. Calculated TMT ratios were used to adjust sample volumes to achieve a 1:1 ratio (mock controls: 127L, 127H; miR-124 inhibitor: 128H, 129L, and miR-124 mimic: 130L, 130H). The combined samples were subjected to a high pH offline fractionation yielding 12 fractions (Hughes et al., 2014), each of those analyzed on a 2 h gradient on Orbitrap Fusion Lumos mass spectrometer (Thermo Fisher). Peptides were separated using an UltiMate 3000 nano RSLC system (Dionex, Thermo Fisher) equipped with a trapping cartridge (Precolumn; C18 PepMap 100, 5 mm, 300 µm i.d. × 5 µm, 100 A˚) and an analytical column (ACCLAIM PEPMAP100 C18, 3 µm, 100 Å, 75 µm i.d. × 15 cm) connected to a nanospray-Flex ion source. The peptides were loaded onto the trap column (30 µl per min) using solvent A (0.1% formic acid) and eluted using a gradient from 2% to 40% Solvent B (0.1% formic acid in acetonitrile) during 2 h (0.3 µl per min). The Orbitrap Fusion Lumos was operated in a positive ion mode with a spray voltage of 2.4 kV and capillary temperature of 275˚C to analyze the peptides. MS spectra with a mass range of 375–1.500 m/z were acquired in profile mode using a resolution of 120,000 [maximum fill time of 50 ms or a maximum of $4 \times 10^5$ ions (automatic gain control, AGC)]. Fragmentation was triggered for 3 s cycle time for peptide-like features with charge states of 2–7 on the MS scan (data-dependent acquisition). Precursors were isolated using the quadrupole with a window of 0.7 m/z and fragmented with a normalized collision energy of 38. Fragment mass spectra were acquired in profile mode and a resolution of 30,000 in profile mode. The maximum fill time was set to 64 ms or an AGC target of $1 \times 10^5$ ions. Dynamic exclusion was set to 45 s.

### 2.12.2 Raw MS Data Processing and Analysis

MS data were analyzed using IsobarQuant (Franken et al., 2015), Mascot V2.4 (Matrix Science, London, United Kingdom) and a reverse UniProt FASTA Homo sapiens (UP000005640) database, including common contaminants. The following modifications were considered: carbamidomethyl (C, fixed), TMT10plex (K, fixed), acetyl (N-term, variable), oxidation (M, variable,) and TMT10plex (N-term, variable). Mass error tolerance for full scan MS spectra was set to 10 ppm and for MS/MS spectra to 0.02 Da. A maximum of two missed cleavages were allowed. A minimum of two unique peptides with a peptide length of at least seven amino acids and a false discovery rate below 0.01 was required on the peptide and protein level, as described (Savitski et al., 2015). From a total of 5,731 identified proteins, 3,785 proteins were quantified. The raw output files of IsobarQuant were processed using the R programming language (R Core Team, 2020). As a quality filter, we only considered proteins quantified with at least two unique peptides. Raw TMT reporter ion intensities ("signal_sum"-columns) were first corrected for batch effects using the "removeBatchEffect" function of the limma package (PMID: 25605792) and further normalized using variance stabilization normalization with the "vsn2" function of the vsn package (Huber et al., 2002). Proteins were tested for differential expression using the limma package (**Supplementary Datasheet 1**). The replicate information was added as a factor in the design matrix given as an argument to the "lmFit" function of limma. The *t*-value output of limma's "topTable" function was used as an input to the "fdrtool" function of the fdrtool package (PMID 18441,000) in order to estimate *p*-values and false discovery rates (fdr) (*q*-values were used). Data normalization for each replicate can be found in **Supplementary Figure S1**, while the relative expression profile of the full proteome dataset is presented in **Supplementary Figure S2** and listed in **Supplementary Datasheet 2**. Proteins were annotated as a hit with an fdr smaller 0.05 and a fold-change of at least 100% and as a candidate with an fdr below 20% and a fold-change of at least 50% (most significant results are presented in **Supplementary Table S2**). The full proteome dataset was classified based on cell component, biological process, and molecular function using Gene Ontology (GO) bioinformatic annotation tool PANTHER with the Overrepresentation Test (version 16.0, release 2020-12-01) (**Supplementary Datasheet 3**). Then, a second GO bioinformatic annotation was performed using the same parameters, but only for the most significant proteins (**Supplementary Table S3**). Homo sapiens GO database (DOI: 10.5281/zenodo.4495804) was used as a reference (Mi et al., 2021), with Fisher's exact test and Bonferroni correction for multiple testing. MS proteomics raw data have been deposited in the ProteomeXchange Consortium *via* the PRIDE database[1] (Perez-Riverol et al., 2019) partner repository with the dataset identifier PXD030315.

### 2.12.3 Construction of the miR-124 Targeting Networks

To create the inflammatory targeting network of miR-124, the subset of 17 differently expressed proteins in microglia, identified in the proteomic analysis and classified as associated with inflammation and innate immunity, were interrogated using the online platform miRNet (Chang et al., 2020). This tool is an open-source platform that comprises eleven miRNA-target prediction databases, including miRTarBase, TarBase, miRecords, SM2mir, Pharmaco-mir, mir2Disease, PhenomiR, StarBase, Epimir, miRDB, and miRanda, mainly focusing on miRNA-target interactions. After defining the interaction tables with hsa-miR-124-3p in the Network Builder menu, the target network was generated and adjusted in the Network Viewer menu, and an image of the generated network was saved. An integrative analysis was also performed in the miRnet.ca platform, using the full proteome dataset with the KEGG database for pathway enrichment through the hypergeometric algorithm for both miRNAs and proteomic data (**Supplementary Figure S3**).

## 2.13 Determination of MMP-2 and MMP-9 Activity by Gelatin Zymography

MMP-2 and MPP-9 activities were determined in the extracellular media of either SWE cells and CHME3 microglia monocultures or those of cocultures by performing an SDS-PAGE zymography using 0.1% gelatin-10% acrylamide gels,

[1]https://www.ebi.ac.uk/pride/archive/projects/PXD030315.

under non-denaturing conditions, as previously described (Cunha et al., 2016). After electrophoresis, gels were washed for 1 h with 50 mM Tris pH 7.4, containing 2.5% Triton-X100, 5 mM $CaCl_2$, and 1 μM $ZnCl_2$, to remove SDS and renature the MMP species. In order to promote gelatin digestion, gels were incubated in the developing buffer (50 mM Tris pH 7.4, 5 mM $CaCl_2$, and 1 μM $ZnCl_2$) at 37°C overnight. Then, gels were stained with 0.5% Coomassie Brilliant Blue R-250 (Sigma-Aldrich) and destained using 30% ethanol/10% acetic acid in $H_2O$ (v/v) to measure enzyme activity. Image acquisition of white bands on a blue background was performed in a ChemiDoc Imaging System (Bio-Rad, Hercules, CA, United States), and further relative quantification by Image Lab analysis software (Bio-Rad). Results are representative of at least three independent experiments.

## 2.14 Silencing Dicer1 in CHME3 Microglia With siRNAs

A pool of siRNAs targeting human Dicer1 was used to silence the Dicer1 expression in CHME3 microglia (SMARTpool: ON-TARGETplus DICER1 siRNA), purchased from Dharmacon®, Thermo Fisher. Briefly, Dicer1 siRNA and the transfection factor (X-tremeGENE, Sigma-Aldrich) were gently mixed in Optimem media (Gibco, Thermo Fisher) and incubated 10 min at RT until transfection. Then, the mixture was added to the cells to perform a final concentration of 50 nM for siRNAs and 100 μM for X-tremeGENE. Timepoints of 12, 24, 48, and 72 h after transfection were tested to select the best results. Dicer-1 inhibition was successfully achieved and confirmed by western blot, and miR-124 silencing validated by RT-qPCR.

## 2.15 Protein Extraction, Quantification, and Western Blot

For western blot analysis, cells and/or EXOs were suspended in cell lysis buffer (Cell Signaling), snap-frozen, and stored at −80°C until use. Protein concentration was measured using BCA Protein Assay Kit (Pierce Biotechnology, Waltham, MA, United States), and equal amounts of protein (30 μg for EXOs and 40 μg for cells) were separated using Tris-Tricine gel, transferred into nitrocellulose membranes (Amersham, Health, Buckinghamshire, United Kingdom), and incubated in blocking buffer [5% (w/v) non-fat dried milk in Tween 20 (0.1%) tween-tris buffer saline (T-TBS)] at RT for 1 h. Membranes were incubated at 4°C overnight with the following primary antibodies diluted in blocking buffer: mouse anti-ALIX (1:1,000, Cell Signaling); goat anti-CD63 (1:1,000, Santa Cruz Biotechnology, Dallas, TX, United States); mouse anti-flotillin-1 (1:1,000, BD Biosciences); rabbit anti-Dicer (1:1,000, Cell Signaling); and mouse anti-β-actin (1: 2,000, Sigma-Aldrich). Then, membranes were incubated with respective HRP-conjugated secondary antibodies also diluted in blocking buffer at room temperature for 1 h: goat anti-mouse (1:2,000); rabbit anti-goat (1:2,000); and goat-anti-rabbit (1:2,000) all from Santa Cruz Biotechnology. WesternBright Sirius® (Advansta, San Jose, CA, United States) was used as chemiluminescent substrate and signal acquired in ChemiDoc Imaging System (Bio-Rad). For relative densitometric analysis of protein bands, the Image Lab analysis software (Bio-Rad) was used.

## 2.16 EXO-Labeling With PKH67 and Incubation With CHME3 Microglia

Freshly isolated EXOs were labeled with the PKH67 Fluorescent Linker Kit (Sigma-Aldrich) to monitor the uptake of SWE-derived EXOs by CHME3 microglia, according to the manufacturer's instructions as we published previously (Pinto et al., 2017). CHME3 microglia were incubated for 24 h with PKH67-labeled EXOs suspended in fresh DMEM supplemented with 1% AB/AM. Cell fixation, additional staining, and fluorescence acquisition/analysis were performed as described above.

## 2.17 Statistical Analysis

Results of at least three independent experiments are presented as mean ± SD. Single comparisons between two conditions were done by Student's *t*-test. In contrast, comparisons between multiple cells/conditions were accomplished by one-way ANOVA, with Bonferroni *post hoc* for multiple comparisons test. Statistical analysis was performed using GraphPad Prism 9 (GraphPad Software Inc., San Diego, CA, United States). Only *p*-values lower than 0.05 were considered statistically significant.

# 3 RESULTS

## 3.1 Upregulation of miR-124 in SWE Cells/EXOs/EXO-Free Secretome Has No Consequences on Cell Viability or Release of Inflammatory miRNAs and Cytokines

We started this study by isolating EXOs from both SH and SWE cells after 24 h incubation, by sequential ultracentrifugation, as we previously described (Fernandes et al., 2018; Garcia et al., 2021). After confirming their round shape surface morphology by TEM, and the presence of the typical EXO-associated markers ALIX, CD63, and flotillin-1 by western blot (**Supplementary Figure S5**), we compared the levels of miR-124 in both SH and SWE cells, as well as in their EXOs and EXO-free secretomes, as schematized in **Figure 1A**. The SWE cells revealed upregulated miR-124, in either cells or in their secretome fractions ($p < 0.05$; **Figure 1B**). Curiously, such increased miR-124 levels in SWE cells, leading to dissemination by the secretome fractions, was not reflected in changes of neuronal cell viability when compared to SH controls (**Figure 1C**), confirming our previous studies (Fernandes et al., 2018). Likewise, no changes were produced, in either inflammatory-associated miRNAs (inflamma-miRNAs), such as miR-146a-5p and miR-155-5p (**Figure 1D**), or

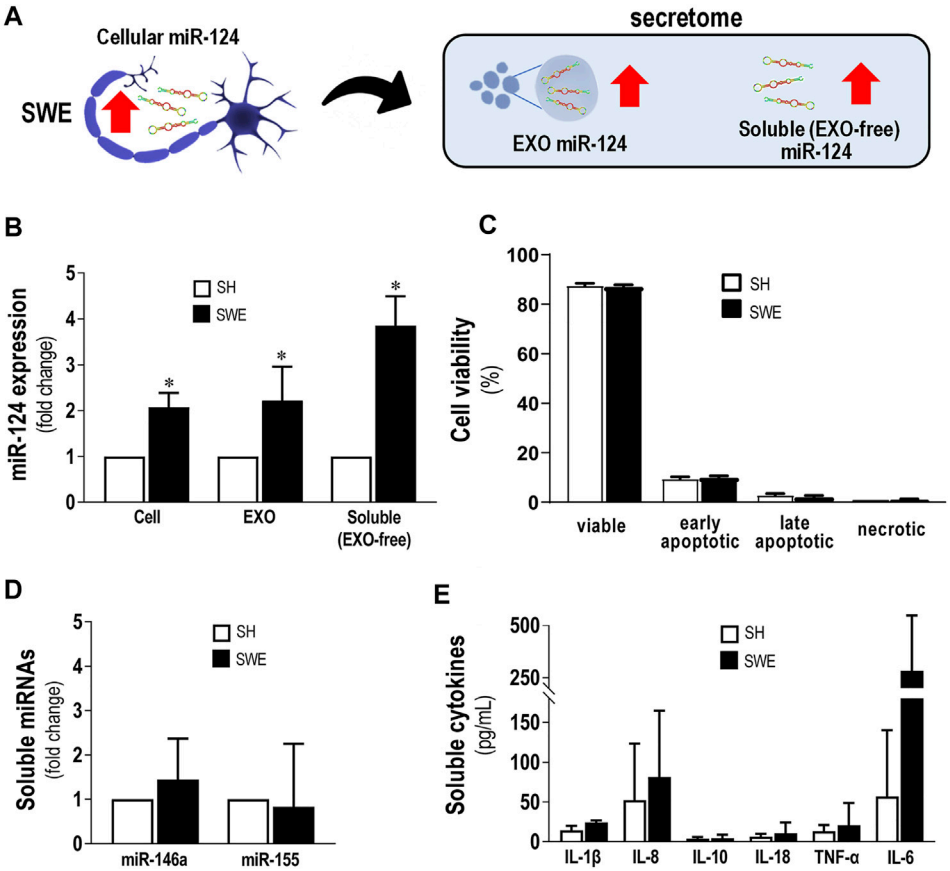


**FIGURE 1 |** Upregulated levels of miR-124 in SWE cells do not modify cell viability or secretion of inflammatory miRNAs and cytokines. Cells were differentiated using 10 μM retinoic acid for 7 days before experiments, as described in the *Materials and Methods* section. **(A)** Schematic representation of miR-124 increase in SWE cells and their secretome, including both exosomal (EXOs) and exosome-free (EXO-free, soluble) fractions. **(B)** Cellular miR-124 expression in SH and SWE cells and their respective EXOs and EXO-free secretome. **(C)** SH and SWE cell viability by the Nexin flow cytometry assay. Four cell populations were distinguished: viable (V-PE and 7-AAD double-negative), early apoptotic (V-PE positive and 7-AAD negative), late apoptotic (V-PE and 7-AAD double-positive), and necrotic cells/cellular debris (V-PE negative and 7-AAD positive). **(D)** Levels of miR-146a and miR-155 in secretomes from SH and SWE cells. **(E)** Profile of inflammatory-associated cytokine levels in the EXO-free secretomes from SH and SWE cells using the LEGENDplex flow cytometry assay. Results are mean ± SD from at least three independent experiments. *$p < 0.05$ *vs*. SH levels, two-tailed Student's *t*-test. miR, miRNA; SH, human SH-SY5Y wild-type neurons; SWE, human SH-SY5Y expressing the APP695 Swedish mutant protein; EXO, Exosomes; IL, interleukin; TNF-α, tumor necrosis factor α.

inflammatory cytokines, such as IL-1β, IL-8, IL-10, IL-18, TNF-α, and IL-6, despite the non-significant elevation observed (**Figure 1E**). In summary, from all the evaluated cellular and extracellular markers, only miR-124 was consistently altered in SWE cells and in their secretome compared to SH counterparts.

Considering the reports on miR-124 properties over microglia immune function (Ponomarev et al., 2011; Yu et al., 2017; Fumagalli et al., 2018), we became interested in investigating whether such increased miR-124 release by SWE cells would have beneficial or harmful effects on the neuro-immune properties of activated microglial cells. For that purpose, we next used the human CHME3 microglia cell line stimulated with IFNγ and evaluated their inflammatory signature, in order to later assess changes induced upon the SWE-CHME3 cocultures.

## 3.2 IFNγ-Treated Microglia (IFNγ-MG) Show a Typical Pro-Inflammatory Profile With Increased Nitrosative Activity and Upregulation of Inflammatory Genes/miRNAs

Significant IFNγ levels were previously identified in AD patients, from mild to severe stages (Belkhelfa et al., 2014). IFNγ has been indicated to be involved in microglia reactivity to Aβ (Meda et al., 1995) and to cause the production of inflammatory cytokines (Abbas et al., 2002; Rock et al., 2005). Herein, we established a human model of activated microglia using the CHME3 human microglia cell line and the stimulation with 50 ng/ml of IFNγ (IFNγ-MG) for 12 and 24 h, as previously described (Spencer et al., 2016). Next, we evaluated iNOS

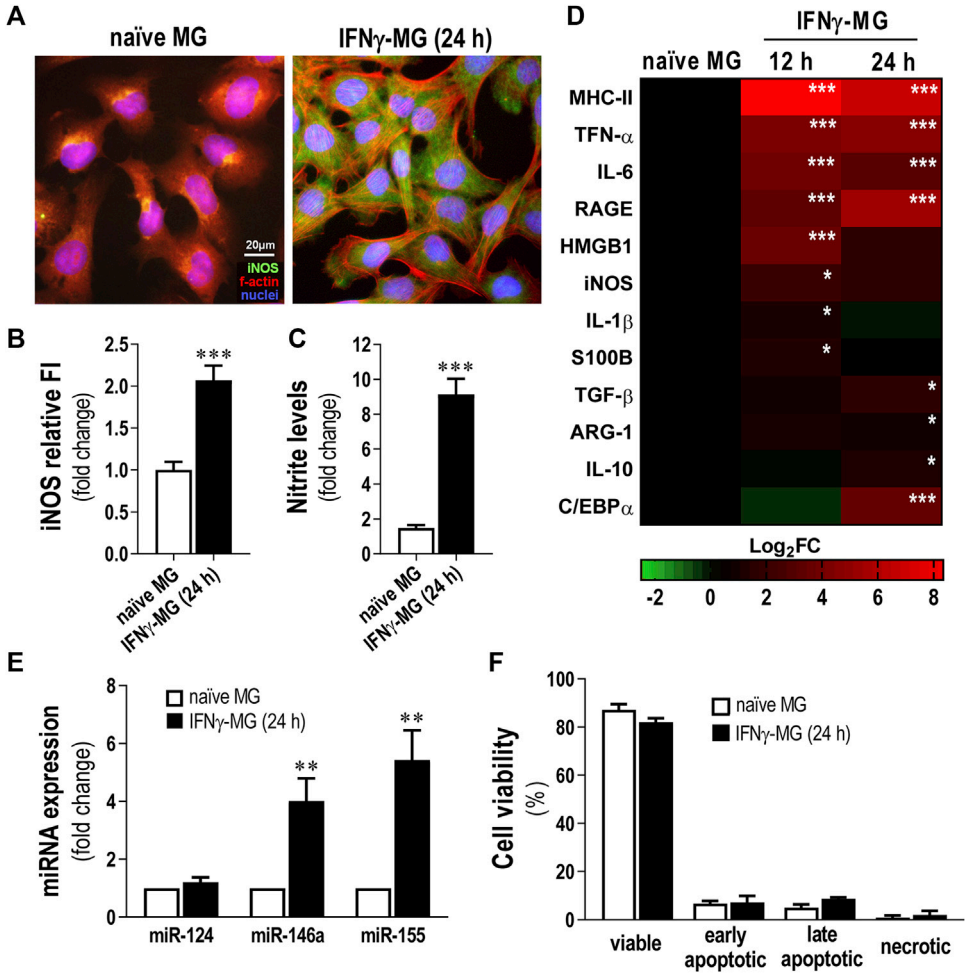


**FIGURE 2 |** Reactive profile of CHME3 human microglia upon stimulation with IFNγ. Human microglia CHME3 were either non-treated (naïve) or stimulated with IFNγ for 12 h or 24 h and assessed for several biomarkers, as indicated in the *Materials and Methods* Section. **(A)** Representative fluorescence images of microglial iNOS (green) and f-actin (red). Cell nuclei are stained with Hoechst 33258 dye (blue). **(B)** Quantification of iNOS relative cell fluorescence intensity (FI). **(C)** Evaluation of nitrite accumulation in the cell media. **(D)** Heatmap representation of inflammatory-associated genes in microglia after 12 and 24 h of IFNγ stimulation. **(E)** Expression levels of the miRNAs associated with inflammation. **(F)** Microglia viability by Nexin flow cytometry assay. Four cell populations were distinguished: viable (V-PE and 7-AAD double-negative), early apoptotic (V-PE positive and 7-AAD negative), late apoptotic (V-PE and 7-AAD double-positive), and necrotic cells/cellular debris (V-PE negative and 7-AAD positive). Results are mean ± SD from at least three independent experiments. $^{**}p < 0.01$ and $^{***}p < 0.001$ *vs*. naïve MG, two-tailed Student's *t*-test. MG; CHME3 human microglia cells; IFNγ-MG, IFNγ-stimulated CHME3 human microglia cells; f-actin, filamentous-actin; iNOS, inducible nitric oxide synthase; miR, miRNA; h, hours; MHC-II, major histocompatibility complex–class II; TNF-α, tumor necrosis factor α; IL, interleukin; RAGE, receptor for advanced glycation end products; HMGB1, high mobility group box protein 1; S100B, S100 calcium-binding protein B; TGF-β, transforming growth factor β; ARG-1, arginase-1; C/EBPα, CCAAT enhancer binding protein α.

immunostaining, monitored nitrite release, and analyzed inflammatory gene expression (**Figures 2A–D**). We also assessed the expression levels of miR-124, as well as of miR-146a and miR-155 in IFNγ-MG, considering their neuro-immune relevance that we previously explored (Fernandes et al., 2018; Garcia et al., 2021) (**Figure 2E**). Evaluation of microglia viability upon IFNγ stimulus was also examined (**Figure 2F**). We confirmed the release of EXOs into the secretome and the presence of their usual protein markers after incubation with IFNγ (**Supplementary Figure S5**). Our results showed that IFNγ promotes inflammatory polarization of CHME3 microglia, noticed by the increase in iNOS immunofluorescence intensity ($p < 0.001$, **Figure 2B**) and the six-fold elevation of nitrite accumulation in the cell media at the same timepoint ($p < 0.001$, **Figure 2C**).

Regarding inflammatory gene expression, IFNγ induced significant overexpression of Major histocompatibility complex (MHC)-II, TNF-α, IL-6, and RAGE ($p < 0.001$), either after 12 or 24 h of stimulation (**Figure 2D**). Other inflammatory genes such as HMGB1 and iNOS peaked after 12 h of treatment with IFNγ ($p < 0.001$ and $p < 0.05$, respectively). On the contrary, genes involved in the pro-regenerative microglial polarization, as TGF-β and IL-10,

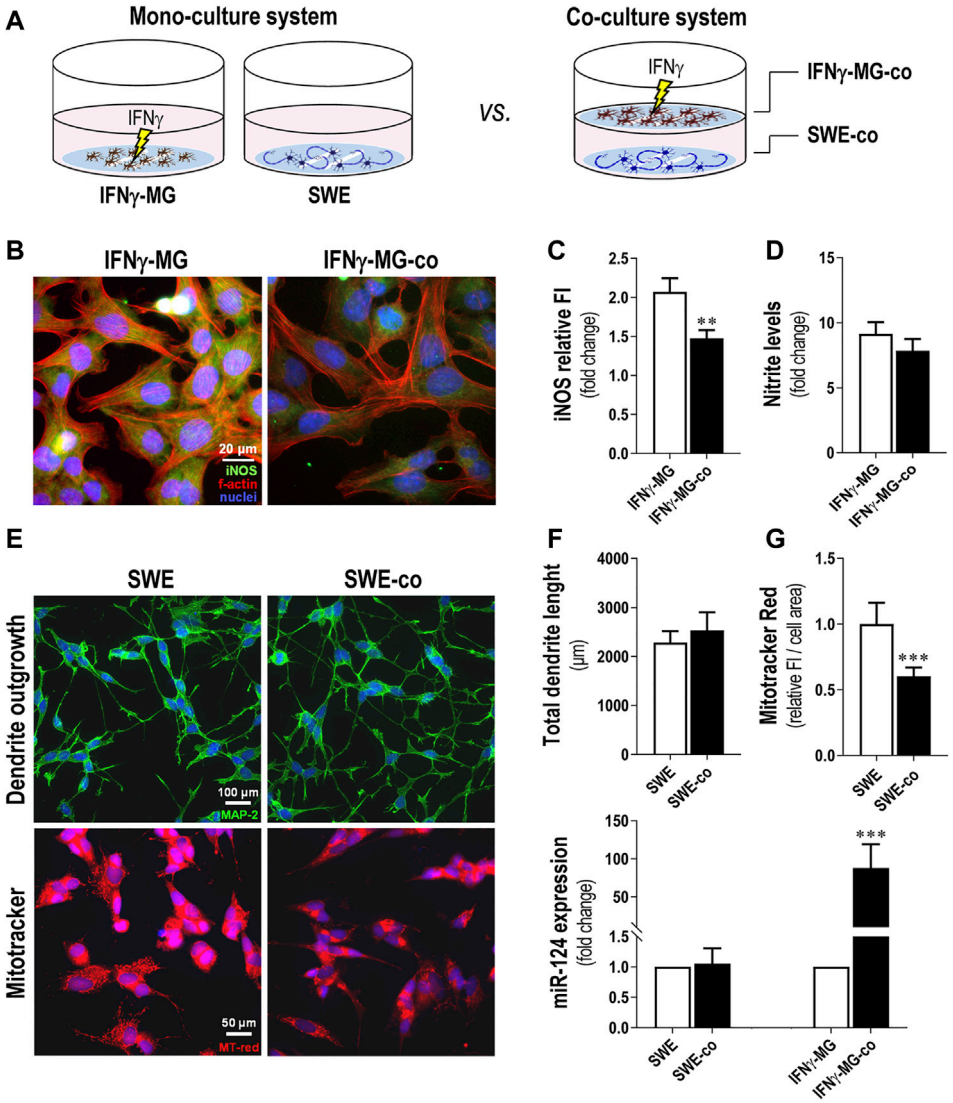


**FIGURE 3 |** Coculture of IFNγ-MG with SWE cells reduces neuronal MitoTracker intensity, while increasing microglial iNOS immunostaining and miR-124 expression levels. SWE cells were differentiated using 10 µM retinoic acid for 7 days before experiments, and CHME3 microglia were pretreated with IFN-γ for 24 h before coculture, as detailed in the *Materials and Methods* section. **(A)** Schematic representation of the coculture establishment. **(B)** Representative fluorescence images of iNOS (green) and f-actin (red) in MG monocultures and cocultures with SWE cells. Cell nuclei were stained with Hoechst 33258 dye (blue). **(C)** Comparison of MG-iNOS relative fluorescence intensity (FI) and **(D)** nitrite accumulation in the cell media when in the monocultures and coculture system with the SWE cells. **(E)** Representative fluorescence images of MAP-2 (green) and MitoTracker (red) in MG monocultures and cocultures with SWE cells. **(F)** Comparison of total dendrite length and **(G)** MitoTracker fluorescence intensity when in the monocultures and the coculture system with the SWE cells. **(H)** Comparison of the miR-124 expression levels in SWE and CHME3 cells monocultures *vs*. cocultures. Results are mean ± SD, obtained from at least three independent experiments. $^{**}p < 0.01$ and $^{***}p < 0.001$ *vs*. respective monocultured cells, two-tailed Student's *t*-test. MG, CHME3 human microglia cells; IFNγ-MG, IFNγ-stimulated CHME3 human microglia cells; SWE, human SH-SY5Y cells expressing the APP695 Swedish mutant protein; co, cocultures; iNOS, inducible nitric oxide synthase; miR, miRNA.

only peaked ($p < 0.01$ and $p < 0.05$, respectively) after 24 h of IFNγ stimulation. In addition, we evaluated the transcription of C/EBPα, which, apart from being a marker of disease-associated microglia contributing to caspase activation and apoptosis (Pan et al., 2013), also constitutes a target of miR-124 in microglia (Ponomarev et al., 2011). We found that C/EBPα was overexpressed after 24 h of IFNγ treatment ($p < 0.001$), suggesting such a timepoint as the most adequate to further evaluate the effects of the SWE-derived miR-124 in coculture. Concerning the miRNA signature, while miR-146a and miR-155 were highly boosted ($p < 0.01$ for both) in IFNγ-MG, miR-124 levels did not change from those found in naïve microglia (**Figure 2E**). Despite the pro-inflammatory profile of IFNγ-MG, our results demonstrated that even after 24 h of IFNγ stimulation, CHME3 viability was not significantly affected (**Figure 2F**), validating the use of such stimulation period in subsequent studies.

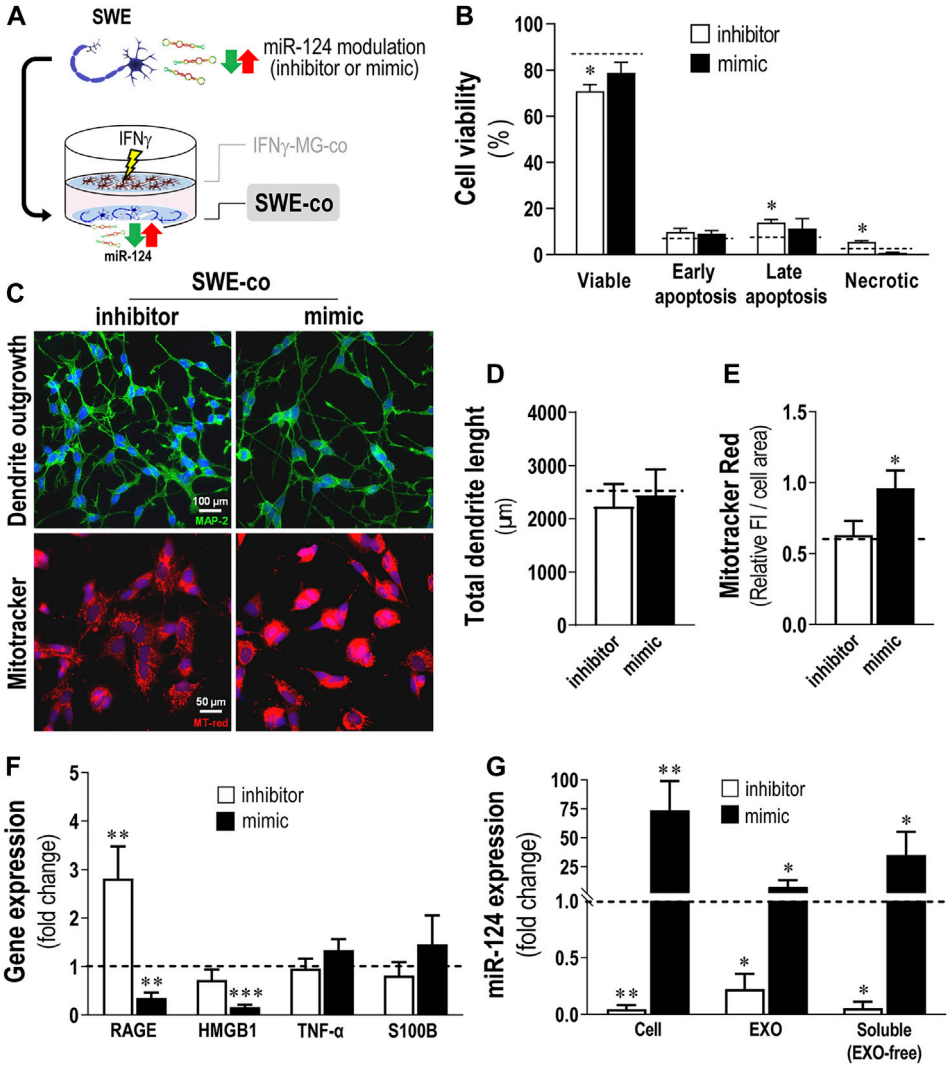


**FIGURE 4 |** Inhibition of miR-124 in SWE cells increases cell death and RAGE gene expression, while the mimic enhances MitoTracker Red intensity and miR-124 cargo in cells and their secretomes, together with a reduction of stress-associated genes, upon coculture with IFNγ-MG. After differentiation, SWE cells were transfected with miR124 inhibitor and mimic, while CHME3 microglia (MG) were treated with IFNγ for 24 h before coculture (IFNγ-MG), as detailed in *Materials and Methods*. **(A)** Schematic representation of the miR-124 modulation, followed by the coculture establishment with IFNγ-MG. **(B)** Cell viability of SWE cells in coculture with IFNγ-MG, assessed by Nexin flow cytometry assay. Four cell populations were distinguished: viable (V-PE and 7-AAD double-negative), early apoptotic (V-PE positive and 7-AAD negative), late apoptotic (V-PE and 7-AAD double-positive), and necrotic cells/cellular debris (V-PE negative and 7-AAD positive). **(C)** Representative fluorescence images of MAP-2 (green) and MitoTracker (red) in SWE cells upon coculture with IFNγ-MG, **(D)** respective evaluation of total dendrite length, and **(E)** quantification of MitoTracker fluorescence intensity (FI). **(F)** Inflammation-associated gene expression levels in SWE cells upon coculture with IFNγ-MG. **(G)** Quantification of miR-124 expression levels in SWE cell monocultures, as well as exosomes (EXOs) and exosome-free (EXO-free, soluble) secretome, 24 h after transfection with the miR-124 inhibitor and mimic *vs*. respective mock controls (dashed line). Results are mean ± SD from at least three independent experiments. $^{*}p < 0.05$, $^{**}p < 0.01$, and $^{***}p < 0.001$ *vs*. mock control (dashed line), one-way ANOVA with the Bonferroni *post hoc* test. SWE, human SH-SY5Y expressing the APP695 Swedish mutant protein; IFNγ-MG, IFNγ-stimulated CHME3 human microglia cells; co, cocultured; miR, miRNA; RAGE, receptor for advanced glycation end products; HMGB1, high mobility group box 1; TNF-α, tumor necrosis; S100B, S100 calcium-binding protein B; EXO, exosomes.

## 3.3 Elevated miR-124 Levels in SWE Cells Determine their Enrichment in IFNγ-MG and Reduce Microglial Nitrosative Activity and Neuronal Mitochondrial Membrane Potential

After characterization of the microglia response to IFNγ, we established a neuronal-microglia coculture with SWE neuroblastoma cells and IFNγ-MG, using the same procedure we previously described (Fernandes et al., 2018). The IFNγ stimulation of microglia was performed during the monoculture and before the coculture with the SWE cells. Therefore, we compared the effects of the cocultures *versus* the monocultures for each cell type, that is SWE and IFNγ-MG cells, as schematized in **Figure 3A**. We noticed that iNOS immunostaining in the IFNγ-MG after the coculture with the

SWE cells (IFNγ-MG-co) was significantly inhibited ($p < 0.01$) when compared with their monocultures (**Figures 3B,C**). Even so, such an effect was not enough to be translated into a significant reduction in the nitrite accumulation, only slightly reduced (**Figure 3D**). SWE cells were also affected by the presence of IFNγ-MG. Despite no alterations in the total dendrite length (**Figure 3E**, top panels, **Figure 3F**), we observed a marked decline ($p < 0.001$) in MitoTracker Red intensity when SWE cells were cocultured with IFNγ-MG (SWE-co) relatively to those in monoculture (**Figure 3E**, bottom panels, **Figure 3G**), suggesting a metabolic shift by the presence of IFNγ-MG cells.

To investigate if miR-124 modified neuron-microglia dynamics, we compared the miR-124 expression levels in both SWE-co and IFNγ-MG-co *versus* the respective monocultured counterparts (**Figure 3H**). Intriguingly, results indicate that while the miR-124 levels in SWE cells remained unchanged regardless of IFNγ-MG presence, the microglial miR-124 levels were highly boosted (nearly 90-fold, $p < 0.001$) in the presence of SWE cells *versus* the IFNγ-MG monocultures. Such data suggest the involvement of neuronal cells in the regulation of miR-124 levels in microglia.

## 3.4 miR-124 Inhibitor Promotes SWE Cell Demise and RAGE Overexpression, While the Mimic Reduces Neuronal Stress Biomarkers, With the Corresponding miR-124 Levels Being Recapitulated in the Secretome

To evaluate the consequences of changing the miR-124 expression levels in the SWE cells when in coculture with IFNγ-MG, we used the neuronal transfection with the miR-124 inhibitor and mimic (**Figure 4A**). Viability of SWE-co after 24 h was slightly but significantly decreased by the miR-124 inhibitor (**Figure 4B**; $p < 0.05$), with late apoptotic and necrotic increased events ($p < 0.05$). Such cytotoxic effect upon miR-124 inhibition was triggered by the presence of IFNγ-MG because no cytotoxic effects were previously detected in SWE monocultures (Garcia et al., 2021).

Many reports support that miR-124 is deeply involved in the regulation of dendrite outgrowth (Yu et al., 2008; Xue et al., 2016; Garcia et al., 2021). In addition, miR-124 was described as a master regulator of neuronal mitochondria activity and localization (Yardeni et al., 2018), capable of inhibiting mitochondrial apoptotic pathways (Xu et al., 2019). Herein, we evaluated how different levels of miR-124 affected the dendrite outgrowth and MitoTracker intensity in SWE-co cells after exposure to IFNγ-MG. Unexpectedly, no significant changes were observed in the total dendrite length, with either the inhibition or the overexpression of miR-124 (**Figure 4C**, top panels, **Figure 4D**). However, our results showed a significant boost in the MitoTracker Red intensity upon the miR-124 mimic *versus* mock control (dashed line) but no changes upon the inhibitor ($p < 0.05$, **Figure 4C**, bottom panels, **Figure 4E**). Remarkably, such upregulation of miR-124 by the mimic led to a recovery of the MitoTracker intensity (shown to be decreased with the coculture, see **Figure 3G**), reestablishing the original values observed in the SWE monocultures.

These effects of miR-124 over the mitochondrial activity of SWE-co cells revealed a potential role also in the neuron-microglia oxidative signaling, which is intrinsically associated with inflammation (Chen et al., 2012; Zarrouk et al., 2012). To explore such a link, we selected a subset of inflammatory-associated genes that we previously identified to be upregulated in SWE cells (Fernandes et al., 2018) and evaluated their expression upon miR-124 modulation (**Figure 4F**). Indeed, results indicate that different miR-124 levels promote disparate effects on SWE-co cells, with the inhibitor inducing RAGE overexpression ($p < 0.01$) and the mimic repressing the expression of both RAGE ($p < 0.01$) and its ligand HMGB1 ($p < 0.001$). Despite the tendency to increase upon the miR-124 mimic, neuronal TNF-α and S100B were not significantly affected by the miR-124 modulation.

Besides confirming the miR-124 modulation consequences in the SWE-co cells, we also assessed whether it was reflected in their EXOs and EXO-free secretome fractions (**Figure 4G**). SWE-co cells showed an impressive reduction of 95% with the inhibitor, while the mimic caused a 70-fold increase in miR-124 levels ($p < 0.01$, **Figure 4G**). Such cellular decrease/increase of miR-124 levels was recapitulated in SWE-co EXOs and EXO-free secretome ($p < 0.05$, in both), confirming a passive diffusion of the neuronal miR-124 into the secretome, previously reported by us (Garcia et al., 2021). In brief, we showed that miR-124 modulation influences SWE-co cell viability, mitochondria dynamics, RAGE-HMGB1 axis, and the amount of miR-124 released into EXOs and EXO-free secretome. Next, we intended to explore the paracrine consequences of modulating neuronal miR-124 levels for IFNγ-MG-co cells.

## 3.5 miR-124-Loaded SWE Cells Regulate the Activation State of IFNγ-MG, While miR-124 Depletion Further Enhances Cell Reactivity, Inflammatory Genes, and miRNAs

In this section, we deeply investigated the consequences of IFNγ-MG of inhibiting/overexpressing miR-124 levels in SWE cells (**Figure 5A**). First, we analyzed the effects on nitrosative activity, which showed no alterations in microglia iNOS immunostaining, despite the significant reduction in nitric oxide (NO) production upon miR-124 mimic modulation (**Figure 5B**, $p < 0.01$). Such NO reduction indicates a direct consequence of neuronal miR-124 overexpression on IFNγ-MG immune properties, previously explored (Ponomarev et al., 2011).

Then, we analyzed the expression of a set of inflammation-associated genes and miRNAs in IFNγ-MG after coculture with SWE cells treated with an inhibitor/mimic of miR-124 (**Figure 5C**). Results confirmed the influence of neuronal miR-124 changes by the inhibitor and mimic on the microglia disparate gene expression profiles. The paracrine signaling by SWE miR-124 inhibition led to microglial overexpression of RAGE ($p < 0.01$), as well as of HMGB1, iNOS, and IL-1β ($p < 0.001$), while repressing microglial IL-10 and ARG-1 gene expression levels ($p < 0.001$), thus hampering pro-resolving

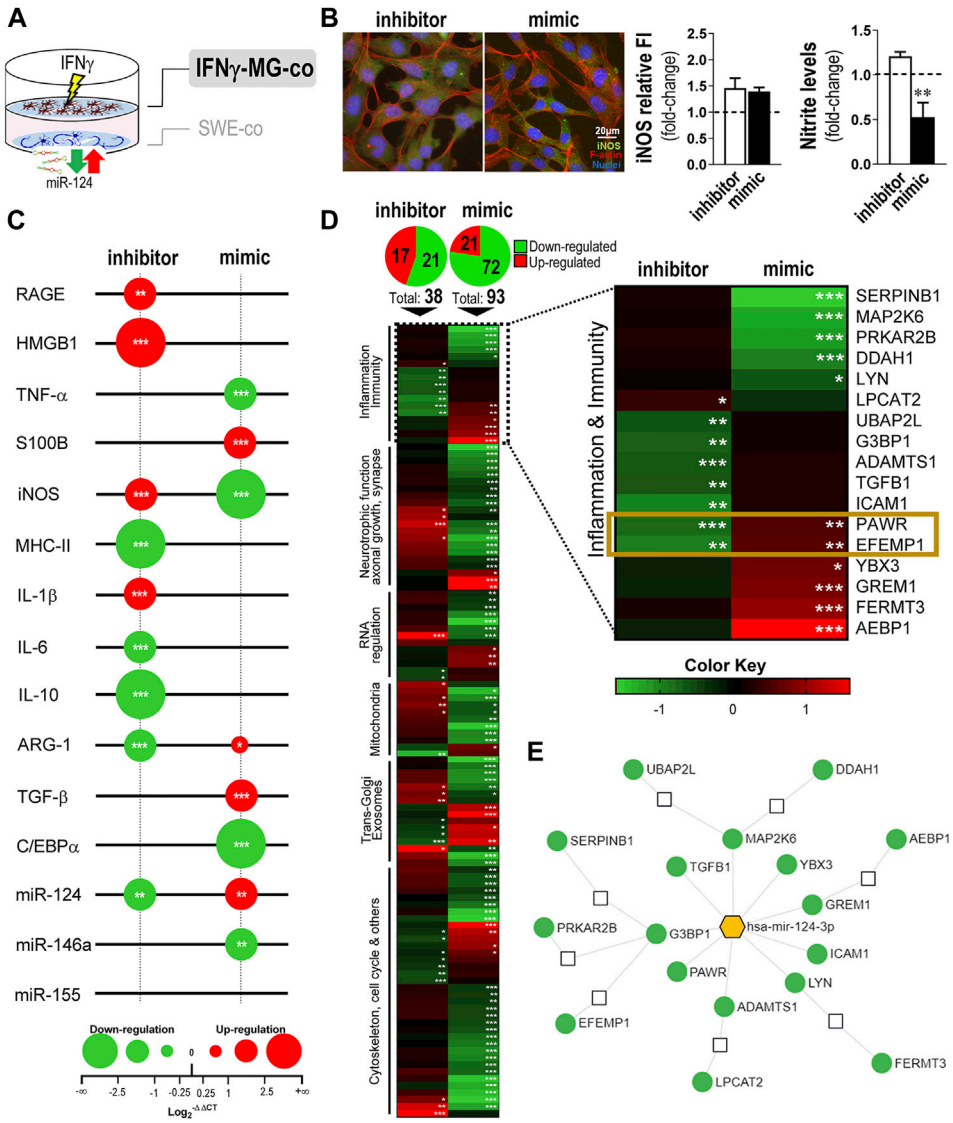


**FIGURE 5 |** Modulation of miR-124 expression levels in SWE cells changes the reactive and proteomic profile in human IFNγ-MG upon established cocultures. After differentiation, SWE cells were transfected with miR124 inhibitor and mimic, while CHME3 microglia were pre-treated with IFNγ for 24 h (IFNγ-MG) before the coculture, as detailed in *Materials and Methods*. **(A)** Schematic representation of the SWE/IFNγ-MG coculture and subsequent indication on microglia effects. **(B)** Representative fluorescence intensity (FI) of iNOS (green) and f-actin (red) in IFNγ-MG cells with quantifications of iNOS relative to FI and nitrite accumulation in cell media, right. Nuclei were stained with Hoechst 33258 dye (blue). **(C)** Bubble plot showing the changes in inflammatory-associated gene/miRNA expression of IFNγ-MG after coculture with inhibitor- and mimic-treated SWE cells. The color of the bubbles indicates downregulated genes (green) or upregulated genes (red), and the size represents the magnitude of each down/upregulation. **(D)** Heatmap representation of 117 proteins identified and quantified by mass spectrometry-based proteomic analysis of IFNγ-MG cells cocultured with SWE (inhibitor *vs*. mimic). A subset of 17 proteins related to innate function and inflammation was highlighted based on their Gene Ontology (GO) classification. Colors indicate downregulated proteins (green) or upregulated proteins (red), and the intensity of each color represents the relative abundance of the indicated protein. Significant proteomic data are detailed in **Supplementary Table S2**. **(E)** Targeting network of miR-124 for each of the 17 highlighted proteins, created in the "miRnet.ca" platform. Results are mean ± SD from at least three independent experiments. $^{*}p < 0.05$, $^{**}p < 0.01$, and $^{***}p < 0.001$ *vs*. IFNγ-MG cocultured with SWE mock control, one-way ANOVA with the Bonferroni *post hoc* test. SWE, human SH-SY5Y expressing the APP695 Swedish mutant protein; MG, CHME3 human microglia cells; IFNγ-MG, IFNγ-stimulated CHME3 human microglia cells; co, cocultured; miR, miRNA; f-actin, filamentous-actin; iNOS, inducible nitric oxide synthase; RAGE, receptor for advanced glycation end products; HMGB1, high mobility group box protein 1; TNF-α, tumor necrosis factor α; S100B, S100 calcium-binding protein B; iNOS, inducible nitric oxide synthase; MHC-II, major histocompatibility complex–class II; IL, interleukin; ARG-1, arginase-1; TGF-β, transforming growth factor β; C/EBPα, CCAAT enhancer binding protein α.

cascades. In contrast, SWE miR-124 upregulation by the mimic inhibited the microglial expression of TNF-α and iNOS, disrupting part of the pro-inflammatory signature stimulated by IFNγ, described in **Figure 2D**. On top of this, the miR-124 mimic in neurons influenced the pro-resolving signature in IFNγ-MG, with significant overexpression of ARG-1 ($p < 0.05$) and TGF-β ($p < 0.001$). Regarding the inflammation-associated miRNAs, their microglial levels

differed according to the dissemination of miR-124 levels from the SWE cells. While the inhibition of miR-124 in SWE cells caused its depletion ($p < 0.01$), the mimic upregulated miR-124 in IFNγ-MG cells ($p < 0.01$) with marked repression of its direct target, the C/EBPα ($p < 0.001$). Furthermore, a significant reduction ($p < 0.01$) was found in the AD-associated miR-146a upon the mimic action on SWE cells (Wang et al., 2016; Ansari et al., 2019) (**Figure 5C**). Surprisingly, no changes were observed in the miR-155 expression, despite being the most upregulated miRNA by the IFNγ stimulus (**Figure 2E**).

To deeper investigate the consequences of the neuronal miR-124 modulation on the neighboring IFNγ-MG cells, we performed a proteomic analysis in these cells after coculture with SWE treated with inhibitor and/or mimic (**Figure 5D** and **Supplementary Figure S2**). Remarkably, from a total of 3,785 quantified proteins in IFNγ-MG, more than a hundred of them were significantly affected by the SWE levels of miR-124 (**Figure 5D**, top and detailed in **Supplementary Table S2**). Curiously, the miR-124 mimic produced a higher impact in IFNγ-MG with 93 differently expressed proteins (DEPs) compared to the 38 DEPs upon the miR-124 inhibitor. From those 93 mimic-dependent DEPs, the large majority (72) was downregulated. This finding indicates that miR-124 overexpression in SWE cells has a predominant effect on inhibiting IFNγ-MG protein expression.

Gene Ontology (GO) annotation for the cell component of DEPs clearly indicates an enrichment on neuron-specific terms, including "synapse," "dendrite," or "growth cone," despite showing enrichment in "extracellular EXOs" and "secretory vesicles" (**Supplementary Table S3**). Even so, those terms were not dominant in the full GO annotation done with the full proteome dataset of IFNγ-MG (**Supplementary Datasheet 3**). In this part, we specifically focused on the immune/inflammatory changes in microglia upon miR-124 modulation. Many protein IDs from the full proteome dataset were annotated in the GO analysis as involved in "immune regulation," "inflammatory response," and "response to stimulus" (**Supplementary Datasheet 3**). Then, we filtered the 17 most differentially expressed proteins changed upon the miR-124 inhibitor, the mimic, or simultaneously in both conditions (**Figure 5D**, right). From these, PRKC apoptosis WT1 regulator (PAWR) and EGF-containing fibulin-like extracellular matrix protein 1 (EFEMP1) were the only two proteins differently expressed with the inhibitor and/or the mimic, showing a direct response to the neuronal miR-124 levels. Both proteins were significantly co-inhibited in microglia upon neuronal miR-124 inhibition (PAWR, $p < 0.001$, and EFEMP1, $p < 0.01$) and co-expressed upon neuronal miR-124 overexpression ($p < 0.01$, for both).

Most of the significant effects were mediated by the miR-124 mimic, including the reduction ($p < 0.001$) of leukocyte elastase inhibitor (SERPINB1) and dual-specificity mitogen-activated protein kinase kinase 6 (MAP2K6), limiting the pro-inflammatory signaling. Additionally, the mimic increased the expression of: 1) Y-box-binding protein 3 (YBX3), a known Granulocyte-macrophage colony-stimulating factor (GM-CSF) regulator ($p < 0.05$) (Coles et al., 1996); 2) gremlin-1 (GREM1) ($p < 0.001$), involved in monocyte chemotaxis (Müller et al., 2014); and 3) fermitin family homolog 3 (FERMT3) ($p < 0.001$), an essential player in hematopoietic cell adhesion and potential NF-kB repressor (Wang et al., 2008; Svensson et al., 2009). In contrast, the neuronal inhibition of miR-124 led to a significant decrease in the transforming growth factor beta-1 proprotein (TGFB1) ($p < 0.01$), a direct precursor of the anti-inflammatory cytokine TGF-β, as an example.

Finally, we used a miRNA functional analysis and system biology network database "miRnet.ca" (Chang et al., 2020) to create a targeting map of miR-124 using the subset of the 17 DEPs involved in microglia innate function (**Figure 5E**). We found that nine DEPs are direct targets of miR-124, while the remaining seem to be indirectly affected through pathways influenced by the direct targets. In addition, we confirmed the impact of miR-124 in the full proteome dataset of IFNγ-MG using the same miRnet.ca database (**Supplementary Figure S3**). Remarkably, miR-124-3p was confirmed as the miRNA better explaining the full proteomic changes detected in IFNγ-MG, through the predicted involvement of several transcription factors, such as C/EBPα, NFATc1, or STAT3, which also constitute major miR-124 targets. Our coculture system was more effective in the identification of relevant microglial proteomic data compared to other studies using monoculture (Ahuja and Lazar, 2021), despite the differences to more advanced experimental models of microglia (Svoboda et al., 2019) (**Supplementary Figure S4**). Nevertheless, the sum of these data elucidates the multi-targeting power of neuronal miR-124 over the microglial proteome.

## 3.6 Secretion of MMP-2 and MMP-9 Decreases When IFNγ-MG is Cocultured With miR-124-Loaded SWE Cells

Matrix metalloproteinase (MMP) dysregulation is implicated in microglia activation, inflammation, and neurodegenerative diseases, such as AD (Könnecke and Bechmann, 2013). Previous studies have shown that low levels of miR-124 upregulated MMP-2 and MMP-9 in bladder cancer cells and favored their invasion (Xu et al., 2013). Herein, the GO analysis for IFNγ-MG-co revealed a 4.4-fold-enrichment in extracellular matrix proteins (**Supplementary Table S3**). Considering these aspects, we next evaluated the activity of MMP-2 and MMP-9, described to play multiple roles in AD (Candelario-Jalil et al., 2011; Wang et al., 2014; Ringland et al., 2021). We collected cell media from monocultures (SWE, naïve MG, and IFNγ-MG) and SWE/IFNγ-MG cocultures (with mock, inhibitor, and mimic of miR-124) as schematized (**Figure 6A**). Then, we evaluated the gelatinase activity of MMP-2 and MMP-9 using gelatin zymography under non-denaturation conditions (**Figure 6B**). While no significant differences were observed between monocultures, SWE/IFNγ-MG cocultures produced significant increases in MMP-9 activity upon transfection with mock and miR-124 inhibitor ($p < 0.05$ for both) compared to the SWE monoculture (**Figure 6C**). Oppositely, the coculture with miR-124-loaded SWE cells (mimic) led to a significant decrease ($p < 0.05$) in the MMP-9 activity compared to the mock coculture, with values close to those observed in the SWE cell monocultures (**Figure 6C**). Regarding MMP-2, we could distinguish between the pro- (72 kDa) and active

(62 kDa) forms in our different experimental conditions (**Figures 6D,E**). Concerning the monocultures, we observed a reduced pro-MMP-2 accumulation in the secretome from naïve MG relative to that of SWE cells ($p < 0.05$, **Figure 6D**). Interestingly, the upregulation of miR-124 in the SWE cells and their coculture with IFNγ-MG determined a reduction of the active MMP-2 accumulation (**Figure 6E**), not observed for the pro-MMP-2. Such deactivation of the MMP-2 and MMP-9 may represent an additional benefit of miR-124 overexpression, which apparently works as an inhibitor reducing their proaggregatory and inflammatory influence in AD.

## 3.7 Elevation of miR-124 in Dicer1-Silenced IFNγ-MG in the Presence of miR-124-Loaded SWE Neurons Indicate Secretome-Mediated Signaling Between Cells

Once we observed a miR-124 boost in IFNγ-MG when cocultured with the SWE neuronal cells (**Figure 3H**) and later that miR-124 up/downregulation levels in IFNγ-MG recapitulated its levels in SWE cells modulated with the miR-124 inhibitor or mimic (**Figure 5C**), we put the hypothesis of a horizontal transfer of miR-124 from SWE cells to IFNγ-MG. To explore such a process, we silenced RNase III endonuclease Dicer1 in IFNγ-MG to block their miRNA production before establishing the coculture, as schematized in **Figure 7A**. After testing different incubation periods, the 24 h one was the most efficient in siRNA-mediated Dicer-1 silencing (siDicer1), as confirmed by western blot (**Figure 7B**). In this condition, we also confirmed massive repression ($p < 0.001$) of miR-124 in IFNγ-MG cells to only 3.4% of the unrepressed control levels (**Figure 7C**). Besides, we confirmed that Dicer1 silencing was maintained even until 72 h after transfection, thus covering the coculture period of 24 h (data not shown).

After establishing the best silencing conditions, we cocultured the SWE cells with Dicer1-silenced IFNγ-MG. Remarkably, miR-124 levels were still increased in siDicer1 microglia upon coculture with the SWE cells, regardless of the type of modulation (mock control: 80.6-fold; inhibitor: 16.7-fold; mimic: 152.4-fold; $p < 0.001$ for all *vs.* naïve microglia) (**Figure 7D**). Noteworthy, such miR-124 increase in siDicer1 microglia was still observed in cocultures with the SWE cells treated with the miR-124 inhibitor ($p < 0.001$). However, the effect, in this case, was inferior to that caused by the mock or mimic (at least $p < 0.01$). Notably, miR-124 in Dicer1-silenced IFNγ-MG cells cocultured with SWE cells treated with miR-124 mimic was upregulated compared to the mock, as expected

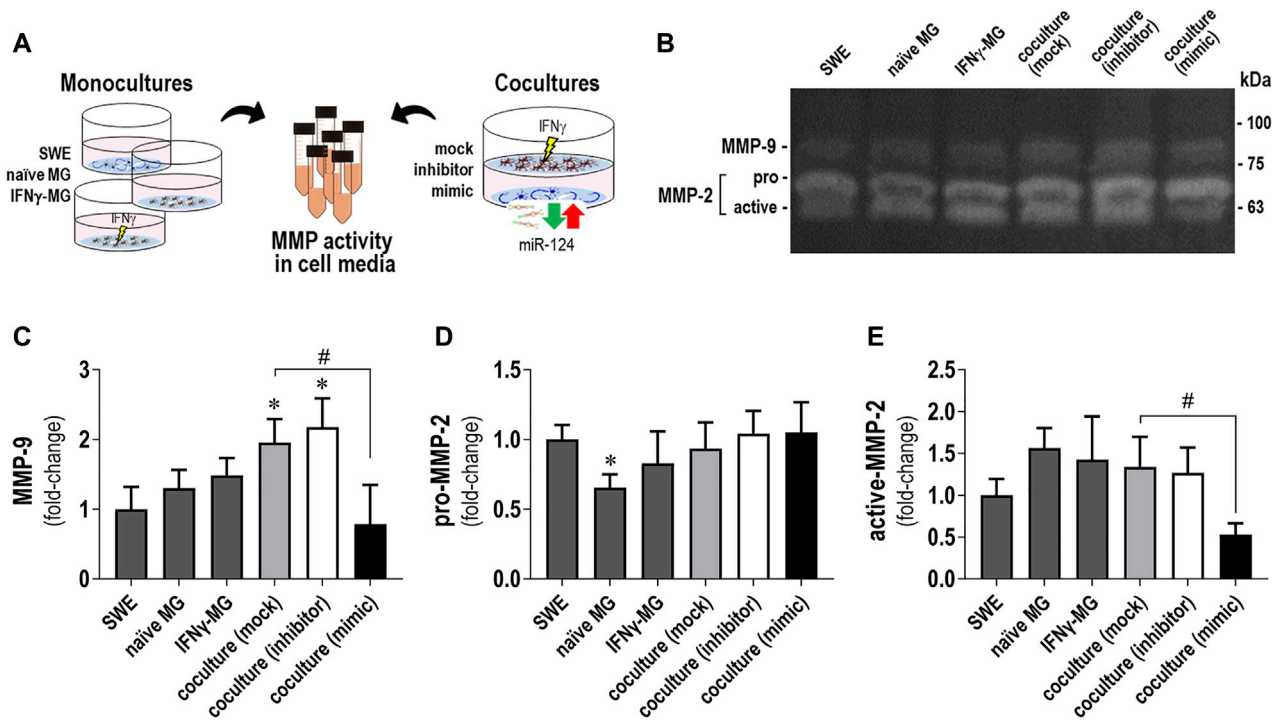


**FIGURE 6 |** Changes in MMP-2 and MMP-9 activities by gelatin zymography in secretomes from SWE and IFNγ-MG cells, in either monocultures or cocultures, are determined by miR-124 expression levels. Cell media from the SWE and IFNγ-MG monocultures and cocultures were collected and analyzed for matrix metalloproteinase (MMP) gelatinase activities, as described in *Materials and Methods*. **(A)** Schematic representation of the experimental conditions (in either monoculture or coculture) and cell media collection. **(B)** Representative images of the gelatin zymography assay showing the gelatinolytic bands of MMP-9 and MMP-2. Discrimination between the pro- and active forms was only possible for MMP-2. **(C)** Quantification of gelatinase activity MMP-9 (±80–90 kDa), **(D)** pro-MMP-2 (72 kDa), and **(E)** active-MMP-2 (62 kDa). Results are mean ± SD from at least three independent experiments. *$p < 0.05$ *vs.* SWE cell secretome, one-way ANOVA with the Bonferroni *post hoc* test; #$p < 0.05$ *vs.* coculture with the SWE mock, two-tailed Student's *t*-test. SWE, human SH-SY5Y cells expressing the APP695 Swedish mutant protein; MG, CHME3 human microglia cells; IFNγ-MG, IFNγ-stimulated CHME3 human microglia cells.

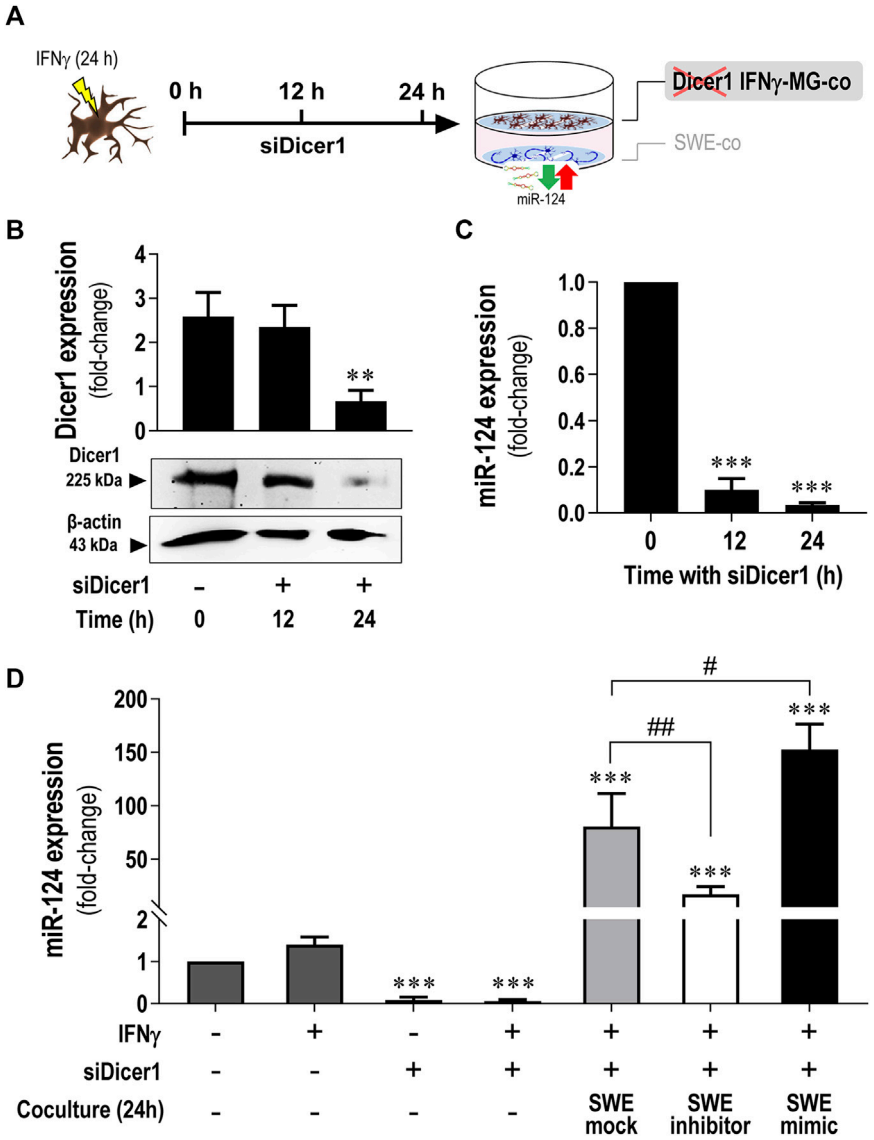


**FIGURE 7 |** Increased miR-124 expression levels are present in Dicer1-silenced IFNγ-MG upon established cocultures with the SWE cells modulated for miR-124. After differentiation, SWE cells were transfected with mock, inhibitor, and mimic of miR-124, while CHME3 microglia were pre-treated with IFNγ (IFNγ-MG) before transfection with Dicer1 siRNAs, as detailed in *Materials and Methods*. **(A)** Schematic representation of siRNA-mediated Dicer1 silencing in IFNγ-MG cells, followed by coculture with miR-124 modulated SWE cells. **(B)** Representative western blot images and relative densitometric quantification of Dicer1 expression in IFNγ-MG after 0 (naïve), 12, and 24 h of Dicer1 siRNA incubation. **(C)** miR-124 expression levels in IFNγ-MG after 0 (naïve), 12, and 24 h of Dicer1 siRNA incubation. **(D)** miR-124 expression levels in IFNγ-MG in monocultures upon the indicated conditions or in coculture with SWE cells modulated for miR-124 after 24 h incubation. Results are mean ± SD from at least three independent experiments. $^{**}p < 0.01$ and $^{***}p < 0.001$ *vs*. naïve MG; $\#\#p < 0.01$ *vs*.IFNγ-MG cocultured with SWE mock, one-way ANOVA with the Bonferroni *post hoc* test. SWE, human SH-SY5Y cells expressing the APP695 Swedish mutant protein; MG, CHME3 human microglial cells; IFNγ-MG, IFNγ-stimulated CHME3 human microglia cells; co, coculture; siDicer1, siRNA-mediated Dicer-1 silencing.

($p < 0.05$). So far, these results confirm the miR-124 paracrine trafficking from neurons to IFNγ-MG.

## 3.8 Transmission of miR-124 Into IFNγ-Microglia Is Mediated by EXOs From the SWE Neurons

EXOs have been described to participate in the clearance and dissemination of misfolded proteins in neurodegenerative disorders, including AD (Eitan et al., 2016; Yuyama and Igarashi, 2017). More recently, they were described as specialized miRNA carriers with a high impact on recipient cells' function (Bell and Taylor, 2016; Brites, 2020). Considering the GO analysis of the cellular component, indicating that miR-124 changes relate to the terms "extracellular exosome" and "secretory vesicle" (**Supplementary Table S3**), along with our previous background on neuronal miR-124 EXO delivery (Fernandes

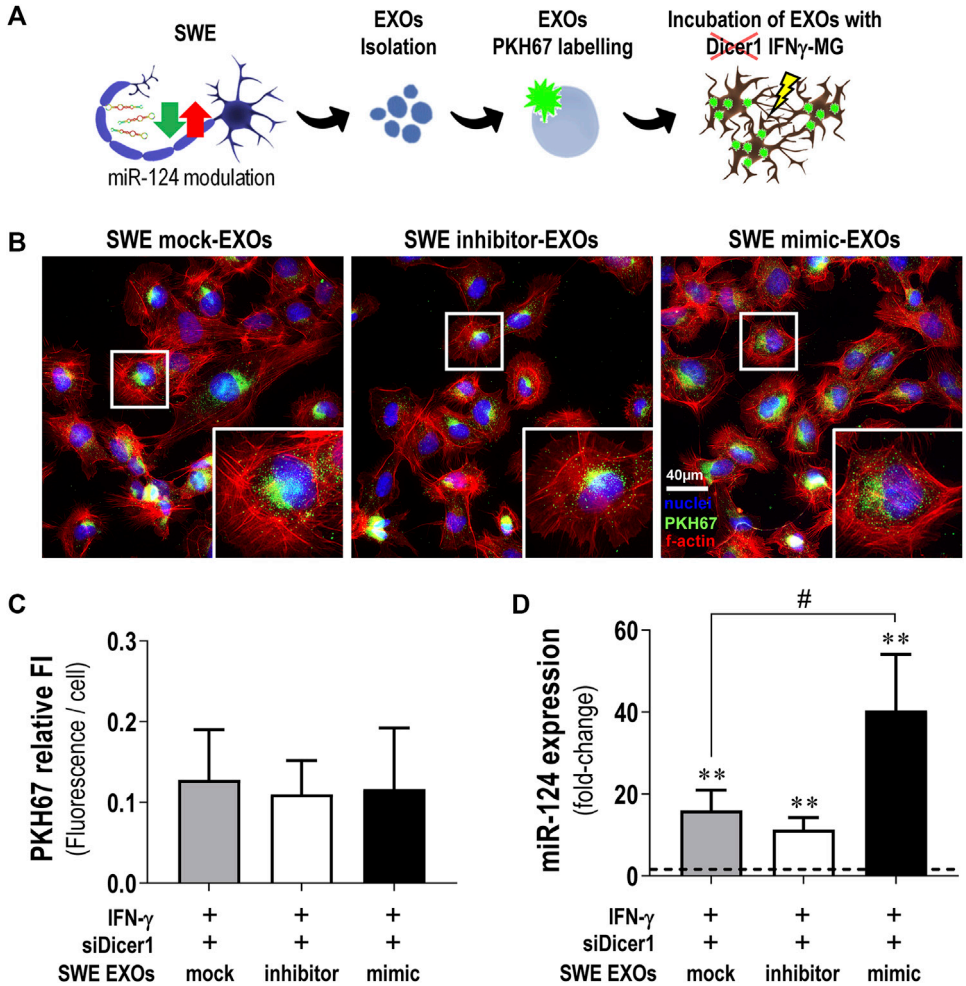


**FIGURE 8 |** SWE-derived EXOs efficiently deliver miR-124 into Dicer1-silenced IFNγ-MG. After differentiation, SWE cells were transfected with mock or miR124 inhibitor and mimic, while CHME3 microglia were treated with IFNγ followed by Dicer-1 siRNAs, as described before. **(A)** Schematic representation of exosome (EXO) isolation from SWE cells expressing different miR-124 levels (mock, inhibitor, and mimic), labeling with the fluorescent probe PKH767, and incubation with Dicer1-silenced IFNγ-MG. **(B)** Representative fluorescence images of PKH67-labelled EXOs collected by Dicer1-silenced IFNγ-MG (green) and f-actin (red). Nuclei were stained with Hoechst 33258 dye (blue). **(C)** Quantification of PKH67 fluorescence intensity (FI) per microglial cell. **(D)** Expression of miR-124 in Dicer1-silenced IFNγ-MG after incubation with SWE-derived EXOs (mock *vs*. inhibitor *vs*. mimic). Results are mean ± SD from at least three independent experiments. $^{**}p < 0.01$ *vs*. naïve MG (dashed line), one-way ANOVA with the Bonferroni *post hoc* test; $\#p < 0.01$ *vs*. siDicer1 silenced IFNγ-MG cocultured with SWE mock exosomes, two-tailed Student's *t*-test. SWE, human SH-SY5Y expressing the APP695 Swedish mutant protein; EXOs, exosomes; IFNγ-MG, IFNγ-stimulated CHME3 human microglia cells; siDicer1, siRNA-mediated Dicer-1 silencing.

et al., 2018; Garcia et al., 2021), we investigated whether EXOs were responsible for the miR-124 trafficking from SWE neurons to IFNγ-MG (**Figure 8**). To do so, we modulated miR-124 levels in SWE cells as before and isolated EXOs from each type of modulation (mock, inhibitor, and mimic) by sequential ultracentrifugation. Then, EXOs were labeled with PKH67 and incubated with Dicer1-silenced IFNγ-MG for 24 h, as schematized in **Figure 8A**. First, we checked if any miR-124 modulations modified the amount of SWE EXOs internalized by IFNγ-MG (**Figures 8B,C**). Results clearly show that SWE EXOs, independent of the modulation with the miR-124 inhibitor or mimic, were equally internalized by Dicer1-silenced IFNγ-MG (**Figure 8C**). Remarkably, after the incubation of the Dicer1-silenced IFNγ-MG with the SWE EXOs, we observed that miR-124 increased in IFNγ-MG (SWE mock-EXO, 16-fold; SWE inhibitor-EXO, 11-fold; SWE mimic-EXO, 40-fold; $p < 0.01$ for all). Such an increase attested the above-described internalization upon coculture with the SWE neuronal cells (**Figure 7D**). Particularly, SWE mimic-EXOs led to 2.5-fold increased levels of miR-124 in the Dicer1-silenced IFNγ-MG ($p < 0.05$) compared to the effect of EXOs from mock control SWE cells. These results confirm the transfer and delivery of miR-124 from SWE cells into the Dicer1-silenced IFNγ-MG, either in coculture (~150-fold) or as cargo in EXOs (~40-fold), supporting its dissemination role.

Interestingly, it seems that the ingested miR-124-enriched EXOs by the Dicer1-silenced IFNγ-MG are mainly

metabolized intracellularly, considering that the EXOs released from these cells evidenced less miR-124 (~25%, $p < 0.001$) in the case of mock, inhibitor, and mimic than those from the naïve microglia (**Supplementary Figure S5**). Our results indicate that the miR-124-loaded EXOs are internalized by the IFNγ-MG, where they target genes involved in the restoration of microglia's steady state without further exosomal sorting and propagation.

## 4 DISCUSSION

This study shows that neuronal miR-124 is a major paracrine regulator of microglia neuro-immune function. By modulating miR-124 levels in SWE cells, using a specific inhibitor and mimic, we produced consistent alterations in the inflammatory signature and polarization status of IFNγ-stimulated microglia and its secretome. Inhibition of neuronal miR-124 accentuated the pro-inflammatory signaling triggered by IFNγ to the point of compromising neuronal viability in coculture. Conversely, neuronal miR-124 overexpression switched the microglia pro-inflammatory signature into a pro-regenerative one, while also inhibiting the activity of MMP-2 and MMP-9 in the secretome of SWE + IFNγ-MG. These findings indicate a miR-124-mediated microglia depolarization in an inflammatory milieu, which must probably rescue their neuroprotective functions, compromised in AD (Könnecke and Bechmann, 2013; von Bernhardi et al., 2015; Bachiller et al., 2018). Moreover, we showed that miR-124 is delivered from neuronal cells into activated microglia (IFNγ-MG), with a substantial part of such trafficking being vehiculated by neuronal EXOs.

Although neurons are the main cells responsible for miR-124 expression in the CNS (Åkerblom et al., 2012), the role of this miRNA in AD neuropathology has always been controversial, with opposite perceptions and different levels reported (Sonntag et al., 2012). Due to these inconsistencies in the literature, there is not yet a clear idea about the role of miR-124 in the AD onset and progression, even though its implication is unquestionable (Han et al., 2020). In that matter, we believe that most of the miR-124 contradictions rely on studies performed with different experimental models, disease stages, and brain regions (Brites, 2020). There is no doubt that miR-124 is important in AD. Increasing studies point to the release of miR-124 from neuronal cells as a major signaling messenger for recipient cells (Veremeyko et al., 2019; Garcia et al., 2021). Microglia are one of those recipient cells known to acquire a homeostatic and reparative phenotype upon miR-124 uptake (Ponomarev et al., 2011; Veremeyko et al., 2019). These findings have been conducted to develop multiple therapeutic approaches in different disease contexts (Saraiva et al., 2016; Chivero et al., 2020). Herein, our objective was to examine the *modus operandi* through which miR-124 regulates neuron-microglia crosstalk. Therefore, we established a coculture system including IFNγ-MG and SWE cells, which we previously demonstrated to recapitulate important AD features and overexpress/release elevated miR-124 levels (Fernandes et al., 2018; Garcia et al., 2021).

The decision of choosing IFNγ to stimulate CHME3 microglia was supported by the involvement of this cytokine in AD pathology, reported in both mild- and severe-stage patients compared to individuals with mild cognitive impairment (MCI) (Belkhelfa et al., 2014). Moreover, IFNγ is involved in microglia activation upon Aβ (Meda et al., 1995) and the expression of multiple chemokines, MHC, signal transducing elements, increased ROS and NO generation (Rock et al., 2005; Spencer et al., 2016). While other stimuli, such as bacterial lipopolysaccharide (LPS), simulate infection-associated defense mechanisms and trigger microglia-mediated neurotoxicity (Chien et al., 2016), IFNγ is a sterile stimulus actively involved in AD pathology, with a neuroimmune role over microglia activation and synaptic activity (Ta et al., 2019). Apart from the above-mentioned rationale, IFNγ was also reported as one of the most suitable cytokines to stimulate the CHME3 microglial cells (aliased as HMC3) (Dello Russo et al., 2018). Accordingly, our data depict much of those aspects of microglial IFNγ stimulation, with increased nitrosative activity, and upregulation of pro-inflammatory cytokines and receptors. Upregulation of MHC-II, IL-6, and iNOS upon IFNγ stimulation was expected considering previous studies (Ta et al., 2019; Zhang et al., 2020). However, iNOS activation may not be sufficient to mediate neurotoxicity, considering the relatively benign outcomes of iNOS if not coactivated with NOX (Mander and Brown, 2005). Moreover, despite the predominance of pro-inflammatory markers, IFNγ also induced a modest reparative/anti-inflammatory signature (elevated TGF-β and IL-10), a consequence that has long been discussed and described as the dual-role of IFNγ in inflammation (Mühl and Pfeilschifter, 2003).

Not surprisingly, the coculture led to mutual adaptations in SWE cells and IFNγ-MG. While microglial iNOS and its end-product NO were described as neuronal killers by inhibiting the neuronal respiratory chain (Bal-Price and Brown, 2001), our data indicate that microglial iNOS is hampered upon coculture. Nevertheless, our results suggest that coculture with IFNγ-MG may compromise mitochondria membrane potential in the SWE cells, thus affecting their oxidative capacity. However, the most interesting finding was the marked miR-124 elevation in IFNγ-MG upon coculture with the SWE cells, strongly suggestive of miR-124 microglial uptake, herein confirmed with Dicer1 knock-down experiments in the activated microglial cells.

Major insights on the relevance of miR-124 levels in neuronal-microglial signaling were further revealed after transfection of the SWE cells with the inhibitor and mimic of miR-124. We showed that miR-124 levels secreted by SWE cells (either *via* EXOs or as a soluble factor) recapitulate intracellular ones, pointing to the passive release of miR-124 into EXOs or EXO-free secretome, as reported in our previous study (Garcia et al., 2021), and also observed in other disease-associated miRNAs (Bell and Taylor, 2016). Moreover, we showed that miR-124 overexpression (with mimic) protects neurons from mitochondrial oxidative injury and stress-associated mediators imposed by the coculture with IFNγ-MG. Such a neuroprotective activity was previously explored in a neurodegenerative context, indicating that miR-124 promotes neurite outgrowth under an inflammatory environment associated with activated macrophages (Hartmann et al., 2015).

On the microglia side, Ponomarev et al. were pioneers in showing that peripheral administration of miR-124 in the mouse model of experimental autoimmune encephalomyelitis (EAE) resulted in systemic deactivation of macrophages, microglia quiescence (a disused designation), reduced activation of myelin-specific T cells, and disease suppression, but miR-124 inhibition caused microglia activation (Ponomarev et al., 2011). They further demonstrated the C/EBPα as a direct target of miR-124. Herein, we demonstrate that miR-124 paracrine signaling from the SWE neuronal cells sustained microglia physiology in the IFNγ context and the mimic repressed the expression of C/EBPα. Upregulation of miR-124 in SWE cells with the mimic also repressed the IFNγ-MG overexpression of iNOS and TNF-α, reduced NO release and inhibited the MMP-2 and MMP-9 activities in the secretome from the coculture, while further stimulating the gene expression of ARG-1 and TGF-β, important for repair. Additionally, TGF-β increase is also correlated with the expression of miR-124 (Lu et al., 2019), corroborating its increased gene expression in IFNγ-MG in coculture with the SWE cells treated with the miR-124 mimic.

Herein, we further demonstrate that miR-124 paracrine signaling from SWE neuronal cells sustained microglia physiology in the IFNγ context. By upregulating miR-124 in SWE cells with the mimic, we repressed the IFNγ-MG overexpression of iNOS and TNF-α, reduced NO release, and inhibited the MMP-2 and MMP-9 activities in the secretome from the coculture, while further stimulating the gene expression of ARG-1 and TGF-β, important for repair.

Although iNOS inhibition *per se* may not confirm neuroprotection due to its synergistic dependence on NADPH oxidase (Mander and Brown, 2005), its combination with TNF-α and MMP inhibitions clearly supports a protective role of miR-124 regulation, whenever its expression levels are downregulated. Such neuroprotective potential of miR-124 was confirmed in the proteomic study by the repression of pro-inflammatory and disease-associated mediators. For instance, MAP2K6 and SERPINB1 were downregulated in IFNγ-MG upon the miR-124 mimic influence. For example, MAP2K6 consists of a direct mediator of p38 phosphorylation, which mediates MAPK pathway activation (Zhu et al., 2001), while SERPINB1 regulates innate immune responses and controls the activity of inflammatory caspases (Choi et al., 2019).

Conversely, the inhibition of miR-124 in SWE cells further induced RAGE, HMGB1, iNOS, and IL-1β in the IFNγ-MG when using the coculture system and inhibited IL-10 and ARG-1, thus favoring a predominant reactive phenotype. Such effects were also confirmed by the proteomic analysis of the DEPs that identified: 1) pro-resolving associated proteins as TGFB1; 2) NF-kB inhibitors as PAWR; and 3) disease-associated markers as EFEMP1. All of them were decreased upon miR-124 inhibition. PAWR (aliased as PAR-4) is a tumor suppressor protein linked to NF-κB and BCL2 direct inhibition (Chakraborty et al., 2001; Yang et al., 2016), also indicated as an AD biomarker involved in the regulation of BACE1-mediated APP processing (Xie and Guo, 2005; Greco et al., 2012). In turn, EFEMP1 (known as fibulin-3) was reported to be involved in glial cell migration and neurite outgrowth in the olfactory nerve (Vukovic et al., 2009), while it decreased in the cerebrospinal fluid (CSF) of AD patients (Khoonsari et al., 2016). Intriguingly, PAWR and EFEMP1 were the only two proteins (from the inflammation/immunity cluster) that showed a direct co-regulation by miR-124 levels. Considering their potential in AD, it becomes crucial to deeply explore their involvement in miR-124 expression levels and their mechanisms of action in future studies.

To highlight that the anti-inflammatory and pro-resolving effects of miR-124 in microglia are at least in part mediated by the C/EBPα and the cytokine receptor IL6R (Hatziapostolou et al., 2011; Ponomarev et al., 2011; Brites, 2020), while C/EBPα was reported to regulate the expression of acute-phase response proteins and the histone deacetylase inhibitor, as well as NF-κB and STAT-3 (Ko et al., 2015). However, further mechanistic studies are needed. By repressing IL6R, miR-124 prevents the priming of microglia by IL-6 (Garner et al., 2018), a multifunctional cytokine that when chronically produced, is involved in the pathogenesis of inflammatory disorders (West et al., 2019). In the case of AD, miR-124, besides influencing the microglia activation state, prevents Aβ production, while reducing tau phosphorylation and synaptic loss, thus having potential as a treatment strategy in AD (Zhao et al., 2021).

By interrogating the miRnet.ca database with the 17 DEPs participating in immune regulation, inflammatory response, and response to stimulus, we found that nine of those are direct targets of miR-124, which confirms the relevance of neuronal-derived miR-124 on the microglia function in an inflammatory and pathological milieu. Furthermore, using the full dataset of proteins identified in our proteomic analysis, it was clear that miR-124 was, by far, the miRNA better explaining the proteomic changes in IFNγ-MG (**Supplementary Figure S4**). In addition, several transcription factors were predicted to be implicated, including C/EBPα, NFATc1, or STAT3, three major miR-124-3p direct targets. In the case of C/EBPα, such a prediction was confirmed in IFNγ-MG by RT-qPCR, showing a marked downregulation upon coculture with mimic-treated SWE cells. Besides miR-124, other miRNAs were also predicted to be engaged, such as miR-1-3p, miR-155-5p, miR-16-5p, miR-125b-5p, or miR-21, and thus of interest in further studies.

Concerning the GO annotation of DEPs, we found an enrichment in neuron-specific terms, such as "synapse," "dendrite," and "growth cone" in the cellular component and "response to axon injury," "regulation of axon extension," and "axon development" in biological processes (**Supplementary Table S3**). Because the coculture setup used in our study prevents neuron-microglia direct contact (Phatnani et al., 2013; Wasilewski et al., 2022), we were surprised to find these neuron-specific GO terms. Interestingly, the induction of neuronal gene expression in microglia was previously recognized, though it remains unclear and would be interesting to address (Veremeyko et al., 2019). However, such terms were not found in the GO annotation of the full proteomic dataset (**Supplementary Datasheet 3**). The comparison of both GO analyses (full dataset *vs.* DEPs) suggests that the enrichment in neuron-specific terms in the DEP dataset is a

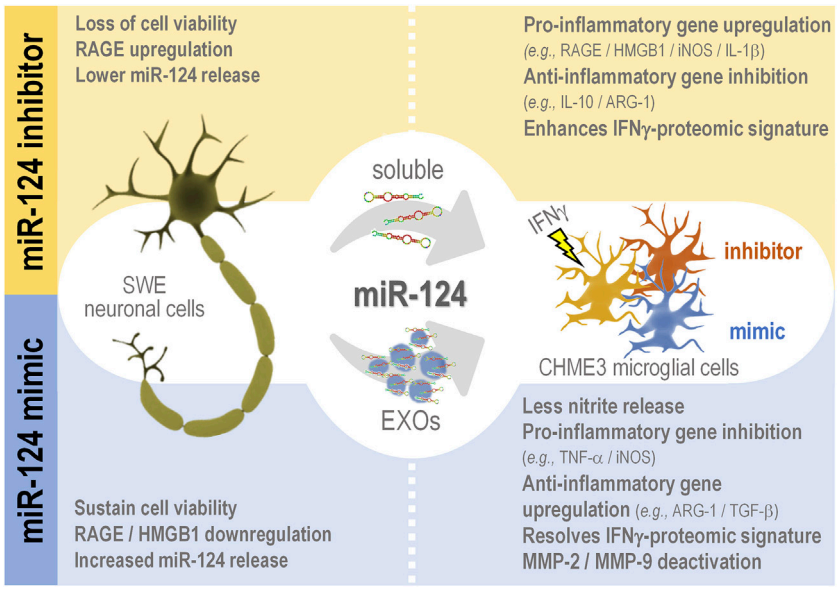


**FIGURE 9 |** Schematic representation of the miR-124 trafficking between SWE cells and IFNγ-MG and consequences associated with miR-124 inhibition (inhibitor) and upregulation (mimic) in each cell type. miR-124 is transferred from the SWE cells to IFNγ-MG *via* neuronal secretome (either free or in EXOs). The neuronal miR-124 inhibition, apart from reducing its levels in SWE cells and their secretome, also compromises cell viability and induces RAGE upregulation upon coculture with IFNγ-MG. Besides the effects in the SWE cells, the miR-124 inhibition leads to paracrine effects in IFNγ-MG, including pro-inflammatory gene expression and IFN-associated proteomic signature. On the contrary, the miR-124 mimic upregulates its expression/release by SWE cells, while sustaining cell viability in the presence of IFNγ-MG cells, which in turn manifest a homeostatic state profile with less nitrosative activity, predominant anti-inflammatory gene/proteomic signature, and reduced extracellular matrix degradation. Considering the progress in the field of EXOs as miRNA carriers to alleviate pathological cellular states in several diseases, EXOs enriched in miR-124 may open a new avenue in therapeutic interventions in AD. miR, miRNA; RAGE, receptor for advanced glycation end products; HMGB1, high mobility group box protein 1; iNOS, inducible nitric oxide synthase; IL, interleukin; ARG-1, arginase-1; TNF-α, tumor necrosis factor α; TGF-β, transforming growth factor β; MMP, metalloproteinase.

consequence of the statistical filtering, and despite being significant, such neuron-specific terms do not represent the most predominant signature in microglia full proteome. Nevertheless, we hypothesize that those terms appeared as a consequence of the microglial involvement in synaptic function (Ta et al., 2019) or simply by the paracrine influence of neuronal cells, which are known to profoundly change the microglial gene expression (Baxter et al., 2021). Alternatively, considering that synaptic proteins are released by neuronal EXOs (Fauré et al., 2006), we cannot discard the hypothesis of microglial uptake of such proteins, a phenomenon described in different studies (Paolicelli et al., 2011; Brioschi et al., 2020). It was suggested to be also associated with epigenetic changes occurring in both cell types during development, and soluble neuronal factors may modify microglial phenotypes and functions and be involved in the AD pathology (Veremeyko et al., 2019).

In the AD context, MMP-2 has been reported to participate in the degradation of the blood–brain barrier (BBB), facilitating the infiltration of inflammatory cells (Candelario-Jalil et al., 2011), while MMP-9 was pointed to accentuate the neurobehavioral deficits in a mouse model of AD (Ringland et al., 2021). Although neither MMP-2 nor MMP-9 are described as miR-124 targets, this study provides the first line of evidence showing that miR-124 overexpression reduces their activity in an AD *in vitro* cell model. However, while the inhibition of MMP-2 and MMP-9 activities was indicated to compromise their potential to degrade Aβ toxic species (Hernandez-Guillamon et al., 2015), their elevation may act as inflammatory components and have a proaggregatory influence on tau oligomerization (Wang et al., 2014).

In the last part of this study, we suppressed the new formation of miRNAs in the IFNγ-MG, including miR-124, by silencing the RNase III endonuclease Dicer1, responsible for canonical miRNA processing. Such silencing allowed us to confirm that most of the miR-124 observed in the cocultures of SWE cells + IFNγ-MG derive from neurons. With the GO enrichment in terms of "extracellular exosome" and "secretory vesicle," we further confirmed that SWE-derived EXOs are major shuttles involved in miR-124 trafficking into microglia. The use of EXOs as miR-124 vehicles has been successfully explored in ischemia (Yang et al., 2017), traumatic brain injury (Yang et al., 2019), and traumatic spinal cord injury (Jiang et al., 2020), as well as in cocaine-mediated microglial activation (Chivero et al., 2020) and Huntington disease (Lee et al., 2017). All these studies converged on the benefits of miR-124, especially by redirecting microglia into a neuroprotective phenotype.

We believe that our study draws attention to the complexity of miRNA-based therapies but overall clarifies their potential as neuropharmacological approaches in the AD field. However, by only using immortalized cell lines, this study must be understood as an opportunity to explore further the potential of miR-124-based strategies in AD, namely, the possibility of developing

miRNA-loaded EXOs (de Abreu et al., 2021) and their future prospects as therapeutics (Munir et al., 2020). Although our coculture system with immortalized cell lines is more advanced than monoculture systems, a big gap still exists between each of them and iPSCs-derived models and/or primary human cells, as depicted in **Supplementary Figure S3**. Hence, it is essential to validate the neuroprotective potential of regulating miR-124 expression levels in more advanced human personalized AD models, as the three-dimensional spheroids and organoids (Pomeshchik et al., 2020; Chen et al., 2021), not forgetting the possibility of new animal models (Baglietto-Vargas et al., 2021; Le Bras, 2021). Future studies should also characterize the entire EXO cargo and use miR-124 cellular probing (fluorescent *in situ* hybridization) to assess its subcellular localization. It is also important to investigate the consequences of Dicer1 silencing on EXO biogenesis and release by microglia because little is known in this regard. Finally, it should be considered that miR-124 has hundreds of direct and indirect targets, as evidenced in our proteomic analysis, which may have off-target effects and benefit as a multitarget approach.

## 5 CONCLUSION

This study provides novel insights into the relevance of miR-124 to sustain nerve cell homeostatic balance in pathological neurodegeneration and associated inflammation. Besides being important to prevent neuronal dysfunction, as shown in advanced AD cell models (Garcia et al., 2021), we established miR-124 as a key player in the paracrine signaling between the SWE neuronal and microglial cells after stimulation with IFNγ (IFNγ-MG), to mimic neuro-immune dysregulation. A schematic summary of the results obtained is depicted in **Figure 9**. Herein, we reveal that low levels of miR-124, upon modulation with its inhibitor, aggravate the reactivity of IFNγ-MG and compromise their neighboring SWE cell viability, as demonstrated by their coculture. In contrast, the upregulation of miR-124 with its mimic, apart from preserving the SWE cell viability in the presence of IFNγ-MG, contributes to prevent excessive microglia activation and plays an inhibitory role in MMP-2 and MMP-9 activation associated with AD progression. Moreover, besides identifying multiple targets of miR-124 in the activated microglia, our proteomic analysis reveals deep changes in the expression of proteins involved in vesicular trafficking, extracellular matrix, and neuro-immune function, as well as of several proteins involved in synaptic function, dendrite outgrowth, and cytoskeleton remodeling. Of note, some proteins involving a neuro-immune function (e.g., EFEMP1 and PAWR) are reported in AD, thus opening a new field for future research.

Together, our results validate the relevance of miR-124 in the maintenance of neuron-microglia homeostatic balance in AD conditions, namely, in the presence of inflammation and microglia activation. Furthermore, we show that SWE-derived EXOs are substantial players in translating miR-124 into IFNγ-MG cells, reprogramming microglia signature, and influencing microglia local responses in health and disease. As therapeutic miRNA-enriched EXOs have been tested as promising therapies in neurodegenerative diseases, we anticipate that miR-124-loaded EXOs may constitute an advance in future AD treatment strategies.

## DATA AVAILABILITY STATEMENT

The datasets presented in this study can be found in online repositories. The names of the repository/repositories and accession number(s) can be found in the article/**Supplementary Material**.

## AUTHOR CONTRIBUTIONS

The study was conceived, designed, and directed by DB, who supervised GG. GG and AF planned and conducted the experiments. GG carried out the cell characterization, miRNA modulation, exosome isolation, microscopic assessments, qRT-PCR, western blot determinations, and original draft preparation. AF was involved in the determination of soluble cytokines and cell viability. FS performed proteomic data analysis and edited the final manuscript and figures. Full data analysis and manuscript writing and editing were performed by GG and DB.

## FUNDING

This study was supported by Fundação para a Ciência e a Tecnologia (FCT) (JPco-fuND/0003/2015, PTDC/MED-NEU/31395/2017, PTDC/MED-NEU/2382/2021, and LISBOA-01-0145-FEDER-031395 to DB; in part by UID/DTP/04138/2019, UIDB/04138/2020, and UIDP/04138/2020 to iMed.ULisboa; and individual fellowships to GG (SFRH/BD/128738/2017 and COVID/BD/151849/2021) from FCT. The funding organization had no role in the study design, data collection and analysis, decision to publish, or manuscript preparation.

## ACKNOWLEDGMENTS

We thank Rui Fernandes and A. R. Malheiro from the Instituto de Investigação e Inovação em Saúde (i3S) and Histology and Electron Microscopy Service (HEMS/IBMC) at the Universidade do Porto, for acquisition and analysis of exosome TEM images. Finally, we also thank Per Haberkant from the EMBL Proteomics Core facility in Heidelberg for additional support with mass spectrometry and data analysis.

## SUPPLEMENTARY MATERIAL

The Supplementary Material for this article can be found online at: https://www.frontiersin.org/articles/10.3389/fphar.2022.833066/full#supplementary-material

## REFERENCES


Abbas, N., Bednar, I., Mix, E., Marie, S., Paterson, D., Ljungberg, A., et al. (2002). Up-regulation of the Inflammatory Cytokines IFN-Gamma and IL-12 and Down-Regulation of IL-4 in Cerebral Cortex Regions of APP(SWE) Transgenic Mice. *J. Neuroimmunol.* 126, 50–57. doi:10.1016/S0165-5728(02)00050-4

Ahuja, S., and Lazar, I. M. (2021). Systems-Level Proteomics Evaluation of Microglia Response to Tumor-Supportive Anti-inflammatory Cytokines. *Front. Immunol.* 12, 3404. doi:10.3389/fimmu.2021.646043

Åkerblom, M., Sachdeva, R., Barde, I., Verp, S., Gentner, B., Trono, D., et al. (2012). MicroRNA-124 Is a Subventricular Zone Neuronal Fate Determinant. *J. Neurosci.* 32, 8879–8889. doi:10.1523/JNEUROSCI.0558-12.2012

An, F., Gong, G., Wang, Y., Bian, M., Yu, L., and Wei, C. (2017). MiR-124 Acts as a Target for Alzheimer's Disease by Regulating BACE1. *Oncotarget* 8, 114065–114071. doi:10.18632/oncotarget.23119

Ansari, A., Maffioletti, E., Milanesi, E., Marizzoni, M., Frisoni, G. B., Blin, O., et al. (2019). miR-146a and miR-181a Are Involved in the Progression of Mild Cognitive Impairment to Alzheimer's Disease. *Neurobiol. Aging* 82, 102–109. doi:10.1016/j.neurobiolaging.2019.06.005

Bachiller, S., Jiménez-Ferrer, I., Paulus, A., Yang, Y., Swanberg, M., Deierborg, T., et al. (2018). Microglia in Neurological Diseases: A Road Map to Brain-Disease Dependent-Inflammatory Response. *Front. Cel. Neurosci.* 12, 488. doi:10.3389/fncel.2018.00488

Baglietto-Vargas, D., Forner, S., Cai, L., Martini, A. C., Trujillo-Estrada, L., Swarup, V., et al. (2021). Generation of a Humanized Aβ Expressing Mouse Demonstrating Aspects of Alzheimer's Disease-like Pathology. *Nat. Commun.* 12, 2421. doi:10.1038/s41467-021-22624-z

Bal-Price, A., and Brown, G. C. (2001). Inflammatory Neurodegeneration Mediated by Nitric Oxide from Activated Glia-Inhibiting Neuronal Respiration, Causing Glutamate Release and Excitotoxicity. *J. Neurosci.* 21, 6480–6491. doi:10.1523/jneurosci.21-17-06480.2001

Baxter, P. S., Dando, O., Emelianova, K., He, X., McKay, S., Hardingham, G. E., et al. (2021). Microglial Identity and Inflammatory Responses Are Controlled by the Combined Effects of Neurons and Astrocytes. *Cell Rep* 34, 108882. doi:10.1016/j.celrep.2021.108882

Belkhelfa, M., Rafa, H., Medjeber, O., Arroul-Lammali, A., Behairi, N., Abada-Bendib, M., et al. (2014). IFN-γ and TNF-α Are Involved during Alzheimer Disease Progression and Correlate with Nitric Oxide Production: a Study in Algerian Patients. *J. Interferon Cytokine Res.* 34, 839–847. doi:10.1089/jir.2013.0085

Bell, E., and Taylor, M. A. (2016). Functional Roles for Exosomal MicroRNAs in the Tumour Microenvironment. *Comput. Struct. Biotechnol. J.* 15, 8–13. doi:10.1016/j.csbj.2016.10.005

Belyaev, N. D., Kellett, K. A., Beckett, C., Makova, N. Z., Revett, T. J., Nalivaeva, N. N., et al. (2010). The Transcriptionally Active Amyloid Precursor Protein (APP) Intracellular Domain Is Preferentially Produced from the 695 Isoform of APP in a {beta}-secretase-dependent Pathway. *J. Biol. Chem.* 285, 41443–41454. doi:10.1074/jbc.M110.141390

Brioschi, S., d'Errico, P., Amann, L. S., Janova, H., Wojcik, S. M., Meyer-Luehmann, M., et al. (2020). Detection of Synaptic Proteins in Microglia by Flow Cytometry. *Front. Mol. Neurosci.* 13, 149. doi:10.3389/fnmol.2020.00149

Brites, D. (2020). Regulatory Function of microRNAs in Microglia. *Glia* 68, 1631–1642. doi:10.1002/glia.23846

Candelario-Jalil, E., Thompson, J., Taheri, S., Grossetete, M., Adair, J. C., Edmonds, E., et al. (2011). Matrix Metalloproteinases Are Associated with Increased Blood-Brain Barrier Opening in Vascular Cognitive Impairment. *Stroke* 42, 1345–1350. doi:10.1161/STROKEAHA.110.600825

Chakraborty, M., Qiu, S. G., Vasudevan, K. M., Rangnekar, V. M., Rangnekar, V. M., and Rangnekar, V. M. (2001). Par-4 Drives Trafficking and Activation of Fas and FasL to Induce Prostate Cancer Cell Apoptosis and Tumor Regression. *Cancer Res.* 61, 7255–7263.

Chang, L., Zhou, G., Soufan, O., and Xia, J. (2020). miRNet 2.0: Network-Based Visual Analytics for miRNA Functional Analysis and Systems Biology. *Nucleic Acids Res.* 48, W244–W251. doi:10.1093/nar/gkaa467

Chen, X., Guo, C., and Kong, J. (2012). Oxidative Stress in Neurodegenerative Diseases. *Neural Regen. Res.* 7, 376–385. doi:10.3969/j.issn.1673-5374.2012.05.009

Chen, X., Sun, G., Tian, E., Zhang, M., Davtyan, H., Beach, T. G., et al. (2021). Modeling Sporadic Alzheimer's Disease in Human Brain Organoids under Serum Exposure. *Adv. Sci.* 8, 2101462. doi:10.1002/advs.202101462

Chien, C. H., Lee, M. J., Liou, H. C., Liou, H. H., and Fu, W. M. (2016). Microglia-Derived Cytokines/Chemokines Are Involved in the Enhancement of LPS-Induced Loss of Nigrostriatal Dopaminergic Neurons in DJ-1 Knockout Mice. *PLoS One* 11, e0151569. doi:10.1371/journal.pone.0151569

Chivero, E. T., Liao, K., Niu, F., Tripathi, A., Tian, C., Buch, S., et al. (2020). Engineered Extracellular Vesicles Loaded with miR-124 Attenuate Cocaine-Mediated Activation of Microglia. *Front. Cel Dev. Biol.* 8, 573. doi:10.3389/fcell.2020.00573

Choi, Y. J., Kim, S., Choi, Y., Nielsen, T. B., Yan, J., Lu, A., et al. (2019). SERPINB1-mediated Checkpoint of Inflammatory Caspase Activation. *Nat. Immunol.* 20, 276–287. doi:10.1038/s41590-018-0303-z

Coles, L. S., Diamond, P., Occhiodoro, F., Vadas, M. A., and Shannon, M. F. (1996). Cold Shock Domain Proteins Repress Transcription from the GM-CSF Promoter. *Nucleic Acids Res.* 24, 2311–2317. doi:10.1093/nar/24.12.2311

Cunha, C., Gomes, C., Vaz, A. R., and Brites, D. (2016). Exploring New Inflammatory Biomarkers and Pathways during LPS-Induced M1 Polarization. *Mediators Inflamm.* 2016, 6986175. doi:10.1155/2016/6986175

de Abreu, R. C., Ramos, C. V., Becher, C., Lino, M., Jesus, C., da Costa Martins, P. A., et al. (2021). Exogenous Loading of miRNAs into Small Extracellular Vesicles. *J. Extracell. Vesicles* 10, e12111. doi:10.1002/jev2.12111

Deczkowska, A., Keren-Shaul, H., Weiner, A., Colonna, M., Schwartz, M., and Amit, I. (2018). Disease-Associated Microglia: A Universal Immune Sensor of Neurodegeneration. *Cell* 173, 1073–1081. doi:10.1016/j.cell.2018.05.003

Dello Russo, C., Cappoli, N., Coletta, I., Mezzogori, D., Paciello, F., Pozzoli, G., et al. (2018). The Human Microglial HMC3 Cell Line: where Do We Stand? A Systematic Literature Review. *J. Neuroinflammation* 15, 259. doi:10.1186/S12974-018-1288-0

Drummond, E., and Wisniewski, T. (2017). Alzheimer's Disease: Experimental Models and Reality. *Acta Neuropathol.* 133, 155–175. doi:10.1007/s00401-016-1662-x

Eitan, E., Hutchison, E. R., Marosi, K., Comotto, J., Mustapic, M., Nigam, S. M., et al. (2016). Extracellular Vesicle-Associated Aβ Mediates Trans-neuronal Bioenergetic and Ca2+-Handling Deficits in Alzheimer's Disease Models. *Npj Aging Mech. Dis.* 2, 16019. doi:10.1038/npjamd.2016.19

Fan, Z., Brooks, D. J., Okello, A., and Edison, P. (2017). An Early and Late Peak in Microglial Activation in Alzheimer's Disease Trajectory. *Brain* 140, 792–803. doi:10.1093/brain/aww349

Fauré, J., Lachenal, G., Court, M., Hirrlinger, J., Chatellard-Causse, C., Blot, B., et al. (2006). Exosomes Are Released by Cultured Cortical Neurones. *Mol. Cel. Neurosci.* 31, 642–648. doi:10.1016/j.mcn.2005.12.003

Fernandes, A., Ribeiro, A. R., Monteiro, M., Garcia, G., Vaz, A. R., Brites, D., et al. (2018). Secretome from SH-Sy5y APPSwe Cells Trigger Time-dependent CHME3 Microglia Activation Phenotypes, Ultimately Leading to miR-21 Exosome Shuttling. *Biochimie* 155, 67–82. doi:10.1016/J.BIOCHI.2018.05.015

Franken, H., Mathieson, T., Childs, D., Sweetman, G. M., Werner, T., Tögel, I., et al. (2015). Thermal Proteome Profiling for Unbiased Identification of Direct and Indirect Drug Targets Using Multiplexed Quantitative Mass Spectrometry. *Nat. Protoc.* 10, 1567–1593. doi:10.1038/nprot.2015.101

Fumagalli, M., Lombardi, M., Gressens, P., and Verderio, C. (2018). How to Reprogram Microglia toward Beneficial Functions. *Glia* 66, 2531–2549. doi:10.1002/glia.23484

Garcia, G., Pinto, S., Cunha, M., Fernandes, A., Koistinaho, J., and Brites, D. (2021). Neuronal Dynamics and miRNA Signaling Differ between SH-Sy5y APPSwe and PSEN1 Mutant iPSC-Derived AD Models upon Modulation with miR-124 Mimic and Inhibitor. *Cells* 10, 2424. doi:10.3390/cells10092424

Garner, K. M., Amin, R., Johnson, R. W., Scarlett, E. J., and Burton, M. D. (2018). Microglia Priming by Interleukin-6 Signaling Is Enhanced in Aged Mice. *J. Neuroimmunol.* 324, 90–99. doi:10.1016/j.jneuroim.2018.09.002

Greco, I., Day, N., Riddoch-Contreras, J., Reed, J., Soininen, H., Kłoszewska, I., et al. (2012). Alzheimer's Disease Biomarker Discovery Using In Silico Literature Mining and Clinical Validation. *J. Transl Med.* 10. doi:10.1186/1479-5876-10-217

Han, D., Dong, X., Zheng, D., and Nao, J. (2020). MiR-124 and the Underlying Therapeutic Promise of Neurodegenerative Disorders. *Front. Pharmacol.* 10, 1555. doi:10.3389/fphar.2019.01555

Hartmann, H., Hoehne, K., Rist, E., Louw, A. M., and Schlosshauer, B. (2015). miR-124 Disinhibits Neurite Outgrowth in an Inflammatory Environment. *Cell Tissue Res* 362, 9–20. doi:10.1007/s00441-015-2183-y

Hatziapostolou, M., Polytarchou, C., Aggelidou, E., Drakaki, A., Poultsides, G. A., Jaeger, S. A., et al. (2011). An HNF4α-miRNA Inflammatory Feedback Circuit Regulates Hepatocellular Oncogenesis. *Cell* 147, 1233–1247. doi:10.1016/j.cell.2011.10.043

Hernandez-Guillamon, M., Mawhirt, S., Blais, S., Montaner, J., Neubert, T. A., Rostagno, A., et al. (2015). Sequential Amyloid-β Degradation by the Matrix Metalloproteases MMP-2 and MMP-9. *J. Biol. Chem.* 290, 15078–15091. doi:10.1074/jbc.M114.610931

Hu, Z., and Li, Z. (2017). miRNAs in Synapse Development and Synaptic Plasticity. *Curr. Opin. Neurobiol.* 45, 24–31. doi:10.1016/J.CONB.2017.02.014

Huber, W., von Heydebreck, A., Sültmann, H., Poustka, A., and Vingron, M. (2002). Variance Stabilization Applied to Microarray Data Calibration and to the Quantification of Differential Expression. *Bioinformatics* 18, S96–S104. doi:10.1093/bioinformatics/18.suppl_1.S96

Hughes, C. S., Foehr, S., Garfield, D. A., Furlong, E. E., Steinmetz, L. M., and Krijgsveld, J. (2014). Ultrasensitive Proteome Analysis Using Paramagnetic Bead Technology. *Mol. Syst. Biol.* 10, 757. doi:10.15252/msb.20145625

Janabi, N., Peudenier, S., Héron, B., Ng, K. H., and Tardieu, M. (1995). Establishment of Human Microglial Cell Lines after Transfection of Primary Cultures of Embryonic Microglial Cells with the SV40 Large T Antigen. *Neurosci. Lett.* 195, 105–108. doi:10.1016/0304-3940(94)11792-H

Jiang, D., Gong, F., Ge, X., Lv, C., Huang, C., Feng, S., et al. (2020). Neuron-derived Exosomes-Transmitted miR-124-3p Protect Traumatically Injured Spinal Cord by Suppressing the Activation of Neurotoxic Microglia and Astrocytes. *J. Nanobiotechnology* 18, 105. doi:10.1186/s12951-020-00665-8

Khoonsari, P. E., Häggmark, A., Lönnberg, M., Mikus, M., Kilander, L., Lannfelt, L., et al. (2016). Analysis of the Cerebrospinal Fluid Proteome in Alzheimer's Disease. *PLoS One* 11, e0150672. doi:10.1371/journal.pone.0150672

Ko, C. Y., Chang, W. C., and Wang, J. M. (2015). Biological Roles of CCAAT/Enhancer-binding Protein delta during Inflammation. *J. Biomed. Sci.* 22, 6. doi:10.1186/s12929-014-0110-2

Könnecke, H., and Bechmann, I. (20132013). The Role of Microglia and Matrix Metalloproteinases Involvement in Neuroinflammation and Gliomas. *Clin. Developmental Immunol.* 2013, 1–15. doi:10.1155/2013/914104

Korecka, J. A., van Kesteren, R. E., Blaas, E., Spitzer, S. O., Kamstra, J. H., Smit, A. B., et al. (2013). Phenotypic Characterization of Retinoic Acid Differentiated SH-Sy5y Cells by Transcriptional Profiling. *PLoS One* 8, e63862. doi:10.1371/journal.pone.0063862

Kumar, S., and Reddy, P. H. (2018). MicroRNA-455-3p as a Potential Biomarker for Alzheimer's Disease: An Update. *Front. Aging Neurosci.* 10, 41. doi:10.3389/FNAGI.2018.00041

Le Bras, A. (2021). A New Mouse Model to Study Late-Onset Alzheimer's Disease. *Lab. Anim.* 50, 151. doi:10.1038/s41684-021-00780-5

Lee, S. T., Im, W., Ban, J. J., Lee, M., Jung, K. H., Lee, S. K., et al. (2017). Exosome-Based Delivery of miR-124 in a Huntington's Disease Model. *J. Mov. Disord.* 10, 45–52. doi:10.14802/jmd.16054

Leng, F., and Edison, P. (2021). Neuroinflammation and Microglial Activation in Alzheimer Disease: where Do We Go from Here? *Nat. Rev. Neurol.* 17, 157–172. doi:10.1038/s41582-020-00435-y

Lu, Y., Zhang, T., Shan, S., Wang, S., Bian, W., Ren, T., et al. (2019). MiR-124 Regulates Transforming Growth Factor-B1 Induced Differentiation of Lung Resident Mesenchymal Stem Cells to Myofibroblast by Repressing Wnt/β-Catenin Signaling. *Dev. Biol.* 449, 115–121. doi:10.1016/j.ydbio.2019.02.010

Mander, P., and Brown, G. C. (2005). Activation of Microglial NADPH Oxidase Is Synergistic with Glial iNOS Expression in Inducing Neuronal Death: a Dual-Key Mechanism of Inflammatory Neurodegeneration. *J. Neuroinflammation* 2, 20. doi:10.1186/1742-2094-2-20

Mastrangelo, M. A., Sudol, K. L., Narrow, W. C., and Bowers, W. J. (2009). Interferon-{gamma} Differentially Affects Alzheimer's Disease Pathologies and Induces Neurogenesis in Triple Transgenic-AD Mice. *Am. J. Pathol.* 175, 2076–2088. doi:10.2353/AJPATH.2009.090059

McGowan, H., Mirabella, V. R., Hamod, A., Karakhanyan, A., Mlynaryk, N., Moore, J. C., et al. (2018). hsa-let-7c miRNA Regulates Synaptic and Neuronal Function in Human Neurons. *Front. Synaptic Neurosci.* 10, 19. doi:10.3389/FNSYN.2018.00019

Meda, L., Cassatella, M. A., Szendrei, G. I., Otvos, L., Baron, P., Villalba, M., et al. (1995). Activation of Microglial Cells by β-amyloid Protein and Interferon-γ. *Nature* 374, 647–650. doi:10.1038/374647a0

Mi, H., Ebert, D., Muruganujan, A., Mills, C., Albou, L. P., Mushayamaha, T., et al. (2021). PANTHER Version 16: A Revised Family Classification, Tree-Based Classification Tool, Enhancer Regions and Extensive API. *Nucleic Acids Res.* 49, D394–D403. doi:10.1093/nar/gkaa1106

Moggridge, S., Sorensen, P. H., Morin, G. B., and Hughes, C. S. (2018). Extending the Compatibility of the SP3 Paramagnetic Bead Processing Approach for Proteomics. *J. Proteome Res.* 17, 1730–1740. doi:10.1021/acs.jproteome.7b00913

Mühl, H., and Pfeilschifter, J. (2003). Anti-inflammatory Properties of Pro-inflammatory Interferon-γ. *Int. Immunopharmacol.* 3, 1247–1255. doi:10.1016/S1567-5769(03)00131-0

Müller, I. I., Chatterjee, M., Schneider, M., Borst, O., Seizer, P., Schönberger, T., et al. (2014). Gremlin-1 Inhibits Macrophage Migration Inhibitory Factor-dependent Monocyte Function and Survival. *Int. J. Cardiol.* 176, 923–929. doi:10.1016/j.ijcard.2014.08.051

Munir, J., Yoon, J. K., and Ryu, S. (2020). Therapeutic miRNA-Enriched Extracellular Vesicles: Current Approaches and Future Prospects. *Cells* 9, 2271. doi:10.3390/cells9102271

Pan, H. C., Yang, C. N., Hung, Y. W., Lee, W. J., Tien, H. R., Shen, C. C., et al. (2013). Reciprocal Modulation of C/EBP-α and C/EBP-β by IL-13 in Activated Microglia Prevents Neuronal Death. *Eur. J. Immunol.* 43, 2854–2865. doi:10.1002/eji.201343301

Paolicelli, R. C., Bolasco, G., Pagani, F., Maggi, L., Scianni, M., Panzanelli, P., et al. (2011). Synaptic Pruning by Microglia Is Necessary for normal Brain Development. *Science* 333, 1456–1458. doi:10.1126/science.1202529

Perez-Riverol, Y., Csordas, A., Bai, J., Bernal-Llinares, M., Hewapathirana, S., Kundu, D. J., et al. (2019). The PRIDE Database and Related Tools and Resources in 2019: Improving Support for Quantification Data. *Nucleic Acids Res.* 47, D442–D450. doi:10.1093/nar/gky1106

Phatnani, H. P., Guarnieri, P., Friedman, B. A., Carrasco, M. A., Muratet, M., O'Keeffe, S., et al. (2013). Intricate Interplay between Astrocytes and Motor Neurons in ALS. *Proc. Natl. Acad. Sci. U S A.* 110, E756–E765. doi:10.1073/pnas.1222361110

Pinto, S., Cunha, C., Barbosa, M., Vaz, A. R., and Brites, D. (2017). Exosomes from NSC-34 Cells Transfected with hSOD1-G93a Are Enriched in Mir-124 and Drive Alterations in Microglia Phenotype. *Front. Neurosci.* 11, 273. doi:10.3389/fnins.2017.00273

Pomeshchik, Y., Klementieva, O., Gil, J., Martinsson, I., Hansen, M. G., de Vries, T., et al. (2020). Human iPSC-Derived Hippocampal Spheroids: An Innovative Tool for Stratifying Alzheimer Disease Patient-specific Cellular Phenotypes and Developing Therapies. *Stem Cel Rep.* 15, 256–273. doi:10.1016/j.stemcr.2020.06.001

Ponomarev, E. D., Veremeyko, T., Barteneva, N., Krichevsky, A. M., and Weiner, H. L. (2011). MicroRNA-124 Promotes Microglia Quiescence and Suppresses EAE by Deactivating Macrophages via the C/EBP-α-PU.1 Pathway. *Nat. Med.* 17, 64–70. doi:10.1038/nm.2266

R Core Team (2020). R: A Language and Environment for Statistical Computing. Available at: https://www.r-project.org/.

Ringland, C., Schweig, J. E., Eisenbaum, M., Paris, D., Ait-Ghezala, G., Mullan, M., et al. (2021). MMP9 Modulation Improves Specific Neurobehavioral Deficits in a Mouse Model of Alzheimer's Disease. *BMC Neurosci.* 22, 39. doi:10.1186/s12868-021-00643-2

Rock, R. B., Hu, S., Deshpande, A., Munir, S., May, B. J., Baker, C. A., et al. (2005). Transcriptional Response of Human Microglial Cells to Interferon-Gamma. *Genes Immun.* 6, 712–719. doi:10.1038/sj.gene.6364246

Saito, Y., and Saito, H. (2012). MicroRNAs in Cancers and Neurodegenerative Disorders. *Front. Genet.* 3, 194. doi:10.3389/fgene.2012.00194

Saraiva, C., Paiva, J., Santos, T., Ferreira, L., and Bernardino, L. (2016). MicroRNA-124 Loaded Nanoparticles Enhance Brain Repair in Parkinson's Disease. *J. Control Release* 235, 291–305. doi:10.1016/j.jconrel.2016.06.005

Savitski, M. M., Wilhelm, M., Hahne, H., Kuster, B., and Bantscheff, M. (2015). A Scalable Approach for Protein False Discovery Rate Estimation in Large Proteomic Data Sets. *Mol. Cel. Proteomics* 14, 2394–2404. doi:10.1074/mcp.M114.046995

Schindelin, J., Arganda-Carreras, I., Frise, E., Kaynig, V., Longair, M., Pietzsch, T., et al. (2012). Fiji: An Open-Source Platform for Biological-Image Analysis. *Nat. Methods* 9, 676–682. doi:10.1038/nmeth.2019

Shirazi, S., Huang, C.-C., Kang, M., Lu, Y., Ravindran, S., and Cooper, L. F. (2021). The Importance of Cellular and Exosomal miRNAs in Mesenchymal Stem Cell Osteoblastic Differentiation. *Sci. Rep.* 11, 1–14. doi:10.1038/s41598-021-85306-2

Sierksma, A., Lu, A., Mancuso, R., Fattorelli, N., Thrupp, N., Salta, E., et al. (2020). Novel Alzheimer Risk Genes Determine the Microglia Response to Amyloid-β but Not to TAU Pathology. *EMBO Mol. Med.* 12, e10606. doi:10.15252/EMMM.201910606

Silva, S. L., Osório, C., Vaz, A. R., Barateiro, A., Falcão, A. S., Silva, R. F., et al. (2011). Dynamics of Neuron-Glia Interplay upon Exposure to Unconjugated Bilirubin. *J. Neurochem.* 117, 412–424. doi:10.1111/j.1471-4159.2011.07200.x

Sonntag, K. C., Woo, T. U., and Krichevsky, A. M. (2012). Converging miRNA Functions in Diverse Brain Disorders: A Case for miR-124 and miR-126. *Exp. Neurol.* 235, 427–435. doi:10.1016/j.expneurol.2011.11.035

Spencer, N. G., Schilling, T., Miralles, F., and Eder, C. (2016). Mechanisms Underlying Interferon-γ-Induced Priming of Microglial Reactive Oxygen Species Production. *PLoS One* 11, e0162497. doi:10.1371/journal.pone.0162497

Sun, Y., Luo, Z. M., Guo, X. M., Su, D. F., and Liu, X. (2015). An Updated Role of microRNA-124 in central Nervous System Disorders: a Review. *Front. Cel. Neurosci.* 9, 193. doi:10.3389/fncel.2015.00193

Svensson, L., Howarth, K., McDowall, A., Patzak, I., Evans, R., Ussar, S., et al. (2009). Leukocyte Adhesion Deficiency-III Is Caused by Mutations in KINDLIN3 Affecting Integrin Activation. *Nat. Med.* 15, 306–312. doi:10.1038/nm.1931

Svoboda, D. S., Barrasa, M. I., Shu, J., Rietjens, R., Zhang, S., Mitalipova, M., et al. (2019). Human iPSC-Derived Microglia Assume a Primary Microglia-like State after Transplantation into the Neonatal Mouse Brain. *Proc. Natl. Acad. Sci. U S A.* 116, 25293–25303. doi:10.1073/pnas.1913541116

Ta, T. T., Dikmen, H. O., Schilling, S., Chausse, B., Lewen, A., Hollnagel, J. O., et al. (2019). Priming of Microglia with IFN-γ Slows Neuronal Gamma Oscillations *In Situ*. *Proc. Natl. Acad. Sci. U. S. A.* 116, 4637–4642. doi:10.1073/pnas.1813562116

Uriarte Huarte, O., Richart, L., Mittelbronn, M., and Michelucci, A. (2021). Microglia in Health and Disease: The Strength to Be Diverse and Reactive. *Front. Cel. Neurosci.* 15, 107. doi:10.3389/fncel.2021.660523

Veremeyko, T., Kuznetsova, I. S., Dukhinova, M., W Y Yung, A., Kopeikina, E., Barteneva, N. S., et al. (2019). Neuronal Extracellular microRNAs miR-124 and miR-9 Mediate Cell-Cell Communication between Neurons and Microglia. *J. Neurosci. Res.* 97, 162–184. doi:10.1002/jnr.24344

Vitek, M. P., Araujo, J. A., Fossel, M., Greenberg, B. D., Howell, G. R., Rizzo, S. J. S., et al. (2020). Translational Animal Models for Alzheimer's Disease: An Alzheimer's Association Business Consortium Think Tank. *Ad&d Transl Res. Clin. Interv.* 6, e12114. doi:10.1002/trc2.12114

von Bernhardi, R., Eugenín-von Bernhardi, L., and Eugenín, J. (2015). Microglial Cell Dysregulation in Brain Aging and Neurodegeneration. *Front. Aging Neurosci.* 7, 124. doi:10.3389/fnagi.2015.00124

Vukovic, J., Ruitenberg, M. J., Roet, K., Franssen, E., Arulpragasam, A., Sasaki, T., et al. (2009). The Glycoprotein Fibulin-3 Regulates Morphology and Motility of Olfactory Ensheathing Cells *In Vitro*. *Glia* 57, 424–443. doi:10.1002/glia.20771

Wang, G., Huang, Y., Wang, L. L., Zhang, Y. F., Xu, J., Zhou, Y., et al. (2016). MicroRNA-146a Suppresses ROCK1 Allowing Hyperphosphorylation of Tau in Alzheimer's Disease. *Sci. Rep.* 6, 26697. doi:10.1038/srep26697

Wang, L., Deng, W., Shi, T., and Ma, D. (2008). URP2SF, a FERM and PH Domain Containing Protein, Regulates NF-kappaB and Apoptosis. *Biochem. Biophys. Res. Commun.* 368, 899–906. doi:10.1016/j.bbrc.2008.02.024

Wang, X., Liu, D., Huang, H. Z., Wang, Z. H., Hou, T. Y., Yang, X., et al. (2018). A Novel MicroRNA-124/PTPN1 Signal Pathway Mediates Synaptic and Memory Deficits in Alzheimer's Disease. *Biol. Psychiatry* 83, 395–405. doi:10.1016/j.biopsych.2017.07.023

Wang, X.-X., Tan, M.-S., Yu, J.-T., and Tan, L. (2014). Matrix Metalloproteinases and Their Multiple Roles in Alzheimer's Disease. *Biomed. Res. Int.* 2014, 1–8. doi:10.1155/2014/908636

Wasilewski, D., Villalba-Moreno, N. D., Stange, I., Glatzel, M., Sepulveda-Falla, D., and Krasemann, S. (2022). Reactive Astrocytes Contribute to Alzheimer's Disease-Related Neurotoxicity and Synaptotoxicity in a Neuron-Astrocyte Co-culture Assay. *Front. Cel. Neurosci.* 15, 540. doi:10.3389/fncel.2021.739411

West, P. K., Viengkhou, B., Campbell, I. L., and Hofer, M. J. (2019). Microglia Responses to Interleukin-6 and Type I Interferons in Neuroinflammatory Disease. *Glia* 67, 1821–1841. doi:10.1002/glia.23634

Xie, J., and Guo, Q. (2005). PAR-4 Is Involved in Regulation of Beta-Secretase Cleavage of the Alzheimer Amyloid Precursor Protein. *J. Biol. Chem.* 280, 13824–13832. doi:10.1074/jbc.M411933200

Xu, X., Li, S., Lin, Y., Chen, H., Hu, Z., Mao, Y., et al. (2013). MicroRNA-124-3p Inhibits Cell Migration and Invasion in Bladder Cancer Cells by Targeting ROCK1. *J. Transl. Med.* 11, 276. doi:10.1186/1479-5876-11-276

Xu, Z., Zhang, K., Wang, Q., and Zheng, Y. (2019). MicroRNA-124 I-mproves F-unctional R-ecovery and S-uppresses Bax-dependent A-poptosis in R-ats F-ollowing S-pinal C-ord I-njury. *Mol. Med. Rep.* 19, 2551–2560. doi:10.3892/mmr.2019.9904

Xue, Q., Yu, C., Wang, Y., Liu, L., Zhang, K., Fang, C., et al. (2016). miR-9 and miR-124 Synergistically Affect Regulation of Dendritic Branching via the AKT/GSK3β Pathway by Targeting Rap2a. *Sci. Rep.* 6, 26781. doi:10.1038/srep26781

Yang, J., Zhang, X., Chen, X., Wang, L., and Yang, G. (2017). Exosome Mediated Delivery of miR-124 Promotes Neurogenesis after Ischemia. *Mol. Ther. Nucleic Acids* 7, 278–287. doi:10.1016/j.omtn.2017.04.010

Yang, K., Shen, J., Chen, S. W., Qin, J., Zheng, X. Y., and Xie, L. P. (2016). Upregulation of PAWR by Small Activating RNAs Induces Cell Apoptosis in Human Prostate Cancer Cells. *Oncol. Rep.* 35, 2487–2493. doi:10.3892/or.2016.4582

Yang, Y., Ye, Y., Kong, C., Su, X., Zhang, X., Bai, W., et al. (2019). MiR-124 Enriched Exosomes Promoted the M2 Polarization of Microglia and Enhanced Hippocampus Neurogenesis after Traumatic Brain Injury by Inhibiting TLR4 Pathway. *Neurochem. Res.* 44, 811–828. doi:10.1007/s11064-018-02714-z

Yardeni, T., Fine, R., Joshi, Y., Gradus-Pery, T., Kozer, N., Reichenstein, I., et al. (2018). High Content Image Analysis Reveals Function of miR-124 Upstream of Vimentin in Regulating Motor Neuron Mitochondria. *Sci. Rep.* 8, 59. doi:10.1038/s41598-017-17878-x

Yu, A., Zhang, T., Duan, H., Pan, Y., Zhang, X., Yang, G., et al. (2017). MiR-124 Contributes to M2 Polarization of Microglia and Confers Brain Inflammatory protection via the C/EBP-α Pathway in Intracerebral Hemorrhage. *Immunol. Lett.* 182, 1–11. doi:10.1016/j.imlet.2016.12.003

Yu, J. Y., Chung, K. H., Deo, M., Thompson, R. C., and Turner, D. L. (2008). MicroRNA miR-124 Regulates Neurite Outgrowth during Neuronal Differentiation. *Exp. Cel Res.* 314, 2618–2633. doi:10.1016/j.yexcr.2008.06.002

Yuyama, K., and Igarashi, Y. (2017). Exosomes as Carriers of Alzheimer's Amyloid-SS. *Front. Neurosci.* 11, 229. doi:10.3389/fnins.2017.00229

Zarrouk, A., Vejux, A., Nury, T., El Hajj, H. I., Haddad, M., Cherkaoui-Malki, M., et al. (2012). Induction of Mitochondrial Changes Associated with Oxidative Stress on Very Long Chain Fatty Acids (C22:0, C24:0, or C26:0)-Treated Human Neuronal Cells (SK-NB-E). *Oxidative Med. Cell Longevity* 2012, 623257. doi:10.1155/2012/623257

Zhang, J., He, H., Qiao, Y., Zhou, T., He, H., Yi, S., et al. (2020). Priming of Microglia with IFN-γ Impairs Adult Hippocampal Neurogenesis and Leads to Depression-like Behaviors and Cognitive Defects. *Glia* 68, 2674–2692. doi:10.1002/glia.23878

Zhao, J., He, Z., and Wang, J. (2021). MicroRNA-124: A Key Player in Microglia-Mediated Inflammation in Neurological Diseases. *Front. Cel. Neurosci.* 15, 451. doi:10.3389/fncel.2021.771898

Zheng, D., Huo, M., Li, B., Wang, W., Piao, H., Wang, Y., et al. (2021). The Role of Exosomes and Exosomal MicroRNA in Cardiovascular Disease. *Front. Cel Dev. Biol.* 8, 1810. doi:10.3389/FCELL.2020.616161

Zhu, X., Rottkamp, C. A., Hartzler, A., Sun, Z., Takeda, A., Boux, H., et al. (2001). Activation of MKK6, an Upstream Activator of P38, in Alzheimer's Disease. *J. Neurochem.* 79, 311–318. doi:10.1046/j.1471-4159.2001.00597.x

**Conflict of Interest:** The authors declare that the research was conducted in the absence of any commercial or financial relationships that could be construed as a potential conflict of interest.

**Publisher's Note:** All claims expressed in this article are solely those of the authors and do not necessarily represent those of their affiliated organizations or those of the publisher, the editors, and the reviewers. Any product that may be evaluated in this article, or claim that may be made by its manufacturer, is not guaranteed or endorsed by the publisher.

frontiers | Frontiers in Neuroscience

REVIEW
published: 09 June 2022
doi: 10.3389/fnins.2022.878296

# Cell Non-autonomous Proteostasis Regulation in Aging and Disease

*Joao Vasco Ferreira*, Ana da Rosa Soares† and Paulo Pereira*

*Proteostasis and Intercellular Communication Lab, Chronic Diseases Research Centre (CEDOC), NOVA Medical School, Faculdade de Ciencias Medicas, Universidade NOVA de Lisboa, Lisbon, Portugal*

Aging is a risk factor for a number of diseases, being the more notorious ones perhaps neurodegenerative diseases such as Alzheimer's and Parkinson's. These and other age-related pathologies are often associated with accumulation of proteotoxic material inside cells, as well as with the accumulation of protein deposits extracellularly. It is widely accepted that this accumulation of toxic proteins trails a progressive decline in the mechanisms that regulate protein homeostasis, or proteostasis, during aging. However, despite significant efforts, the progress in terms of novel or improved therapies targeting accumulation of proteotoxic material has been rather limited. For example, clinical trials for new drugs aimed at treating Alzheimer's disease, by preventing accumulation of toxic proteins, have notoriously failed. On the other hand, it is becoming increasingly apparent that regulation of proteostasis is not a cell autonomous process. In fact, cells rely on complex transcellular networks to maintain tissue and organ homeostasis involving endocrine and paracrine signaling pathways. In this review we will discuss the impact of cell non-autonomous proteostasis mechanisms and their impact in aging and disease. We will focus on how transcellular proteostasis networks can shed new light into stablished paradigms about the aging of organisms.

**Keywords: proteostasis, molecular chaperones, transcellular, misfolding, proteotoxicity**

OPEN ACCESS

***Edited by:***
*Valle Palomo,*
*Spanish National Research Council (CSIC), Spain*

***Reviewed by:***
*Ehud Cohen,*
*Hebrew University of Jerusalem, Israel*
*Anat Ben-Zvi,*
*Ben-Gurion University of the Negev, Israel*

****Correspondence:***
*Joao Vasco Ferreira*
*joao.ferreira@nms.unl.pt*

***†Present address:***
*Ana da Rosa Soares,*
*Instituto de Medicina Molecular João Lobo Antunes, Faculdade de Medicina, Universidade de Lisboa, Lisboa, Portugal*

***Specialty section:***
*This article was submitted to Neuropharmacology, a section of the journal Frontiers in Neuroscience*

***Received:*** *17 February 2022*
***Accepted:*** *18 May 2022*
***Published:*** *09 June 2022*

***Citation:***
*Ferreira JV, da Rosa Soares A and Pereira P (2022) Cell Non-autonomous Proteostasis Regulation in Aging and Disease. Front. Neurosci. 16:878296. doi: 10.3389/fnins.2022.878296*

## INTRODUCTION

### Preserving the Proteome

By continuous accumulation of random DNA mutations, selection by survival and reproduction rate, organisms evolved by piecemeal modification of their proteins. In time, proteins increased in variety and complexity, allowing for more intricate enzymatic processes and ever more sophisticated protein assemblies. However, as an extraordinary diverse collection of proteins emerged, organisms struggled to preserve proteome functionality, as higher complexity often compromises structural integrity of proteins. We now know that organisms, from bacteria and archaea to mammals, have developed intricate mechanisms that assist in protein maintenance and quality control, by tightly controlling protein synthesis, supporting the folding of individual proteins and assembly of protein complexes, as well as disposing of damaged or otherwise unwanted ones. This includes, for example, the ribosome-associated quality control factors during synthesis, the aid in folding and support in conformation offered by molecular chaperones or the proteolytic mechanisms that eliminate those proteins rendered obsolete (Balch et al., 2008; Powers et al., 2009; Labbadia and Morimoto, 2015b; Balchin et al., 2016; Deuerling et al., 2019; Jayaraj et al., 2020; Morimoto, 2020; Rebeaud et al., 2021). These and other mechanisms involved in governing protein homeostasis, or proteostasis, comprise an extensive network or around 2000 proteins in humans (Klaips et al., 2018; Hipp et al., 2019). Thus, at the cellular level, a network of proteostasis mechanism is in place to minimize error and maximize efficiency. A malfunction of

these mechanisms is extremely detrimental to cellular health and proteostasis loss is often associated with aging and disease.

However, the damage associated to proteostasis breakdown is hardly confined to a group of cells or tissue in an organism. While approaches to the contribution of proteostasis to disease have mostly assumed that regulation of proteostasis networks in living organisms is a cell autonomous process, an overwhelming amount of evidences, gathered over the years, show that organisms organize a proteostasis response a in an integrated, cell non-autonomous level, as well (Taylor et al., 2014; Desdin-Mico and Mittelbrunn, 2017; Takeuchi, 2018; Miles et al., 2019; Miller et al., 2020; Morimoto, 2020). This response involves communication between different cell types, tissues and organs. The advantages of a transcellular proteostasis regulation appear to be manifold. For example, sensorial tissues detect environmental changes that boost proteostasis in sensitive or essential cells for the organism to survive in new and challenging conditions. On the other hand, stress induced proteostasis activation in one tissue can stimulate proteostasis mechanisms in distant tissues, in preparation for stresses to come. Additionally, proteostasis machinery components can be spared from more proteostasis competent cells and delivered to less resilient ones, while cells with failing proteostasis networks can transfer unwanted proteins to neighboring cells and be relieved from the burden (Taylor et al., 2014; Desdin-Mico and Mittelbrunn, 2017; Takeuchi, 2018; Miles et al., 2019; Miller et al., 2020; Morimoto, 2020).

## Protein Synthesis and the Origin of Protein Misfolding

Most proteins need to reach a defined tridimensional structure, or folding conformation, to attain biological function (Hipp et al., 2019). However, the folding kinetics of proteins is constantly being challenged (Morimoto, 2020). While generally the folded (or native) state is thermodynamically favored, often proteins endure challenges that promote additional kinetically stable non-native states (Hipp et al., 2019). Right from the start, biosynthetic errors, which are inherent to protein synthesis, can obstruct protein folding and promote loss of function or toxic gain of function (Morimoto, 2020). Even when successfully translated, specific regions within proteins can be thermodynamically unstable and inherently hard to maintain in the appropriate folding conformation, without assistance from molecular chaperones to maintain conformational stability (Demarest et al., 2002; Dunker et al., 2008; Uversky et al., 2008; Hipp et al., 2019). However, harsh environmental conditions and stresses such as high temperatures and oxidation, as well as additional forms of post-translational modification, are the major drivers for defective folding kinetics. Additionally, a crowded intracellular space promotes non-native interactions and facilitates protein unfolding (Ellis and Minton, 2006; Morimoto, 2020). In humans, cells contain more than 10.000 different proteins with ranging conformational stabilities (Kulak et al., 2017). Moreover, some proteins can reach millions of copies per cell (Ghaemmaghami et al., 2003). Also, individuals within a population contain single-nucleotide variations that may further hinder the folding kinetics of proteins (Lek et al., 2016). Overall, all these different contexts are likely to result in large amounts of metastable polypeptides, with tendency to misfold and create toxic oligomers and aggregates. Therefore, protein conformation and abundance must be strictly controlled, to ensure proper cellular signaling, maintain metabolic flow and the correct assembly of molecular machinery responsible for complex cellular functions such as DNA replication, oxidative phosphorylation and protein synthesis itself.

## Proteome Preservation by Molecular Chaperones

During evolution, as proteins increased in complexity to execute new or more intricate tasks, polypeptide folding efficiency dropped. In fact, the folded conformation of proteins is generally very perilous such that a substantial number of copies of a given protein can exist in partially unfolded states (Hipp et al., 2019). To hold proteome stability and maintain proteins functionally active, molecular chaperones emerged, a family of highly conserved proteins that act by directly interacting with the unstructured polypeptides backbones of proteins in non-native conformations (Hartl, 1996; Rebeaud et al., 2021). The emergence of molecular chaperones supported the structural evolution of proteins into more complex molecules, capable of executing new or improved biological functions. Molecular chaperones can be subdivided into different sub-families (Hartl et al., 2011; Kim Y. E. et al., 2013; Balchin et al., 2016; Carra et al., 2017; Lee et al., 2018). By the direct interaction with client proteins and the hydrolysis of ATP, molecular chaperones improve the folding kinetics of *de novo* synthesized proteins, prevent unfolding and counteract oligomerization/aggregation of polypeptides in non-native conformations.

When under stress, cells can boost the expression of chaperones through specific transcriptions factors such as Heat Shock Factor 1 (HSF1). In steady state, an abundance of inactive chaperones bind to HSF1 to block its activity. Under stress, a surge in chaperone demand titrates chaperones away from HSF1, releasing the transcription factor to command the synthesis of new molecular chaperones (Zou et al., 1998; Anckar and Sistonen, 2011; Zheng et al., 2016; Gomez-Pastor et al., 2018).

Moreover, chaperones are also important in deciding if a client protein has exhausted its time for folding and should be degraded, by coupling molecular chaperones with the ubiquitin-proteasome and autophagy/lysosomal pathways through the ubiquitin ligase CHIP, that binds molecular chaperones and adds ubiquitin chains to client proteins, triggering their degradation (Marques et al., 2006; Ferreira et al., 2013, 2015; Elia et al., 2019; Moran Luengo et al., 2019; Finley and Prado, 2020).

## Elimination of Misfolded Proteins

Elimination of proteins is essential for proteome stability in two major ways, one by adjusting the levels of proteins so they are kept in soluble concentrations (Ciryam et al., 2013, 2015), and a second one by avoiding accumulation of faulty or obsolete proteins (Hipp et al., 2019). Proteins can be degraded by the ubiquitin-proteasome pathway (UPS), whereby proteins

tagged with a polyubiquitin chain, conjugated by covalently attaching single ubiquitin moieties by the lysine at position 48, are recognized by the 26S proteasome for degradation (Ciechanover, 1994). Additionally, proteins can be degraded by the autophagic-lysosomal pathway (ALP), a collection of mechanisms that allows for the degradation of individual proteins as well as protein complexes, organelles and even protein aggregates (Ferreira et al., 2013, 2015; Finkbeiner, 2020). Both UPS and ALP directly or indirectly need ATP and use molecular chaperones both to detect unwanted protein species and unfold proteins prior to degradation. Over the years evidences have shown that, in many instances, ALP also uses ubiquitination as a signal for degradation (Kirkin et al., 2009; Ferreira et al., 2013, 2015; Finkbeiner, 2020). While lysine 48 conjugated ubiquitin chains are a signal for proteasomal degradation, lysine 63 and other ubiquitin chains may be a signal for ALP degradation.

## Aging and Proteostasis Decline

Deregulation of the mechanisms governing proteostasis leads to protein malfunction and the formation of toxic protein oligomers and aggregates. There is a strong correlation between proteostasis decline and aging, such that is a feature of many age-related diseases such as Alzheimer's Disease, Parkinson's Disease, Age-related Macular Degeneration, Amyotrophic Lateral Sclerosis, and others (Morimoto, 2020). Thus, maintaining proteostasis is essential for organismal health. However, a genetically encoded aging component is evident in *C. elegans* where a sharp change in protein abundance and increase in protein aggregation is clear upon reaching the reproductive age (Walther et al., 2015). Moreover, maintaining proteostasis is energetically costly as well. Both molecular chaperones activity and proteolysis consume ATP. The high energetic cost is consistent with the "disposable soma" theory, whereby organisms might often trade longevity for reproduction, likely by decreasing proteostasis robustness to save energy in favor of progeny generation (Hsin and Kenyon, 1999; Ben-Zvi et al., 2009; Shemesh et al., 2013; Labbadia and Morimoto, 2015a). Additional evidences nonetheless suggest that while there are trade-offs between the soma and the germline, they are not purely based on energy availability (Sala and Morimoto, 2022), as we will discuss later.

In parallel to programmed proteostasis decline, protein aggregation by itself can cause the misfolding of additional proteins in its vicinity, a compound effect exacerbated by post-translation modifications triggered by environmental stress that slowly overburdens proteostasis mechanisms and leads to proteostasis loss (Morimoto, 2020). The combination of programmed decline of proteostasis and environmental stress creates the aging phenotype. The collapse of the proteostasis networks will lead to the accumulation of misfolded, damaged and obsolete proteins, some of which will end up oligomerizing and even aggregating. This phenotype is particularly damaging to post-mitotic cells that cannot use asymmetric cell division to dilute and distribute protein toxicity.

In *C. elegans*, the onset of proteostasis mechanisms failure happens early in life (Ben-Zvi et al., 2009). Chronic expression of misfolded proteins in age-onset neurodegenerative disease leads to accumulation of misfolded species and aggregates that overwhelm proteostasis as a basis of cellular dysfunction (Gidalevitz et al., 2006; Douglas and Dillin, 2010). However, the expression of different aggregation-prone proteins, such as amyloid β or polyQ35 leads to a similar, but not identical, chaperone network activation (Brehme et al., 2014). Surprisingly, chaperone induction upon the expression of aggregative proteins can have opposite effects. For example, torsins 1 and 2 mitigate the toxicity of HD-associated polyQ stretches and the ALS-causing mutated superoxide dismutase 1 (SOD-1), but exacerbate the proteotoxicity of A-beta (Boocholez et al., 2022). This apparent heterogenicity in proteome protection mechanisms reflects the intricacy of age-related diseases and highlights the complexity of developing putative therapeutic approaches.

# CELL NON-AUTONOMOUS COORDINATION OF PROTEOSTASIS

A focus on the study of proteostasis at the cellular level has led to models of proteostasis regulation that skew to cell autonomy. However, in recent years, mounting evidences also indicate that there are mechanisms in place to support a systemic, intercellular and inter tissue, cell non-autonomous variety of networked proteostasis. On one side, pathways regulating systemic proteostasis may control organismal adaptation to stress, by modulating or boosting proteostasis networks in a more even and synchronized manner. On the other, these mechanisms may negatively impact proteostasis by coordinating aging progression and disseminating disease into other cells, tissues and organs. Understanding these mechanisms of systemic proteostasis may offer new and improved ways of boosting proteostasis to mitigate the effects of aging, including the possibility of refining organismal proteostasis by targeting only a small number of cells.

## Systemic Activation of Heat Shock Response

The heat shock response (HSR) is primarily modulated by HSF1, from the heat shock factor (HSF) transcription factor family. HSFs react to increases in temperature, as well as other stresses that can negatively impact protein folding, to recover proteostasis by increasing the amount of available molecular chaperones (Akerfelt et al., 2010).

In a living organism, protection from heat shock also involves changes in behavior, such as moving away from high temperatures. In *C. elegans*, studies in thermolocomotion showed that increasing temperatures activate a pair of amphid finger (AFD) neurons and their postsynaptic amphid Y (AIY) interneurons. In turn, AIY interneurons signal to motor neurons in the muscle wall to promote the movement of organisms away from restrictive temperatures. Surprisingly, inhibition of AFD signaling prevents the HSF-mediated induction of Heat Shock Protein 70 (HSP70) in various non-neuronal tissues of the worm's body following heat shock, in a process shown to be mediated by serotonin. Additionally, activation of AFD neurons by optogenetics is sufficient to activate HSF1, increase

the expression of HSP70 in the whole organism and suppress protein aggregation in muscle tissue (Mori and Ohshima, 1995; Hobert et al., 1997; Inada et al., 2006; Prahlad et al., 2008; Ramot et al., 2008; Prahlad and Morimoto, 2011; Sugi et al., 2011; Tatum et al., 2015).

On the other hand, however, even in the absence of AFD neurons, worms can still activate HSF-1 upon exposure to different stressors, such as the heavy metal cadmium (Prahlad et al., 2008), while AFD incompetent worms were still able to activate the expression of molecular chaperones upon tissue specific expression of polyQ aggregates (Prahlad and Morimoto, 2011). In fact, animals with WT thermosensory neurons express basal levels of chaperones despite the chronic accumulation of misfolded proteins, while retaining their ability to respond to acute heat stress (Prahlad and Morimoto, 2011; Maman et al., 2013). On the other hand mutations in thermosensory neuronal signaling inverts this response, such that chaperone induction in AFD incompetent animals now occurs when misfolded proteins are chronically expressed, but is dampened in response to acute heat stress (Prahlad and Morimoto, 2011; Maman et al., 2013). Therefore, thermosensory neurons are likely to act as neuronal switches for the control of chaperone expression in *C. elegans*, allowing tissues within the organism to maintain optimal levels of chaperones for normal function and yet respond to transient exposures to environmental stress by up-regulating chaperones (Prahlad and Morimoto, 2011; Maman et al., 2013). However, these evidences also highlight that the ability to respond to heat comes at the expense of proteostasis (Prahlad and Morimoto, 2011; Maman et al., 2013). In addition, these observations suggest that systemic proteostasis regulation in *C. elegans* might depend on the particular stress context. Whether this means that different stressors activate different neurons to mediate a proteostasis response, or rather that some stressors preferentially activate cell autonomous mechanisms while others activate cell non-autonomous ones is still a matter of debate.

This might be explained by the fact that additional neurons and neurotransmitters might be implicated in HSR regulation. For example, chemosensory neurons expressing the GPCR thermal receptor 1 (gtr-1) are also involved in systemic HSR activation, as well as inhibiting resistance to stress associated with expression of misfolded proteins (Hobert and Ruvkun, 1998; Beverly et al., 2011; Maman et al., 2013). On the other hand, at the neuromuscular junction, GABA and cholinergic signaling from stimulatory motor neurons can decrease aggregation of polyQ repeats in muscle cells, while the signaling from inhibitory motor neurons acts opposingly to increase polyQ repeats aggregation (Garcia et al., 2007).

Additionally, germline ablation, both in *C. elegans* and drosophila prevents proteostasis collapse in the whole body. This happens because the germline signals to somatic tissues to repress proteome protection, mainly associated to HSF1 inability to bind chaperone promotor regions in the DNA (Flatt et al., 2008; Labbadia and Morimoto, 2015a). However, additional evidences indicate that the impact of reproduction on longevity might be more complex than anticipated (Sala and Morimoto, 2022). For example, the targeted ablation of germ cells leads to lifespan extension, while the abolishment of both germ and somatic gonad cells at the same time fails to do so (Hsin and Kenyon, 1999). In fact, germline ablation acts by activating the longevity gene DAF-19/FOXO in the intestine, through lipophilic hormone signaling (Berman and Kenyon, 2006). In addition, post-translational modifications such as SUMOylation appear to be involved in germline regulation of lifespan (Moll et al., 2018). As far as in vertebrates, a study in zebrafish recently showed that sterile males are more resistant to stress (Chen et al., 2020). Overall, data suggests that there are trade-offs between germline and somatic proteostasis maintenance, even if specific signaling events, rather than solely energetic trade-offs, appear to modulate the longevity of somatic tissues regulated by the germline. In addition, systemic proteostasis regulation appears to involve mechanism of proteome protection as well as, in specific situations, mechanisms of proteostasis depression.

## Systemic Activation of the Endoplasmic Reticulum Unfolded Protein Response

Cell non-autonomous control of proteostasis extends to the UPR$^{ER}$. During protein synthesis, proteome surveillance is mainly sustained by the unfolded protein response of the endoplasmic reticulum (UPR$^{ER}$). When protein misfolding surpasses a certain threshold, excess misfolded proteins displace the UPR$^{ER}$ inhibitory chaperone BiP and bind directly to specific membrane receptors: the activating transcription factor 6, the inositol-requiring protein 1, and protein kinase RNA-like ER kinase, leading to the activation of three separate signaling pathways. These conserved pathways have a compound effect that potentiates protein folding such as augmenting ER cisternal space to reduce protein overcrowding, promoting degradation of unwanted proteins, reducing translation and increasing the expression of proteins with the ability to promote and assist protein folding, referred as molecular chaperones (Ron and Walter, 2007; Taylor et al., 2014). However, deletirious mutations of the octamine receptor 1 from *C. elegans* neurons induce increased expression of UPR$^{ER}$ canonical genes, IRE-1 and X-box Binding Protein 1 (XBP-1), in the whole body (Sun et al., 2012). On the other hand, XBP-1 overexpression in neurons triggers ER chaperone BiP activation both in neurons and the intestine, counteracting the age-related decline of the UPR$^{ER}$ and promoting longevity (Taylor and Dillin, 2013). Intriguingly, a change in lipid metabolism and an increase in oleic acid is needed to activate systemic UPR$^{ER}$ when expressing XBP-1 in neurons (Imanikia et al., 2019). In addition, inhibition of neuropeptide secretion by glial cells expressing XBP-1 inhibits UPR$^{ER}$ activation in distant tissues as well (Frakes et al., 2020). In fact, neuropeptides seem to regulate systemic proteostasis in neurons (Boocholez et al., 2022).

Interestingly, induction of the UPR$^{ER}$ in non-neuronal tissues is activated in *C. elegans* after pathogen infection, in a mechanism mediated by sensory neurons. In mice, XBP-1 expression in pro-opio-melanocortin neurons activates XBP1 in the liver, resulting in an improved liver function (Williams et al., 2014). In tumor cell lines, UPR$^{ER}$ activation under stress leads to upregulation of UPR$^{ER}$ and production of pro-inflammatory cytokines in macrophages, whereas conditioned media from

tumor cells induces UPR$^{ER}$ in dendritic cells, leading to a suppressive phenotype that impairs T cell proliferation and facilitates tumor growth (Mahadevan et al., 2012). The systemic activation of UPR$^{ER}$ strongly emphasizes the importance of maintaining efficiency of proteins synthesis in a synchronized and cell-non-autonomous fashion in the whole body.

## Systemic Activation of the Unfolded Protein Response of the Mitochondria

Maintaining healthy mitochondria is vital for cell fitness. They are fundamental for energy production, primarily through oxidative phosphorylation. However, the mitochondria electron transport chain is not 100% efficient and leaks electrons that are unable to fully reduce oxygen to form water at cytochrome c oxidase, leading to only partial reduction of oxygen to form the anion superoxide. Thus, mitochondria activity is a major source of reactive oxygen species (ROS). ROS damages proteins and promotes protein misfolding. Accumulation of protein damage impairs mitochondrial activity and overloads to mitochondrial chaperone machinery, to which mitochondria respond by degrading damaged proteins using the mitochondria protease caseinolytic peptidase P (CLPP; Pellegrino et al., 2013). Subsequently, the cleaved peptide products from CLPP action are exported to the cytosol by half transporter 1, that is present at the mitochondrial membrane. Peptide export from mitochondria acts upon the activating transcription factor associated with stress 1, to trigger expression of Unfolded Protein Response of the Mitochondria (UPR$^{mito}$) related chaperones (Haynes et al., 2010).

While there are many ways in which the mitochondria ROS can increase *C. elegans* lifespan, including by activating either the hypoxia inducible transcription factor 1 alpha (Lee et al., 2010) or the transcription factor daf-16/FOXO (Senchuk et al., 2018), as well as by lowering ATP production to induce "slow aging" (Yee et al., 2014), lifespan can be extended in a systemic fashion, through cell-non-autonomous regulation of UPR$^{mito}$. Depletion from neurons of the cco-1 protein, a component of the mitochondria electron transport chain, is sufficient to activate UPR$^{mito}$ in the gut, as well as increased lifespan (Durieux et al., 2011). Depletion of cco-1 in the whole organism leads to the same increase in the lifespan in the worm (Durieux et al., 2011). Interestingly, depletion of cco-1 from body wall cells has the opposite effect, reducing lifespan (Durieux et al., 2011). This observation indicates that similar stresses applied to different areas of the body do not wield the same proteome protective measures, and that efficiency of systemic proteostasis activation might depend on both the type of stress and the tissue that is most affected by stress.

On the other hand, expression of Huntington causing protein in polyQ 40-repeat protein in neurons activates the expression of mitochondrial HSP70 (mtHSP70) in the gut of *C. elegans*, in a process mediated by serotonin (Berendzen et al., 2016). Other groups found additional factors that mediate systemic UPR$^{mito}$ activation in *C. elegans*, such as Wnt signaling and neuropeptide FLP-2 (Shao et al., 2016; Zhang et al., 2018).

In mammals, fibroblast growth factor 21 is responsible for signaling to peripheral tissues upon mitochondrial damage in muscle cells, leading to resistance to obesity and improved insulin sensitivity, which might indicate a systemic activation of UPR$^{mito}$ (Kim K. H. et al., 2013).

## Transcellular Chaperone Signaling

Other forms of cell non-autonomous proteostasis regulation involve molecular chaperone signaling that is unrelated to HSF-1 activation. For example, in *C. elegans* specific over-expression of HSP90 in the gut or in neurons protects against misfolding of myosin and amyloid β aggregation in the muscles of the body wall. In neurons, for example, this happens because HSP90 overexpression leads to PQM-1 activation (zinc finger transcription factor) and subsequent HSP90 upregulation in distant tissues by glutamatergic signaling (Taylor and Dillin, 2013; van Oosten-Hawle et al., 2013; O'Brien et al., 2018).

A second form of transcellular chaperone signaling is the direct secretion of molecular chaperones by cells. Initial evidence in mice showed that overexpression of HSP40 in one brain region of polyQ diseased animals lead to the elimination of inclusion bodies in other parts of the brain (Popiel et al., 2012). In drosophila, expression of HSP70 and HSP40 in muscles and fat cells prevented eye degeneration caused by polyQ proteins (Warrick et al., 1999; Kazemi-Esfarjani and Benzer, 2000). These initial observations eventually lead to the discovery that molecular chaperones are secreted to the extracellular space, encased inside a subtype of extracellular vesicles called exosomes (Takeuchi et al., 2015). Exosomes are small extracellular vesicles that are present in virtually all biological fluids and circulate in the blood stream. However, not all chaperones are secreted *via* this non-canonical secretory pathway, only cytosolic ones. Exosomes loaded with cytosolic chaperones are able to get endocytosed by other cells and suppress aggregate formation by polyQ proteins. In drosophila, inhibition of exosome secretion from muscle and fat cells expressing HSP70 and HSP40 suppressed eye regeneration (Takeuchi et al., 2015).

The molecular basis for the loading and secretion of chaperones *via* exosomes is still unclear. However, reports show that depletion of HSC70 from cells decreases HSP40 presence in exosomes (Kampinga and Craig, 2010). Additionally, a recent paper demonstrates that HSC70, and potentially other chaperones that directly interact with HSC70 (such as HSP40, HSP90, and others), are loaded into nascent exosomes by a mechanism dependent on the endo-lysosomal transmembrane receptor LAMP2A (Ferreira et al., 2022). These observations indicate that there is a conserved molecular mechanism for the loading and transfer of molecular chaperones *via* exosomes, with the potential to boost proteostasis in a cell non-autonomous way.

## Transcellular Transfer of Proteotoxic Material

The secretion of misfolded, oligomerized, and/or aggregated material to the extracellular space by vesicles, particularly by exosomes, has been proposed as a new major pathway for the disposal of unwanted proteins. Overburden cells with

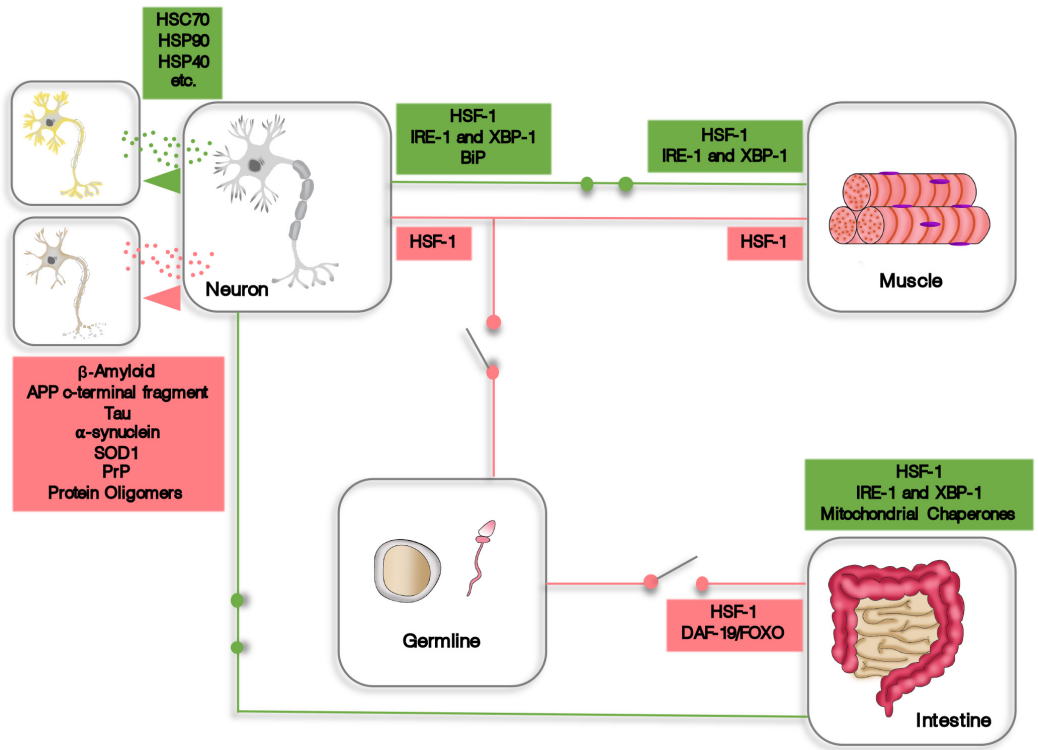


**FIGURE 1 |** A schematic representation of some aspects of cell non-autonomous proteostasis. Expression of HSF-1, XBP-1, and other components of the proteostasis machinery is induced (green circuits) or repressed (red circuits) in one tissue or organ by endocrine signaling originating from distant cells. In addition, cells and tissues can transfer proteostasis machinery or dispose of proteotoxic material using extracellular vesicles.

falling proteostasis capabilities would secrete unwanted and toxic protein material encased inside exosomes. Exosomes originate from multivesicular endosomal compartments and are therefore at the crossroads between protein degradation by the lysosome and vesicle secretion. Analysis of the protein cargo of exosomes supports this hypothesis. Misfolded and prion proteins (PrP) are released in exosomes (Guo et al., 2015), particularly the ones implicated in neurodegenerative diseases such as Huntington's, Alzheimer's and Parkinson's disease, including amyloid β, APP C-terminal fragments, Tau, α-synuclein, SOD1, and the PrP (Fevrier et al., 2004; Rajendran et al., 2006; Perez-Gonzalez et al., 2012; Saman et al., 2012; Grad et al., 2014). Additionally, oligomerized proteins have been shown to be secreted by exosomes upon ubiquitin ligase CHIP inactivation (Ferreira et al., 2019). While the initial effect of the secretion of these proteins might be beneficial, particularly for post-mitotic cells such as neurons and the retina pigmented epithelium, in some instances and over time, such mechanisms could do more harm than good, participating in the spreading of disease rather than in the dilution of the proteotoxic burden.

The mechanisms that regulate the loading of proteotoxic material into nascent exosomes are still a matter of debate. One way this could happen is through the trapping of misfolded proteins bound to the molecular chaperone HSC70, that is included in exosomes, either through the interaction with LAMP2A or by attaching to lipids, in the endosomal limiting membrane, where exosomes are formed (Sahu et al., 2011; Ferreira et al., 2022).

## CONCLUDING REMARKS

While there is still much to be discovered regarding cell non-autonomous proteostasis, there are definitely an overwhelming amount of evidences showing that organisms can build up from cellular based proteostasis mechanisms to a fully integrated and systemic proteostasis network, encompassing the whole body. These transcellular coordinated responses involve endocrine and paracrine intercellular and intertissue communication, either through signaling molecules or by the material exchange of proteostasis machinery and proteotoxic peptides *via* extracellular vesicles (**Figure 1**). Intriguingly, integrated proteostasis networks can function as synchronized proteome protector mechanisms and, opposingly, coordinate proteostasis decline, such as in the example of the germline signaling to inhibit HSF1 activity. These evidences highlight the complexity and intricacy of organismal proteostasis and how important the study of cell non-autonomous proteostasis is. Therefore, we do believe that future research aimed at mitigating the effects of aging should focus on the systemic aspects of

proteostasis to generate new options for innovative and more targeted therapeutic strategies.

## AUTHOR CONTRIBUTIONS

JF conceptualized and wrote and proofread the manuscript. AR and PP conceptualized and proofread the manuscript. All authors contributed to the article and approved the submitted version.

## FUNDING

This study was supported by the "Programa Operacional Regional de Lisboa-FEDER/ Project 02/SAICT/2020/072552," and iNOVA4Health – UIDB/04462/2020 and UIDP/04462/2020, and by the Associated Laboratory LS4FUTURE (LA/P/0087/2020), two programs financially supported by Fundação para a Ciência e Tecnologia / Ministério da Ciência, Tecnologia e Ensino Superior.

## REFERENCES

Akerfelt, M., Morimoto, R. I., and Sistonen, L. (2010). Heat shock factors: integrators of cell stress, development and lifespan. *Nat. Rev. Mol. Cell Biol.* 11, 545–555. doi: 10.1038/nrm2938

Anckar, J., and Sistonen, L. (2011). Regulation of HSF1 function in the heat stress response: implications in aging and disease. *Annu. Rev. Biochem.* 80, 1089–1115. doi: 10.1146/annurev-biochem-060809-095203

Balch, W. E., Morimoto, R. I., Dillin, A., and Kelly, J. W. (2008). Adapting proteostasis for disease intervention. *Science* 319, 916–919.

Balchin, D., Hayer-Hartl, M., and Hartl, F. U. (2016). In vivo aspects of protein folding and quality control. *Science* 353:aac4354. doi: 10.1126/science.aac4354

Ben-Zvi, A., Miller, E. A., and Morimoto, R. I. (2009). Collapse of proteostasis represents an early molecular event in Caenorhabditis elegans aging. *Proc. Natl. Acad. Sci. U S A.* 106, 14914–14919. doi: 10.1073/pnas.0902882106

Berendzen, K. M., Durieux, J., Shao, L. W., Tian, Y., Kim, H. E., Wolff, S., et al. (2016). Neuroendocrine coordination of mitochondrial stress signaling and proteostasis. *Cell* 166, 1553–63e10. doi: 10.1016/j.cell.2016.08.042

Berman, J. R., and Kenyon, C. (2006). Germ-cell loss extends C. elegans life span through regulation of DAF-16 by kri-1 and lipophilic-hormone signaling. *Cell* 124, 1055–1068. doi: 10.1016/j.cell.2006.01.039

Beverly, M., Anbil, S., and Sengupta, P. (2011). Degeneracy and neuromodulation among thermosensory neurons contribute to robust thermosensory behaviors in Caenorhabditis elegans. *J. Neurosci.* 31, 11718–11727. doi: 10.1523/JNEUROSCI.1098-11.2011

Boocholez, H., Marques, F. C., Levine, A., Roitenberg, N., Siddiqui, A. A., Zhu, H., et al. (2022). Neuropeptide signaling and SKN-1 orchestrate differential responses of the proteostasis network to dissimilar proteotoxic insults. *Cell Rep.* 38:110350. doi: 10.1016/j.celrep.2022.110350

Brehme, M., Voisine, C., Rolland, T., Wachi, S., Soper, J. H., Zhu, Y., et al. (2014). A chaperome subnetwork safeguards proteostasis in aging and neurodegenerative disease. *Cell Rep.* 9, 1135–1150. doi: 10.1016/j.celrep.2014.09.042

Carra, S., Alberti, S., Arrigo, P. A., Benesch, J. L., Benjamin, I. J., Boelens, W., et al. (2017). The growing world of small heat shock proteins: from structure to functions. *Cell Stress Chaperones* 22, 601–611. doi: 10.1007/s12192-017-0787-8

Chen, H. Y., Jolly, C., Bublys, K., Marcu, D., and Immler, S. (2020). Trade-off between somatic and germline repair in a vertebrate supports the expensive germ line hypothesis. *Proc. Natl. Acad. Sci. U S A.* 117, 8973–8979. doi: 10.1073/pnas.1918205117

Ciechanover, A. (1994). The ubiquitin-proteasome proteolytic pathway. *Cell* 79, 13–21.

Ciryam, P., Kundra, R., Morimoto, R. I., Dobson, C. M., and Vendruscolo, M. (2015). Supersaturation is a major driving force for protein aggregation in neurodegenerative diseases. *Trends Pharmacol. Sci.* 36, 72–77. doi: 10.1016/j.tips.2014.12.004

Ciryam, P., Tartaglia, G. G., Morimoto, R. I., Dobson, C. M., and Vendruscolo, M. (2013). Widespread aggregation and neurodegenerative diseases are associated with supersaturated proteins. *Cell Rep.* 5, 781–790. doi: 10.1016/j.celrep.2013.09.043

Demarest, S. J., Martinez-Yamout, M., Chung, J., Chen, H., Xu, W., Dyson, H. J., et al. (2002). Mutual synergistic folding in recruitment of CBP/p300 by p160 nuclear receptor coactivators. *Nature* 415, 549–553. doi: 10.1038/415549a

Desdin-Mico, G., and Mittelbrunn, M. (2017). Role of exosomes in the protection of cellular homeostasis. *Cell Adh. Migr.* 11, 127–134. doi: 10.1080/19336918.2016.1251000

Deuerling, E., Gamerdinger, M., and Kreft, S. G. (2019). Chaperone interactions at the ribosome. *Cold Spring Harb. Perspect. Biol.* 11:a033977. doi: 10.1101/cshperspect.a033977

Douglas, P. M., and Dillin, A. (2010). Protein homeostasis and aging in neurodegeneration. *J. Cell Biol.* 190, 719–729.

Dunker, A. K., Silman, I., Uversky, V. N., and Sussman, J. L. (2008). Function and structure of inherently disordered proteins. *Curr. Opin. Struct. Biol.* 18, 756–764. doi: 10.1016/j.sbi.2008.10.002

Durieux, J., Wolff, S., and Dillin, A. (2011). The cell-non-autonomous nature of electron transport chain-mediated longevity. *Cell* 144, 79–91. doi: 10.1016/j.cell.2010.12.016

Elia, L. P., Mason, A. R., Alijagic, A., and Finkbeiner, S. (2019). Genetic regulation of neuronal progranulin reveals a critical role for the autophagy-lysosome pathway. *J. Neurosci.* 39, 3332–3344. doi: 10.1523/JNEUROSCI.3498-17.2019

Ellis, R. J., and Minton, A. P. (2006). Protein aggregation in crowded environments. *Biol. Chem.* 387, 485–497.

Ferreira, J. V., da Rosa Soares, A., Ramalho, J., Maximo Carvalho, C., Cardoso, M. H., Pintado, P., et al. (2022). LAMP2A regulates the loading of proteins into exosomes. *Sci. Adv.* 8:eabm1140. doi: 10.1126/sciadv.abm1140

Ferreira, J. V., Fofo, H., Bejarano, E., Bento, C. F., Ramalho, J. S., Girao, H., et al. (2013). STUB1/CHIP is required for HIF1A degradation by chaperone-mediated autophagy. *Autophagy* 9, 1349–1366. doi: 10.4161/auto.25190

Ferreira, J. V., Rosa Soares, A., Ramalho, J. S., Ribeiro-Rodrigues, T., Maximo, C., Zuzarte, M., et al. (2019). Exosomes and STUB1/CHIP cooperate to maintain intracellular proteostasis. *PLoS One* 14:e0223790. doi: 10.1371/journal.pone.0223790

Ferreira, J. V., Soares, A. R., Ramalho, J. S., Pereira, P., and Girao, H. (2015). K63 linked ubiquitin chain formation is a signal for HIF1A degradation by Chaperone-Mediated Autophagy. *Sci. Rep.* 5:10210. doi: 10.1038/srep10210

Fevrier, B., Vilette, D., Archer, F., Loew, D., Faigle, W., Vidal, M., et al. (2004). Cells release prions in association with exosomes. *Proc. Natl. Acad. Sci. U S A.* 101, 9683–9688. doi: 10.1073/pnas.0308413101

Finkbeiner, S. (2020). The autophagy lysosomal pathway and neurodegeneration. *Cold Spring Harb. Perspect. Biol.* 12:a033993.

Finley, D., and Prado, M. A. (2020). The proteasome and its network: engineering for adaptability. *Cold Spring Harb. Perspect. Biol.* 12:a033985. doi: 10.1101/cshperspect.a033985

Flatt, T., Min, K. J., D'Alterio, C., Villa-Cuesta, E., Cumbers, J., Lehmann, R., et al. (2008). Drosophila germ-line modulation of insulin signaling and lifespan. *Proc. Natl. Acad. Sci. U S A.* 105, 6368–6373. doi: 10.1073/pnas.0709128105

Frakes, A. E., Metcalf, M. G., Tronnes, S. U., Bar-Ziv, R., Durieux, J., Gildea, H. K., et al. (2020). Four glial cells regulate ER stress resistance and longevity via neuropeptide signaling in C. elegans. *Science* 367, 436–440. doi: 10.1126/science.aaz6896

Garcia, S. M., Casanueva, M. O., Silva, M. C., Amaral, M. D., and Morimoto, R. I. (2007). Neuronal signaling modulates protein homeostasis in Caenorhabditis elegans post-synaptic muscle cells. *Genes Dev.* 21, 3006–3016. doi: 10.1101/gad.1575307

Ghaemmaghami, S., Huh, W. K., Bower, K., Howson, R. W., Belle, A., Dephoure, N., et al. (2003). Global analysis of protein expression in yeast. *Nature* 425, 737–741. doi: 10.1038/nature02046

Gidalevitz, T., Ben-Zvi, A., Ho, K. H., Brignull, H. R., and Morimoto, R. I. (2006). Progressive disruption of cellular protein folding in models of polyglutamine diseases. *Science* 311, 1471–1474. doi: 10.1126/science.1124514

Gomez-Pastor, R., Burchfiel, E. T., and Thiele, D. J. (2018). Regulation of heat shock transcription factors and their roles in physiology and disease. *Nat. Rev. Mol. Cell Biol.* 19, 4–19. doi: 10.1038/nrm.2017.73

Grad, L. I., Yerbury, J. J., Turner, B. J., Guest, W. C., Pokrishevsky, E., O'Neill, M. A., et al. (2014). Intercellular propagated misfolding of wild-type Cu/Zn superoxide dismutase occurs via exosome-dependent and -independent mechanisms. *Proc. Natl. Acad. Sci. U S A.* 111, 3620–3625. doi: 10.1073/pnas.1312245111

Guo, B. B., Bellingham, S. A., and Hill, A. F. (2015). The neutral sphingomyelinase pathway regulates packaging of the prion protein into exosomes. *J. Biol. Chem.* 290, 3455–3467. doi: 10.1074/jbc.M114.605253

Hartl, F. U. (1996). Molecular chaperones in cellular protein folding. *Nature* 381, 571–579.

Hartl, F. U., Bracher, A., and Hayer-Hartl, M. (2011). Molecular chaperones in protein folding and proteostasis. *Nature* 475, 324–332. doi: 10.1038/nature10317

Haynes, C. M., Yang, Y., Blais, S. P., Neubert, T. A., and Ron, D. (2010). The matrix peptide exporter HAF-1 signals a mitochondrial UPR by activating the transcription factor ZC376.7 in C. elegans. *Mol. Cell* 37, 529–540. doi: 10.1016/j.molcel.2010.01.015

Hipp, M. S., Kasturi, P., and Hartl, F. U. (2019). The proteostasis network and its decline in ageing. *Nat. Rev. Mol. Cell Biol.* 20, 421–435. doi: 10.1038/s41580-019-0101-y

Hobert, O., and Ruvkun, G. (1998). A common theme for LIM homeobox gene function across phylogeny? *Biol. Bull.* 195, 377–380. doi: 10.2307/1543153

Hobert, O., Mori, I., Yamashita, Y., Honda, H., Ohshima, Y., Liu, Y., et al. (1997). Regulation of interneuron function in the C. elegans thermoregulatory pathway by the ttx-3 LIM homeobox gene. *Neuron* 19, 345–357. doi: 10.1016/s0896-6273(00)80944-7

Hsin, H., and Kenyon, C. (1999). Signals from the reproductive system regulate the lifespan of C. elegans. *Nature* 399, 362–366.

Imanikia, S., Sheng, M., Castro, C., Griffin, J. L., and Taylor, R. C. (2019). XBP-1 Remodels Lipid Metabolism to Extend Longevity. *Cell Rep.* 28, 581–9e4. doi: 10.1016/j.celrep.2019.06.057

Inada, H., Ito, H., Satterlee, J., Sengupta, P., Matsumoto, K., and Mori, I. (2006). Identification of guanylyl cyclases that function in thermosensory neurons of Caenorhabditis elegans. *Genetics* 172, 2239–2252. doi: 10.1534/genetics.105.050013

Jayaraj, G. G., Hipp, M. S., and Hartl, F. U. (2020). Functional modules of the proteostasis network. *Cold Spring Harb. Perspect. Biol.* 12:a033951. doi: 10.1101/cshperspect.a033951

Kampinga, H. H., and Craig, E. A. (2010). The HSP70 chaperone machinery: J proteins as drivers of functional specificity. *Nat. Rev. Mol. Cell Biol.* 11, 579–592. doi: 10.1038/nrm2941

Kazemi-Esfarjani, P., and Benzer, S. (2000). Genetic suppression of polyglutamine toxicity in Drosophila. *Science* 287, 1837–1840. doi: 10.1126/science.287.5459.1837

Kim, K. H., Jeong, Y. T., Oh, H., Kim, S. H., Cho, J. M., Kim, Y. N., et al. (2013). Autophagy deficiency leads to protection from obesity and insulin resistance by inducing Fgf21 as a mitokine. *Nat. Med.* 19, 83–92. doi: 10.1038/nm.3014

Kim, Y. E., Hipp, M. S., Bracher, A., Hayer-Hartl, M., and Hartl, F. U. (2013). Molecular chaperone functions in protein folding and proteostasis. *Annu. Rev. Biochem.* 82, 323–355. doi: 10.1146/annurev-biochem-060208-092442

Kirkin, V., McEwan, D. G., Novak, I., and Dikic, I. (2009). A role for ubiquitin in selective autophagy. *Mol. Cell* 34, 259–269.

Klaips, C. L., Jayaraj, G. G., and Hartl, F. U. (2018). Pathways of cellular proteostasis in aging and disease. *J. Cell Biol.* 217, 51–63. doi: 10.1083/jcb.201709072

Kulak, N. A., Geyer, P. E., and Mann, M. (2017). Loss-less nano-fractionator for high sensitivity, high coverage proteomics. *Mol. Cell Proteom.* 16, 694–705. doi: 10.1074/mcp.O116.065136

Labbadia, J., and Morimoto, R. I. (2015a). Repression of the heat shock response is a programmed event at the onset of reproduction. *Mol. Cell* 59, 639–650. doi: 10.1016/j.molcel.2015.06.027

Labbadia, J., and Morimoto, R. I. (2015b). The biology of proteostasis in aging and disease. *Annu. Rev. Biochem.* 84, 435–464. doi: 10.1146/annurev-biochem-060614-033955

Lee, C., Kim, H., and Bardwell, J. C. A. (2018). Electrostatic interactions are important for chaperone-client interaction in vivo. *Microbiology* 164, 992–997. doi: 10.1099/mic.0.000676

Lee, S. J., Hwang, A. B., and Kenyon, C. (2010). Inhibition of respiration extends C. elegans life span via reactive oxygen species that increase HIF-1 activity. *Curr. Biol.* 20, 2131–2136. doi: 10.1016/j.cub.2010.10.057

Lek, M., Karczewski, K. J., Minikel, E. V., Samocha, K. E., Banks, E., Fennell, T., et al. (2016). Analysis of protein-coding genetic variation in 60,706 humans. *Nature* 536, 285–291. doi: 10.1038/nature19057

Mahadevan, N. R., Anufreichik, V., Rodvold, J. J., Chiu, K. T., Sepulveda, H., and Zanetti, M. (2012). Cell-extrinsic effects of tumor ER stress imprint myeloid dendritic cells and impair CD8(+) T cell priming. *PLoS One* 7:e51845. doi: 10.1371/journal.pone.0051845

Maman, M., Carvalhal Marques, F., Volovik, Y., Dubnikov, T., Bejerano-Sagie, M., and Cohen, E. (2013). A neuronal GPCR is critical for the induction of the heat shock response in the nematode C. elegans. *J. Neurosci.* 33, 6102–6111. doi: 10.1523/JNEUROSCI.4023-12.2013

Marques, C., Guo, W., Pereira, P., Taylor, A., Patterson, C., Evans, P. C., et al. (2006). The triage of damaged proteins: degradation by the ubiquitin-proteasome pathway or repair by molecular chaperones. *FASEB J.* 20, 741–743. doi: 10.1096/fj.05-5080fje

Miles, J., Scherz-Shouval, R., and van Oosten-Hawle, P. (2019). Expanding the organismal proteostasis network: linking systemic stress signaling with the innate immune response. *Trends Biochem. Sci.* 44, 927–942. doi: 10.1016/j.tibs.2019.06.009

Miller, H. A., Dean, E. S., Pletcher, S. D., and Leiser, S. F. (2020). Cell non-autonomous regulation of health and longevity. *Elife* 9:e62659. doi: 10.7554/eLife.62659

Moll, L., Roitenberg, N., Bejerano-Sagie, M., Boocholez, H., Carvalhal Marques, F., Volovik, Y., et al. (2018). The insulin/IGF signaling cascade modulates SUMOylation to regulate aging and proteostasis in Caenorhabditis elegans. *Elife* 7:e38635. doi: 10.7554/eLife.38635

Moran Luengo, T., Mayer, M. P., and Rudiger, S. G. D. (2019). The Hsp70-Hsp90 chaperone cascade in protein folding. *Trends Cell Biol.* 29, 164–177. doi: 10.1016/j.tcb.2018.10.004

Mori, I., and Ohshima, Y. (1995). Neural regulation of thermotaxis in Caenorhabditis elegans. *Nature* 376, 344–348. doi: 10.1038/376344a0

Morimoto, R. I. (2020). Cell-nonautonomous regulation of proteostasis in aging and disease. *Cold Spring Harb. Perspect. Biol.* 12:a034074. doi: 10.1101/cshperspect.a034074

O'Brien, D., Jones, L. M., Good, S., Miles, J., Vijayabaskar, M. S., Aston, R., et al. (2018). A PQM-1-mediated response triggers transcellular chaperone signaling and regulates organismal proteostasis. *Cell Rep.* 23, 3905–3919. doi: 10.1016/j.celrep.2018.05.093

Pellegrino, M. W., Nargund, A. M., and Haynes, C. M. (2013). Signaling the mitochondrial unfolded protein response. *Biochim. Biophys. Acta* 1833, 410–416.

Perez-Gonzalez, R., Gauthier, S. A., Kumar, A., and Levy, E. (2012). The exosome secretory pathway transports amyloid precursor protein carboxyl-terminal fragments from the cell into the brain extracellular space. *J. Biol. Chem.* 287, 43108–43115. doi: 10.1074/jbc.M112.404467

Popiel, H. A., Takeuchi, T., Fujita, H., Yamamoto, K., Ito, C., Yamane, H., et al. (2012). Hsp40 gene therapy exerts therapeutic effects on polyglutamine disease mice via a non-cell autonomous mechanism. *PLoS One* 7:e51069. doi: 10.1371/journal.pone.0051069

Powers, E. T., Morimoto, R. I., Dillin, A., Kelly, J. W., and Balch, W. E. (2009). Biological and chemical approaches to diseases of proteostasis deficiency. *Annu. Rev. Biochem.* 78, 959–991. doi: 10.1146/annurev.biochem.052308.114844

Prahlad, V., and Morimoto, R. I. (2011). Neuronal circuitry regulates the response of Caenorhabditis elegans to misfolded proteins. *Proc. Natl. Acad. Sci. U S A.* 108, 14204–14209. doi: 10.1073/pnas.1106557108

Prahlad, V., Cornelius, T., and Morimoto, R. I. (2008). Regulation of the cellular heat shock response in Caenorhabditis elegans by thermosensory neurons. *Science* 320, 811–814. doi: 10.1126/science.1156093

Rajendran, L., Honsho, M., Zahn, T. R., Keller, P., Geiger, K. D., Verkade, P., et al. (2006). Alzheimer's disease beta-amyloid peptides are released in association with exosomes. *Proc. Natl. Acad. Sci. U S A.* 103, 11172–11177. doi: 10.1073/pnas.0603838103

Ramot, D., MacInnis, B. L., and Goodman, M. B. (2008). Bidirectional temperature-sensing by a single thermosensory neuron in C. elegans. *Nat. Neurosci.* 11, 908–915. doi: 10.1038/nn.2157

Rebeaud, M. E., Mallik, S., Goloubinoff, P., and Tawfik, D. S. (2021). On the evolution of chaperones and cochaperones and the expansion of proteomes across the Tree of Life. *Proc. Natl. Acad. Sci. U S A.* 118:e2020885118. doi: 10.1073/pnas.2020885118

Ron, D., and Walter, P. (2007). Signal integration in the endoplasmic reticulum unfolded protein response. *Nat. Rev. Mol. Cell Biol.* 8, 519–529.

Sahu, R., Kaushik, S., Clement, C. C., Cannizzo, E. S., Scharf, B., Follenzi, A., et al. (2011). Microautophagy of cytosolic proteins by late endosomes. *Dev. Cell* 20, 131–139. doi: 10.1016/j.devcel.2010.12.003

Sala, A. J., and Morimoto, R. I. (2022). Protecting the future: balancing proteostasis for reproduction. *Trends Cell Biol.* 32, 202–215. doi: 10.1016/j.tcb.2021.09.009

Saman, S., Kim, W., Raya, M., Visnick, Y., Miro, S., Saman, S., et al. (2012). Exosome-associated tau is secreted in tauopathy models and is selectively phosphorylated in cerebrospinal fluid in early Alzheimer disease. *J. Biol. Chem.* 287, 3842–3849. doi: 10.1074/jbc.M111.277061

Senchuk, M. M., Dues, D. J., Schaar, C. E., Johnson, B. K., Madaj, Z. B., Bowman, M. J., et al. (2018). Activation of DAF-16/FOXO by reactive oxygen species contributes to longevity in long-lived mitochondrial mutants in Caenorhabditis elegans. *PLoS Genet.* 14:e1007268. doi: 10.1371/journal.pgen.1007268

Shao, Y. F., Wang, C., Xie, J. F., Kong, X. P., Xin, L., Dong, C. Y., et al. (2016). Neuropeptide S ameliorates olfactory spatial memory impairment induced by scopolamine and MK801 through activation of cognate receptor-expressing neurons in the subiculum complex. *Brain Struct. Funct.* 221, 3327–3336. doi: 10.1007/s00429-015-1103-y

Shemesh, N., Shai, N., and Ben-Zvi, A. (2013). Germline stem cell arrest inhibits the collapse of somatic proteostasis early in Caenorhabditis elegans adulthood. *Aging Cell* 12, 814–822. doi: 10.1111/acel.12110

Sugi, T., Nishida, Y., and Mori, I. (2011). Regulation of behavioral plasticity by systemic temperature signaling in Caenorhabditis elegans. *Nat. Neurosci.* 14, 984–992. doi: 10.1038/nn.2854

Sun, J., Liu, Y., and Aballay, A. (2012). Organismal regulation of XBP-1-mediated unfolded protein response during development and immune activation. *EMBO Rep.* 13, 855–860. doi: 10.1038/embor.2012.100

Takeuchi, T. (2018). Non-cell autonomous maintenance of proteostasis by molecular chaperones and its molecular mechanism. *Biol. Pharm. Bull.* 41, 843–849. doi: 10.1248/bpb.b18-00141

Takeuchi, T., Suzuki, M., Fujikake, N., Popiel, H. A., Kikuchi, H., Futaki, S., et al. (2015). Intercellular chaperone transmission via exosomes contributes to maintenance of protein homeostasis at the organismal level. *Proc. Natl. Acad. Sci. U S A.* 112, E2497–E2506. doi: 10.1073/pnas.1412651112

Tatum, M. C., Ooi, F. K., Chikka, M. R., Chauve, L., Martinez-Velazquez, L. A., Steinbusch, H. W. M., et al. (2015). Neuronal serotonin release triggers the heat shock response in C. elegans in the absence of temperature increase. *Curr. Biol.* 25, 163–174. doi: 10.1016/j.cub.2014.11.040

Taylor, R. C., and Dillin, A. (2013). XBP-1 is a cell-nonautonomous regulator of stress resistance and longevity. *Cell* 153, 1435–1447.

Taylor, R. C., Berendzen, K. M., and Dillin, A. (2014). Systemic stress signalling: understanding the cell non-autonomous control of proteostasis. *Nat. Rev. Mol. Cell Biol.* 15, 211–217. doi: 10.1038/nrm3752

Uversky, V. N., Oldfield, C. J., and Dunker, A. K. (2008). Intrinsically disordered proteins in human diseases: introducing the D2 concept. *Annu. Rev. Biophys.* 37, 215–246. doi: 10.1146/annurev.biophys.37.032807.125924

van Oosten-Hawle, P., Porter, R. S., and Morimoto, R. I. (2013). Regulation of organismal proteostasis by transcellular chaperone signaling. *Cell* 153, 1366–1378.

Walther, D. M., Kasturi, P., Zheng, M., Pinkert, S., Vecchi, G., Ciryam, P., et al. (2015). Widespread proteome remodeling and aggregation in aging C. elegans. *Cell* 161, 919–932.

Warrick, J. M., Chan, H. Y., Gray-Board, G. L., Chai, Y., Paulson, H. L., and Bonini, N. M. (1999). Suppression of polyglutamine-mediated neurodegeneration in Drosophila by the molecular chaperone HSP70. *Nat. Genet.* 23, 425–428. doi: 10.1038/70532

Williams, K. W., Liu, T., Kong, X., Fukuda, M., Deng, Y., Berglund, E. D., et al. (2014). Xbp1s in Pomc neurons connects ER stress with energy balance and glucose homeostasis. *Cell Metab.* 20, 471–482. doi: 10.1016/j.cmet.2014.06.002

Yee, C., Yang, W., and Hekimi, S. (2014). The intrinsic apoptosis pathway mediates the pro-longevity response to mitochondrial ROS in C. elegans. *Cell* 157, 897–909. doi: 10.1016/j.cell.2014.02.055

Zhang, Q., Wu, X., Chen, P., Liu, L., Xin, N., Tian, Y., et al. (2018). The mitochondrial unfolded protein response is mediated cell-non-autonomously by retromer-dependent WNT signaling. *Cell* 174, 870–83e17. doi: 10.1016/j.cell.2018.06.029

Zheng, X., Krakowiak, J., Patel, N., Beyzavi, A., Ezike, J., Khalil, A. S., et al. (2016). Dynamic control of Hsf1 during heat shock by a chaperone switch and phosphorylation. *Elife* 5:e18638. doi: 10.7554/eLife.18638

Zou, J., Guo, Y., Guettouche, T., Smith, D. F., and Voellmy, R. (1998). Repression of heat shock transcription factor HSF1 activation by HSP90 (HSP90 complex) that forms a stress-sensitive complex with HSF1. *Cell* 94, 471–480. doi: 10.1016/s0092-8674(00)81588-3

**Conflict of Interest:** The authors declare that the research was conducted in the absence of any commercial or financial relationships that could be construed as a potential conflict of interest.

**Publisher's Note:** All claims expressed in this article are solely those of the authors and do not necessarily represent those of their affiliated organizations, or those of the publisher, the editors and the reviewers. Any product that may be evaluated in this article, or claim that may be made by its manufacturer, is not guaranteed or endorsed by the publisher.

frontiers | Frontiers in Pharmacology

BRIEF RESEARCH REPORT
published: 26 July 2022
doi: 10.3389/fphar.2022.897056

# GABA Receptor Agonists Protect From Excitotoxic Damage Induced by AMPA in Oligodendrocytes

*Laura Bayón-Cordero*[1,2,3], *Blanca Isabel Ochoa-Bueno*[1,2,3], *Asier Ruiz*[1,2,3], *Marina Ozalla*[2], *Carlos Matute*[1,2,3] *and María Victoria Sánchez-Gómez*[1,2,3]*

[1]*Laboratory of Neurobiology, Achucarro Basque Center for Neuroscience, Leioa, Spain,* [2]*Department of Neurosciences, University of the Basque Country (UPV/EHU), Leioa, Spain,* [3]*Centro de Investigación Biomédica en Red de Enfermedades Neurodegenerativas (CIBERNED), Leioa, Spain*

Oligodendrocytes are the myelin forming cells of the central nervous system, and their vulnerability to excitotoxicity induced by glutamate contributes to the pathogenesis of neurological disorders including brain ischemia and neurodegenerative diseases, such as multiple sclerosis. In addition to glutamate receptors, oligodendrocytes express GABA receptors (GABAR) that are involved in their survival and differentiation. The interactions between glutamate and GABAergic systems are well documented in neurons, under both physiological and pathological conditions, but this potential crosstalk in oligodendrocytes has not been studied in depth. Here, we evaluated the protective effect of GABAR agonists, baclofen ($GABA_B$) and muscimol ($GABA_A$), against AMPA-induced excitotoxicity in cultured rat oligodendrocytes. First, we observed that both baclofen and muscimol reduced cell death and caspase-3 activation after AMPA insult, proving their oligoprotective potential. Interestingly, analysis of the cell-surface expression of calcium-impermeable GluR2 subunits in oligodendrocytes revealed that GABAergic agonists significantly reverted GluR2 internalization induced by AMPA. We determined that baclofen and muscimol also impaired AMPA-induced intracellular calcium increase and subsequent mitochondrial membrane potential alteration, ROS generation, and calpain activation. However, AMPA-triggered activation of Src, Akt, JNK and CREB was not affected by baclofen or muscimol. Overall, our results suggest that GABAR activation initiates alternative molecular mechanisms that attenuate AMPA-mediated apoptotic excitotoxicity in oligodendrocytes by interfering with expression of GluR subunits in membranes and with calcium-dependent intracellular signaling pathways. Together, these findings provide evidence of GABAR agonists as potential oligodendroglial protectants in central nervous system disorders.

**Keywords: GABA receptor, oligodendrocyte, AMPA, baclofen, muscimol, excitotoxicity, multiple sclerosis**

OPEN ACCESS

***Edited by:***
*Valle Palomo,*
*IMDEA Nanociencia, Spain*

***Reviewed by:***
*Yong Li,*
*Shanghai Jiao Tong University, China*
*Melinda Fitzgerald,*
*Curtin University, Australia*

***Correspondence:**
*María Victoria Sánchez-Gómez*
*vicky.sanchez@ehu.eus*

***Specialty section:***
*This article was submitted to Neuropharmacology, a section of the journal Frontiers in Pharmacology*

***Received:*** *15 March 2022*
***Accepted:*** *06 June 2022*
***Published:*** *26 July 2022*

***Citation:***
*Bayón-Cordero L, Ochoa-Bueno BI, Ruiz A, Ozalla M, Matute C and Sánchez-Gómez MV (2022) GABA Receptor Agonists Protect From Excitotoxic Damage Induced by AMPA in Oligodendrocytes. Front. Pharmacol. 13:897056. doi: 10.3389/fphar.2022.897056*

## INTRODUCTION

Oligodendrocytes are the myelin forming cells in the central nervous system (CNS), and they express multiple neurotransmitter receptors, including glutamate receptors (GluR) (Yoshioka et al., 1995; Matute et al., 1997; McDonald et al., 1998). Excitotoxic damage induced in oligodendrocytes by overactivation of glutamate receptors leads to oligodendrocyte death, and it is a contributor to the

pathogenesis of CNS-related disorders including ischemia, traumatic brain injury, and neurodegenerative diseases such as multiple sclerosis, where oligodendrocyte death is a well-known pathological hallmark (Matute et al., 2001; Matute et al., 2006; Matute et al., 2007). Excitotoxicity is associated with sustained activation of glutamate ionotropic receptors, in particular α-amino-3-hydroxy-5-methyl-4-isoxazolepropionate (AMPA) and kainate receptors, sensitive to activation with these agonists. In oligodendrocytes, AMPA-activated GluR receptors are mainly formed by GluR1-4 subunits (Matute et al., 2007).

Excitotoxic insults to oligodendrocytes are dependent on calcium entry through ionotropic GluRs, which alters calcium homeostasis, induces changes in mitochondrial function and activates apoptotic pathways involving caspases-9 and -3, leading to oligodendroglial cell death (Galluzzi et al., 2009; Sánchez-Gómez et al., 2011; Simonishvili et al., 2013). In these excitotoxic processes, calcium is an essential signaling molecule that affects pivotal cellular mechanisms. The increase in cytosolic calcium levels directly targets the mitochondria, leading to an alteration in the polarization of the mitochondrial membrane (Duchen, 2000) and causing overproduction of reactive oxygen species (ROS) and reduced cell survival (Sánchez-Gómez et al., 2003; Ness et al., 2004; Suski et al., 2018; Singh et al., 2019). Alterations in calcium levels also affect calpain activity. Calpains are calcium dependent cysteine proteases that are ubiquitously expressed as two isoforms, μ- and m-calpain, which are activated by micromolar and millimolar concentrations of calcium, respectively. The potential role of calpains in cell death is indicated by a growing list of substrates, including Bax, p53, PARP, Src, Akt, JNK, and CREB, whose proteolytic cleavage activity has been characterized as crucial in oligodendrocyte excitotoxicity, acute hypoxia, traumatic brain injury, and chronic degeneration (Trinchese et al., 2008; Sánchez-Gómez et al., 2011; Barateiro et al., 2012; Hossain et al., 2013; Wang et al., 2013; Jantzie et al., 2016; Zhang et al., 2017).

While glutamate is the main excitatory neurotransmitter in the CNS, γ-aminobutyric acid (GABA) is the major inhibitory neurotransmitter. Excitatory-inhibitory signal balance is necessary to ensure proper functioning of cells, therefore, correct crosstalk between glutamate and GABAergic signaling is essential (Kantamneni, 2015). Oligodendrocyte progenitor cells receive both excitatory inputs mediated by glutamate and inhibitory signals mediated by GABA (Lin and Bergles, 2004; Káradóttir et al., 2008; Kukley et al., 2008), which supports the importance of these neurotransmitters in the fate and function of the oligodendroglial lineage. Along this line, it has been described that increasing GABAergic action can prevent excitotoxicity and oligodendrocyte loss following preterm birth by creating a normal balance of inhibition-excitation (Shaw et al., 2021).

Disturbances in GABAergic signaling are found in several injury conditions, such as stroke or epilepsy (Bai et al., 2021), which gives insight into their potential relevance in the progression of these disorders. Oligodendrocytes express the two main GABA receptors (GABAR), ionotropic $GABA_AR$ and metabotropic $GABA_BR$ (Serrano-Regal et al., 2020), and the relevance of GABARs for oligodendrocyte functionality has become clear in recent years (reviewed in Serrano-Regal et al., 2020; Bai et al., 2021). GABARs are related to myelination and neuroprotection in the CNS, given the link between $GABA_AR$ signaling disruption or downregulation and reduced myelination observed *in vivo* (Zonouzi et al., 2015; Kalakh and Mouihate, 2019), or the decreased myelination following $GABA_AR$ activation observed in organotypic slices (Hamilton et al., 2017), and considering the remyelinating capacity of $GABA_BR$ agonist baclofen following spinal cord injury (Serrano-Regal et al., 2022).

Here, we investigated the impact of $GABA_A$ and $GABA_BR$ agonists, muscimol and baclofen, respectively, in AMPA-mediated excitotoxicity using primary cultures of cortical rat brain-derived oligodendrocytes, mimicking the excitotoxic insults through moderate activation of AMPA receptors. Our results provide evidence of the protective effect of baclofen and muscimol from AMPA-induced excitotoxic death of oligodendrocytes through modulation of cell-surface GluR2 AMPA subunit expression in these cells, as well as by regulating the subsequent cytosolic calcium overload calpain activation and mitochondrial dysfunction.

# MATERIALS AND METHODS

## Animal Ethic Statement

The animal study was approved by the internal Animal Ethics Committee of the University of the Basque Country (UPV/EHU) and the European Communities Council Directive. All efforts were made to minimize animal suffering and the number of animals used. Sprague-Dawley rats of both sexes were used for the experiments.

## Rat Brain Oligodendrocyte Primary Culture and Excitotoxicity Induction

Oligodendrocyte progenitor cell (OPC) culture was obtained from newborn Sprague-Dawley rat mixed glial cultures as previously described (Sánchez-Gómez et al., 2018). Isolated OPCs were seeded onto poly-D-lysine-coated coverslips and cultured at 37°C with 5% $CO_2$ in SATO differentiation medium for 2–3 days, to promote maturation into oligodendrocytes (Canedo-Antelo et al., 2018). Excitotoxic conditions were recreated using oligodendrocytes by exposure to cyclothiazide (CTZ; 100 μM; Tocris) for 10 min before incubation with AMPA (10 μM; Tocris) for 30 min (Sánchez-Gómez and Matute, 1999; Sánchez-Gómez et al., 2011). After incubation with AMPA, the medium was changed to remove the stimulus and for treatments with baclofen or muscimol; these GABAergic drugs were added again after AMPA removal to maintain their effect until the end of the experiment.

## Cell Viability Assay

Cultured oligodendrocytes were exposed to excitotoxicity and 24 h later, they were loaded with calcein-AM (1 μM; Invitrogen) for 30 min at 37°C. Fluorescence was measured in a Synergy H4 hybrid reader fluorimeter (Bio-Tek Instruments), with excitation at 485 nm and emission at 528 nm.

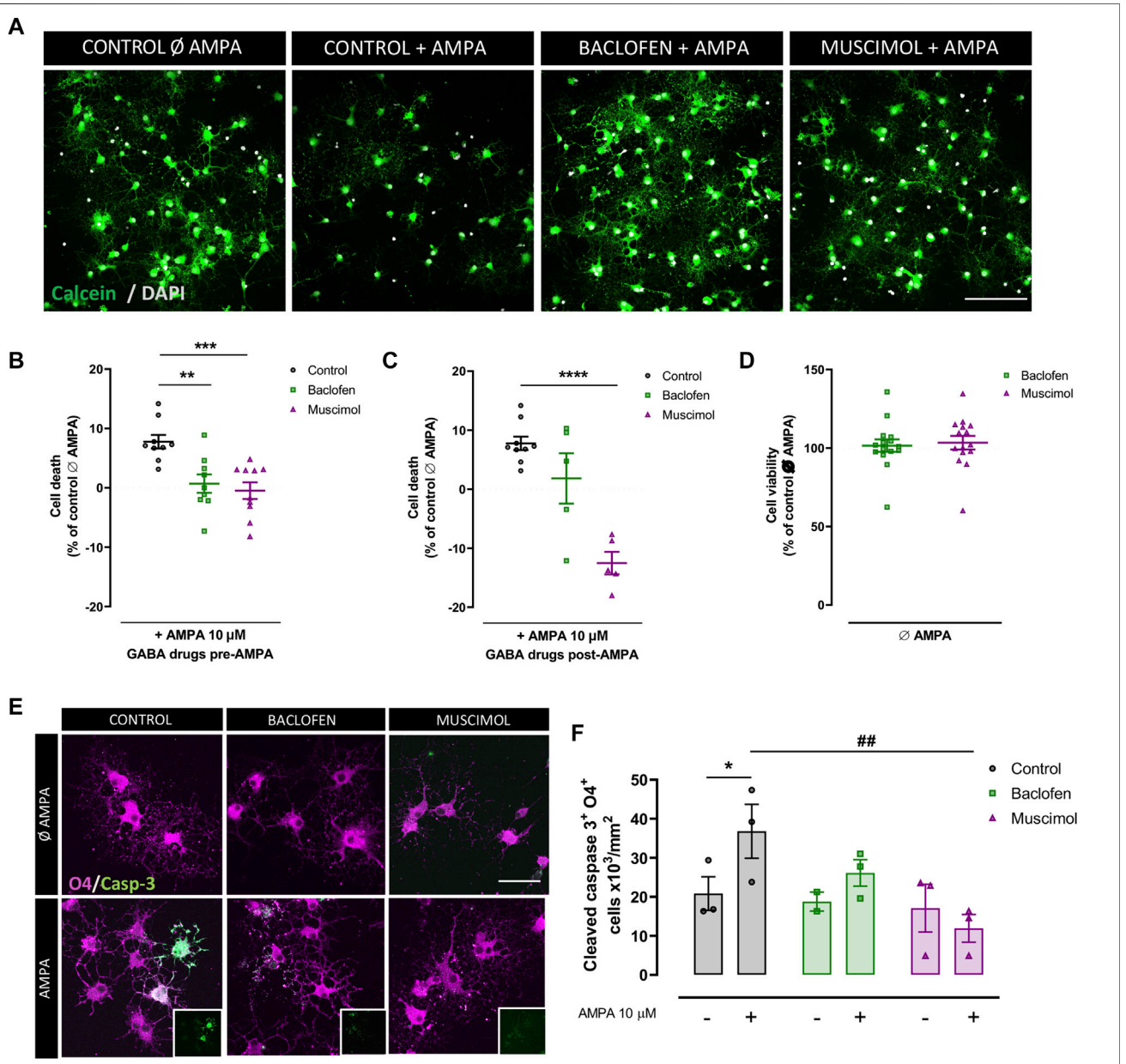


**FIGURE 1 | Baclofen and muscimol reduce cell death AMPA-induced excitotoxicity in oligodendrocytes**. **(A)** Representative images from viability assays of oligodendrocytes treated with CTZ and AMPA plus baclofen or muscimol added before the excitotoxic insult. Cells are labeled with calcein (green) and DAPI (blue). Scale bar: 100 µm. **(B, C)** Percentage of death oligodendrocytes after 24h in cultures treated with baclofen or muscimol 30 min before or after exposure to CTZ and AMPA, respectively. All conditions were normalized to calcein values from untreated cells, which was considered as 0% of cell death. **(D)** No cell death was observed in oligodendrocytes treated with baclofen or muscimol and analyzed 24 h later. All conditions were normalized to calcein values from untreated cells, which was considered as 100% of cell viability. Data are shown as mean ± SEM of at least 5 independent experiments. **p<0.01, ***p<0.001, ****p<0.0001 vs. control, one-way ANOVA. **(E)** Representative images of oligodendrocytes treated with CTZ and AMPA plus baclofen or muscimol added before the excitotoxic insult, and labeled with rabbit anti-cleaved caspase 3 (green) and IgG anti-O4 (magenta). Scale bar: 50 µm. **(F)** Number of cleaved caspase 3- and O4-positive cells per area. Data are shown as mean ± SEM of at least 2 independent experiments. *p<0.05 vs. control Ø AMPA; ##p<0.01 vs. control; one-way ANOVA.

## Western Blotting

Isolated oligodendrocytes were scraped into RIPA buffer supplemented with EDTA and protease inhibitor cocktail (Thermo Scientific). Samples were diluted in sodium dodecyl sulfate sample buffer and boiled for 8 min at 100°C. Protein extracts were separated by size through SDS-PAGE in 4%–20% Criterion TGX precast gels and then transferred to Trans-Blot Turbo Midi Nitrocellulose or PVDF Transfer Packs (Bio-Rad). Membranes were blocked with 5% BSA (Sigma-Aldrich) or phosphoBLOCKER reagent (Cell Biolabs) and incubated with

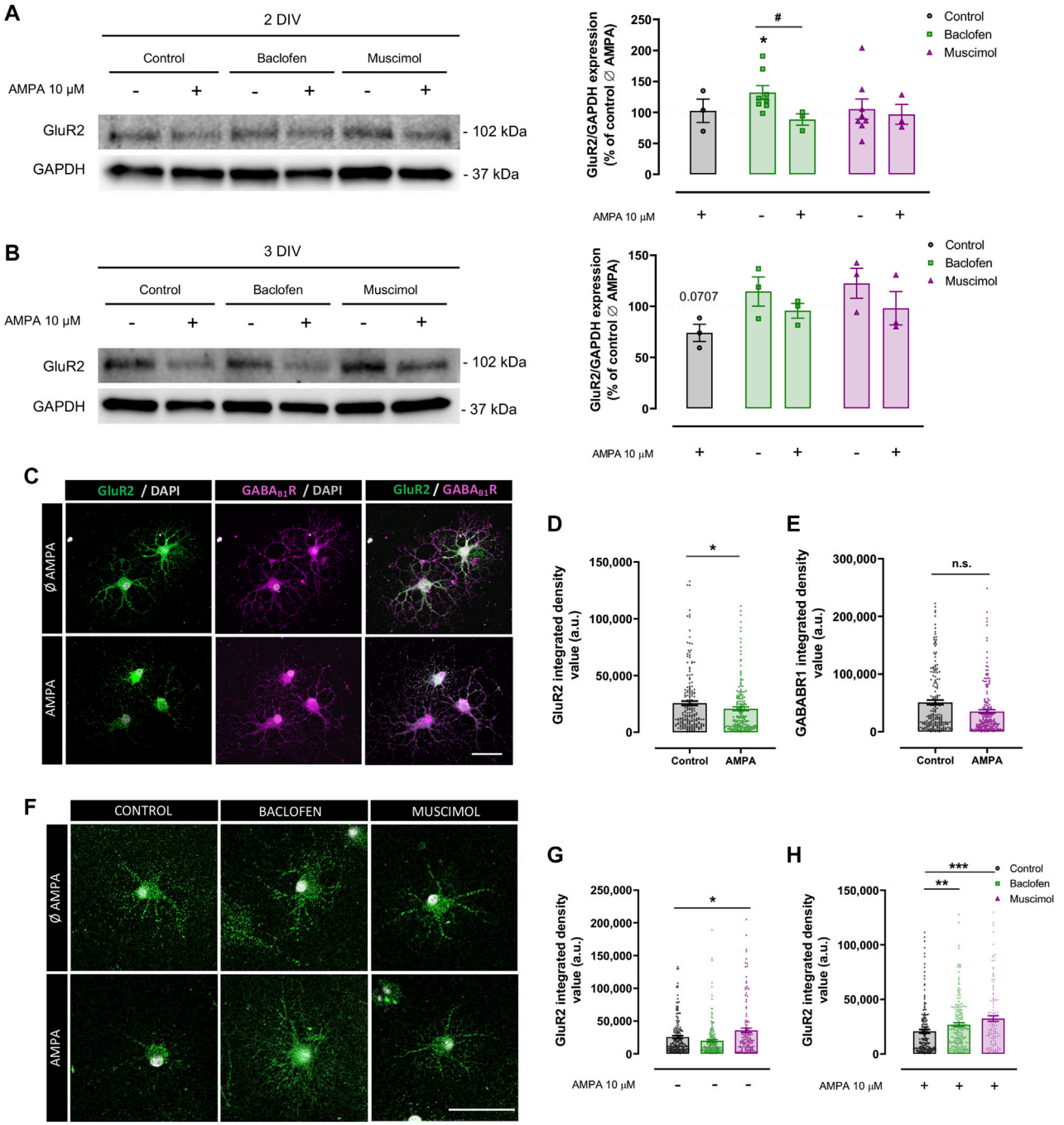


**FIGURE 2 | Baclofen and muscimol reduce downregulation of cell-surface GluR2 subunit levels induced by AMPA in oligodendrocytes**. **(A)** Western blot of GluR2 total protein levels normalized to GAPDH in oligodendrocytes treated daily with baclofen or muscimol and analyzed at day 2 in vitro (2DIV), 24 h after exposure to AMPA. **(B)** Western blot of GluR2 total protein levels in oligodendrocytes treated daily with baclofen or muscimol and analyzed at day 3 in vitro (3DIV), 24 h after exposure to AMPA. In both A and B, all conditions were normalized to control values from non-treated cultures. Data are shown as the mean ± SEM of at least 3 independent experiments. *p<0.05 vs. control Ø AMPA; #p<0.05 vs. control; one-way ANOVA. **(C, F)** Representative images of sum representation **(C)** or single stack **(F)** of oligodendrocytes treated or not with AMPA and/or baclofen or muscimol and stained with mouse anti-GluR2 extracellular (green) and/or rabbit anti- GABA$_B$R1 extracellular (magenta) and DAPI (grey). Scale bar: 50 µm. **(D, E)** Integrated density values of GluR2 or GABAB$_R$1 fluorescence signal, respectively. **(G, H)** Integrated density values of GluR2 in oligodendrocytes under different treatments. Data are shown as the mean ± SEM of at least 123 individual cells. *p<0.05, **p<0.01, ***p<0.001 vs. control without or with AMPA respectively; one-way ANOVA for multiple experimental groups comparisons; unpaired t test for two experimental group comparison.

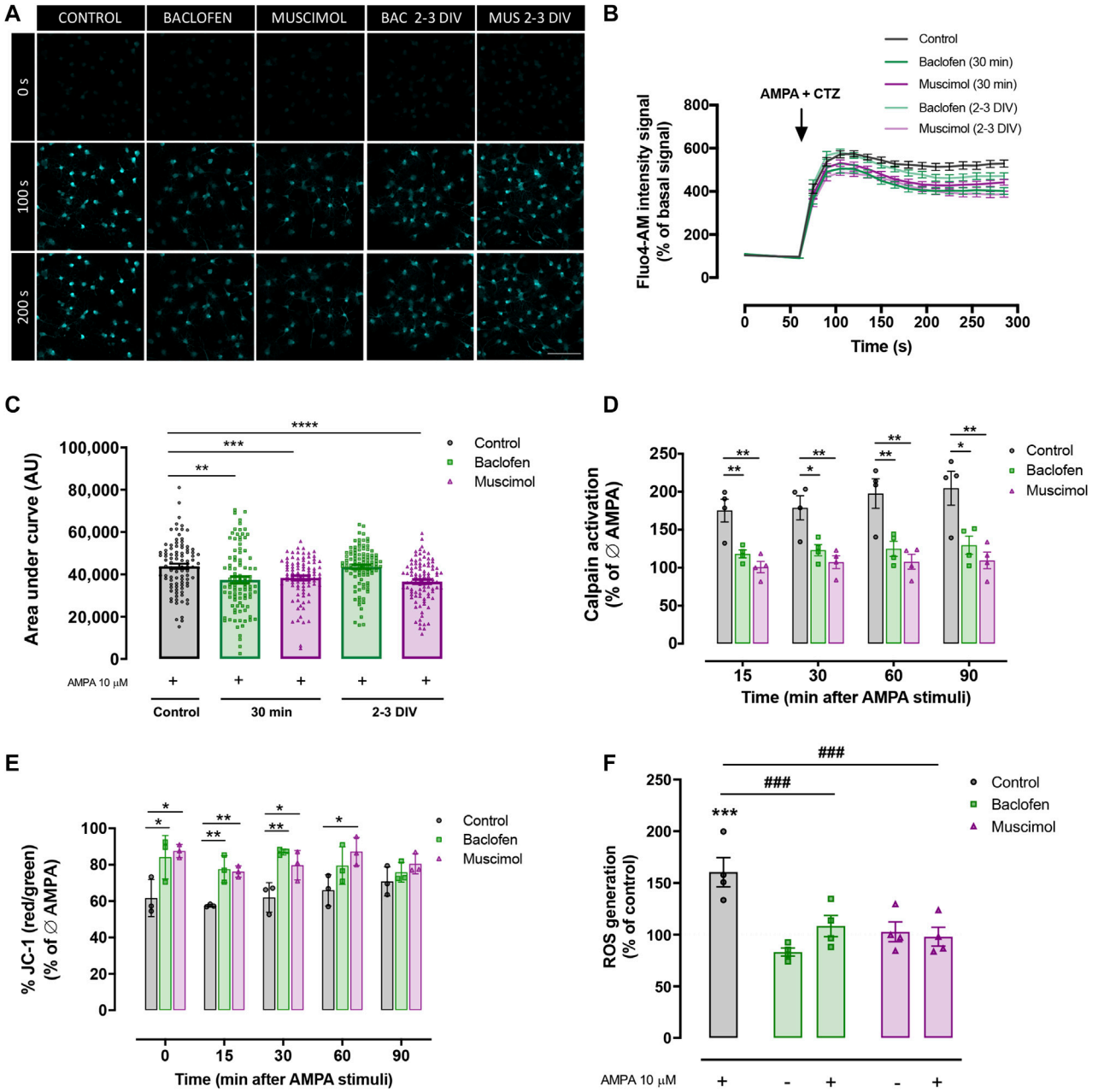


**FIGURE 3 | Baclofen and muscimol modulate AMPA-induced calcium signaling and mitochondrial alterations**. **(A)** Representative images of Ca2+ responses to CTZ and AMPA in cells loaded with Fluo4-AM at 0 s, 100 s and 200 s of recording. **(B)** Recordings of Ca2+ responses to CTZ and AMPA in control oligodendrocytes (black trace), treated with baclofen or muscimol for 30 min before exposure to AMPA (green and magenta traces respectively, bold) or treated daily with baclofen or muscimol until the analysis (green and magenta traces respectively, soft). **(C)** Area under the curve of calcium recordings for each condition. Data are shown as violin plots indicating the median and quartiles of at least 88 cells from 4 independent experiments. **p<0.01, ***p<0.001, ****p<0.0001 vs. control; one-way ANOVA. **(D)** Calpain activity detected using the Calpain-Glo Protease Assay in oligodendrocytes treated with baclofen or muscimol 30 min pre-AMPA and analyzed 30 min after CTZ and AMPA stimulus. All conditions were normalized to controls without AMPA treatment. Data are shown as the mean mean ± SEM of 4 independent experiments. *p<0.05, **p<0.01 vs. control; one-way ANOVA. **(E)** Mitochondrial membrane potential monitored in oligodendrocytes loaded with JC-1 probe. All conditions were normalized to controls without AMPA treatment. Data are shown as the mean ± SEM of 3 independent experiments. *p<0.05, **p<0-01 vs. control; one-way ANOVA. **(F)** Intracellular levels of ROS in oligodendrocytes treated with baclofen or muscimol for 30 min before adding AMPA and analyzed 30 min after AMPA stimulus. Cell were loaded with CM-H2DCFDA probe and the values were normalized with calcein signal. All conditions were normalized to control values in cultures without AMPA treatment. Data are shown as the mean ± SEM of 4 independent experiments. ***p<0.001 vs. control Ø AMPA; ###p<0.001 vs. control; one-way ANOVA.

the following primary antibodies: rabbit anti-pSrc (#2101), anti-Src (#2109), anti-pAkt (#9271), anti-Akt (#9272), anti-pJNK (#9251), anti-JNK (#9252), anti-pCREB (#9198) (1:1000; all from Cell Signaling) and mouse anti-pJNK (#sc-6254), anti-JNK (#sc-7345) (1:500; both from Santa Cruz), anti-CREB (#9104) and anti-GAPDH (#mab374; Merck). Horseradish peroxidase-conjugated goat anti-rabbit or sheep anti-mouse (1: 2000; Cell Signaling) were used as secondary antibodies. Protein band signals were developed using SuperSignal West Femto chemiluminescent substrate detection kit (Thermo Scientific) and images were acquired with a ChemiDoc MP image system (Bio-Rad). For incubation with primary antibodies against the total portion of the protein, antibodies against phosphorylated proteins were stripped by incubation in Restore Western Blot stripping buffer (Thermo Scientific). Ponceau Red staining, GAPDH, or the total portion of the protein was used for normalization of the signal.

## Immunofluorescence and Image Analysis

Oligodendrocytes were fixed in 4% paraformaldehyde for 20 min at RT. For cleaved caspase-3 detection, membranes were permeabilized in blocking solution containing 0.1% Triton X-100 and 4% normal goat serum in PBS and then labeled with rabbit anti-cleaved caspase-3 (1:500; Cell Signaling; #9661) and mouse IgM anti-O4 (1:100; R&D Systems; #MAB1326) overnight at 4°C. Then, cells were incubated with goat anti-rabbit IgG Alexa Fluor-488 (1:500; Invitrogen; #A11034), goat anti-mouse IgM TXRed (1:500; Thermo Scientific, #401296). For detection of the N-terminal extracellular domains of GluR2 and $GABA_{B1}R$, cells were blocked using 2% normal goat serum. Primary antibodies, mouse anti-GluR2 extracellular (1:1500; Merck, #MAB397) and rabbit anti-$GABA_{B1}$ extracellular (1:200; Alomone, #AGB-001) were added for 1 h at 37°C, after which the cells were incubated with goat anti-mouse IgG Alexa Fluor-488 and goat anti-rabbit IgG Alexa Fluor-594 (1:500; Invitrogen; #A11001 and ##A11012 respectively). 4′,6-diamidino-2-phenylindole (DAPI; 4 μg/ml; Sigma-Aldrich) was used for nuclear staining and coverslips were mounted using ProLong™ Gold anti-fade reagent (Invitrogen).

Images were acquired using a 40X oil-immersion objective (numerical aperture 1.3) on an inverted Zeiss LSM800 confocal microscope (Analytical and High Resolution Microscopy Service in Biomedicine, UPV/EHU) for cleaved caspase-3 analysis or a Leica TCS STED CW SP8 confocal microscope (Achucarro Basque Center for Neuroscience) for receptor expression analysis. Image analysis was performed using ImageJ software (National Institute of Health). For receptor expression quantification, individual cells were selected as regions of interest (ROIs) and the integrated density value was measured for each ROI. In this case, ten fields of view were quantified per biological replicate. For cleaved caspase-3 quantification, seven fields of view were quantified per biological replicate.

## Cytosolic Calcium Imaging

Cytosolic calcium levels in oligodendocytes were measured as described previously (Ruiz et al., 2014). Briefly, cells were incubated with Fluo4-AM (1 mM; Molecular Probes, Invitrogen) for 30 min at 37°C, and then exposed to AMPA (10 μM) plus CTZ (100 μM). Fluorescence was imaged through a 40X objective (numerical aperture 1.3) on an inverted Zeiss LSM800 confocal microscope (Analytical and High Resolution Microscopy Service in Biomedicine, UPV/EHU) at an acquisition rate of 1 frame/15 s for 5 min. For data analysis, a population of 15–25 cells per coverslip was selected and the oligodendrocyte soma was selected as ROI. Calcium levels are expressed as F/F0 ± SEM (%), in which F represents the fluorescence value for a given time point and F0 represents the mean of the resting fluorescence level. Background values were subtracted in all cases. The area under the curve of accumulated calcium levels (Fluo4-AM fluorescence increase) was calculated during the time course.

## Mitochondrial Membrane Potential Gradient Measurement

Oligodendrocytes were exposed to excitotoxicity and loaded with 5,5′,6,6′-tetrachloro-1,1′,3,3′-tetraethylbenzimidazolcarbocyanine iodide (JC-1; 3 μM; Invitrogen) for 15 min at 37°C. After changing medium, the coverslips were washed with HBSS without phenol red and transferred to a different plate. Fluorescence was monitored every 15 min for 2 h using a Synergy H4 hybrid reader fluorimeter (Bio-Tek Instruments), with excitation at 485 nm and emission at 528 nm for green (monomeric form, cytosol) and at 620 nm for red fluorescence (aggregated form, mitochondrial matrix). Changes in the mitochondrial potential gradient are indicated by the red/green ratio.

## Measurement of Intracellular Reactive Oxygen Species

Cells were loaded with 5-(and 6)-chloromethyl-2 ′,7-dichlorodihydro fluorescein diacetate acetyl ester (CM-H2DCFDA; 10 μM; Invitrogen) for 30 min at 37°C. Fluorescence was measured using a Synergy H4 hybrid reader fluorimeter (Bio-Tek Instruments), with excitation and emission at 485 and 528 nm, respectively. ROS production values were normalized using the calcein-AM probe (1 μM) in duplicate wells seeded under the same conditions.

## Calpain Activity Assay

Calpain activity was measured in oligodendrocytes using the Calpain-Glo protease assay (Promega) and luminescence was monitored after excitotoxicity exposure every 15 min for 90 min using a Synergy H4 hybrid reader fluorimeter-luminometer (Bio-Tek Instruments).

## Statistical Analysis

Statistical analysis was performed using GraphPad Prism software version 8.0. All data are expressed as the mean ± SEM. The number of biological replicates per experiment is indicated in each case and experiments were performed at least twice. For comparisons between multiple experimental groups, one-way analysis of variance (ANOVA) with Fisher's LSD test was applied, unpaired *t* test was used for comparisons

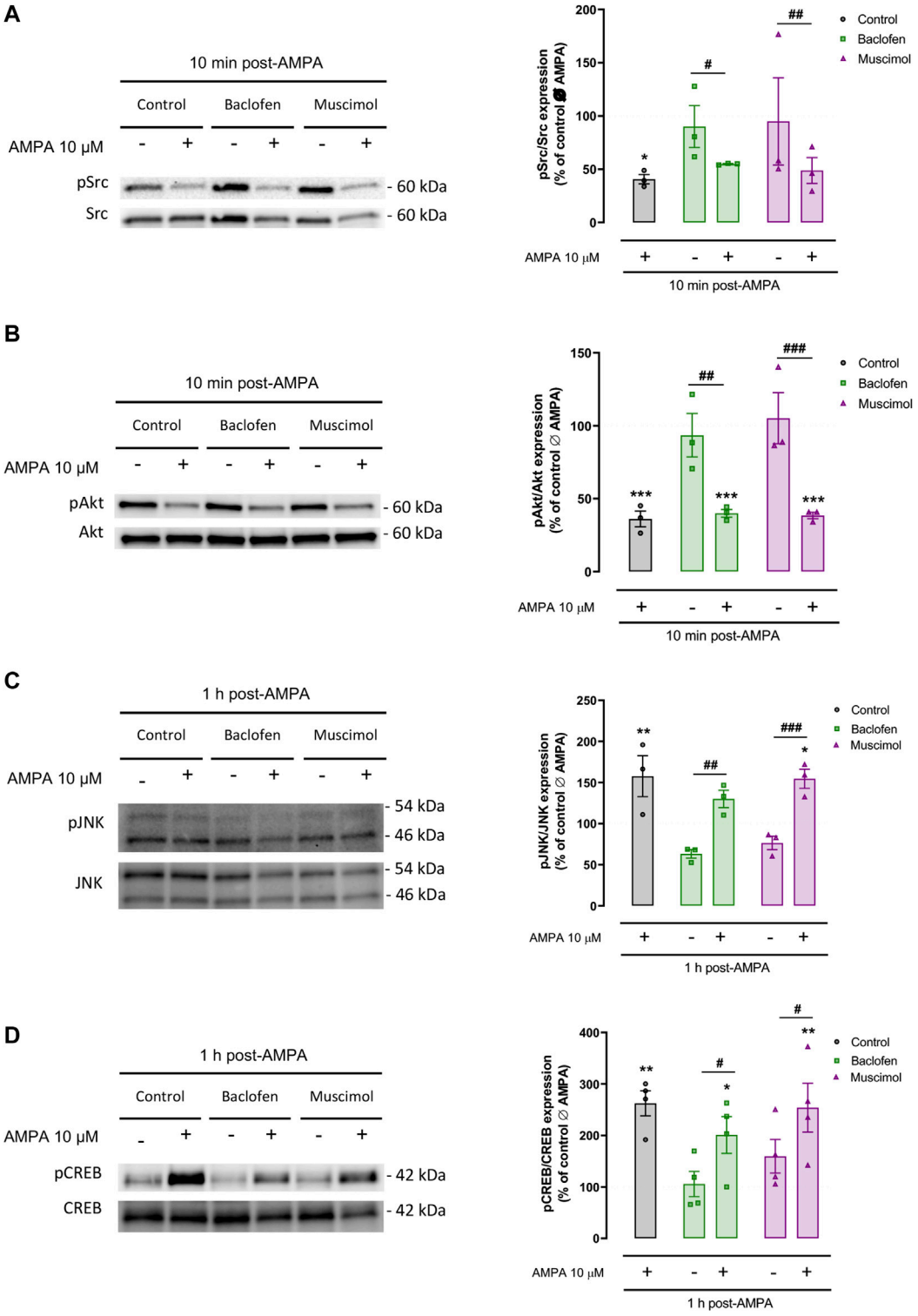


**FIGURE 4 | Baclofen and muscimol do not modulate AMPA-activated Src, Akt, JNK and CREB signaling pathways**. Western blot of phosphorylated Src **(A)**, Akt **(B)**, JNK **(C)** and CREB **(D)** protein levels, normalized to the total protein, in oligodendrocytes treated with baclofen or muscimol before exposure to AMPA, and analyzed 10 min or 1 h after AMPA stimulus. All conditions were normalized to values from untreated cells, which was considered as 100% of phosphorylated protein expression levels. Data are shown as the mean ± SEM of at least 3 independent experiments. *p<0.05, **p<0.01, ***p<0.001 vs. control Ø AMPA; #p<0.05, ##p<0.01, ###p<0.001 vs. ØAMPA one-way ANOVA.

between two experimental groups, and $p<0.05$ was considered significant.

# RESULTS

## Baclofen and Muscimol Attenuate Excitotoxic Cell Death in Oligodendrocytes

To assess the protective effect of the $GABA_AR$ agonist, muscimol, and the $GABA_BR$ agonist, baclofen, in oligodendrocyte excitotoxicity, we first mimicked the excitotoxic signal in vitro through administration of CTZ and AMPA (we will refer to AMPA addition as the excitotoxic signal), and we analyzed cell viability using the calcein-AM probe (**Figures 1A–D**). When baclofen and muscimol were added 30 min before AMPA and maintained after AMPA stimulus (pre-AMPA), both drugs reduced the percentage of cell death caused by AMPA (**Figure 1B**), while muscimol alone effectively attenuated excitotoxic cell death when added only after AMPA (post-AMPA) (**Figure 1C**). Moreover, neither baclofen nor muscimol caused any variation in cell viability in the absence of AMPA (**Figure 1D**), showing that neither of these GABAR agonists presented toxicity against oligodendrocytes in vitro. The most reproducible protective effect was observed when drugs were added 30 min before and maintained during AMPA stimulus, thus, further analyses were mainly performed following this drug treatment protocol.

Given the link between AMPAR overactivation and apoptosis activation (Sánchez-Gómez et al., 2003, Sánchez-Gómez et al.,2011; Canedo-Antelo et al., 2018), we next evaluated whether baclofen and muscimol reduced the expression of cleaved caspase-3 in O4-positive oligodendrocytes (**Figures 1E,F**). We verified that the AMPA-induced increase in cleaved caspase-3 was not significantly altered by baclofen addition, but was attenuated by muscimol treatment (**Figure 1F**). Thus, selective activation of GABAR in oligodendrocytes with baclofen or muscimol protected them from excitotoxic damage induced by AMPA; muscimol seemed to be primarily responsible for reducing the caspase-dependent apoptotic pathway.

## Baclofen and Muscimol Reduce GluR2 Subunit Internalization Induced by AMPA in Oligodendrocytes

Next, we explored the mechanisms through which baclofen and muscimol could be exerting their protective effect against AMPA-induced damage in oligodendrocytes. Taking into account the increasing evidence that GABARs play an important role in modulating the expression and function of GluRs (Kantamneni, 2015; Shaw et al., 2021), we initially assessed whether GABAergic drugs caused alterations in the expression of GluRs in oligodendrocytes under excitotoxicity insults. We focused on the $Ca^{2+}$-impermeable GluR2 subunit, which is expressed in oligodendrocytes and whose cell-surface expression presents differential levels in response to AMPAR activation (Hossain et al., 2014; Harlow et al., 2015). To evaluate that response, AMPA stimulus was added to oligodendrocytes at 1 or 2DIV, and sample collection was performed 24 h later, at 2 or 3DIV (**Figure 2**). In these experiments, baclofen or muscimol was added daily until AMPA stimulus, and maintained after its removal. Protein expression analysis by immunoblot of the total protein fraction at 2DIV did not reveal any differences in the expression of GluR2 in cells treated with AMPA compared with control; baclofen or muscimol did not modify this situation (**Figure 2A**). Interestingly, GluR2 expression at 2DIV was higher following baclofen treatment, but this increase was reversed when baclofen addition was combined with AMPA. At 3DIV, we observed a non-significant decrease in the total expression of GluR2 in cells treated with AMPA (**Figure 2B**).

Considering that these analyses had been performed with total protein extracts, we proposed to specifically assess the GluR2 subunit located on the extracellular side of the membrane in oligodendrocytes at 3DIV by immunofluorescence assay (**Figures 2C,F**). We found that AMPA provoked a significant decrease in extracellular GluR2 level, indicating that AMPA stimulation caused internalization of GluR2 (**Figures 2C,D**). In parallel, we did not detect significant alterations in the density of extracellular $GABA_{B1}R$ in AMPA-treated oligodendrocytes compared to control cells (**Figures 2C,E**). We then evaluated the impact of baclofen or muscimol treatments on extracellular GluR2 expression and observed that, in the absence of AMPA, muscimol but not baclofen led to higher levels of cell-surface GluR2 expression (**Figures 2F,G**). However, in the presence of the excitotoxic effect, both drugs reduced the downregulation of extracellular GluR2 subunits induced by AMPA, although the effect caused by muscimol was more robust than baclofen (**Figures 2F,H**). These results suggest that baclofen and muscimol maintain extracellular membrane GluR2 levels in oligodendrocytes subjected to AMPA, which could give them greater resistance to the excitotoxic stimulus.

## Baclofen and Muscimol Compromise Calcium Signaling Caused by Excitotoxicity in Oligodendrocytes

Increased calcium uptake is a common feature of excitotoxic damage in oligodendrocytes, which leads to a series of events resulting in cell stress and eventually cell death (Sánchez-Gómez and Matute 1999). Considering this, we monitored changes in intracellular calcium levels in response to AMPA stimulus, to determine whether baclofen or muscimol were able to reduce calcium uptake in response to AMPA. We induced an acute AMPA stimulus during cell recording and combined it with baclofen or muscimol added daily until the day of recording (2-3 DIV), or added 30 min before recording (**Figures 3A–C**). Representative measurements from live imaging showed that AMPA notably increased the fluorescence signal that positively correlated with intracellular calcium concentration (**Figure 3A**). We observed that oligodendrocyte incubation with baclofen or muscimol 30 min before AMPA reduced the magnitude of calcium uptake driven by AMPA, while treatment during 2-3 DIV with these drugs resulted in muscimol but not baclofen reducing the calcium response (**Figures 3B,C**). These data indicate that baclofen and muscimol reduce calcium influx induced by AMPA-mediated GluR activation in oligodendrocytes, after both chronic and acute pretreatment.

Among the damaging consequences of disruption of calcium homeostasis due to excitotoxic insults is the enhancement of calcium-dependent calpain protease activity, leading to an activation of apoptotic pathways (Sánchez-Gómez et al., 2011; Zhang et al., 2017). With the aim of elucidating whether baclofen or muscimol affected AMPA-induced calpain activity, we used the Calpain-Glo protease assay and determined calpain activation from 15 to 90 min after AMPA, in the absence or presence of GABAergic agonists 30 min before (**Figure 3D**). Our results showed that AMPA-induced calpain activation was reduced when combined with baclofen or muscimol at all analyzed time points. In addition, we evaluated the mitochondrial parameters that are altered in excitotoxicity because of calcium influx, such as mitochondrial membrane potential and ROS generation. First, the JC-1 probe was used to assess changes in the mitochondrial membrane potential gradient in oligodendrocytes exposed to AMPA in the presence or absence of GABAergic drugs, and the analysis was performed from 0 to 90 min after AMPA (**Figure 3E**). We observed that the presence of either baclofen or muscimol were able to prevent the reduction of mitochondrial membrane potential caused by AMPA, from 0 to 60 min after AMPA stimulus. ROS generation was measured using the CM-H2DCFDA probe and the analysis revealed how baclofen and muscimol prevented the increase in ROS levels caused by AMPA incubation (**Figure 3F**). Taken together, these results indicate that baclofen and muscimol can prevent AMPA-triggered calcium signaling in oligodendrocytes through calpain activation and mitochondrial dysfunction.

## Baclofen and Muscimol Do Not Interfere With Src, Akt, JNK, or CREB Activated by AMPA in Oligodendrocytes

Lastly, we determined whether the protective effects of baclofen or muscimol affected the activation of key molecules in several AMPA-driven signaling pathways in oligodendrocytes. We checked the phosphorylation levels of Src protein kinase, Akt, JNK and CREB in the presence or absence of baclofen or muscimol 30 min before AMPA, and analyzed 10 min or 1 h after AMPA stimulus (**Figure 4**). Immunoblot analysis proved that AMPA treatment strongly diminished phosphorylated Src (pSrc; **Figure 4A**) and Akt levels (pAkt; **Figure 4B**) assessed at a shorter time point (10 min after AMPA stimulus). However, pretreatment with GABAergic agonist did not modify either the basal expression in the absence of AMPA or the changes observed after toxic insult. Similarly, we showed that pJNK (**Figure 4C**) and pCREB expression (**Figure 4D**) were increased following AMPA addition (analyzed 1 h after); but, GABAergic drugs did not modulate this activation (**Figure 4B**). Overall, our results indicate that baclofen and muscimol are not able to restore the changes provoked by AMPA in the tested molecular signaling pathways under our analytical conditions.

# DISCUSSION

Glial cells constitute the vast majority of CNS cells. As described above, oligodendrocytes and myelin are vulnerable to enhanced glutamate signals, and glutamate-induced glial cell death is highly relevant for the pathophysiology of CNS diseases (Stys, 2004; Matute et al., 2006; Micu et al., 2006; Matute et al., 2007; Matute and Ransom, 2012; Fern and Matute, 2019). In humans, white matter (WM) constitutes about half of the CNS volume, which is a greater proportion than in other mammals, including those typically used for animal experiments. This feature may have misrepresented the importance of WM damage for the outcome of CNS diseases such as multiple sclerosis in humans, (Matute, 2011). Mature oligodendrocytes ensheathe axons, potential sources of high glutamate levels, and, they are therefore vulnerable to excitotoxicity. For that reason, the search for drugs that protect oligodendrocytes from this damage will provide novel agents to treat WM injury in the CNS. $GABA_B$ and $GABA_AR$ agonists have been described as displaying neuroprotective roles (Tu et al., 2010; Wei et al., 2012; Hleihil et al., 2021), and recent reports have outlined their importance in oligodendrocyte functionality, proliferation, differentiation and remyelination (Zonouzi et al., 2015; Kalakh and Mouihate, 2019; Serrano-Regal et a., 2020a; Serrano-Regal et al., 2020b; Bai et al., 2021; Serrano-Regal et al., 2022). Here, we demonstrate that baclofen and muscimol, $GABA_B$ and $GABA_AR$ agonists, respectively, exert a protective role in the oligodendrocyte response to glutamate-induced excitotoxicity, by alleviating the damage caused by this insult enhancing the presence of calcium-impermeable GluR2 subunits on the oligodendroglial cell surface.

Previous studies have established that cell-surface expression of GluR2 subunits in OPCs could be reduced by AMPA treatment (Hossain et al., 2014; Harlow et al., 2015), and similarly, we observed that moderate overactivation of AMPAR in mature oligodendrocytes downregulated the expression of GluR2 subunits in the cell membrane. This event is a crucial step in the onset of the excitotoxic program, as the calcium conductance of AMPARs differs markedly depending on whether the GluR2 subunit is a component of the membrane receptor (Hollmann et al., 1991; Jayakar and Dikshit, 2004). Calcium-permeable receptor channels are formed by GluR1, GluR3 or GluR4 subunits, whereas GluR2 subunits restrict calcium entry by rendering the receptor impermeable to calcium. In oligodendrocytes, calcium permeability of AMPARs was shown to be inversely correlated with the abundance of GluR2 subunits on the surface (Deng et al., 2006), indicating that GluR2 is critical for controlling oligodendroglial excitotoxicity.

In this work, we found that the sustained activation of GABARs with baclofen or muscimol stabilized calcium-impermeable GluR2 subunits on the surface of oligodendrocytes. We hypothesize that this stabilization mediates the protective role of baclofen and muscimol, which could prevent the consequent mitochondrial dysfunction through a reduction in calcium influx, the activation of calpain and oligodendrocyte death induced by AMPA. GABAR activation by its agonists may lead to an increase in GABAergic activity that must be neutralized by a decrease in glutamatergic activity, which in this case is achieved by stabilization of GluR2 in the cell membrane and consequent decrease in calcium influx. These compensatory mechanisms could achieve equilibrium in

neurotransmitter receptor expression to stabilize the response to synaptic activity. Thus, our results demonstrate that GABAergic drugs alter GluR2 trafficking mechanisms induced by AMPA, most likely through downregulation of endocytosis and/or endosomal recycling of GluR2 subunits. It is also possible that GABAR activation provokes intracellular signals that strengthen interactions between GluR2 subunits and cytoskeletal proteins, providing a more powerful anchoring of the receptor to the membrane. A clear interplay between GABA and glutamate receptors has been previously indicated in neurons, where treatment with baclofen was shown to affect the expression, activity and signaling of glutamate receptors under physiological and pathological conditions, restoring excitatory/inhibitory imbalance (Kantamneni, 2015). However, this close relationship between GABA and GluRs expressed in oligodendrocytes had not been described so far, and a thorough assessment of the molecules and pathways involved in this connection will be necessary, as well as determining its relevance in pathological conditions.

Focusing on the intracellular signaling triggered by the activation of AMPARs in oligodendrocytes, it is well accepted that the increase in cytoplasmic calcium is the key event (Sánchez-Gómez and Matute, 1999), and both baclofen and muscimol reduce the AMPA-induced calcium influx in oligodendrocytes. This reduction in intracellular calcium was observed in combination with a decrease in alterations of mitochondrial membrane potential, ROS production, and calpain activity all promoted by AMPA. ROS formation is closely related to alterations in the mitochondrial membrane potential, and leads to damages in DNA, proteins and lipids, resulting in progressive harmful events leading to cell dysfunction (Suski et al., 2018). Thus, the reduction in mitochondrial membrane potential alteration and consequent reduction in the levels of ROS caused by GABAergic drugs reinforces the role of baclofen and muscimol on cell survival and protection against excitotoxicity. Calpain activation is also known to induce cell dysfunction by proteolytic cleavage of various targets involved in apoptotic or necrotic pathways in addition to causing direct alterations in mitochondria (Mansouri et al., 2006; Sánchez-Gómez et al., 2011). Among the proteins targeted by calpain, we find Src protein kinase, which is cleaved by these proteases generating a truncated fragment that induces cell death in neurons and is related to inactivation of Akt signaling (Hossain et al., 2013). Src and Akt are mediators of key survival signaling pathways, and our results showed their early inactivation after AMPA stimulus (10 min). Moreover, we have previously described that AMPA triggered JNK and CREB activation (Canedo-Antelo et al., 2018); other authors have also shown the involvement of calpains in the processing of these molecules (Trinchese et al., 2008; Bollino et al., 2015; Messaoud et al., 2015). However, baclofen and muscimol did not seem to modulate these signaling mechanisms, at least during the times analyzed, despite reducing AMPA-induced calpain activity. Therefore, the molecules and/or pathways involved in the protective effect of baclofen or muscimol from excitotoxic damage caused by AMPA have not yet been determined. Further investigations are necessary to clarify the molecules and pathways involved in the oligoprotection exerted by baclofen or muscimol. The signaling axis involving Smac/DIABLO or p38 could be a promising target, given its relevance in calpain-targeted activity (Bollino et al., 2015; Messaoud et al., 2015).

GluR2 overexpression in OPCs favors not only OPC proliferation, but also oligodendrocyte regeneration following demyelinating brain injury, which suggests that suppressing AMPAR calcium signaling in OPCs could help to promote myelin repair (Khawaja et al., 2021). In this context, the restoration of cell-surface levels of GluR2 subunits in oligodendrocytes after AMPA insult, induced by baclofen and muscimol, could be relevant for the regenerative response after CNS damage and we endorse these drugs as promising tools for limiting oligodendrocyte death and myelin damage in demyelinating diseases.

Interestingly, we have observed that the muscimol effect is more homogeneous and robust than baclofen. Muscimol was able to reduce AMPA-induced cell death when applied after AMPA stimulus, increase GluR2 cell-surface expression even in the absence of AMPA, and reduce AMPA-associated calcium uptake when added 2-3 DIV before the recordings. This more consistent effect, independent of the time or duration of drug treatment, may be related to the faster response that ionotropic $GABA_AR$ activation causes in ion trafficking, compared to the metabotropic $GABA_BR$ (Frangaj and Fan, 2018). Nevertheless, given the positive neuroprotective effect resulting from co-activation of GABA receptors using muscimol and baclofen (Wei et al., 2012), a combination of GABAR agonists baclofen and muscimol may lead to a synergistic effect more powerful than the one exerted by each drug alone.

In conclusion, the present study shows how GABAR agonists, baclofen and muscimol, affect AMPA-induced excitotoxicity in oligodendrocytes by modulating calcium-related signaling and reducing cell death. Further analyses will clarify the exact mechanism of action of baclofen and muscimol to disrupt AMPA-induced damaging effect in oligodendrocytes and will confirm the observed protective effect of these drugs using in vivo models of CNS diseases related to excitotoxicity, including brain ischemia, or demyelinating diseases such as multiple sclerosis.

## DATA AVAILABILITY STATEMENT

The raw data supporting the conclusions of this article will be made available by the authors, without undue reservation.

## ETHICS STATEMENT

The animal study was reviewed and approved by Comité de Ética en la Investigación de la Universidad del País Vasco (UPV/EHU).

## AUTHOR CONTRIBUTIONS

MVS-G, LB-C, and CM designed the experiments. LB-C, MVS-G, BO-B, AR, and MO conducted the experiments. LB-C wrote the manuscript with input from all authors.

## FUNDING

This work was supported by the University of Basque Country (COLAB20/02), the Ministry of Science, Innovation and Universities (PID 2019-108465RB-100), the Basque government (ITI203-19 and 2021333019), and CIBERNED (CB06/05/0076). LB-C is a pre-doctoral fellow from the Basque government. BO-B is a pre-doctoral fellow from the Ministry of Universities (FPU20/06365).

## ACKNOWLEDGMENTS

We thank Zara Martínez for her technical support and Dr. Laura Escobar for her expert assistance with the Leica TCS STED SP8 laser scanning confocal microscope in the Achucarro Basque Center for Neuroscience. We also thank Dr. Patricia Aspichueta for kindly allowing us the use of the ChemiDoc MP Image System. Support provided by SGIker from the University of the Basque Country (UPV/EHU) (Animal Unit and Analytical and High-Resolution Microscopy in Biomedicine) is also gratefully acknowledged.

## REFERENCES

Bai, X., Kirchhoff, F., and Scheller, A. (2021). Oligodendroglial GABAergic Signaling: More Than Inhibition!. *Neurosci. Bull.* 37 (7), 1039–1050. doi:10.1007/s12264-021-00693-w

Barateiro, A., Vaz, A. R., Silva, S. L., Fernandes, A., and Brites, D. (2012). ER Stress, Mitochondrial Dysfunction and Calpain/JNK Activation Are Involved in Oligodendrocyte Precursor Cell Death by Unconjugated Bilirubin. *Neuromolecular Med.* 14 (4), 285–302. doi:10.1007/s12017-012-8187-9

Ben Messaoud, N., Yue, J., Valent, D., Katzarova, I., and López, J. M. (2015). Osmostress-induced Apoptosis in Xenopus Oocytes: Role of Stress Protein Kinases, Calpains and Smac/DIABLO. *PLoS One* 10 (4), e0124482. doi:10.1371/journal.pone.0124482

Bollino, D., Balan, I., and Aurelian, L. (2015). Valproic Acid Induces Neuronal Cell Death through a Novel Calpain-dependent Necroptosis Pathway. *J. Neurochem.* 133 (2), 174–186. doi:10.1111/jnc.13029

Canedo-Antelo, M., Serrano, M. P., Manterola, A., Ruiz, A., Llavero, F., Mato, S., et al. (2018). Inhibition of Casein Kinase 2 Protects Oligodendrocytes from Excitotoxicity by Attenuating JNK/p53 Signaling Cascade. *Front. Mol. Neurosci.* 11, 333. doi:10.3389/fnmol.2018.00333

Deng, W., Yue, Q., Rosenberg, P. A., Volpe, J. J., and Jensen, F. E. (2006). Oligodendrocyte Excitotoxicity Determined by Local Glutamate Accumulation and Mitochondrial Function. *J. Neurochem.* 98 (1), 213–222. doi:10.1111/j.1471-4159.2006.03861.x

Duchen, M. R. (2000). Mitochondria and Calcium: from Cell Signalling to Cell Death. *J. Physiol.* 529 Pt 1 (Pt 1), 57–68. doi:10.1111/j.1469-7793.2000.00057.x

Fern, R., and Matute, C. (2019). Glutamate Receptors and White Matter Stroke. *Neurosci. Lett.* 694, 86–92. doi:10.1016/j.neulet.2018.11.031

Frangaj, A., and Fan, Q. R. (2018). Structural Biology of GABAB Receptor. *Neuropharmacology* 136 (Pt A), 68–79. doi:10.1016/j.neuropharm.2017.10.011

Galluzzi, L., Blomgren, K., and Kroemer, G. (2009). Mitochondrial Membrane Permeabilization in Neuronal Injury. *Nat. Rev. Neurosci.* 10 (7), 481–494. doi:10.1038/nrn2665

Hamilton, N. B., Clarke, L. E., Arancibia-Carcamo, I. L., Kougioumtzidou, E., Matthey, M., Káradóttir, R., et al. (2017). Endogenous GABA Controls Oligodendrocyte Lineage Cell Number, Myelination, and CNS Internode Length. *Glia* 65 (2), 309–321. doi:10.1002/glia.23093

Harlow, D. E., Saul, K. E., Komuro, H., and Macklin, W. B. (2015). Myelin Proteolipid Protein Complexes with αv Integrin and AMPA Receptors *In Vivo* and Regulates AMPA-dependent Oligodendrocyte Progenitor Cell Migration through the Modulation of Cell-Surface GluR2 Expression. *J. Neurosci.* 35 (34), 12018–12032. doi:10.1523/JNEUROSCI.5151-14.2015

Hleihil, M., Vaas, M., Bhat, M. A., Balakrishnan, K., and Benke, D. (2021). Sustained Baclofen-Induced Activation of GABA B Receptors after Cerebral Ischemia Restores Receptor Expression and Function and Limits Progressing Loss of Neurons. *Front. Mol. Neurosci.* 14, 726133. doi:10.3389/fnmol.2021.726133

Hollmann, M., Hartley, M., and Heinemann, S. (1991). Ca2+ Permeability of KA-AMPA-Ggated Glutamate Receptor Channels Depends on Subunit Composition. *Science* 252 (5007), 851–853. doi:10.1126/science.1709304

Hossain, M. I., Roulston, C. L., Kamaruddin, M. A., Chu, P. W., Ng, D. C., Dusting, G. J., et al. (2013). A Truncated Fragment of Src Protein Kinase Generated by Calpain-Mediated Cleavage Is a Mediator of Neuronal Death in Excitotoxicity. *J. Biol. Chem.* 288 (14), 9696–9709. doi:10.1074/jbc.M112.419713

Hossain, S., Liu, H. N., Fragoso, G., and Almazan, G. (2014). Agonist-induced Down-Regulation of AMPA Receptors in Oligodendrocyte Progenitors. *Neuropharmacology* 79, 506–514. doi:10.1016/j.neuropharm.2013.12.020

Jantzie, L. L., Winer, J. L., Corbett, C. J., and Robinson, S. (2016). Erythropoietin Modulates Cerebral and Serum Degradation Products from Excess Calpain Activation Following Prenatal Hypoxia-Ischemia. *Dev. Neurosci.* 38 (1), 15–26. doi:10.1159/000441024

Jayakar, S. S., and Dikshit, M. (2004). AMPA Receptor Regulation Mechanisms: Future Target for Safer Neuroprotective Drugs. *Int. J. Neurosci.* 114 (6), 695–734. doi:10.1080/00207450490430453

Kalakh, S., and Mouihate, A. (2019). Enhanced Remyelination during Late Pregnancy: Involvement of the GABAergic System. *Sci. Rep.* 9 (1), 7728. doi:10.1038/s41598-019-44050-4

Kantamneni, S. (2015). Cross-talk and Regulation between Glutamate and GABAB Receptors. *Front. Cell. Neurosci.* 9, 135. doi:10.3389/fncel.2015.00135

Káradóttir, R., Hamilton, N. B., Bakiri, Y., and Attwell, D. (2008). Spiking and Nonspiking Classes of Oligodendrocyte Precursor Glia in CNS White Matter. *Nat. Neurosci.* 11 (4), 450–456. doi:10.1038/nn2060

Khawaja, R. R., Agarwal, A., Fukaya, M., Jeong, H. K., Gross, S., Gonzalez-Fernandez, E., et al. (2021). GluA2 Overexpression in Oligodendrocyte Progenitors Promotes Postinjury Oligodendrocyte Regeneration. *Cell. Rep.* 35 (7), 109147. doi:10.1016/j.celrep.2021.109147

Kukley, M., Kiladze, M., Tognatta, R., Hans, M., Swandulla, D., Schramm, J., et al. (2008). Glial Cells Are Born with Synapses. *FASEB J.* 22 (8), 2957–2969. doi:10.1096/fj.07-090985

Lin, S. C., and Bergles, D. E. (2004). Synaptic Signaling between Neurons and Glia. *Glia* 47 (3), 290–298. doi:10.1002/glia.20060

Mansouri, B., Henne, W. M., Oomman, S. K., Bliss, R., Attridge, J., Finckbone, V., et al. (2006). Involvement of Calpain in AMPA-Induced Toxicity to Rat Cerebellar Purkinje Neurons. *Eur. J. Pharmacol.* 557 (2-3), 106–114. doi:10.1016/j.ejphar.2006.11.032

Matute, C., Alberdi, E., Domercq, M., Pérez-Cerdá, F., Pérez-Samartín, A., and Sánchez-Gómez, M. V. (2001). The Link between Excitotoxic Oligodendroglial Death and Demyelinating Diseases. *Trends. Neurosci.* 24 (4), 224–230. doi:10.1016/s0166-2236(00)01746-x

Matute, C., Alberdi, E., Domercq, M., Sánchez-Gómez, M. V., Pérez-Samartín, A., Rodríguez-Antigüedad, A., et al. (2007). Excitotoxic Damage to White Matter. *J. Anat.* 210 (6), 693–702. doi:10.1111/j.1469-7580.2007.00733.x

Matute, C., Domercq, M., and Sánchez-Gómez, M. V. (2006). Glutamate-mediated Glial Injury: Mechanisms and Clinical Importance. *Glia* 53 (2), 212–224. doi:10.1002/glia.20275

Matute, C. (2011). Glutamate and ATP Signalling in White Matter Pathology. *J. Anat.* 219 (1), 53–64. doi:10.1111/j.1469-7580.2010.01339.x

Matute, C., and Ransom, B. R. (2012). Roles of White Matter in Central Nervous System Pathophysiologies. *ASN Neuro* 4 (2), e00079. doi:10.1042/AN20110060

Matute, C., Sánchez-Gómez, M. V., Martínez-Millán, L., and Miledi, R. (1997). Glutamate Receptor-Mediated Toxicity in Optic Nerve Oligodendrocytes. *Proc. Natl. Acad. Sci. U. S. A.* 94 (16), 8830–8835. doi:10.1073/pnas.94.16.8830

McDonald, J. W., Althomsons, S. P., Hyrc, K. L., Choi, D. W., and Goldberg, M. P. (1998). Oligodendrocytes from Forebrain Are Highly Vulnerable to AMPA/kainate Receptor-Mediated Excitotoxicity. *Nat. Med.* 4 (3), 291–297. doi:10.1038/nm0398-291

Micu, I., Jiang, Q., Coderre, E., Ridsdale, A., Zhang, L., Woulfe, J., et al. (2006). NMDA Receptors Mediate Calcium Accumulation in Myelin during Chemical Ischaemia. *Nature* 439 (7079), 988–992. doi:10.1038/nature04474

Ness, J. K., Scaduto, R. C., Jr., and Wood, T. L. (2004). IGF-I Prevents Glutamate-Mediated Bax Translocation and Cytochrome C Release in O4+ Oligodendrocyte Progenitors. *Glia* 46, 183–194. doi:10.1002/glia.10360

Ruiz, A., Alberdi, E., and Matute, C. (2014). CGP37157, an Inhibitor of the Mitochondrial Na+/Ca2+ Exchanger, Protects Neurons from Excitotoxicity by Blocking Voltage-Gated $Ca^{2+}$ Channels. *Cell death. Dis.* 5 (4), e1156. doi:10.1038/cddis.2014.134

Sánchez-Gómez, M. V., Alberdi, E., Ibarretxe, G., Torre, I., and Matute, C. (2003). Caspase-dependent and Caspase-independent Oligodendrocyte Death Mediated by AMPA and Kainate Receptors. *J. Neurosci.* 23 (29), 9519–9528. doi:10.1523/JNEUROSCI.23-29-09519.2003

Sánchez-Gómez, M. V., Alberdi, E., Pérez-Navarro, E., Alberch, J., and Matute, C. (2011). Bax and Calpain Mediate Excitotoxic Oligodendrocyte Death Induced by Activation of Both AMPA and Kainate Receptors. *J. Neurosci.* 31 (8), 2996–3006. doi:10.1523/JNEUROSCI.5578-10.2011

Sánchez-Gómez, M. V., and Matute, C. (1999). AMPA and Kainate Receptors Each Mediate Excitotoxicity in Oligodendroglial Cultures. *Neurobiol. Dis.* 6 (6), 475–485. doi:10.1006/nbdi.1999.0264

Sánchez-Gómez, M. V., Serrano, M. P., Alberdi, E., Pérez-Cerdá, F., and Matute, C. (2018). Isolation, Expansion, and Maturation of Oligodendrocyte Lineage Cells Obtained from Rat Neonatal Brain and Optic Nerve. *Methods Mol. Biol.* 1791, 95–113. doi:10.1007/978-1-4939-7862-5_8

Serrano-Regal, M. P., Bayón-Cordero, L., Ordaz, R. P., Garay, E., Limon, A., Arellano, R. O., et al. (2020). Expression and Function of GABA Receptors in Myelinating Cells. *Front. Cell. Neurosci.* 14, 256. doi:10.3389/fncel.2020.00256

Serrano-Regal, M. P., Luengas-Escuza, I., Bayón-Cordero, L., Ibarra-Aizpurua, N., Alberdi, E., Pérez-Samartín, A., et al. (2020). Oligodendrocyte Differentiation and Myelination Is Potentiated via GABAB Receptor Activation. *Neuroscience* 439, 163–180. doi:10.1016/j.neuroscience.2019.07.014

Serrano-Regal, M. P., Bayón-Cordero, L., Chara, J. C., Tepavcevic, V., Ochoa-Bueno, B. I., Matute, C., et al. (2022). *GABABR Agonist Baclofen Promotes Central Nervous System Remyelination*. bioRxiv Prepr.doi:10.1101/2022.01.28.478233

Shaw, J. C., Crombie, G. K., Palliser, H. K., and Hirst, J. J. (2021). Impaired Oligodendrocyte Development Following Preterm Birth: Promoting GABAergic Action to Improve Outcomes. *Front. Pediatr.* 9, 618052. doi:10.3389/fped.2021.618052

Simonishvili, S., Jain, M. R., Li, H., Levison, S. W., and Wood, T. L. (2013). Identification of Bax-Interacting Proteins in Oligodendrocyte Progenitors during Glutamate Excitotoxicity and Perinatal Hypoxia-Ischemia. *ASN Neuro* 5 (5), e00131. doi:10.1042/AN20130027

Singh, A., Kukreti, R., Saso, L., and Kukreti, S. (2019). Oxidative Stress: a Key Modulator in Neurodegenerative Diseases. *Molecules* 24 (8), 1583. doi:10.3390/molecules24081583

Stys, P. K. (2004). White Matter Injury Mechanisms. *Curr. Mol. Med.* 4 (2), 113–130. doi:10.2174/1566524043479220

Suski, J., Lebiedzinska, M., Bonora, M., Pinton, P., Duszynski, J., and Wieckowski, M. R. (2018). Relation between Mitochondrial Membrane Potential and ROS Formation. *Methods Mol. Biol.* 1782, 357–381. doi:10.1007/978-1-4939-7831-1_22

Trinchese, F., Fa', M., Liu, S., Zhang, H., Hidalgo, A., Schmidt, S. D., et al. (2008). Inhibition of Calpains Improves Memory and Synaptic Transmission in a Mouse Model of Alzheimer Disease. *J. Clin. Investig.* 118 (8), 2796–2807. doi:10.1172/JCI34254

Tu, H., Xu, C., Zhang, W., Liu, Q., Rondard, P., Pin, J.-P., et al. (2010). GABAB Receptor Activation Protects Neurons from Apoptosis via IGF-1 Receptor Transactivation. *J. Neurosci.* 30 (2), 749–759. doi:10.1523/JNEUROSCI.2343-09.2010

Wang, C. Y., Xie, J. W., Wang, T., Xu, Y., Cai, J. H., Wang, X., et al. (2013). Hypoxia-triggered M-Calpain Activation Evokes Endoplasmic Reticulum Stress and Neuropathogenesis in a Transgenic Mouse Model of Alzheimer's Disease. *CNS Neurosci. Ther.* 19 (10), 820–833. doi:10.1111/cns.12151

Wei, X. W., Yan, H., Xu, B., Wu, Y. P., Li, C., and Zhang, G. Y. (2012). Neuroprotection of Co-activation of GABA Receptors by Preventing Caspase-3 Denitrosylation in KA-Induced Seizures. *Brain Res. Bull.* 88 (6), 617–623. doi:10.1016/j.brainresbull.2012.05.008

Yoshioka, A., Hardy, M., Younkin, D. P., Grinspan, J. B., Stern, J. L., and Pleasure, D. (1995). Alpha-amino-3-hydroxy-5-methyl-4-isoxazolepropionate (AMPA) Receptors Mediate Excitotoxicity in the Oligodendroglial Lineage. *J. Neurochem.* 64 (6), 2442–2448. doi:10.1046/j.1471-4159.1995.64062442.x

Zhang, Y., Liu, N. M., Wang, Y., Youn, J. Y., and Cai, H. (2017). Endothelial Cell Calpain as a Critical Modulator of Angiogenesis. *Biochim. Biophys. Acta. Mol. Basis. Dis.* 1863 (6), 1326–1335. doi:10.1016/j.bbadis.2017.03.021

Zonouzi, M., Scafidi, J., Li, P., McEllin, B., Edwards, J., Dupree, J. L., et al. (2015). GABAergic Regulation of Cerebellar NG2 Cell Development Is Altered in Perinatal White Matter Injury. *Nat. Neurosci.* 18 (5), 674–682. doi:10.1038/nn.3990

**Conflict of Interest:** The authors declare that the research was conducted in the absence of any commercial or financial relationships that could be construed as a potential conflict of interest.

**Publisher's Note:** All claims expressed in this article are solely those of the authors and do not necessarily represent those of their affiliated organizations, or those of the publisher, the editors and the reviewers. Any product that may be evaluated in this article, or claim that may be made by its manufacturer, is not guaranteed or endorsed by the publisher.

# Advantages of publishing in Frontiers

**OPEN ACCESS**
Articles are free to read for greatest visibility and readership

**FAST PUBLICATION**
Around 90 days from submission to decision

**HIGH QUALITY PEER-REVIEW**
Rigorous, collaborative, and constructive peer-review

**TRANSPARENT PEER-REVIEW**
Editors and reviewers acknowledged by name on published articles

**Frontiers**
Avenue du Tribunal-Fédéral 34
1005 Lausanne | Switzerland

**Visit us:** www.frontiersin.org
**Contact us:** frontiersin.org/about/contact

**REPRODUCIBILITY OF RESEARCH**
Support open data and methods to enhance research reproducibility

**DIGITAL PUBLISHING**
Articles designed for optimal readership across devices

**FOLLOW US**
@frontiersin

**IMPACT METRICS**
Advanced article metrics track visibility across digital media

**EXTENSIVE PROMOTION**
Marketing and promotion of impactful research

**LOOP RESEARCH NETWORK**
Our network increases your article's readership